The influence of N6-methyladenosine (m^6A) RNA methylation on synaptic function and local protein synthesis

Braulio Martinez De La Cruz

BSc (Hons)

Thesis submitted to The University of Nottingham for the degree of Doctor of Philosophy

June 2019

Declaration

I declare that this thesis is the result of my own work which has been mainly undertaken during my period of registration for this degree at The University of Nottingham. Any content that is not my own or the product of a collaboration has been properly acknowledged in the text. I have complied with the word limit for my degree.

_____

Signed: Braulio Martinez De La Cruz

Date: 28th June, 2019

Abstract

Leading theories on learning and memory postulate the importance of strengthening specific synaptic pathways, communication of post- and pre-synaptic terminals, and dendritic local protein synthesis. RNA-binding proteins which recognise epigenomic N6-methyladenosine (m^6A) messenger RNA modifications can regulate a number of molecular functions including polyribosome loading, RNA decay, splicing, and translation. To investigate whether and how synaptic plasticity may be regulated by m^6A RNA processing, three approaches were undertaken.

First, I analysed m^6A-sequencing data of human grey matter, white matter, and fetal tissue to identify transcripts that were m^6A-methylated in human brain, as well as the biological processes and diseases enriched in this data. Several transcripts whose protein product is important in synaptic structure and function, particularly neurotransmitter receptors, were found to be methylated. The most highly enriched gene ontology terms included “synapses” and “nervous system development,” suggesting a function for m^6A methylation in plasticity.

Second, I performed immunofluorescent assays on quiescent and activated neuronal cell lines to examine changes in colocalisation of m^6A modifications with m^6A-binding proteins at synapses. Colocalisation of m^6A and YTHDF1, YTHDF3, and ALKBH5 at synapses all increased significantly after 15 minutes of glutamate receptor activation. Changes were also observed 24 hours after activation. These results suggest the

binding of these proteins to m^{6}A-mRNAs responds to plasticity processes and is time-dependent.

Third, abundance of m^{6}A-modified RNA and expression of YTHDF1/YTHDF3 in the cerebellum, frontal and cingulate gyrus cortex, and hippocampus of normal and neurological disease-affected human brain was examined. Using machine learning quantitative analysis, I found m^{6}A abundance and YTH protein expression to be differently dysregulated in each region and neuronal population of brain affected by Parkinson's disease, Lewy Body Dementia, and cognitive defects.

Overall, these findings provide evidence highlighting the importance of m^{6}A-mediated regulation of local protein synthesis at synapses, providing a clearer understanding of the processes involved in normal synaptic and neuronal function and how m^{6}A regulation may contribute to the pathophysiology of brain disease.

Acknowledgements

First and foremost, I would like to express my gratitude to my primary supervisor, Dr. Helen M. Knight, for providing me the opportunity to work in a novel and exciting project and trusting me with its development. Throughout my PhD, her supervision and discussions have helped me develop into a better researcher. I would also like to thank my co-supervisors Dr. Ian Macdonald and Dr. Rupert Fray for their guidance, comments, and support over the years.

I am also thankful to all our current and former lab members including Dr. Miles Flitton, Dr. Maria Koromina, Maria Isabel Haig, Nicholas Reilly, and Eleanor Bellows. Their assistance in learning some methods and above all, their companionship through this project helped motivate me to do my best.

Special thanks go to every member of the University of Nottingham's SLIM facility. They trained me in the use of various microscopic techniques, tissue preparation, and image analysis. In particular, I would like to thank Dr. Chris Gell and Dr. Robert Markus, whom I worked with most closely to analyse confocal and super resolution images, respectively.

I would also like to express my gratitude to CONACYT and the University of Nottingham for funding my PhD. Their support made this possible.

On a personal note, I would like to thank my parents, Dr. Gerardo Martinez Suzuki and Dr. Maribell De La Cruz Lopez, and my grandfather, Dr. Julio Cesar De La Cruz, for teaching me the importance of a scientific mind and helping me achieve my dream of studying in the UK. I thank my family as whole for their support and care through these years. I also thank my girlfriend, Dr. Brenda Canales, for her love and support and the great moments we have lived together through the course of our PhDs.

Finally, I would like to dedicate my work to the memory of my grandmother Olga Suzuki, who taught me kindness and piousness. I keep you with me despite the distance.

Table of Contents

List of Figures

List of Tables

Abbreviations

CA *Cornu ammonis*
LTP Long-term potentiation
NMDA N-methyl-D-aspartate
VGluT1 Vessicle Glutamate Transporter 1
PSD Post-synaptic density
CaMKII Ca2+/calmodulin-dependent protein kinase
PKC Protein kinase C
E-LTP Early long-term potentiation
L-LTP Late long-term potentiation
RNA Ribonucleic acid
mRNA Messenger ribonucleic acid
tRNA Transfer ribonucleic acid
AMPA α-amino-3-hydroxy-5-methyl-4-isoxazolepropionic acid
BDNF Brain-derived neurotrophic factor
FMRP Fragile X mental retardation protein
CYFPI1 Cytoplasmic FMRP-interacting protein 1
eIF4 Eukaryotic initiation factor 4
TDP-43 Transactive response DNA binding protein
FXS Fragile X syndrome
FXR1 Fragile X-related protein 1
FXR2 Fragile X-related protein 2
PD Parkinson's disease
AD Alzheimer's disease
LBD Lewy body dementia
MCI Mild cognitive impairment
CB Cerebellum
CG Cingulate gyrus
PFC Prefrontal cortex
HIP Hippocampus
SNCA alpha-synuclein
APOE Apolipoprotein E
m^6A N6-methyladenosine RNA modification
UTR Untranslated region of mRNA
HEPG2 Hepatic G2 immortalised cell line
m^1A N1-methyladenosine RNA modification
m^6A_m N6,2′-O-dimethyladenosine
METTL3 Methyltransferase-like protein 3
METTL14 Methyltransferase-like protein 14
WTAP Wilms-associated tumour protein
SAM S-adenosine methionine
FTO Fat mass and obesity-associated protein
ALKBH5 Alpha-ketoglutarate-dependent dioxygenase alkB homolog 5
YTHDF YTH domain family
YTHDC YTH domain-containing
hnRNP heterogeneous nuclear ribonucleoprotein
RNP Ribonucleoprotein
STEM Scanning transmission electron microscopy
ICC Immunocytochemistry
IHC Immunohistochemistry

DMEM Dulbecco's modified Eagle medium
dbcAMP Dibutyryl-cyclic-adenosine-monophosphate
cAMP Cyclic-adenosine-monophosphate
DMSO Dimethyl sulfoxide
HBSS Hank's balanced salt solution
PFA Paraformaldehyde
DAPI 4′,6-diamidino-2-phenylindole
PBS Phosphate buffer solution
SRM Super resolution microscopy
SIM Structured illumination microscopy
PCC Pearson's correlation coefficient
ANOVA Analysis of variance
DAB 3,3′-Diaminobenzidine
FFPE Formalin-fixed paraffin-embedded
NA Numerical aperture
GFAP Glial fibrillary acidic protein
BSA Bovine serum albumin
TRIS Trisaminomethane
HOMER Hypergeometric Optimization of Motif EnRichment
DAVID Database for Annotation, Visualization and Integrated Discovery
NGS Next-generation sequencing
m^{6}A-seq m^{6}A next-generation sequencing
PCW Post-conception week
TSS Transcription start site
TTS Transcription termination site
GO Gene ontology
BPD Bipolar disorder
ADHD Attention deficit hyperactivity disorder
DNA Deoxyribonucleic acid
FRET Förster resonance energy transfer
GL Granular cell layer
PL Purkinje cell layer
ML Molecular layer
SUB Subiculum
DG Dentate Gyrus
CRISPR Clustered regularly interspaced short palindromic repeats

Chapter 1:

Introduction

1.1 Cognition, Learning, and Memory

Today's neuroscience is a merger of neurophysiology, anatomy, developmental biology, cell and molecular biology, and cognitive psychology. Neuroscience as we understand it today is grounded on the idea, first stated by Hippocrates in the fourth century BC, that the study of the mind begins with the brain. By studying this organ's physical properties, we seek to understand its emerging properties, such as thought.

One of the brain's functions is cognition. Cognition can be defined as "the collection of mental processes and activities used in perceiving, remembering, thinking, and understanding, as well as the act of using these processes (Ashcraft & Radvansky, 2014)." Learning is also an important function of the human brain. It can be defined as the process by which we gain knowledge. This can include knowledge of events, of our immediate surroundings, of other people, etc. Learning is also essential to human life. Memory is a third function of the brain to help us understand the mind. It can be defined as "the process by which that knowledge is encoded, stored, and later retrieved (Kandel et al., 2000) . This way we can see how learning and memory are related, as it is the former that obtains information for memory to work with.

Memory is particularly important in research, as memory performance tests are often used to evaluate cognition. Memory is subdivided into explicit (conscious) and implicit (non-conscious), with explicit memory further divided into: episodic, which deals with specific

events; and semantic, which deals with facts or other forms of knowledge (Kandel et al., 2000).

Memory is theorised to be a four-process function (Ashcraft & Radvansky, 2014). After the perception of stimuli, the first process is encoding. Encoding is the transformation of physical stimuli into spatiotemporal patterns of neuronal activation. Afterwards, the information must be stabilised through the process of consolidation. Consolidation is both synaptic, occurring within a few hours and consisting of long-term potentiation of synapses; and systematic, by which hippocampus-dependent memories transition to being independent by forming new connections in the neocortex that have the same potentiation pattern as in the hippocampus. Through long-term potentiation, the process of storage occurs. Storage is a passive process in which information can be maintained as long-term, short-term, or sensory memory. The last process of memory is retrieval. Retrieval consists of reactivation of the neural network where a memory was stored and moving a memory from long to short-term memory for a while. None of these four processes is fully understood and they are all targets of modern neuroscience research.

Impaired memory is a critical early symptom of many brain diseases, most commonly neurodegeneration. For example, impaired memory is the chief characteristic of Alzheimer's disease, which is the most common form of dementia and represents 60-70% of cases (Duthey, 2013). According to a 2018 report by the National Office of Statistics, there are currently around 24 million individuals in the UK appropriately

aged for the onset of neurodegenerative disease (UK Statistics, 2018). This amounts to 37% of the country's population. In the UK alone, it is estimated that dementia costs the economy £17 billion per year (Medical Research Council, 2019).

Other forms of brain disease affect cognition and perception. Disorders such as mental retardation, mild cognitive impairment, autism, and schizophrenia all represent human and economic costs. As such, research into the bases of cognition, learning, and memory has become paramount to the work of academia and governments.

1.2 The hippocampal formation

The hippocampal formation is a functional system which has long been studied and associated to information processing, learning, and memory. Hippocampal volume has been shown to correlate with species differences in cognition (Shultz & Dunbar, 2010). This is one example of why the hippocampus is widely considered to be an adept model for a heuristic approach to neuroscience research.

While many types of explicit memory exist, they are all connected to the hippocampal formation since it helps form associations in the neocortex. It holds information while "constructing memories" in other areas and slowly releasing that information to be stored in new connections. The hippocampal formation is therefore essential for all memory processes.

In relation to the hippocampal formation's function as the system in charge of memory is the theory of the hippocampus as a spatial map. This theory, first put forward in 1971 by O'Keefe and Dostrovsky,

proposes that the hippocampus can create cognitive maps in order to arrange concepts and locations. Based on the lateralisation of the human brain, the proposal says that the left side of the brain creates semantic maps, while the right side of the brain creates spatial maps. The first evidence supporting this theory was the discovery of place-coded neurons in rats. Rats in an unknown free-moving environment were found to have specific hippocampal neurons firing only at specific sites, suggesting that a conceptualisation of the environment had been formed in the rat brain's hippocampus after only one time seeing their new environment. The theory has since expanded to humans with the assumption that a semantic cognitive map can be developed, too, in order to know which part of a narrative goes first or to be able to visualize a story in which characters move. This is one example of physical phenomena in hippocampal cells which has served to explain how our minds work and which has demonstrated the essential role of the hippocampus in daily life (O'Keefe & Dostrovsky, 1971; O'Keefe & Nades, 1979).

The organization of the hippocampal formation is likely key to its unique role in memory processing. It is composed of the entorhinal cortex, subiculum, the dentate gyrus, and the *cornu ammonis* (subdivided into CA1, CA2, CA3, and CA4 fields). The system is unique in many ways and part of what makes the hippocampal formation stand out from neocortical regions is that information in this system flows unidirectionally. As opposed to most connections between brain structures, the hippocampal formation does not demonstrate reciprocal

signalling between its components. Rather, there is a flow of information similar to a cycle (**Figure 1.1**). The flow of information is as follows: the entorhinal cortex acts as the receptor of information and disseminates this information to the dentate gyrus in a connection called the performant pathway. The dentate gyrus then connects to the CA3 field. This field in turn, communicates with CA1 by stretching its neuronal processes across CA2. After reaching CA1, the non-reciprocity rule is increasingly lax, as CA1 will communicate with both the subiculum and the entorhinal cortex, which will form a connection with both. This is a basic summary of the way information flows in the hippocampal formation but it is important to remember that each structure will contribute to the hippocampal function in its own unique way.

For example, a big species-specific feature is that the human entorhinal complex appears to be associated with stronger interconnections with the associational areas of the neocortex, which are also more developed in humans. This supports the idea of the entorhinal cortex being the receptor of information in the hippocampal formation, as well as suggesting that in humans, non-motor and non-sensory information is important to the hippocampus's function (Andersen et al., 2006). Moreover, a study of the entorhinal cortex's involvement in memory-related disease has shown that this is one of the first structures to be affected by β-amyloid plaques in Alzheimer's disease (Hoesen et al., 1991).

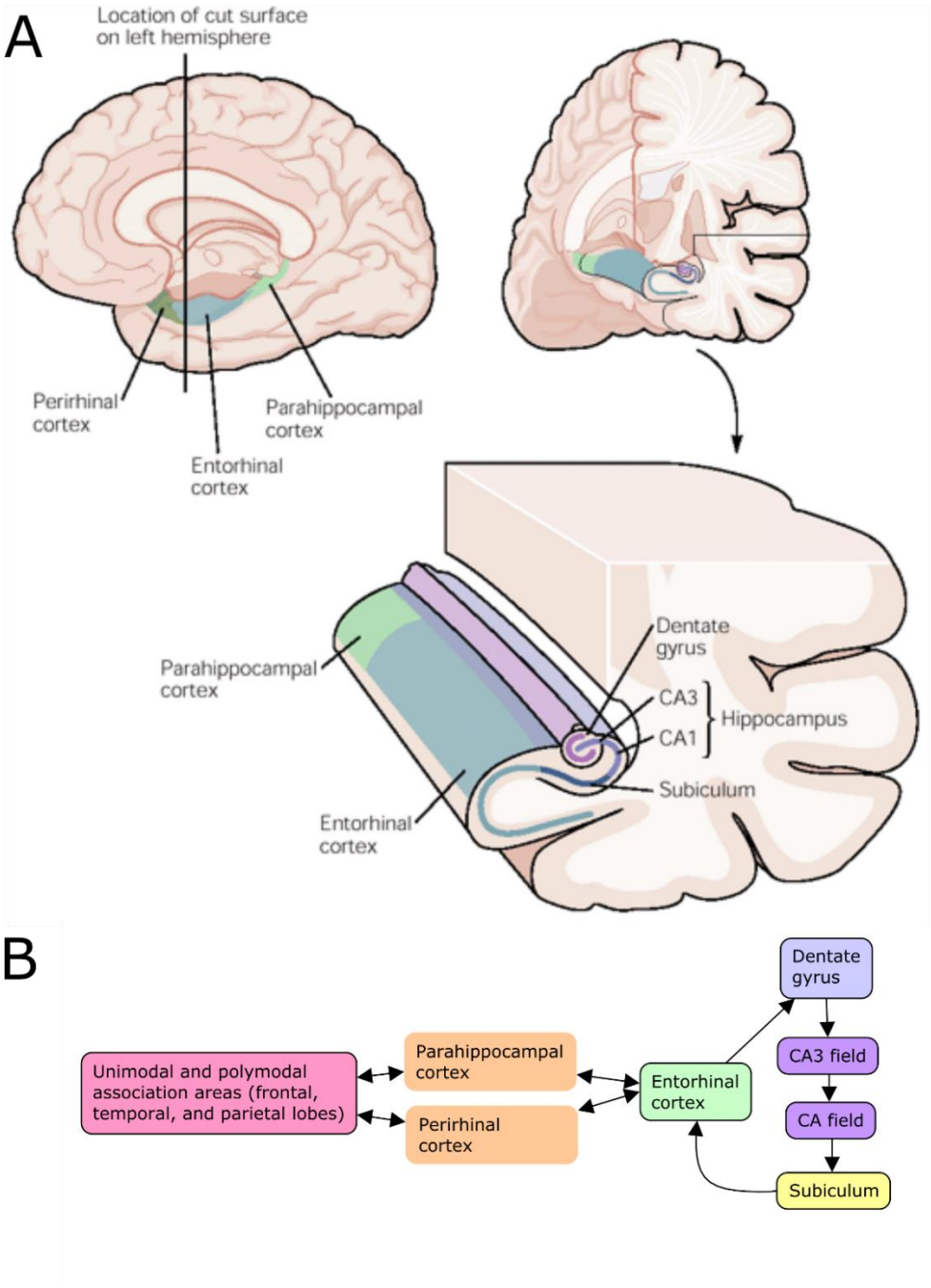

Figure 1.1 Anatomy and flow of information in the hippocampus. A) Sagittal (left) and coronal (right) views of the hippocampus within normal human brain. Adapted from Kandel et al., 2000. B) Diagram depicting the flow of information received and transmitted by the hippocampus. This information is unique as it is transmitted in a non-reciprocal manner.

The dentate gyrus, too, has very specific and important functions: neurogenesis and information relay. Consider that the hippocampal formation is the last system to receive information from the visual association cortex and other areas that gather sensory information. Using this information as stimulus, the hippocampal formation then stimulates cells with similar information to make connections amongst themselves so that, for example, the face of a friend will also bring back memories of their height, voice, or other characteristics (Kandel et al., 2000). This is the result of adult-hippocampal neurogenesis, the process by which neural stem cells from the dentate gyrus differentiate into neurons, being specially high in and around the dentate gyrus, which contributes to hippocampal function through disambiguation of similar input patterns initially received by the entorhinal cortex and passed on to the dentate gyrus. This process of clarifying signals is called pattern separation. It is notable that even after pattern separation, some connection remains between information and cells that store this information create associations between themselves. In this way, a friend's face is invariantly attached to memories of time spent with said friend (Oomen et al., 2014).

Association memory in the dentate gyrus is still not fully understood. Some reports have proposed neurogenesis in the dentate gyrus is key to the association of time and memories (Aimone et al., 2006). Others have persistently observed propagation of long-term potentiation (LTP, see **1.3.3**) through dentate gyrus synapses to be a feature of associative memory (Christie & Abraham, 1992; Levy & Steward, 1979).

The other two major components of memory are both part of the hippocampus. The CA3 field, which is located next to the dentate gyrus, has been hypothesised to be largely involved in the formation of contextual memories (Ramamoorthi et al., 2011). The CA3 field acts as an association matrix which enables all elements that constitute a memory – taste, sound, sight, smell, location, time – to be assembled together and made into a single memory. Simultaneously, some studies suggest the CA3 field can accentuate one of these elements of a memory during recall, a process dependent on the presence of N-methyl-D-aspartate (NMDA) receptors (Nakazawa, 2002). Human CA3 size has also been found to predict the quality of memory recall, suggesting the link between CA3 and associative memory is strong (Chadwick et al., 2014).

Next, the CA1 field is hypothesised to prepare a memory for long-term storage in the neocortex through the process of consolidation – the process by which an initial pattern of temporary neuronal activation is transformed into a permanent memory trace manifested as changes in the pattern of synaptic interconnectivity (Parkin, 1996). Additionally, rapid NMDA-dependent dendritic morphogenesis in CA1 neurons has been strongly associated with the retrieval of contextual memories and spatial maps, making this region critical to learning (Burgess et al., 2002; Chen et al., 2010; Ji & Maren, 2008; Tsien et al., 1996).

The functions of these two neuronal populations within the hippocampus have been supported by studies in patients with lesions. Initially, a study was published about a patient named RB, who had a stroke in the

temporal lobe which left him with a marked inability to form new long-term memories but only a small issue recalling memories from before his lesion. Post-mortem studies of RB showed that the damage was restricted to the CA1 field of the hippocampus (Zola-Morgan et al., 1986). Other patients, named GD, LM, and WH, all had small lesions to the CA1 field, but the latter two had more extensive damage that covered the CA2 and CA3 fields. GD, with a similar lesion to the original RB patient, showed amnesia consistent with RB. LM and WH showed the same problems with creating new memories but also showed a decreased ability in recalling contextual aspects of memories they had not lost. Additionally, LM and WH were unable to remember the 15 and 25 years before their injuries, respectively (Parkin, 1996). More recently, neuroimaging studies continue to support the role of CA1 in long-term memory formation and have found that autobiographical memory is also impaired following CA1 lessions (Bartsch et al., 2011).

1.2 Neuronal populations of the hippocampus

Why do different regions of the hippocampus have different functions? A clue towards answering this question lays in the unique cytology and cytoarchitecture of the hippocampus and its subfields.

The hippocampal formation has one principal cell type: pyramidal cells. Pyramidal cells are named so because of the shape of their cell body, or soma. They feature a large apical dendrite (protruding from the top of the pyramid shape), multiple basal dendrites, and the presence of dendritic spines. This cell type is present in all hippocampal formation structures.

The differences between the fields of the hippocampus lie in the size of their pyramidal shapes and the density of their populations. The CA3 field is densely populated with large pyramidal cells whose dendrites vary considerably in length. CA3 pyramidal cells receive their input from the mossy fibres of the dentate gyrus. CA2 only differs from CA3 because it receives input only from the latter (Andersen et al., 2006). CA1 however, has small pyramidal cells whose long length and number of dendrites are homogeneous. CA1 receives its input from CA2 and the entorhinal cortex (Pyapali et al., 1998).

Some other cell types in the hippocampal formation include interneurons and glial cells for relaying information and supporting pyramidal cells, respectively. In the dentate gyrus, there is also a granule cell layer which is the principal area of adult neurogenesis (Ming & Song, 2011). This cell type is characterised by small, rounded somata.

From this information, we surmise that since cells are all the same type, the differences in function of each field in the hippocampal formation could be partly attributed to their cytoarchitectural organisation. Therefore, to understand learning and memory, one approach is to research pyramidal cells and hippocampal cytoarchitecture, including neuronal pathways.

1.3 Synaptic bases of memory

1.3.1 Synapses

Neurons are electrically excitable. They receive and transmit electrical impulses known as action potentials to other neurons. Action potentials are propagated throughout the cell membrane due to the opening of voltage-gated channels, principally sodium. The inside of the cell has a negative charge at rest, known as the resting membrane potential, and the sudden, transient influx of positively charged Na^+ ions results in a depolarisation of the negative membrane potential. The points at which action potentials are transmitted from one neuron to another are known as synapses (Chen & Lui, 2019; Catterall & Few, 2008).

Synapses are the points of connection between two neuronal cells. The two most researched types are excitatory and inhibitory synapses, although three other types have been more prominent recently (Klemann & Roubos, 2011). The term synapse has changed from referring only to the space in between cells to reflect the three areas involved in communications: the presynaptic terminal, the synaptic cleft, and the postsynaptic terminal (Kandell et al., 2000).

After the presynaptic terminal is reached by a propagating action potential, voltage-gated calcium channels at the plasma membrane open up and the calcium flows into the cell. The influx of these ions trigger the fusion of neurotransmitter-filled vesicles (e.g. glutamate, dopamine) and the pre-synaptic end's plasma membrane. This process of exocytosis results in neurotransmitters being released into the synaptic cleft

(Sullivan & Schweizer, 2015). Vesicle Glutamate Transporters (VGluT) are one of the protein families which aid in the transport of the excitatory neurotransmitter glutamate into synaptic vesicles, and there are three classes numbered 1 to 3. VGluT proteins are classical pre-synaptic markers (Fremeau et al., 2004).

The synaptic cleft is the short intercellular space in which neurotransmitters (transiently), mineral ions (Ca^{2+}, K^{+}, Na^{+}, etc.), and even some moving neurotransmitter receptors are found. The synaptic cleft permits the augmentation, inhibition, or even stopping of an electrical impulse between neuronal cells. Without it, the neural networks could not function as we know it.

The postsynaptic terminal is called a dendrite or dendritic spine. Dendritic spines are short branches of a dendrite of approximately 1 µm in length and whose shape and size is determined by synaptic activity. The postsynaptic terminal's cellular membrane is populated with neurotransmitter receptors and other integral membrane proteins that together compose the Post-Synaptic Density (PSD). Once these receptors interact with appropriate neurotransmitters, signalling cascades are activated which relay an action potential to the cell body (called soma) and ultimately to its own axon and presynaptic terminal (Kandel et al., 2000).

1.3.2 Synaptic plasticity

Synaptic plasticity is the experience-dependent process by which changes in synaptic activity result in changes in the structure and

function of synapses. It is one of the key processes thought to underlie memory and learning (Takeuchi et al., 2013). One of the ways in which synaptic plasticity is induced is through the establishment of long-term potentiation, although there are other forms of plasticity. These include long-term depression and synaptic depression.

Changes in synaptic plasticity stem from changes in the expression of various proteins important to synaptic communication. One form of plasticity involves the “strengthening” of a synapse, referring to an increase in expression of proteins which facilitate synaptic transmission, as well as an increase in the size of synaptic terminals through F-actin expression. Other proteins whose expression changes during synaptic plasticity include neurotransmitter receptors, transporter proteins, cell adhesion proteins, translation initiation factors, protein kinases, etc (Ho et al., 2011). The strengthening of synapses is principally mediated through long-term potentiation, which induces local protein synthesis at both synaptic terminals and vesicle formation at the pre-synapse.

1.3.3 Long-term potentiation

The main theory explaining how memories are physically stored in the human brain proposes that memories are encoded as differing patterns of synaptic activation. This idea is termed “engram” or “memory trace (Redondo & Morris, 2011).” This raises the question of how engrams are stored, strengthened through stimulus repetition, and recalled when needed.

The lead hypothesis to answer such questions is long-term potentiation (LTP). Long-term potentiation can be broadly defined as the phenomenon in which brief high-frequency synaptic stimulation in the hippocampus results in a long-lasting increase in synaptic strength, or synaptic plasticity (Nicoll & Roche, 2013). Note that long-term potentiation is not completely understood and is one of the main objects of study in memory research. By strengthening the communication between two neuronal cells, it is believed that long-term potentiation facilitates further synaptic activation when receiving the same stimuli.

The molecular biology of LTP is not certain. However, LTP roughly follows the pathway summarised in **Figure 1.2**. First, high-frequency stimuli at the presynaptic terminal induce the release of L-glutamate. Glutamate is the brain's most common neurotransmitter and its release is a critical first step in synaptic plasticity. Second, NMDA receptors in the postsynaptic terminal bind to L-glutamate and open up their channels. Next, Ca^{2+} flows through these channels and into the cell, which activates kinases CaMKII and PKC (Sutton & Schuman, 2006). These two enzymes cause early LTP (E-LTP; which lasts 1-3 hours after the stimulus), with proteins being synthesized from previously available mRNAs. At this point, it is hypothesized that a process named "synaptic tagging" (see section 1.3.5 below) takes place, signalling this specific synapse for continued growth (Frey & Morris, 1997). Later, late LTP (L-LTP) continues and newly transcribed mRNAs are transported to the synapse and translated (Bliss & Collingridge, 1993).

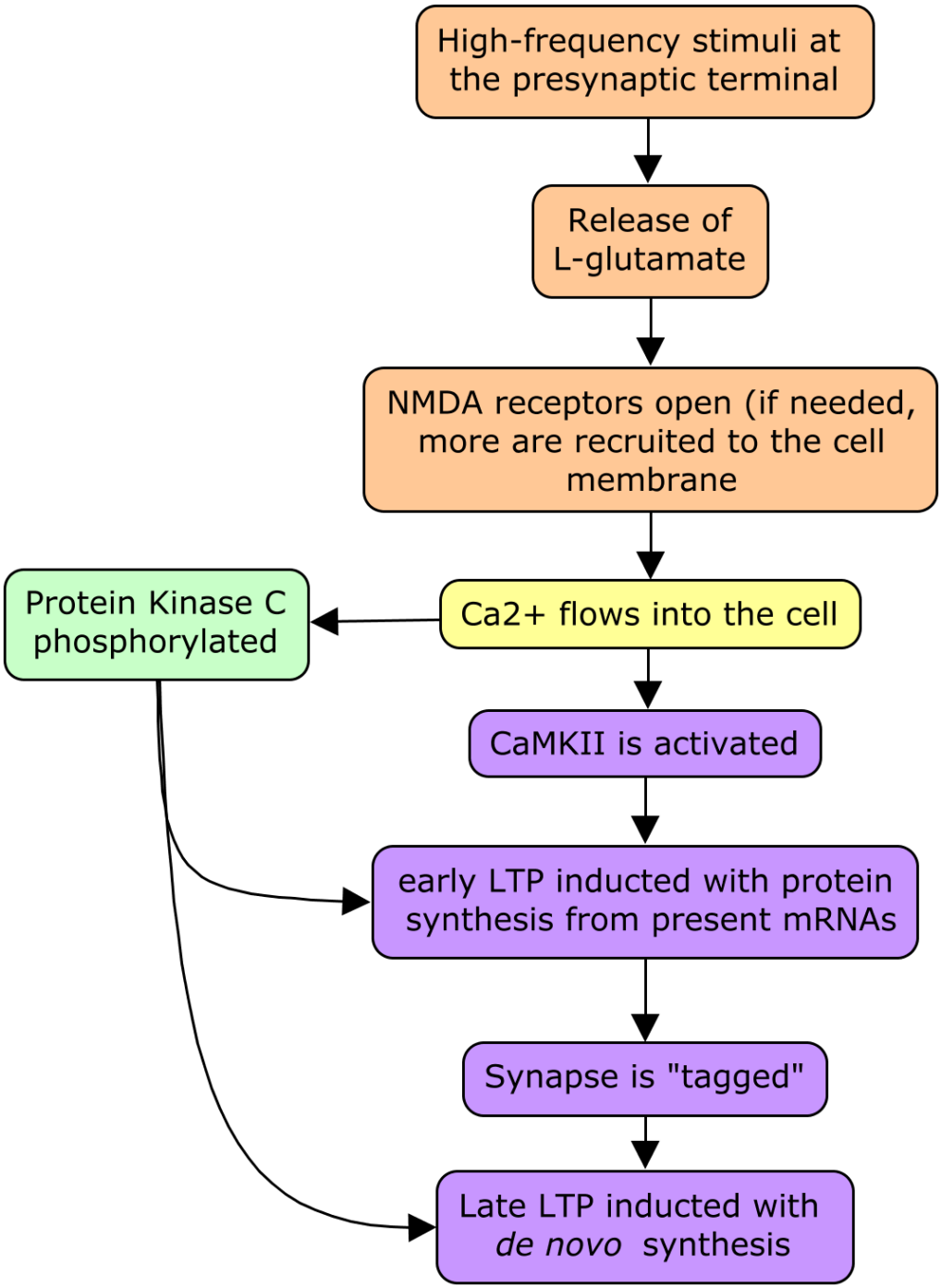

Figure 1.2 Schematic of events leading to long-term potentiation (LTP). Stimuli encoded as electrical impulses reach the presynaptic terminal, which releases L-Glutamate. NMDA receptors (or other glutamate receptors, if needed) are activated and a cascading signalling pathway is initiated. Protein synthesis in early LTP results from translation of messenger RNAs that were previously there. Afterwards, the synapse is tagged and this primes it for late LTP and protein synthesis from newly-transcribed mRNAs.

1.3.4 Local protein synthesis at the synapse

Various experiments have set out to determine if protein synthesis is essential to LTP and if so, what the relative importance of localized translation is in comparison to translation in the cell body. Five principal methods have been used to this end: (1) inhibition of protein synthesis, (2) genetic targeting of translation efficiency, (3) imaging of local translation reporters, (4) prevention of dendritic targets from being translated (i.e. CaMKII), and (5) profiling the mRNA populations in dendritic spines (Sutton & Schuman, 2006).

One way protein synthesis has surprised researchers is that it is mostly localized to individual dendritic spines and can quickly respond to changes in postsynaptic requirements (Cougot et al., 2008). When inhibited, for example, NMDA receptors can be replaced by newly expressed Ca^{2+}-permeable AMPA receptors (another glutamate receptor) and later on be removed to accommodate the appropriate NMDA receptors, possibly influenced by N-cadherin (Jungling et al., 2006; Nicoll & Roche, 2013; van Stegen et al., 2017). Subsequently, experiments looking at mRNA populations localized in dendritic spines support the importance of protein synthesis as an essential part of plasticity. There is currently no consensus on the number of transcripts localised to dendritic spines. In these studies, researchers have reported highly variable numbers of mRNA species in rodent brain, with the latest reports estimating 400-2550 different mRNAs (Cajigas et al., 2012a; Lein et al., 2007; Poon et al., 2006).

Furthermore, it seems the importance of local protein synthesis in synaptic plasticity and LTP is time-dependent. Studies have repeatedly observed long-term memory deficits when local protein synthesis is inhibited in the first three to eight hours following training (Frey & Morris, 1997). However, translation after said time frame did not have permanent effects, as neuron-wide protein translation ameliorates any deficits (Fonseca et al., 2006). One of the key targets for such research has been brain-derived neurotrophic factor (BDNF), whose expression has been shown to induce structural and functional changes characteristic of plasticity (Lu et al., 2008). Taken together, these observations suggest that in the study of plasticity, the role of local protein synthesis over the short timeframe of a few hours is likely to be more important than that over the considerably longer lifespan of a memory.

1.3.5 Synaptic tagging

The suggestion that local protein synthesis is not constant during the lifespan of an engram necessitates a different mechanism for LTP to be maintained. Similarly, observations that early LTP can be induced in synapses without necessarily inducing late LTP suggests there is a decisive mechanism that signals which synapses will continue expressing LTP. Is this signalling dependent on a protein or some other macromolecule? Is it perhaps due to elongated neurotransmitter release? Could it be a mark involved in protein synthesis, present before and after the deciding step? One possible hypothesis which addresses this question is the synaptic tagging and capture hypothesis (Frey & Morris, 1997; Redondo et al., 2010).

The overall idea of synaptic tagging is that induction of early LTP creates only the *potential* for a lasting change in synaptic efficacy, but not a commitment to late LTP. That is to say, early LTP does not guarantee that a memory will leave short-term memory (Redondo & Morris, 2011). Therefore, Frey and Morris suggest that in between the stages of LTP, there must be "a short-lived protein-synthesis-independent synaptic 'tag' at the potentiated synapse which sequesters the relevant protein(s) to establish late LTP (Frey & Morris, 1997)."

Originally, the synaptic tagging hypothesis assumed that there was no protein translation at an individual synapse level and proteins were necessarily trafficked from the cell body to dendritic spines. Given the advances in the last two decades, there is belief now that this is not accurate (Cajigas et al., 2012a; Cougot et al., 2008; Sutton & Schuman, 2006) and so, the possibility that the tag is related to protein synthesis is borne. Moreover, experiments have shown that depotentiated synapses can regain late LTP after a short period without stimulation, suggesting the "tag" a persistent molecule (Sajikumar & Frey, 2004). In addition, experiments inhibiting translation before inducing early LTP through tetanus induction have been successful at blocking only late LTP (Redondo et al., 2010), strongly suggesting the tag is involved in translation. Taken as a whole, these new findings suggest that synapses are tagged in a process closely linked to local protein synthesis of *de novo* transcripts which occurs between the establishments of E-LTP and L-LTP.

1.3.6 FMRP and fragile X syndrome

Fragile X Mental Retardation Protein (FMRP) is a polyribosome-associated RNA-binding protein that binds specifically to a purine quartet motif (Schaeffer, 2001; Tamanini et al., 1996). It binds to mRNAs outside the nucleus and, as part of a complex including CYFIP1 and translation initiation factor eIF4E, silences and transports transcripts to the synapse (De Rubeis et al., 2013; Napoli et al., 2008). At the same time, polyribosomes are bound to the FMRP complex and repressed (Darnell et al., 2011).

FMRP is thought to be necessary for dendritic local protein synthesis and normal synaptic development. The FMRP complex has been found to associate with other RNA-binding proteins such as TDP-43 to co-repress translation of neurotransmitter receptors and other synaptic structural proteins ultimately impacting synaptogenesis and the formation of dendritic spines (Majumder et al., 2016). Additionally, it has been observed that translocation of polyribosomes and mRNAs to the synapse by the FMRP complex is initiated by metabotropic glutamate receptor activation exclusively (Antar, 2004). As mentioned before, glutamate is the brain's most common neurotransmitter and its release is thus a critical first step in synaptic plasticity.

Loss of such an important protein for synaptic development is likely to have a tremendous impact. Indeed, loss of function mutations in FMRP's corresponding *FMR1* gene result in Fragile X Syndrome (FXS), which is the most common inherited form of autism and intellectual disability. At

the cellular level, FXS is characterised by increased dendritic spine density and abnormal expression of structural proteins, which can be rescued by inhibition of actin cytoskeleton formation (Dolan et al., 2013).

This may explain why there are two related proteins, FXR1 and FXR2, which interact with FMRP and can partially form similar complexes (Zhang et al., 1995). However, despite the presence of these two proteins, loss of function mutations FMRP's corresponding *FMR1* gene are not compensatory in developing human prenatal tissue or *Fmr1*-knockout mice (Agulhon et al., 1999; Antar & Bassell, 2003).

These observations suggest that FMRP has a specialised function in mRNA repression that related proteins do not have. One possibility is that FMRP binds to post-transcriptional modifications such as methylation marks, while FXR1 and FXR2 do not. Indeed, FMRP and m^6A methylation share a similar purine-rich motif (Chang et al., 2017; Schaeffer, 2001).

1.4 Human brain disease

1.4.1 Parkinson's disease

Parkinsonism is a term that include several closely-related syndromes. These are characterised by resting tremors, bradykinesia, and rigidity, among other symptoms. Parkinson's disease (PD) is the most common form of Parkinsonism and the second most common neurodegenerative disorder, affecting 2-3% of the global population 65 years of age or above (Poewe et al., 2017). In PD, motor deficits are one of the first clinical symptoms of the disease, followed by final-stage deficits in cognition

(Halliday et al., 2014). Although research has identified at least 8 genes which are associated with PD, the familial component of this disease appears not to be predictive of the majority of cases. Rather, most cases of PD are idiopathic (Goldman & Fahn, 2015).

The neuropathology of PD is progressive. The first sign of PD pathology is the loss of dopaminergic neurons in the *substantia nigra*, a structure in the midbrain which plays a role in movement (Halliday et al., 2014). Recent studies have found that there are also early signs of neurodegeneration in the cerebellum, which coordinates voluntary movement. Anatomical connections between the cerebellum and *substantia nigra* were dysfunctional likely due to dopaminergic degeneration. Also, pronounced progressive Purkinje cell loss was observed in the cerebellum (Wu & Hallett, 2013). These changes are thought to explain early symptoms of PD such as tremors and restricted movement.

After the disease progresses, aberrant expression and/or degradation of alpha-synuclein results in abnormal aggregates within cells called Lewy bodies. The presence and spread of these inclusions through all cortical regions of the brain are the hallmark pathology of final stage PD (Schulz-Schaeffer, 2010). Probing the correlation between Lewy body prevalence and neuronal loss in PD has resulted in contradicting evidence. (Fuchs et al., 2008; Gründemann et al., 2008; Tan et al., 2005).

Furthermore, characterisation of Lewy bodies has found that the alpha-synuclein protein these are made of is normal, disproving hypotheses

that Lewy bodies were prion-like inclusions. Also, there is no current consensus on how Lewy bodies affect neurons. One study found Lewy bodies were preferentially located to pre-synaptic regions and induced dendritic spine degeneration on the post-synaptic side, possibly as a result of impaired neurotransmitter release (Kramer & Schulz-Schaeffer, 2007).

Parkinson's disease is a multi-factorial disease with many unanswered questions. At this point, what seems to be most likely is that loss of dopaminergic neurons and aberrant alpha-synuclein are two critical factors. In the future, research which link these two factors, such as synaptogenesis and dopamine/receptor expression, may elucidate the root processes of PD (Mattson & Magnus, 2006).

1.4.2 Lewy body dementia

Lewy Body Dementia (LBD) is a parkinsonian syndrome which shares many of its neuropathological features with PD and Alzheimer's Disease (AD). Patients suffering from LBD experience visual hallucinations, memory deficits, and movement disorders.

The main neuropathological feature of LBD is, of course, the widespread presence of Lewy bodies. In LBD, these aggregates are first present in the cortical regions of the brain rather than the basal ganglia. Similar to AD, amyloid-beta and tau accumulation is also observed in early-stage LBD (Hansen et al., 1998). The combination of these protein aggregates leads to neuronal cell death and cortical atrophy in LBD patients.

Depending on the site of aggregates, visual hallucinations and memory deficits can vary in severity (Dickson et al., 2008).

There has been a debate whether LBD and PD are separate disorders or simply two forking set of symptoms arising from the same aetiology. The current classification of the diseases is based on clinical symptoms. LBD patients present dementia-like deficits first (memory loss, attention deficit, visual hallucinations), whereas early-stage PD is manifested through motor disorders such as tremors. Studies into their biological differences have found that LBD and PD differ most in selective vulnerability of certain neuronal populations (Jellinger & Korczyn, 2018). In LBD, neuronal loss is more pronounced in cortical regions, while PD causes severe neuronal death in the *substantia nigra* and cerebellum (Tsuboi & Dickson, 2005).

There appears to be a more pronounced genetic influence in LBD. Although the majority of cases are sporadic, just as with PD, a recent study looking at *SNCA* and *APOE* variants has estimated the heritable component of LBD to be 36% (Guerreiro et al., 2018). The same group also compared genetic variants between patients with LBD, PD, and AD and found that although LBD is most clinically similar to PD, it is a genetically distinct disease equally correlated to AD and PD (Guerreiro et al., 2016).

To summarise, LBD is a disease that combines many of the genetic, neuropathological, and clinical characteristics of PD and AD. A large component of its aetiology appears to arise from changes in alpha-

synuclein transcription and translation, therefore suggesting regulatory mechanisms of such processes may also be dysfunctional.

1.4.3 Mild Cognitive Impairment

Mild Cognitive Impairment (MCI) is a condition defined by a measured cognitive decline which is greater than expected for one's age and education level. It is often considered a transitional state between a normal cognitive state and dementia (Gauthier et al., 2006).

MCI is generally a clinical classification. Some hesitate to consider it a separate state from dementia, but observations that many MCI patients do not progress to have AD and some even regress to a normal cognitive state have convinced the scientific community of its value as a distinct syndrome. Additionally, MCI and AD differ in the type of cognitive deficits observed with the largest difference being that MCI patients perform significantly higher, almost indistinguishable from control individuals, in full-scale IQ tests compared to AD (Petersen et al., 1999).

Longitudinal studies have found that about 12% of MCI patients progress to AD each year and that the rate of decline is accelerated with age (Petersen et al., 1999). There are some predictive biomarkers for progression from MCI to AD. One of these is the presence of the *APOE-ε4* allele, which has previously been widely associated with AD incidence (Corder et al., 1993; Elias-Sonnenschein et al., 2011). Another risk factor is increased BDNF serum levels, in which a progressive increase has been observed from healthy to MCI to AD individuals (Angelucci et al., 2010). Interestingly, both APOE and BDNF are proteins which have

widely been shown to impact upon synaptic plasticity (Chen et al., 2010; Leal et al., 2014).

As MCI is symptomatically similar to AD, it is likely that amyloid deposition and neurofibrillary tangle formation also plays a role. The current consensus is that MCI patients have intermediate amounts of AD pathological markers across the frontal and temporal lobes post-mortem (Bennett et al., 2005; Gauthier et al., 2006).

There is currently a dearth of knowledge regarding the altered molecular biology which results in MCI. Additionally, current studies often present issues in their classification of MCI individuals. As such, reliable diagnostic biomarkers are needed for the continuation of MCI research, especially in post-mortem tissue.

1.4.4 Paediatric ependymoma

Ependymomas are the third most common central nervious system tumour type in childhood, accounting for up to 12% of brain cancer in children. In childhood, grade I tumours are less common than in adults, exemplifying their threat to life. Despite advancement in treatment, these tumours have a recurrence rate of 50%, particularly when resection is limited by obstructions during surgery as most ependymomas are chemo-resistent (Zeng et al., 2017). To date, cell lines and animal models of these tumour type have failed to reflect the perseverance of these tumours. In recent years, breakthroughs into the genetics of ependymomas have revealed nine distinct subtypes which are spread throughout three different anatomic compartments, and more recently,

subgroups have been found based on transcriptomic profiling (Khatua et al., 2017).

Ependymomas arise from ependymal cells, thin neuroepithelial lining of the brain's ventricular system. Classic examples of this tumour are characterised by rosette and pseudorosette structures surrounding vascular features and low cellularity. Other more aggressive forms of the tumour are called anaplastic ependymomasand have higher cellularity, frequent mitosis, and variable degrees of vascular proliferation. The histopathological identification of ependymomas, however, is remarkably unreliable with as much as 69% discordance between neuropathologists (Ellison et al., 2011). As such, paediatric ependymoma diagnosis and treatment are areas where urgent research is needed.

1.4.5 Paediatric glioblastoma

Glioblastomas are one of the deadliest types of tumour. The median survival for all glioblastoma patients is just one year with a five year survival rate of less than 5%, with some suggesting this figure to be an overestimation (McLendon & Halperin, 2003). Glioblastomas develop from glial cells and sometimes astrocytomas. They are characterised by high cellularity, high amounts of mitosis, cellular pleomorphism, necrotic areas, and cellular hypertrophy. Due to these characteristics, glioblastoma growth is aggressive and manifests rapidly without recognizable signs of early symptoms (Sturm et al., 2014).

As with other brain tumours, the grading of paediatric glioblastomas is generally high, yet these have not been extensively studied in children.

Some large-scale research consortiums, such as The Cancer Genome Atlas, have attempted to understand the genetic origin of glioblastomas. These studies have resulted in the subcharacterisation of glioblastomas into thee subtypes (Phillips et al., 2006). These subtypes are predictive of prognosis, highlighting the importance of genetic profiling of these tumours. Furthermore, the importance of epigenetics in glioblastoma has recently been highlighted *in vitro*, in which RNA modifications were identified as a requirement for cell differentiation (Cui et al., 2017).

1.5 Epigenetics

1.5.1 N6-methyladenosine

The epigenetic influence of a methyl group (CH_3) added to DNA has been well documented. Its role in regulating protein expression through transcription revolves around the coiling and uncoiling of histones, as well as its function as a substrate in enzymatic activity (Jones, 2012). Similarly, the methylation of messenger RNA has been recently observed to be a key regulator of translation.

It has long been known that methylation also occurs at nucleoside bases like in mRNA and tRNA. For example, mRNA's capping mechanism ostensibly consists of methylation of the N_7 position of the first mRNA base. However, it was not until after the 1970s and the characterisation of new mRNA modifications that N6-methyladenosine (m^6A) was characterised, though this discovery was shelved until recent years (Schibler et al., 1977; Wei & Moss, 1977). m^6A RNA modification involves the addition of a methyl group to the sixth nitrogen of an adenosine. It is

now known to be the most common internal RNA modification (Fray & Simpson, 2015; Meyer & Jaffrey, 2014; Yue et al., 2015). The prevalence of this modification has been estimated to be between 0.1-0.4% of all adenosine residues and is widely conserved amongst eukaryotic species (Dominissini et al., 2012; Fu et al., 2014).

Notably, m^6A does is not randomly distributed within an mRNA transcript. Sequencing and annotation studies performed in various cell lines from both human and mouse show a preference of m^6A to be inserted near stop codons. The 3' UTR and coding sequence are also common m^6A sites but notably the 5' UTR m^6A methylation is rare (Dominissini et al., 2012; Meyer et al., 2012). As shown in **Figure 1.3**, there is considerable species and tissue-dependent variability in sites m^6A methylation. Due to this non-random distribution of m^6A marks, the idea of dynamic m^6A methylation arose and has led to further research regarding the function of m^6A within translation and its larger biological role, which are currently unclear.

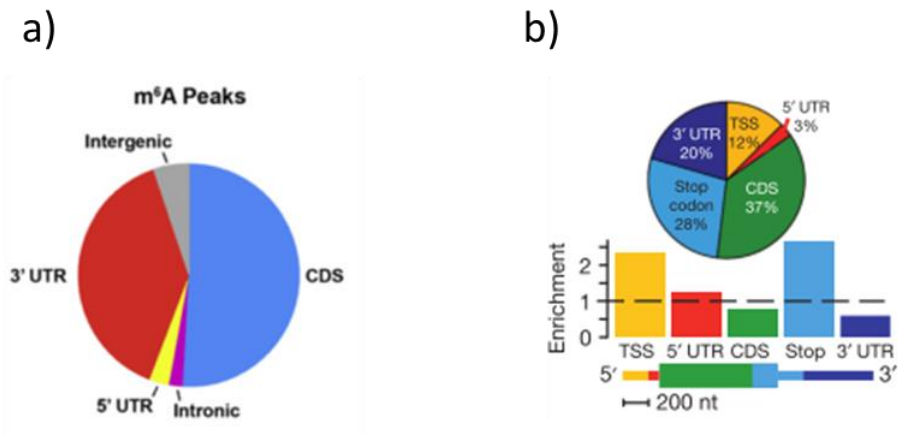

Figure 1.3 Tissue-dependent variability of m^{6}A topology. a) Pie chart shows the distribution of m^{6}A peaks in five gene segments. mRNA from human liver cell line HEPG2. b) Pie chart of m^{6}A peaks in each of five non-overlapping segments. In the middle, the relative enrichment of m^{6}A peaks across transcript segments is shown. Bottom shows a schematic of five segments. mRNA from mouse brain. Adapted from Meyer et al., 2012 and Dominissini et al., 2012.

m^{6}A's function has been elucidated by several studies associating these modifications with different developmental and disease states. Low m^{6}A levels have been found to result in developmental deficits and abnormalities in the *Arabidopsis* plant (Bodi et al., 2012), In *Drosophila*, loss of m^{6}A was a critical factor in sex determination (Haussmann et al., 2016). In humans, it has been observed that during development, m^{6}A is highly expressed in embryos (Yue et al., 2015). Complementing these studies, high expression of m^{6}A modifications has been found to affect embryonic stem cell differentiation and development (Geula et al., 2015; Wang et al., 2014c). Methylation was also found to be a key influence in tumourigenesis (Cui et al., 2017).

Likewise, it has been demonstrated that in response to various cellular stresses like heat shock or glucose depravation, adenosine residues in 3' UTR and 5' UTR are preferentially m^6A methylated (Engel et al., 2018; Zhou et al., 2015a). m^6A has also been shown to regulate nuclear RNA processing and splicing (Ke et al., 2017).

Most importantly, m^6A modifications have been shown to regulate translation through the binding of specific proteins, which will be detailed below (Wang et al., 2015). Even the presence of an m^6A mark within a transcript has been found to cause structural changes to a transcript. These changes, in turn, affect translation by limiting the space in which RNA-binding proteins may attach to a transcript. The removal and addition of an m^6A mark for this purpose has thus been termed an m^6A switch (Liu et al., 2015).

Overall, the breadth of research in recent years surrounding m^6A methylation has shown that this modification may impact many unrelated functions. Observations like this remain restricted by *in vitro* studies and limited tissue variability in other research. Currently, the number of studies regarding m^6A modifications in humans is limited but growing.

Related research has found modifications similar to m^6A. The first of these is called N1-methyladenosine (m^1A). Studies have revealed that unlike to m^6A, m^1A is enriched in the 5' UTR region of mRNA transcripts (Li et al., 2016). Older studies reported that under alkaline conditions, m^1A can convert to m^6A through a process called Dimroth rearrangement, which introduces noise to m^6A measurements

(Dominissini et al., 2016; Macon & Wolfenden, 1968). Another mark similar to m^6A is N6-2'-O-dimethyladenosine (m^6A_m), which is also located in 5' UTR and is associated with mRNA stability and longevity (Mauer et al., 2017). The discovery of these two modifications also suggested some previous m^6A research was actually related to m^1A and m^6A_m (Linder et al., 2015; Wei et al., 2018). This serves as a precautionary tale for future research.

1.5.2 m^6A-interacting proteins

With the topology of the m^6A modification discovered and its methyltransferase complex described, the idea of dynamic methylation comes to mind. In a dynamic model of methylation that is analogous to DNA methylation, three elements are required: "writers," "erasers," and "readers."

Writers catalyse the addition of m^6A onto a transcript. This process is not spontaneous but rather requires an enzymatic complex that binds to a consensus sequence DRACH where D = A, G, or U, R = purine, H = pyrimidine (Linder et al., 2015). The enzymatic complex is composed of the methyltransferases METTL3 and METTL14, which are docked together by Wilms-associated Tumour Protein (WTAP). Simultaneously, S-Adenosine Methionine (SAM), a common methyl donor, will draw near the enzyme complex as the latter reaches an mRNA consensus sequence and binds to its adenosine (Ping et al., 2014). While both methyltransferase enzymes are independently active *in* vitro, METTL3 is reported to be the catalytic component of this complex, as knockdown of

its corresponding gene will invariably result in apoptosis while silencing METTL14 will only result in moderately reduced methylation levels (Dominissini et al., 2012; Fu et al., 2014). This model is illustrated in **Figure 1.4**. It is likely that this model is incomplete and more unidentified proteins influence the m^6A methyltransferase complex, as it has been recently found that methylation in *Arabidopsis* requires the E3 ubiquitin ligase HAKAI (Růžička et al., 2017).

Eraser proteins are enzymes which get rid of (or "erase") the modification. These enzymes are called demethylases. The fat mass and obesity-associated protein (FTO) was the first m^6A eraser discovered (Hess et al., 2013; Jia et al., 2011). FTO is an enzyme originally linked to body weight regulation and subsequently to several phenotypic mutations. For example, it was discovered that a loss of function mutation in the FTO protein lead to postnatal retardation, malformations, and multiple dysmorphisms (Boissel et al., 2009). Presence of FTO in axons has been linked to adult neurogenesis and memory formation in mouse brain but a functional model has yet to be proposed (Li et al., 2017b; Walters et al., 2017). Furthermore, it is unknown whether it is FTO's role as an m^6A demethylase which impact these processes or its role in adipogenesis and energy homeostasis (Claussnitzer et al., 2015; Livingstone et al., 2016).

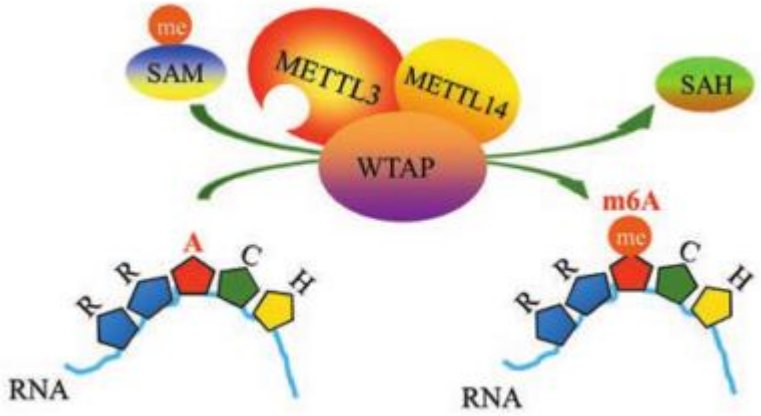

Figure 1.4 Schematic of the m^{6}A methyltransferase complex. METTL3, bound to METTL14 and WTAP, is attracted to the consensus sequence in an mRNA transcript. SAM acts as a methyl donor, after which METTL3 converts adenosine to N6-methyladenosine. Following this, the complex releases the now-methylated transcript. Adapted from Ping et al., 2014.

The second eraser, ALKBH5, is part of the same family of the Fe(II) and α–ketoglutarate-dependent family of proteins. While both erasers have had their function validated through knockout and *in vitro* experiments, ALKBH5 has been further validated through the identification of mRNA species in direct immunoprecipitation experiments, which makes it part of the mRNA-bound proteome and suggests very tight interaction with RNA chains (Zheng et al., 2013a). ALKBH5 and demethylation have been shown to have functional effects in pre-mRNA splicing, mouse spermatogenesis and fertility, and tumourigenicity (Zhang et al., 2017; Zheng et al., 2013b; Zhou et al., 2018).

The last element to discuss is m^{6}A readers. Readers are proteins that recognize the m^{6}A RNA modification and thus display an m^{6}A-dependent function. Readers include YTHDF1, YTHDF2, YTHDF3, YTHDC1,

YTHDC1, HNRNPC, HNRNPA2B1, and more, and are all reported to have distinct functions. The most important subset of m^6A readers is the YTH domain family. These are proteins which contain a specialised domain that strongly binds to m^6A by recognising the modification and creating a small hydrophobic aromatic cage between them (Luo & Tong, 2014; Xu et al., 2014, 2015).

The first protein in YTH domain family, YTHDF1, also facilitates translation of an m^6A-marked transcript, though it uses a very different mechanism. YTHDF1 will selectively recognize m^6A-modified transcripts (preferentially near their stop codon) and promote ribosome loading of these mRNAs. A single m^6A molecule can then, through YTHDF1-chaperoned interaction, be translated by many ribosomes at a time. Some studies have also shown that the same YTHDF1 protein will interact with initiation factors to facilitate translation (Wang et al., 2015). YTHDF1 has recently been linked to axon growth, suggesting a role in neuronal development and possibly memory formation (Zhuang et al., 2019). It is also the first m^6A-binding protein to be targeted for therapeutic anti-tumour immunity (Han et al., 2019). These publications point to YTHDF1 as the prime protein of interest in the application of our knowledge of m^6A methylation.

Another reader, YTHDF2, has been reported to have a significant effect in transcript expression through an arresting mechanism. Once bound to the m^6A modification, YTHDF2 will relocate the bound transcript from the translatable pool to a ribonucleoprotein (also known as RNP or P-body), a processing body in which the components of RNA degradation are

closely localized and where RNA decay happens. Afterwards, YTHDF2 will also move the bound mRNA to mRNA decay sites, making it a fundamental reader in the heightened expression and decay of transcripts during cellular stress (Wang et al., 2014a). Other studies have implicated YTHDF2 as a leading factor in the increased expression of m^6A-methylated transcripts during cellular stress, with research pointing at a competitive interaction between YTHDF2 and FTO during these events (Wang et al., 2015). Upon heat shock, YTHDF2 will relocate from the cytoplasm to the nucleus and preserve m^6A-methylated transcripts by stopping FTO from binding to them (Zhou et al., 2015b).

One more reader protein, YTHDF3, has also been shown to directly influence translation in the cytoplasm. YTHDF3 has been found to perform the functions of both YTHDF1 and YTHDF2 (Li et al., 2017a; Shi et al., 2017). It is currently unknown what determines the mechanism of action of YTHDF3 and this has been proposed as a focus of future research (Meyer & Jaffrey, 2017).

Other readers have been reported to have functions that have been less thoroughly characterised. For example, hnRNPC is a protein which selectively binds "m^6A switches," loops of mRNA that have been opened up by this modification. hnRNPC recognizes this "switch" and acts as a coenzyme for YTHDF2 and possibly other RNA-binding proteins that would otherwise not be able to access the RNA structure (Liu et al., 2015). Furthermore, hnRNPA2B1 is an essential protein that binds m^6A-methylated transcripts and assists their transportation from the cell nucleus (Alarcón et al., 2015). Finally, there is also eIF3, a translation-

initiation factor that has recently been shown to read m^{6}A residues in order to initiate cap-independent translation in otherwise untranslatable transcripts (Meyer et al., 2015).

The list of m^{6}A writers, erasers, and readers has been growing for the past few years and will undoubtedly grow larger in the future as more proteins are found which interact with the dynamic m^{6}A modification. Currently identified m^{6}A-binding proteins are summarised in **Table 1.1**.

Type	Protein	Function
Writers	**METTL3**	Methyltransferase
	METTL14	Methyltransferase adaptor
	WTAP	Localisation to nuclear speckles
	Virilizer	Unknown effect
	RBM15	Targets specific DRACH motifs
	HAKAI	Unknown effect
Erasers	**ALKBH5**	m^{6}A demethylation
	FTO	m^{6}A$_m$ demethylation
Readers	**YTHDF1**	Ribosome loading
	YTHDF2	Regulates mRNA stability
	YTHDF3	Controls translation efficiency and RNA stability
	YTHDC1	Pre-mRNA splicing
	YTHDC2	Unknown effect
	eIF3	Cap-independent translation
	HNRNPA2B1	Splicing
	HNRNPC	m^{6}A switches

Table 1.1 List of identified m^{6}A-interacting proteins and their known functions. All known parts of the m^{6}A methyltransferase complex are listed.

1.6 Aims of the project

Synaptic plasticity and long-term potentiation are part of the leading model describing the physical bases of memory in the hippocampal formation. The synaptic tag and capture hypothesis aims to explain a missing link in this model by proposing a “tag” that signals a synapse to undergo late LTP and create a persistent memory.

We hypothesize that synaptic plasticity and late LTP are established partly through local protein synthesis from m^6A-methylated mRNAs, which are likely to be enriched for synaptically-relevant proteins. In turn, these transcripts interact with m^6A-binding proteins to undergo changes in translation efficiency, stability, or methylation state. As such, we expect m^6A modifications and their related proteins to be located in synapses of neuronal cells.

The specific aims of this project were:

I. To investigate the distribution of m^6A methylation in the human brain transcriptome and a possible common function of these transcripts.
II. To identify the location of m^6A within neuronal cells and mouse hippocampus.
III. To assess the colocalisation of m^6A with m^6A-binding proteins at synaptic compartments before and after neuronal activation of neuronal cell lines.
IV. To assess the colocalisation of m^6A and m^6A-binding proteins with active ribosomes at the synapse.

V. To characterise the distribution of m^6A methylation and m^6A-binding proteins in four regions of healthy and diseased adult human brain, as well as in brain tumours.

Chapter 2:

Materials and Methods

2.1 Materials

2.1.1 Next-Generation Sequencing Data

Previously, Dominissini et al. (2012) published m^6A-sequencing data of normal human brain. This dataset was accessed and downloaded from the Methyltranscriptome Database (MeT-DB; https://whistle-epitranscriptome.com/metdb_v2/html/index.php).

A second human brain-derived m^6A-sequencing dataset was generated in collaboration with the Children's Brain Tumour Research Centre and Deep Seq Facility.

2.1.2 Formalin-Fixed and Paraffin Embedded Human Brain Sections

Human brain sections were obtained from three different sources and held under a Human Tissue Act 2004 license. The tissue is accessed through the Nottingham Health Science Biobank (NHSB) project number ACP000101and approval for the project was awarded by the chair of the committee.

2.1.2.1 Healthy Individuals

Non-affected, healthy brain tissue samples, were obtained from the Nottingham Health Science Biobank. The demographic details are presented in **Table 2.1**. Individuals were at an advanced age at the time of death (mean 85 years, ranging from 63-99 years old) but otherwise the brains were classified as non-disease affected by a neuropathologist. Tissue from 6 different brain regions was received: caudate nucleus, cerebellum, cingulate gyrus, hippocampus, middle frontal gyrus, occipital cortex.

Case ID	Diagnosis	Age	Sex
NP22/06	Normal brain	99	Female
NP41/06	Mild age-related change. Normal brain	92	Female
NP62/06	Minor, age-related, changes. Normal.	86	Male
NP85/07	Normal brain	63	Male

Table 2.1 Human brain tissue from healthy individuals used in this study. Age is shown in years.

2.1.2.2 Neuropathology-affected Individuals

The tissue in **Table 2.2** was obtained from the Multiple Sclerosis and Parkinson's Tissue Bank at Imperial College London. These samples had a mean age of 82.5 years and ranged from 63-104 years old. Regions received included cerebellum, cingulate gyrus, frontal cortex, and hippocampus.

Case ID	Diagnosis	Age	Sex
PD687	Parkinson's disease	86	Male
PD793	Parkinson's disease	75	Female
PD898	Parkinson's disease	84	Male
PD115	Lewy Body Dementia	63	Male
PD120	Lewy Body Dementia	83	Female
PD332	Lewy Body Dementia	77	Male
C045	Mild cognitive impairment	77	Male
PD715	Mild cognitive impairment	86	Male
PDC07	Mild cognitive impairment	104	Female
PD65	Mild cognitive impairment	84	Female
PDC111	Mild cognitive impairment	88	Female

Table 2.2 Human brain tissue from individuals with various brain diseases used in this study. Age is shown in years.

2.1.2.3 Brain Cancer Individuals

The tissue in **Table 2.3** was obtained from paediatric patients with a brain tumour characterised as an ependymoma or a glioblastoma. Ependymomas are tumours originating from the neuroepithelial lining of the brain, which is associated with neuroregeneration. Glioblastomas are one of the most aggressive types of cancer and originate from glial cells which are prevalent throughout the brain. Sections were provided by the Children's Brain Tumour Research Centre of the University of Nottingham.

Case ID	Diagnosis	Age	Sex
PN01/04922A	Ependymoma	N/A	N/A
03/20064B	Ependymoma	N/A	N/A
06/1477	Ependymoma	N/A	N/A
94/9860A	Ependymoma	N/A	N/A
97/4274A2	Ependymoma	N/A	N/A
90-6570	Glioblastoma	70	Male
H06.0480B2	Glioblastoma	54	Female
H01.2862B1	Glioblastoma	43	Female

Table 2.3 Human brain tissue from paediatric patients with one of two brain tumour types. Age is shown in months.

2.1.2.4 Human Brain Tissue for m^{6}A-sequencing

Human grey matter, white matter, and fetal brain samples were obtained from the Children's Cancer and Leukaemia Group (CCLG) by the University of Nottingham's Children's Brain Tumour Research Centre and results were provided to the author. Full consent and ethical approval was obtained for their use in this study from the CCLG and local ethical and Trent Medical Review and Ethics Committee approval (06/MRE04/86). Foetal brain RNA age 22-30 weeks was acquired from clontech #636526.

2.1.2 Cell Lines

Human rhabdomyosarcoma line TE671 cells were obtained as a gift from Dr. Ian Mellor's lab. An initial population of human neuroblastoma cell line SH-SY5Y cells were purchased from Sigma-Aldrich (94030304),

which sources these cell line from the European Collection of Authenticated Cell Cultures (ECACC).

Differentiated ReNcell CX human neural progenitor cells were also obtained in collaboration with Dr. Ian Mellor and Mahmoud Sherif, who purchased them from Merck Millipore (SCC007).

2.1.3 Antibodies

A variety of antibodies were purchased or gifted to use in immunocytochemistry, immunohistochemistry, and STEM immunogold labelling. Details of these antibodies are shown in **Table 2.4**.

Type	Code	Source	Target	Raised In	Raised Against	ICC Dilution	IHC-DAB Dilution	STEM
Primary	ab12093	Abcam	PSD95	Goat	Human	1:100	-	-
Primary	ab110139	Abcam	VGluT1	Goat	Human	1:100	-	-
Primary	-	Rupert Fray	m^6A	Mouse	Human	1:250	1:50	-
Primary	sc-8424	Santa Cruz Biotech	N-cadherin	Mouse	Human	1:50	1:50	-
Primary	MAB377	Millipore	NeuN	Mouse	Mammals	-	1:100	-
Primary	MABE343	Millipore	Puromycin	Mouse	Human	1:10,000	-	-
Primary	sc-377119	Santa Cruz Biotech	YTHDF3	Mouse	Human	1:100	1:200	-
Primary	16837-1-AP	Protein Tech	ALKBH5	Rabbit	Human	1:100	-	-
Primary	ABE1013	Merck Millipore	ALKBH5	Rabbit	Human	1:200	-	-
Primary	ab47811	Abcam	Dcp1a	Rabbit	Human	1:250	-	-
Primary	HPA010122	Sigma Aldrich	DLG4	Rabbit	Human	1:250	-	-
Primary	HPA050118	Sigma Aldrich	FMR1	Rabbit	Human	1:250	-	1:25
Primary	RM-2125-S	Thermo Fisher	GFAP	Rabbit	Human	1:250	1:25	-
Primary	G5922	Sigma Aldrich	GW182	Rabbit	Human	1:500	-	-
Primary	ab31645	Abcam	hnRNPA2B1	Rabbit	Human	1:1000	-	-

Primary	R225	Cell Signalling Technology	L7A	Rabbit	Human	1:250	-	-
Primary	E1610S	New England Biolabs	m^6A	Rabbit	Human	1:1000	1:250	-
Primary	ab190886	Abcam	m^6A	Rabbit	Mammals	1:250	1:250	1:25
Primary	ab72311	Abcam	VGluT1	Rabbit	Human	1:500	-	-
Primary	ab99080	Abcam	YTHDF1	Rabbit	Human	1:100	1:75	1:25
Secondary	ab150105	Abcam	Alexa Fluor 488	Donkey	Mouse	1:500	-	-
Secondary	SAB4600175	Sigma Aldrich	Alexa Fluor 647	Donkey	Goat	1:300	-	-
Secondary	ab175471	Abcam	Alexa Fluor 568	Goat	Rabbit	1:500	-	-
Secondary	G7277	Sigma Aldrich	5 nm Gold IgG	Goat	Rabbit	-	-	1:50

Table 2.4 List of antibodies used for immunocytochemistry (ICC), immunohistochemistry (IHC), and scanning transmission electron microscopy (STEM) immunogold labelling with their appropriate dilutions, if tested.

2.1.3 General Reagents

Reagent	Supplier
B-27 Supplement	ThermoFisher Scientific
BSA	VWR
Dibutyryl cyclic AMP (dbcAMP)	Sigma-Aldrich
DMEM medium	ThermoFisher Scientific
DMEM/F12 1:1 medium	Sigma-Aldrich
DMSO	Sigma-Aldrich
Ethanol	Honeywell
Fetal bovine serum (FBS)	ThermoFisher Scientific
Fluo4-AM	ThermoFisher Scientific
Glutaraldehyde	Sigma-Aldrich
Hank's Buffered Saline Solution	Sigma-Aldrich
10 M HCl solution	Honeywell
HEPES Buffer	ThermoFisher Scientific
L-Glutamine	ThermoFisher Scientific
10 M NaOH solution	Honeywell
Neurobasal medium	ThermoFisher Scientific
4% Paraformaldehyde	Sigma-Aldrich
PBS	ThermoFisher Scientific
Penicilin/Streptomycin	ThermoFisher Scientific
20% Pluronic Acid	Sigma-Aldrich
Probenecid	Sigma-Aldrich
Retinoic acid (RA)	Sigma-Aldrich
Sodium Citrate	Sigma-Aldrich
Trigene	Sigma-Aldrich
TRIS	Sigma-Aldrich
Triton X-100	Sigma-Aldrich
Trypsin/EDTA solution	ThermoFisher Scientific
Tween-20	Sigma-Aldrich
Xylene	Sigma-Aldrich

Table 2.5 List of general reagents and suppliers.

2.2 Methods

2.2.1 Cell culture

TE671 and SH-SY5Y cells were cultured under standard conditions in complete Dulbecco's Modified Eagle Medium (DMEM) and complete DMEM/F12 (1:1) Nutrient Mixture Medium, respectively. Cells were subcultured once per week and maintained until a passage number of ten, after which a fresh vial of frozen cells stored in liquid nitrogen would be cultured to replace the older plates.

2.2.2 Cell Differentiation

To differentiate cells, plates were allowed to grow until approximately 90% confluency and then subcultured onto 12 mm coverslips. Growth media was then replaced with differentiation media. Each cell type had a specific differentiation media: serum-free DMEM for TE671 cells and Neurobasal medium supplemented with 0.5 mM GlutaMAX, 2% v/v B-27 supplement, and 1% Penicillin/Streptomycin (10,000 U/ml) for SH-SY5Y cells. Finally, one of two differentiation compounds was added at the appropriate concentration depending on the cell type and experiment. The first compound was Dibutyryl-cyclic-adenosine-monophosphate (dbcAMP), which mimics the action of cAMP and promotes neurite growth and extension, and this was added to a final concentration of 400 µM for TE671 cells and 1mM for SH-SY5Y. The other compound, Retinoic Acid, is a vitamin A derivative widely used as an SH-SY5Y differentiator and was hence only used in these cells and at a final

concentration of 10 µM. Cells were allowed to differentiate for 24 hours, at which point neurite extension and growth was evident.

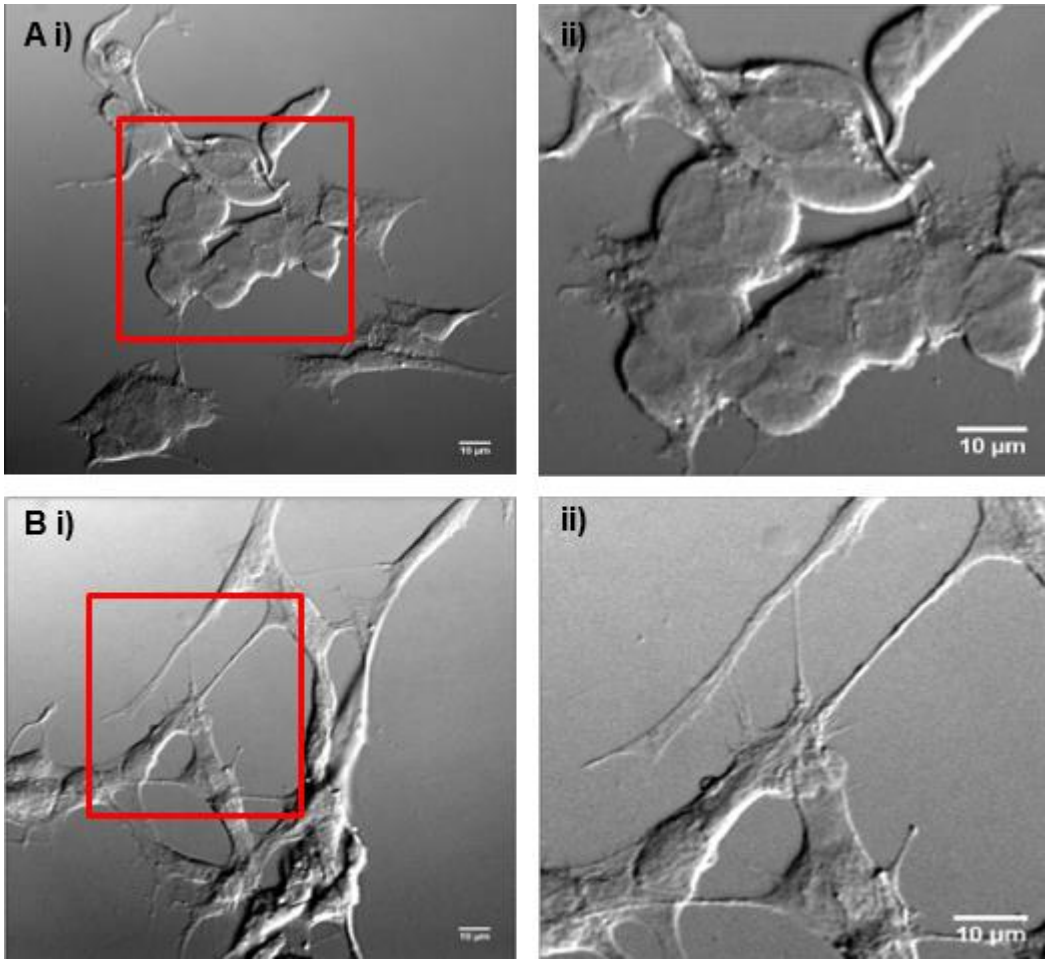

Figure 2.1 dbcAMP differentiation of SH-SY5Y cells. A) Undifferentiated cells grow in clusters with few neurites of short length. B) Once differentiated, cells spread out, take a pyramidal shape, and grow thin long neurites between each other. 40x magnification. Images on the right are enlarged views of selected regions from images on the left.

2.2.3 Neuronal Activation

To activate metabotropic or ionotropic receptors, TE671 and SH-SY5Y were differentiated as described above and 100 µM NMDA or 30 mM KCl was added to their media. Cells were left in this state for either 15 minutes or 24 hours, times analogous to early and late long-term potentiation, respectively. To stop this process, agonist-containing media was removed and cells were fixed.

2.2.4 Calcium Imaging

Calcium imaging was performed to confirm cellular response to receptor activation compounds. First, 22 mm round coverslips were cultured with TE671 and SH-SY5Y cells. Fluorescent calcium indicator Fluo4-AM was diluted in a solution of 22.8 µl DMSO, 22.8 µl 20% pluronic acid, and 10 ml of the appropriate culture media for a final Fluo4-AM concentration of 100 µM. This culture medium was added to the cells and these were incubated at 37°C for 45 minutes in the dark, followed by washes with HBSS and a 30 minute incubation at the same temperature. Coverslips were then loaded on a LSM710 confocal microscope with a 40x water objective (Carl Zeiss, Germany). Image acquisition was set up to capture a new single-channel image every two seconds for a total of 3 minutes. After a few frames, 50 µl of NMDA or KCl were added at the appropriate concentration. For each cell type, one coverslip was treated with buffer to rule out mechanical activation of the cells by the addition of any liquid.

2.2.5 Ribopuromycilation

A ribopuromycilation assay was performed to examine actively translating ribosomes following the protocol described by David et al., 2011; David et al., 2012. Differentiated TE671 cells were treated with Puromycin, a protein synthesis inhibitor, and Emetine, a chain elongation inhibitor at a final concentration of 18.4 µM and 208 µM, respectively. Cells were incubated at 37°C (5% CO_2) for 5 minutes and washed thrice with 1xPBS. Cells were immediately fixed using 4% Paraformaldehyde and permeabilised for 15 minutes using labelling buffer (0.05% Saponin, 10mM Glycine, 5% Fetal Bovine Serum in 1 x PBS). Immunolabelling was then conducted using an anti-Puromycin antibody (see **Table 2.4**).

2.2.6 Immunocytochemistry

After cells were cultured and treated (when applicable) in 12 mm coverslips, they were fixed for 10 minutes using 4% Paraformaldehyde and washed thrice in 1xPBS. This was followed by permeabilisation using 0.2% Triton X-100 and three more washing steps. Once fixed, cells were incubated with primary antibodies (see **Table 2.4**) for two hours. After washing, cells were incubated with Alexa Fluor-conjugated secondary antibodies for one hour. Coverslips with immunostained cells were mounted using Fluoroshield DAPI (Sigma-Aldrich, F6057) medium and sealed.

2.2.7 Structured Illumination Microscopy

For Super Resolution Microscopy, cells were differentiated on square high-precision 22 x 22 mm coverslips (Zeiss, 474030-9020-000) and

post-fixed following immunocytochemistry for 10 minutes in 4% PFA and washed in PBS before mounting using CFM3 non-hardening medium (CitiFluor, Pennsylvania, CFM3-25). Slides were kept at room temperature and imaged in a Zeiss ELYRA PS.1 microscope (Carl Zeiss, Germany) with a controlled temperature module at 27°C using a Plan Apochromat 63x/1.4 oil DIC M27 objective with Zeiss Immersol™ 518F (30°C) oil (Zeiss, 444960-0000-000). Using stack scan mode, two tracks were setup for lasers 488nm and 561 nm, both at 25% laser power and with 100 ms exposure times. SRM SIM grating periods were 28.0 µm and 34.0 µm for green and red tracks, respectively. Bandpass filters used were BP420-480 + BP 495-550 + LP 650 for green and BP 420-480 + BP 570-640 + LP 740 for red. Multiple Z-stacks were captured for all experiments. With the objective of correcting channel shift in the data, coverslips with and without cells were cultured and 100 nm TetraSpeck Microspheres (ThermoFisher Scientific, T7279) were added. Z-stacks of these coverslips were captured using the same settings as experimental samples. These beads are excited by multiple laser wavelengths and thus are the gold standard tool to verify channel shift.

2.2.8 Confocal Microscopy

Cells were visualised at room temperature using a confocal LSM880C microscope (Carl Zeiss, Germany). Confocal images were captured at a 12-bit depth and with consistent power, wavelength, and detector gain settings across all samples using a 40x EC-Plan Neofluar (NA= 1.3) and 63x Plan-Apo (NA = 1.4) oil objectives.

2.2.9 Fluorescent Image Analysis

Channel shift correction on SIM data was performed using both 100 nm TetraSpeck Microspheres and marker-based alignment in Zen Black 2012 software under the supervision of Dr. Robert Markus. Colocalisation analysis, 3D modelling, and movies were generated using the Zen Black colocalisation and 3D modules, respectively.

For confocal data, quantitative localisation was performed in FIJI software using an in-house methodology which followed the principles outlined by Fletcher et al., (2010). A three channel approach was used to select synapse-specific regions. The third channel, the synaptic marker, was manually thresholded to eliminate background noise and converted to an 8-bit mask image to create regions of interest which encompassed only pre-/post-synaptic areas. Using FIJI's Coloc2 plug-in colocalisation analysis tool, colocalisation between the remaining two channels was evaluated at the 8-bit mask created. Pearson's Correlation Coefficients (PCC) were recorded. PCC is a standard measurement in fluorescent microscopy used to assess colocalisation between signals from two different channels. Values range from -1, indicating exclusion, to 1, which indicates a perfect correlation between the two channels. Values close to zero imply there is no linear correlation.

2.2.10 Statistics of Fluorescent Microscopy Data

Statistical significance was calculated for confocal microscopy data using the GraphPad Prism software by analysing the mean differences between PCC values obtained from image analysis. Results probing the

colocalisation of m^6A and a related protein at PSD95/VGluT1 sites were analysed with a two-way ANOVA with multiple comparisons. Results from ribopuromycilation experiments were analysed with an unpaired *t*-test. Finally, results from neuronal stem cell experiments were analysed with an ordinary one-way ANOVA with multiple comparisons.

2.2.11 Rat Brain Tissue Preparation

Rat brain was extracted by a licensed technician and tissue was fixed in 4% PFA and placed on a roller mixer for 48 hours. For dehydration and clearing, a Leica TP1020 tissue processor (Germany) was used to dip the tissue in increasing concentrations of ethanol followed by xylene (see details in **Table 2.6**). Tissue was left in xylene overnight and then infiltrated with paraffin as an embedding agent, positioned sagittally relative to where it would be cut. The tissue-wax cassette was left on a cold plate overnight to solidify. Tissue was cut using a Leica RM2145 microtome (Germany) and attached to glass slides.

Reagent	Time (mins)
70% Ethanol	15
90% Ethanol	15
100% Ethanol	15
100% Ethanol	15
100% Ethanol	30
100% Ethanol	45
Xylene	20
Xylene	20
Xylene	45
Wax	30
Wax	30
Wax	45

Table 2.6 Dehydration, clearing, and paraffin wax infiltration times for the processing of tissue.

2.2.12 3,3′-Diaminobenzidine (DAB) Immunohistochemistry

DAB stain immunohistochemistry was performed using a Vectastain Elite ABC Kit (Vector Labs, USA) on formaldehyde-fixed paraffin-embedded (FFPE) rat whole brain sections to optimise antibody dilutions and consequentially on FFPE human occipital cortex sections. Sections were dewaxed and rehydrated by immersion in two xylene containers for three minutes each followed by two immersions in absolute ethanol and a further two in 70% ethanol for three minutes each. Next, antigen retrieval was performed in sodium citrate (pH 6.0) in a steamer for 45 minutes. Protein blocking was performed using diluted normal horse serum for 1 hour. Endogenous peroxidases were blocked by covering sections in 3% hydrogen peroxide in 1 x PBS solution for 30 mins. Endogenous avidin, biotin, and biotin receptors were blocked by incubating sections in Avidin D for 15 minutes followed by Biotin for a further 15 mins (Avidin/Biotin Blocking Kit, Vector Labs).

Primary antibodies (see **Table 2.4**) were diluted in 0.2% Triton X-100 in 1 x PBS to further permeabilised tissue and sections were incubated overnight. The next day, sections were washed and covered in horse-raised universal secondary antibody diluted in normal horse serum and incubated for 1 hour. Subsequently, sections were washed and incubated with Vectastain ABC Reagent, a biotin detection system, for 30 minutes. Finally, tissue was incubated with ImmPACT DAB Substrate until the appropriate staining intensity was obtained (see **Table 2.7** for details). Sections were then counterstained in Haematoxylin for one minute and blued using Scott's Tap Water. Finally, sections were

dehydrated by dipping 10 times in a gradient of 2 x 70% ethanol, 2 x 100% ethanol, and 2 x Xylene. Sections were mounted on slides using ImmunoHistoMount mounting media (Sigma-Aldrich, USA) and then sealed.

Target	Time (sec)
m^6A	20
YTHDF1	120
YTHDF3	60
N-cadherin	45
NeuN	60
GFAP	45

Table 2.7 DAB substrate incubation times in brain tissue.

2.2.13 Brightfield Microscopy

Images of immunostained tissue were captured using the Micro Manager open-source microscope controller software (www.micro-manager.org ; Edelstein et al., 2010) and an Axioplan microscope (Carl Zeiss, Germany). Images were captured using a 5x air objective (NA = 0.15) and a 20x air objective (NA = 0.5) with exposure times of 20 ms and 35 ms respectively. After imaging each slide with each objective, a blank image was captured and used to white balance all other experimental images using a macro created by the University of Nottingham SLIM imaging unit staff which adjusts the blank image to white and applies the same degree of colour intensity change to other images to reflect the tissue's real colour. The default settings were used in this macro and raw and white-balanced data was saved.

2.2.14 Image Analysis of IHC Using Machine Learning

With the objective of reducing researcher bias during data analysis, the ilastik open-source image classification and segmentation software was used (www.ilastik.org ; Sommer et al, 2011; reviewed in Kan, 2017). ilastik uses machine learning algorithms to automatically (but under supervision) find and quantify features in an image. To achieve this in immunohistochemistry-DAB data, five selected images with clear, isolated DAB staining (GFAP and m^6A) were input. All feature selection algorithms were set at a threshold of $\sigma = 1.0$. Two labels were used in the training module, one to teach it brown DAB staining and one to teach it to exclude blue haematoxylin staining. After training, all experimental images were batched processed and resulted in probability maps, i.e. images showing all areas the software predicts are DAB-stained, were exported as .tiff files and opened in FIJI.

2.2.15 IHC-DAB Statistics

Mean pixel intensity values were calculated for each IHC-DAB image using FIJI's Measure command and recorded. Statistical significance was calculated with an unpaired *t*-test in GraphPad Prism, which was also used to generate graphs.

2.2.16 Tissue Preparation for Scanning Transmission Electron Microscopy (STEM)

To perform STEM microscopy, a mouse hippocampus which had been fixed with 3% PFA/0.1% Glutaraldehyde in 0.1M phosphate buffer through perfusion was obtained, dehydrated, and polymerised in araldite.

200 nm sections were cut using a Leica EM UC6/FC6 cryoultramicrotome and mounted on graphene oxide grids, which were chosen to stabilise sections and allow longer dwell times or more repeated acquisitions during imaging.

2.2.17 Immunogold Labelling

Tissue-mounted grids were placed in 1% BSA in 1 x PBS for 5 minutes and then 15 minutes in 1% BSA, 10% goat serum in 1 x PBS. Grids were incubated overnight at 4°C with primary antibodies in 1% BSA, 5% goat serum in 1 x PBS at the appropriate dilution (see **Table 2.4**). After three washes with 1% BSA in 1 x PBS and one in 1% BSA, 0.25% Tween 20, the gold nanoparticle-conjugated secondary antibody was centrifuged for 5 min at a 2,000 G force to remove clumped antibodies. The supernatant antibodies were diluted in a solution of 1% BSA, 0.25% Tween 20, 1% TRIS in 1 x PBS and incubated for 4 hours at 4°C followed by three 5 min washes with 1% TRIS, 1% BSA in 1 x PBS. Finally, grids were jet washed thrice and dried.

2.2.18 Scanning Transmission Electron Microscopy

Scanning TEM images were obtained on a JEOL 2100F TEM operating at 200kV, equipped with JEOL bright field and dark field detectors. Images were acquired and processed using Gatan Digital Micrograph software and the open source FIJI software (Schindelin et al., 2012).

By use of the diffuse, high angle annular diffracted electrons in STEM, the contrast mechanism for the subsequent image is significantly proportional to the atomic number Z ^ 1.6-1.9 per atom (Hartel et al.,

1996). This makes small, heavy labelling nanoparticles, e.g. 5 or 10nm gold nanoparticles, much higher contrast than the significantly higher volume biological material. As the orientation of the structure does not significantly affect the contrast, this mode of imaging is also ideal for tilt series analysis of three dimensional nanoscale structures.

Due to the transient nature of the rastered STEM beam, the use of graphene oxide film as a heat and charge conductive, low contrast support can significantly stabilise insulating biological sections for use in STEM imaging and mapping, allowing longer dwell times of up to 10 ms per pixel or more repeated acquisitions of the same region.

2.2.19 m^6A-sequencing of Human Brain

The University of Nottingham's Deep Seq next generation sequencing facility performed the RNA preparation and m^6A-sequencing for this project. 40-50 mg of snap frozen tissue was used for RNA extraction. Ribo-depleted RNA was fragmented to 100bp. 1/10 volume of fragmented RNA was separated to use as input control. Remaining RNA (9/10; 200-300ng) was divided into two equal fractions for m^6A immunoprecipitation in duplicate.

Immunoprecipitation was performed using an anti-m^6A antibody (Abcam, ab151230). Total RNA (input control) or m6A IP RNA was used for creation of double stranded cDNA, which was used to generate Sequencing libraries NEBNext® Ultra II DNA Library Prep Kit for Illumina (NEB, E7645S) according to manufacturer's instructions. Libraries were pooled at desired concentrations and sequenced according to

manufacturer's instructions using Illumina NextSeq500 platform to generate approx. 40-50million 75bp PE reads per sample (Illumina, FC-404-2002).

Pre-processing of reads was performed using the FASTX programme. Reads were aligned to the human genome (build GRCh37/hg19) using Tophat2 (Kim, Pertea et al. 2013) with default settings. m^6A-tagged regions were identified using the exomePeak calling algorithm (Zhang et al., 2008) with the input library as background.

2.2.20 m^6A-sequencing Data Annotation and Gene Ontology

Next-generation sequencing data obtained from homogenised human brain tissue was downloaded from the Methylation Database (MeT-DB). N6-methyladenosine (m^6A) peaks from this dataset and the human brain-derived data generated by this project were annotated to eight non-overlapping transcript segments using HOMER (Salk Institute, USA) and a combination of bioinformatics tools as previously described. These segments were: intron, exon, transcription termination site (TTS), transcription start site (TSS), 3' UTR, 5' UTR, non-coding, and intergenic. Transcripts were then split into lists according to their region of methylation and these, together with the full lists of annotated peaks per tissue sample, were analysed using DAVID's Functional Annotation Clustering tool to discern possible tissue- and region-specific functions for methylation.

In a separate analysis, a published highly-specific list of transcripts found in neuropil was obtained from Cajigas et al. (2012) and compared with

both annotated datasets for further analysis. A new list of synaptically-located m^{6}A-methylated transcripts was created from the genes found in both datasets. Again, DAVID's Functional Annotation Clustering tool was used to assess a possible common function of these transcripts based on tissue and region of methylation.

All subsequent analysis of m^{6}A topology, methylated transcripts, and gene ontology was performed using Microsoft Excel and BioVenn (www.biovenn.nl ; Hulsen et al., 2008).

Chapter 3:

Bioinformatic analysis of brain-derived m^6A-sequencing data

In this chapter, I would like to extend my sincerest thanks to my research group co-workers, Dr. Miles Flitton and Dr. Maria Koromina, whose guidance in using R to run HOMER greatly facilitated this work. I also appreciate the high quality work of the University of Nottingham's Deep Seq facilities. Finally, I thank Dr. Anbarasu Lourdusamy, who performed the motif analysis presented below.

3.1 Preface

The phenomenon that RNA, like DNA, could be methylated at the sixth nitrogen of an adenosine base was first discovered and characterised in the 1970s (Desrosiers et al., 1974). Two sequencing studies published in 2012 by Meyer et al. and Dominissini et al. have since revived the field of m^6A. In this chapter, the results of NGS m^6A-sequencing in human brain tissue are presented. These results attempt to understand the distribution of m^6A modification in brain-derived mRNA, what these transcripts do, and how methylation changes in tissue types and even cell compartments.

3.2 Results

3.2.1 Analysis of human methylated brain transcripts

To characterise the m^6A methylome in grey and white matter from the human parahippocampus as well as PCW 20-33 fetal brain, high throughput m^6A-seq was performed (**Appendix 1**). A total of 9579 high confidence peaks were identified in 5298 coding transcripts in human parahippocampus grey matter tissue, 14064 peaks in 6968 coding transcripts in parahippocampus white matter tissue, and 14249 peaks in 6730 coding transcripts in foetal brain. The number of non-coding mRNAs identified in grey matter, white matter, and fetal brain tissue were 851, 1460, and 1262, respectively. The most enriched m^6A binding motif in all samples was found to be GGAC, which is consistent with the previously reported RRACH motif (Schibler et al., 1977; Bailey, T., 2011; **Figure 3.1**).

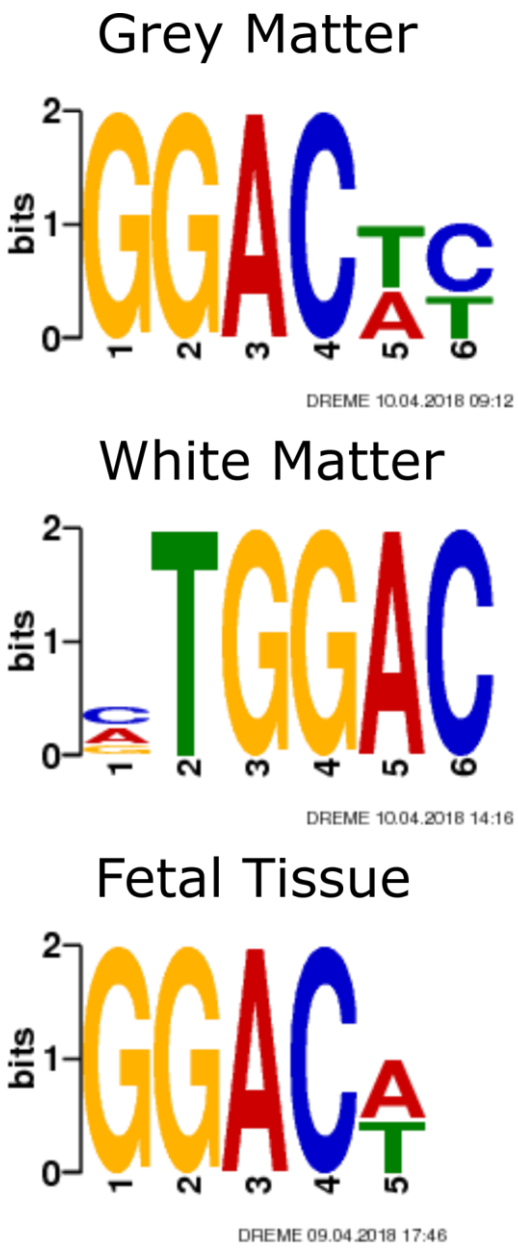

Figure 3.1 Top motif in human brain m^{6}A-sequencing data. The most common motif in all samples was found to be GGAC, as expected. Consensus logos were generated using DREME software.

m^6A methylation was predominantly present at exons (~45%) and 3' UTR (~30%) and this did not vary significantly between tissue samples (**Figure 3.2 A-C**). The mean number of methylation peaks per transcript was approximately two. Specifically, grey matter tissue had a mean methylation rate of 1.81 m^6A marks per methylated mRNA, white matter had 2.02, and fetal brain tissue 1.93. There was a 50-25-25 percent split in transcripts with one, two, or more m^6A peaks (**Figure 3.2 D**). Finally, transcripts were identified in all samples with at least double the average methylation marks and found 473, 869, and 833 in grey matter, white matter, and fetal tissue, respectively. These hypermethylated transcripts had a maximum of 28 m^6A marks and almost all encoded for prototocadherins (**Table 3.1**).

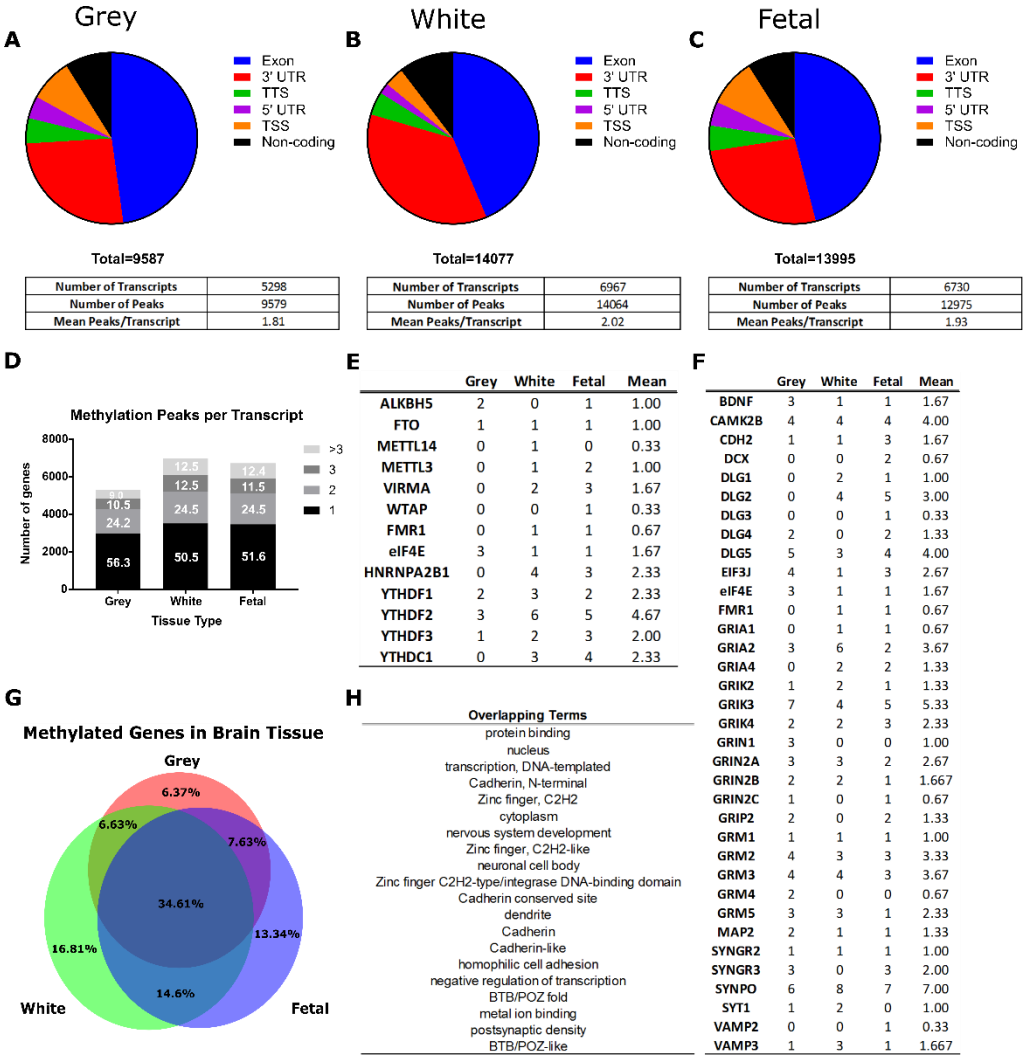

	Grey	White	Fetal	Mean
ALKBH5	2	0	1	1.00
FTO	1	1	1	1.00
METTL14	0	1	0	0.33
METTL3	0	1	2	1.00
VIRMA	0	2	3	1.67
WTAP	0	0	1	0.33
FMR1	0	1	1	0.67
eIF4E	3	1	1	1.67
HNRNPA2B1	0	4	3	2.33
YTHDF1	2	3	2	2.33
YTHDF2	3	6	5	4.67
YTHDF3	1	2	3	2.00
YTHDC1	0	3	4	2.33

	Grey	White	Fetal	Mean
BDNF	3	1	1	1.67
CAMK2B	4	4	4	4.00
CDH2	1	1	3	1.67
DCX	0	0	2	0.67
DLG1	0	2	1	1.00
DLG2	0	4	5	3.00
DLG3	0	0	1	0.33
DLG4	2	0	2	1.33
DLG5	5	3	4	4.00
EIF3J	4	1	3	2.67
eIF4E	3	1	1	1.67
FMR1	0	1	1	0.67
GRIA1	0	1	1	0.67
GRIA2	3	6	2	3.67
GRIA4	0	2	2	1.33
GRIK2	1	2	1	1.33
GRIK3	7	4	5	5.33
GRIK4	2	2	3	2.33
GRIN1	3	0	0	1.00
GRIN2A	3	3	2	2.67
GRIN2B	2	2	1	1.667
GRIN2C	1	0	1	0.67
GRIP2	2	0	2	1.33
GRM1	1	1	1	1.00
GRM2	4	3	3	3.33
GRM3	4	4	3	3.67
GRM4	2	0	0	0.67
GRM5	3	3	1	2.33
MAP2	2	1	1	1.33
SYNGR2	1	1	1	1.00
SYNGR3	3	0	3	2.00
SYNPO	6	8	7	7.00
SYT1	1	2	0	1.00
VAMP2	0	0	1	0.33
VAMP3	1	3	1	1.667

Figure 3.2 Peak annotation and gene ontology analysis of m^{6}A-sequencing data from grey matter, white matter, and fetal human brain samples. A-C) Topological distribution of m^{6}A within a transcript and the average number of peaks per transcript per sample. D) Number of detected m^{6}A peaks per transcript. Percentages are superimposed on bar graphs. All samples showed a 50-25-25 percentage of transcripts with 1, 2, or more peaks, respectively. E) Summary table shows transcripts of m^{6}A writers, readers, and erasers are themselves methylated. F) Transcripts that encode for synaptic structure, function, and receptors were found to be methylated. G) The overlap of methylated transcripts between grey matter, white matter, and fetal brain tissue is low, displaying a high variability according to tissue type and developmental stage. H) Top 20 significant GO terms indicate methylated transcript enrichment for protein binding, cadherins, and neuronal terms.

	Grey	White	Fetal	Mean
PCDH1	6	5	6	5.67
PCDH10	5	5	4	4.67
PCDH11X	0	1	5	2.00
PCDH11Y	1	5	4	3.33
PCDH12	0	1	2	1.00
PCDH17	8	7	7	7.33
PCDH18	1	2	2	1.67
PCDH19	4	3	5	4.00
PCDH20	8	6	6	6.67
PCDH7	3	3	3	3.00
PCDH8	4	1	7	4.00
PCDH9	4	1	3	2.67
PCDHA1	2	0	2	1.33
PCDHA10	0	0	4	1.33
PCDHA11	1	0	3	1.33
PCDHA12	0	0	5	1.67
PCDHA13	0	0	2	0.67
PCDHA2	0	0	4	1.33
PCDHA3	1	1	2	1.33
PCDHA4	4	1	5	3.33
PCDHA5	1	0	6	2.33
PCDHA6	1	1	3	1.67
PCDHA7	0	0	3	1.00
PCDHA8	0	0	1	0.33
PCDHA9	0	0	4	1.33
PCDHAC1	2	2	3	2.33
PCDHAC2	3	1	2	2.00
PCDHB1	0	21	28	16.33
PCDHB10	0	2	3	1.67
PCDHB11	4	1	7	4.00
PCDHB12	6	1	7	4.67
PCDHB13	1	1	2	1.33
PCDHB14	8	8	7	7.67
PCDHB15	1	2	4	2.33
PCDHB16	0	1	5	2.00
PCDHB18P	0	1	0	0.33

PCDHB19P	5	2	0	2.33
PCDHB2	2	3	8	4.33
PCDHB3	2	2	2	2.00
PCDHB4	4	3	2	3.00
PCDHB5	4	0	3	2.33
PCDHB6	2	4	5	3.67
PCDHB7	0	0	2	0.67
PCDHB9	1	1	5	2.33
PCDHGA1	1	0	2	1.00
PCDHGA10	1	1	3	1.67
PCDHGA11	1	1	5	2.33
PCDHGA12	1	3	3	2.33
PCDHGA2	0	0	2	0.67
PCDHGA3	1	0	1	0.67
PCDHGA4	1	1	2	1.33
PCDHGA5	2	2	5	3.00
PCDHGA6	1	3	5	3.00
PCDHGA7	1	0	3	1.33
PCDHGA9	1	3	2	2.00
PCDHGB2	0	1	2	1.00
PCDHGB3	0	0	3	1.00
PCDHGB4	0	1	2	1.00
PCDHGB5	1	2	3	2.00
PCDHGB6	0	1	4	1.67
PCDHGB7	0	2	4	2.00
PCDHGC3	2	2	3	2.33
PCDHGC4	4	0	2	2.00
PCDHGC5	3	24	26	17.67

Table 3.1 Number of m^6A peaks per protocadherin-encoding transcript in grey matter, white matter, and fetal tissue. 64 Protocadherins were found to be methylated more than average (~2 peaks per transcript) in at least one tissue type in a majority of cases.

Data also indicated that all currently known proteins involved in m^{6}A methylation (Meyer & Jaffrey, 2017; Patil et al., 2018) are themselves modified. This suggests a role for m^{6}A autoregulation in which methylation modifies the amount of writer, reader, and eraser proteins available and thus their cumulative effect on m^{6}A methylation (**Figure 3.2 E**). m^{6}A readers were found to have a higher than average number of methylation modifications per transcript (mean of 2.73), especially YTHDF2 which had an average of 4.67 marks per transcript across samples. In contrast, eraser protein transcripts were found on average to have only one modification, whilst transcripts corresponding to the methyltransferase complex had an even lower average of 0.83. Lastly, newly proposed candidate readers, FMRP and EIF4E (Chang et al., 2017; Meyer et al., 2015), each had a lower than average number of modifications with 0.67 and 1.67.

In addition, transcripts relating to synaptic structure and activity were also multi-modified methylated and in many cases whole classes of protein family members were modified (**Figure 3.2 F**). For example, *CAMK2B*, involved in synaptic spine formation and a classic marker of LTP, had a mean of 4.0 modifications in all tissue samples whereas *DLG2* and *DLG5*, both part of the post-synaptic density structure, have an average of 3.0 and 4.0 modification sites, respectively. All glutamate subunit receptors were found to be modified with *GRIN2A* (2.67) and *GRIK3* (5.33) being most prominent. Finally, although *CDH2*, the transcript from which neuronal cadherin is translated, has an average number of m^{6}A

marks, 22 different precursor protocadherin transcripts were highly methylated with an average of 4.5 marks per transcript and a maximum of 9.0 (**Table 3.1**). Taken together, these results suggest that m^6A readers undergo self-regulation by m^6A and that this modification is more numerous in structural and functional synaptic transcripts.

Gene ontology functional annotation of modified transcripts revealed that the most enriched biological processes in grey matter tissue were nervous system specific, e.g. synapse, axon, and nervous system development (**Table 3.2**). In contrast, white matter tissue was enriched for processes associated the nucleus and cytoplasm, like transcription and ubiquitylation. In accordance with a previous report by Yoon et al. (2017), foetal tissue showed enrichment for transcripts which are associated with nervous system development but this analysis also found enrichment of organelle and nucleus-associated transcripts. (**Table 3.2**). Interestingly, only about one third of significant terms were shared across all samples, indicating high variability in which transcripts are modified (**Figure 3.2G**), and these included processes such as neuronal development, dendritic structure and function, ion channel binding, neurotransmitter signalling pathways, and N-cadherin domains (**Figure 3.2H**). This suggests that the most conserved functions of m^6A methylation in brain tissue are related to neuronal development and cell adhesion.

GO Term	Enrichment *p* Value	Fold Enrichment	m^6A Transcripts	Transcripts in Term
Hippocampal Grey Matter				
Phosphoprotein	4.10E-62	1.26	2335	8246
Synapse	5.10E-22	2.02	162	357
Cell junction	2.70E-17	1.75	188	459
Protein binding	1.40E-15	1.10	2292	8785
Ubiquitin-like conjugation	6.90E-15	1.35	514	1705
Axon	1.20E-14	2.02	105	222
Nervous system development	2.80E-13	1.83	124	287
Postsynaptic membrane	4.00E-13	1.99	98	298
Alternative splicing	1.50E-12	1.09	2579	10587
Chemical synaptic transmission	8.50E-12	1.86	105	240
Hippocampal White Matter				
Phosphoprotein	4.40E-76	1.24	3097	8246
Alternative splicing	8.10E-37	1.13	3622	10587
Nucleus	6.00E-32	1.21	1928	5244
Zinc-finger	3.70E-30	1.4	756	1781
Protein binding	8.50E-29	1.11	3156	8785
Transcription regulation	1.50E-28	1.33	942	2332
Transcription	2.10E-28	1.33	964	2398
Zinc	2.60E-22	1.29	917	2348
Ubl conjugation	4.20E-22	1.34	695	1705
Isopeptide bond	7.00E-19	1.4	479	1132
Fetal Whole Brain				
Protein binding	7.75E-43	1.14	3424	8785
Nucleus	1.60E-31	1.19	2157	5415
Transcription, DNA-templated	1.31E-25	1.31	873	1955
Nucleoplasm	3.00E-22	1.24	1157	2784
Cytoplasm	2.08E-18	1.14	2001	5222
Nervous system development	2.24E-18	1.74	170	287
Poly(A) RNA binding	1.25E-17	1.34	519	1129
Neuronal cell body	1.41E-15	1.66	175	315
Dendrite	1.96E-13	1.58	178	335
Cell adhesion	1.57E-12	1.82	98	158

Table 3.2 Gene ontology functional annotation of m^6A-modified transcripts in grey and white matter in the adult para hippocampus and foetal brain. The top ten enriched terms by ascending *p*-value are shown for each tissue type.

Currently, it is known that m^6A is distributed across all regions of a transcript but it is unknown whether this is random. To address this question, transcripts were separated per sample according to their region of methylation. For the purpose of simplicity, 5' and Transcription Start Sites (-1kb to +100 bp from start codon) annotations were combined into one, as well as 3' UTR and Transcription Termination Site (-100 bp to +1kb from end codon). DAVID Gene Ontology analysis was performed and it was found that in all three samples, the number of common biological functions between transcripts methylated in different regions was very low with a maximum of 5% of significant functions being shared (**Figure 3.3 A-C**). Investigating further, it was observed that 5' UTR/TSS-methylated transcripts encoded for neuron-specific terms such as "synapse" and "axon", as well as "methylation" in both DNA and RNA (**Figure 3.3D**). In contrast, exon-methylated transcripts were most significantly enriched for cadherins, other cell adhesion-related proteins, transcription, and signalling pathway regulation (**Figure 3.3E**). Lastly, 3' UTR/TTS-methylated transcripts were most enriched for a combination of housekeeping functions like potassium channels, cell junctions, protein binding, and regulation of protein transport but also neuronal terms like synapse, post-synaptic membrane, and neuronal cell body; (terms similar to those from the 5' UTR/TSS list; **Figure 3.3F**). These results indicate that the region of methylation correlates to the biological function of a transcript's protein product.

A

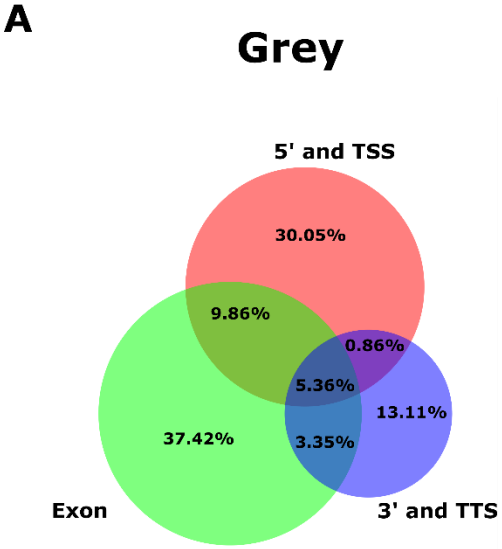

B

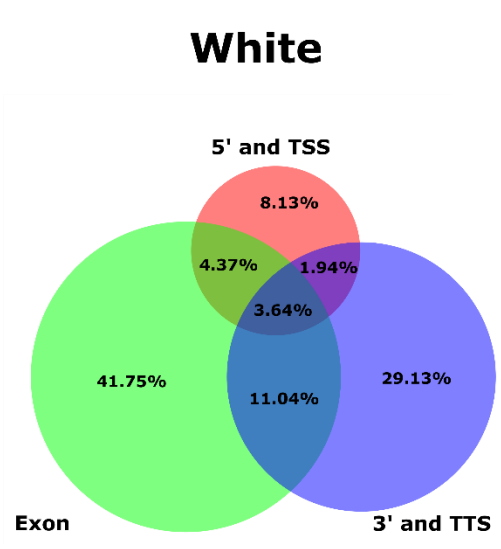

C

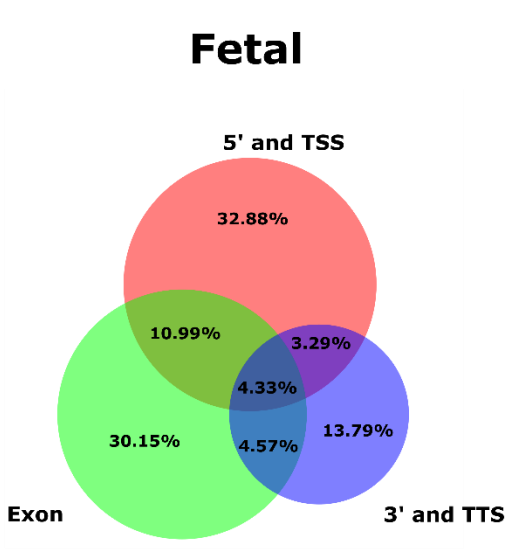

D

Term
Phosphoprotein
Synapse
Axon
Postsynaptic density
Neuronal cell body
Postsynaptic membrane
Postsynaptic cell membrane
Dendrite
Methylation
Neurogenesis

E

Term
Phosphoprotein
domain:Cadherin 6
domain:Cadherin 5
IPR013164:Cadherin, N-terminal
domain:Cadherin 4
domain:Cadherin 3
domain:Cadherin 2
domain:Cadherin 1
zinc finger region:C2H2-type 2
Transcription regulation

F

Term
Phosphoprotein
Potassium channel
Cell junction
Synapse
Golgi apparatus
Protein binding
Positive regulation of positive chemotaxis
Postsynaptic membrane
Protein homooligomerization
Neuronal cell body

Figure 3.3 Region of methylation correlates to enriched biological function. m^6A-sequencing results were separated by region of methylation and then analysed using DAVID's Functional Annotation tool to obtain the dataset's gene ontology. A-C) Overlap of GO terms between transcripts methylated at the 5' UTR/TSS, exon, or 3' UTR/TTS regions in grey matter, white matter, or fetal brain tissue. In all cases, the GO terms shared between all transcripts were ≤5%, suggesting distinct biological functions. D-F) Top 10 significant GO terms of transcripts methylated at the 5'UTR.TSS (D), exon (E), or 3'UTR/TTS (F).

Finally, m^6A's prevalence in all transcripts and what this could mean in terms of disease lead to the investigation of transcript enrichment in disease classes. DAVID's functional annotation tool indicated that m^6A-methylated transcripts in all samples' transcript lists were enriched for psychological and neurological disease classes as their top two terms. Further investigation using DAVID's OMIM (Online Mendelian Inheritance in Man) disease database revealed Schizophrenia as the most significant ($p < 0.0001$) disease related to m^6A-methylated transcripts, with at least 251 methylated transcripts related to the disease found in all samples, e.g. *BNDF*, *GRIK4*, and *GRM3*. Other neurological disorders such as bipolar, psychosis, epilepsy, Tourette syndrome, and Alzheimer's disease were found in all three tissue samples. Alzheimer's disease was especially interesting due to the high number of methylated transcripts (253) found in the term. These transcripts included APOE and SNCA, well-studied proteins related to dementia. Besides brain disease, one other type of disorder found in the gene ontology of all samples was substance abuse of alcohol, tobacco, and marijuana with these terms having a fold enrichment of up to 2.2. Lastly, weight gain and lipid metabolism-related terms were enriched in all samples with a fold enrichment of approximately 1.4. **Table 3.3** summarises these results.

GO Term	Enrichment *p* Value	Fold Enrichment	m^6A Transcripts	Transcripts in Term
Hippocampal Grey Matter				
Schizophrenia	6.11E-09	1.38	251	785
Weight Gain	2.19E-06	1.82	56	133
Schizophrenia; schizoaffective disorder; bipolar disorder	5.41E-05	3.45	12	15
Several psychiatric disorders	1.37E-04	1.41	98	299
Marijuana Abuse, Psychosis, Substance-Induced	1.42E-04	2.20	23	45
Alcohol consumption	2.74E-04	1.63	49	130
Fibrinogen	3.97E-04	1.56	54	149
Epilepsy	5.34E-04	1.87	29	67
Bipolar Disorder	1.17E-03	1.29	122	407
Alzheimer's disease	6.93E-03	1.15	253	950
Hippocampal White Matter				
Schizophrenia	2.49E-04	1.18	296	785
Weight Gain	4.67E-04	1.46	62	133
Several psychiatric disorders	1.33E-03	1.27	121	299
Tobacco Use Disorder	1.47E-03	1.07	1034	3034
Alcoholism	2.35E-03	1.19	193	509
Bipolar Disorder	2.82E-03	1.21	157	407
Cholesterol, LDL	3.17E-03	1.19	183	483
Alcohol consumption	4.44E-03	1.38	57	130
Stroke	4.57E-03	1.17	202	542
Tourette syndrome	5.28E-03	3.14	7	7
Fetal Whole Brain				
Schizophrenia	1.41E-04	1.18	313	785
Tobacco Use Disorder	2.16E-04	1.08	1104	3034
High-density lipoprotein Cholesterol	3.84E-04	1.95	23	35
Weight Gain	6.99E-04	1.43	64	133
Alcoholism	3.89E-03	1.17	201	509
Marijuana Abuse, Psychosis, Substance-Induced	5.09E-03	1.65	25	45
Cholesterol, HDL	6.37E-03	1.18	172	434
Huntington disease-like	7.25E-03	2.97	7	7
Conduct Disorder	8.03E-03	1.78	18	30
Alcohol consumption	9.75E-03	1.32	58	130

Table 3.3 Top ten GO disease terms from grey matter, white matter, and fetal brain. Lists of m^6A-methylated transcripts were most significantly enriched for Schizophrenia in all samples, followed by other neurological diseases, substance abuse disorders, and weight-related terms.

3.2.2 Analysis of synaptically located methylated transcripts from human brain

Using a set of bioinformatic tools (see **Chapter 2**), the above m^6A sequencing data was cross-referenced with a published list of mRNAs located at the neuropil of rat hippocampus (Cajigas et al., 2012) to create a list of synaptically-located m^6A methylated transcripts. Following the same annotation and gene ontology analysis as before, the following results were obtained.

In total, grey matter was found to have 1407 peaks annotating to 774 protein-coding genes, white matter had 1800 peaks annotating to 886 genes, and fetal brain had 1871 peaks corresponding to 983 genes. Consistently, the proportion of total methylated transcripts overlapping with the list of neuropil-derived mRNAs was found to be approximately 15%. The distribution of m^6A peaks across transcripts was also consistent with 45-50% of peaks located in the exon of transcripts and approximately 30% in the 3' UTR (**Figure 3.4 A-C**). The mean number of m^6A peaks per transcript (two) did not change significantly compared to the whole-tissue transcript list. Likewise, the percentage of transcripts with one, two, or more m^6A marks was still split 50-25-25 (**Figure 3.4D**).

One observed change is that the percentage of transcripts that were methylated in all three samples increased to approximately 40%, suggesting less variation of transcript methylation when compared to the whole cell (**Figure 3.4E**). Analysing overlapping GO terms for lists of synaptically-located m^6A-methylated transcripts (sorted by largest to

smallest *p* value), there is a clear enrichment of neuronal functions. As expected, the synaptic lists are strongly enriched for transcripts encoding for proteins important in synaptic function and structure. There is also an enrichment for proteins important in neuronal cell growth, development, and adhesion, as well as for the overall development of the nervous system (**Figure 3.4F**). This is in contrast with the overlapping terms of whole tissues, in which terms such as “protein binding” and “nucleus” were more prevalent than neuronal terms. Taken together, these results suggest that methylation of transcripts found in the synapse is consistent between tissue types and important to the proper function and development of this compartment.

A notable difference is that the transcripts of m^6A writers, readers, and erasers are rarely found in these lists (**Table 3.4**). Only one transcript encoding for a reader is found to be methylated, YTHDC1. Likewise, it was found that one m^6A writer’s transcript, METTL14 was methylated in white matter synapses. Interestingly, both YTHDC1 and METTL14 have been reported to be located in the nucleus and were therefore not expected in this list.

	Grey	White	Fetal	Mean
ALKBH5	0	0	0	0.00
FTO	1	1	1	1.00
METTL14	0	2	0	0.67
METTL3	0	0	0	0.00
VIRMA	0	0	0	0.00
WTAP	0	0	1	0.33
FMR1	0	0	1	0.33
HNRNPA2B1	0	0	0	0.00
YTHDF1	0	0	0	0.00
YTHDF2	0	0	0	0.00
YTHDF3	0	0	0	0.00
YTHDC1	0	1	2	1.00

Table 3.4 Transcripts encoding for m^{6}A-related proteins are rarely found at the synapses of grey matter, white matter, or fetal brain Summary table shows transcripts of m^{6}A writers, readers, and erasers and how many m^{6}A marks they have in each tissue type.

A

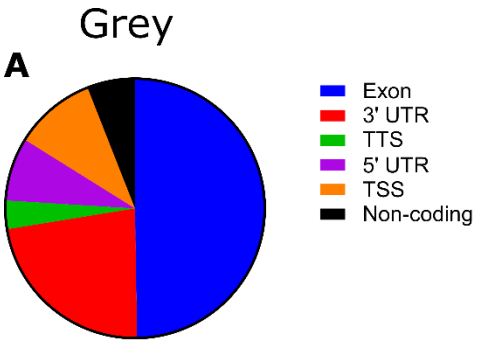

Total=1407

Number of Transcripts	774
Number of Peaks	1407
Mean Peaks/Transcript	1.82

B

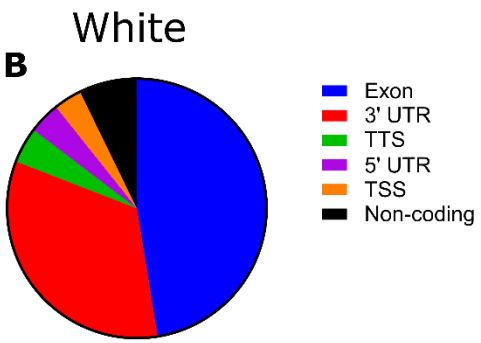

Total=1800

Number of Transcripts	886
Number of Peaks	1800
Mean Peaks/Transcript	2.03

C

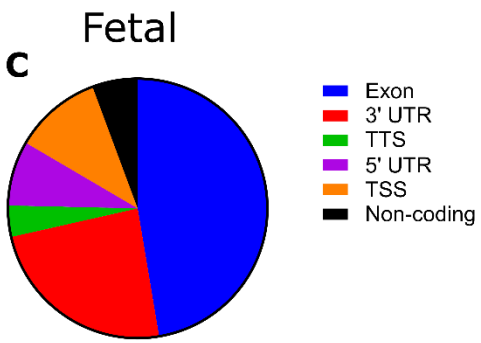

Total=1871

Number of Transcripts	983
Number of Peaks	1871
Mean Peaks/Transcript	1.90

D

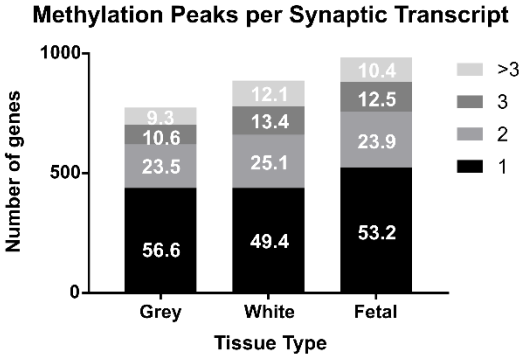

E

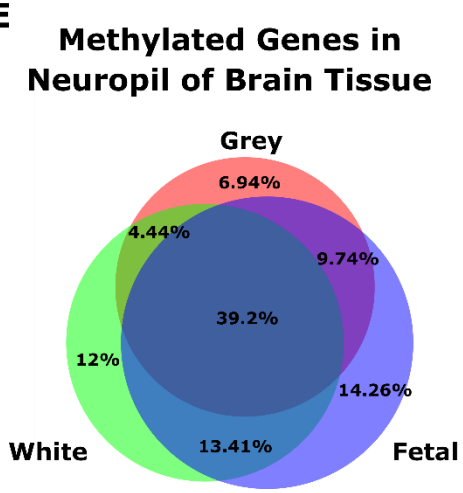

F

Overlapping Terms
Synapse
Phosphoprotein
Cell junction
Postsynaptic cell membrane
Postsynaptic density
Membrane
Transport
Axon
Ion transport
Voltage-gated potassium channel complex
Chemical synaptic transmission
Ion channel
Potassium transport
Neuronal cell body
Neuron projection
Dendritic spine
Potassium
Nervous system development
Alternative splicing

Figure 3.4 HOMER peak annotation and DAVID Functional Annotation Analysis of lists of synaptically-located m^{6}A-transcripts found in grey matter, white matter, and fetal brain. A-C) Topological distribution of m^{6}A within a transcript and the average number of peaks per transcript per sample. D) Number of detected m^{6}A peaks per transcript. Percentages are superimposed on bar graphs. All samples showed a 50-25-25 percentage of transcripts with 1, 2, or more peaks, respectively. E) Overlap of synaptically-located m^{6}A-transcripts is around 40%, displaying the high variability across synapses of different brain tissues. F) The top 20 significant GO terms show a clear trend towards the normal functioning and growth of synapses and neuronal cells.

3.2.3 Analysis of total human brain methylated brain transcripts

Previously, Dominissini et al., (2012) published the first m^6A-sequencing data, originating from commercially available total RNA of human adult brain. However, the analysis of this data was restricted to motif analysis and peak distribution across transcripts. These data were analysed using this project's methods to serve as a positive control and to obtain information regarding total human brain m^6A-methylation.

In total, 1863 peaks annotating to 1530 transcripts were found. Thus, the mean number of m^6A peaks per transcript was only 1.22. The distribution of peaks across transcripts was different, as well, with 65% of peaks in exons, 23% in 3' UTR, and only 1.6% in 5' UTR (**Figure 3.5A**). The fraction of transcripts with only one m^6A mark was substantially larger than previous datasets with 83% (**Figure 3.5B**). These results suggest that the methylation profile of the adult human brain as a whole is different to that of the cerebrum's two components or a developing fetal brain.

The gene ontology of m^6A-methylated transcripts was investigated using DAVID's functional annotation tool. As before, top enriched terms related to cellular adhesion (particularly through cadherin proteins), neuronal function and development, and regulation of transcription (**Figure 3.5C**).

Given that cellular adhesion and cadherins were once more a highly enriched common function for methylated transcripts, these transcripts were further investigated. **Table 3.5** lists 15 cadherin or protocadherin methylated transcripts. Although these were not highly methylated, this

protein family remains an important target of methylation across all analysed samples.

Gene	m^6A peaks
CDH18	1
CDH20	1
PCDH1	1
PCDH17	2
PCDH7	2
PCDH9	2
PCDHA7	1
PCDHAC2	2
PCDHB14	1
PCDHGA1	1
PCDHGA2	1
PCDHGA3	1
PCDHGA5	1
PCDHGC3	1
PCDHGC5	2

Table 3.5 Cadherin and protocadherin methylated transcripts.

Despite multiple differences between the results of this analysis compared to that of previous analyses, m^6A reader proteins were still found to be methylated. All three YTHDF proteins' transcripts were methylated once in the exon region. This finding suggests self-regulation of YTH proteins is a well-conserved feature. Finally, it was found that ALKBH1, a DNA demethylase that binds to the DNA equivalent of m^6A, was also methylated.

A

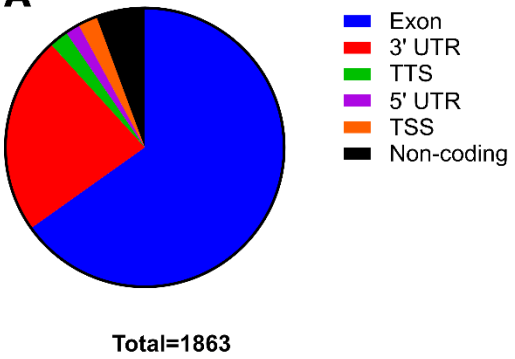

Number of Transcripts	1530
Number of Peaks	1863
Mean Peaks/Transcript	1.22

B

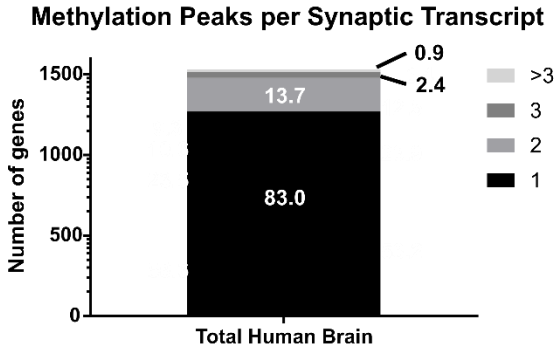

C

Term	Count	PValue
BTB/POZ-like	38	2.01E-10
BTB/POZ fold	38	9.98E-10
Zinc finger, C2H2-like	89	4.59E-08
Zinc finger, C2H2	90	1.95E-07
Zinc finger C2H2-type/integrase DNA-binding domain	82	2.95E-07
Positive regulation of synapse assembly	18	3.36E-07
Regulation of transcription, DNA-templated	149	3.73E-07
Transcription, DNA-templated	183	6.61E-07
Axon	35	2.78E-06
Nucleus	424	3.15E-06
Metal ion binding	186	4.11E-06
Delayed rectifier potassium channel activity	12	1.19E-05
Voltage-gated potassium channel complex	19	1.21E-05
Negative regulation of neuron apoptotic process	24	1.69E-05
Nucleic acid binding	99	1.81E-05
Transcription factor activity, sequence-specific DNA binding	97	1.91E-05
Potassium ion transport	18	2.09E-05
Ubiquitin-protein transferase activity	43	2.54E-05
Protein ubiquitination	46	2.61E-05

Figure 3.5 Analysis of HOMER peak annotation and DAVID functional annotation of m^{6}A-methylated transcripts in the adult human total RNA, as published by Dominissini et al. A) Topological distribution of m^{6}A within a transcript and the average number of peaks per transcript. B) Number of detected m^{6}A peaks per transcript. Percentages are superimposed on bar graphs. C) Top 20 significant GO terms show methylated transcripts are enriched for cellular adhesion, neuronal function and development, and regulation of transcription.

As in a previous analysis, transcripts were also separated based on their region of methylation - binning 5' UTR together with TSS and 3' UTR with TTS – and gene ontology analysis was performed (**Table 3.6**). The majority of GO terms from 5'UTR/TSS-methylated transcripts were related to different element-binding protein domains or DNA transcription, with "Glial cell differentiation" being the exception. Exon-methylated transcripts returned terms related zinc finger structural protein motifs, the common BTB/POZ domain, and cadherins. There was little variability in this region. 3' UTR/TTS meanwhile was annotated to a combination of synaptic (synapse, postsynaptic membrane, neuronal signal transduction, etc.), protein regulation (i.e. protein phosphorylation, protein activity), and transcription terms. In this last region, it was observed that the most significant terms were synaptic terms, while protein regulation and transcription were less significant.

GO Term	Enrichment p Value	Fold Enrichment	m^6A Transcripts	Transcripts in Term
5' UTR/TSS				
mTOR signaling pathway	9.80E-03	18.73	3	58
WWE domain, subgroup	1.12E-02	175.08	2	4
WWE	1.27E-02	152.38	2	4
Cysteine persulfide intermediate	1.57E-02	123.85	2	6
Protein homodimerization activity	1.84E-02	3.24	7	730
Metal-binding	2.15E-02	1.75	17	3640
WWE domain	3.58E-02	53.87	2	13
Glial cell differentiation	3.93E-02	48.96	2	14
Metal ion-binding site:Iron-sulfur (4Fe-4S)	4.40E-02	43.71	2	17
Rhodanese	5.41E-02	35.38	2	21
Exon				
Phosphoprotein	5.11E-19	1.35	493	8246
Zinc-finger	9.22E-13	1.83	144	1781
BTB/POZ-like	1.52E-10	3.90	32	180
BTB/POZ fold	6.12E-10	3.69	32	190
Transcription	8.53E-10	1.59	168	2398
Zinc finger, C2H2-like	1.44E-09	2.13	74	762
Transcription regulation	1.91E-09	1.58	163	2332
Zinc finger region:C2H2-type 4	2.20E-09	2.32	61	588
Zinc finger region:C2H2-type 3	2.81E-09	2.25	64	636
Zinc finger region:C2H2-type 5	3.24E-09	2.36	58	550
3' UTR/TTS				
Nucleosome assembly protein (NAP)	2.81E-04	15.16	5	20
Synapse	1.20E-03	3.52	15	181
Ion channel	2.73E-03	2.52	15	359
Sulfotransferase activity	3.26E-03	8.06	5	37
Postsynaptic membrane	3.69E-03	3.02	11	211
Neuronal signal transduction	4.29E-03	28.75	3	6
Positive regulation of synapse assembly	4.37E-03	5.57	6	62
Endoplasmic reticulum	4.75E-03	1.82	26	828
Establishment of protein localization	4.94E-03	7.19	5	40
Protein phosphorylation	6.24E-03	2.14	17	456

Table 3.6 Top ten GO terms from m^6A-sequence adult human brain total RNA separated based on region of methylation.

As with previous lists of methylated transcripts, a gene ontology analysis was performed and the disease category was investigated (**Table 3.7**). It was found that the top significant disease GO term for this list was tobacco use disorder with 264 transcripts found within this term. This was followed by weight-related and other substance abuse terms. Neurological terms such as major depressive disorder and ADHD were found to have a higher fold enrichment but be less significant when compared to the analysis of other datasets, suggesting variability depending on tissue. Notably, Schizophrenia was a highly significant term in newly generated hippocampal grey and white matter but was not found in this analysis.

GO Term	Enrichment *p* Value	Fold Enrichment	m^6A Transcripts	Transcripts in Term
Tobacco Use Disorder	8.1E-06	1.26	264	3034
Cholesterol, HDL	7.3E-04	1.64	49	434
Weight Gain	4.3E-03	2.08	19	133
Alcohol consumption	7.7E-03	2.01	18	130
Body Mass Index	8.6E-03	1.46	48	479
Methamphetamine Abuse	9.6E-03	5.59	5	13
Lower Back Pain	1.4E-02	14.53	3	3
Carotid Artery Diseases	1.7E-02	2.23	12	78
Major depressive disorder	1.8E-02	2.67	9	49
ADHD	1.8E-02	2.91	8	40

Table 3.7 Top ten GO disease terms from adult human brain total RNA. This list of m^6A-methylated transcripts was most significantly enriched for tobacco use disorder, followed by weight-related and other substance abuse terms. Neurological disease is present in this list with major depressive disorder and ADHD as significant terms.

3.2.4 Analysis of synaptically located methylated transcripts from total human brain

To investigate what methylated transcripts from Dominissini et al.'s previously published dataset were likely to be found at synapses, the list of transcripts was cross-referenced with Cajigas et al.'s (2012) list of proteins found at the neuropil. This list was analysed as before and transcripts showed a very similar m^6A-methylation topology with 69% of m^6A marks at exons, 23% at 3' UTR, and 1.7% at 5' UTR (**Figure 3.6A**). The fractions of transcripts with one, two, or more marks was also consistent skewing towards 83% of transcripts having a single peak (**Figure 3.6B**).

Transcripts in this list showed enrichment for similar functions as total adult brain RNA. These terms include synapses, post-synaptic membranes, cell junctions, voltage-gated ion channels, and neuronal cell adhesion (related to cadherin). Interestingly, enrichment of positive regulation of both pre- and post-synaptic compartments was observed, suggesting methylated transcripts are found at both synaptic terminals.

Finally, although transcripts encoding m^6A readers were found in the total adult human brain RNA list, none of these were found to be methylated in the synaptically-located list.

A

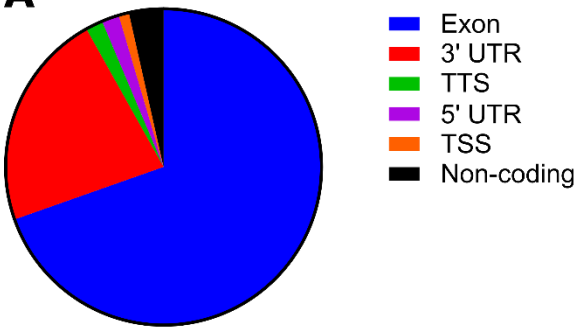

Number of Transcripts	1530
Number of Peaks	1863
Mean Peaks/Transcript	1.22

B

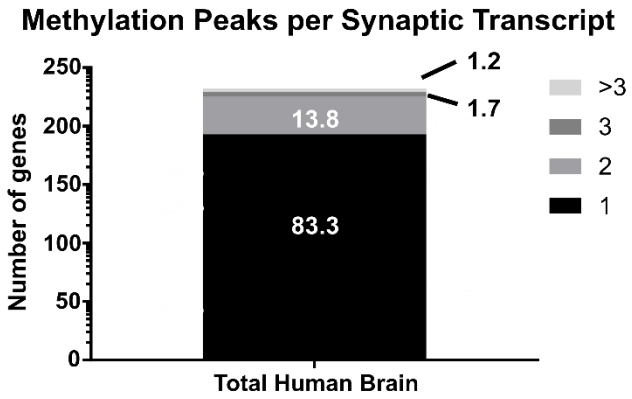

C

Term	Count	PValue
Potassium channel, voltage dependent, Kv	9	6.06E-10
Synapse	22	6.59E-10
Phosphoprotein	139	6.91E-10
Potassium ion transport	12	6.73E-09
Potassium channel	11	9.61E-09
Delayed rectifier potassium channel activity	9	1.26E-08
BTB/POZ-like	15	3.05E-08
Voltage-gated potassium channel activity	10	4.27E-08
Potassium transport	12	7.51E-08
Voltage-gated potassium channel complex	11	1.16E-07
Ion channel	19	1.30E-07
Postsynaptic membrane	15	3.25E-07
Ion transport domain	11	5.06E-07
Postsynaptic cell membrane	13	8.55E-07
Cell junction	21	9.27E-07
Voltage-gated channel	12	1.02E-06
Membrane	119	2.52E-06
Dendrite	17	3.73E-06
Positive regulation of synapse assembly	8	1.30E-05

Figure 3.6 Analysis of HOMER peak annotation and DAVID functional annotation of synaptically-located m^{6}A-methylated transcripts in the adult human total RNA, as published by Dominissini et al. A) Topological distribution of m^{6}A within a transcript and the average number of peaks per transcript. B) Number of detected m^{6}A peaks per transcript. Percentages are superimposed on bar graphs. C) Top 20 significant GO terms show methylated transcripts are enriched for synaptic terms, potassium and voltage-gated channel activity, and cell junctions.

3.3 Discussion

Using next-generation sequencing and a novel m^6A-specific antibody, the epitranscriptome of adult human and fetal brain was elucidated in this study. It was confirmed that m^6A methylation is a common modification which is added to a transcript at the GGAC (or DRACH; Meyer & Jaffrey, 2017; Linder et al., 2015) motif and that can be detected across all regions of a transcript, preferably at the 3' UTR and exon (Meyer et al., 2012; Dominissini et al, 2012).

Similarly to a previous report by Chang et al. (2017) in whole mouse brain, m^6A-sequencing analysis in human hippocampal grey and white matter found that the mean number of m^6A marks per transcript was approximately two. Across analyses of four different complete tissue datasets and four synaptically-located datasets, this number did not change. This was contrary to expectations, as it was hypothesised that global methylation levels would vary depending on tissue type, age, and location of transcripts. However, the number of m^6A marks observed in specific transcripts did vary, e.g. transcripts that were hypermethylated in one tissue type only had the average number of methylation events in another one. The variability of a specific transcript's methylation suggests that this is a mechanism that adapts to its environment, at least across tissue types and developmental stage.

Interestingly, new functional annotation evidence was found to support the hypothesis that a transcript's region of methylation is indicative of its corresponding protein's function. This effect was observed in both newly

generated datasets from grey matter, white matter, and fetal brain, as well as from new analysis of previously published data from adult human brain total RNA (Dominissini et al., 2012). More specifically, it was observed that in all datasets, transcripts whose protein product is important to synaptic function were m^6A-methylated in the 3' UTR/TTS region. More importantly, newly generated m6A-sequencing data performed using a more specific antibody than previous reports showed the 5' UTR/TSS was more enriched for synaptic function. For example, some transcripts were found to be involved in the positive regulation of synaptic transmission, the positive regulation of synapse assembly, and the postsynaptic membrane formation. Taken together, these terms suggest these transcripts are important in the formation and growth of new synapses.

Moreover, because these terms were consistent across fetal and adult brain (including grey and white matter), it points to m^6A methylation being a permanent mechanism used in neurons and the synapse. One possible way that m^6A methylation could support this function is through readers YTHDF1 and YTHDF3 ribosome loading transcripts to accelerate production of proteins in response to synaptic activation. These two reader proteins have been observed in dissociated hippocampal neurons and mouse hippocampus (Merkurjev et al., 2018; Shi et al., 2018) but experimental evidence of their function at these sites is yet to be presented, which becomes especially important due to contradicting reports of YTHDF3's role in ribosome loading and transcript decay (Shi et al., 2017; Wang et al., 2014; Li et al., 2017).

The discovery that transcripts of m^{6}A readers, writers, and erasers are themselves m^{6}A-modified gives way to an even finer control mechanism of protein expression. This represents a second level in which expression of these proteins is modified to amplify their regulatory effect on translation. The first of these levels is the enhancement of transcript translation or decay simply through the presence of m^{6}A within a transcript and the subsequent binding of readers or erasers to this mark. The second level of regulation modulates the first by affecting the number of reader/eraser/writer proteins. Evidence supporting this includes the consistent methylation of YTHDF1 and YTHDF3 in all tissue types and the singularly high (~5 marks per transcript) methylation of YTHDF2, which suggests the number of YTHDF2 proteins is critical for speedy transcript decay. While this is a new finding, more research into the effects of altered methylation in m^{6}A reader proteins will be needed to discern the level of importance of m^{6}A self-regulation.

m^{6}A autoregulation may also prove to be a valuable therapeutic target in neurological disease, as it is more effective to modify the expression of readers, writers, and erasers than to target protein products themselves. A recent study supports this idea as Han et al. found that YTHDF1-defficient mice had more effective anti-tumour immunity compared to wild type mice as a reduced rate of translation of a certain mRNA species proved more effective in preventing tumour growth than the elimination of said mRNA (Han et al., 2019).

It has been previously reported that m^{6}A is sensitive to external stimuli such as cellular stress through heat shock and starvation (Zhou et al.,

2015; Engel et al., 2018; Meyer et al, 2015) and thus possibly other types of external stimuli. It is also basic knowledge that the synapse, particularly the post-synaptic compartment responds to electrochemical stimuli. Together with gene ontology analysis indicating the synapse as an enriched biological term, this has led to the hypothesis that m^6A methylation is an important regulatory mechanism of synaptic function. To begin investigating this, the present study's datasets were cross-referenced with a published list of transcripts found in the neuropil of mouse brain. In grey matter, white matter, and fetal brain data, roughly 40% of all synaptically-located transcripts were found. This clear enrichment of m^6A-methylation in synaptic transcripts provides a basis for the exploration of m^6A's role in synaptic function through functional experiments.

The proposed use of m^6A methylation as part of the regulation of synapses would logically lead to a search for possible targets, transcripts whose regulation would impact upon synaptic development. In **Figure 3.2F**, some synapse-related transcripts were found to be methylated. These transcripts were all included in the "synapse" category of the gene ontology analysis. They include pre- and post-synaptic markers (VAMP and DLG proteins), a majority of ionotropic and metabotropic glutamate receptors (including those for AMPA, kainate, and NMDA), brain growth factor BDNF, and classic plasticity marker CAMK2B. Since these are all proteins that respond to and mediate the activation of a synapse, it would be interesting to explore how m^6A methylation changes after synaptic transmission and also how these transcripts interact with m^6A reader,

eraser, and writer proteins. These observations may be able to answer how the synapse uses m^{6}A methylation to respond to changes in its environment, which type of m^{6}A-interacting protein is most important, and whether changes in transcript methylation are transient or are conserved to mediate future responses to stimuli.

Moreover, transcripts from an important class of cellular adhesion proteins, cadherins, was found to be methylated. These transcripts included *CDH2*, which encodes N-cadherin, the principal cell adhesion protein in neuronal tissue, and 64 protocadherin subunits (**Tables 3.1** and **3.5**). N-cadherin in particular has been shown to be able to regulate AMPA-receptor availability, transsynaptically regulate short- and long-term plasticity at glutamatergic synapses, and to be able to induce retroactive signalling from the post-synaptic side to the pre-synapse (Ju et al., 2006; Tai et al., 2008; van Stegen et al., 2017). The finding that N-cadherin transcripts are highly methylated in fetal brain tissue suggests that m^{6}A reader-mediated regulation of its translation is important in the development of the human brain. Meanwhile, protocadherins are believed to mainly cluster and anchor two cell compartments together, and, in the context of neuronal tissue, protocadherins stabilise synapses (Jang et al., 2017). In summary, the m^{6}A-mediated fine-tuning of cadherin protein expression is an important part of the growth and stabilisation of a synapse.

The evidence presented here suggests that m^{6}A is important in normal synaptic function. Thus, it was expected that when probing the disease category of gene ontology analysis for all four datasets, brain-related

diseases were the top targets. Schizophrenia, Bipolar Disorder, Alzheimer's, and Tourette Syndrome were some of the most significantly enriched diseases (with Parkinson's Disease being less enriched but still significant), but there were also substance abuse and eating disorder terms. As with most neurological diseases, it is believed that alterations in synaptic formation, growth, and stabilisation over time are involved in these conditions. It is possible that reduction of m^6A activity over time leads to synaptic degeneration and these diseases but more evidence is needed to determine the molecular mechanism and timing through which m^6A affects the synapse.

However, if that were to be proven, another common trait of almost all of these neurological diseases is that they have been associated with impulse control disorder (Rodriguez-Violante et al., 2018), an important characteristic of substance abuse and eating disorders. The genetic mechanism behind these impulse control disorders is widely debated, but observations have been made that low dopamine receptor availability and decreased levels of dopamine are common in ADHD, persistent gambling, and other impulse control disorders (Voon et al., 2017; Brewer et al., 2008; Comings et al., 1997). Coincidentally, transcripts encoding for dopamine receptors DRD1, DRD4, and DRD5 were all found to be m^6A methylated, perhaps putting them forward as therapeutic targets in the future. Currently, although an association between m^6A and impulse control disorders through changes in dopamine receptor translation is tempting, it will be critical to first establish the fundamental role of m^6A in normal synaptic function.

Despite the fact that the discoveries presented here have been consistent across all datasets, there have also been discrepancies. Grey matter, white matter, and fetal brain samples have a different number of m^6A peaks and different methylated transcripts, and they share ~35% of transcripts. This is evidence that m^6A methylation varies across tissue types and developmental stage, suggesting that methylation is important in cell specialisation. In fact, it has been previously reported that m^6A global levels, as mediated by writer METTL3 and eraser ALKBH5, influence cell differentiation or tumourigenicity with increased or decreased levels of methylation, respectively (Geula et al., 2015; Zhang et al., 2017; Cui et al., 2017). Thus, this is a likely explanation for the overall differences in methylation between these three tissue types. The changes in specific transcript methylation will have to be further investigated, although it is likely to be partly due to the cellular response to each tissue's environment.

Bioinformatic analysis was also performed on a previously published dataset by Dominissini et al. (2012) to serve as a positive control of our peak annotation in an independent sample. Because the original authors had not looked at the data's gene ontology, this analysis was also performed to obtain information about m^6A methylation in whole adult human brain. The overall gene ontology results for this independent sample were similar to those of newly generated datasets. However, there were also important differences such as the lack of synaptic terms in the gene ontology of 5' UTR/TSS-methylated transcripts and the underrepresentation of neurological terms in disease gene ontology.

Furthermore, it was unexpected that this data set originating from whole adult brain (and thus including more tissue types and tissue volume) contained the least m^6A peaks. In this study, published in early 2012, one of the earliest m^6A-specific antibodies was used. Contrary to proper publishing guidelines, the authors have only listed the source of this antibody as “Synaptic Systems” without a product code or host species. Since the provider has four anti-m^6A products, this has made it difficult to verify which antibody was used. However, ensuring the specificity of antibodies that will bind only to the methylated N6 position of adenine has been a problem in this nascent field, and although progress has been made, it is well known that older antibodies are less specific (binding to closely related modifications m^1A and m^6A_m) and thus peak calling algorithms may have missed true but low m^6A peaks (Mauer et al., 2016; Dominissini et al, 2016; Safra et al., 2017; Linder et al., 2015). These issues may explain why their data contains less than half the number of peaks in newly sequenced data and why some transcripts are only found to be “methylated” in this dataset, thus altering gene ontology analysis.

There are limitations in this bioinformatic analysis that should be addressed in future work. The first and foremost is that although the samples selected as part of the current study’s m^6A-sequencing attempted to cover different tissue types and developmental stages, it is important to increase the number of biological replicates to ensure methylation is consistent within each tissue type and also increase technical replicates of the same sample to test possible issues with the antibody and m^6A-seq technology. Another way to further this research

would be by sequencing more brain regions with very different functions (grey matter and white matter here are both from temporal lobe) and by looking at more stages of development. For example, fetal brain sequencing was performed on RNA from a fetus aged 22-30 weeks but brain development begins four weeks after conception and does not stop until adulthood. It would be interesting, for example, to sequence adolescent brain and compare it to diseases with impulse control disorders.

Another limitation of this study is that m^6A-sequencing is does not quantify mRNA expression, thus there is no observable difference between tissue having just one copy of a specific methylated transcript or multiple. This represents an issue as we seek to understand the differences between highly methylated transcripts and those with a single m^6A mark. One idea is that there may be more transcripts with single m^6A marks and fewer transcripts with multiple marks, and that the abundance of these will impact protein production. A recent study proposes that slow transcription resulting in few copies of a specific mRNA species results in high co-transcriptional m^6A methylation and low translation efficiency - possibly due to quick transcript decay mediated by YTHDF2 - and that the opposite occurs with fast transcription, in this case mediated by YTHDF1 (Slobodin et al., 2017). Although this is a possible explanation why 50% of transcripts only have a single m^6A mark (**Figure 3.2D**), this cannot currently be supported due to m^6A-sequencing's limitations. In future studies, quantitative approaches

should be used to determine whether there are differences in transcription corresponding to differential m^6A methylation.

Finally, although we already know that 1 in 200 bases in mRNA is m^6A-modified, more analysis is needed to assess a possible correlation between size of a transcript region and the number of modifications in it. Although this correlation does not seem to exist in the promoter or 5' UTR region, it is not certain if the overrepresentation of methylation in the 3' UTR is relative to its size. The high number of m^6A marks at or near the stop codon would suggest this relationship is not random and further analysis could verify that.

Overall, the bioinformatic analysis of m^6A-sequencing data from human brain tissue has provided valuable insight into m^6A self-regulation, methylation of synaptic functional and structural transcripts, and an association between m^6A methylation and neurological disease. Although it is possible that m^6A methylation is used in different ways in other organs, its fine-tuning of translation, sensitivity to stimulus, and proven association with neurological disease make it a likely participant in normal synaptic growth, learning, and memory.

Chapter 4:

Investigating the localisation of m^6A modifications in neuronal cells

For their microscopy training and assistance in analysing super resolution and scanning TEM data, I would like to extend my gratitude to Dr. Robert Markus of the School of Life Sciences Imaging department and Dr. Michael Fay of the Nanoscale and Microscale Research Centre. Likewise, I thank Denise McLean for her training in the preparation of samples for electron microscopy. The work in this chapter would not have been possible without them.

4.1 Preface

Results presented in Chapter 3 showed significant enrichment of m^6A modifications present in transcripts associated with neuron-specific functions and structures, such as synaptic transmission and the post-synaptic density. Following on from these results, the work presented in this chapter consists of antibody-based microscopy of m^6A modifications in human differentiated neuronal cell lines and mouse hippocampus. These results were intended to investigate the subcellular location of m^6A-modified transcripts in neuronal cells and assess interaction between these mRNAs and proteins associated with m^6A methylation dynamics.

4.2 Results

4.2.1 Anti-m^{6}A antibodies bind to the same target located in the cytoplasm of neuronal cells

To perform immunocytochemistry using two novel anti-m^{6}A antibodies generated by two different manufacturers and ensure comparability between these results, immunofluorescence of both antibodies was assessed for overlap in signal. Immunocytochemistry was performed using anti-mouse and anti-rabbit m^{6}A antibodies on differentiated TE671 cells (**Figure 4.1**). Visually, the overlap of the green and red channels is represented by yellow colouring. The Pearson's Colocalisation Coefficient was found to be 0.96. Manders' M1 and M2 coefficients, which assess overlap of one channel only at regions covered by the other channel (i.e. colocalisation of green channel only at red channel areas), were both 1.00. Together with the high affinity and high specificity tests performed by the antibodies' manufacturers (e.g. ELISA, IP-MS), these results demonstrate that these two novel antibodies reliably and consistently bind to m^{6}A-modified transcripts.

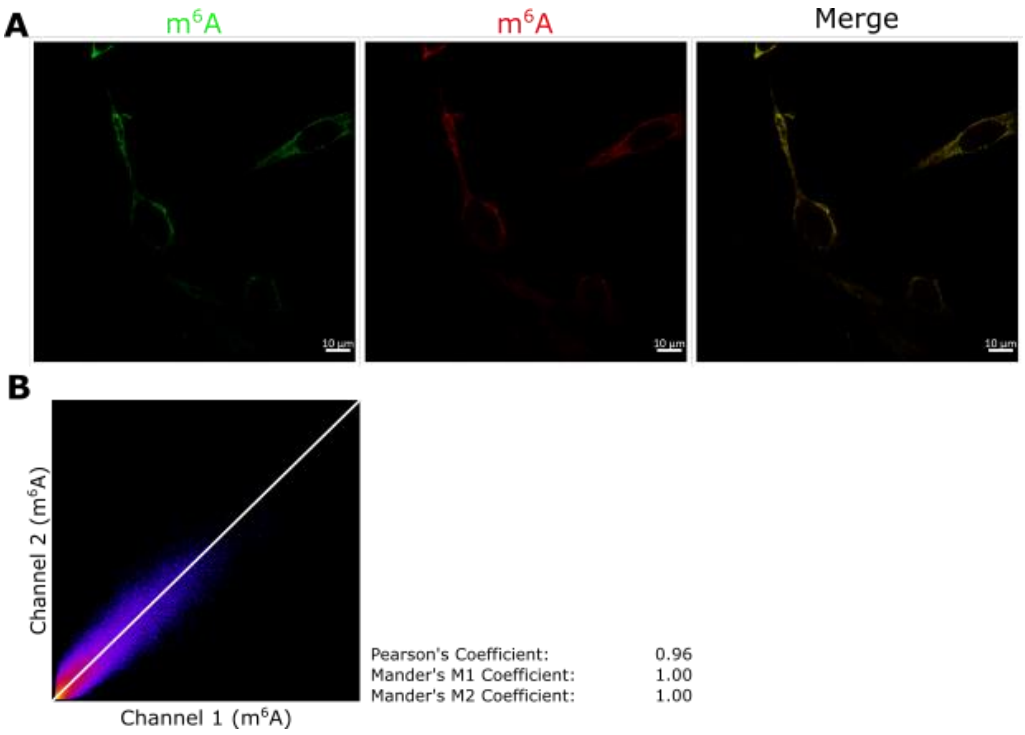

Figure 4.1 Correlation between fluorescent signals of two m^{6}A antibodies. A mouse polyclonal antibody generated in-lab by the Fray lab and a commercially available rabbit monoclonal antibody from Abcam (ab190886). A) Visual comparison of these antibodies showing overlap in yellow in differentiated TE671 cells. B) 2D intensity histogram shows high colocalisation and similar fluorescence intensity between the two antibodies. A 0.96 PCC indicates a very high correlation. Mander's M1 and M2 coefficients, which assess overlap of one channel only at regions covered by the other channel (i.e. colocalisation of green channel only at red channel areas), show a perfect degree of colocalisation (Zinchuk et al., 2007).

4.2.2 m^{6}A colocalises with pre- and post-synaptic markers

The initial hypothesis that m^{6}A RNA modifications would contribute to neuronal function was supported by the bioinformatic analysis of m^{6}A-sequencing data presented in Chapter 3. To further investigate this relationship, an *in vitro* approach was selected. Using neuronal cell lines TE671 and SH-SY5Y and differentiating these cells, an immunocytochemistry protocol was performed to visualise the location of m^{6}A in these cells relative to the defining structure of neuronal cells: the synapse. Both the pre- and post-synaptic compartments were visualised using VGluT1 and PSD95/DLG4 antibodies as their respective markers.

As shown in **Figure 4.2** (left side), m^{6}A-modified transcripts were found to be abundant in the cytoplasm and neuronal processes of cells. However, the nucleus of these cells showed little immunofluorescence. This finding confirms that m^{6}A modifications are found in all areas of the cell where transcripts can be found and are not restricted to one compartment. Furthermore, double labelling of m^{6}A and VGluT1 (**Figure 4.2A**), as well as m^{6}A and DLG4 (**Figure 4.2B**) showed evidence of co-localisation in both cell lines. Quantification of the overlap between m^{6}A-modified transcripts and VGluT1 returned a Pearson's Correlation Coefficient (PCC, also abbreviated as R) of 0.62 in SH-SY5Y cells and 0.67 in TE671 cells. The same analysis performed on m^{6}A's overlap with DLG4 resulted in higher PCC values of 0.81 and 0.78 for SH-SY5Y and TE671 cells, respectively. These findings show that m^{6}A-modified RNA

is present at both sides of the synapse and suggest higher abundance in the post-synaptic compartment.

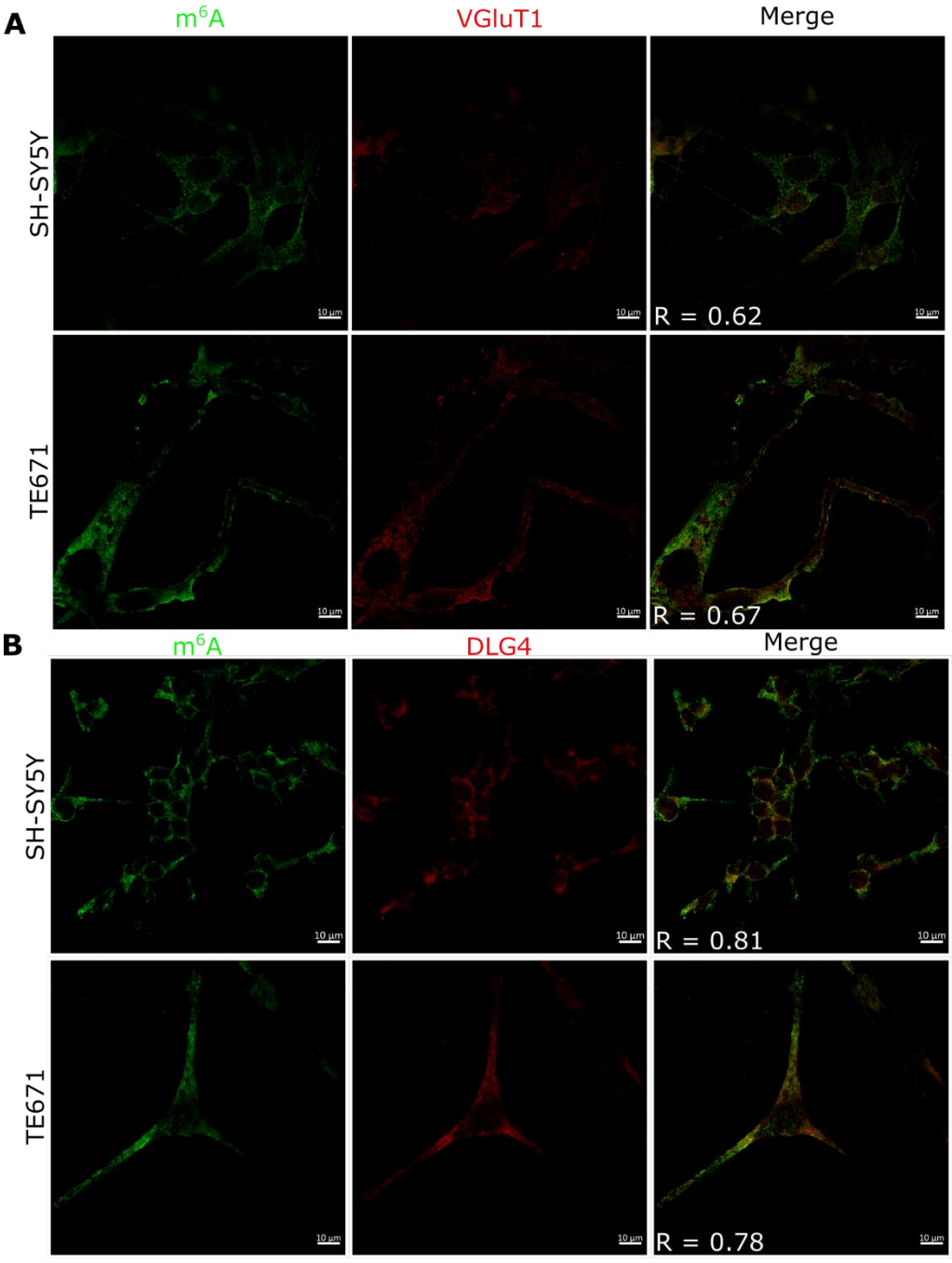

Figure 4.2 m^{6}A colocalises with pre- and post-synaptic markers in differentiated neuronal cell lines. Colocalisation was observed in the neuronal processes of differentiated neuronal cell lines at synaptic sites. n = 10. A) m^{6}A and pre-synaptic marker VGluT1 show some colocalisation (seen in yellow) in processes. Pearson's Correlation Coefficients, presented as R values, approximate 0.6. B) m^{6}A and the post-

synaptic marker DLG4 show more evidence of colocalisation, especially in processes. Pearson's Correlation Coefficients, seen as R values, approximate 0.8, suggesting there are more m^6A modifications at the post-synapse.

4.2.3 m^{6}A-modified transcripts colocalise with cytoplasmic reader YTHDF1, ribosomes, and P-body components

To investigate the possible role and interactions of m^{6}A-modifed transcripts, double-labelling immunocytochemistry was performed on differentiated SH-SY5Y cells to assess colocalisation with m^{6}A readers YTHDF1 and hnRNPA2B1, as well as neuronal P-body components Dcp1a and GW182. It was observed that YTHDF1 immunofluorescence was found in the cytoplasm around the nucleus but also in the far away neuronal processes (**Figure 4.3A**). Colocalisation analysis with anti-m^{6}A signal returned PCC values averaging 0.78, a high value indicating a close relation between the two markers. Unexpectedly, low immunoreactivity was observed in the nucleus. Experiments with m^{6}A and hnRNPA2B1, an m^{6}A reader involved in pre-mRNA processing, showed normal m^{6}A immunofluorescence and an almost entirely nuclear hnRNPA2B1 signal (**Figure 4.3B**). Colocalisation between these two markers was therefore drastically low with a PCC mean of only 0.04.

Reports which investigated the effect of m^{6}A modifications on mRNA fate found that the YTHDF1 reader functioned by recognising m^{6}A within a transcript and recruiting ribosomes (Wang et al., 2015; Meyer & Jaffrey, 2017). Therefore, the colocalisation of m^{6}A-modified transcripts and ribosomal marker L7A was studied. m^{6}A immunofluorescence was found consistent with previous experiments, while that of L7A was found to be well-defined, showing a punctate signal, and common throughout the cytoplasm (**Figure 4.3C**). PCC values for this experiment averaged 0.49, which is lower than that of m^{6}A and YTHDF1. This suggests that although

m^{6}A-modified transcripts may be bound to YTHDF1, not all of these were being translated at the point the experiment was performed.

Finally, YTHDF2 has been reported to affect mRNA stability by binding to m^{6}A and transporting transcripts to P-bodies, sites of mRNA turnover mediated by multiple enzymes. Due to the large size of P-bodies, two different enzymes, Dcp1a and GW182, were selected from opposite ends of this structure to assess colocalisation with m^{6}A-modified transcripts. Experiments immunolabelling Dcp1a had punctate immunofluorescence that was most prevalent around the nucleus of cells, although this was also observed with lower intensity in neuronal processes (**Figure 4.3D**). The mean of PCC values was 0.40, suggesting colocalisation is common. In similar experiments, GW182 immunofluorescence was observed throughout cells. GW182 appears in the cytoplasm, neuronal processes, and even nuclei (**Figure 4.3E**), consistent with its independent role in gene silencing, as well as a component of P-bodies. The PCC average was 0.64. Taken together, these results indicate that colocalisation of m^{6}A-modified transcripts and P-bodies is common, although both elements can function independently of each other.

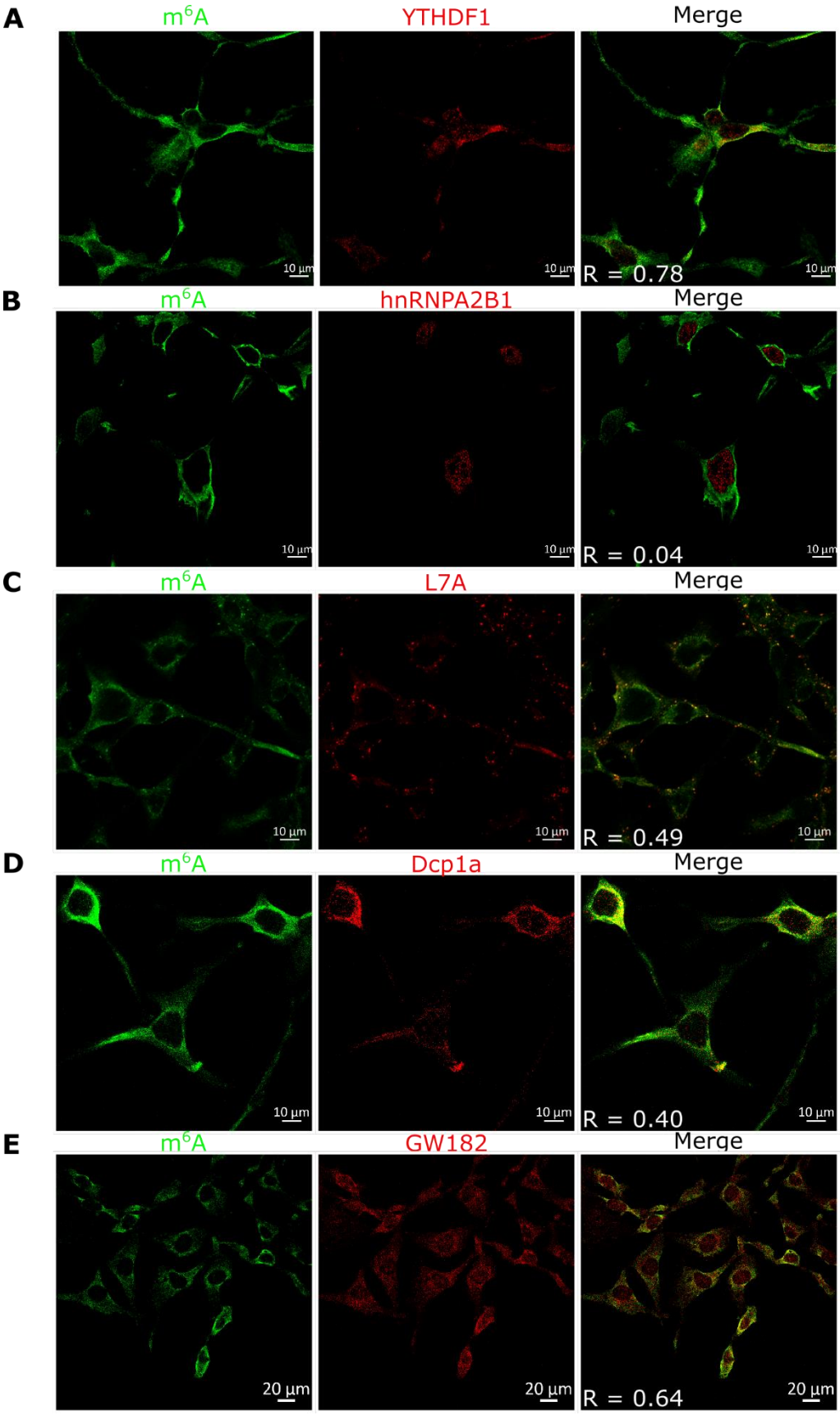

Figure 4.3 Colocalisation between m^{6}A-modified transcripts and m^{6}A-binding proteins, ribosomes, and P-body components in differentiated SH-SY5Y neuronal cells. n = 10.

PCC values were used as a measure of colocalisation. A) m^{6}A and YTHDF1 colocalise with a PCC of 0.78, suggesting YTHDF1 binds to and transports m^{6}A-modified transcripts in neuronal cells. B) m^{6}A and hnRNP2AB1 do not colocalises, as one is located in cytoplasm and the other in nuclei. PCC of 0.04 indicates almost no correlation. C) m^{6}A and ribosomes are commonly colocalised (PCC = 0.49) near the nucleus and in neuronal processes. D-E) m^{6}A-modified transcripts colocalise with and are likely degraded by P-bodies. PCC of 0.4 for Dcp1a and 0.64 for GW182 suggest that decapping and silencing are common processes undergone by m^{6}A-modified transcripts.

4.2.4 SIM super resolution microscopy confirms m^{6}A interactions with readers and erasers at nanoscale

To confirm previous observations regarding the location of m^{6}A-modified transcripts at synaptic regions, Structured Illumination Microscopy (SIM) was used to visualise differentiated SH-SY5Y cells, making this the first study to look at mRNA modifications at super resolution. This technique increased XY resolution three-fold, allowing for the identification of independent fluorescence events up to 80 nm apart vs 250 nm when compared to confocal microscopy. Colocalisation between m^{6}A modifications and synaptic markers VGluT1 and DLG4 at this increased resolution was still observed in many cases (shown as yellow areas). In many cases where overlap was not apparent, immunofluorescent puncta of each marker were found next to each other and within 1 µm, the approximate size of dendritic spines (**Figure 4.4A-B**).

Consistent with results from section 4.2.3, colocalisation of m^{6}A modifications with cytoplasmic reader proteins is most commonly observed. **Figure 4.4C** shows overlap of m^{6}A and YTHDF1 at neuronal connections between cells with a resolution of 80 nm. Another m^{6}A reader protein, YTHDF3, was also found overlapping with m^{6}A-modified transcripts at a 90 nm resolution (**Figure 4.4D**). However, colocalisation events in this last experiment were slightly less common than with YTHDF1.

Colocalisation between m^{6}A and demethylase, i.e. “m^{6}A eraser”, ALKBH5 was also evaluated. ALKBH5 was located mostly in the nucleus

but immunoreactivity was also observed in the cytoplasm (**Figure 4.4E**). Colocalisation with m^{6}A modifications was apparent in a few cases at neuronal processes, all within a resolution of 120 nm.

Finally, Dcp1a, a decapping protein found in P-bodies, did not appear to overlap with anti-m^{6}A signal often. **Figure 4.4F** shows that m^{6}A and Dcp1a immunofluorescence was found all throughout the cell but at a resolution of 110 nm, only a few rare instances of colocalisation were apparent. Some of the captured images suggested that there were many instances of m^{6}A immunofluorescence surrounding Dcp1a signal, but more experiments would be needed to confirm this. This result suggests that observations made of the colocalisation between m^{6}A and Dcp1a at lower resolutions may present some false positive results.

Taken together, results from super resolution experiments suggest m^{6}A-mediated regulation of translation is important at pre- and post-synaptic sites, and that in differentiated but quiescent, i.e. non activated neuronal cells, the roles of reader proteins YTHDF1 and YTHDF3 are more prominent than that of eraser protein ALKBH5.

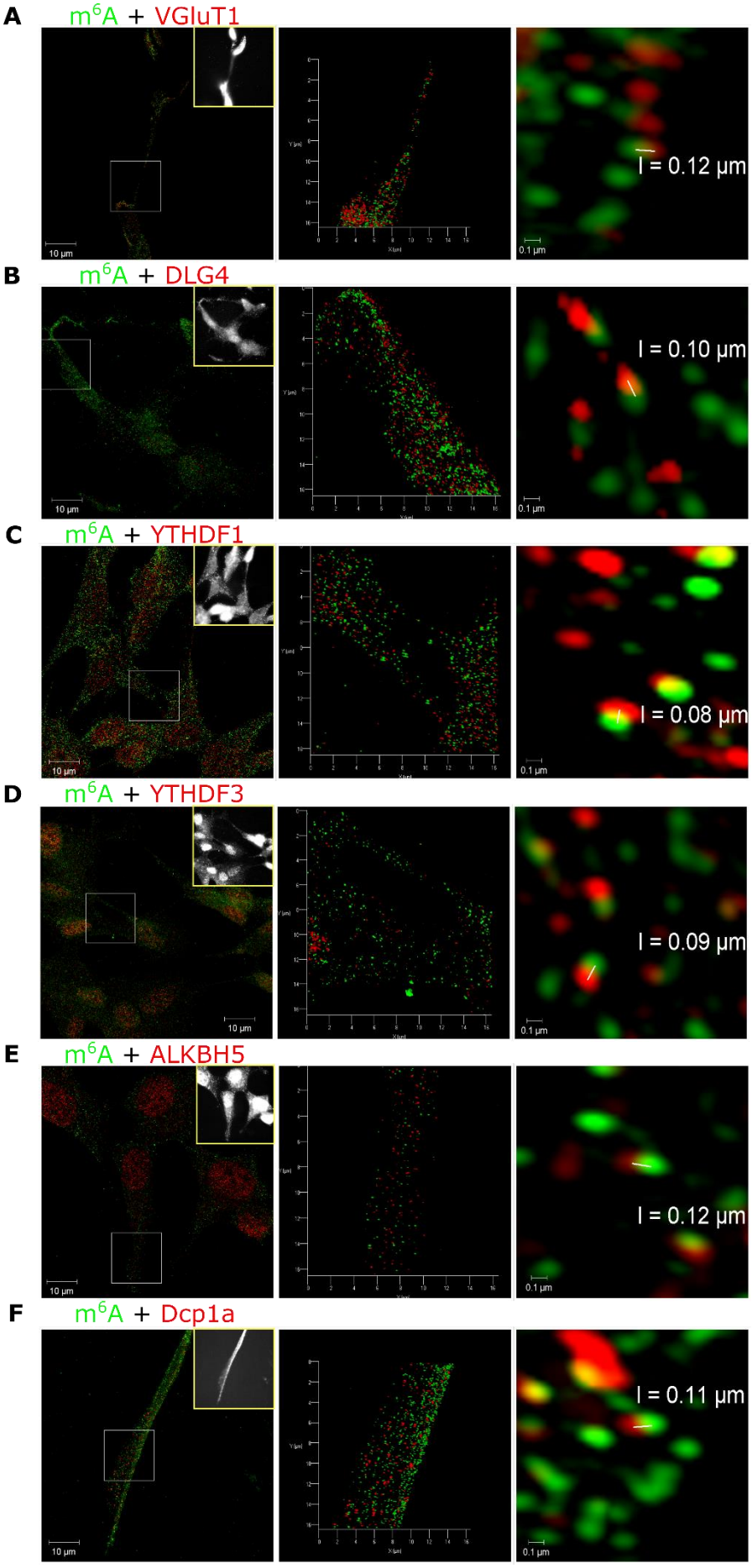
A
m6A + VGluT1
l = 0.12 µm
B
m6A + DLG4
l = 0.10 µm
C
m6A + YTHDF1
l = 0.08 µm
D
m6A + YTHDF3
l = 0.09 µm
E
m6A + ALKBH5
l = 0.12 µm
F
m6A + Dcp1a
l = 0.11 µm

Figure 4.4 SIM super resolution microscopy exhibits colocalisation of m^{6}A-modified transcripts with synaptic markers, m^{6}A-binding proteins, and P-bodies. Differentiated SH-SY5Y cells were immunolabelled and imaged at resolutions of up to 80 nm. n = 5 for each experiment. Left panels are maximum intensity projections of sample images. Middle panels are 3D models of regions of interest. Right panels show the resolution at which two fluorescent puncta can be discerned. A-B) m^{6}A modifications overlap with pre- and post-synaptic markers or are found within 1 µm, the average length of a dendritic spine. C-D) Colocalisation of m^{6}A modifications is most prevalent with YTHDF1 while also being commonly observed with YTHDF3. E) ALKBH5 immunoreactivity is concentrated in the nucleus but lower amounts of it are found within the cytoplasm and at neuronal processes. Colocalisation with m^{6}A is m^{6}A but obvious. F) m^{6}A modifications did not often overlap with Dcp1a despite both having high amounts of immunofluorescence throughout the cytoplasm.

Three-dimensional models were created for select images of each experiment (images from **Figure 4.4**). These models, shown in **Figure 4.5**, allowed for further meticulous analysis of instances where colocalisation was observed. **Figures 4.5A-B** show rare instances where colocalisation is apparent when viewed from one angle, but a large distance of at least 100 nm is then discovered when rotated over the x axis. Although a majority of colocalisation events were found to be true in a 3D space, this is a demonstration that real, high-confidence colocalisation is difficult to observe in 2D images and careful 3D analysis is needed.

Conversely, the rest of the models in **Figure 4.5** demonstrate instances where colocalisation from a 2D perspective was correct and 3D modelling details how this interaction occurs. Immunofluorescent signal from m^6A readers YTHDF1 and YTHDF3, as well as eraser ALKBH5, are observed to be engulfing the anti-m^6A signal (**Figures 4.5C-E**). This is especially clear between m^6A and YTHDF3 and suggests that despite m^6A being tagged by primary and secondary antibodies, readers and erasers still have access to the m^6A modification.

Lastly, the model generated from experiments with Dcp1a also showed contact between markers. Notably, Dcp1a appeared to be in contact with at least two distinct m^6A modifications. Consistent with previous observations, there were a high number of m^6A modifications surrounding relatively few Dcp1a proteins, which could suggest modifications at other sites of the same transcript or multiple transcripts in one P-body.

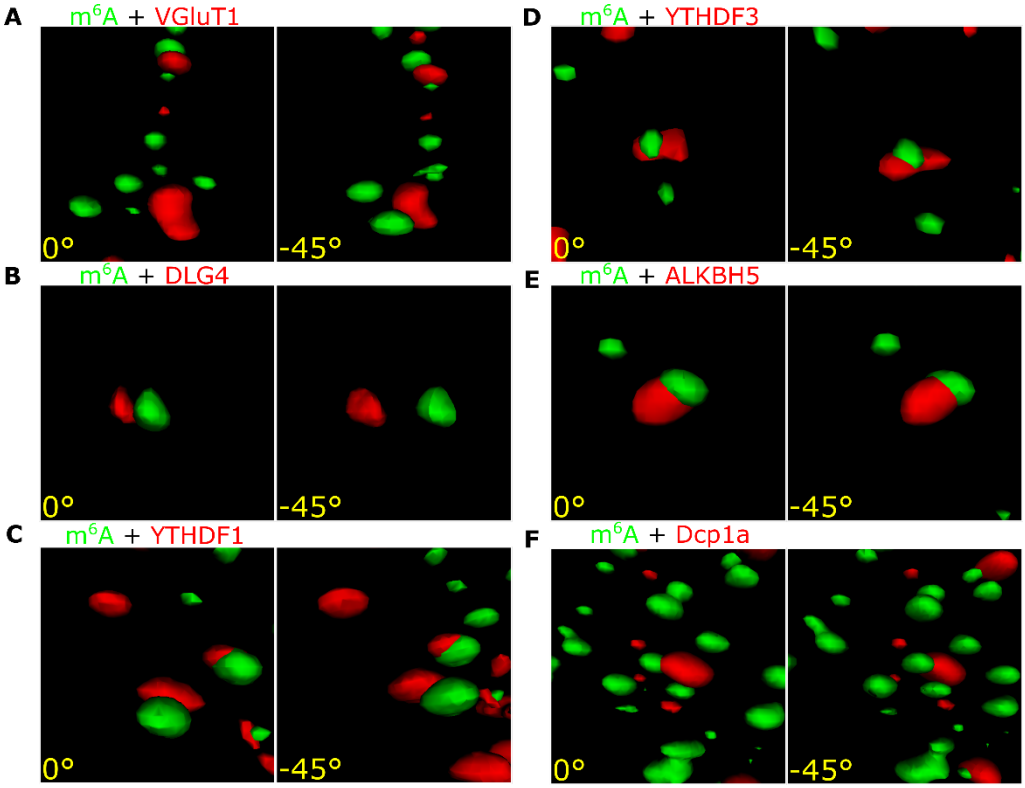

Figure 4.5 3D models of SIM images reveal true protein-m^{6}A interactions and false overlaps. 3D models were generated from images in Figure 4.4. Images were rotated on the x-axis only. A-B) Some rare instances of colocalisation between m^{6}A and pre-/post-synaptic markers in a 2D image were found to be false positives when rotated. C-E) m^{6}A readers YTHDF1 and eraser ALKBH5 were found to engulf m^{6}A modifications one at a time, with YTHDF3 providing the clearest example. These interactions were consistent in 3D. F) Dcp1a was found to also have true, 3D colocalisation. Curiously, interaction between two m^{6}A marks and one Dcp1a protein was the norm.

4.2.5 Scanning TEM reveals the location of m^{6}A-modified transcripts and YTHDF1 within a synapse

To examine the localisation of m^{6}A-modified transcripts at the nano resolution within single synapses and pre/post-synaptic compartments in primary brain tissue scanning TEM imaging was performed on mouse hippocampus immunolabelled with nanogold particle-conjugated antibodies. In the CA3 and CA4 regions of the hippocampus, m^{6}A-modified transcripts were evident at post-synaptic regions (**Figure 4.6A-B**), although in lower quantities than expected based off immunocytochemistry in neuronal cells. m^{6}A-modified transcripts were also apparent in the cell body of cells (**Figure 4.6B**, orange), consistent with results from experiments on neuronal cell lines. Furthermore, m^{6}A modifications were also found in small, nascent synapses (**Figure 4.6B**, arrow) which were identified based on their shape and size (Ahmari & Smith, 2002; Santuy et al., 2018). These results confirm the location of m^{6}A modifications at mature and nascent synapses and serve as the first use of scanning TEM to look at RNA modifications in brain.

Additionally, the YTHDF1 reader protein, was also found to be located at both synaptic terminals (**Figure 4.6C-D**) in similar quantities. The pre-synaptic terminal showed aggregates of YTHDF1 immunoreactivity while post-synaptic YTHDF1 showed a wider distribution throughout the compartment and no clumping. YTHDF1 was also observed in high numbers and with a spread out distribution at the dendrite from which the post-synapse emerged, suggesting a role in which YTHDF1 may need to be mobilised between post-synaptic compartments, i.e. dendritic spines.

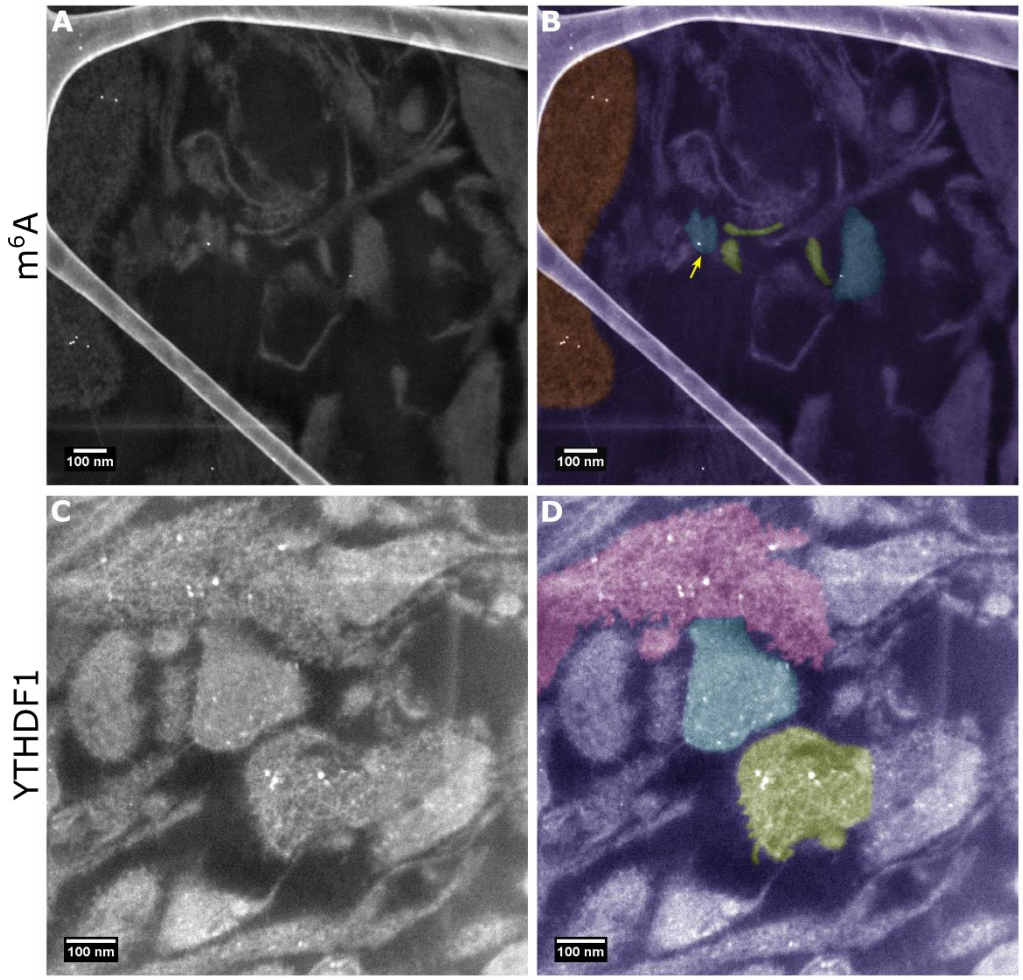

Figure 4.6 Scanning TEM reveals the presence of m^{6}A-modified transcripts and m^{6}A reader protein YTHDF1 at the synapses of CA3/CA4 pyramidal neurons from mouse hippocampus. n = 4. A-B) m^{6}A was detected in the post-synaptic region (blue) in low numbers. No nanogold particles were detected in identified pre-synaptic areas (green). m^{6}A was also found in cell bodies (orange). C-D) YTHDF1 was detected in both synaptic compartments with visible clustering in the pre-synapse and spread out signal in the post-synapse. YTHDF1 was also found in large numbers in the dendrite from which the post-synaptic compartment originated (pink), suggesting a role for YTHDF1 movement between synapses.

4.3 Discussion

Previous work regarding m^{6}A modifications has focused on m^{6}A-sequencing and pull-down assays to identify m^{6}A-methylated transcripts (Bodi et al., 2010; Meyer et al., 2012; Dominissini et al., 2012; Linder et al., 2015), m^{6}A-binding proteins (Jia et al., 2011; Wang et al., 2014; Shi et al., 2017), and the effects of global reduction of m^{6}A levels (Batista et al., 2014; Geula et al., 2015; Haussmann et al., 2016). The present work makes use of highly specific, novel m^{6}A antibodies to visualise for the first time the location of modified transcripts within cells and elucidate their *in vivo* interactions. Using different microscopic techniques, it has been found that m^{6}A-modified transcripts concentrate at the cytoplasm around the nucleus and neuronal processes, giving rise to the possibility that m^{6}A modifications are involved in neuron-specific functions such as synaptic transmission and plasticity.

The hypothesis that m^{6}A modifications may have a special role in neuronal cells is supported by experiments which found them to colocalise with synaptic markers, with a slight increase in the post-synaptic compartment. This finding inevitably brings to the fore reports identifying m^{6}A modifications as a regulatory mechanism of translation (Wang et al., 2015; Liu et al., 2015) and questions about the effects that such a mechanism can have on local protein synthesis at the synapse.

Because m^{6}A modifications are not by themselves catalytic, the first step towards providing evidence to answer such questions is to identify molecules with which m^{6}A-modified transcripts may interact. Colocalisation between m^{6}A-modified transcripts and readers, erasers,

ribosomes, and P-bodies was assessed. The findings in this study at spatial resolutions of up to 80 nm suggest that readers YTHDF1 and YTHDF3 are interacting with m^{6}A modifications. This is supported by qualitative observations in confocal and super-resolution microscopy (including 3D modelling) and quantitatively by PCCs. These two reader proteins have been proposed to be involved in ribosome loading of m^{6}A-modified transcripts (Wang et al., 2015; Meyer & Jaffrey, 2017), resulting in increased translation of methylated transcripts.

Likewise, colocalisation between m^{6}A-modified transcripts and ribosomal marker L7A was found to be very common. These findings suggest that m^{6}A, the most common internal mRNA modification, is an important mechanism of global translation in cells. However, because L7A is only one protein subunit out of 80 in eukaryotic ribosomes (De La Cruz et al., 2015), these findings do not conclusively prove that all colocalisation between m^{6}A modifications and L7A is related to active translation. Also, since there are higher PCC values for m^{6}A and YTHDF1 experiments than m^{6}A and L7A, this suggests some m^{6}A-modifed transcripts are bound to YTHDF1 but not yet being translated. One possible explanation for this is that YTHDF1 promotes translation by recruiting initiation factors eIF3A and eIF3B and ribosomes (Wang et al., 2014; Wang et al., 2015), both processes which represent an extra step before initiating translation and during which there would be YTHDF1-m^{6}A interactions without a nearby ribosome. Another possibility is that there may be some level of translation repression performed by other proteins that, while not blocking YTHDF1 binding, keep ribosomes from binding to the m^{6}A-

modified transcript during transport to distant neuronal processes where m^6A was also observed. One such mechanism of translational repression during synaptic transport is mediated by the FMRP-CYFIP1-eIF4 complex (Napoli et al., 2008).

Images of ALKBH5 represent the first time this m^6A eraser has been demonstrated to be located outside of the nucleus and, to the best of the author's knowledge, the first time it has been found in neuronal processes. Furthermore, super resolution microscopy revealed that there is some colocalisation between ALKBH5 and m^6A-modified transcripts, which was confirmed by 3D modelling, at a resolution of at least 120 nm. It has been previously shown that global levels of m^6A methylation can be modified in cells undergoing external stress stimuli like heat shock or starvation (Zhou et al., 2015; Zhou et al., 2018), but these changes were assumed to take place solely in the nucleus. The current findings suggest that changes in the number of methylation marks happen not just in *de novo* transcripts in the nucleus but also in cytoplasmic, translation-ready mRNAs. As such, more research is needed to discover what drives ALKBH5 activity in the cytoplasm and how transcripts are selected to undergo demethylation.

The overlap of m^6A modifications and P-body markers was also studied. Two reasons exist behind this experimental design. One,, quantifying this overlap would provide a baseline for how many m^6A-modified transcripts are degraded by P-bodies rather than endonuclease cleavage or other mRNA decay pathways. Two, one more known m^6A reader is YTHDF2, which acts upon methylated mRNA by transporting it to P-bodies (Liu et

al., 2015; Wang et al., 2014). At the beginning of this study, there were no available YTHDF2-specific antibodies, and as such, a decision was made to study colocalisation of YTHDF2 and m^{6}A modifications by proxy, using markers of proteins known to associate with YTHDF2.

By performing confocal microscopy, it was observed that m^{6}A modifications and two P-body markers, Dcp1a and GW182, colocalised with PCC values of 0.4 and 0.64, respectively. Due to further investigation into GW182's possible location outside of P-bodies and its role in mRNA silencing through miRNA recruitment (thus possibly blocking m^{6}A sites; Kulkarni et al., 2010), as well as a report by Mauer et al., (2017) that other decapping proteins interacted with similar mRNA modifications, later experiments focusing on P-bodies used Dcp1a as the only marker. One of these experiments, which assessed m^{6}A-modified transcripts and Dcp1a colocalisation using super resolution microscopy, provided further confirmation that these two molecules interact, at least within 110 nm. 3D modelling using these images showed that Dcp1a was in contact with two m^{6}A sites in a transcript, questioning whether transcripts with more than one mark are more likely to be degraded. Another explanation for the relative abundance of m^{6}A modifications relative to the number of Dcp1a proteins based on the large size of P-bodies and current literature on the subject may suggest that these instances, although quite common, were simply due to Dcp1a binding to the mRNA 5' cap while other P-body proteins are also acting on it. Further research involving co-immunoprecipitation and m^{6}A-sequencing of Dcp1a-bound transcripts is needed to resolve this issue.

One final experiment was performed to try to pinpoint the location of m^6A and YTHDF1 within a synapse. Due to the inherent difficulties in performing electron microscopy on biological tissue (e.g. burn in, tearing, fixing artifacts, etc.; Hartell et al., 1996) combined with difficulties of gold immunolabelling, this work was limited to four different antibodies. As shown in section 4.2.5, only two of these antibodies worked well. This is a well-known problem with this technique, as only highly stable antibodies are likely to be imaged (Hermann et al., 1996).

Despite these issues, the CA3/CA4 mouse hippocampal region was identified and its pyramidal neurons exhibited immunogold labelling of m^6A modifications and YTHDF1. m^6A was observed at very low quantities at synapses, a result which partially clashes with the abundant m^6A signal observed in both confocal and super resolution microscopy. However, the location of m^6A-modified transcripts within 1 µm of the post-synaptic density and in the cytoplasm of neuronal cell bodies was consistent with previous experiments. Due to time restraints, it was impossible to verify these results by using a different anti-m^6A antibody, but this is one experiment that is planned in the short-term.

YTHDF1 was found to be in the same location within post-synaptic compartments (dendritic spines) as m^6A modifications. It was also found in the pre-synapse and at dendrites. The spread of YTHDF1 is consistent with the location of local protein synthesis and is likely due to its involvement in regulation of translation. Being at the dendrite, YTHDF1 proteins may be able to translocate to other synapses when recruited, as polyribosomes are thought to do (Ostroff et al., 2002; Graber et al., 2013;

Schuman et al., 2006), which would suggest YTHDF1 (and possibly other readers) must either be bound to m^{6}A-modified transcripts or some unknown agent prevents recognition of m^{6}A by YTHDF1 until an appropriate time and then recruits it to the correct synapse.

This study is not without limitations. Research of novel molecules using immunological approaches is limited by the availability and quality of antibodies (Sewell et al., 2017; Almagro et al., 2018). First and foremost, this work was made possible by the isolation of a unique, highly specific anti-m^{6}A antibody by Dr. Rupert Fray's laboratory. However, other antibodies like the aforementioned anti-YTHDF2 were unavailable throughout the timeframe of this study. Others, like ALKBH5 and YTHDF3, were slowly made available but had not been tested for immunofluorescent techniques, making this study one of the first to optimise their use for immunocytochemistry (see Annex for optimisation). The quality of antibodies also impacted their use in certain experiments. As previously mentioned, only two out of four tested antibodies worked for immunogold labelling. In the case of SIM super resolution microscopy, the low quality of these first-generation antibodies meant that the signal to noise ratio was lower than expected, making SIM reconstruction and the identification of "true" signal more difficult. However, in both scanning TEM and SIM, the expertise of senior staff members was used to ensure data was not misrepresented and results shown here were of the highest possible quality.

The selection of targets for immunofluorescence suggested some proteins should be ignored. Previously, m^{6}A writers METTL3 and

METTL14 and the m^{6}A methylation complex have been reported to be nuclear (Ping et al., 2014; Meyer & Jaffrey, 2014), which resulted in the exclusion of writers from the present work. FTO, an m^{6}A eraser, was also excluded as it has been shown to localise to dendrites in a single-labelling experiment (Walters et al., 2017). Most importantly, FTO has been associated with many different functions like energy homeostasis, adipogenesis, DNA repair, tRNA demethylation, etc. leading to varied diseases such as diabetes, heart failure, and acute myeloid leukemia (Jia et al., 2008; Claussnitzer et al., 2015; Wei et al., 2018). Also, FTO's role as an m^{6}A demethylase has recently been disputed with reports claiming it preferentially binds to another mRNA modification, m^{6}A$_m$, *in vivo* (Mauer et al., 2017) and another study saying it acts on non-mRNA species (Wei et al., 2018). As such, ALKBH5 was chosen as an eraser for these experiments based on its functional characterisation and reported high levels of m^{6}A demethylase activity in *in vivo* models (Zheng et al., 2013).

One other issue was that it was not possible to quantitatively measure colocalisation in super resolution data as the manufacturer's software contained bugs which tried to include false fluorescence (i.e. noise) in the calculation of PCCs. This was later found to be partly due to the low signal to noise ratio mentioned above and a decision was made to only measure colocalisation qualitatively in this data to avoid misrepresentation of results.

Here new evidence is provided of the location of m^{6}A-modified transcripts and its interactions. The evidence presented in this chapter suggests that

m^{6}A readers YTHDF1/3, the ALKBH5 eraser, and P-bodies interact with methylated transcripts in neuronal cells and at their processes, suggesting that not only is m^{6}A used to regulate translation and mRNA decay but these transcripts' may be demethylated in the cytoplasm to modify mRNA fate. Scanning TEM also demonstrated that m^{6}A readers may be recruited to different synapses and are located where local protein synthesis takes place following neuronal activation (Martin et al., 2000; Martin, 2004; Steward & Schuman, 2001). These two conclusions lead to the hypothesis that m^{6}A methylation in neuronal cells is a regulatory mechanism of translation that is used in local protein synthesis and is modified as a response to an unknown stimulus.

Chapter 5:

Spatiotemporal effects of m^6A methylation at the synapse

The work presented in this chapter was, in part, performed by Maria Isabel Haig, whose guidance and support throughout is greatly appreciated. To establish the method of colocalisation analysis at synapses, the advice and assistance of Dr. Chris Gell of the School of Life Sciences Imaging department was essential. I am also thankful to Mahmoud Sherif for the gift of differentiated neural stem cells and to the Mellor lab for agonist dilutions.

5.1 Preface

Following on from results in Chapter 4 which found m^6A-modified transcripts at synapses, the work in the chapter attempts to investigate the interactions of m^6A modifications with m^6A-binding proteins in this compartment. Since synapses are also the site of local protein synthesis which is initiated after synaptic activation, the changes in m^6A dynamics following agonistic receptor activation are also investigated. These same questions are researched throughout neural stem cell development to ponder the merit of this method of quick, time-sensitive control of translation. These results as a whole are intended to shed light on the methods of synaptic response to stimulus and its ensuing growth and, if logical, integrate these findings with the synaptic tagging and capture hypothesis proposed by Frey & Morris (1997).

5.2 Results

5.2.1 m^{6}A modifications colocalise with readers and erasers at the synapse

In Chapter 4, it was demonstrated that m^{6}A-modified RNA localised to the synapse, with a higher abundance at the post-synaptic compartment. To investigate the dynamics of m^{6}A modifications specifically at synapses, a triple labelling immunocytochemical approach was utilised. Differentiated SH-SY5Y and TE671 cells were immunolabelled with a combination of antibodies which specifically bind to m^{6}A RNA modifications, an m^{6}A reader/eraser or P-body marker, and pre- (VGluT1) or post-synaptic (PSD-95) markers. Results showed colocalisation between these markers at varying levels.

YTHDF1 and YTHDF3, reader proteins of the YTH domain family were found to colocalise with m^{6}A-modified transcripts at both the pre- and post-synaptic compartments. Colocalisation of m^{6}A and YTHDF1 (**Figure 5.1A**), observed as white and light pink colouring, was punctate in the pre-synapse and relatively sparse. In the post-synaptic terminal, however, more areas of colocalisation were apparent in neuronal processes. YTHDF3, a second reader protein, showed high colocalisation with m^{6}A modifications at both pre- and post-synaptic domains (**Figure 5.1B**). This effect was higher in the post-synaptic terminal, where colocalisation is throughout most neuronal processes and cell bodies. Overall, the brightness of YTHDF1 immunostaining, which has a correlates with its abundance, was much lower than that of YTHDF3. This suggests there are fewer YTHDF1 proteins than YTHDF3.

More YTHDF3 protein may explain why proteins with similar ribosome-loading functions have different levels of colocalisation. These results suggest YTHDF1 and YTHDF3 reader proteins often interact with m^{6}A-modified transcripts at synapses.

Other markers' colocalisation with m^{6}A modifications was not so clear. Dcp1a was chosen as the sole P-body marker for these experiments due to possible confounding effects of other markers. Colocalisation between m^{6}A-modified transcripts and Dcp1a was obvious only at the post-synaptic compartment in low numbers (**Figure 5.1C**). Due to the sparse and punctate immunostaining of the Dcp1a antibody, colocalisation in these images was restricted to a few clear light pink puncta. As discussed in an earlier chapter, ALKBH5 immunofluorescence in quiescent cells is low in the cytoplasm, which would make colocalisation at the synapse even rarer. Indeed, it was found that m^{6}A-modified transcripts only scarcely overlap with ALKBH5, with more of these instances occurring at the post-synapse (**Figure 5.1D**). Due to the scarcity of these events, it would be interesting to find what special circumstances cause demethylation of transcripts at synapses. These two results suggest that, in non-activated cells, degradation and demethylation of m^{6}A-modified transcripts at synapses is non-essential.

Finally, a recent report by Chang et al., (2017) found almost all Fragile X Mental Retardation Protein (FMRP) binding targets are m^{6}A-methylated and proposes this protein as an m^{6}A reader in charge of transcript transport to the synapse. Thus, colocalisation of m^{6}A-modified transcripts and FMRP at the synapse was also assessed. No overlapping signal was

clearly observed at the pre-synaptic terminal and colocalisation was exceedingly rare at the post-synaptic region (**Figure 5.1E**). This negative result is in line with FMRP's reported location near the nucleus in neurons with dormant synapses (Majumder et al., 2017; Antar & Bassell, 2003).

Together, these results support the idea that translation of m^6A-modified transcripts at the synapse is regulated by YTHDF1 and YTHDF3. Low colocalisation with Dcp1a and ALKBH5 suggests degradation by P-bodies and demethylation of these same transcripts is not common and may require a very specific set of circumstances to be effected. Alongside low colocalisation of methylated transcripts and FMRP, which is known to react to synaptic changes, these results posit the manipulation of synapses to assess changes in m^6A-regulated translation as a logical next step in the current project.

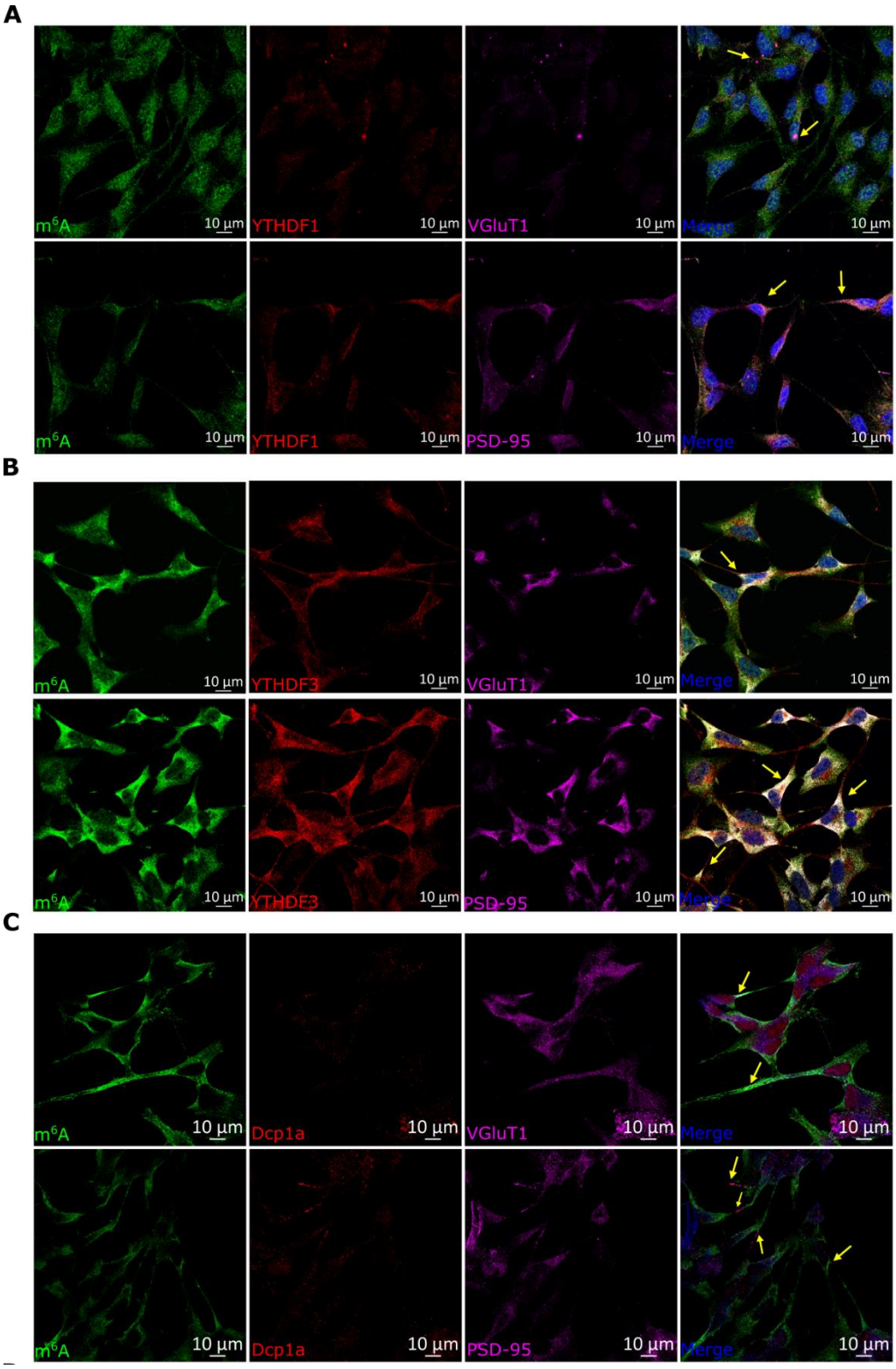
A
m6A
10 μm
YTHDF1
10 μm
VGluT1
10 μm
Merge
10 μm
m6A
10 μm
YTHDF1
10 μm
PSD-95
10 μm
Merge
10 μm
B
m6A
10 μm
YTHDF3
10 μm
VGluT1
10 μm
Merge
10 μm
m6A
10 μm
YTHDF3
10 μm
PSD-95
10 μm
Merge
10 μm
C
m6A
10 μm
Dcp1a
10 μm
VGluT1
10 μm
Merge
10 μm
m6A
10 μm
Dcp1a
10 μm
PSD-95
10 μm
Merge
10 μm

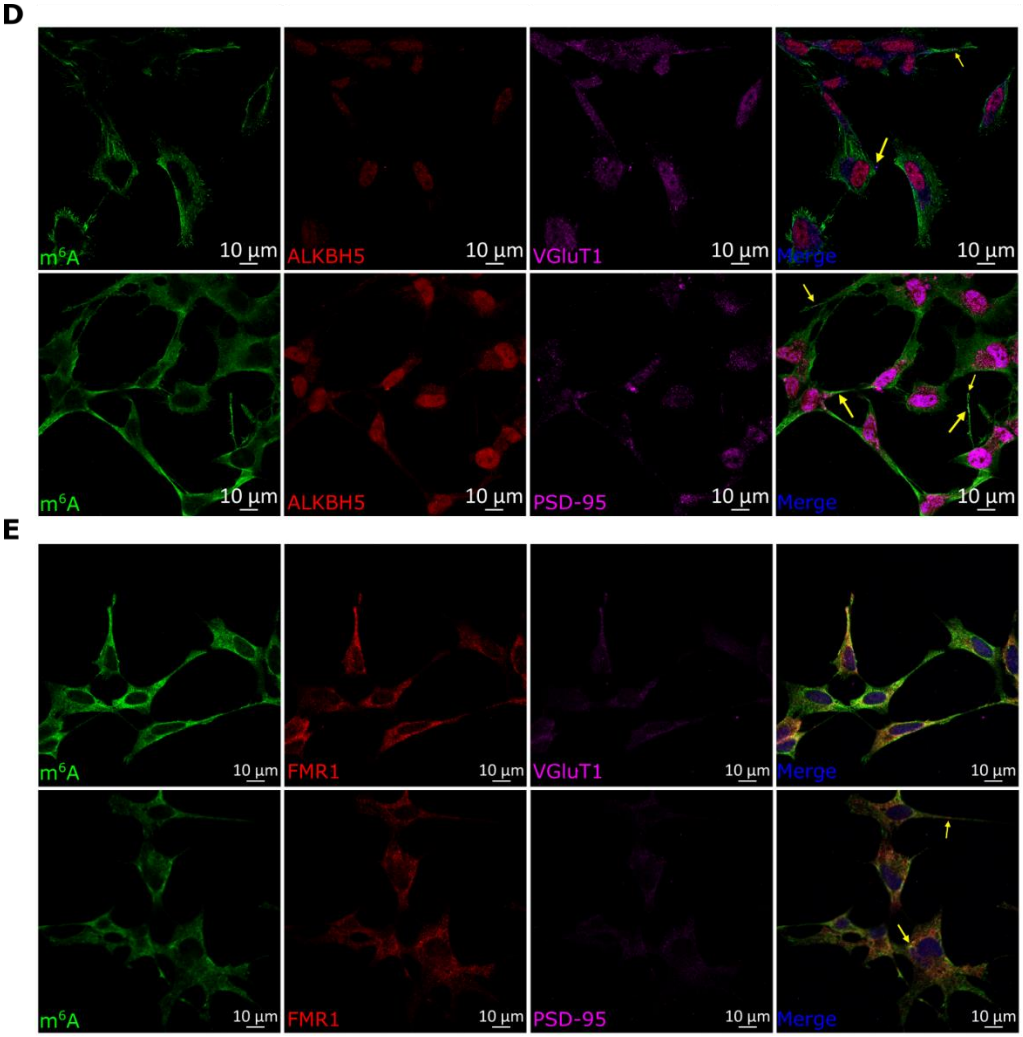

Figure 5.1 Methylated mRNAs colocalises with m^{6}A readers, P-bodies, and erasers in differentiated neuronal cells. A) Overlap of m^{6}A and YTHDF1, represented as white colouring, was only clearly visible at the post-synapse. B) m^{6}A and YTHDF3 very clearly overlap at both synaptic terminals. C-D) Other markers show colocalisation that is less strong and sparse throughout cells at both pre- and post-synaptic terminals. Arrows show clear areas of colocalisation. E) FMRP is not observed at pre-synaptic areas and colocalisation with m^{6}A is only noticeable near the nucleus (lower arrow) or in a single instance at a neuronal process (upper arrow), a rarity which is consistent with FMRP's reported cytoplasmic location in the absence of synaptic activation. Scale bar = 10 µm.

5.2.2 Protein interaction with m^{6}A-modified transcripts at the synapse is time- and activation state-dependent

Following on from the triple-labelling immunocytochemistry presented in section 5.2.1 and based on reports that m^{6}A methylation responds to external stimuli such as heat shock and starvation (Zhou et al., 2015; Meyer et al., 2015), experiments which stimulate long-term potentiation (LTP) and modify the system were designed and conducted. To examine the spatiotemporal changes of interactions between m^{6}A-modified transcripts and markers of interest, two differentiated neuronal cell lines, SH-SY5Y and TE671, were activated with NMDA or KCl (stimulating ionotropic NMDA receptors and voltage-gated ion channels, respectively) at two different time points (15 minutes or 24 hours) analogous to early and late LTP, respectively. This experimental design is summarised in **Figure 5.4F**. Cellular response to these activation compounds was confirmed by calcium imaging using Fluo4-AM as a reporter (**Figure 5.2**).

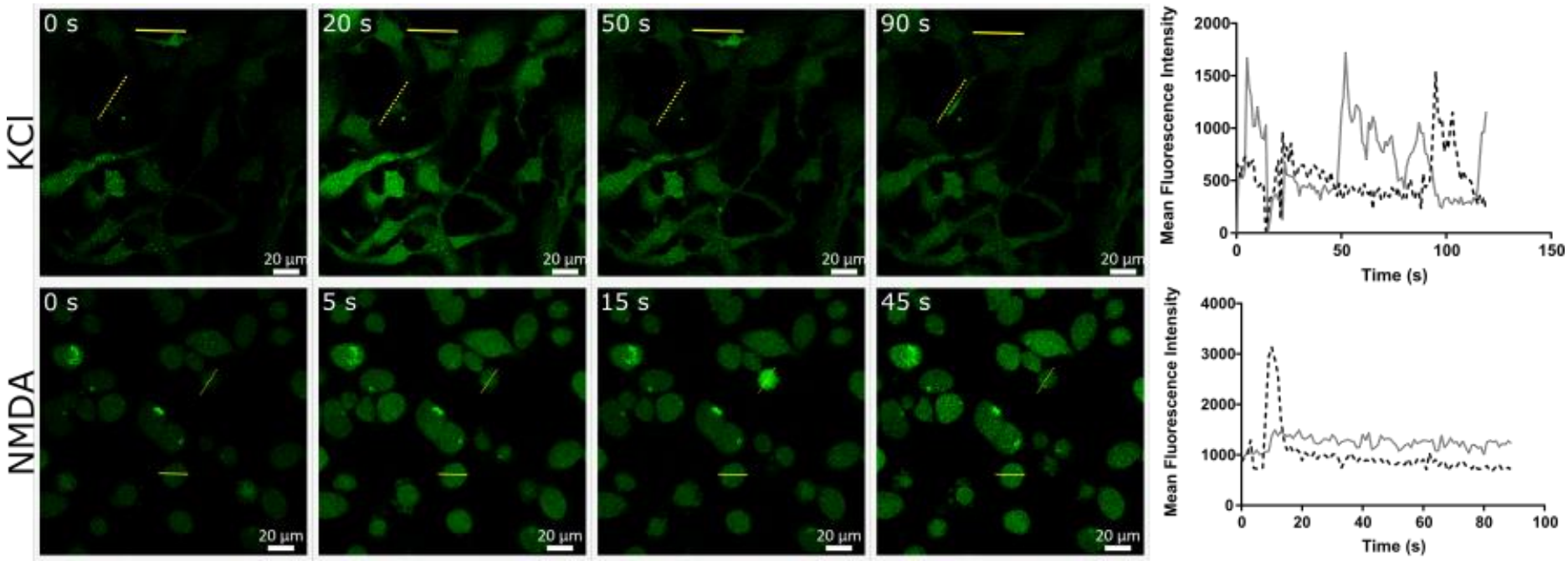

Figure 5.2 Calcium imaging confirms activation of differentiated TE671 (shown) and SH-SY5Y cells. Differentiated TE671 cells were cultured and a calcium imaging protocol using Fluo4-AM was performed. Using KCl and NMDA as agonists, ion channels or glutamate receptors, respectively, were activated shortly after commencing live imaging. Both compounds elicited a response observed as periodic increases in fluorescence at different cellular compartments. Images are shown at different time points. Mean fluorescence over a line profile was calculated across time and plotted on the right. A large dip in fluorescence near the beginning of the protocol indicates the time at which compounds were added and light was blocked in the microscope. Scale bar = 20 µm.

The first difference observed in activated cells was that immunofluorescence from anti-VGluT1 and anti-PSD-95 was not as widespread as in inactive cells. Instead, signal from these markers seemed to consolidate into fewer areas, often in the form of puncta, and these areas were in turn brighter (**Figure 5.3**). These changes signal higher protein expression of synaptic markers, a consequence of the growth and strengthening of synapses during plasticity.

When assessing colocalisation between m^6A and other markers of interest at synaptic sites, it proved difficult to visually detect differences between experiments performed on inactive and active cells (**Figure 5.3**). One exception of this was the colocalisation of m^6A and FMRP at post-synaptic sites following 15 mins of NMDA treatment. In this case, colocalisation, shown by white or light pink areas, was increased following activation.

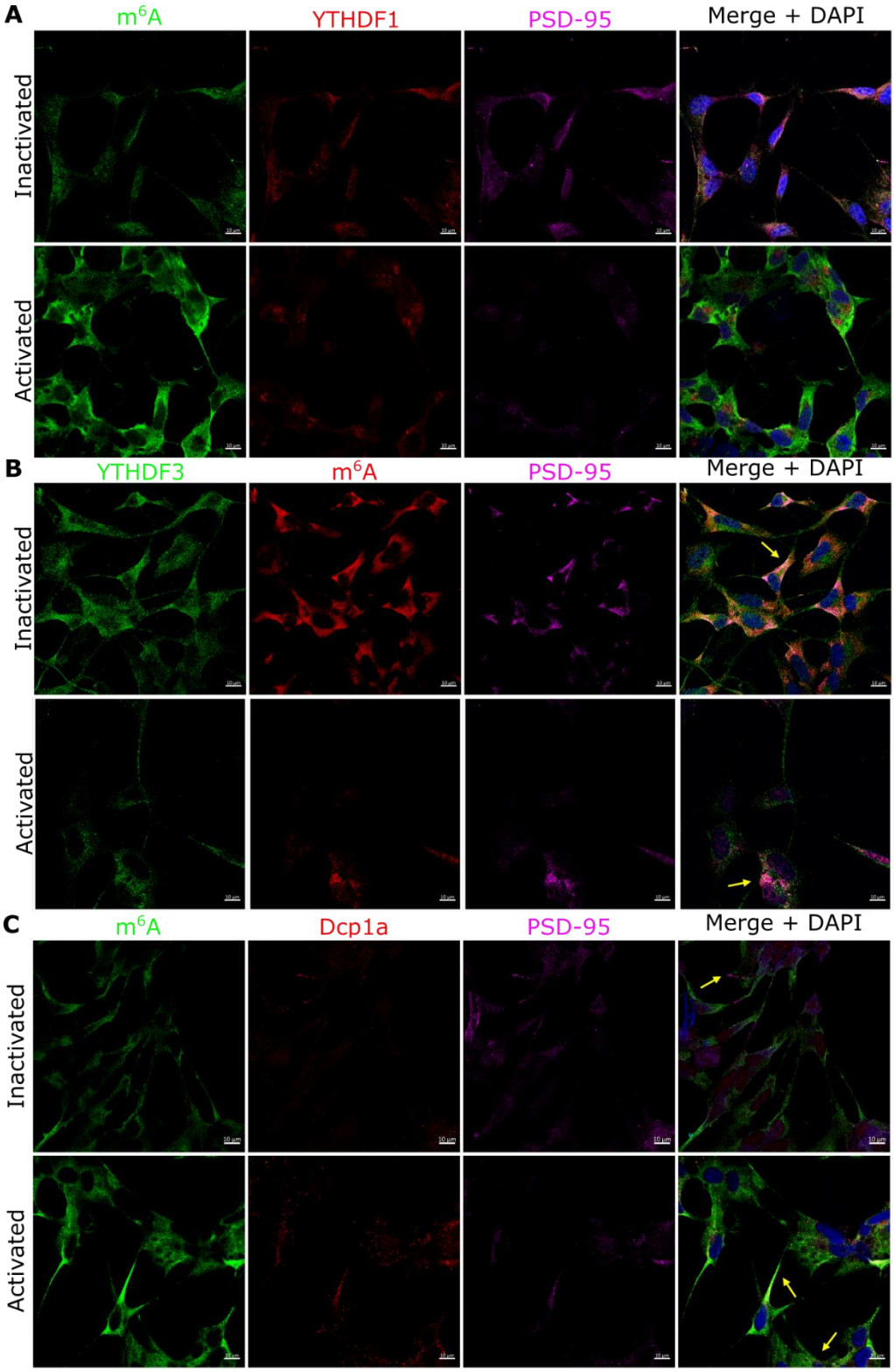
A
m6A
YTHDF1
PSD-95
Merge + DAPI
Inactivated
Activated
B
YTHDF3
m6A
PSD-95
Merge + DAPI
Inactivated
Activated
C
m6A
Dcp1a
PSD-95
Merge + DAPI
Inactivated
Activated

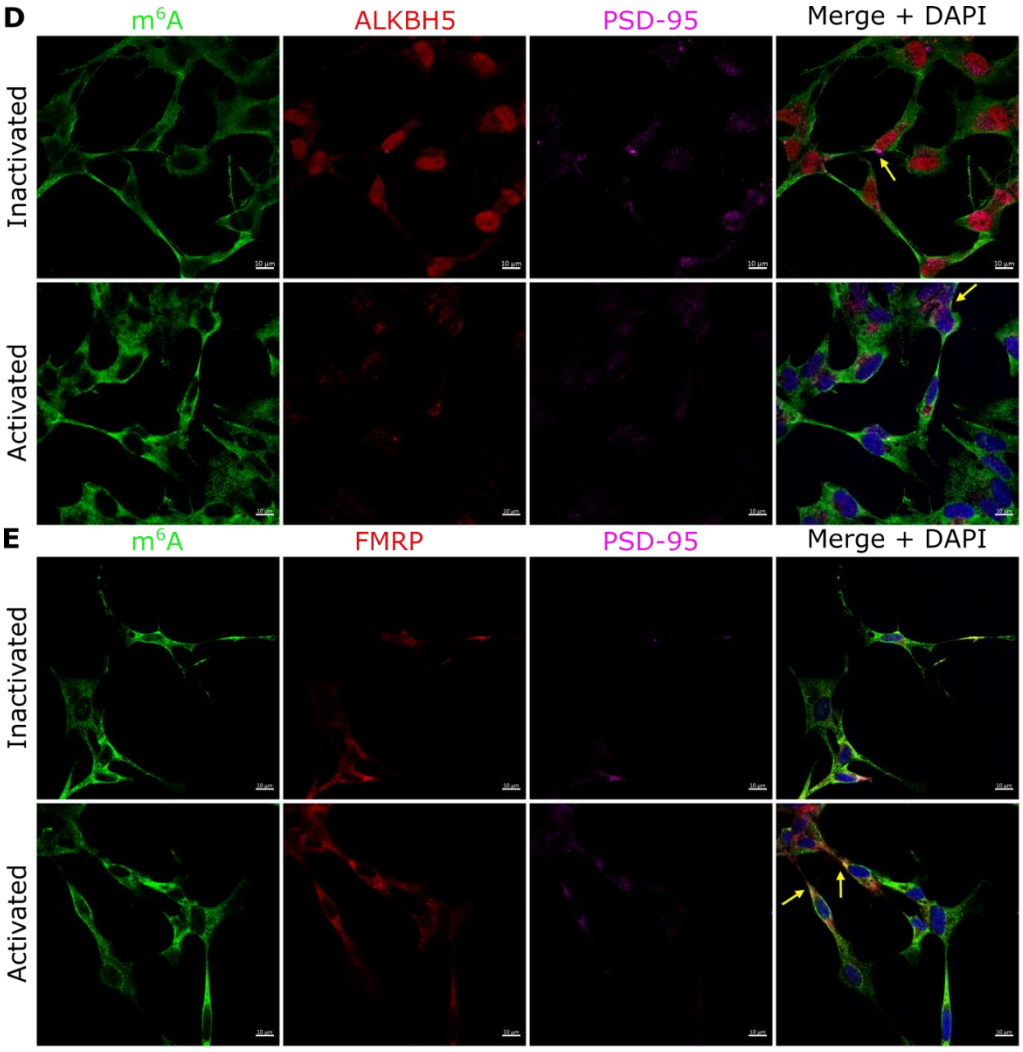

Figure 5.3 Neuronal activation changes overlap between m^{6}A and related proteins at the post-synapse. Triple labelling immunocytochemistry was performed on differentiated TE671 and SH-SY5Y (shown) cells to quantify the difference in colocalisation between m^{6}A-modified transcripts and m^{6}A readers (A, B), P-bodies (C), and erasers (D) after either 15 mins (shown) or 24 hours of receptor activation using NMDA (shown) or KCl. Arrows point to cases of clear overlap, if any. Immunofluorescence of PSD-95 was consolidated into brighter, well-defined, and less numerous puncta following neuronal activation. E) FMRP overlap with m^{6}A increased following activation, as shown by white and light pink colouring around the cytoplasm and neuronal processes (arrows). Scale bar = 10 µm.

Quantitative analysis was performed on all experiments and collated in **Figures 5.4-5.5**. Results were generally consistent between activation compounds and time after activation in both cell lines, suggesting the type of synaptic activation does not affect the colocalisation between m^6A modifications and most of the studied proteins. Some exceptions that followed glutamatergic activation only were also found, including ALKBH5 and FMRP colocalisation with m^6A-modified transcripts.

Significant differences were found in colocalisation of m^6A-modified transcripts and m^6A-interacting proteins before and after neuronal activation. Colocalisation of methylated mRNAs with YTHDF1 and YTHDF3 proteins ($p < 0.05$ for SH-SY5Y and $p < 0.005$ for TE671 in both experiments) significantly increased at 15 minutes after activation with NMDA and KCl and then remains high, although not statistically significant, 24 hours after activation (**Figure 5.4A-B**). Mean PCC values from these experiments were as high as 0.48 for YTHDF1 and 0.55 for YTHDF3, indicating strong colocalisation. This suggests involvement of these reader proteins in regulating m^6A-mediated local protein translation is more critical for short term plasticity processes.

In contrast, colocalisation with Dcp1a, a marker of RNA decay sites, was significantly increased ($p < 0.05$) only after 24 hours (**Figure 5.4C**) suggesting that at least some modified transcripts are degraded after late LTP. Indeed, the mean PCC values for these experiments were between 0.32-0.38, indicating moderate colocalisation. Since the half-life of specific mRNA species can vary by many hours (Greenberg, 1972), these results suggest degradation of transcripts by P-bodies, including

m^{6}A-methylated ones, is a persistent process and may explain a relatively modest colocalisation at any one time.

Following NMDA activation, there is significant increase in colocalisation of modified transcripts with the eraser protein, ALKBH5 ($p < 0.00005$) in both cell lines (**Figure 5.4D**). . In the long term, there are some significant changes where PCC values are close to zero, indicating no correlation. This new discovery suggests 'demethylation' by eraser proteins is part of the mechanism modulating local protein synthesis following short term (E-LTP) synaptic activation.

Finally, the Fragile X Mental Retardation Protein (FMRP) has previously been shown to transport transcripts to post-synaptic sites following NMDA receptor activation (Darnell et al., 2011; Tamanini et al., 1996; Ascano et al., 2012; Napoli et al., 2008; Antar et al., 2004) and to repress translation by stalling mRNA-linked ribosomes. FMRP has also been recently reported as a potential 'reader' m^{6}A-binding protein (Chang et al., 2017). To gain further insight into FMRP's association with m^{6}A regulatory mechanisms during early plasticity processes, an assessment was made whether FMRP colocalises with m^{6}A mRNAs at synapses, and whether the activation of neuronal cells changes this relationship. As with other reader proteins, we found that colocalisation in non-activated cells was modest with a PCC of 0.25 at post-synaptic sites. After activation with NMDA, FMRP colocalisation with m^{6}A-methylated transcripts was found to increase significantly to mean PCC values of 0.5 ($p < 0.05$ in SH-SY5Y cells and $p < 0.005$ in TE671 cells) (**Figure 5.4E**). However, as expected, activation by KCl did not cause a significant change in

FMRP overlap with modified transcripts. These results suggest that FMRP is involved in an m^6A-regulatory mechanism influencing short term plasticity only at activated glutamatergic synapses.

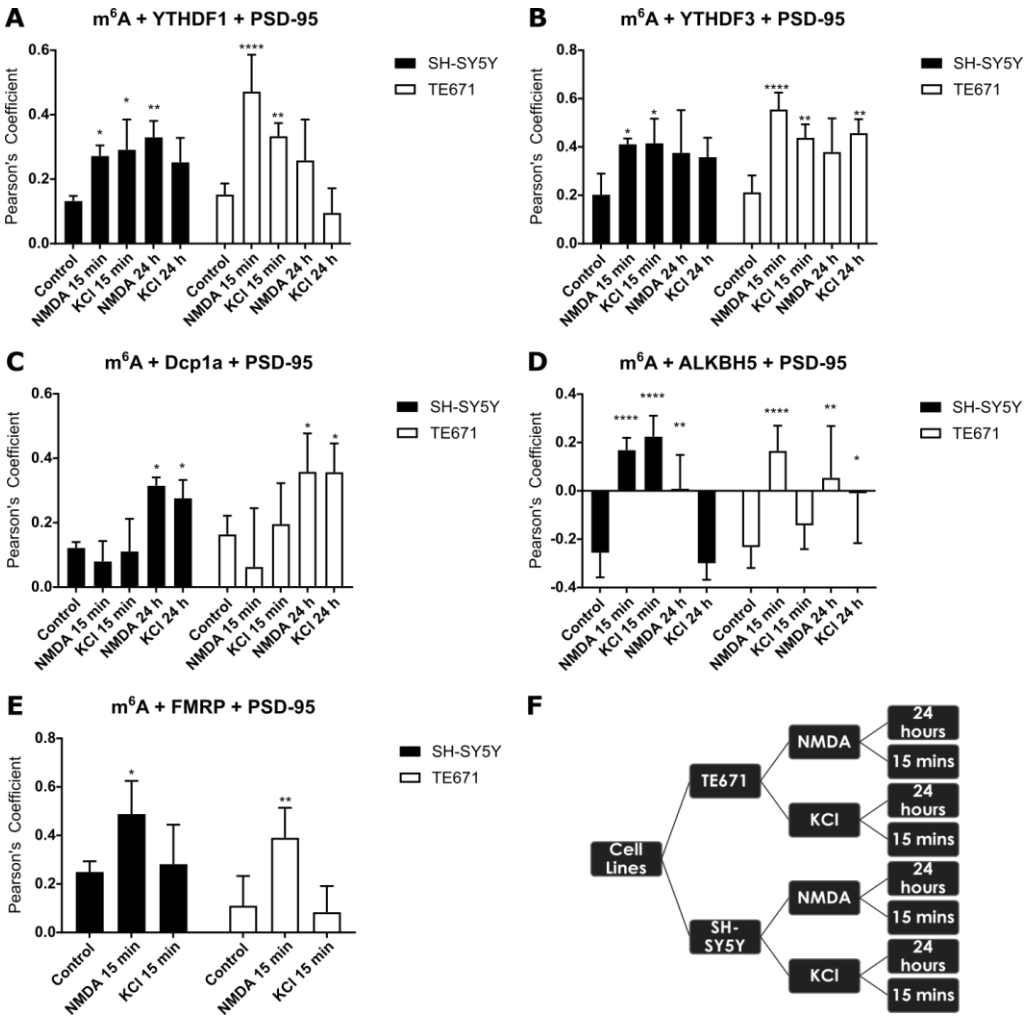

Figure 5.4 Colocalisation of m^{6}A modifications and related proteins at post-synaptic areas in differentiated SH-SY5Y and TE671 cells. Bar graphs show the mean Pearson's Correlation Coefficient (PCC) for m^{6}A and an m^{6}A-binding protein at post-synaptic areas. A-B) m^{6}A and YTHDF1/3 colocalisation increases significantly after short-term activation. C) Colocalisation with Dcp1a increases after 24 hours, suggesting degradation of transcripts is only important in the long-term. D) ALKBH5 overlaps with m^{6}A modifications more often following short-term activation, with NMDA having the same effect in both cell lines. In the long term, there are some significant changes where PCC values are close to zero, indicating no correlation. F) Experimental design for activation experiments. All experiments were repeated twice and at least ten images were captured each time (n = 4), resulting in approximately 700 confocal images captured. A two-way ANOVA was used to calculate statistical significance. Error bars denote 95% CI. * $p \leq 0.05$, ** $p \leq 0.005$, *** $p \leq 0.0005$, **** $p \leq 0.00005$.

The same experiments were performed to quantify colocalisation at the pre-synaptic terminal (**Figure 5.5**). However, only two m^{6}A-related proteins appear to interact with methylated transcripts in this region. First, YTHDF3 colocalisation with modified transcripts significantly increased following 15 minute activation ($p < 0.00005$ with both compounds) and also after 24 hours ($p < 0.05$ and $p < 0.005$ for NMDA and KCl activation, respectively (**Figure 5.5B**). Notably, this significant increase was only observed in differentiated TE671 cells, where PCC values were relatively high at approximately 0.5.

Likewise, overlap of m^{6}A modifications and eraser protein ALKBH5 was significantly increased following short term activation with both compounds and in both differentiated TE671 ($p < 0.005$ and $p < 0.0005$ for NMDA and KCl-mediated activation) and SH-SY5Y cells ($p < 0.0005$ with both compounds). After 24 hours, negative correlations were observed, indicating exclusion between the two markers (**Figure 5.5D**). These results suggest that previously observed m^{6}A-methylated transcripts undergo demethylation trans-synaptically. Furthermore, demethylation appears to be more important in the short term to either initiate or maintain the potentiation of a synapse through some unknown mechanism.

Notably, colocalisation of m^{6}A modifications and YTHDF1, Dcp1a, or FMRP at the pre-synaptic terminal was not found to change significantly following synaptic activation by either compound or in either cell line (**Figure 5.5A,C,E**) . Taken together, results at the pre-synaptic terminal suggest that there is discrimination of YTHDF1 and YTHDF3 at specific

cellular compartments. Additionally, findings suggest P-body degradation of mRNAs at pre-synapses is not dependent on the potentiation of this compartment. Lastly, results showing a lack of change after activation in experiments involving FMRP are consistent with reports that this protein translocates only to dendritic spines following NMDA activation (Antar et al., 2004).

Overall, the results from these experiments demonstrate an effect of neuronal activation upon the m^6A-mediated dynamics of mRNA colocalisation with m^6A readers, erasers, and P-bodies. The probable interaction of m^6A-modified transcripts and these proteins is likely to impact upon mRNA transport, translation, and degradation involved in the growth and strengthening of synapses.

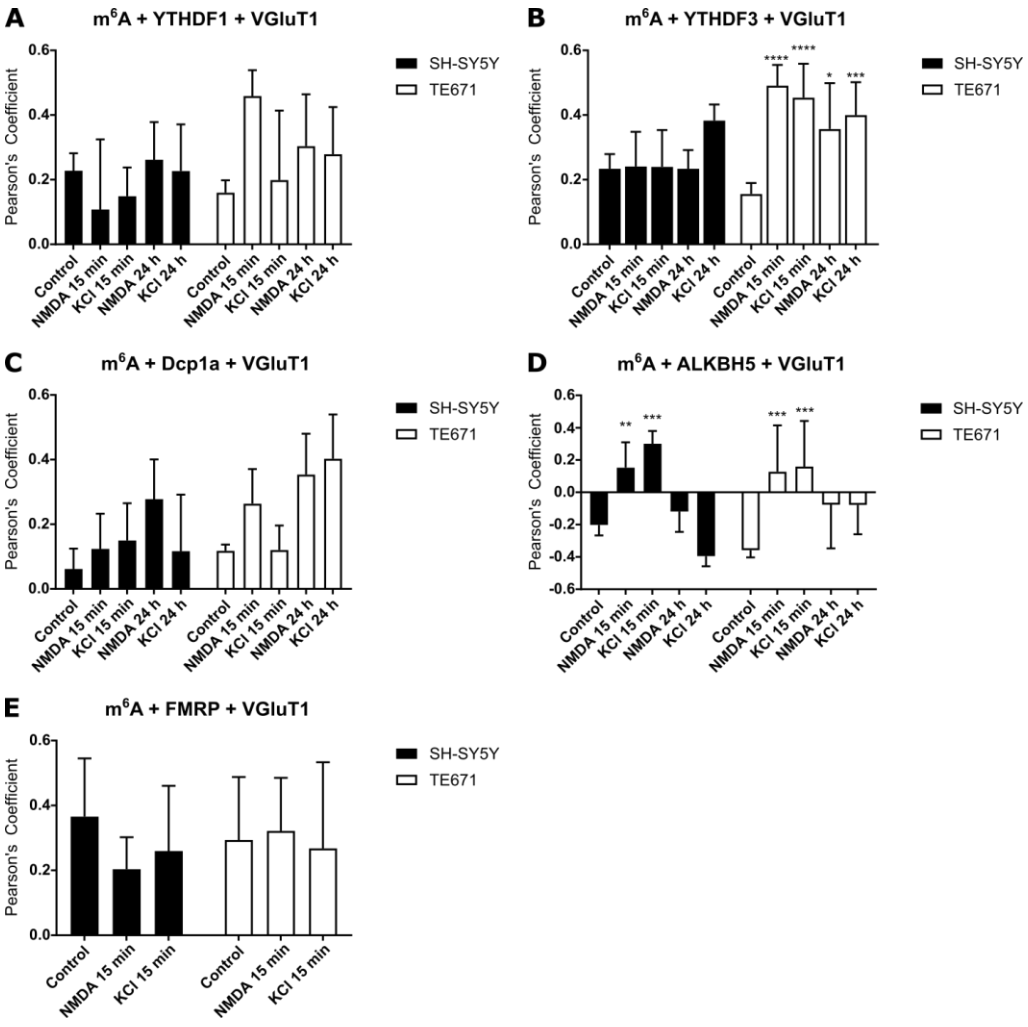

Figure 5.5 Colocalisation of m^{6}A modifications and related proteins at pre-synaptic areas in differentiated SH-SY5Y and TE671 cells. The differences depend on length of activation rather than agonist. Bar graphs showing the mean Pearson's Correlation Coefficient (PCC) for m^{6}A and an m^{6}A-binding protein at post-synaptic areas. A) No change in colocalisation of m^{6}A and YTHDF1 at pre-synaptic sites. B) Colocalisation of m^{6}A-modified transcripts and YTHDF3 is significantly increase at pre-synapses of differentiated TE671 cells following activation by either compound at both time points. C) No change in colocalisation of m^{6}A and Dcp1a at pre-synaptic sites. D) ALKBH5 and methylated transcripts colocalise more following short-term activation, an effect observed also at the post-synapse. E) No change in colocalisation of m^{6}A and FMRP at pre-synaptic sites. A two-way ANOVA was used to calculate statistical significance. Error bars denote 95% CI. * $p \leq 0.05$, ** $p \leq 0.005$, *** $p \leq 0.0005$, **** $p \leq 0.00005$.

5.2.3 Colocalisation of active ribosomes at the synapse with m^{6}A modifications and m^{6}A-binding proteins increases following neuronal activation

Given that previous findings demonstrated an increase in colocalisation between m^{6}A-modified transcripts and proteins known to affect translation following short-term glutamatergic activation, experiments were next performed to investigate whether these proteins associated with active ribosomes at synapses. Using a ribopuromycilation protocol with protein synthesis inhibitors, active translation was stalled in differentiated TE671 cells before and after short-term activation of NMDA receptors. Such active ribosomes were immunolabelled with anti-Puromycin, along with antibodies for m^{6}A modifications, reader YTHDF1, eraser ALKBH5, or P-body marker Dcp1a. Given local protein synthesis occurs at dendritic spines, PSD-95 was chosen as a third target for these experiments and used to quantify changes at post-synaptic sites only.

Visually, the activation state of cells did not appear to modify anti-Puromycin immunofluorescence throughout whole cells (**Figure 5.6**). This was confirmed by quantification of mean fluorescence intensity values across control and activated cells, which returned a *p*-value of ~0.48 (**Figure 5.7**). Immunofluorescence of other markers remained consistent with previous results.

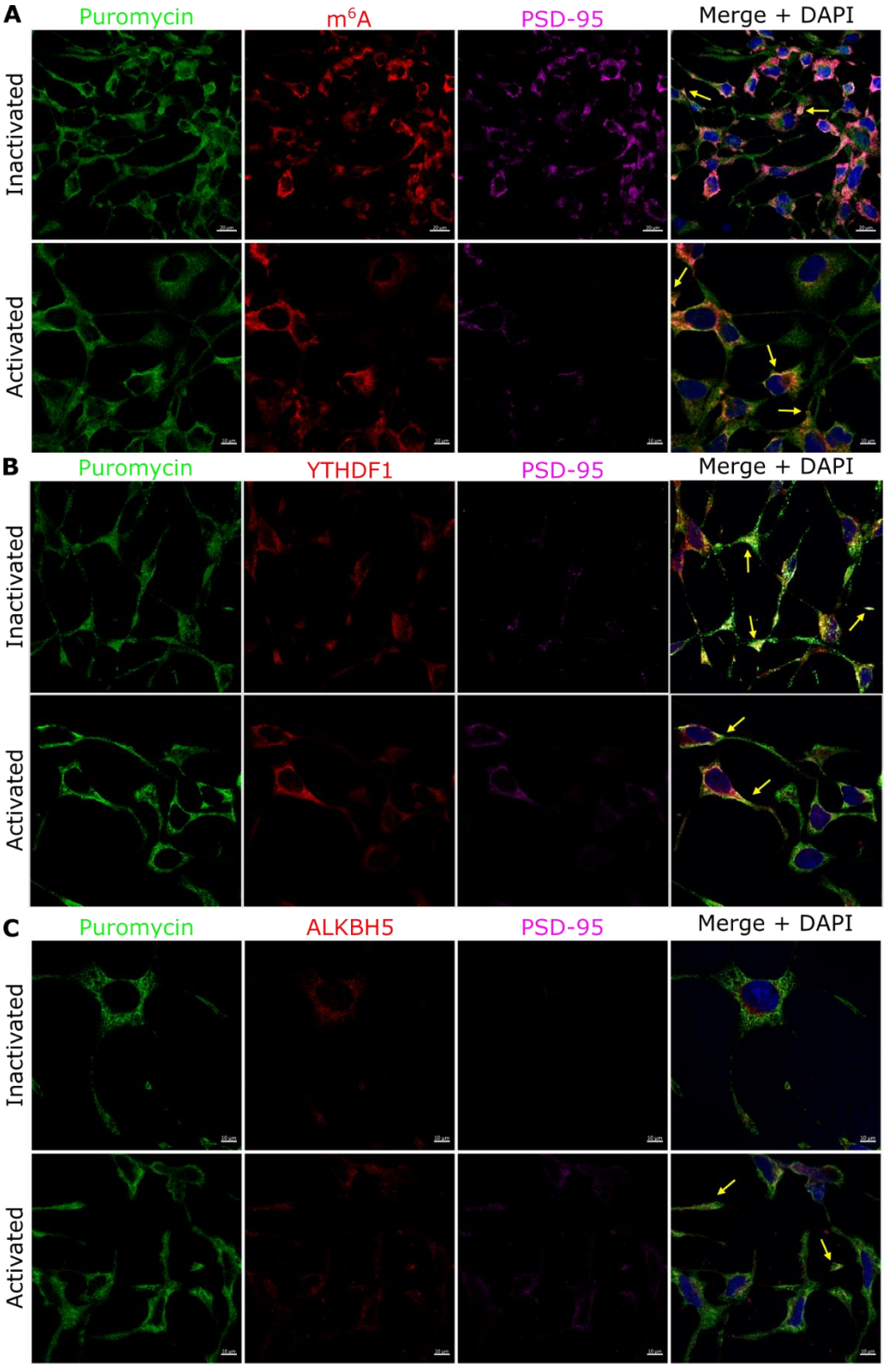
A
Puromycin
m6A
PSD-95
Merge + DAPI
Inactivated
Activated
B
Puromycin
YTHDF1
PSD-95
Merge + DAPI
Inactivated
Activated
C
Puromycin
ALKBH5
PSD-95
Merge + DAPI
Inactivated
Activated

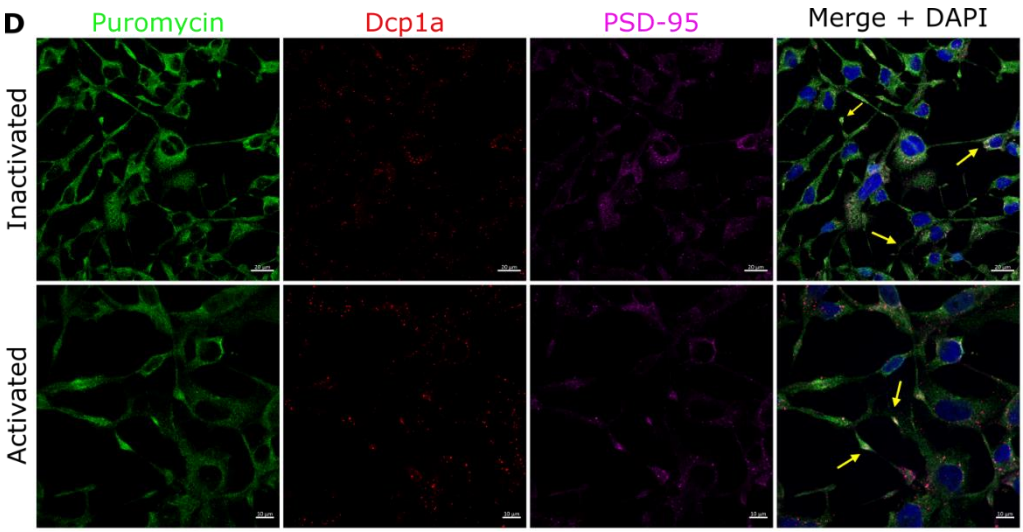

Figure 5.6 Colocalisation of active ribosomes and m^{6}A modifications/m^{6}A-binding proteins at synaptic areas in response to short NMDA receptor activation in differentiated TE671 cells. Cells were differentiated and treated with emetine followed by Puromycin to arrest translation and tag active ribosomes. There was little observable difference between inactive and active neuronal cells in the amount or intensity of signal from anti-puromycin. Changes in colocalisation between the red and green channels at PSD-95 were difficult to visually assess. Arrows point to cases of clear overlap, if any. Scale bar = 10 µm.

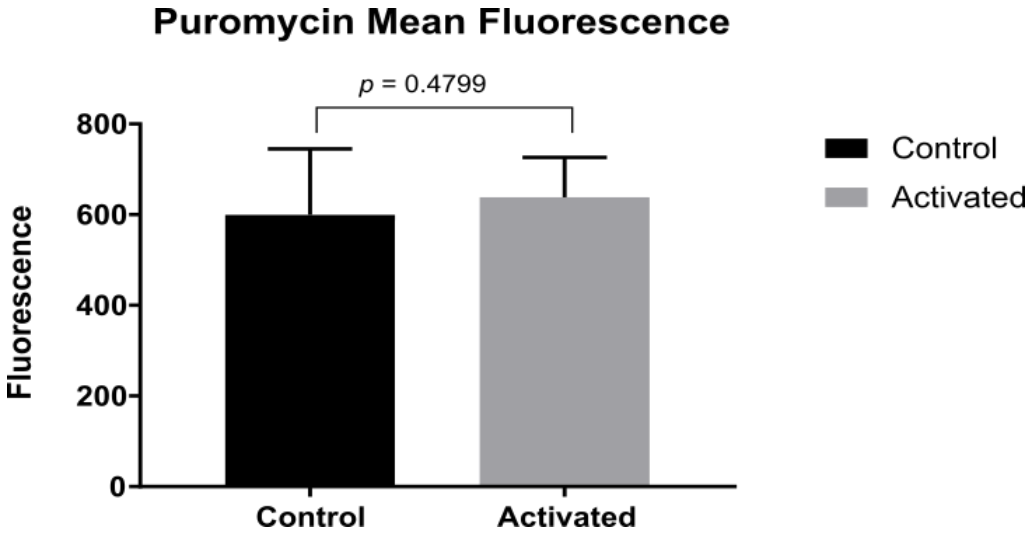

Figure 5.7 Neuronal activation has no effect on abundance of active ribosomes. The mean fluorescence of control and activated cells was calculated using FIJI on ten randomly selected images for each case. No statistically significant difference was observed between them.

Quantification of colocalisation between anti-Puromycin and other markers at post-synaptic sites significantly differed between inactive and NMDA-activated cells. There were significant increases in colocalisation of active ribosomes at post synaptic sites and m^6A-modified transcripts ($p < 0.0005$; **Figure 5.8A**), as well as reader YTHDF1 ($p < 0.0005$**; Figure 5.8B**) and eraser ALKBH5 ($p < 0.005$; **Figure 5.8C**). As YTHDF1 is a polyribosome loader of m^6A-methylated transcripts, this result is consistent with current literature. However, the increase in overlapping ALKBH5 and active polyribosomes is a novel finding which strengthens suggestions of a role for demethylation during local protein synthesis underlying plasticity. Finally, colocalisation with Dcp1a, in contrast, was significantly reduced ($p < 0.00005$) after activation which is consistent with a lack of mRNA decapping and degradation occurring during local protein synthesis.

Collectively, these results suggest there is moderate interaction between active ribosomes, m^6A-methylated transcripts, and m^6A-binding proteins at synapses. Furthermore, synaptic activation appears to be a trigger for these interactions which are likely involved in the regulation of local protein synthesis at synapses and thus their strength as a whole.

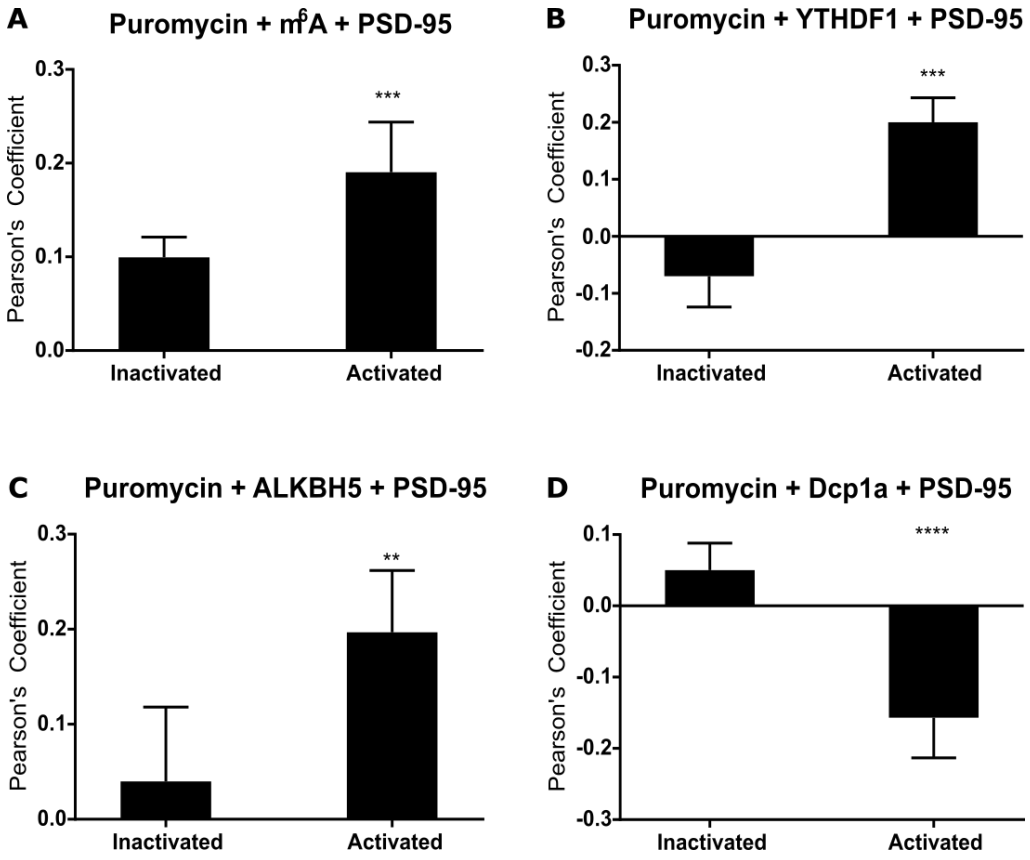

Figure 5.8 NMDA receptor activation induces post-synaptic changes. NMDA receptor activation induces post-synaptic changes in interactions between m^{6}A modifications and related proteins in ribopuromycilated cells (n = 4). Colocalisation of active ribosomes and m^{6}A modifications/related proteins was quantified in differentiated TE671 cells that were NMDA-activated for 15 minutes before fixing or inactive. A) m^{6}A-modified transcripts overlapped with active ribosomes significantly more often, suggesting translation of methylated transcripts is activity-dependent. B) YTHDF1, a ribosome-loading m^{6}A reader, colocalised with active ribosomes significantly more following activation. C) ALKBH5 colocalises significantly more with active ribosomes. D) The correlation between Puromycin and Dcp1a becomes negative following activation and local protein synthesis.

5.2.4 m^6A modification abundance and dynamics at synapses change during development

m^6A methylation has previously been studied during proliferation and differentiation in both embryonic and glioblastoma stem cells (Batista et al., 2014; Wang et al., 2014; Chen et al., 2015; Cui et al., 2017; Zhang et al., 2017). Here, human primary neuronal stem cells (NSCs) were utilised to assess the abundance of m^6A modified transcripts and their proximity to YTH readers and ALKBH5 erasers at the synapse during differentiation. These parameters were recorded at three different time points: before differentiation, one day after differentiation (i.e. early differentiation), and 14 days after differentiation (i.e. fully differentiated).

As shown in **Figure 5.9**, m^6A abundance was found to be very low, perhaps absent, in undifferentiated and early differentiated cells. However, in fully differentiated 14 day cells, m^6A abundance increases dramatically when compared with previous time points.

As before, colocalisation of m^6A-methylated mRNAs with YTHDF1, YTHDF3 and Dcp1a at post-synaptic regions was quantified at all time points. A significant increase was observed in colocalisation between m^6A-modified transcripts and YTHDF1 ($p < 0.0005$), as well as with Dcp1a ($p < 0.00005$), at 14 days of differentiation. In contrast, the opposite effect, a significant decrease in colocalisation, was observed between m^6A and YTHDF3 ($p < 0.005$).

These results suggest that YTHDF1-mediated ribosome-loading is an important part of neuronal development, putting it forward as one

mechanism by which m^6A affects cell differentiation or tumorigenesis. Notably, none of these experiments showed a significant change in colocalisation between the undifferentiated and early differentiated samples, possibly suggesting that m^6A dynamics are one of the latter changes in the differentiation process.

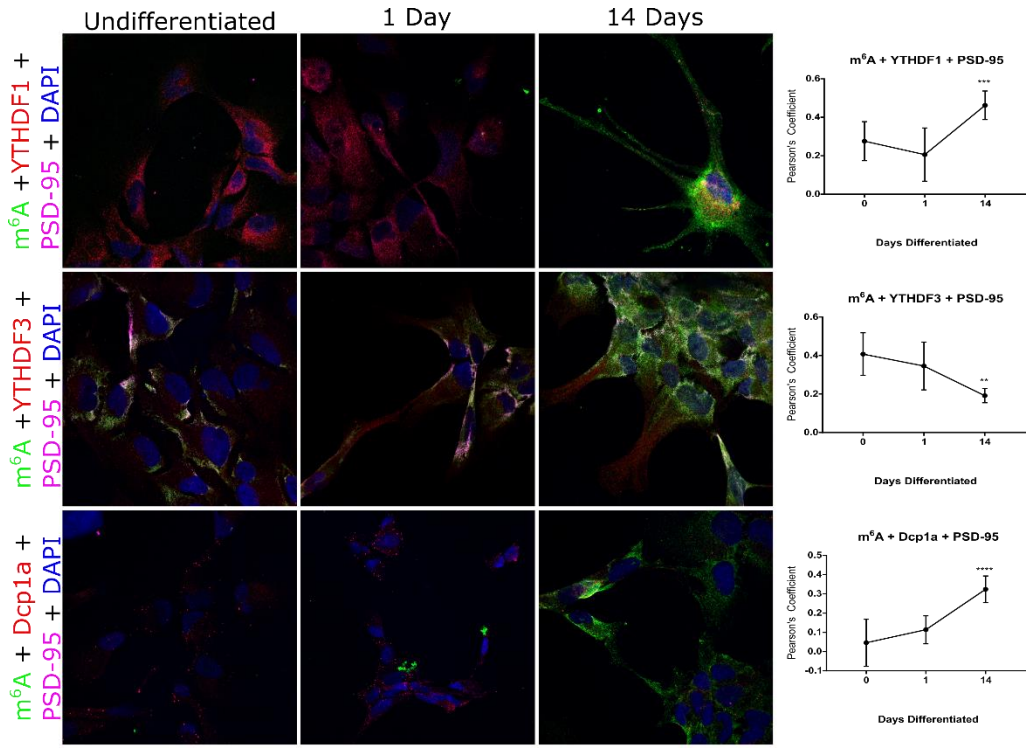

Figure 5.9 m^{6}A abundance and dynamics change during differentiation of human primary neuronal stem cells. m^{6}A (green) abundance increases throughout time. Arrows point to cases of clear overlap, if any. Colocalisation of m^{6}A and proteins of interest (red) was quantified at post-synaptic sites (magenta) and the Pearson's Correlation Coefficient is shown for each set of experiments on the right (n = 2). Colocalisation between m^{6}A modifications and reader YTHDF1 significantly increases at the final time point. The same effect is observed with Dcp1a. However, m^{6}A and YTHDF3 colocalisation significantly decreases. An ordinary one-way ANOVA was used to calculate statistical significance. Error bars denote 95% CI. * $p \leq 0.05$, ** $p \leq 0.005$, *** $p \leq 0.0005$.

5.2.5 N-cadherin abundance positively correlates with m^{6}A modifications and ribosomes at dendritic spines

Bioinformatic analysis of m^{6}A-sequencing data presented in Chapter 3 showed an enrichment of transcripts encoding for the cadherin family of cell adhesion proteins in brain-derived m^{6}A-methylated mRNA. To further investigate the role of RNA methylation in cadherin regulation, triple labelling immunocytochemistry was performed using anti-N-cadherin, anti-m^{6}A, and anti-L7A (ribosomal marker). This time, Phalloidin was used to stain F-actin bundles characteristic of dendritic spines, sites of neuronal contact.

Overlap of N-cadherin and m^{6}A was investigated as m^{6}A-modified transcripts were previously (Chapter 4) observed close to the active zone, i.e. the edge of the synapse. **Figure 5.10A** shows N-cadherin and m^{6}A immunofluorescence is abundant throughout neuronal cells, including at neuronal processes and dendritic spines (indicated by arrows). Zooming in on these dendritic spines (see inset) there is apparent colocalisation of the m^{6}A modifications and N-cadherin. Mean PCC values for these experiments were 0.38 in both cell lines, indicating medium levels of colocalisation (**Figure 5.10B**). The close proximity of m^{6}A modifications and N-cadherin suggest translation of cadherin transcripts may not occur at the head of dendritic spines, as is the case with most transcripts. Since the active zone is also where N-cadherin is expressed, an advantage of this would be perhaps to reduce transport times of the protein product.

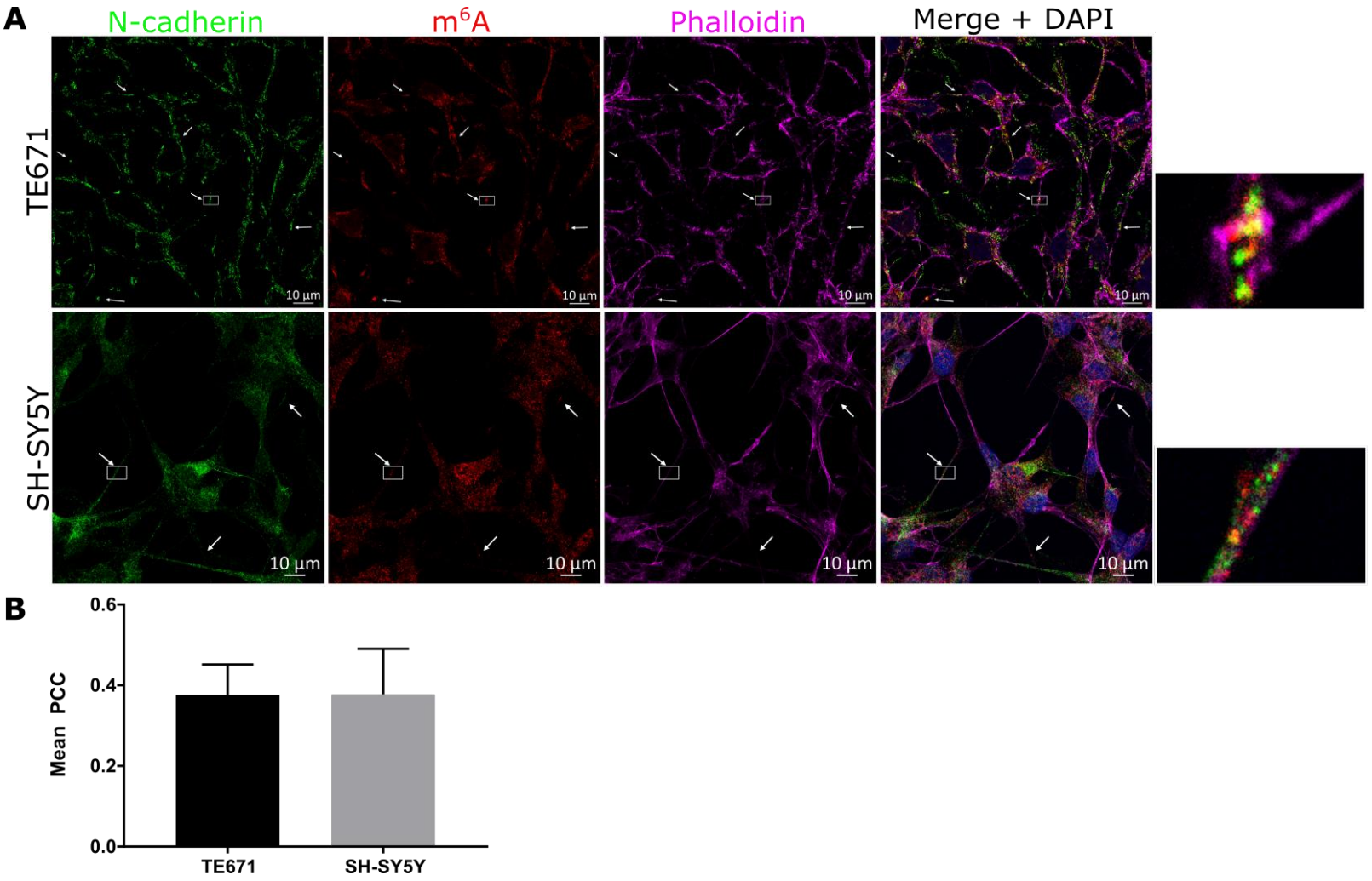
A
N-cadherin
m6A
Phalloidin
Merge + DAPI
TE671
SH-SY5Y
10 µm
B
Mean PCC
0.6
0.4
0.2
0.0
TE671
SH-SY5Y

Figure 5.10 N-cadherin and m^{6}A modifications colocalise at dendritic spines. To determine the relationship between m^{6}A-modified transcripts and N-cadherin at dendritic spines, triple labelling immunohistochemistry was performed using antibodies specific for m^{6}A modifications and N-cadherin, as well as Phalloidin. A) Image analysis found that there is colocalisation of m^{6}A modifications and N-cadherin at dendritic spines in differentiated neuronal cell lines. This effect was observed in many neuronal processes, as marked by white arrows. As shown on the insets on the right, N-cadherin was observed to be more abundant than m^{6}A modifications and all throughout dendrites. B) Quantifications of this overlap returned PCC values of ~0.38 for both cell lines, indicating medium level colocalisation (n = 4). These results suggest that m^{6}A-modified transcripts are located much closed to the edge of synapses than would be expected.

Due to the unusual location of m^{6}A-modified transcripts found in these experiments, the location of ribosomes relative to N-cadherin was also investigated. **Figure 5.11** shows colocalisation of N-cadherin and ribosomal marker L7A within various dendritic spines (arrows). Despite colocalisation being rarer in this experiment, it is still clearly close to the edge of some spines (**Figure 5.11A** insets), suggesting movement of ribosomes through these structures. Quantitative colocalisation analysis of m^{6}A modifications and N-cadherin returned PCC values of ~0.27 and ~0.26 for SH-SY5Y and TE671 cell, respectively (**Figure 5.11B**). This level of colocalisation suggest that there is a low level of ribosomal movement through spines to be close to the active zone.

Additionally, further quantitative analysis was performed by selecting sites of abundant N-cadherin (based on high fluorescence) to ask whether there is a relationship between ribosomes at dendritic spines and high N-cadherin expression. This analysis returned a mean PCC of 0.02, which means there is no apparent correlation.

Taken together, these results provide evidence that certain m^{6}A-modified transcripts are located much closer to the edge of synapses than would be expected by conventional theories on local protein synthesis (Rangaraju et al., 2017; Sutton & Schuman, 2006). These results also provide evidence that ribosomes can be found at the same location, meaning these are likely translating the aforementioned methylated transcripts. Further research is needed to investigate what causes these observations.

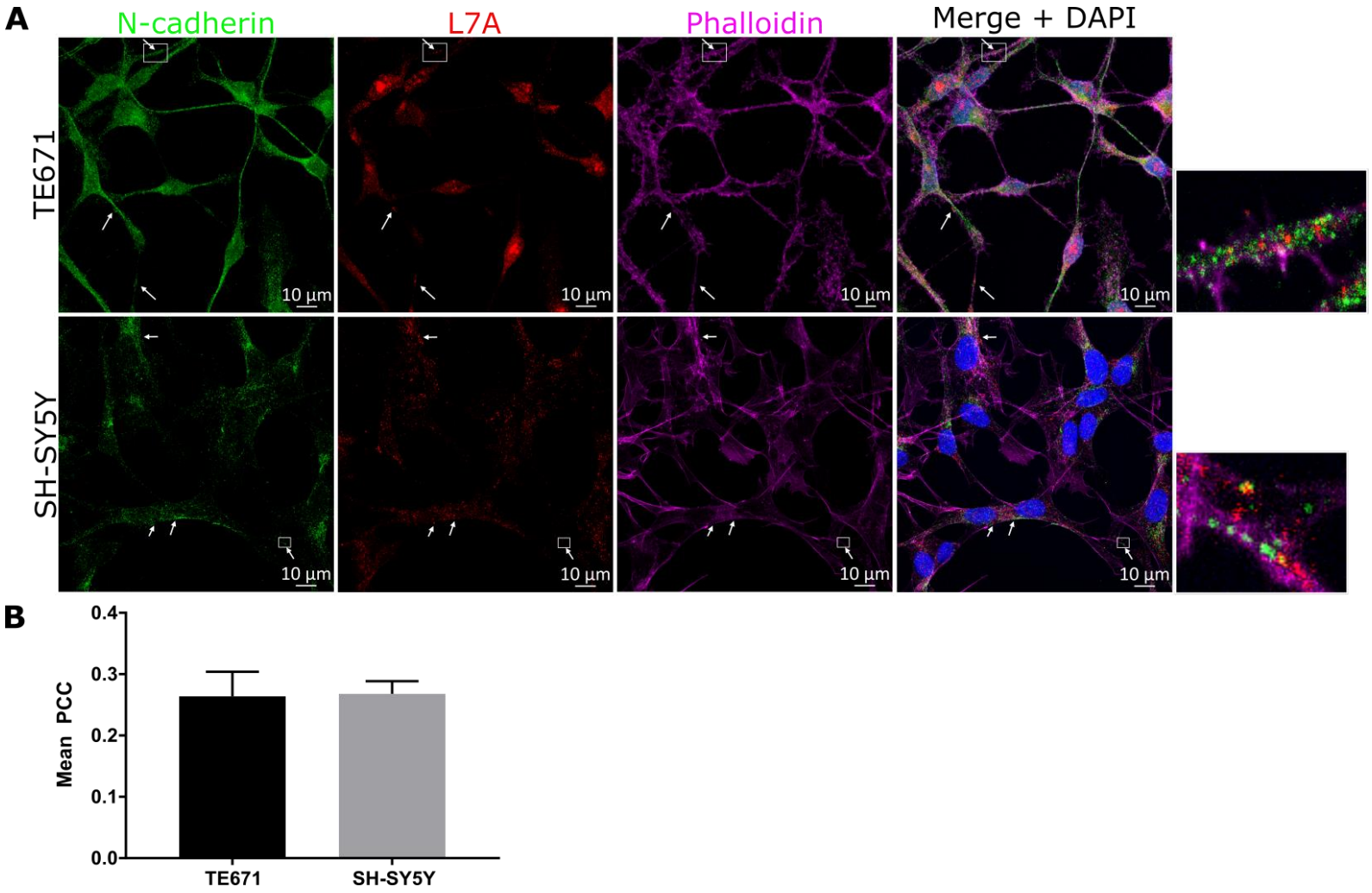
A
N-cadherin
L7A
Phalloidin
Merge + DAPI
TE671
SH-SY5Y
10 µm
B
Mean PCC
0.4
0.3
0.2
0.1
0.0
TE671
SH-SY5Y

Figure 5.11 N-cadherin colocalises with ribosomes at dendritic spines. To investigate the function of m^{6}A-modified transcripts near N-cadherin, colocalisation with ribosomal marker L7A was assessed in differentiated TE671 and SH-SY5Y cells. A) Overlap of these markers occurred at neuronal processes and dendritic spines (white arrows), which were identified as bundles of F-actin (stained by Phalloidin). N-cadherin was found to be abundant, as was L7A. However, colocalisation of these markers was not as common. B) Quantification of overlap between m^{6}A modifications and N-cadherin at dendritic spines gave PCC values of 0.26 for TE671 cells and 0.27 for SH-SY5Y, indicating low levels of colocalisation (n = 4). These findings suggest that there are ribosomes close to the edge of the synapse and that these are responsible for translation of previously found m^{6}A-modified transcripts at that site.

5.3 Discussion

Local protein synthesis induced by neuronal activation is a time-sensitive process which is responsible for synaptic plasticity and therefore learning and memory. The results presented in this chapter suggest that following synaptic activation, local transcripts undergo translation regulated by their m^6A methylation status and the function of m^6A readers and erasers. These local transcripts are also later degraded or demethylated within time scales corresponding to early/late LTP and are consistent with previous information about mRNA stability in neurons and the half-life of mRNAs (Bolognani, 2008; Sharova, 2009). These findings are also likely to happen *in vivo* based on the identification of m^6A erasers FTO and ALKBH5 in rat models in cerebral cortex and primary neurons (Li et al., 2017; Chang et al., 2017).

In the current study, neuronal activation experiments showed that there was a change in colocalisation between m^6A modifications and proteins of interest. Two of these tested proteins were m^6A readers YTHDF1 and YTHDF3, which consistently interacted with m^6A-methylated transcripts following short-term activation. Given current leading theories about post-synaptic local protein synthesis during LTP, the use of these two proteins to augment translation of m^6A-tagged transcripts would facilitate fast protein expression needed to strengthen synapses. This discovery is thus an important step towards the manipulation of synaptic protein expression and therapy for neurodegenerative diseases characterised by synaptic loss. An example of this type of therapy is yet to be demonstrated but more and more, the involvement of m^6A-binding

proteins in cancer is being studied (Han et al., 2019). The lack of similar research investigating neuronal disease remains an opportunity for future studies.

Throughout this research, ALKBH5, the eraser protein, has provided unexpected results. This includes the discovery that it is located in the cytoplasm and interacts with m^6A-methylated transcripts shortly following neuronal activation rather than being involved in transcript degradation. It is difficult to reconcile a mechanism in which both YTH reader proteins interact with the m^6A mark while demethylation occurs, but one possibility is that the eraser and reader function consecutively. If this were the case, more research is needed to decipher the temporal order of m^6A reader and eraser function.

A high proportion (>95%) of FMRP targets in mouse brain have recently been shown to be highly methylated with ~3.3 m^6A marks per target transcript compared to <2 in other transcripts (Chang et al., 2017). This suggests that FMRP is an m^6A reader which, as part of an RNA-binding complex with CYFIP1, eIF4E, and polyribosomes (Napoli et al., 2008; Darnell & Klann, 2013), silences and transports methylated transcripts to the synapse. It is currently unknown how FMRP detaches at the synapse from its complex, but Chang et al. (2017) proposed m^6A methylation is involved either by the addition or removal of m^6A modifications. The present immunocytochemistry experiments show ALKBH5 solely interacts with m^6A shortly after NMDA activation, an effect also observed between m^6A and FMRP. Therefore, the answer to how FMRP detaches from its mRNA silencing complex may be demethylation activity of

ALKBH5 which reduces but does not completely erase methylation. A change in m^6A methylation numbers is then likely to affect the binding stability of the FMRP complex, freeing transcripts to initiate translation by local polyribosomes.

An increase was also observed in colocalisation of active ribosomes and ALKBH5 following NMDA receptor activation. It is possible then that once FMRP unbinds, translation is modified when YTHDF1 or YTHDF3 read the remaining m^6A marks. This may mean readers compete with ALKBH5 to avoid further demethylation. Under this model, defects in m^6A-binding proteins may also contribute to Fragile X syndrome by altering translation efficiency. Further research identifying specific m^6A-methylated transcripts bound by FMRP and live imaging of these mRNAs and proteins is needed to confirm this model.

Subsequently, ALKBH5 colocalisation with m^6A modifications at the pre-synapse was also observed to increase significantly following NMDA receptor activation. Since this result was found to be consistent across cell lines and activation compounds, it suggests that demethylation is also a critical part of pre-synaptic growth, too. Local protein translation at the pre-synapse remains unexplored in comparison to the contribution of translation at post-synaptic compartments, but it has been shown to contribute to maintenance of nascent synapses undergoing LTP (Akins et al., 2009). Pre-synaptic protein synthesis has also been reported to affect neurotransmitter release (Younts et al., 2016), a critical part of synaptic transmission. Thus, demethylation of transcripts may function similarly to what is proposed to occur in the post-synaptic compartment,

wherein a change in numbers of m^{6}A marks modulates translation of transcripts that impact upon the expression of pre-synaptic proteins and continuation of LTP through repeated synaptic transmission. Furthermore, at this compartment a similar change in colocalisation of YTHDF3 was observed in at least one cell line, suggesting this m^{6}A reader also modulates translation in this compartment through ribosome loading.

A unique result in this study was the increase in colocalisation of m^{6}A-methylated transcripts and the P-body marker, Dcp1a, at post-synaptic compartments following neuronal activation. This change was only observed after 24 hours, simulating late-LTP. The uniquely long half-life of mRNA in human brain has been previously described as advantageous for plasticity for two reasons: mRNAs may be shared between synapses that receive input and mRNAs may remain translationally silent at a dendritic spine until activation of its synapse (Kosik, 2016). Since there is no methyltransferase (i.e. writer) activity at synapses, the finding that m^{6}A-methylated transcripts move to P-bodies for degradation at approximately the same time that *de novo* transcripts from the nucleus are transported to potentiated synapses (Schuman et al., 2006; Martin, 2004) strongly suggests that m^{6}A methylation is a necessary feature of the requisite mRNAs to begin plasticity. A new question which arises from this finding is how these transcripts initially avoid being degraded through YTHDF2-mediated transport to P-bodies. Currently, little *in vivo* research looking at YTHDF2 has been conducted and the answer may simply lie in YTHDF2 expression at synapses being

characteristic of late-LTP. Further research is necessary as dysregulation of YTHDF2:YTHDF1 protein expression ratios could in some cases lead to synaptic depression rather than potentiation.

The translational state of ribosomes at post-synaptic compartments before and after short-term potentiation was also investigated. In this section, it was found that in non-activated cells, there is little colocalisation between active ribosomes and m^{6}A modifications, reader YTHDF1, eraser ALKBH5, or Dcp1a. The changes following NMDA receptor activation were consistent with previous results, suggesting m^{6}A-methylated transcripts are actively translated after activation and that this process is aided by YTHDF1 and ALKBH5. Colocalisation with Dcp1a was, as predicted, reduced as interaction between P-bodies and ribosomes would be detrimental to cells by degrading transcripts ready for translation. Notably, all results showed lower PCC values when compared to previous experiments and this is likely due to saturation of ribosomes. While m^{6}A is the most common internal mRNA modification, there are other transcripts that would also be translated at this time and thus represent competition for available ribosomes. Still, these results strengthen findings that m^{6}A-dependent translation at post-synaptic compartments is sensitive to NMDA receptor activation.

Yoon et al. (2017) have previously reported that m^{6}A methylation is important for temporal control of mammalian neurogenesis. Their results support the above findings in neuronal stem cells, which showed m^{6}A methylation is nearly absent in undifferentiated stem cells but abundance peaks late during differentiation and development. The absence of m^{6}A

throughout most of the cytoplasm of undifferentiated cells suggests RNA methylation is part of a late stage development mechanism for fine-tuning of global translation. Publically available microarray data from the Human Brain Atlas (http://hbatlas.org/) shows a similar pattern for m^6A writers METTL3 and METTL14 in the hippocampus brain region. Furthermore, observations that m^6A and YTHDF1/Dcp1a colocalisation increased throughout time at post-synaptic compartments suggests methylation is also critical for synaptic plasticity. The timing of this increase in m^6A methylation coincides with an increase in spine formation, NMDA receptors, and CaMKII expression levels (Lohmann & Kessels, 2014).

In addition, in these neuronal stem cells, YTHDF1 was identified as the critical m^6A reader during development. Coupled with results in differentiated immortalised cell lines, these findings propose YTHDF1 is the principal m^6A reader to modulate translation and that YTHDF3, which is thought to be functionally similar to YTHDF1 and YTHDF2 (Shi et al., 2017), is highly expressed after cells have matured.

Cell adhesion proteins, in particular cadherins, are uniquely poised at synapses to mediate synaptic plasticity. This protein family is characterised by its trans-synaptic location, its persistent expression at nascent and mature synapses, and its ability to initiate internal signalling cascades (Tai et al., 2008). N-cadherin's involvement with methylation and translation was investigated and it was found that m^6A modifications colocalise with N-cadherin at the synapse of neuronal cell lines. It was also observed that the L7A ribosomal subunit colocalised with N-cadherin, too, albeit with a weaker correlation. These results were

unexpected as local protein synthesis is thought to occur at the base of dendritic spines, at distances of ~1 µm from the synaptic membrane where N-cadherin is located. However, these findings suggest that a subset of ribosomes and m^6A-methylated transcripts are located much closer to N-cadherin.

It would be informative to continue investigating the spatial relationship between m^6A modifications and N-cadherin. One hypothesis is that the m^6A-modified transcripts found near the active zone transcripts encode for cadherins and protocadherins, mRNAs which, in Chapter 3, were prevalent in m^6A-sequencing of human brain tissue (Dominissini et al., 2012). These transcripts were found to be highly methylated, sometimes having up to 27 m^6A marks. Especially high methylation may work similarly to a peptide chain's signal recognition particle (SRP), which would flag transcripts for co-translational translocation towards the membrane, resulting in quicker transmembrane integration of cadherins (Walter and Blobel, 1983). This would, in turn, benefit N-cadherin-mediated regulation of short-term plasticity (Jungling et al., 2006). To begin investigating this, synthetic highly m^6A-methylated RNAs with either a fluorescent or biotin tag could be live imaged through time in an *in vitro* model to test whether they are translated at unique sites. Extensive research is needed to determine whether there is a unique relationship between cadherin expression and m^6A methylation and what are the processes involved.

A number of issues are worthy of note as limitations in this study. The first one is that, as discussed before, research of novel molecules using

immunological approaches is limited by the availability and quality of antibodies (Sewell et al., 2017; Almagro et al., 2018). This was demonstrated by the use of a new anti-m^{6}A antibody used for experiments of N-cadherin and m^{6}A colocalisation. This antibody, which had only been tested as part of an m^{6}A-sequencing kit, was supplied by New England Biolabs and proved to be noticeably better (punctate, uniquely high signal-to-noise ratio of fluorescence) in immunocytochemistry than any other commercial antibody. However, due to production issues, the amount of available antibody was extremely low and as such it was not viable to use it for activation experiments.

As mentioned before, the unavailability of good YTHDF2 antibodies proved to be a more costly limitation. P-body marker Dcp1a was chosen as a proxy to study YTHDF2 because these structures are the target of YTHDF2-mediated m^{6}A-binding. Unfortunately, by doing this, it was impossible to observe changes in YTHDF2 abundance at the synapse which may have helped explain the long lives of mRNAs.

Another issue which would be interesting to address in future studies is the timing of neuronal activation. Two time points were chosen to simulate early and late phase LTP, but the extremely fast protein expression and movement of proteins and transcripts which characterises LTP is not fully explored by the current method. Due to bleaching of immunofluorescence in these first generation antibodies, live imaging was not possible. However, when better antibodies are developed in the future, it would be interesting to revisit these experiments using live cell imaging and activating neurons while being

imaged. In this way, individual m^{6}A-binding proteins could be tracked for hours. This in itself would be limited by the number of labels commonly available for live cell imaging being limited to two, although methods to add more labels are being explored (Chen et al., 2018).

Another limitation is that colocalisation observed by confocal microscopy is a relative measure. Colocalisation means that two fluorescent puncta are located within a distance smaller than the optical resolution of the instrument. With confocal microscopy, that distance is ~200 nm (Pike et al., 2017). This means that colocalisation does not always mean interaction. One method to verify the interactions observed here would be using FRET microscopy, which is especially useful to discover protein-protein interactions as it causes an observable change in fluorescence only when two markers of interest are interacting within 8 nm (Padilla-Parra, 2012). Another technique that may be used to confirm protein-protein or protein-mRNA interactions would be coimmunoprecipitation, although this was limited in the current study by the ability to isolate both stable and activated synapses.

Finally, one last issue in this work was the limited numbers in two techniques. In the case of ribopuromycilation experiments, the method proved toxic to differentiated SH-SY5Y cells. These cells would die and change morphology during the procedure, resulting in very few images comparable to those using differentiated TE671 cells. This thus limited reproduction of results as in other experiments. Also, since neural stem cell differentiation is a long and careful process, the number of cells gifted

by collaborators was limited to two cell populations per condition. This likewise affected the number of time points that were studied.

To conclude, m^6A methylation has been identified as a fine-tuning mechanism of active translation at synapses which is principally mediated by YTH proteins and responds to synaptic stimuli to help recruit mRNAs to the synapse via FMRP and promote synaptic growth and development. Evidence is also provided that FMRP release of mRNA follows demethylation by ALKBH5 and that ALKBH5 may act in the pre-synaptic compartment. It has been observed that the fate of m^6A methylated transcripts in synapses is dependent on time of receptor activation. Finally, the current study provides evidence that m^6A is observed only during late neuronal stem cell development. Taken together, these findings represent the first investigation into the dynamics of m^6A methylation in stable and developing synapses.

Chapter 6:

Characterisation of m^6A methylation in normal and diseased human brain

I would like to thank Dr. Chris Gell for his invaluable assistance in developing an unbiased quantitative method to assess DAB-stained immunohistochemistry. I would also like to thank Djordje Gveric and Steve Gentleman from the Parkinson's UK brain bank for providing the valuable tissue and associated clinical information.

6.1 Preface

Results from the previous chapter strongly suggest that local protein synthesis regulated by m^6A methylation is key to synaptic development and neuronal communication. In this chapter, I aim to assess the prevalence of m^6A modifications and m^6A readers in normal human brain. Given that early stage neurodegenerative disease is characterised by deficits in synaptic transmission (Bereczki et al., 2018), I also examine the state of m^6A methylation in Parkinson's disease, Lewy Body Dementia, and Mild Cognitive Impairment. Lastly, m^6A methylation deficits have been associated with tumourigenicity in human cancer stem-like cells, so two human brain tumour types (ependymoma and glioblastoma) were also analysed (Cui et al., 2017). The results of this chapter are intended to provide insight of the epitranscriptomic changes of neurodegenerative disease and brain cancer to serve as the basis for future study of disruption in disease and the development of therapies.

6.2 Results

6.2.1 Cerebellum

m^6A modifications were shown in previous chapters to be highly abundant in brain tissue. Immunohistochemistry using 3,3′-Diaminobenzidine (DAB) as a reporter was performed on cerebellum from healthy control individuals and tissue from individuals affected with three different neurological diseases (**Figure 6.1**): Parkinson's Disease (PD), Lewy Body Dementia (LBD), and Mild Cognitive Impairment (MCI).

The colour intensity of DAB staining has a non-linear positive correlation with marker expression. To complement observations from these experiments, quantitative analysis of mean DAB staining intensity (but not staining area) in whole regions was performed by selecting all positively stained cells in an image and using FIJI's Measure command, resulting in an intensity integer value for each image. See sections 2.2.12-2.2.14 for more details.

Immunohistochemical characterisation of m^6A methylation abundance and YTHDF1/YTHDF3 expression in cerebellum was described for each of the three layers of the cerebellar cortex's microanatomy. These layers include the outermost molecular layer (ML), the narrow Purkinje cell layer (PL), and the thick granular cell layer (GL). These three layers contain specialised cells and processes.

Immunoreactivity in control unaffected individuals showed m^6A modifications are abundant in all layers of the cerebellum with medium to high staining intensity observed. Specifically, abundance of m^6A

modifications was observed around the nucleus of inhibitory interneurons in the molecular layer (**Figure 6.1**). Reactivity varied from cell to cell and cells that show reactivity have medium to high expression. However, not all cells in this layer were reactive. Processes originating from Purkinje cells and identified by their thickness extend into the molecular layer and were clearly reactive, displaying medium abundance of m^6A modifications.

In the Purkinje layer, large Purkinje cells are easily identifiable and display medium m^6A modification abundance. Curiously, processes stemming from Purkinje cells are not always stained continuously and immunoreactivity seems to be mostly cytoplasmic in this layer. A few Bergmann glia are found between Purkinje cells and show high m^6A abundance.

Finally, the cerebellar granular layer of control individuals had medium expression. Some variability was observed in this layer with some patches of cells being more darkly stained.

Comparing PD samples against controls, quantitative analysis of expression of m^6A modifications, performed by machine-learning software, was not significant ($p > 0.19$). This is likely because only the Purkinje layer showed differences in expression. Cells in this layer showed m^6A modifications in the proximal area of processes near the cytoplasm. However, abundance in the cytoplasm was not apparent.

Overall, abundance of m^6A modifications in LBD and MCI-affected tissue was significantly higher than in control samples ($p < 0.001$ and $p <$

0.0001, respectively). However, in LBD and MCI tissue, reactivity in Purkinje cells was not observed.

Taken together, these results suggest global changes in m^{6}A methylation in cerebellum are features of neurological disease. Furthermore, Purkinje cell m^{6}A methylation appears to be a highly dysregulated process.

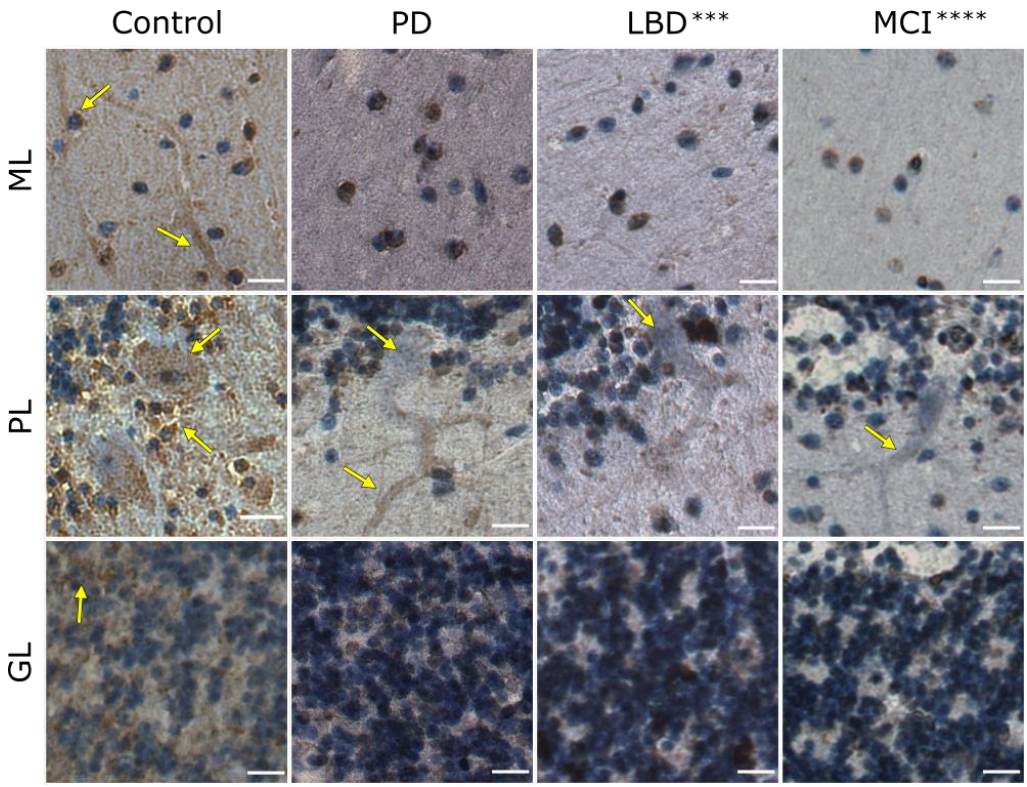

Figure 6.1 Abundance of m^{6}A-modified transcripts changes in neurological disease-affected cerebellum. m^{6}A-modified transcripts are expressed in all principal layers of the cerebellum. However, changes between control and disease samples are more obvious in the middle layer or Purkinje cells. LBD and MCI samples showed a significant increase in overall expression of m^{6}A-modified transcripts. Arrows point to sites where differential expression was observed between samples. n = 3 for each condition. *** $p \leq 0.001$, **** $p \leq 0.0001$. Scale bar = 20 μm.

Normal brain immunoreactivity for m^6A reader protein YTHDF1 was high (**Figure 6.2**). YTHDF1 expression in the molecular layer of cerebellum was high, as demonstrated by dark DAB staining in the cytoplasm of small neurons. However, some small neurons also showed little reactivity, perhaps suggesting that YTHDF1 expression changes in these cells. Also in the molecular layer, Purkinje cell processes were observed to highly express YTHDF1. Consistent with this, in the Purkinje layer, Purkinje cells displayed especially high reactivity of YTHDF1 both in the cytoplasm and proximal neuronal processes. Finally, the granular cell layer of healthy cerebellum once again showed a variation of marker expression. Most of the cytoplasm of these granular cells had medium strength immunoreactivity but some small areas in which expression was much higher were observed.

YTHDF1 immunohistochemistry in PD-affected individuals generally showed reduced expression in cerebellum. Overall, expression of YTHDF1 tissue was reduced significantly ($p < 0.01$) beginning with null immunoreactivity in the small neurons of the molecular layer and faint staining of processes. Purkinje cells were found not to express YTHDF1, while the small cells between Purkinje cells, known as Bergmann glia, had normal expression levels. In contrast, the granular cell layer had very low expression.

LBD samples had normal expression in the molecular and granular layers, resulting in an overall non-significant difference when compared with control samples ($p > 0.35$). However, in LBD, proximal processes in the Purkinje layer were non-reactive for YTHDF1 and cytoplasmic

expression of YTHDF1 varied between from low to high expression in Purkinje cells.

Subsequently, MCI individuals had reduced YTHDF1 expression in the molecular and granular layers ($p < 0.05$), but Purkinje layer cells stained normally in the cytoplasm and proximal neuronal processes. The variability in YTHDF1 expression amongst all samples, be they healthy or affected, suggests that control mechanisms of YTHDF1 are differentially affected by defects in each of neurological disease.

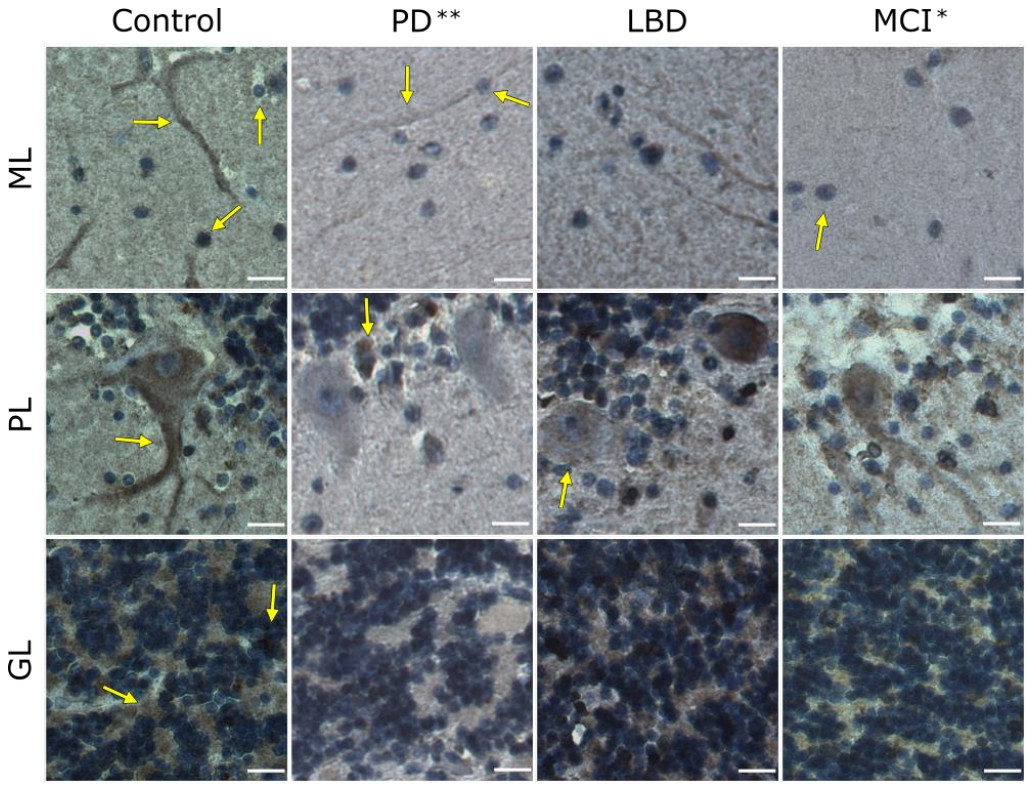

Figure 6.2 Expression of YTHDF1 changes in neurological disease-affected cerebellum. YTHDF1 is expressed in all principal layers of the cerebellum. PD and MCI samples showed a significant decrease in overall expression of m^6A-modified transcripts. Arrows point to sites where differential expression was observed between samples. n = 3 for each condition. * $p \leq 0.05$, ** $p \leq 0.01$. Scale bar = 20 μm.

Despite their similar function, YTHDF3 immunohistochemistry differed from that of YTHDF1 (**Figure 6.3**). Generally, YTHDF3 staining had very low background reactivity, suggesting specific regional differences in protein expression. Average reactivity in normal samples was of medium intensity. In the molecular layer, staining around small neuronal nuclei was common and expression was high. Light Purkinje process staining is also apparent in this layer. In these samples, it appeared YTHDF3 expression was higher in areas of the molecular layer closest to the Purkinje layer. YTHDF3 reactivity was not apparent in Purkinje cells' cytoplasm. A few Bergmann glia in the PL showed medium intensity staining but most were non-reactive. Lastly, expression in the granular layer was generally of medium intensity with lighter patches observed.

Samples from affected individuals showed expression levels similar to control individuals in the molecular layer, higher in the granular layer, and varied in the Purkinje layer. These changes in expression added up to quantitatively significant increases in all diseases ($p < 0.001$ for all). In this last layer, Purkinje cells in PD samples had either null or very low YTHDF3 immunoreactivity. LBD cerebellum contained Purkinje cells in which YTHDF3 expression was generally low and consistent in the cytoplasm of all Purkinje cells but no proximal neuronal process staining was observed. Finally, MCI samples showed some variability. Some Purkinje cells in this tissue were highly reactive in the cytoplasm and proximal neuronal processes, but other cells had medium or low YTHDF3 expression. In these latter cells, neuronal cell processes were not observed to be reactive.

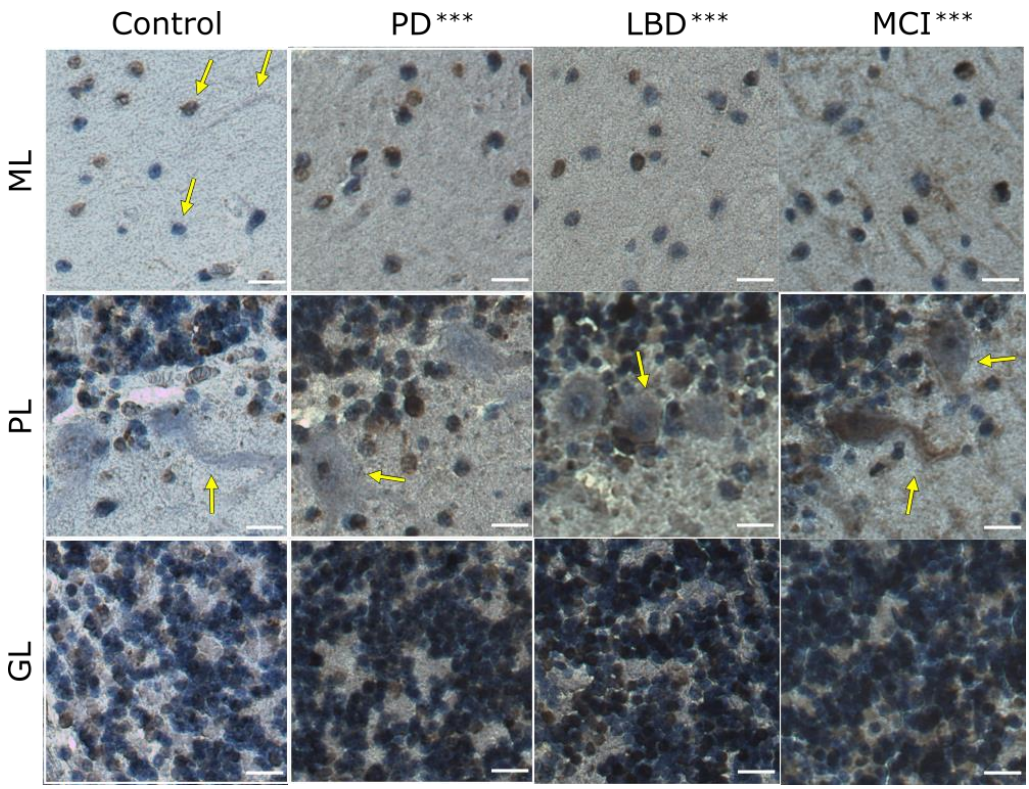

Figure 6.3 Expression of YTHDF3 changes in neurological disease-affected cerebellum. YTHDF3 is expressed in all principal layers of the cerebellum. YTHDF3 expression varies in all layers of disease cerebellum. PD, LBD, and MCI samples all showed a significant increase in overall expression of YTHDF3. Arrows point to sites where differential expression was observed between samples. n = 3 for each condition. *** $p \leq 0.001$. Scale bar = 20 μm.

6.2.2 Cingulate Gyrus

Immunohistochemistry was also performed on tissue samples of the cingulate gyrus (**Figure 6.4**). This area of the brain is part of the limbic system, an area of the brain responsible for emotional and behavioural responses. It is reported to be one of the first areas to accumulate alpha synuclein aggregates both at synapses and forming spherical entities called Lewy bodies (Hansen et al., 1998). The cingulate gyrus is a cortical region and its microanatomy is separated into six distinct layers with unique cell populations.

The abundance of m^6A modifications in normal brain samples was of medium intensity. Layer I contains glia cells and neuronal processes, all which presented high abundance of m^6A methylation. Layers II and IV, which consist of relatively small, densely packed excitatory granular neurons, both had high reactivity for m^6A modifications, although Layer IV had some larger cells with only medium staining. In Layer III, small pyramidal cells were observed to have m^6A-methylated mRNAs both in the cytoplasm surrounding the nucleus and their neuronal processes. Immunoreactivity in the cytoplasm was darker than in processes. Layer V, consisting of large pyramidal neurons had high abundance in throughout the cytoplasm and neuronal processes. In these cells, m^6A methylation was high enough that it traced the shape of the whole cell. Layer VI, which contains a mix of pyramidal and other neuron types, had medium staining of m^6A modifications.

Next, samples from PD-affected individuals were found to have a global reduction in m^6A methylation ($p < 0.0001$). This changes is more obvious in Layers III-VI affecting all types of neurons. Notably, while staining intensity is lighter in pyramidal cells of Layers III and V, the processes extending from these cells have the same darkness as their cytoplasm, indicating that although m^6A levels may be reduced, the spatial distribution of modifications has remained equal.

Compared with PD samples, the opposite effect is observed in LBD-affected individuals. There is a global increase of m^6A methylation ($p < 0.0001$). This results in fewer non-reactive cells in Layers I and II compared to control samples. In Layer III, uniform longer process staining is observed. In Layer V of LBD tissue, a notable decrease in the number of reactive pyramidal neuron processes is observed despite an overall increase in expression of m^6A modifications in these cells.

Tissue from individuals with MCI did not show a clear trend in all cortical layers, although overall m^6A methylation in the cingulate gyrus was also increased ($p < 0.01$). Specifically, Layers I, II, and IV were observed to abundance of m^6A modifications comparable to control samples and also have more non-reactive cells, although it has not been possible to quantify this last observation. There was a clear change in immunoreactivity observed in Layer V, where only a few large pyramidal neuron processes were stained.

Overall, these results provide evidence that there are clear changes to global m^6A methylation levels associated with different neurological

diseases. Results also suggest there is a reduction of pyramidal neuron processes staining in diseases, such as LBD and MCI, characterised by cognitive and synaptic deficits.

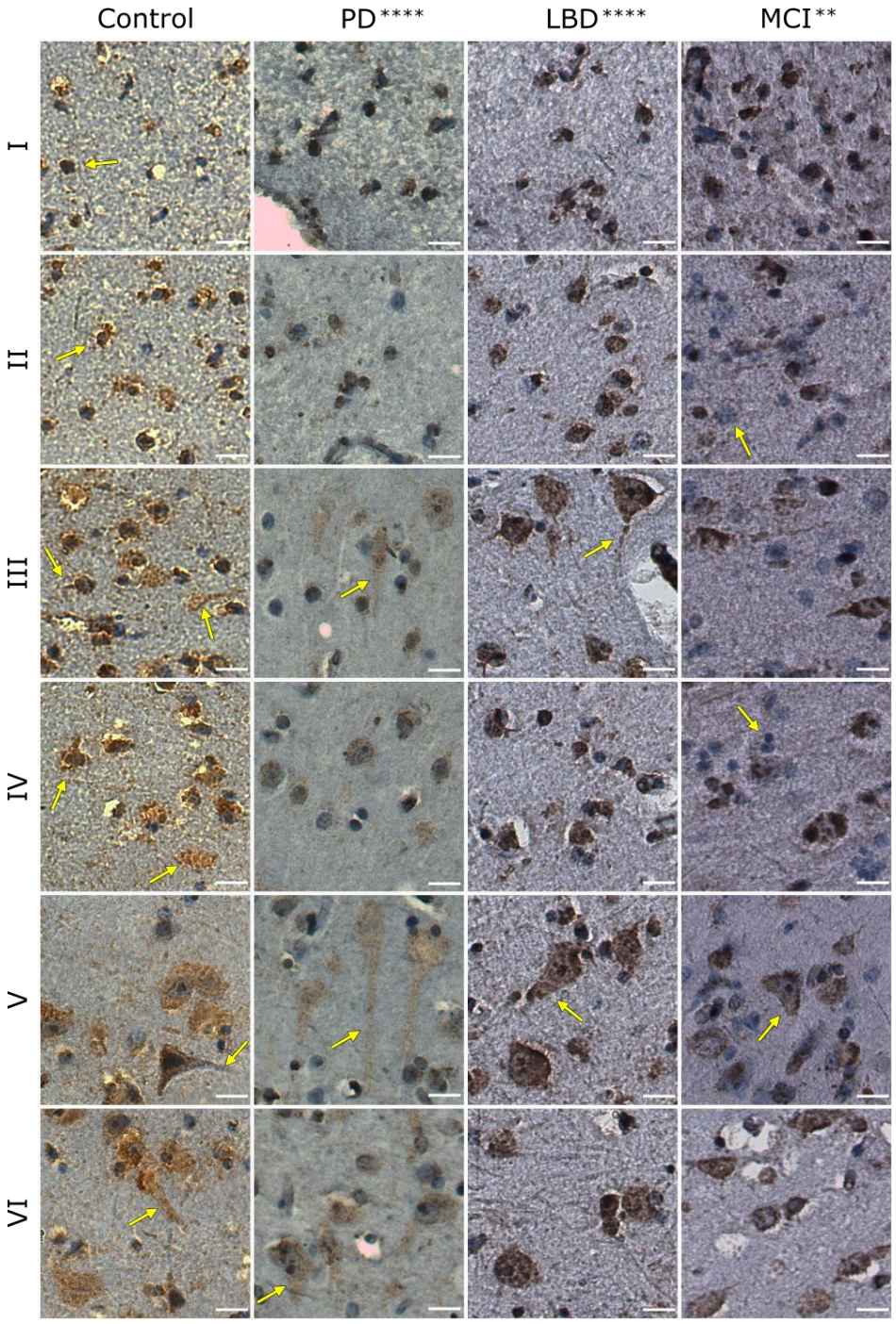

Figure 6.4 Expression of m^{6}A-modified transcripts varies by cortical layer and cell population of cingulate gyrus and changes in disease. m^{6}A-modified transcripts are expressed in all cells of all six cortical layers and the processes of pyramidal neurons. Sites and levels of m^{6}A-modified transcript abundance significantly change in disease. Overall expression decreases in PD and increases in LBD and MCI. Arrows point to sites where differential expression was observed between samples. n = 3 for each condition.** $p \leq 0.01$, **** $p \leq 0.001$. Scale bar = 20 µm.

The prevalence of m^6A reader protein YTHDF1 in the cingulate gyrus was also characterised (**Figure 6.5**). In control tissue, YTHDF1 expression was found to be low. Layers I and II of the cingulate gyrus reveal that although a majority of small cells are non-reactive, cells that did stain for YTHDF1 had high YTHDF1 immunoreactivity. In Layer III, small pyramidal neurons had high cytoplasmic expression of this protein, although only the base of processes were clearly observed. Expression in Layer IV small neurons was irregular, with some presenting all colour intensities from null to high immunoreactivity. Layer V large pyramidal neurons showed high levels of expression that were consistently located in the side of the cytoplasm opposite to the axon (polarised). Subsequently, Layer VI cells also had medium YTHDF1 expression levels that did not vary from one cell type to another.

YTHDF1 expression in disease-affected tissue was reduced. PD cingulate gyrus had a global reduction of YTHDF1 staining compared to unaffected controls ($p < 0.05$). This was most notable in Layer III, where pyramidal cell staining was low and did not delineate the cell's shape and processes, as opposed to the high and extensive staining observed in normal tissue. One other change was observed in Layer V, where low reactivity was spread throughout the cytoplasm and base of pyramidal neuron processes rather than the polarised medium immunoreactivity observed in normal tissue.

Other diseases had no overall differences in colour intensity ($p = 0.83$ and $p = 0.06$ for MCI) and few changes in a layer per layer analysis. LBD samples were found to have normal YTHDF1 expression in Layers I and

II. However, in other layers, immunoreactivity and expression patterns remained consistent with controls. Likewise, MCI samples only changed in Layers III and V, where immunoreactivity was lower and processes were not stained. All other cortical layers in MCI tissue were normal.

Taken together, these results present consistent changes in expression levels of YTHDF1 and m^6A methylation abundance, at least in PD and MCI affected tissue (this latter being non-significant in these samples). This suggests a link between the control of m^6A methylation levels and YTHDF1 protein translation and localisation.

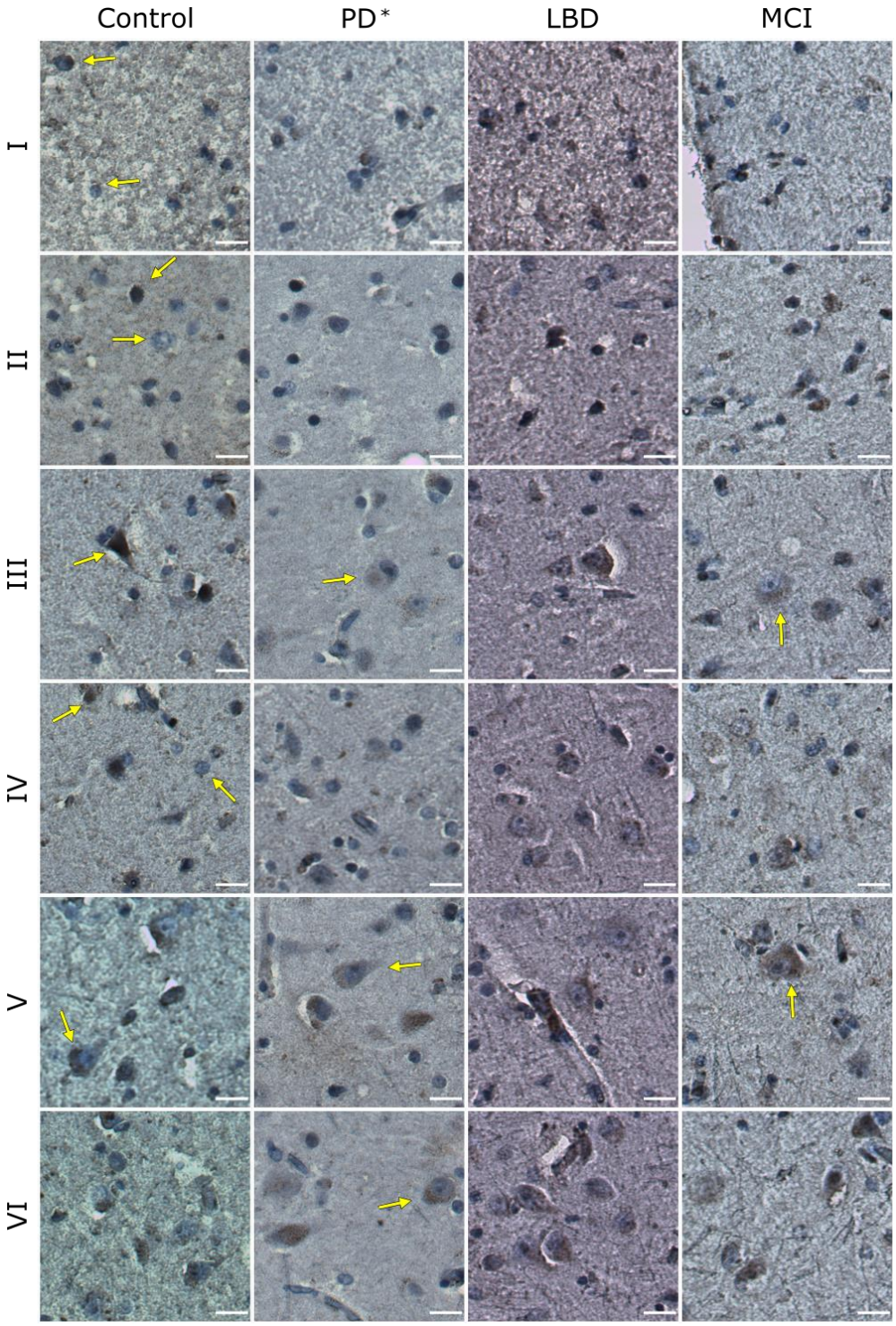

Figure 6.5 YTHDF1 expression varies by cortical layer and cell population of cingulate gyrus and changes in disease. YTHDF1 was expressed in all cells of all six cortical layers and pyramidal neurons. Sites and levels of YTHDF1 expression significantly change in disease. Overall expression was reduced in PD. Arrows point to sites where differential expression was observed between samples. n = 3 for each condition.* $p \leq 0.05$. Scale bar = 20 µm.

Next, YTHDF3 expression in the cingulate gyrus was characterised (**Figure 6.6**). In normal tissue, it was revealed that expression of this m^6A reader was high in all layers. Layers I, II, and IV all had dark DAB staining in the cytoplasm of small neurons. Layers III, V, and VI also contained pyramidal neurons with dark cytoplasmic staining. In pyramidal cells, neuronal process staining was not apparent in any layer. Combined with YTHDF1's characterisation, this result provides evidence of a difference in expression and location of YTH proteins in pyramidal neurons of the cingulate gyrus.

DAB staining of YTHDF3 in neurological disease-affected samples once more showed differences in global cortical expression depending on the tissue sample. Cingulate gyrus from PD individuals presented a global reduction in YTHDF3 immunoreactivity compared to controls ($p < 0.001$). This reduction was consistently observed in every cortical layer. Pyramidal neurons in Layers III and V showed more staining across the neuronal body, including the base of cells' axons. Meanwhile, YTHDF3 expression in LBD tissue saw a global increase ($p < 0.0001$) but no obvious differences in expression patterns. YTHDF3 immunoreactivity in MCI samples showed the same expression patterns as controls but quantitative analysis indicated an overall decrease in expression ($p < 0.001$). Changes in this disease tissue included an increase in non-reactive cells of Layer II, as well as high pyramidal cell expression in the cytoplasm and processes of Layers III and V.

Overall, these results suggest that YTHDF3 expression patterns and changes in normal and disease tissue follow those of m^6A methylation, similar to YTHDF1.

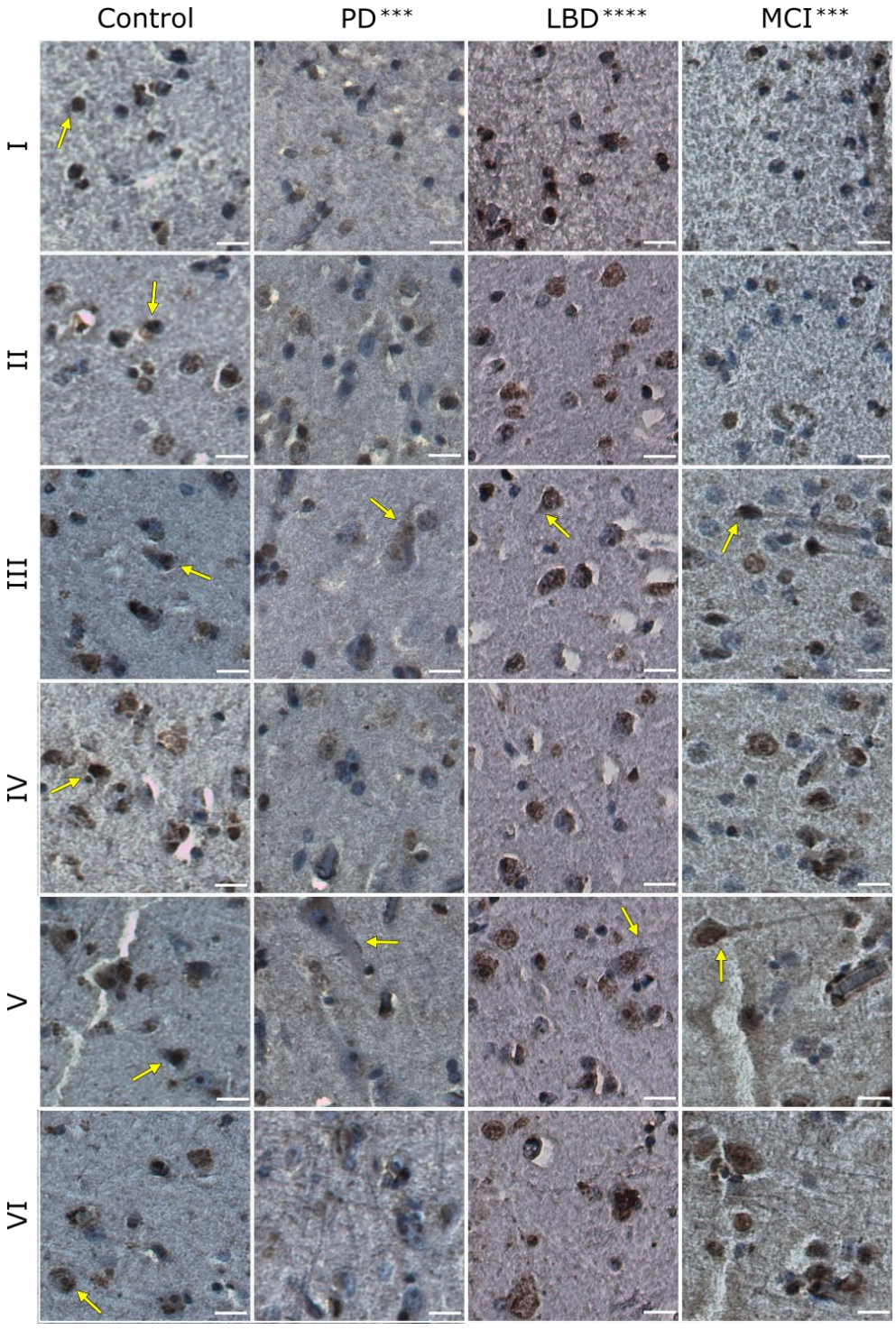

Figure 6.6 YTHDF3 expression varies by cortical layer and cell population of cingulate gyrus and changes in disease. YTHDF3 was expressed in all cells of all six cortical layers and pyramidal neurons. Sites and levels of YTHDF3 expression significantly change in disease. Overall expression decreased in PD and MCI but increased in LBD. Arrows point to sites where differential expression was observed between samples. n = 3 for each condition. *** $p \leq 0.001$, **** $p \leq 0.0001$. Scale bar = 20 μm.

6.2.3 Prefrontal Cortex

Immunohistochemistry was also performed in sections of prefrontal cortex. This area of the brain is implicated in complex behaviours such as planning, personality, decision making, and memory. Neuronal models of these behaviours involve the creation and pruning of synapses, therefore it is important to study mechanisms which may affect such processes, such as abundance of m^6A-modified transcripts and expression of m^6A readers.

m^6A methylation immunohistochemistry of the prefrontal cortex in control unaffected sections revealed generally medium immunostaining (**Figure 6.7**). Most small neurons in Layer I and II were highly abundant for m^6A modifications in the cytoplasm. Layer III also had medium immunoreacitivity of m^6A in the cytoplasm and neuronal processes of pyramidal cells. Layer IV, although the same cell type as Layer II, was found to have medium intensity staining. Layer V large pyramidal neurons had the same medium staining pattern observed in Layer III, evident in the cytoplasm and processes. In Layer VI, experiments revealed medium intensity staining in all cell types. These results suggest a difference in m^6A methylation levels between pyramidal cells of the prefrontal cortex and cingulate gyrus, with the former's cells showing process staining far more clearly.

Sections from disease-affected individuals revealed differences in methylation levels consistent with previous findings from cortical areas of the cingulate gyrus but staining localisation was generally unaffected. PD

samples saw a large decrease in m^6A modification abundance compared to controls ($p < 0.05$) but notably, expression in pyramidal neuron processes did not disappear. LBD samples showed a clear increase in m^6A methylation levels in both cytoplasm and processes of cells ($p < 0.01$).

Subsequently, changes in MCI-affected sections revealed an overall decrease in m^6A methylation levels in the whole cortex ($p < 0.01$) but mixed observations per neuronal layer. Layers I, II, and V all had a reduction of m^6A modification expression. Layer V in particular showed a further decrease in immunoreactivity in neuronal processes, the only instance in which process staining saw a difference. Layers III, IV, and VI, on the other hand, all showed varying degrees of increases in m^6A modification immunoreactivity. Pyramidal neurons in Layer VI of MCI samples showed a staining pattern similar to pyramidal cells in cingulate gyrus affected tissue, where m^6A expression was localised to the cytoplasm opposite a cell's axon (polarised). These results provide further evidence that there are differential effects on abundance of m^6A methylation associated with specific neurological diseases.

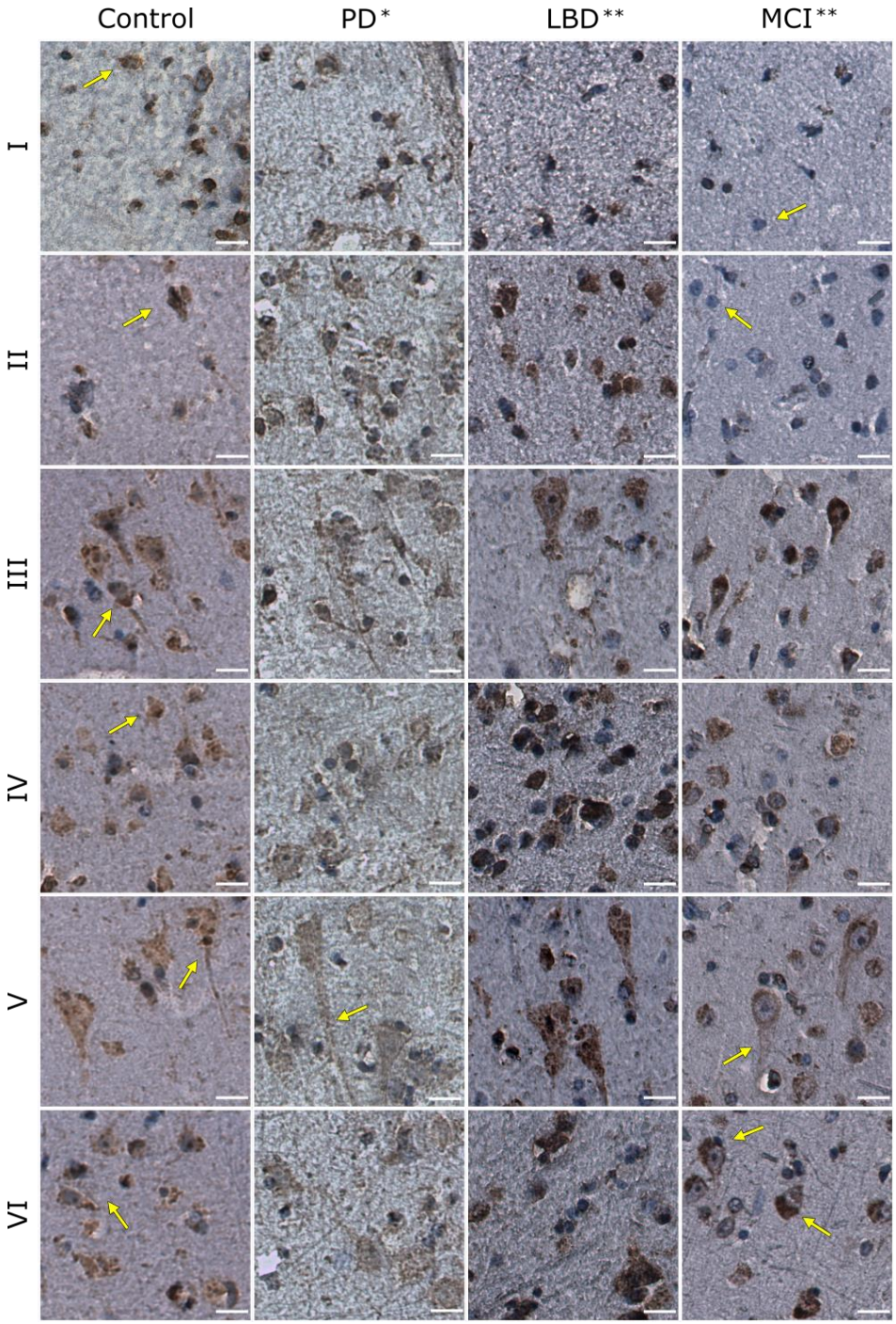

Figure 6.7 Abundance of m^{6}A-modified transcripts varies by layer and cell population of the frontal cortex and changes in disease. m^{6}A-modified transcripts are expressed in all cells of all six cortical layers and the processes of pyramidal neurons. Sites and levels of m^{6}A-modified transcripts significantly change in disease. Overall expression decreases in PD and MCI but increases in LBD. Arrows point to sites where differential expression was observed between samples. n = 3 for each condition. * $p \leq 0.05$, ** $p \leq 0.01$. Scale bar = 20 µm.

YTHDF1 immunohistochemistry revealed global low expression of this protein, consistent with what was seen in cingulate gyrus (**Figure 6.8**). Layers I and II were the exceptions as they both showed dark staining of cells. Layers III-VI showed rare dark staining but many non-reactive cells. This was especially notable in pyramidal cells of Layers III and V, where no process staining was detected. In Layer V, specifically, areas of immunoreactivity had a polarised pattern.

Expression levels in affected tissue presented reduced immunoreactivity in many layers but quantitative analysis showed no significant changes in colour intensity over the whole cortex compared to controls ($p > 0.15$, $p > 0.79$, and $p > 0.3$ for PD, LBD, and MCI respectively). PD samples were notable in that YTHDF1 immunoreactivity in pyramidal cells of Layers III and V, while still reduced, covered a larger area of the cytoplasm, ending at the base of neuronal processes. A reduction of YTHDF1 staining in LBD Layers I and II was not clearly discernible, but all other layers showed low reactivity or many more non-reactive cells. Once more, pyramidal neurons in Layers III and V were unique in that, although many were non-reactive, if they were stained, the colour intensity was high. Finally, MCI sections again had mixed expression changes. Layers I, II, and IV, which are characterised by their granular cell populations, all showed normal expression of YTHDF1. However, Layers III, V, and VI all had a reduction of immunoreactivity. Once more, it was observed that pyramidal cells in Layer V were mostly non-reactive but the few exceptions to this had high YTHDF1 expression.

Overall, changes in YTHDF1 expression in pyramidal cells appear to be most consistent with previous results for the cingulate gyrus. These results suggest that YTHDF1 may have a role in this cell type that is specifically affected in neurological disease.

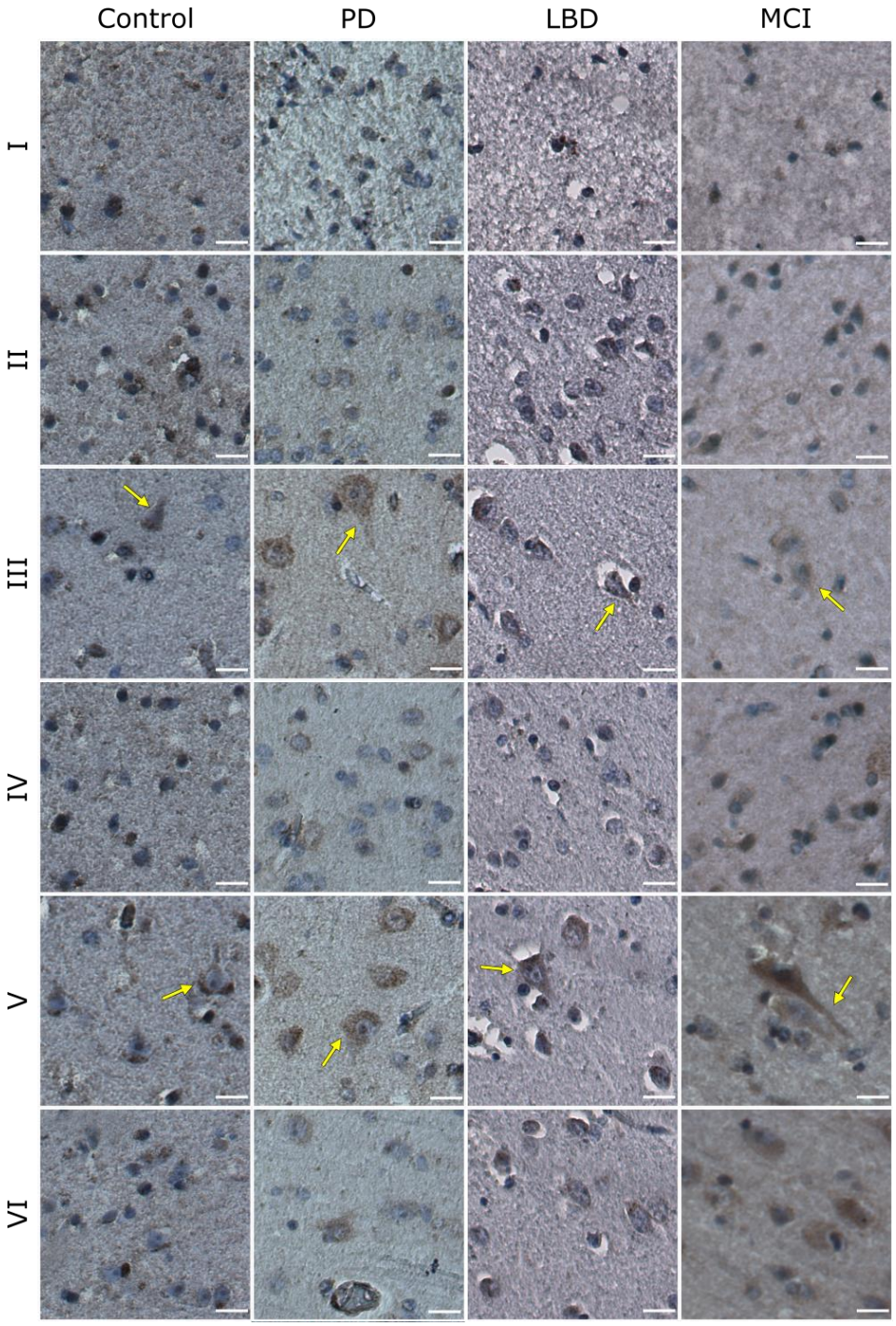

Figure 6.8 YTHDF1 expression varies by cortical layer and cell population of cingulate gyrus and changes in disease. YTHDF1 was expressed in all cells of all six cortical layers and pyramidal neurons. Sites and levels of YTHDF1 expression appear to change in disease, although this was not significant in a quantitative analysis. Arrows point to sites where differential expression was observed between samples. However, no global differences in staining were significant. n = 3 for each condition. Scale bar = 20 µm.

Lastly, YTHDF3 expression in normal brain was also characterised (**Figure 6.9**). Dark cytoplasmic staining was observed in Layers I-IV. Cells in Layer V, however, had reduced medium staining levels in the cytoplasm of large pyramidal neurons. Layer VI saw a large number of non-reactive cells, with light to medium colouring in cells expressing YTHDF3. Overall, YTHDF3 appears to be highly expressed in human prefrontal cortex.

Changes of YTHDF3 expression in neurological disease-affected tissue were consistent with changes in levels of m^6A methylation. Compared with unaffected controls, there were differences in the global expression of YTHDF3 in PD and LBD tissue ($p < 0.05$ for both). PD samples showed an overall decrease in DAB staining of YTHDF3 and polarised staining pattern in Layer V pyramidal neurons. In contrast, LBD prefrontal cortex showed an overall increase in YTHDF3 expression, as well as an increase in reactive cells. Polarised staining in Layer V was also observed in these sections. Lastly, MCI-affected sections saw no changes in Layers I-V. Layer VI showed more prevalent reactivity in all cell types and a slight increase in staining intensity.

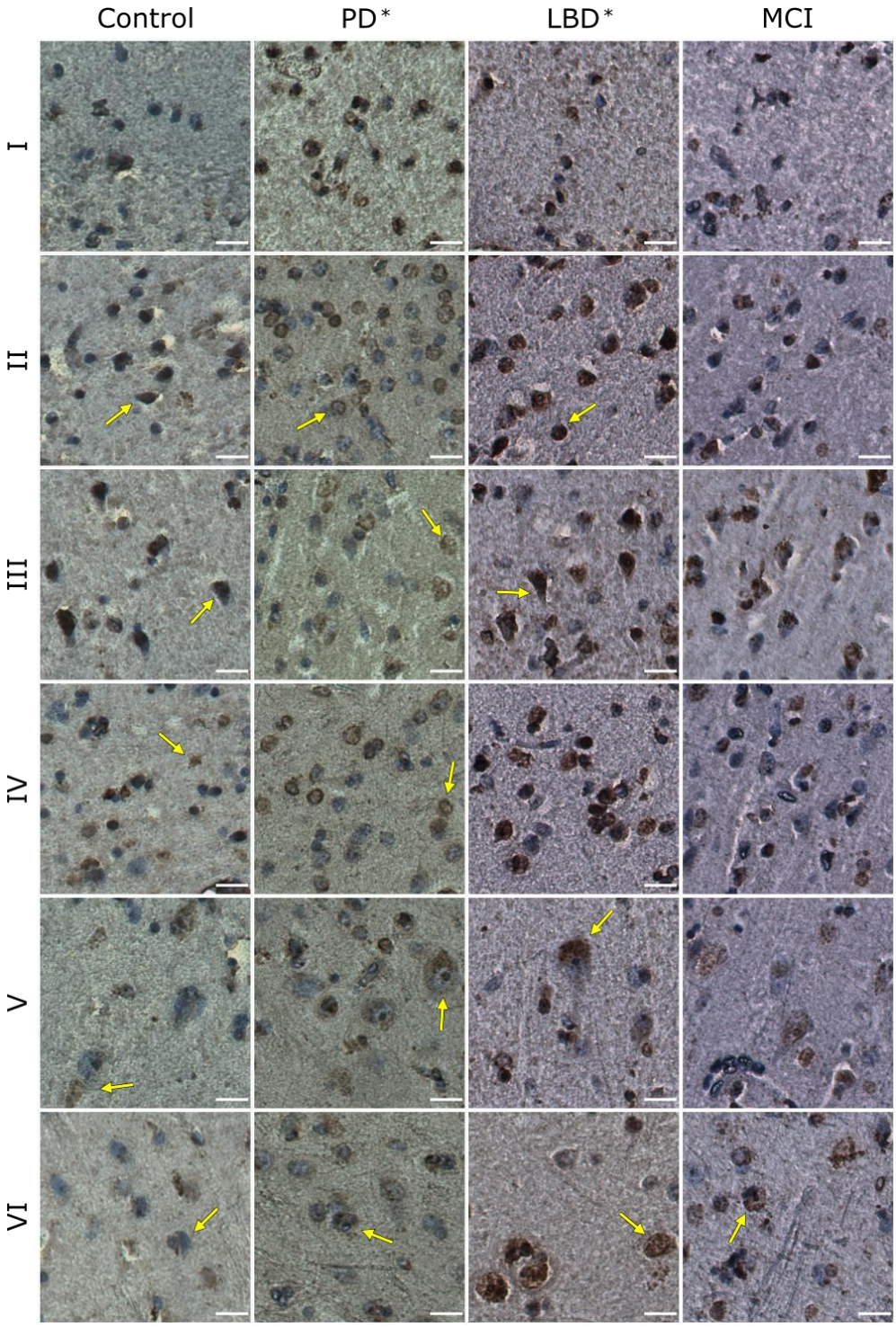

Figure 6.9 YTHDF3 expression varies by cortical layer and cell population of cingulate gyrus and changes in disease. YTHDF3 was expressed in all cells of all six cortical layers and pyramidal neurons. Sites and levels of YTHDF3 expression significantly change in disease. Overall expression decreased in PD but increased in LBD. Arrows point to sites where differential expression was observed between samples. n = 3 for each condition. * $p \leq 0.05$. Scale bar = 20 μm.

6.2.4 Hippocampus

The last brain region to be characterised was the hippocampus. This area of the brain plays a major role in the formation and consolidation of memory. The part of the hippocampus assessed here was the hippocampal formation, which is a compound structure containing the dentate gyrus (DG), subsections of the hippocampus proper or *cornu ammonis* (CA4-CA1), and the subiculum (SUB). Effective communication between these fields requires formation and pruning of synapses, and thus expression of m^6A modifications and m^6A reader proteins was studied to evaluate their potential involvement in this process of plasticity.

As before, immunohistochemistry was performed using an anti-m^6A antibody (**Figure 6.10**). This revealed prevalent immunoreactivity of m^6A-modified RNA and medium to high staining in all subregions, beginning with the dentate gyrus. Large areas of granular cell cytoplasm were observed to be reactive, as well as some of their processes.

In the CA4 region, there were medium levels of methylation in large pyramidal cells and inhibitory basket cells. In both cell types, neuronal processes were m^6A-reactive with the same colour intensity. Levels of m^6A modifications were also medium in CA3/CA2 pyramidal cells, consistent with previous regions.

In CA1 pyramidal cells, there was some variation of abundance levels. m^6A modification immunoreactivity in this region was medium in some cells or high in others with no discernible pattern. All pyramidal cells

(identified by the presence of a blue-stained nucleus) in the CA1 field showed cytoplasmic and process immunoreactivity, making this an area of particularly prevalent m^6A modification abundance. Finally, abundance levels in the subiculum were medium, although few processes were found to be reactive.

Taken together, the high prevalence of m^6A modifications in all fields of the hippocampal formation suggests a potentially important role in normal synaptic function. Furthermore, consistent staining of neuronal processes in CA field pyramidal neurons suggests that one of the roles of this mRNA modification involves neuron to neuron sites of communication, i.e. synapses.

Global levels and subcellular areas of m^6A modification abundance saw differences in disease-affected tissue. In PD, m^6A-methylated mRNA was reduced compared to controls ($p < 0.0001$). PD dentate gyrus colour intensity was lower and no processes were observed to be reactive. PD CA4 and CA3/CA2 pyramidal cell processes were less often reactive. Despite overall reduction in abundance, CA1 immunohistochemistry showed m^6A-modified transcripts were still in most processes.

Overall, global levels of m^6A modifications were significantly enhanced in LBD-affected sections ($p < 0.0001$). Apart from this, expression patterns in all hippocampal fields were consistent with controls, including process staining.

However, m^6A methylation profiles seem to be more dysregulated in MCI hippocampal formation. In these samples, quantitative analysis revealed

an overall decrease in expression levels ($p < 0.0001$). This includes a decrease in methylation levels in the dentate gyrus and all CA fields. Moreover, the dentate gyrus also contained many non-reactive granular cells and presented no process immunoreactivity. Process staining in pyramidal cells was stunted in all CA fields, most surprisingly in the CA1 field where very few cells were found to have m^6A modifications. Subsequently, the subiculum in these samples showed an increase in m^6A methylation levels but few processes were reactive.

These drastic changes in methylation in neurological disease, particularly in MCI samples, suggest that m^6A methylation is a key mechanism of RNA processing that is dysregulated in the hippocampus. Disruption to m^6A modifications at neuronal processes raises the question of how these methylated mRNA molecules are transported to synaptic sites.

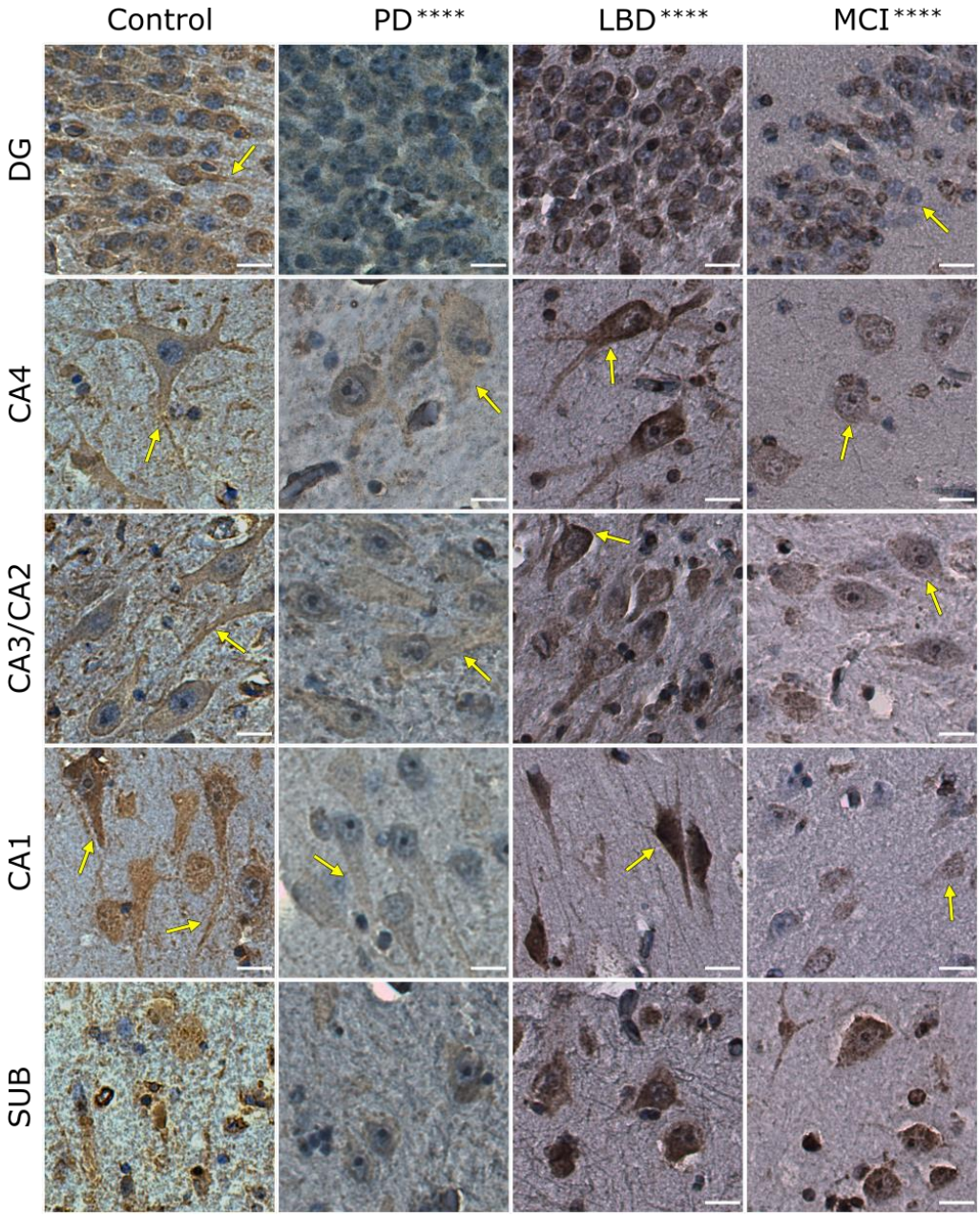

Figure 6.10 m^{6}A-modified transcripts are highly abundant in the hippocampal formation of healthy and diseased hippocampus.m^{6}A-modified transcripts were found to be highly prevalent in granular cells of the dentate gyrus and pyramidal neuron cytoplasm and processes. Immunohistochemistry in disease samples found changes in global m^{6}A levels and neuronal process staining. Overall abundance decreased in PD and MCI but increased in LBD. Arrows point to sites where differential expression was observed between samples. n = 3 for each condition. **** $p \leq 0.0001$. Scale bar = 20 µm.

Immunohistochemistry of m^6A reader YTHDF1 in normal brain revealed generally low expression across the whole hippocampal formation (**Figure 6.11**). The dentate gyrus showed low cytoplasmic immunoreactivity in all granular cells. The cytoplasm of CA4 cells showed high colour intensity, although the areas of reactivity were restricted to the perimeter of the nucleus. In CA3/CA2 and CA1 pyramidal neurons, in contrast, YTHDF1 immunoreactivity was observed in the cytoplasm and some neuronal processes. Expression of YTHDF1 in CA1 pyramidal neurons was prevalent, although staining intensity varied from low to high between cells. Finally, the subiculum presented low YTHDF1 expression, mainly in the cytoplasm of small neurons. Overall, these experiments suggest that YTHDF1 expression is highest in pyramidal neurons of the *cornu ammonis* fields.

YTHDF1 expression in the hippocampal formation changed significantly in disease-affected tissue. PD tissue saw an increase in expression in the dentate gyrus and CA fields compared to controls ($p < 0.0001$). PD CA4 and CA3/CA2 pyramidal neurons showed immunoreactivity in larger areas of the cytoplasm and neuronal processes. In the CA1 field, YTHDF1 staining was low and exclusively cytoplasmic in most cells with overexpression a few pyramidal cells.

There was also a global increase of YTHDF1 expression in LBD tissue ($p < 0.0001$). LBD CA4 pyramidal cells showed YTHDF1 localised to larger areas of the cytoplasm and the base of axons. In all CA fields from LBD-affected brain, YTHDF1 expression was increased.

Contrary to changes in other diseases, immunohistochemistry on tissue from MCI-affected patients revealed a dramatic global decrease in YTHDF1 expression throughout the hippocampal formation ($p < 0.01$). Dentate gyrus, CA4, CA3/CA2, and subiculum cells all presented low or null immunoreactivity. Once again, expression in the CA1 field of diseased tissue varied between cells. Most of these pyramidal neurons had very low cytoplasmic expression of YTHDF1. A few cells, however, had normal staining intensity and patterning.

Overall, changes in YTHDF1 expression in neurological disease-affected hippocampal formation were unique. These results suggest that YTHDF1 expression is increased in Parkinsonism but decreased in cognitive disorders. Additionally, variation in YTHDF1 expression in CA1 pyramidal neurons appears to be normal but is accentuated in neurological disease.

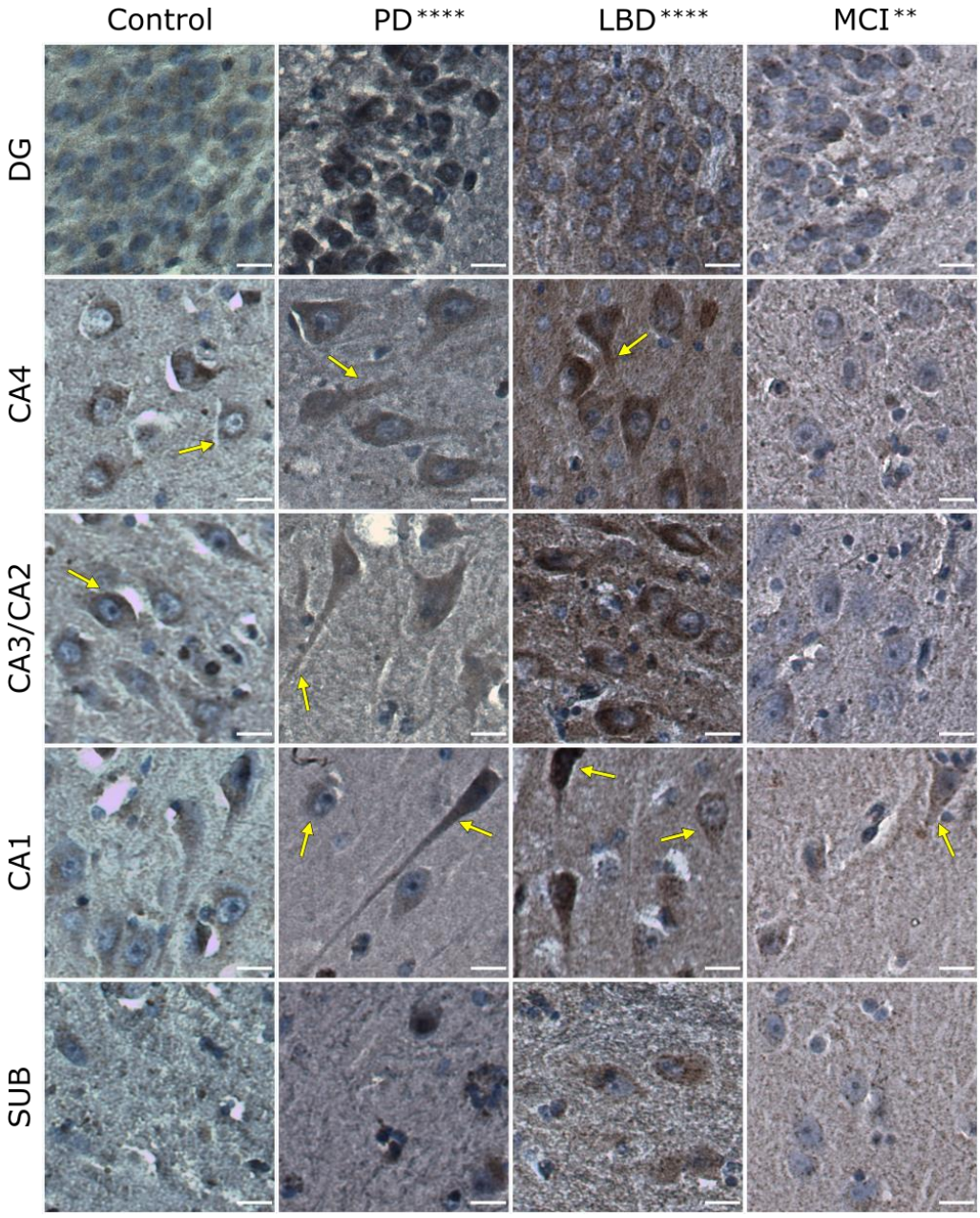

Figure 6.11 YTHDF1 is highly expressed in the hippocampal formation of healthy and diseased hippocampus. YTHDF1 was highly expressed in granular cells of the dentate gyrus and pyramidal neuron cytoplasm and processes. Immunohistochemistry in disease samples found changes in global YTHDF1 expression and neuronal process staining. Overall expression increased in PD and LBD but decreased in MCI. Arrows point to sites where differential expression was observed between samples. n = 3 for each condition. ** $p \leq 0.01$, **** $p \leq 0.0001$. Scale bar = 20 μm.

Finally, YTHDF3 expression was also evaluated (**Figure 6.12**). Immunohistochemistry revealed that YTHDF3 was generally highly expressed in small areas of the cytoplasm. In the dentate gyrus, many granular cells were non-reactive. Process staining was not apparent in pyramidal neurons of any of the CA fields. However, in these cells, YTHDF3 has a unique ring-like pattern of immunoreactivity. Subsequently, neurons in the subiculum varied between non-reactive and high YTHDF3 expression. These experiments suggest that YTHDF3 localisation is limited to the cytoplasm in pyramidal cells.

Characterisation of YTHDF3 expression in diseased tissue was highly variable. In PD, for example, quantitative analysis indicated a global increase of YTHDF3 immunoreactivity ($p < 0.0001$). For example, abundance in the dentate gyrus and CA3/CA2 increased. All other regions remained unaffected.

Observations in LBD-affected samples signalled an increase in immunoreactivity in the dentate gyrus and all CA fields which was not backed up by quantitative analysis ($p > 0.07$). Furthermore, some CA1 field pyramidal neurons highly expressed YTHDF3 in neuronal processes.

Lastly, YTHDF3 immunoreactivity in MCI did not significantly change compared to control tissue ($p > 0.89$).

Overall, the variability in results of YTHDF3 immunohistochemistry in diseased tissue makes it difficult to see a trend. Perhaps the most consistent features of these experiments are the larger areas of reactivity

in PD and LBD samples followed by the ringed staining pattern in CA pyramidal neurons.

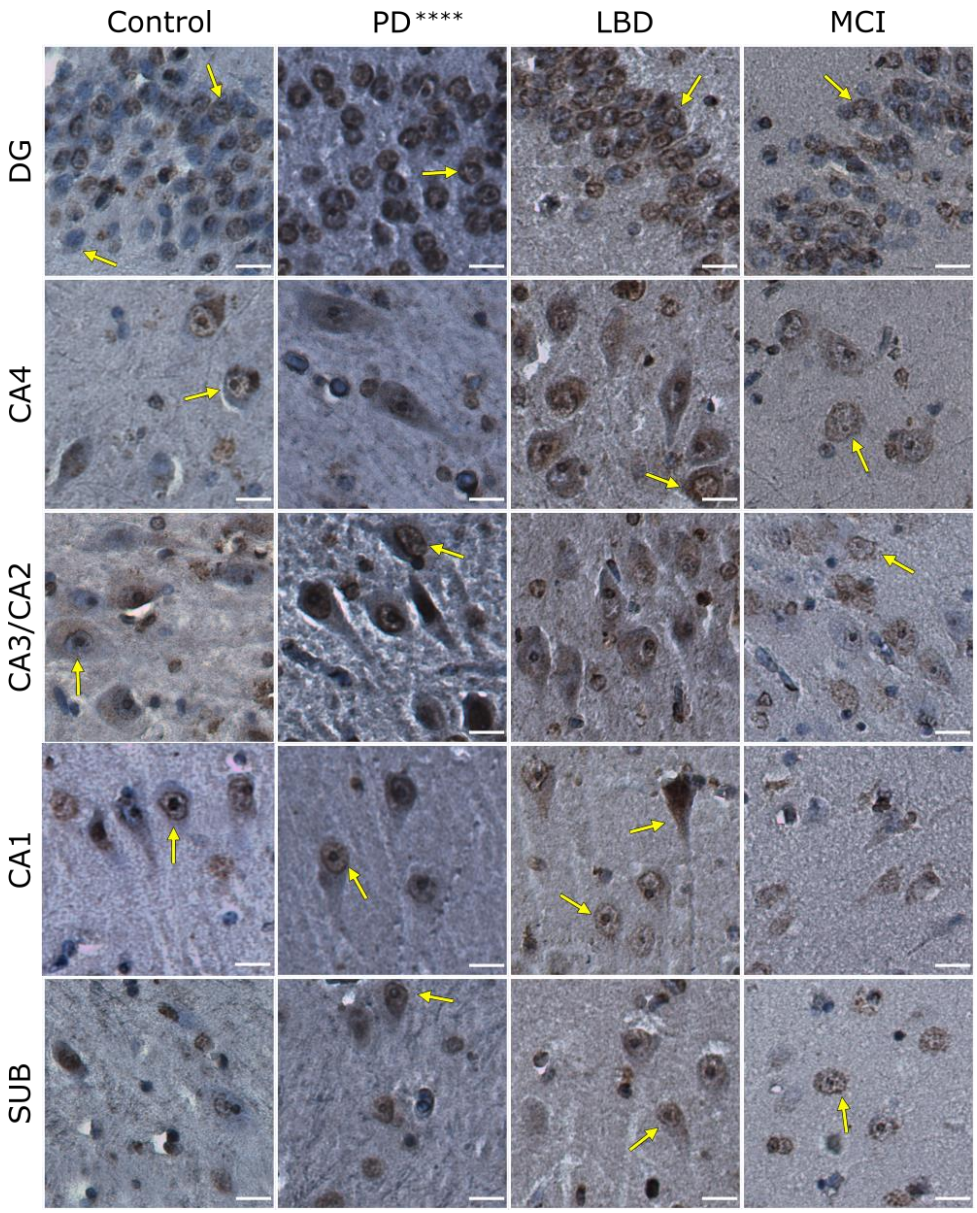

Figure 6.12 YTHDF3 is highly expressed in the hippocampal formation of healthy and diseased hippocampus. YTHDF3 was highly expressed in granular cells of the dentate gyrus and pyramidal neuron cytoplasm. YTHDF3 showed unique ring-like staining in CA fields of both healthy and diseased hippocampus. Immunohistochemistry in disease samples found changes in global YTHDF3 expression and neuronal process staining. Overall expression increased in PD and LBD. Arrows point to sites where differential expression was observed between samples. n = 3 for each condition. **** $p \leq 0.0001$. Scale bar = 20 µm.

6.2.5 Ependymoma and Glioblastoma

Additionally, m^6A methylation levels were characterised in two different type of tumours found in the central nervous system. One of these was ependymoma, which is derived from neuroepithelial cells called ependyma which line the cerebrospinal fluid's (CSF) ventricular system of the brain. This is a tumour that grows slowly but has a poor prognosis due to malignant cell propagation through CSF (Khatua et al., 2017).

Immunohistochemistry using the same anti-m^6A antibody was performed in primary ependymoma (**Figure 6.13**). Expression of m^6A modifications was highly variable throughout areas of the tumour with areas showing either medium or low staining. A high fraction of tumour cells, approximately half, were non-reactive. This was consistent between areas of primary tumours. Rosettes in primary ependymoma, a hallmark structure consisting of tumour cells surrounding empty lumen (Reni et al., 2017), were found to contain a few cells which had higher m^6A immunoreactivity (**Figure 6.13A**, arrow). Rosettes had a consistent number of non-reactive cells relative to the rest of the tumour.

m^6A prevalence in recurrent ependymomas, derived from the same individuals as primary tumours, was also characterised. Overall, m^6A immunoreactivity in these tumours was decreased compared to primary tumours ($p < 0.0001$) and the number of non-reactive cells was increased relative to primary tumours. m^6A abundance across the tumour was consistent. A large pseudorosette (similar to a rosette; **Figure 6.13C**,

arrow) showed that m^6A expression did not change in the cells around this structure.

Endothelial cells surrounding blood vessels in both types of ependymomas also showed differences in expression (**Figure 6.13B** and **D**, arrows). In primary tumours, these cells had high immunostaining but had very low reactivity in recurrent tumours. This may be due to the differences observed in the rest of the tumours or may be influenced by tumour progression.

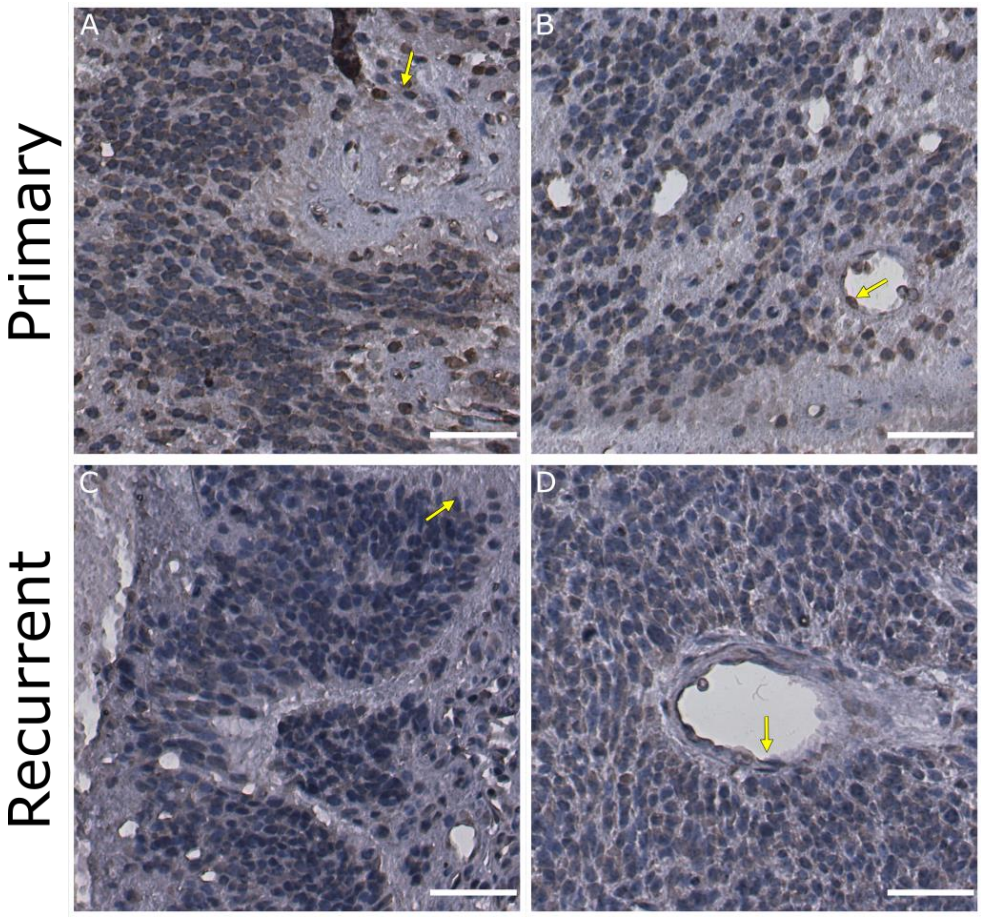

Figure 6.13 m^6A modification levels in ependymomas are decreased in recurrent tumours. Primary ependymoma IHC-DAB shows low levels of m^6A-modified transcripts. In primary tumours (top), arrows point to cells in rosettes (A) and endothelial cells (B) were found to highly express m^6A, while similar structures (C, D) in recurrent tumours did not show such abundance. n = 2 for each condition. Scale bar = 50 µm.

Experiments were also performed on primary paediatric glioblastoma tumours. Glioblastomas are fast-growing tumours with a median survival of one year and the role of m^6A methylation has previously been studied in glioblastoma stem-like cells (Batista & Yang, 2017). In this study, m^6A methylation was studied in human childhood glioblastoma for the first time.

The profile of m^6A modifications in glioblastoma was observed to resemble that of primary ependymoma. Quantitative analysis revealed mean pixel intensity values of 138 and 135 in ependymoma and glioblastoma primary tumours, respectively. Glioblastoma samples also exhibited variability in expression (medium to high) and a high number of non-reactive cells.

Some classic features of childhood glioblastoma were identified in which to assess m^6A methylation expression (Maher & Bachoo, 2015). Anaplastic cells, in which cellular organisation is in disarray, covered most of the tumour and did not show much variation in staining (**Figure 6.14A**). Microvascular proliferation was identified and it was found that in glioblastomas, endothelial cells surrounding vessels did not have a high level of m^6A methylation, in contrast with ependymomas. Furthermore, mitotic cells were identified and found to consistently express m^6A modifications (**Figure 6.14B**). Lastly, pseudopalisading necrosis (Rong et al., 2006), acellular areas surrounded by parallel-facing tumour cells, revealed a high proportion of non-reactive cells (**Figure 6.14C**).

Taken together, immunohistochemistry in brain tumours suggests a progressive downregulation of m^6A methylation. Results suggest there is variation across tumour-specific structures, which may influence their formation. Further experiments could be complemented by use of m^6A-binding proteins and markers of tumour progression such as p53 or Ki67 in order to understand the possible function of m^6A methylation through the different stages of cancer.

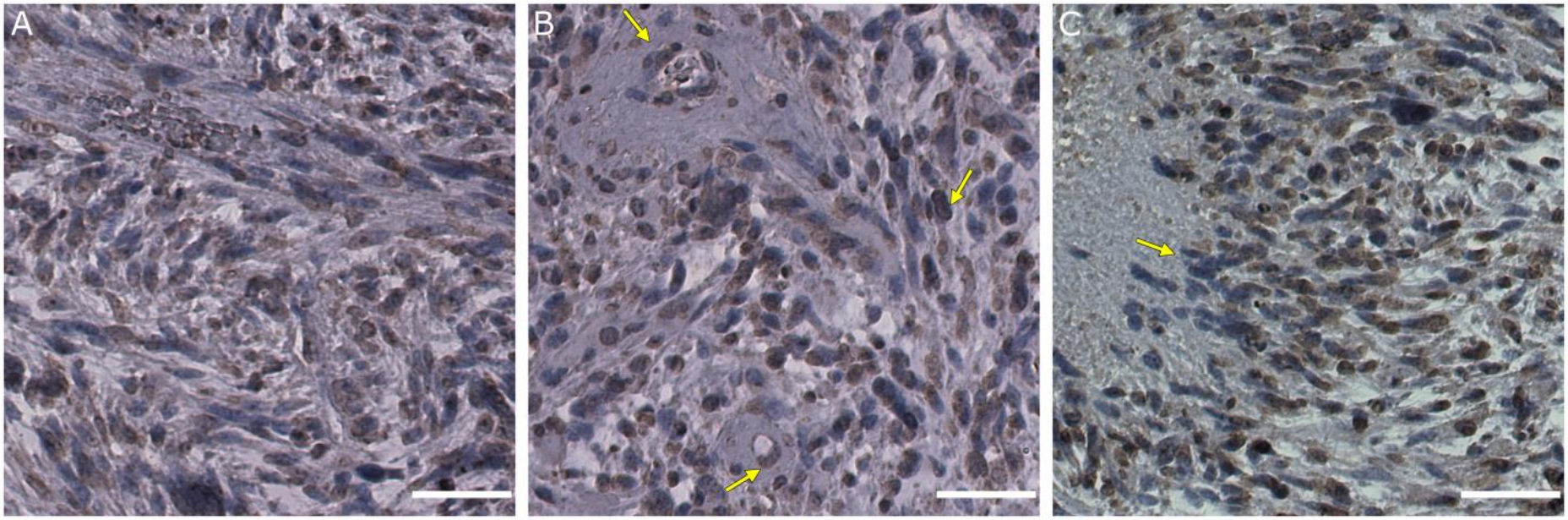

Figure 6.14 m^{6}A modification abundance changes throughout primary glioblastomas. Abundance of m^{6}A varied from null to high in paediatric glioblastoma. Hallmark structures of anaplasia (A) and mitotic cells (B) showed medium to high expression, while microvascular proliferation (B) and pseudopalisading necrosis (C) presented low or no m^{6}A modifications. n = 2. Scale bar = 50 µm.

6.3 Discussion

Post-transcriptional modifications have previously been shown to be essential in the regulation of translation in cells (Dominissini, 2014) and normal organism development (Bodi et al., 2012), but thus far research has not satisfactorily bridged the gap how m^6A-mediated regulation of translation is reflected in human neurobiology. Here, the first work is presented attempting to understand how m^6A modifications and related proteins are expressed in healthy human brain and what defects in methylation correlate to neurodegeneration and neuro-oncological disease. **Table 6.1** summarises the quantitatively significant changes (compared to controls) observed throughout the immunohistochemistry of PD, LBD, and MCI affected tissue.

		m^6A	YTHDF1	YTHDF3
Parkinson's Disease	CB		-	+
	CG	-	-	-
	PFC	-		-
	HIP	-	+	+
Lewy Body Dementia	CB	+	-	+
	CG	+		+
	PFC	+		+
	HIP	+	+	+
Mild Cognitive Impairment	CB	+	-	+
	CG	+		-
	PFC	-		
	HIP	-	-	

Table 6.1 Summary table of the changes in m^6A abundance and YTHDF1/YTHDF3 expression in immunohistochemistry of affected tissue, compared to controls. CB = Cerebellum, CG = Cingulate Gyrus, PFC = Prefrontal Cortex, HIP = Hippocampus.

There is growing evidence which suggests the cerebellum may play a role in the pathology of Parkinsonism (including PD and LBD), cognitive disorders, and other diseases with similar symptoms (Louis, 2016; Wu & Hallett, 2013). Therefore, m^6A, YTHDF1, and YTHDF3 were examined in the cerebellum, and one key feature observed was that Purkinje cells and Purkinje cell processes both clearly showed abundance of all three markers. However, Purkinje cells were all clearly different in disease tissue with a near total disappearance of process staining and inconsistent cytoplasmic staining. m^6A methylation depletion in Purkinje cell processes are consistent with findings of synaptic defects and Purkinje neuron loss in parkinsonism (Rolland et al., 2007; Takada et al., 1993) which would suggest a reduction in translation or other m^6A-mediated RNA processing. Moreover, these neuronal losses are thought to be initiated by pathological changes to dopaminergic projections received by the cerebellum (Kishore et al., 2014), neuron to neuron contacts in which defects in m^6A methylation and m^6A readers might result in a loss of dopaminergic receptor expression.

Another factor possibly contributing to a change in receptor expression is the high expression of YTHDF1 in normal human brain followed by a near total loss of YTHDF1 in disease tissue, at least in Purkinje processes. High expression of this protein in normal brain suggests that YTHDF1-mediated regulation of translation of m^6A-modified transcripts is highly important to the healthy cerebellum and its motor functions. A loss in YTHDF1 expression could thus easily lead to dysregulation of

protein expression in all parts of Purkinje cells, first contributing to synaptic defects and possibly to cell death.

Due to the severity of this defect, it is interesting that YTHDF3 was found to be expressed in Purkinje cells only in disease tissue. Part of the current understanding of this protein is that it can perform the same functions as YTHDF1 and YTHDF2 (Shi et al., 2017; Wang et al., 2014b). Therefore, it is possible that YTHDF3 may be expressed in disease-affected cerebellum as a compensatory mechanism for YTHDF1. Curiously, reduction of m^6A-modified transcripts would suggest expression of YTHDF3 is unnecessary. If this were the case, then YTHDF3 may have some other unknown role. Further research could test this by creating YTHDF1-knockdown Purkinje cells in a model organism and assessing whether YTHDF3 expression is increased in the absence of any other dementia-related effects.

Currently, there is no clear known common cause of sporadic Parkinson's disease or Lewy Body Dementia. However, protein aggregates composed of α-synuclein are a feature of both conditions, forming abnormal deposits at both pre- and post- synaptic sites that have been shown to be toxic in PD and LBD (Colom-Cadena et al., 2017; Schulz-Schaeffer, 2010) and correlating with survival (Irwin et al., 2017). It seems that some of the only differences between these two diseases are the areas of cell loss and timing of Lewy body formation. In PD, cell loss is more severe in the midbrain and hindbrain (Pedersen et al., 2005; Tsuboi & Dickson, 2005), possibly influenced by neurotransmitter and corresponding receptor loss (Halliday et al., 2014). Meanwhile, LBD is

defined by the early onset of Lewy bodies in cortical regions but in PD, these neuropathological changes may not develop for up to 20 years (Ruffmann et al., 2016).

Such differences are supported in the current study by immunohistochemistry in cortical regions which revealed similar findings between them. In general, it was observed that m^{6}A-modified transcripts were less abundant in PD, more abundant in LBD, and effects varied in MCI. The finding that m^{6}A-modified RNA is abundant in the cortex of LBD individuals but not in PD suggests that m^{6}A methylation is involved in the overexpression of α-synuclein which leads to the formation of Lewy bodies.

Further supporting this hypothesis, the gene encoding for α-synuclein, *SNCA*, was previously found to be methylated in human adult brain (Chapter 3). Subsequently, expression of m^{6}A-modified transcripts and m^{6}A readers in cortical regions, while low, remained higher than in the cerebellum. This suggests that synaptic dysfunction and cell death caused by loss of neurotransmitter receptors are stalled by translation of remaining m^{6}A-modified transcripts. Taken together, it appears differences in m^{6}A methylation levels between PD and LBD correlate to the regional progression of each disease.

Additionally, YTH protein levels positively correlated with changes in m^{6}A methylation. In fact, it was found that YTHDF1 remains normal in PD (YTHDF3 only slightly reduced), increasing the expression of methylated transcripts.

One more recurrent difference observed in cortical layers was the change in m^{6}A methylation in pyramidal cells and their neuronal processes. In cortical layers III and V, which contain pyramidal neurons, changes in staining of m^{6}A readers extended beyond abundance and included differences in neuronal processes and cytoplasm. Generally, m^{6}A readers were located in neuronal processes in normal brain, but PD and LBD cortices showed much reduced expression and sometimes polarised localisation of both readers. Previous reports have found selective neuronal loss in pyramidal and other neurons of the motor cortex and midbrain (MacDonald & Halliday, 2002; Surmeier et al., 2017), finding that common characteristics included high levels of arborisation and long axons, such as the ones in cortical pyramidal neurons. Changes in m^{6}A-mediated maintenance of processes and synapses may have significant repercussions in the connectivity and cell viability of the cortex and thus may be one factor in cognitive and behavioural changes characterising these diseases.

Observations in the hippocampus differed from other regions. Despite significant changes in abundance of m^{6}A-modified transcripts and expression of m^{6}A readers, staining of neuronal processes was conserved in pyramidal neurons in the CA fields of PD and LBD samples. Although the hippocampus in Parkinson's disease and Lewy Body Dementia is associated with atrophy and reduced volume (Camicioli et al., 2003; Laakso et al., 1996), these effects are not as pronounced as they are in Alzheimer's disease (AD). In fact, selective neuronal loss in PD and LBD is reportedly subdued in the hippocampus, relative to other

brain regions (Mattson & Magnus, 2006). Results from m^{6}A immunohistochemistry suggest that methylation is one regulatory process that is also protected in these diseases and is possibly a causative factor in the preservation of synapses and pyramidal cells.

Along a decrease in overall atrophy, regions of the hippocampal formation also undergo differential atrophy (Mak et al., 2016). The abundance of m^{6}A methylation and expression of m^{6}A readers were particularly consistent in CA1 neuronal processes across healthy and disease individuals. However, some CA3/CA2 processes did not express m^{6}A readers. This finding is consistent with reports that CA1 pyramidal neurons are spared from degeneration (von Gunten et al., 2005) but CA3/CA2 neurons were found to have the most significant cell loss (Dickson et al., 1991; Mak et al., 2016).

Furthermore, it has been reported that glutamatergic, dopaminergic, cholinergic neurons of the CA1 field are highly protected in PD and LBD (Hall et al., 2014), in contrast to a characteristic cell loss in Alzheimer's disease (Bobinski et al., 1998). The main receptor subunits for each of these neurotransmitters have been found to be methylated (Chapter 3), which suggests that even in disease tissue, m^{6}A methylation is an important regulatory mechanism of neurotransmitter receptor expression. The conservation of m^{6}A modifications are thus a possible protective mechanism in neurons of the hippocampal formation.

m^{6}A reader expression was found to increase in PD and LBD hippocampus. Alongside variations in overall m^{6}A methylation levels, this

change in disease tissue suggests that YTHDF1 and YTHDF3 are needed to increase the rate of translation of m^{6}A-modified transcripts and maintain normal protein levels in these cells. However, expressions of methyltransferases, i.e. m^{6}A writers, and demethylases, i.e. erasers, have not yet been studied in neurodegenerative disease.

It is also possible that the differences observed are the result of m^{6}A writer genetic mutations. This is less likely to be the case as there is little current evidence in neurodegenerative disease of changes in expression of proteins whose transcripts are m^{6}A-modified, such as dopamine receptors or BDNF (Calabresi et al., 2013; Mercado et al., 2017). To evaluate these possibilities, further research could assess expression of m^{6}A writers and m^{6}A-modified synaptically-enriched proteins, including neurotransmitter receptors, in control, PD, and LBD tissue.

Although differential neuropathology is common across regions in neurodegenerative disease, there is also the possibility that a global dysregulation is an initial factor. Rare familial mutations within the gene, *HNRNPA2B1*, which encodes an m^{6}A reader that mediates m^{6}A-dependent RNA processing events, are reported to cause neurodegenerative conditions such as multisystem proteinopathy and ALS (Alarcón et al., 2015; Kim et al., 2013; Liu et al., 2015). Furthermore, the protein HNRNPA2B1 has been shown to be involved in the formation of 'liquid droplets', a process described as the rapidly assemble and disassemble of protein aggregates and RNA in response to changes in the cellular environment (Lin et al., 2015; Zhang et al., 2015).Such behaviour is reminiscent of the formation of alpha-synuclein aggregates

which plague all regions of PD and LBD brain with different severity, and suggests that m^{6}A methylation mechanisms could control gene expression of hub proteins which form protein aggregates.

For the first time, m^{6}A expression was assessed in primary and recurrent human brain tumours. These results were consistent with previous work which indicated m^{6}A methylation is decreased in glioblastoma stem-like cells (Cui et al., 2017; Zhang et al., 2017). Despite an overall dysregulation of m^{6}A methylation, evidenced by a high number of non-reactive tumour cells, primary tumours were found to have areas of high or low m^{6}A modification expression. It has previously been reported that human lung cancer cells show high levels of m^{6}A writer METTL3 (Lin et al., 2016). Although this report suggested METTL3 promotes translation in these cells, no other evidence of such activity has been published. It may be, then, that the different levels of m^{6}A methylation observed across primary tumours in this study are partly due to aberrant METTL3 expression impacting its principal role as a methyltransferase. Further research characterising METTL3 expression and mutations in its corresponding gene may elucidate the reasons for such highly variable m^{6}A expression.

Tumour heterogeneity represents a significant challenge in the development of effective treatment strategies, a problem which would arise during the development of therapeutic control of m^{6}A methylation in primary tumours. Attempts at maintaining normal levels of m^{6}A-modified transcripts through gene or drug therapies would likely induce overexpression of m^{6}A modifications and result in tissue death or other

unknown disadvantages. However, the finding that recurrent tumours were much more homogenous in their expression of m^{6}A modifications posit them as better targets for such therapies.

In glioblastomas, pseudopalisading necrosis was found to be surrounded by cells with depleted m^{6}A methylation. Such glioblastoma structures are associated with the deadlier later stages of the disease and therefore, studying the genetic or epigenetic abnormalities in these cells may be key in understanding the progressive dysregulation of m^{6}A methylation and its related functions in glioblastomas.

Recently, YTHDF1-deficient mice were found to have an elevated anti-tumour response, although m^{6}A methylation was not investigated in their study (Han et al., 2019). Such approaches are likely to be the first applications of our knowledge of m^{6}A methylation in disease and will guide future development of therapies. Given further research into the m^{6}A epitranscriptome of any of the diseases studied here, pathological m^{6}A-modified transcripts could be identified. Indeed a lab with which my lab collaborate has already identified several pathways which are specifically dysregulated in childhood brain tumours (unpublished data). Thus, modulation of such proteins through the manipulation of m^{6}A methylation dynamics may rescue the normal phenotype. It is important to note that although current research has targeted m^{6}A readers, any m^{6}A-related proteins may serve as new targets.

Problematically, while such therapies may be useful in localised cancers, the heterogeneous pathology of neurological disease would likely result

in a situation where the amelioration of one deficit could result in deterioration of another cellular process. As the understanding of m^6A methylation and its effects on disease is broadened, new therapeutic approaches such as targeted genome or perhaps even epitranscriptome editing will be essential for practical use.

Overall, the present work presents compelling evidence that PD and LBD are characterised by changes in m^6A methylation. However, these observations are currently only a correlation and much more research is needed to prove a mechanistic cause of disease by atypical m^6A methylation. One of the first steps in this research will be to sequence the m^6A epitranscriptome in specific regions of diseased brain. This data must then be mined to identify transcript families enriched for m^6A modifications which are unique to disease. Alpha-synuclein and dopamine receptors are examples of terms which may be examined in PD and LBD.

The use of a novel way to quantify DAB immunohistochemistry in this study, while being blind to disease status and automated by software, proved successful. Traditional methods of evaluating these experiments consist of binary confirmation of staining or rely on observations by one or more trained individuals and the assignment of a perceived staining intensity, which is plagued by observed bias and often irreproducible. Newer methods include simple measuring using image analysis tools in which a handful of circular regions of interest are measured and assigned a value (Nguyen et al., 2013). However, this once again is biased by the selection of regions of interest in an image and ignores areas of the cell

which may not fit nicely in a circular region of interest. The method developed here was derived from this last protocol but the Ilastik image classification software was trained to discriminate DAB and background stains (Sommer et al., 2011). This novel method attempted to reduce researcher bias by uncoupling the selection and measurement of regions of interest from the analysis of quantitative data. Overall, *a priori* observations made by the researchers matched quantitative results, as can be observed in all figures of this chapter. Thus, it was possible to calculate statistical differences, with the caveat that IHC-DAB is an inherently non-linear, semi-quantitative staining method.

One weakness in the current study pertains to the amount and type of human tissue available. The number of sections available for each disease, including tumours, was limited and as such, ALKBH5 (m^6A eraser) immunohistochemistry was not performed. High expression of ALKBH5 has been suggested as a factor in glioblastoma stem-like cell tumourigenicity (Zhang et al., 2017). Likewise, m^6A eraser, FTO, has been implicated in memory processes in the prefrontal cortex and fear memory in mice hippocampus (Walters et al., 2017; Widagdo et al., 2016). ALKBH5 is also implied by my own research in this thesis to be involved in synaptic plasticity and thus learning and memory. As such, it is probable that perturbed m^6A eraser expression is a factor in human neurological disease. A short-term goal should be to broaden the present study to include m^6A eraser and m^6A writer immunohistochemistry and diseases characterised by more severe memory deficits.

Finally, throughout this study, individuals characterised as having Mild Cognitive Impairment showed no trend in differences. Despite not being shown here, it was often found that one of three MCI individuals had no changes compared with normal brain. One issue with these individuals may be that, although the patients presented with slight cognitive deficits in life, they were not assigned a formal diagnosis of Mild Cognitive Impairment by a physician. Rather, these samples were classified as such due to their cognitive test results and some slight pathophysiological changes apparent in post-mortem tissue. One of the problems with classifying MCI post-mortem is that the disease does not have many physiological markers and is assumed to be just a prodromal stage of other neurodegenerative diseases. The only two currently accepted markers are amyloid-beta deposition and tau-positive neurofibrillary tangles, and these characteristics were inconsistent across brain regions of MCI samples and individuals. Currently, there are no agreed upon levels of pathophysiological changes in an MCI diagnosis other than the expectation that these should not be as severe as in AD. Taken together, it is unknown if the tissue studied would have detectable changes in m^6A methylation at this stage or if what was observed are true results. In the future, more stringent selection of tissue would be required to study m^6A methylation in MCI, although it would be recommendable to focus on AD as a disease with memory impairment.

In this chapter, evidence has been provided that m^6A methylation and m^6A reader expression are perturbed in neurological disease and cancer. These changes were characterised in each neuronal population of 4

different regions with varying functions, as well as in two different paediatric tumours. The findings suggest that m^6A methylation and readers are consistently upregulated in LBD and downregulated in PD. MCI hippocampus was found to be depleted of these markers. Finally, a progressive downregulation of m^6A-modified RNA was observed in paediatric tumours. Taken together, these findings provide a basis for the development of future therapies for these diseases.

Chapter 7:

Discussion

7.1 General Discussion

The central dogma of molecular biology, the idea that genetic information flows from DNA to RNA to protein, has been found to be more complex than anticipated. In the past decades, researchers have learned that there are further regulatory mechanisms for each of these steps. DNA has several types of methylation and proteins have post-translational modifications with a plethora of effects on protein stability. Most recently, post-transcriptional modifications on RNA have emerged as critical regulators of translation. Amongst these, m^6A methylation has been found to be a quickly reversible process that responds to environmental stimuli. As such, m^6A methylation may be involved in specialised stimulus-dependent cellular processes.

Our current understanding of synaptic plasticity proposes it is driven by local protein synthesis of dormant mRNA transcripts at dendritic spines (Martin et al., 2000). I initially hypothesised that synaptic plasticity and late LTP are established partly through local protein synthesis from dendritically-localised m^6A-methylated mRNAs, which are likely to be enriched for synaptically-relevant proteins. In turn, these transcripts may then interact with m^6A-binding proteins which mediate changes in translation efficiency, stability, or methylation state. Therefore, I predicted that m^6A modifications and their related proteins to be located in synapses of neuronal cells.

Throughout this project, evidence that supports m^6A methylation as a fine-tuning mechanism of active translation which is principally mediated by YTH proteins and responds to synaptic stimuli to help recruit mRNAs

to the synapse via FMRP ultimately promoting synaptic growth and development. Evidence was shown that FMRP release of mRNA occurs in tandem with demethylation by ALKBH5. The fate of m^6A methylated transcripts at synapses was observed to be time-dependent. Evidence was provided that m^6A methylation is also a factor in late stem cell development and that dysregulation of m^6A methylation levels and the localisation of these marks is a salient feature of neurodegenerative disease.

7.2 m^6A-sequencing presents several pathological targets

The results presented in Chapter 3 revealed novel m^6A-sequencing performed on human brain tissue. Some of the observations made from this data has already been discussed in that chapter, but as the project advanced, more observations made from m^6A-sequencing were emphasised.

For instance, it was found that many of the transcripts typically associated with neurodegenerative disease were hypomethylated in normal brain. Alpha-synuclein (*SNCA*), amyloid precursor protein (*APP*), and Apolipoprotein E (*APOE*), all involved in dementia, were all found to have one m^6A mark, most commonly at the transcription start site (5' UTR). This low level of methylation, i.e. below the average of 2 m^6A marks per transcript, implies that large changes in translation efficiency of these mRNAs are not commonly controlled by m^6A modifications.

As discussed before, aberrant alpha-synuclein expression resulting in formation of Lewy bodies is the main neuropathological feature of

Parkinsonism, including Parkinson's disease and Lewy Body Dementia (Schulz-Schaeffer, 2010). Together with the aberrant m^6A methylation observed in imunohistochemical analysis of the diseased tissue in Chapter 6, these two observations suggest a link between changes in m^6A methylation of alpha-synuclein transcripts and Lewy body formation in disease.

APP and APOE are two protein markers of Alzheimer's disease. Increases in APP expression are well-documented to correlate with dementia and that this change in expression occurs early in the cascade of events leading to amyloid plaque formation (Matsui et al., 2007; Ovchinnikov et al., 2018). In APOE's case, contradictory reports make it unclear whether APOE protein numbers are significantly higher compared to controls but the function of this protein in fat metabolism in the brain suggests protein levels are also a factor in dementia (Kim et al., 2009). Aberrant m^6A methylation in one or both of these transcripts would also modify expression to pathological levels.

Subsequently, many other synaptic markers of cognitive decline were found to be methylated (Bereczki et al., 2018). Most prominently, glutamate receptors, such as NMDA, Kainate, and AMPA receptors, were found to be highly methylated. These receptors' expression is known to be altered in neurodegenerative disease (Hondius et al., 2016; Lerma & Marques, 2013). Given observations made in neuronal activation experiments of Chapter 5, it is likely that the availability of these receptors is regulated by m^6A methylation of their corresponding transcripts. As observed in immunohistochemical experiments, global

m^{6}A levels change in disease and, crucially, the location of m^{6}A-modified transcripts moves away from synapses in some diseases. These changes in disease are likely to lead to abnormalities in glutamate receptor expression through altered splicing, translation efficiency, or transcript stability. Also, they may involve decreased expression or, at least in schizophrenia, result in overexpression of glutamate receptors because these transcripts are not properly degraded through YTHDF2-binding. More research is needed using manipulatable models of disease and m^{6}A-sequencing of disease tissue.

In isolation, m^{6}A-sequencing suggested a prominent role for m^{6}A modifications in biological processes such as synapse formation or intracellular signal induction. Indeed, it was confirmed by imaging in neuronal cell lines and human tissue that m^{6}A modifications are located at synapses and react to synaptic stimuli. To study other gene ontology terms such as phosphoproteins will require biochemical approaches rather than imaging, but the implication that m^{6}A modifications affect the expression of these post-translationally modified proteins is an exciting prospect. This would provide a mechanism by which signal transduction cascades all throughout the cell could be controlled and another mechanism by which m^{6}A methylation may relate to diseases such as cancer and stress-induced disease.

In this project, I was aware that m^{6}A methylation's impact on translation in all areas of neurons could mean that transcripts enriched at the synapse could be obscured by more general, homeostasis-relevant transcripts. I attempted to address this possible skew of data by

combining our list of m^{6}A-modified transcripts with synaptically-located transcripts (Cajigas et al., 2012b). This analysis resulted in similar results as the whole-cell transcript list with the differences being that synaptic gene ontology terms were more significant than before. However, as the field moves forward, I believe one limitation is that published lists of synaptic transcripts do not agree with each other. In a recent paper, investigators addressed this by using the twelve most-cited lists of transcripts (Merkurjev et al., 2018a). Few researchers have the time or funding to repeat a whole-transcriptome analysis twelve times, and indeed, most choose one database. This means that conclusions may be based on incorrect results, highlighting the need for a unified, single list of synaptic transcripts. More likely, approaches that physically separate synapses, such as synaptosome preparation, will be important for more location-specific sequencing. Furthermore, no current list derived from human synapses exists, suggesting that some human-specific nuance is also lost in these analyses.

The m^{6}A-sequencing data presented here is ultimately the basis for future work. Nearly seven thousand transcripts were found to be m^{6}A-methylated, which means that we now know more about the regulation of ~30% of human genes. Many major markers of disease are found in this data, and hopefully it will serve as a starting point for further research into the effects of specific m^{6}A-modified transcripts in the brain.

7.3 A model of m^{6}A-mediated synaptic development

The enrichment of m^{6}A-methylated transcripts at dendrites and their response to synaptic activation to strengthen the synapse as a whole –

through increased translation of structural and adhesion proteins – is consistent with the idea of synaptic tagging proposed by Frey & Morris (Frey & Morris, 1997).

Local protein synthesis following neuronal activation is a time-sensitive process which is responsible for synaptic plasticity, learning, and memory. Results suggest that following synaptic activation, local transcripts undergo translation which is influenced by their m^6A methylation status and availability of m^6A reader and eraser protein function. These local transcripts are also later degraded or demethylated at times which correspond to changes in transcript dynamics during early/late LTP and are consistent with previous information about mRNA stability in neurons and the half-life of mRNAs (Bolognani & Perrone-Bizzozero, 2008; Sharova et al., 2008).

It is currently unknown how FMRP, a suggested m^6A reader, detaches at the synapse from its complex. One possibility is that an increase or decrease in methylation following synaptic stimulus may impact its binding affinity (Chang et al., 2017). This project shows ALKBH5 interacts with m^6A only shortly after NMDA activation, an effect also observed between m^6A and FMRP. Therefore, the data suggests FMRP detaches due to demethylation activity of ALKBH5 which reduces but does not completely erase methylation.

An increase in colocalisation of active ribosomes and ALKBH5 was also observed. Therefore, once FMRP unbinds through demethylation, translation by the ribosomes in the FMRP complex initiates and is

increased when YTHDF1/3 reads the remaining m^{6}A marks. Thus, defects in m^{6}A-binding proteins may also contribute to Fragile X syndrome. As found in m^{6}A-sequencing data, readers and erasers were methylated, suggesting a mechanism of autoregulation. One use for autoregulation of ALKBH5 would then be to control the start of local protein synthesis following synaptic activity. Further research is needed to confirm this model (**Figure 7.1**).

As previously mentioned, the finding that m^{6}A writer, eraser, and reader proteins are translated from m^{6}A-methylated transcripts also represents an interesting new regulatory mechanism. Through this autoregulation, m^{6}A-methylation has two levels of control over translation. Like a microscope's coarse and fine focus, translation efficiency (and other reader functions) can be coarsely enhanced through the presence of m^{6}A modifications on a transcript. Fine control of this enhancement can be achieved by controlling the number of m^{6}A-binding proteins available. For example, if m^{6}A methylation increases protein expression by 50% but a neuron must only up-regulate its GRIK4 (a Kainate receptor) production by 25%, methylating GRIK4 transcripts and demethylating half of YTHDF1/YTHDF3 transcripts may be one way to achieve this. The therapeutic control of such a mechanism would be a paramount achievement in treating diseases characterised by protein deficiencies or overexpression, such as neurodegeneration.

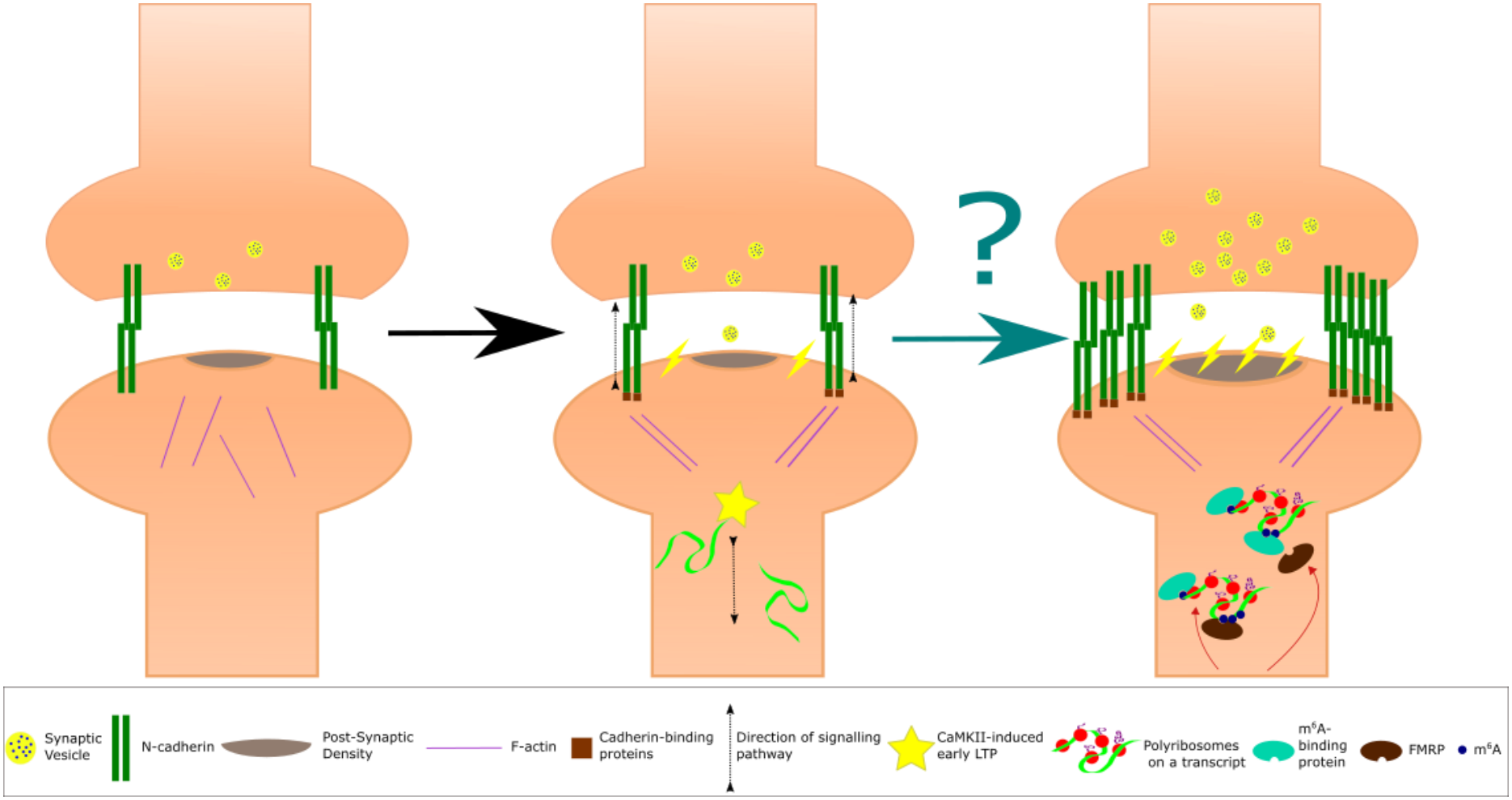
?
Synaptic Vesicle
N-cadherin
Post-Synaptic Density
F-actin
Cadherin-binding proteins
Direction of signalling pathway
CaMKII-induced early LTP
Polyribosomes on a transcript
m6A-binding protein
FMRP
m6A

Figure 7.1 Proposed model of action of m^6A at a synapse. An inactive synapse (left) is stimulated (middle) by external stimuli. We propose that after repeated stimulus within the next three hours (right), m^6A-tagged transcripts are transported by Fragile X Mental Retardation Protein (FMRP) from dendrites into the dendritic spine of the postsynaptic compartment. Once inside the dendritic spine, an m^6A binding protein, most likely ALKBH5, modifies the number of m^6A marks, causing FMRP to detach and allowing YTH reader proteins to bind to modifications.

7.4 Dysregulation of m^{6}A methylation and its implications in disease

The model described above provides an explanation for the mechanism through which dysregulation of m^{6}A methylation results in synaptic defects. In this model, decreased m^{6}A methylation results in reduced transportation of mRNAs to synapses and/or translation inefficiency at these sites. Given the importance of a quick response to synaptic stimulation, these deficits ultimately prevent the increased expression of synaptic proteins and synaptic strengthening characteristic of LTP. In schizophrenia, for example, abnormal modulation of NMDA-dependent plasticity, suggested here to be m^{6}A-dependent, is thought to cause dysconnectivity between brain regions. Similarly, increases in m^{6}A methylation could result in too much synaptic growth, called "hyperconnectivity," a feature of autism (Supekar et al., 2013).

In Chapter 6, most examined regions showed global changes in m^{6}A abundance and YTHDF1/YTHDF3 expression. Such global deficits have been associated with defects in development and spinogenesis (Bodi et al., 2012; Merkurjev et al., 2018b). Furthermore, the model in **Figure 7.1** suggests that single dysregulation, not just depletion, of methylation or any one m^{6}A-binding protein is enough to result in abnormal synaptic plasticity.

The m^{6}A methyltransferase complex also plays a key role in control of synaptic plasticity, as abnormal methylation of specific transcripts may affect translation at the synapse thus having functional effects on neuron

to neuron connectivity. More research is needed to understand how this complex is influenced by the environment and how the methylation status of specific transcripts is decided. These findings would provide a basis for the development of m^6A methylation therapies for brain disease.

Synaptic plasticity is believed to be the root of the brain's complex functions. A mechanism such as m^6A RNA methylation which may regulate plasticity is therefore likely to affect most brain functions in different measures. Whether in neurodegeneration, cognition, brain trauma, or neurodevelopmental disease, these findings suggest the role of m^6A methylation in each context is one factor worth investigating.

7.5 Future perspectives

In such a novel field, future directions are broad.

First of all, research has focused on the functional understanding of m^6A methylation. In building the basis of this field, the questions asked were first about the effects of m^6A/m^6A writer depletion in various models (Bodi et al., 2012; Dominissini et al., 2012; Lin et al., 2016; Zhou et al., 2015a). Then, a number of m^6A readers were (Liu et al., 2015; Meyer et al., 2015; Shi et al., 2017; Wang et al., 2015; Xiao et al., 2016). Currently, the field is moving towards the dynamic m^6A epitranscriptome in disease (Cui et al., 2017; Widagdo et al., 2016; Zhang et al., 2017). In this explosive growth, only a few researchers have looked to characterise the proteins which allow m^6A methylation's versatility. The methyltransferase complex has been investigated further and the basis of YTH domain's

recognition of m^{6}A modifications has been detailed (Liu et al., 2016; Růžička et al., 2017).

One of the basic unanswered questions in m^{6}A research is why YTHDF3 appears to have two very different functions which are redundant with YTHDF1 and YTHDF2. Redundancy of protein function is sometimes observed in plants when the proteins have different patterns of expression. A recent study showed that in *Arabidopsis*, single knockout mutants did not exhibit any obvious phenotypic changes due to redundant m^{6}A readers (Arribas-Hernández et al., 2018). However, neither that study nor this thesis project found redundant m^{6}A readers to have different patterns of expression. In fact, expression of all YTHDF readers appears to be equal in healthy organisms, with the only observed change being that YTHDF2 relocate into the nucleus upon heat shock (Zhou et al., 2015a). However, in Chapter 6, we observed an upregulation of YTHDF3 and downregulation of YTHDF1.

Another question regarding YTH reader proteins is how they “choose” which transcripts to bind to. These proteins all share the YTH domain and thus its ability to form an aromatic cage when binding to an m^{6}A mark at a specific sequence. One hypothesis is that differences in protein folding may make these proteins have slightly different affinities for different binding sites. Thus, competition between proteins would tend to pair a specific sequence with the YTH protein with the highest affinity. Another possibility is that YTH readers are switched on through phosphorylation in response to specific environmental conditions, a possibility that fits with “phosphoproteins” being highly enriched in m^{6}A-

sequencing. More detailed research of m^6A motifs, together with pull-down approaches could test this in the future.

Here, sequencing was performed on a single sample of three different tissue types. Due to the dynamic nature of m^6A RNA modifications, it is likely that some of the transcripts found to be methylated were only transiently methylated as an adaptation to the local environment at the time of the individual's death, i.e. their methylation state might have normally been reversed. It will first be important to increase sample numbers of brain-derived m^6A-sequencing to learn of the variation in m^6A methylated transcripts. Future characterisation of m^6A methylation profiles in disease will also be critical to our understanding of how these modifications impact upon cellular processes. There may be various applications for this knowledge, including using global methylation levels or methylation status of specific transcripts as biomarkers of disease progression.

It is possible to envisage the development of m^6A-RNA editing in the near future. Indeed, a system of guided RNA editing has already been developed for the targeted adenosine to inosine (A-to-I) editing, another post-transcriptional modification. A CRISPR-based system was developed in which Cas13b was fused to the protein responsible for A-to-I conversion (Cox et al., 2017). A similar system could be developed for control of m^6A methylation in specific RNAs. Such a system could be fused to an eraser and target conserved sequences surrounding sites of m^6A methylation or m^6A switches (Liu et al., 2015). The demethylation of specific RNAs would allow for the application of knowledge generated

from disease studies. Transcripts that are hypermethylated in disease can be demethylated through m^{6}A RNA editing to rescue a normal phenotype *in vivo*.

There are some advantages to m^{6}A RNA editing over CRISPR-Cas9 cleavage of m^{6}A writers, for example. First, a possible m^{6}A RNA editing system would not break a transcript and thus would not be dependent on endogenous repair mechanisms to have the desired effect. Thus, m^{6}A RNA editing would be inherently functional in all types of cells, including neuronal and tumour cells. Second, the transient nature of mRNA means any effects can be easily reversed. This would make m^{6}A RNA editing useful for treating time-restrained cellular changes, such as local inflammation. More importantly, it could be used to prevent the disease progression of neurological disorders characterised by protein accumulation. Some examples of these include aggregation of alpha-synuclein in Parkinsonism and amyloid-beta in Alzheimer's, both of which, under the current model, could be reduced by demethylation of their transcripts.

One more unanswered question is whether and how the cell can control aberrant m^{6}A methylation. Is there "quality assurance" of methylation before nuclear export? Demethylases were mostly found within the nucleus under normal conditions, ideally positioning them for such a mechanism (Chapters 4 and 5, Zheng et al., 2013). However, in Chapter 3, the number of methylation marks was shown to be highly variable, with up to 28 modifications found in some transcripts. As such, it does not seem that simply having multiple m^{6}A marks signals repair of

methylation. In the future, understanding this process may further develop our understanding of m^6A writer and reader function.

7.6 Conclusions

Synaptic plasticity and epigenetic modifications are two areas of research in which fundamental mechanisms of are not yet fully understood. In synaptic plasticity, activity- and time-dependent changes combine to strengthen the synapse, but these changes involve many different processes. Local protein synthesis is one of these processes and in this project, evidence has been provided that m^6A methylation is an important regulator of its outcome. Furthermore, detailed m^6A-sequencing data is provided to analyse exactly which transcripts require m^6A modifications for effective translation at the synapse. This information, together with the dysregulation of m^6A methylation levels and previous genetic research, can be used to find transcripts which have been previously associated with disease states. Overall, this project is a starting point to understand the epigenetic mechanisms which fine-tune synaptic plasticity and how these mechanisms are affected in disease. In the future, this study may serve as the basis for development of epigenetic therapies that may lead to the improvement of public health and quality of life.

Chapter 8:

Bibliography

Agulhon, C., Blanchet, P., Kobetz, A., Marchant, D., Faucon, N., Sarda, P., Moraine, C., Sittler, A., Biancalana, V., Malafosse, A., & Abitbol, M. (1999). Expression of FMR1, FXR1, and FXR2 Genes in Human Prenatal Tissues. *Journal of Neuropathology and Experimental Neurology*, *58*(8), 867–880. https://doi.org/10.1097/00005072-199908000-00009

Aimone, J. B., Wiles, J., & Gage, F. H. (2006). Potential role for adult neurogenesis in the encoding of time in new memories. *Nature Neuroscience*, *9*(6), 723–727. https://doi.org/10.1038/nn1707

Alarcón, C. R., Goodarzi, H., Lee, H., Liu, X., Tavazoie, S., & Tavazoie, S. F. (2015). HNRNPA2B1 Is a Mediator of m(6)A-Dependent Nuclear RNA Processing Events. *Cell*, *162*(6), 1299–1308. https://doi.org/10.1016/j.cell.2015.08.011

Andersen, P., Morris, R. G. M., Amaral, D., Bliss, T. V. P., & O'Keefe, J. (2006). *The Hippocampus Book* (1st ed.). Oxford University Press.

Angelucci, F., Spalletta, G., di Iulio, F., Ciaramella, A., Salani, F., Colantoni, L., Varsi, A. E., Gianni, W., Sancesario, G., Caltagirone, C., & Bossù, P. (2010). Alzheimer's disease (AD) and Mild Cognitive Impairment (MCI) patients are characterized by increased BDNF serum levels. *Current Alzheimer Research*, *7*(1), 15–20. http://www.ncbi.nlm.nih.gov/pubmed/20205668

Antar, L. ., & Bassell, G. . (2003). Sunrise at the Synapse: The FMRP mRNP Shaping the Synaptic Interface. *Neuron*, *37*(4), 555–558. https://doi.org/10.1016/S0896-6273(03)00090-4

Antar, L. N. (2004). Metabotropic Glutamate Receptor Activation Regulates Fragile X Mental Retardation Protein and Fmr1 mRNA Localization Differentially in Dendrites and at Synapses. *Journal of Neuroscience*, *24*(11), 2648–2655. https://doi.org/10.1523/JNEUROSCI.0099-04.2004

Arribas-Hernández, L., Bressendorff, S., Hansen, M. H., Poulsen, C., Erdmann, S., & Brodersen, P. (2018). An m 6 A-YTH Module Controls Developmental Timing and Morphogenesis in Arabidopsis . *The Plant Cell*, *30*(5), 952–967. https://doi.org/10.1105/tpc.17.00833

Ashcraft, M. H., & Radvansky, G. A. (2014). *Cognition* (6th ed.). Pearson.

Bartsch, T., Döhring, J., Rohr, A., Jansen, O., & Deuschl, G. (2011). CA1 neurons in the human hippocampus are critical for autobiographical memory, mental time travel, and autonoetic consciousness. *Proceedings of the National Academy of Sciences of the United States of America*, *108*(42), 17562–17567. https://doi.org/10.1073/pnas.1110266108

Batista, P. J., & Yang, Y.-G. (2017). *The RNA Modification N6-methyladenosine and Its Implications in Human Disease*. https://doi.org/10.1016/j.gpb.2017.03.002

Bennett, D. A., Schneider, J. A., Bienias, J. L., Evans, D. A., & Wilson, R. S. (2005). Mild cognitive impairment is related to Alzheimer disease pathology and cerebral infarctions. *Neurology*, *64*(5), 834–841. https://doi.org/10.1212/01.WNL.0000152982.47274.9E

Bereczki, E., Branca, R. M., Francis, P. T., Pereira, J. B., Baek, J.-H., Hortobágyi, T., Winblad, B., Ballard, C., Lehtiö, J., & Aarsland, D. (2018). Synaptic markers of cognitive decline in neurodegenerative diseases: a proteomic approach. *Brain*, *141*(2), 582–595. https://doi.org/10.1093/brain/awx352

Bliss, T. V. P., & Collingridge, G. L. (1993). A Synaptic Model of Memory: Long-Term Potentiation in the Hippocampus. *Nature*, *361*, 31–39. https://doi.org/10.1038/361031a0

Bobinski, M., de Leon, M. J., Tarnawski, M., Wegiel, J., Bobinski, M., Reisberg, B., Miller, D. C., & Wisniewski, H. M. (1998). Neuronal and volume loss in CA1 of the hippocampal formation uniquely predicts duration and severity of Alzheimer disease. *Brain Research*, *805*(1–2), 267–269. https://doi.org/10.1016/S0006-8993(98)00759-8

Bodi, Z., Zhong, S., Mehra, S., Song, J., Graham, N., Li, H., May, S., & Fray, R. G. (2012). Adenosine Methylation in Arabidopsis mRNA is Associated with the 3' End and Reduced Levels Cause Developmental Defects. *Frontiers in Plant Science*, *3*(March), 48. https://doi.org/10.3389/fpls.2012.00048

Boissel, S., Reish, O., Proulx, K., Kawagoe-Takaki, H., Sedgwick, B., Yeo, G. S. H., Meyre, D., Golzio, C., Molinari, F., Kadhom, N., Etchevers, H. C., Saudek, V., Farooqi, I. S., Froguel, P., Lindahl, T., O'Rahilly, S., Munnich, A., & Colleaux, L. (2009). Loss-of-Function Mutation in the Dioxygenase-Encoding FTO Gene Causes Severe Growth Retardation and Multiple Malformations. *The American*

Journal of Human Genetics, *85*(1), 106–111. https://doi.org/10.1016/J.AJHG.2009.06.002

Bolognani, F., & Perrone-Bizzozero, N. I. (2008). RNA–protein interactions and control of mRNA stability in neurons. *Journal of Neuroscience Research*, *86*(3), 481–489. https://doi.org/10.1002/jnr.21473

Burgess, N., Maguire, E. A., & O'Keefe, J. (2002). The Human Hippocampus and Spatial and Episodic Memory. *Neuron*, *35*(4), 625–641. https://doi.org/10.1016/S0896-6273(02)00830-9

Cajigas, I. J., Tushev, G., Will, T. J., Tom Dieck, S., Fuerst, N., & Schuman, E. M. (2012a). The Local Transcriptome in the Synaptic Neuropil Revealed by Deep Sequencing and High-Resolution Imaging. *Neuron*, *74*(3), 453–466. https://doi.org/10.1016/j.neuron.2012.02.036

Cajigas, I. J., Tushev, G., Will, T. J., Tom Dieck, S., Fuerst, N., & Schuman, E. M. (2012b). The Local Transcriptome in the Synaptic Neuropil Revealed by Deep Sequencing and High-Resolution Imaging. *Neuron*, *74*(3), 453–466. https://doi.org/10.1016/j.neuron.2012.02.036

Calabresi, P., Castrioto, A., Di Filippo, M., & Picconi, B. (2013). New experimental and clinical links between the hippocampus and the dopaminergic system in Parkinson's disease. *The Lancet Neurology*, *12*(8), 811–821. https://doi.org/10.1016/S1474-4422(13)70118-2

Camicioli, R., Moore, M. M., Kinney, A., Corbridge, E., Glassberg, K., & Kaye, J. A. (2003). Parkinson's disease is associated with hippocampal atrophy. *Movement Disorders*, *18*(7), 784–790. https://doi.org/10.1002/mds.10444

Chadwick, M. J., Bonnici, H. M., & Maguire, E. A. (2014). CA3 size predicts the precision of memory recall. *Proceedings of the National Academy of Sciences*, *111*(29), 10720–10725. https://doi.org/10.1073/PNAS.1319641111

Chang, M., Lv, H., Zhang, W., Ma, C., He, X., Zhao, S., Zhang, Z.-W., Zeng, Y.-X., Song, S., Niu, Y., & Tong, W.-M. (2017). Region-specific RNA m(6)A methylation represents a new layer of control in the gene regulatory network in the mouse brain. *Open Biology*, *7*(9), 170166. https://doi.org/10.1098/rsob.170166

Chen, Y., Durakoglugil, M. S., Xian, X., & Herz, J. (2010). ApoE4 reduces glutamate receptor function and synaptic plasticity by selectively impairing ApoE receptor recycling. *Proceedings of the National Academy of Sciences*, *107*(26), 12011–12016. https://doi.org/10.1073/pnas.0914984107

Christie, B. R., & Abraham, W. C. (1992). Priming of associative long-term depression in the dentate gyrus by θ frequency synaptic activity. *Neuron*, *9*(1), 79–84. https://doi.org/10.1016/0896-6273(92)90222-Y

Claussnitzer, M., Dankel, S. N., Kim, K.-H., Quon, G., Meuleman, W., Haugen, C., Glunk, V., Sousa, I. S., Beaudry, J. L., Puviindran, V.,

Abdennur, N. A., Liu, J., Svensson, P.-A., Hsu, Y.-H., Drucker, D. J., Mellgren, G., Hui, C.-C., Hauner, H., & Kellis, M. (2015). FTO Obesity Variant Circuitry and Adipocyte Browning in Humans. *The New England Journal of Medicine*, *373*(10), 895–907. https://doi.org/10.1056/NEJMoa1502214

Colom-Cadena, M., Pegueroles, J., Herrmann, A. G., Henstridge, C. M., Muñoz, L., Querol-Vilaseca, M., Martín-Paniello, C. S., Luque-Cabecerans, J., Clarimon, J., Belbin, O., Núñez-Llaves, R., Blesa, R., Smith, C., McKenzie, C.-A., Frosch, M. P., Roe, A., Fortea, J., Andilla, J., Loza-Alvarez, P., … Lleó, A. (2017). Synaptic phosphorylated α-synuclein in dementia with Lewy bodies. *Brain*, *140*(12), 3204–3214. https://doi.org/10.1093/brain/awx275

Corder, E. H., Saunders, A. M., Strittmatter, W. J., Schmechel, D. E., Gaskell, P. C., Small, G. W., Roses, A. D., Haines, J. L., & Pericak-Vance, M. A. (1993). Gene dose of apolipoprotein E type 4 allele and the risk of Alzheimer's disease in late onset families. *Science*, *261*(5123), 921–923. https://doi.org/10.1126/science.8346443

Cougot, N., Bhattacharyya, S. N., Tapia-Arancibia, L., Bordonne, R., Filipowicz, W., Bertrand, E., & Rage, F. (2008). Dendrites of Mammalian Neurons Contain Specialized P-Body-Like Structures That Respond to Neuronal Activation. *Journal of Neuroscience*, *28*(51), 13793–13804. https://doi.org/10.1523/JNEUROSCI.4155-08.2008

Cox, D. B. T., Cox, D. B. T., Gootenberg, J. S., Abudayyeh, O. O.,

Franklin, B., & Kellner, M. J. (2017). RNA editing with CRISPR-Cas13. *Science*, *0180*(October), 1–15. https://doi.org/10.1126/science.aaq0180

Cui, Q., Shi, H., Ye, P., Li, L., Qu, Q., Sun, G., Sun, G., Lu, Z., Huang, Y., Yang, C.-G., Riggs, A. D., He, C., & Shi, Y. (2017). m6A RNA Methylation Regulates the Self-Renewal and Tumorigenesis of Glioblastoma Stem Cells. *Cell Reports*, *18*(11), 2622–2634. https://doi.org/10.1016/J.CELREP.2017.02.059

Darnell, J. C., Van Driesche, S. J., Zhang, C., Hung, K. Y. S., Mele, A., Fraser, C. E., Stone, E. F., Chen, C., Fak, J. J., Chi, S. W., Licatalosi, D. D., Richter, J. D., & Darnell, R. B. (2011). FMRP stalls ribosomal translocation on mRNAs linked to synaptic function and autism. *Cell*, *146*(2), 247–261. https://doi.org/10.1016/j.cell.2011.06.013

De Rubeis, S., Pasciuto, E., Li, K. W., Fernández, E., Di Marino, D., Buzzi, A., Ostroff, L. E., Klann, E., Zwartkruis, F. J. T., Komiyama, N. H., Grant, S. G. N., Poujol, C., Choquet, D., Achsel, T., Posthuma, D., Smit, A. B., & Bagni, C. (2013). CYFIP1 Coordinates mRNA Translation and Cytoskeleton Remodeling to Ensure Proper Dendritic Spine Formation. *Neuron*, *79*(6), 1169–1182. https://doi.org/10.1016/J.NEURON.2013.06.039

Dickson, D. W., Dubois, B., Emre, M., Fahn, S., Farmer, J. M., Galasko, D., Goetz, C. G., Growdon, J. H., Hardy, J., Heutink, P., Kosaka, K., Lee, V. M., Leverenz, J. B., Masliah, E., Mckeith, I. G., Olanow, C. W., Ravina, B. M., Singleton, A. B., & Tanner, C. M. (2008). DLB and

PDD boundary issues: diagnosis , treatment , molecular pathology , and biomarkers. *Neurology*, *68*(11), 812–819. https://doi.org/10.1212/01.wnl.0000256715.13907.d3

Dickson, D. W., Ruan, D., Crystal, H., Mark, M. H., Davies, P., Kress, Y., & Yen, S. H. (1991). Hippocampal degeneration differentiates diffuse Lewy body disease (DLBD) from Alzheimer's disease: light and electron microscopic immunocytochemistry of CA2-3 neurites specific to DLBD. *Neurology*, *41*(9), 1402–1409. https://doi.org/10.1212/wnl.41.9.1402

Dolan, B. M., Duron, S. G., Campbell, D. A., Vollrath, B., Rao, B. S. S., Ko, H.-Y., Lin, G. G., Govindarajan, A., Choi, S.-Y., & Tonegawa, S. (2013). Rescue of fragile X syndrome phenotypes in Fmr1 KO mice by the small-molecule PAK inhibitor FRAX486. *Proceedings of the National Academy of Sciences*, *110*(14), 5671–5676. https://doi.org/10.1073/pnas.1219383110

Dominissini, D. (2014). Roadmap to the epitranscriptome. *Science*, *346*(6214), 1192. https://doi.org/10.1126/science.aaa1807

Dominissini, D., Moshitch-Moshkovitz, S., Schwartz, S., Salmon-Divon, M., Ungar, L., Osenberg, S., Cesarkas, K., Jacob-Hirsch, J., Amariglio, N., Kupiec, M., Sorek, R., & Rechavi, G. (2012). Topology of the human and mouse m6A RNA methylomes revealed by m6A-seq. *Nature*, *485*(7397), 201–206. https://doi.org/10.1038/nature11112

Dominissini, D., Nachtergaele, S., Moshitch-Moshkovitz, S., Peer, E.,

Kol, N., Ben-Haim, M. S., Dai, Q., Di Segni, A., Salmon-Divon, M., Clark, W. C., Zheng, G., Pan, T., Solomon, O., Eyal, E., Hershkovitz, V., Han, D., Doré, L. C., Amariglio, N., Rechavi, G., & He, C. (2016). The dynamic N1-methyladenosine methylome in eukaryotic messenger RNA. *Nature*, 1–21. https://doi.org/10.1038/nature16998

Duthey, B. (2013). *Background Paper 6.11 Alzheimer Disease and other Dementias*. https://www.who.int/medicines/areas/priority_medicines/BP6_11Alzheimer.pdf

Elias-Sonnenschein, L. S., Viechtbauer, W., Ramakers, I. H. G. B., Verhey, F. R. J., & Visser, P. J. (2011). Predictive value of APOE- 4 allele for progression from MCI to AD-type dementia: a meta-analysis. *Journal of Neurology, Neurosurgery & Psychiatry*, *82*(10), 1149–1156. https://doi.org/10.1136/jnnp.2010.231555

Ellison, D. W., Kocak, M., Figarella-Branger, D., Felice, G., Catherine, G., Pietsch, T., Frappaz, D., Massimino, M., Grill, J., Boyett, J. M., & Grundy, R. G. (2011). Histopathological grading of pediatric ependymoma: reproducibility and clinical relevance in European trial cohorts. *Journal of Negative Results in BioMedicine*, *10*(1), 7. https://doi.org/10.1186/1477-5751-10-7

Engel, M., Eggert, C., Kaplick, P. M., Eder, M., Röh, S., Tietze, L., Namendorf, C., Arloth, J., Weber, P., Rex-Haffner, M., Geula, S., Jakovcevski, M., Hanna, J. H., Leshkowitz, D., Uhr, M., Wotjak, C.

T., Schmidt, M. V, Deussing, J. M., Binder, E. B., & Chen, A. (2018). The Role of m6A/m-RNA Methylation in Stress Response Regulation. *Neuron*, *99*(2), 389-403.e9. https://doi.org/10.1016/j.neuron.2018.07.009

Fonseca, R., Nägerl, U. V., & Bonhoeffer, T. (2006). Neuronal activity determines the protein synthesis dependence of long-term potentiation. *Nature Neuroscience*, *9*(4), 478–480. https://doi.org/10.1038/nn1667

Fray, R. G., & Simpson, G. G. (2015). The Arabidopsis epitranscriptome. *Current Opinion in Plant Biology*, *27*, 17–21. https://doi.org/10.1016/J.PBI.2015.05.015

Fremeau, R. T., Voglmaier, S., Seal, R. P., & Edwards, R. H. (2004). VGLUTs define subsets of excitatory neurons and suggest novel roles for glutamate. In *Trends in Neurosciences* (Vol. 27, Issue 2, pp. 98–103). Elsevier Ltd. https://doi.org/10.1016/j.tins.2003.11.005

Frey, U., & Morris, R. G. M. (1997). Synaptic tagging and long-term potentiation. *Nature*, *385*. https://doi.org/10.1038/385533a0

Fu, Y., Dominissini, D., Rechavi, G., & He, C. (2014). Gene expression regulation mediated through reversible m^6A RNA methylation. *Nature Reviews. Genetics*, *15*(5), 293–306. https://doi.org/10.1038/nrg3724

Fuchs, J., Tichopad, A., Golub, Y., Munz, M., Schweitzer, K. J., Wolf, B., Berg, D., Mueller, J. C., & Gasser, T. (2008). Genetic variability in the SNCA gene influences α-synuclein levels in the blood and brain.

The FASEB Journal, *22*(5), 1327–1334. https://doi.org/10.1096/fj.07-9348com

Gauthier, S., Reisberg, B., Zaudig, M., Petersen, R. C., Ritchie, K., Broich, K., Belleville, S., Brodaty, H., Bennett, D., Chertkow, H., Cummings, J. L., de Leon, M., Feldman, H., Ganguli, M., Hampel, H., Scheltens, P., Tierney, M. C., Whitehouse, P., & Winblad, B. (2006). Mild cognitive impairment. *The Lancet*, *367*(9518), 1262–1270. https://doi.org/10.1016/S0140-6736(06)68542-5

Geula, S., Mor, N., Levanon, E. Y., Massarwa, R., Moshitch-Moshkovitz, S., Rechavi, G., Dominissini, D., Amit, I., Salmon-Divon, M., Mansour, A. A., Krupalnik, V., Stern-Ginossar, N., Ben-Haim, M. S., Amariglio, N., Zerbib, M., Kol, N., Novershtern, N., Chomsky, E., Peer, E., … Rais, Y. (2015). m6A mRNA methylation facilitates resolution of naïve pluripotency toward differentiation. *Science*, *347*(6225), 1002–1006. https://doi.org/10.1126/science.1261417

Goldman, J. S., & Fahn, S. (2015). Genetics of Parkinson Disease and Related Diseases. In *Rosenberg's Molecular and Genetic Basis of Neurological and Psychiatric Disease* (5th ed., pp. 769–778). Elsevier. https://doi.org/10.1016/B978-0-12-410529-4.00068-1

Gründemann, J., Schlaudraff, F., Haeckel, O., & Liss, B. (2008). Elevated α-synuclein mRNA levels in individual UV-laser-microdissected dopaminergic substantia nigra neurons in idiopathic Parkinson's disease. *Nucleic Acids Research*, *36*(7), e38. https://doi.org/10.1093/nar/gkn084

Guerreiro, R., Escott-Price, V., Darwent, L., Parkkinen, L., Ansorge, O., Hernandez, D. G., Nalls, M. A., Clark, L., Honig, L., Marder, K., van der Flier, W., Holstege, H., Louwersheimer, E., Lemstra, A., Scheltens, P., Rogaeva, E., St George-Hyslop, P., Londos, E., Zetterberg, H., … Bras, J. (2016). Genome-wide analysis of genetic correlation in dementia with Lewy bodies, Parkinson's and Alzheimer's diseases. *Neurobiology of Aging*, *38*, 214.e7-214.e10. https://doi.org/10.1016/j.neurobiolaging.2015.10.028

Guerreiro, R., Ross, O. A., Kun-Rodrigues, C., Hernandez, D. G., Orme, T., Eicher, J. D., Shepherd, C. E., Parkkinen, L., Darwent, L., Heckman, M. G., Scholz, S. W., Troncoso, J. C., Pletnikova, O., Ansorge, O., Clarimon, J., Lleo, A., Morenas-Rodriguez, E., Clark, L., Honig, L. S., … Bras, J. (2018). Investigating the genetic architecture of dementia with Lewy bodies: a two-stage genome-wide association study. *The Lancet Neurology*, *17*(1), 64–74. https://doi.org/10.1016/S1474-4422(17)30400-3

Hall, H., Reyes, S., Landeck, N., Bye, C., Leanza, G., Double, K., Thompson, L., Halliday, G., & Kirik, D. (2014). Hippocampal Lewy pathology and cholinergic dysfunction are associated with dementia in Parkinson's disease. *Brain*, *137*(9), 2493–2508. https://doi.org/10.1093/brain/awu193

Halliday, G. M., Leverenz, J. B., Schneider, J. S., & Adler, C. H. (2014). The neurobiological basis of cognitive impairment in Parkinson's disease. *Movement Disorders*, *29*(5), 634–650.

https://doi.org/10.1002/mds.25857

Han, D., Liu, J., Chen, C., Dong, L., Liu, Y., Chang, R., Huang, X., Liu, Y., Wang, J., Dougherty, U., Bissonnette, M. B., Shen, B., Weichselbaum, R. R., Xu, M. M., & He, C. (2019). Anti-tumour immunity controlled through mRNA m6A methylation and YTHDF1 in dendritic cells. *Nature*, *566*(7743), 270–274. https://doi.org/10.1038/s41586-019-0916-x

Hansen, L. A., Daniel, S. E., Wilcock, G. K., & Love, S. (1998). Frontal cortical synaptophysin in Lewy body diseases: relation to Alzheimer's disease and dementia. *Journal of Neurology, Neurosurgery & Psychiatry*, *64*(5), 653–656. https://doi.org/10.1136/jnnp.64.5.653

Haussmann, I. U., Bodi, Z., Sanchez-Moran, E., Mongan, N. P., Archer, N., Fray, R. G., & Soller, M. (2016). m6A potentiates Sxl alternative pre-mRNA splicing for robust Drosophila sex determination. *Nature*, *540*(7632), 301–304. https://doi.org/10.1038/nature20577

Hess, M. E., Hess, S., Meyer, K. D., Verhagen, L. a W., Koch, L., Brönneke, H. S., Dietrich, M. O., Jordan, S. D., Saletore, Y., Elemento, O., Belgardt, B. F., Franz, T., Horvath, T. L., Rüther, U., Jaffrey, S. R., Kloppenburg, P., & Brüning, J. C. (2013). The fat mass and obesity associated gene (Fto) regulates activity of the dopaminergic midbrain circuitry. *Nature Neuroscience*, *16*(8), 1042–1048. https://doi.org/10.1038/nn.3449

Ho, V. M., Lee, J.-A., & Martin, K. C. (2011). The Cell Biology of Synaptic

Plasticity. *Science*, *334*(6056), 623–628. https://doi.org/10.1126/science.1209236

Hoesen, G. W. Van, Hyman, B. T., & Damasio, A. R. (1991). Entorhinal Cortex Pathology in Alzheimer ' s Disease. *Hippocampus*, *1*(1), 1–8. https://doi.org/10.1002/hipo.450010102

Hondius, D. C., van Nierop, P., Li, K. W., Hoozemans, J. J. M., van der Schors, R. C., van Haastert, E. S., van der Vies, S. M., Rozemuller, A. J. M., & Smit, A. B. (2016). Profiling the human hippocampal proteome at all pathologic stages of Alzheimer's disease. *Alzheimer's & Dementia*, *12*(6), 654–668. https://doi.org/10.1016/J.JALZ.2015.11.002

Irwin, D. J., Grossman, M., Weintraub, D., Hurtig, H. I., Duda, J. E., Xie, S. X., Lee, E. B., Van Deerlin, V. M., Lopez, O. L., Kofler, J. K., Nelson, P. T., Jicha, G. A., Woltjer, R., Quinn, J. F., Kaye, J., Leverenz, J. B., Tsuang, D., Longfellow, K., Yearout, D., … Trojanowski, J. Q. (2017). Neuropathological and genetic correlates of survival and dementia onset in synucleinopathies: a retrospective analysis. *The Lancet Neurology*, *16*(1), 55–65. https://doi.org/10.1016/S1474-4422(16)30291-5

Jellinger, K. A., & Korczyn, A. D. (2018). Are dementia with Lewy bodies and Parkinson's disease dementia the same disease? *BMC Medicine*, *16*(1), 34. https://doi.org/10.1186/s12916-018-1016-8

Ji, J., & Maren, S. (2008). Differential roles for hippocampal areas CA1 and CA3 in the contextual encoding and retrieval of extinguished

fear. *Learning & Memory (Cold Spring Harbor, N.Y.)*, *15*(4), 244–251. https://doi.org/10.1101/lm.794808

Jia, G., Fu, Y., Zhao, X., Dai, Q., Zheng, G., Yang, Y., Yi, C., Lindahl, T., Pan, T., Yang, Y.-G., & He, C. (2011). N6-Methyladenosine in nuclear RNA is a major substrate of the obesity-associated FTO. *Nature Chemical Biology*, *7*(12), 885–887. https://doi.org/10.1038/nchembio.687

Jones, P. A. (2012). Functions of DNA methylation: islands, start sites, gene bodies and beyond. *Nature Reviews Genetics*, *13*. https://doi.org/10.1038/nrg3230

Jungling, K., Eulenburg, V., Moore, R., Kemler, R., Lessmann, V., & Gottmann, K. (2006). N-Cadherin Transsynaptically Regulates Short-Term Plasticity at Glutamatergic Synapses in Embryonic Stem Cell-Derived Neurons. *Journal of Neuroscience*, *26*(26), 6968–6978. https://doi.org/10.1523/jneurosci.1013-06.2006

Kandel, E. R., Schwartz, J., & Jessell, T. (2000). *Principles of Neural Science* (4th ed.). McGraw-Hill Education.

Ke, S., Pandya-Jones, A., Saito, Y., Fak, J. J., Vågbø, C. B., Geula, S., Hanna, J. H., Black, D. L., Darnell, J. E., & Darnell, R. B. (2017). m(6)A mRNA modifications are deposited in nascent pre-mRNA and are not required for splicing but do specify cytoplasmic turnover. *Genes & Development*, *31*(10), 990–1006. https://doi.org/10.1101/gad.301036.117

Khatua, S., Ramaswamy, V., & Bouffet, E. (2017). Current therapy and

the evolving molecular landscape of paediatric ependymoma. *European Journal of Cancer*, *70*, 34–41. https://doi.org/10.1016/j.ejca.2016.10.013

Kim, H. J., Kim, N. C., Wang, Y.-D., Scarborough, E. A., Moore, J., Diaz, Z., MacLea, K. S., Freibaum, B., Li, S., Molliex, A., Kanagaraj, A. P., Carter, R., Boylan, K. B., Wojtas, A. M., Rademakers, R., Pinkus, J. L., Greenberg, S. A., Trojanowski, J. Q., Traynor, B. J., … Taylor, J. P. (2013). Mutations in prion-like domains in hnRNPA2B1 and hnRNPA1 cause multisystem proteinopathy and ALS. *Nature*, *495*(7442), 467–473. https://doi.org/10.1038/nature11922

Kim, J., Basak, J. M., & Holtzman, D. M. (2009). The role of apolipoprotein E in Alzheimer's disease. *Neuron*, *63*(3), 287–303. https://doi.org/10.1016/j.neuron.2009.06.026

Kishore, A., Meunier, S., & Popa, T. (2014). Cerebellar Influence on Motor Cortex Plasticity: Behavioral Implications for Parkinson's Disease. *Frontiers in Neurology*, *5*, 68. https://doi.org/10.3389/fneur.2014.00068

Klemann, C. J. H. M., & Roubos, E. W. (2011). The gray area between synapse structure and function-Gray's synapse types I and II revisited. *Synapse*, *65*(11), 1222–1230. https://doi.org/10.1002/syn.20962

Kramer, M. L., & Schulz-Schaeffer, W. J. (2007). Presynaptic -Synuclein Aggregates, Not Lewy Bodies, Cause Neurodegeneration in Dementia with Lewy Bodies. *Journal of Neuroscience*, *27*(6), 1405–

1410. https://doi.org/10.1523/JNEUROSCI.4564-06.2007

Laakso, M. P., Partanen, K., Riekkinen, P., Lehtovirta, M., Helkala, E. L., Hallikainen, M., Hänninen, T., Vainio, P., & Soininen, H. (1996). Hippocampal volumes in Alzheimer's disease, Parkinson's disease with and without dementia, and in vascular dementia: An MRI study. *Neurology*, *46*(3), 678–681. https://doi.org/10.1212/WNL.46.3.678

Leal, G., Comprido, D., & Duarte, C. B. (2014). BDNF-induced local protein synthesis and synaptic plasticity. *Neuropharmacology*, *76*, 639–656. https://doi.org/10.1016/j.neuropharm.2013.04.005

Lein, E. S., Hawrylycz, M. J., Ao, N., Ayres, M., Bensinger, A., Bernard, A., Boe, A. F., Boguski, M. S., Brockway, K. S., Byrnes, E. J., Chen, L., Chen, L., Chen, T.-M., Chi Chin, M., Chong, J., Crook, B. E., Czaplinska, A., Dang, C. N., Datta, S., … Jones, A. R. (2007). Genome-wide atlas of gene expression in the adult mouse brain. *Nature*, *445*(7124), 168–176. https://doi.org/10.1038/nature05453

Lerma, J., & Marques, J. M. (2013). Kainate Receptors in Health and Disease. *Neuron*, *80*(2), 292–311. https://doi.org/10.1016/j.neuron.2013.09.045

Levy, W. B., & Steward, O. (1979). Synapses as associative memory elements in the hippocampal formation. *Brain Research*, *175*(2), 233–245. https://doi.org/10.1016/0006-8993(79)91003-5

Li, A., Chen, Y.-S., Ping, X.-L., Yang, X., Xiao, W., Yang, Y., Sun, H.-Y., Zhu, Q., Baidya, P., Wang, X., Bhattarai, D. P., Zhao, Y.-L., Sun, B.-F., & Yang, Y.-G. (2017a). Cytoplasmic m6A reader YTHDF3

promotes mRNA translation. *Cell Research*, *27*(3), 444–447. https://doi.org/10.1038/cr.2017.10

Li, L., Zang, L., Zhang, F., Chen, J., Shen, H., Shu, L., Liang, F., Feng, C., Chen, D., Tao, H., Xu, T., Li, Z., Kang, Y., Wu, H., Tang, L., Zhang, P., Jin, P., Shu, Q., & Li, X. (2017b). Fat mass and obesity-associated (FTO) protein regulates adult neurogenesis. *Human Molecular Genetics*, *26*(13), 2398–2411. https://doi.org/10.1093/hmg/ddx128

Li, X., Xiong, X., Wang, K., Wang, L., Shu, X., Ma, S., & Yi, C. (2016). Transcriptome-wide mapping reveals reversible and dynamic N1-methyladenosine methylome. *Nature Chemical Biology*, *February*. https://doi.org/10.1038/nchembio.2040

Lin, S., Choe, J., Du, P., Triboulet, R., Gregory, R. I., Lin, S., Choe, J., Du, P., Triboulet, R., & Gregory, R. I. (2016). The m6A Methyltransferase METTL3 Promotes Translation in Human Cancer Cells Article The m 6 A Methyltransferase METTL3 Promotes Translation in Human Cancer Cells. *Molecular Cell*, *62*(3), 335–345. https://doi.org/10.1016/j.molcel.2016.03.021

Lin, Y., Protter, D. S. W., Rosen, M. K., & Parker, R. (2015). Formation and Maturation of Phase-Separated Liquid Droplets by RNA-Binding Proteins. *Molecular Cell*, *60*(2), 208–219. https://doi.org/10.1016/j.molcel.2015.08.018

Linder, B., Grozhik, A. V, Olarerin-George, A. O., Meydan, C., Mason, C. E., & Jaffrey, S. R. (2015). Single-nucleotide-resolution mapping of

m6A and m6Am throughout the transcriptome. *Nat Methods*, *12*(8), 767–772. https://doi.org/10.1038/nmeth.3453

Liu, K., Ding, Y., Ye, W., Liu, Y., Yang, J., Liu, J., & Qi, C. (2016). *Structural and Functional Characterization of the Proteins Responsible for 6 -Methyladenosine Modification and Recognition*. 306–318.

Liu, N., Dai, Q., Zheng, G., He, C., Parisien, M., & Pan, T. (2015). N(6)-methyladenosine-dependent RNA structural switches regulate RNA-protein interactions. *Nature*, *518*(7540), 560–564. https://doi.org/10.1038/nature14234

Livingstone, K. M., Celis-Morales, C., Papandonatos, G. D., Erar, B., Florez, J. C., Jablonski, K. A., Razquin, C., Marti, A., Heianza, Y., Huang, T., Sacks, F. M., Svendstrup, M., Sui, X., Church, T. S., Jääskeläinen, T., Lindström, J., Tuomilehto, J., Uusitupa, M., Rankinen, T., … Mathers, J. C. (2016). FTO genotype and weight loss: systematic review and meta-analysis of 9563 individual participant data from eight randomised controlled trials. *BMJ (Clinical Research Ed.)*, *354*, i4707. https://doi.org/10.1136/bmj.i4707

Louis, E. D. (2016). Essential Tremor: A Common Disorder of Purkinje Neurons? *Neuroscientist*, *22*(2), 108–118. https://doi.org/10.1177/1073858415590351

Lu, Y., Christian, K., & Lu, B. (2008). BDNF: A key regulator for protein synthesis-dependent LTP and long-term memory? *Neurobiology of*

Learning and Memory, *89*(3), 312–323. https://doi.org/10.1016/J.NLM.2007.08.018

Luo, S., & Tong, L. (2014). Molecular basis for the recognition of methylated adenines in RNA by the eukaryotic YTH domain. *Proceedings of the National Academy of Sciences of the United States of America*, *111*(38), 13834–13839. https://doi.org/10.1073/pnas.1412742111

MacDonald, V., & Halliday, G. M. (2002). Selective loss of pyramidal neurons in the pre-supplementary motor cortex in Parkinson's disease. In *Movement Disorders* (Vol. 17, Issue 6, pp. 1166–1173). John Wiley & Sons, Ltd. https://doi.org/10.1002/mds.10258

Macon, J. B., & Wolfenden, R. (1968). 1-Methyladenosine. Dimroth rearrangement and reversible reduction. *Biochemistry*, *7*(10), 3453–3458. https://doi.org/10.1021/bi00850a021

Maher, E. A., & Bachoo, R. M. (2015). Glioblastoma. In R. N. Rosenberg & J. M. Pascual (Eds.), *Rosenberg's Molecular and Genetic Basis of Neurological and Psychiatric Disease : Fifth Edition* (5th ed., pp. 909–917). Elsevier Science & Technology. https://doi.org/10.1016/B978-0-12-410529-4.00078-4

Majumder, P., Chu, J.-F., Chatterjee, B., Swamy, K. B. S., & Shen, C.-K. J. (2016). Co-regulation of mRNA translation by TDP-43 and Fragile X Syndrome protein FMRP. *Acta Neuropathologica*, *132*(5), 721–738. https://doi.org/10.1007/s00401-016-1603-8

Mak, E., Su, L., Williams, G. B., Watson, R., Firbank, M., Blamire, A., &

O'Brien, J. (2016). Differential atrophy of hippocampal subfields: A comparative study of dementia with lewy bodies and Alzheimer disease. *American Journal of Geriatric Psychiatry*, *24*(2), 136–143. https://doi.org/10.1016/j.jagp.2015.06.006

Martin, K. C., Barad, M., & Kandel, E. R. (2000). Local protein synthesis and its role in synapse-specific plasticity. *Current Opinion in Neurobiology*, *10*(5), 587–592. https://doi.org/10.1016/S0959-4388(00)00128-8

Matsui, T., Ingelsson, M., Fukumoto, H., Ramasamy, K., Kowa, H., Frosch, M. P., Irizarry, M. C., & Hyman, B. T. (2007). Expression of APP pathway mRNAs and proteins in Alzheimer's disease. *Brain Research*, *1161*, 116–123. https://doi.org/10.1016/J.BRAINRES.2007.05.050

Mattson, M. P., & Magnus, T. (2006). Ageing and neuronal vulnerability. *Nature Reviews Neuroscience*, *7*(4), 278–294. https://doi.org/10.1038/nrn1886

Mauer, J., Luo, X., Blanjoie, A., Jiao, X., Grozhik, A. V., Patil, D. P., Linder, B., Pickering, B. F., Vasseur, J.-J., Chen, Q., Gross, S. S., Elemento, O., Debart, F., Kiledjian, M., & Jaffrey, S. R. (2017). Reversible methylation of m6Am in the 5′ cap controls mRNA stability. *Nature*, *541*(7637), 371–375. https://doi.org/10.1038/nature21022

McLendon, R. E., & Halperin, E. C. (2003). Is the long-term survival of patients with intracranial glioblastoma multiforme overstated?

Cancer, *98*(8), 1745–1748. https://doi.org/10.1002/cncr.11666

Medical Research Council. (2019). *Neurodegenerative diseases and dementia - Funding - Medical Research Council*. https://mrc.ukri.org/funding/science-areas/neurosciences-mental-health/our-science-and-contacts-nmhb/neurodegenerative-diseases-and-dementia/

Mercado, N. M., Collier, T. J., Sortwell, C. E., & Steece-Collier, K. (2017). BDNF in the Aged Brain: Translational Implications for Parkinson's Disease. *Austin Neurology & Neurosciences*, *2*(2). http://www.ncbi.nlm.nih.gov/pubmed/29726549

Merkurjev, D., Hong, W.-T., Iida, K., Oomoto, I., Goldie, B. J., Yamaguti, H., Ohara, T., Kawaguchi, S., Hirano, T., Martin, K. C., Pellegrini, M., & Wang, D. O. (2018a). Synaptic N6-methyladenosine (m6A) epitranscriptome reveals functional partitioning of localized transcripts. *Nature Neuroscience*, *21*(7), 1004–1014. https://doi.org/10.1038/s41593-018-0173-6

Merkurjev, D., Hong, W. T., Iida, K., Oomoto, I., Goldie, B. J., Yamaguti, H., Ohara, T., Kawaguchi, S. ya, Hirano, T., Martin, K. C., Pellegrini, M., & Wang, D. O. (2018b). Synaptic N6-methyladenosine (m6A) epitranscriptome reveals functional partitioning of localized transcripts. *Nature Neuroscience*, 1–11. https://doi.org/10.1038/s41593-018-0173-6

Meyer, K. D., & Jaffrey, S. R. (2014). The dynamic epitranscriptome: N6-methyladenosine and gene expression control. *Nature Reviews.*

Molecular Cell Biology, *15*(5), 313–326. https://doi.org/10.1038/nrm3785

Meyer, K. D., & Jaffrey, S. R. (2017). Rethinking m6A Readers, Writers, and Erasers. *Annual Review of Cell and Developmental Biology*, *33*, 319–342. https://doi.org/10.1146/annurev-cellbio-100616-060758

Meyer, K. D., Patil, D. P., Zhou, J., Pestova, T. V, Qian, S., Jaffrey, S. R., Meyer, K. D., Patil, D. P., Zhou, J., Zinoviev, A., Skabkin, M. A., Elemento, O., Pestova, T. V, Qian, S., & Jaffrey, S. R. (2015). *5′ UTR m6A Promotes Cap-Independent Translation*. 999–1010. https://doi.org/10.1016/j.cell.2015.10.012

Meyer, K. D., Saletore, Y., Zumbo, P., Elemento, O., Mason, C. E., & Jaffrey, S. R. (2012). Comprehensive analysis of mRNA methylation reveals enrichment in 3′ UTRs and near stop codons. *Cell*, *149*(7), 1635–1646. https://doi.org/10.1016/j.cell.2012.05.003

Ming, G., & Song, H. (2011). Adult Neurogenesis in the Mammalian Brain: Significant Answers and Significant Questions. *Neuron*, *70*(4), 687–702. https://doi.org/10.1016/J.NEURON.2011.05.001

Nakazawa, K. (2002). Requirement for Hippocampal CA3 NMDA Receptors in Associative Memory Recall. *Science*, *297*(5579), 211–218. https://doi.org/10.1126/science.1071795

Napoli, I., Mercaldo, V., Boyl, P. P., Eleuteri, B., Zalfa, F., De Rubeis, S., Di Marino, D., Mohr, E., Massimi, M., Falconi, M., Witke, W., Costa-Mattioli, M., Sonenberg, N., Achsel, T., & Bagni, C. (2008). The Fragile X Syndrome Protein Represses Activity-Dependent

Translation through CYFIP1, a New 4E-BP. *Cell*, *134*(6), 1042–1054. https://doi.org/10.1016/J.CELL.2008.07.031

Nguyen, D., Zhou, T., Shu, J., & Mao, J.-H. (2013). Quantifying chromogen intensity in immunohistochemistry via reciprocal intensity. *Protocol Exchange*, *2*(1). https://doi.org/10.1038/protex.2013.097

Nicoll, R. A., & Roche, K. W. (2013). Neuropharmacology Long-term potentiation : Peeling the onion. *Neuropharmacology*, *74*, 18–22. https://doi.org/10.1016/j.neuropharm.2013.02.010

O'Keefe, J., & Dostrovsky, J. (1971). The hippocampus as a spatial map. Preliminary evidence from unit activity in the freely-moving rat. *Brain Research*, *34*(1), 171–175. https://doi.org/10.1016/0006-8993(71)90358-1

O'Keefe, J., & Nades, L. (1979). O ' Keefe & Nadel : Hippocampus as cognitive map. *Behavioral and Brain Sciences*, *2*(4), 487–533. https://doi.org/10.1017/S0140525X00063949

Ovchinnikov, D. A., Korn, O., Virshup, I., Wells, C. A., & Wolvetang, E. J. (2018). The Impact of APP on Alzheimer-like Pathogenesis and Gene Expression in Down Syndrome iPSC-Derived Neurons. *Stem Cell Reports*, *11*(1), 32–42. https://doi.org/10.1016/J.STEMCR.2018.05.004

Parkin, A. J. (1996). Human memory : The hippocampus is the key. *Current Biology*, *6*(12), 1583–1585. https://doi.org/10.1016/S0960-9822(02)70778-1

Pedersen, K. M., Marner, L., Pakkenberg, H., & Pakkenberg, B. (2005). No global loss of neocortical neurons in parkinson's disease: A quantitative stereological study. *Movement Disorders*, *20*(2), 164–171. https://doi.org/10.1002/mds.20289

Petersen, R. C., Smith, G. E., Waring, S. C., Ivnik, R. J., Tangalos, E. G., & Kokmen, E. (1999). Mild Cognitive Impairment. *Archives of Neurology*, *56*(3), 303. https://doi.org/10.1001/archneur.56.3.303

Phillips, H. S., Kharbanda, S., Chen, R., Forrest, W. F., Soriano, R. H., Wu, T. D., Misra, A., Nigro, J. M., Colman, H., Soroceanu, L., Williams, P. M., Modrusan, Z., Feuerstein, B. G., & Aldape, K. (2006). *Molecular subclasses of high-grade glioma predict prognosis , delineate a pattern of disease progression , and resemble stages in neurogenesis*. *March*, 157–173. https://doi.org/10.1016/j.ccr.2006.02.019

Ping, X.-L., Sun, B.-F., Wang, L., Xiao, W., Yang, X., Wang, W.-J., Adhikari, S., Shi, Y., Lv, Y., Chen, Y.-S., Zhao, X., Li, A., Yang, Y., Dahal, U., Lou, X.-M., Liu, X., Huang, J., Yuan, W.-P., Zhu, X.-F., … Yang, Y.-G. (2014). Mammalian WTAP is a regulatory subunit of the RNA N6-methyladenosine methyltransferase. *Cell Research*, *24*(2), 177–189. https://doi.org/10.1038/cr.2014.3

Poewe, W., Seppi, K., Tanner, C. M., Halliday, G. M., Brundin, P., Volkmann, J., Schrag, A.-E., & Lang, A. E. (2017). Parkinson disease. *Nature Reviews Disease Primers*, *3*(1), 17013. https://doi.org/10.1038/nrdp.2017.13

Poon, M. M., Choi, S.-H., Jamieson, C. A. M., Geschwind, D. H., & Martin, K. C. (2006). Identification of Process-Localized mRNAs from Cultured Rodent Hippocampal Neurons. *Journal of Neuroscience*, *26*(51), 13390–13399. https://doi.org/10.1523/JNEUROSCI.3432-06.2006

Pyapali, G. K., Sik, A., Penttonen, M., Buzsaki, G., & Turner, D. A. (1998). Dendritic Properties of Hippocampal CA1 Pyramidal Neurons in the Rat : Intracellular Staining In Vivo and In Vitro. *Journal of Comparative Neurology*, *352*(January 1997), 335–352. https://doi.org/10.1002/(SICI)1096-9861(19980216)391:3<335::AID-CNE4>3.0.CO;2-2

Ramamoorthi, K., Fropf, R., Belfort, G. M., Fitzmaurice, H. L., McKinney, R. M., Neve, R. L., Otto, T., & Lin, Y. (2011). Npas4 Regulates a Transcriptional Program in CA3 Required for Contextual Memory Formation. *Science*, *334*(6063), 1669–1675. https://doi.org/10.1126/science.1208049

Redondo, R. L., & Morris, R. G. M. (2011). *Making memories last : the synaptic tagging and capture hypothesis*. *12*(January). https://doi.org/10.1038/nrn2963

Redondo, R. L., Okuno, H., Spooner, P. A., Frenguelli, B. G., Bito, H., & Morris, R. G. M. (2010). Synaptic Tagging and Capture : Differential Role of Distinct Calcium / Calmodulin Kinases in Protein Synthesis-Dependent Long-Term Potentiation. *Journal of Neuroscience*, *30*(14), 4981–4989. https://doi.org/10.1523/JNEUROSCI.3140-

09.2010

Reni, M., Mazza, E., Zanon, S., Gatta, G., & Vecht, C. J. (2017). Central nervous system gliomas. *Critical Reviews in Oncology/Hematology*, *113*, 213–234. https://doi.org/10.1016/J.CRITREVONC.2017.03.021

Rolland, A.-S., Herrero, M.-T., Garcia-Martinez, V., Ruberg, M., Hirsch, E. C., & François, C. (2007). Metabolic activity of cerebellar and basal ganglia-thalamic neurons is reduced in parkinsonism. *Brain*, *130*, 265–275. https://doi.org/10.1093/brain/awl337

Rong, Y., Durden, D. L., Van Meir, E. G., & Brat, D. J. (2006). 'Pseudopalisading' Necrosis in Glioblastoma: A Familiar Morphologic Feature That Links Vascular Pathology, Hypoxia, and Angiogenesis. *Journal of Neuropathology & Experimental Neurology*, *65*(6), 529–539. https://doi.org/10.1097/00005072-200606000-00001

Ruffmann, C., Calboli, F. C. F., Bravi, I., Gveric, D., Curry, L. K., de Smith, A., Pavlou, S., Buxton, J. L., Blakemore, A. I. F., Takousis, P., Molloy, S., Piccini, P., Dexter, D. T., Roncaroli, F., Gentleman, S. M., & Middleton, L. T. (2016). Cortical Lewy bodies and Aβ burden are associated with prevalence and timing of dementia in Lewy body diseases. *Neuropathology and Applied Neurobiology*, *42*(5), 436–450. https://doi.org/10.1111/nan.12294

Růžička, K., Zhang, M., Campilho, A., Bodi, Z., Kashif, M., Saleh, M., Eeckhout, D., El-Showk, S., Li, H., Zhong, S., Jaeger, G. De,

Mongan, N. P., Hejátko, J., Helariutta, Y., & Fray, R. G. (2017). Identification of factors required for m6A mRNA methylation in Arabidopsis reveals a role for the conserved E3 ubiquitin ligase HAKAI. *New Phytologist*, *215*(1), 157–172. https://doi.org/10.1111/nph.14586

Sajikumar, S., & Frey, J. U. (2004). Resetting of 'synaptic tags' is time- and activity-dependent in rat hippocampal CA1 in vitro. *Neuroscience*, *129*(2), 503–507. https://doi.org/10.1016/J.NEUROSCIENCE.2004.08.014

Schaeffer, C. (2001). The fragile X mental retardation protein binds specifically to its mRNA via a purine quartet motif. *The EMBO Journal*, *20*(17), 4803–4813. https://doi.org/10.1093/emboj/20.17.4803

Schibler, U., Kelley, D. E., & Perry, R. P. (1977). Comparison of methylated sequences in messenger RNA and heterogeneous nuclear RNA from mouse L cells. *Journal of Molecular Biology*, *115*(4), 695–714. https://doi.org/10.1016/0022-2836(77)90110-3

Schulz-Schaeffer, W. J. (2010). The synaptic pathology of α-synuclein aggregation in dementia with Lewy bodies, Parkinson's disease and Parkinson's disease dementia. *Acta Neuropathologica*, *120*(2), 131–143. https://doi.org/10.1007/s00401-010-0711-0

Sharova, L. V, Sharov, A. A., Nedorezov, T., Piao, Y., Shaik, N., & Ko, M. S. H. (2008). *Database for mRNA Half-Life of 19 977 Genes Obtained by DNA Microarray Analysis of Pluripotent and*

Differentiating Mouse Embryonic Stem Cells. https://doi.org/10.1093/dnares/dsn030

Shi, H., Wang, X., Lu, Z., Zhao, B. S., Ma, H., Hsu, P. J., Liu, C., & He, C. (2017). YTHDF3 facilitates translation and decay of N6-methyladenosine-modified RNA. *Cell Research*, *27*(3), 315–328. https://doi.org/10.1038/cr.2017.15

Shultz, S., & Dunbar, R. (2010). Species Differences in Executive Function Correlate With Hippocampus Volume and Neocortex Ratio Across Nonhuman Primates. *Article in Journal of Comparative Psychology*. https://doi.org/10.1037/a0018894

Sommer, C., Straehle, C., Köthe, U., & Hamprecht, F. A. (2011). *Ilastik: Interactive learning and segmentation toolkit*. https://doi.org/10.1109/ISBI.2011.5872394

Sturm, D., Bender, S., Jones, D. T. W., Lichter, P., Grill, J., Becher, O., Hawkins, C., Majewski, J., Jones, C., Costello, J. F., Iavarone, A., Aldape, K., Brennan, C. W., Jabado, N., & Pfister, S. M. (2014). Paediatric and adult glioblastoma: multiform (epi)genomic culprits emerge. *Nature Reviews Cancer*, *14*(2), 92–107. https://doi.org/10.1038/nrc3655

Sullivan, J. M., & Schweizer, F. E. (2015). Neurotransmitter Release from Presynaptic Terminals. *ELS*, 1–7. https://doi.org/10.1002/9780470015902.a0000285.pub2

Supekar, K., Uddin, L. Q., Khouzam, A., Phillips, J., Gaillard, W. D., Kenworthy, L. E., Yerys, B. E., Vaidya, C. J., & Menon, V. (2013).

Brain Hyperconnectivity in Children with Autism and its Links to Social Deficits. *Cell Reports*, *5*(3), 738–747. https://doi.org/10.1016/j.celrep.2013.10.001

Surmeier, D. J., Obeso, J. A., & Halliday, G. M. (2017). Selective neuronal vulnerability in Parkinson disease. *Nature Reviews. Neuroscience*, *18*(2), 101–113. https://doi.org/10.1038/nrn.2016.178

Sutton, M. A., & Schuman, E. M. (2006). *Review Dendritic Protein Synthesis , Synaptic Plasticity , and Memory*. *127*, 49–58. https://doi.org/10.1016/j.cell.2006.09.014

Takada, M., Sugimoto, T., & Hattori, T. (1993). MPTP neurotoxicity to cerebellar Purkinje cells in mice. *Neuroscience Letters*, *150*(1), 49–52. https://doi.org/10.1016/0304-3940(93)90105-T

Takeuchi, T., Duszkiewicz, A. J., & Morris, R. G. M. (2013). The synaptic plasticity and memory hypothesis: encoding, storage and persistence. *Philosophical Transactions of the Royal Society B: Biological Sciences*, *369*(1633), 20130288–20130288. https://doi.org/10.1098/rstb.2013.0288

Tamanini, F., Meijer, N., Verheij, C., Willems, P. J., Galjaard, H., Oostra, B. A., & Hoogeveen, A. T. (1996). FMRP is associated to the ribosomes via RNA. *Human Molecular Genetics*, *5*(6), 809–813. https://doi.org/10.1093/hmg/5.6.809

Tan, E.-K., Chandran, V. R., Fook-Chong, S., Shen, H., Yew, K., Teoh, M.-L., Yuen, Y., & Zhao, Y. (2005). *Alpha-Synuclein mRNA*

Expression in Sporadic Parkinson's Disease. https://doi.org/10.1002/mds.20391

Tsien, J. Z., Huerta, P. T., & Tonegawa, S. (1996). The Essential Role of Hippocampal CA1 NMDA Receptor–Dependent Synaptic Plasticity in Spatial Memory. *Cell*, *87*(7), 1327–1338. https://doi.org/10.1016/S0092-8674(00)81827-9

Tsuboi, Y., & Dickson, D. W. (2005). Dementia with Lewy bodies and Parkinson's disease with dementia: Are they different? *Parkinsonism & Related Disorders*, *11*, S47–S51. https://doi.org/10.1016/J.PARKRELDIS.2004.10.014

UK Statistics. (2018). *Overview of the UK population - Office for National Statistics*. https://www.ons.gov.uk/peoplepopulationandcommunity/populationandmigration/populationestimates/articles/overviewoftheukpopulation/november2018

van Stegen, B., Dagar, S., & Gottmann, K. (2017). Release activity-dependent control of vesicle endocytosis by the synaptic adhesion molecule N-cadherin. *Scientific Reports*, *7*(1), 40865. https://doi.org/10.1038/srep40865

von Gunten, A., Kövari, E., Rivara, C.-B., Bouras, C., Hof, P. R., & Giannakopoulos, P. (2005). Stereologic analysis of hippocampal Alzheimer's disease pathology in the oldest-old: Evidence for sparing of the entorhinal cortex and CA1 field. *Experimental Neurology*, *193*(1), 198–206.

https://doi.org/10.1016/J.EXPNEUROL.2004.12.005

Walters, B. J., Mercaldo, V., Gillon, C. J., Yip, M., Neve, R. L., Boyce, F. M., Frankland, P. W., & Josselyn, S. A. (2017). The Role of The RNA Demethylase FTO (Fat Mass and Obesity-Associated) and mRNA Methylation in Hippocampal Memory Formation. *Neuropsychopharmacology*, *4231*(10), 1502–1510. https://doi.org/10.1038/npp.2017.31

Wang, X., Lu, Z., Gomez, A., Hon, G. C., Yue, Y., Han, D., Fu, Y., Parisien, M., Dai, Q., Jia, G., Ren, B., Pan, T., & He, C. (2014a). N6-methyladenosine-dependent regulation of messenger RNA stability. *Nature*, *505*(7481), 117–120. https://doi.org/10.1038/nature12730

Wang, X., Lu, Z., Gomez, A., Hon, G. C., Yue, Y., Han, D., Fu, Y., Parisien, M., Dai, Q., Jia, G., Ren, B., Pan, T., & He, C. (2014b). *N6-methyladenosine-dependent regulation of messenger RNA stability*. https://doi.org/10.1038/nature12730

Wang, X., Zhao, B. S., Roundtree, I. A., Lu, Z., Han, D., Ma, H., Weng, X., Chen, K., Shi, H., & He, C. (2015). N6-methyladenosine Modulates Messenger RNA Translation Efficiency. *Cell*, *161*(6), 1388–1399. https://doi.org/10.1016/j.cell.2015.05.014

Wang, Y., Li, Y., Toth, J. I., Petroski, M. D., Zhang, Z., & Zhao, J. C. (2014c). LETTER N6-methyladenosine modification destabilizes developmental regulators in embryonic stem cells. *Nature Cell Biology*, *16*(2), 1–10. https://doi.org/10.1038/ncb2902

Wei, C.-M., & Moss, B. (1977). Nucleotide sequences at the N6-

methyladenosine sites of HeLa cell messenger ribonucleic acid. *Biochemistry*, *16*(8), 1672–1676. https://doi.org/10.1021/bi00627a023

Wei, J., Liu, F., Lu, Z., Fei, Q., Ai, Y., He, P. C., Shi, H., Cui, X., Su, R., Klungland, A., Jia, G., Chen, J., & He, C. (2018). Differential m6A, m6Am, and m1A Demethylation Mediated by FTO in the Cell Nucleus and Cytoplasm. *Molecular Cell*, *71*(6), 973-985.e5. https://doi.org/10.1016/J.MOLCEL.2018.08.011

Widagdo, X. J., Zhao, X. Q., Kempen, X. M., Tan, X. M. C., Ratnu, V. S., Wei, W., Leighton, L., Spadaro, P. A., Edson, J., Anggono, X. V., & Bredy, X. T. W. (2016). *Experience-Dependent Accumulation of N6-Methyladenosine in the Prefrontal Cortex Is Associated with Memory Processes in Mice*. *36*(25), 6771–6777. https://doi.org/10.1523/JNEUROSCI.4053-15.2016

Wu, T., & Hallett, M. (2013). The cerebellum in Parkinson's disease. *Brain*, *136*(3), 696–709. https://doi.org/10.1093/brain/aws360

Xiao, W., Adhikari, S., Xiao, W., Adhikari, S., Dahal, U., Chen, Y., Hao, Y., Sun, B., & Sun, H. (2016). Nuclear m6A Reader YTHDC1 Regulates mRNA Splicing. *Molecular Cell*, *61*(4), 507–519. https://doi.org/10.1016/j.molcel.2016.01.012

Xu, C., Liu, K., Ahmed, H., Loppnau, P., Schapira, M., & Min, J. (2015). Structural Basis for the Discriminative Recognition of N6-Methyladenosine RNA by the Human YT521-B Homology Domain Family of Proteins. *The Journal of Biological Chemistry*, *290*(41),

24902–24913. https://doi.org/10.1074/jbc.M115.680389

Xu, C., Wang, X., Liu, K., Roundtree, I. A., Tempel, W., Li, Y., Lu, Z., He, C., & Min, J. (2014). Structural basis for selective binding of m6A RNA by the YTHDC1 YTH domain. *Nature Chemical Biology*, *10*(11), 927–929. https://doi.org/10.1038/nchembio.1654

Yue, Y., Liu, J., & He, C. (2015). *RNA N 6-methyladenosine methylation in post-transcriptional gene expression regulation*. https://doi.org/10.1101/gad.262766

Zeng, Z.-D., Liu, F.-L., & Li, S.-X. (2017). Recent perspectives of ependymomas (childhood brain tumors). *European Review for Medical and Pharmacological Sciences*, *21*(4 Suppl), 13–19. https://www.europeanreview.org/wp/wp-content/uploads/13-19-Recent-perspectives-of-Ependymomas-childhood-brain-tumors.pdf

Zhang, H., Elbaum-Garfinkle, S., Langdon, E. M., Taylor, N., Occhipinti, P., Bridges, A. A., Brangwynne, C. P., & Gladfelter, A. S. (2015). RNA Controls PolyQ Protein Phase Transitions. *Molecular Cell*, *60*(2), 220–230. https://doi.org/10.1016/j.molcel.2015.09.017

Zhang, S., Zhao, B. S., Zhou, A., Lin, K., Zheng, S., Lu, Z., Chen, Y., Sulman, E. P., Xie, K., Bögler, O., Majumder, S., He, C., & Huang, S. (2017). m6A Demethylase ALKBH5 Maintains Tumorigenicity of Glioblastoma Stem-like Cells by Sustaining FOXM1 Expression and Cell Proliferation Program. *Cancer Cell*, *31*(4), 591-606.e6. https://doi.org/10.1016/J.CCELL.2017.02.013

Zhang, Y., O'Connor, J. P., Siomi, M. C., Srinivasan, S., Dutra, A.,

Nussbaum, R. L., & Dreyfuss, G. (1995). The fragile X mental retardation syndrome protein interacts with novel homologs FXR1 and FXR2. *The EMBO Journal*, *14*(21), 5358–5366. https://doi.org/10.1002/J.1460-2075.1995.TB00220.X

Zheng, G., Arne Dahl, J., Niu, Y., Fu, Y., Klungland, A., Yang, Y.-G., & He, C. (2013a). Sprouts of RNA epigenetics. *RNA Biology*, *10*(6), 915–918. https://doi.org/10.4161/rna.24711

Zheng, G., Dahl, J. A., Niu, Y., Fedorcsak, P., Huang, C.-M., Li, C. J., Vågbø, C. B., Shi, Y., Wang, W.-L., Song, S.-H., Lu, Z., Bosmans, R. P. G., Dai, Q., Hao, Y.-J., Yang, X., Zhao, W.-M., Tong, W.-M., Wang, X.-J., Bogdan, F., … He, C. (2013b). ALKBH5 Is a Mammalian RNA Demethylase that Impacts RNA Metabolism and Mouse Fertility. *Molecular Cell*, *49*(1), 18–29. https://doi.org/10.1016/j.molcel.2012.10.015

Zheng, G., Dahl, J. A., Niu, Y., Fedorcsak, P., Huang, C., Li, C. J., Vågbø, C. B., Shi, Y., Wang, W.-L., Song, S., Lu, Z., Bosmans, R. P. G., Dai, Q., Hao, Y., Yang, X., Zhao, W.-M., Tong, W., Wang, X., Bogdan, F., … He, C. (2013c). ALKBH5 Is a Mammalian RNA Demethylase that Impacts RNA Metabolism and Mouse Fertility. *Molecular Cell*, *49*(1), 18–29. https://doi.org/10.1016/j.molcel.2012.10.015

Zhou, J., Wan, J., Gao, X., Zhang, X., Jaffrey, S. R., & Qian, S.-B. (2015a). Dynamic m6A mRNA methylation directs translational control of heat shock response. *Nature*, *526*(7574), 591–594. https://doi.org/10.1038/nature15377

Zhou, J., Wan, J., Gao, X., Zhang, X., Jaffrey, S. R., & Qian, S. (2015b). *Dynamic m6A mRNA methylation directs translational control of heat shock response*. https://doi.org/10.1038/nature15377

Zhou, J., Wan, J., Shu, E., Hess, M. E., Br€, J. C., & Correspondence, S.-B. Q. (2018). N6-Methyladenosine Guides mRNA Alternative Translation during Integrated Stress Response. *Molecular Cell*, *69*, 636-647.e7. https://doi.org/10.1016/j.molcel.2018.01.019

Zhuang, M., Li, X., Zhu, J., Zhang, J., Niu, F., Liang, F., Chen, M., Li, D., Han, P., & Ji, S.-J. (2019). The m6A reader YTHDF1 regulates axon guidance through translational control of Robo3.1 expression. *Nucleic Acids Research*. https://doi.org/10.1093/nar/gkz157

Zola-Morgan, S., Squire, L. R., & Amaralt, D. G. (1986). Human Amnesia and the Medial Temporal Region: Enduring Memory Impairment Following a Bilateral Lesion Limited to Field CA1 of the Hippocampus. In *The Journal of Neurosci*. http://www.jneurosci.org/content/jneuro/6/10/2950.full.pdf

Appendix

Appendix 1. Annotation of m^{6}A peaks from grey matter.

Gene name	m^{6}A peaks
A1BG	5
A3GALT2	3
A4GALT	1
AAR2	3
AASS	2
AATBC	1
ABCA11P	2
ABCA4	1
ABCB9	1
ABCC10	2
ABCC3	2
ABCC5-AS1	1
ABCF3	1
ABHD15	3
ABHD16B	3
ABHD17A	2
ABHD17B	1
ABHD8	1
ABI2	3
ABL1	1
ABRAXAS2	1
ABT1	1
ABTB1	5
ABTB2	1
ACACA	1
ACADS	2
ACADVL	1
ACAT2	2
ACBD6	1
ACER2	3
ACHE	1
ACKR3	1
ACP6	2
ACSF3	1
ACSL3	1
ACSS1	1
ACTB	2
ACTG1	2
ACTG1P4	2
ACTL8	2
ACTN1-AS1	3
ACTR1B	1
ACTR2	1
ACVR1	1
ADAL	1
ADAM11	1
ADAM1A	2
ADAM22	1
ADAM30	4
ADAMTS8	1
ADAP1	2
ADAR	3
ADARB1	1
ADARB2	1
ADARB2-AS1	1
ADAT1	1
ADCK2	2
ADCY3	1
ADCY5	4
ADCY7	1
ADCY8	2
ADCY9	1
ADCYAP1R1	2
ADD1	1
ADD2	1
ADGRA1	3
ADGRB1	1
ADGRB2	1
ADGRB3	2
ADGRG3	2
ADGRL2	2
ADGRL3	1
ADGRL3-AS1	3
ADGRV1	2
ADIRF	1
ADNP	2
ADO	1
ADORA2A	1
ADPGK-AS1	2
ADPRHL1	1
ADPRHL2	2
ADRA1A	4
ADRA1B	1
ADRA1D	2
ADRA2A	4
ADRA2C	6
ADRB1	2
ADRM1	2
ADSL	3
ADSSL1	1
AFAP1-AS1	2
AFAP1L2	2
AFDN	1
AFF1	1
AFF2	1
AFF4	1
AFG3L1P	7
AGAP2	1
AGAP2-AS1	5
AGER	1
AGK	2
AGMAT	1
AGO1	1
AGO3	1
AGPAT1	1
AGPAT4	1
AGPAT4-IT1	1
AGT	2
AGTPBP1	1
AHCYL2	2
AHDC1	6
AHNAK	#
AHNAK2	6
AHSA1	1
AHSA2P	4
AJAP1	2
AJM1	2
AK1	1
AK5	1
AK7	1
AKAP10	1
AKAP11	2
AKAP12	2
AKAP2	2
AKAP5	2
AKAP6	3
AKAP8	1
AKIP1	1
AKNA	1
AKTIP	1
ALCAM	1
ALDH1A3	3
ALDH1B1	2
ALDH3A1	1
ALDH3A2	1
ALDH5A1	1
ALDOA	2
ALG1	2
ALG12	2
ALG1L	2
ALK	1
ALKBH1	1
ALKBH2	2
ALKBH4	2
ALKBH5	2
ALOX15	2
ALPK3	3
ALS2	1
ALS2CR12	1
ALX3	1
ALX4	1
AMBP	1
AMBRA1	1
AMD1	1
AMER2	3
AMER3	2
AMFR	3
AMIGO1	3
AMIGO3	1
AMMECR1L	1
AMN	4
AMOT	1
AMOTL1	1
AMPD2	1
AMT	4
AMZ1	6
AMZ2P1	1
ANAPC7	1
ANGPTL2	1
ANK1	2
ANK2	6

ANK3	2	AQP12A	2	ARL6IP1	1	ATG4D	1
ANKLE1	1	AQP4	2	ARL6IP4	3	ATG9A	1
ANKLE2	3	ARAP1	1	ARL8A	1	ATIC	1
ANKRD11	1	ARAP1-AS2	1	ARMC1	1	ATL1	1
ANKRD19P	2	ARAP2	2	ARMC5	6	ATMIN	2
ANKRD2	1	ARC	4	ARMCX2	1	ATOH7	1
ANKRD33B	9	AREL1	1	ARMCX3	2	ATP10A	1
ANKRD34A	2	ARF6	1	ARMCX5-GPRASP2	3	ATP1A1-AS1	1
ANKRD39	2	ARFGAP2	1	ARMH4	1	ATP1A3	1
ANKRD40	2	ARFGAP3	1	ARPC4	2	ATP1B1	3
ANKRD46	1	ARFIP2	1	ARPC5L	1	ATP1B3	1
ANKRD49	1	ARHGAP1	2	ARPP21	1	ATP2A2	2
ANKRD50	1	ARHGAP12	1	ARRDC2	3	ATP2B1	1
ANKRD63	4	ARHGAP20	2	ARSA	1	ATP2B1-AS1	2
ANKRD9	2	ARHGAP21	3	ARSB	1	ATP2B4	1
ANKS6	2	ARHGAP22	1	ARTN	2	ATP2C2-AS1	1
ANO10	1	ARHGAP23	4	ARX	1	ATP5MF	2
ANO8	2	ARHGAP26	1	ASAH2	1	ATP5PO	1
ANXA2P1	1	ARHGAP26-IT1	1	ASB1	1	ATP6V0A4	4
AP1G2	1	ARHGAP27	1	ASB13	3	ATP6V0C	3
AP1M1	1	ARHGAP27P1-BPTFP1-KPNA2P3	1	ASB6	7	ATP6V0E2	2
AP3B2	1	ARHGAP32	1	ASB8	1	ATP6V0E2-AS1	2
AP3M2	2	ARHGAP33	2	ASCL2	1	ATP8B2	1
AP4S1	1	ARHGAP35	3	ASCL3	1	ATP8B5P	1
AP5B1	4	ARHGAP4	1	ASCL5	1	ATRN	1
AP5S1	2	ARHGAP5	1	ASF1A	1	ATRNL1	1
AP5Z1	3	ARHGAP5-AS1	1	ASGR1	1	ATXN1	1
APAF1	1	ARHGDIA	2	ASIC2	2	ATXN1L	5
APBA1	1	ARHGEF25	1	ASIC3	2	ATXN7L3	2
APBA2	3	ARHGEF26	1	ASIC4	1	ATXN7L3B	4
APBB1	1	ARHGEF3	1	ASMT	2	AUNIP	3
APC	1	ARHGEF4	2	ASMTL-AS1	1	AUP1	1
APC2	1	ARHGEF9	1	ASPDH	2	AURKAIP1	1
APCDD1	2	ARID1A	2	ASPH	1	AURKC	3
APEH	8	ARID1B	2	ASPHD1	3	AUTS2	1
APH1B	1	ARID5B	2	ASPHD2	2	AVL9	1
APLNR	4	ARIH1	3	ASPRV1	1	AXIN1	1
APLP1	1	ARL14EP	1	ASXL1	3	AXIN2	2
APLP2	1	ARL2BP	1	ASXL2	2	AZI2	2
APOA1	3	ARL4C	4	ASXL3	1	B3GALNT1	4
APOD	1	ARL4D	1	ATCAY	2	B3GALT1	1
APOE	1	ARL5A	1	ATF4	2	B3GALT6	3
APOL2	1	ARL5C	1	ATF5	1	B3GAT1	5
APOLD1	3	ARL6	1	ATG13	2	B3GAT2	1
APP	1			ATG14	4	B3GNT2	2
AQP11	2			ATG16L2	1		

B3GNT4	5	BHLHB9	1	BRSK1	1	C19orf44	2
B3GNT7	1	BHLHE22	1	BSCL2	1	C19orf47	2
B3GNT9	6	BHLHE40-AS1	2	BSG	1	C19orf54	1
B3GNTL1	2	BHLHE41	1	BSN-DT	5	C19orf70	2
B4GALNT4	1	BICD1	1	BTBD11	1	C19orf71	1
B4GALT2	1	BICD2	2	BTBD17	1	C19orf81	5
B4GALT7	2	BICDL1	1	BTBD2	2	C1orf115	2
B4GAT1	2	BICRAL	1	BTBD3	1	C1orf123	2
BAALC	1	BIN1	1	BTBD7	1	C1orf189	1
BAALC-AS1	1	BIRC2	1	BTBD9-AS1	7	C1orf198	2
BACE1	1	BIRC3	1	BTD	2	C1orf216	3
BACE1-AS	1	BIRC6	2	BUD31	2	C1orf35	1
BAG1	1	BLCAP	2	C10orf105	1	C1orf50	2
BAG5	1	BLOC1S3	1	C10orf82	5	C1orf56	1
BAIAP2-DT	2	BLOC1S4	2	C10orf90	1	C1orf74	1
BAIAP3	1	BMI1	1	C11orf24	1	C1QB	2
BAMBI	2	BMP6	1	C11orf42	3	C1QBP	1
BANF1	1	BMP7	1	C11orf68	1	C1QC	1
BAP1	2	BMP8A	1	C11orf87	1	C1QL2	2
BASP1	2	BMPR2	1	C11orf91	5	C1QL3	1
BASP1-AS1	1	BMS1P20	1	C11orf94	2	C1QTNF12	1
BATF3	1	BMS1P22	1	C11orf95	3	C1R	2
BAZ1B	1	BNIP1	1	C11orf96	2	C20orf144	4
BCAN	1	BNIP3	1	C12orf43	1	C20orf173	1
BCAR3	3	BNIPL	1	C12orf49	1	C20orf27	1
BCDIN3D	3	BOD1L1	1	C12orf57	1	C21orf2	1
BCKDK	2	BOK-AS1	2	C12orf76	1	C22orf23	1
BCL11A	1	BOLA1	1	C14orf132	6	C22orf24	3
BCL11B	2	BOLA3	3	C14orf180	1	C22orf31	2
BCL2	3	BOLA3-AS1	1	C15orf39	2	C22orf39	1
BCL2L1	2	BORCS6	3	C15orf59	3	C2CD2L	3
BCL2L13	3	BPTF	1	C15orf61	1	C2CD4C	4
BCL2L14	1	BRAP	1	C16orf72	3	C2orf42	2
BCL2L2	2	BRD1	1	C16orf86	3	C2orf71	1
BCORL1	2	BRD2	6	C16orf91	1	C2orf81	4
BCR	2	BRD3OS	3	C16orf92	1	C3orf18	2
BCS1L	1	BRD4	1	C17orf107	2	C3orf20	1
BDNF	3	BREA2	3	C17orf50	1	C3orf58	2
BEAN1-AS1	1	BRF1	2	C17orf51	1	C3orf80	3
BEGAIN	1	BRF2	7	C17orf58	1	C4orf19	6
BEND3P3	5	BRICD5	5	C17orf67	1	C4orf51	1
BEND4	1	BRINP1	2	C17orf80	1	C5orf24	1
BET1L	1	BRINP2	1	C18orf25	1	C5orf30	1
BEX3	1	BRMS1	1	C19orf24	1	C5orf64	3
BHLHA15	9	BRPF1	1	C19orf25	6	C6orf120	2
BHLHA9	1	BRPF3	2	C19orf33	1	C6orf226	1

C6orf47	3	CAMK2D	1	CCDC24	1	CDC42EP3	1
C6orf62	2	CAMKK2	1	CCDC28B	1	CDC42EP4	1
C7orf26	1	CAMLG	1	CCDC32	1	CDC42SE2	1
C7orf43	2	CAMSAP1	5	CCDC34	1	CDCA7L	1
C8orf58	1	CAMSAP2	1	CCDC57	1	CDH10	1
C8orf76	1	CAMTA1	2	CCDC70	3	CDH18	1
C8orf82	2	CAMTA2	1	CCDC71	2	CDH2	1
C9orf129	2	CAND1	2	CCDC71L	2	CDH20	1
C9orf131	1	CAND2	2	CCDC74B	2	CDH23	2
C9orf153	1	CANT1	1	CCDC80	1	CDH6	1
C9orf16	1	CAPN10	1	CCDC85A	1	CDH8	2
C9orf24	1	CAPN10-DT	3	CCDC85B	1	CDIPTOSP	1
C9orf3	1	CAPN11	1	CCDC88C	1	CDK11B	2
C9orf72	2	CAPN12	1	CCDC89	1	CDK12	2
CA10	1	CAPN13	1	CCDC92	1	CDK13	2
CA4	2	CAPN6	1	CCDC96	3	CDK17	1
CA5BP1	1	CAPRIN2	1	CCK	3	CDK18	1
CAB39	1	CAPS	1	CCKBR	1	CDK20	1
CABLES1	4	CARD9	2	CCND3	1	CDK3	2
CABP1	2	CASKIN1	3	CCNI2	1	CDK5R1	3
CABP7	1	CASKIN2	1	CCNK	1	CDK5R2	2
CACNA1A	1	CASP16P	2	CCNL1	1	CDK5RAP1	1
CACNA1C-AS1	3	CASS4	1	CCNL2	1	CDK5RAP2	1
CACNA1E	2	CASTOR1	1	CCNO	1	CDK9	1
CACNA1G	1	CAVIN2	3	CCNQ	2	CDKAL1	1
CACNA1G-AS1	1	CBARP	1	CCSER1	1	CDKL2	1
CACNA1I	2	CBLN2	2	CD14	1	CDPF1	1
CACNB3	2	CBLN4	1	CD180	4	CDR2	2
CACNG1	3	CBR1	1	CD200	1	CDRT15	1
CACNG3	3	CBR4	1	CD22	1	CDRT4	2
CACTIN	1	CBX4	3	CD2BP2	4	CDS1	1
CACTIN-AS1	2	CBX6	4	CD320	2	CDS2	1
CACUL1	1	CBX7	2	CD34	4	CDV3	1
CACYBP	1	CBX8	3	CD40	1	CDYL	1
CADM2	2	CCAR2	4	CD58	1	CEBPA	2
CADM3-AS1	2	CCDC115	1	CD74	1	CEBPA-DT	1
CALHM2	2	CCDC127	1	CD83	1	CEBPB	1
CALM1	2	CCDC137	1	CD8A	1	CEBPB-AS1	3
CALM3	2	CCDC138	1	CD93	1	CEBPD	2
CALML4	1	CCDC144CP	1	CDAN1	1	CEBPG	1
CALY	1	CCDC151	1	CDC25C	1	CELF5	2
CAMK1	1	CCDC154	4	CDC37L1	1	CELP	1
CAMK1D	1	CCDC177	2	CDC42BPA	1	CELSR2	3
CAMK2A	1	CCDC183	1	CDC42BPB	1	CELSR3	5
CAMK2B	3	CCDC184	3	CDC42BPG	1	CEND1	1
		CCDC188	3	CDC42EP2	2	CENPA	2

CENPB	2	CHRAC1	1	CLEC19A	1	COL16A1	2
CENPBD1P1	4	CHRM1	1	CLEC3B	1	COL6A3	1
CENPI	1	CHRM3-AS1	1	CLIP1-AS1	1	COL8A2	1
CENPO	2	CHRM4	3	CLIP2	1	COL9A3	2
CENPV	1	CHRM5	1	CLIP3	1	COLGALT1	2
CENPX	1	CHRNA2	2	CLN5	1	COLGALT2	4
CEP170B	3	CHRNA4	5	CLPB	1	COMMD5	4
CEP192	1	CHRNB2	4	CLSTN3	2	COMMD8	1
CEP350	1	CHST1	3	CLTA	1	COMP	3
CEP68	2	CHST10	4	CLTB	1	COPS2	1
CERCAM	1	CHST12	2	CLTCL1	1	COQ6	3
CERK	1	CHST14	3	CLUAP1	1	COQ8A	2
CERS1	3	CHST15	3	CLVS1	1	CORO2B	1
CERS6	1	CHST2	2	CLVS2	1	CORO6	7
CES2	2	CHST3	1	CMAS	1	COX14	1
CES4A	2	CHST5	5	CMTM1	1	COX4I1	1
CES5AP1	1	CHST7	2	CMTM3	1	COX6A1	1
CFAP298	1	CHSY1	1	CNDP1	3	COX7A2L	1
CFAP53	2	CHSY3	1	CNFN	1	COX7B	1
CFAP69	1	CHTF8	1	CNIH2	1	COX7B2	1
CFD	1	CIAO1	1	CNIH3	3	CPE	1
CFL1	1	CIB1	4	CNKSR2	1	CPEB4	1
CFP	1	CIC	4	CNNM1	2	CPLANE2	4
CGGBP1	3	CINP	1	CNNM2	2	CPLX2	1
CGRRF1	1	CIP2A	1	CNNM3	1	CPNE1	3
CH17-340M24.3	1	CIPC	1	CNNM3-DT	1	CPS1-IT1	1
CH25H	1	CIRBP-AS1	2	CNNM4	1	CPSF4L	1
CHAC1	1	CISD1	1	CNOT3	1	CPT1C	1
CHADL	6	CISD3	1	CNOT7	2	CPTP	1
CHD1	1	CITED2	2	CNP	2	CRAT37	3
CHD5	2	CITED4	3	CNPY3	1	CRB2	6
CHD6	1	CKAP4	2	CNR1	5	CREBBP	1
CHD7	1	CKB	1	CNRIP1	1	CREBL2	1
CHD8	1	CKM	1	CNST	1	CREBZF	2
CHD9	2	CKMT2	4	CNTD2	1	CREG2	1
CHDH	3	CLBA1	2	CNTF	2	CRHR1	1
CHERP	1	CLCC1	1	CNTN2	4	CRIM1	1
CHGA	3	CLCN3	1	CNTNAP2	1	CRIP2	2
CHGB	1	CLCN4	3	CNTNAP5	2	CRIPAK	2
CHKA	1	CLCN6	1	COA3	1	CRMP1	1
CHL1	2	CLDN12	1	COA5	2	CRTAP	2
CHL1-AS1	2	CLDN20	2	COA7	2	CRTC1	4
CHMP1B	1	CLDN34	1	COG1	1	CRYM-AS1	1
CHMP4B	2	CLDN5	4	COG3	1	CSAD	1
CHMP6	3	CLEC14A	2	COL11A2	1	CSE1L	1
CHPF	4	CLEC18B	2	COL14A1	1	CSF1	1

CSF1R	3	CYBA	1	DDX56	1	DLGAP2-AS1	1
CSGALNACT1	1	CYBC1	3	DDX6	1	DLGAP4	2
CSNK1A1	1	CYCSP52	1	DEDD2	2	DLK2	1
CSNK1E	1	CYHR1	2	DEF6	1	DLX6	1
CSNK1G2-AS1	4	CYP17A1	5	DEGS1	1	DMAC1	1
CSPG4	4	CYP1B1	2	DEGS2	1	DMPK	2
CSPG5	1	CYP26B1	1	DENND2A	1	DMRTB1	1
CSRNP1	2	CYP2T1P	2	DENND3	1	DNAAF2	3
CSRNP2	1	CYP2W1	1	DENND4B	1	DNAJA1	1
CSRNP3	5	CYP46A1	3	DENND5A	1	DNAJB1	1
CSRP1	2	CYREN	2	DEPDC7	1	DNAJB12	2
CSTB	1	CYTH2	1	DEPP1	1	DNAJB2	2
CSTF2T	3	D2HGDH	2	DERL1	1	DNAJB5-DT	3
CTB-178M22.2	3	DAB2IP	4	DEXI	6	DNAJC17	1
CTBP1-AS	2	DACT1	2	DFFA	1	DNAJC25	1
CTBP1-DT	3	DACT3	3	DGCR11	3	DNAJC30	3
CTBP2	2	DAGLB	1	DGCR5	3	DNAJC5	1
CTDP1	3	DALRD3	3	DGCR8	1	DNAL4	1
CTDSP2	1	DAO	2	DGCR9	6	DNASE1	2
CTNNA1	3	DAP	2	DGKE	1	DNASE1L2	1
CTNNB1	1	DAPK3	2	DGKQ	3	DNASE2	2
CTNND1	2	DAW1	2	DGKZ	2	DNER	1
CTRC	2	DAXX	1	DHCR24	3	DNM1	1
CTSA	2	DBNDD1	1	DHODH	1	DNM1L	1
CTSB	1	DBNDD2	2	DHRS7B	1	DOCK4	1
CTSC	1	DCAF16	1	DHRS7C	1	DOCK4-AS1	1
CTSL	1	DCHS1	2	DHX34	3	DOCK9-AS1	1
CTTN	4	DCHS2	1	DHX36	1	DOHH	1
CTU1	1	DCLK1	1	DHX58	3	DOK1	1
CTXN1	1	DCLK2	3	DICER1	3	DOK4	1
CUEDC1	1	DCP2	1	DIDO1	1	DOLPP1	3
CUL1	1	DCT	1	DIO2-AS1	5	DOPEY1	1
CUL9	1	DCTD	3	DIP2A	2	DOPEY2	1
CUTC	1	DDAH2	2	DIRAS1	4	DPF1	2
CWF19L1	1	DDC	1	DIRAS2	2	DPH3P1	1
CX3CL1	2	DDHD1	1	DISC1	2	DPH7	1
CX3CR1	2	DDIT4	2	DISP2	6	DPM2	3
CXCR5	2	DDN-AS1	3	DISP3	3	DPP10	1
CXorf36	1	DDX11L5	2	DKK3	3	DPP3	1
CXXC4-AS1	1	DDX19A	4	DLAT	2	DPP7	2
CXXC5	3	DDX23	1	DLC1	3	DPY19L2P2	3
CYB561	5	DDX24	2	DLEU7	2	DPY19L2P3	1
CYB561D1	2	DDX31	4	DLEU7-AS1	1	DPYSL2	1
CYB5D1	1	DDX3X	1	DLG3-AS1	1	DPYSL4	3
CYB5D2	4	DDX41	3	DLG4	1	DR1	1
		DDX51	1	DLG5	5		

DRD1	2	EDNRB	1	EMILIN3	2	ERLNC1	1
DRG1	1	EEF1D	2	EML3	1	ERVFRD-1	1
DRGX	1	EEF1G	3	EML6	2	ERVK13-1	2
DSE	3	EEPD1	1	EMSY	1	ERVK3-1	#
DSN1	#	EFCAB14	2	EMX1	5	ESYT3	4
DST	2	EFCAB14-AS1	1	EMX2	1	ETNPPL	1
DSTYK	1	EFCAB6	2	ENDOG	4	ETS2	2
DTNA	1	EFCAB6-AS1	1	ENDOU	1	ETV4	1
DTNB	1	EFCAB8	1	ENDOV	1	ETV5	3
DTNBP1	3	EFHC1	4	ENGASE	2	EVA1B	1
DTX1	2	EFHD2	1	ENHO	2	EVI2A	1
DTX3	2	EFNB2	1	ENO1	1	EVPL	1
DTYMK	1	EFNB3	1	ENO2	1	EXOC3	1
DUS2	1	EFS	1	ENOPH1	1	EXOC3-AS1	2
DUS3L	1	EGF	1	ENSA	1	EXOC5	1
DUSP1	2	EGFLAM	1	EP300	2	EXOC8	2
DUSP14	1	EGLN1	3	EP300-AS1	3	EXOSC6	2
DUSP16	1	EGLN2	2	EP400	2	EXT1	3
DUSP2	1	EGLN3	1	EP400P1	1	EXT2	1
DUSP26	2	EGR1	2	EPAS1	2	EXTL1	2
DUSP3	2	EGR2	1	EPB41	3	EXTL3	4
DUSP4	1	EGR3	2	EPC2	2	EZH2	1
DUSP5	1	EGR4	1	EPDR1	2	F2RL3	3
DUSP6	1	EHBP1L1	1	EPG5	1	F3	1
DUSP7	3	EHD2	3	EPHA3	1	F7	1
DUSP8	1	EHD3	3	EPHA4	6	FAAP100	3
DVL2	2	EID1	3	EPHA5-AS1	1	FABP5	1
DVL3	1	EID2B	3	EPHA6	1	FADD	2
DYNC1H1	4	EIF1	1	EPHA8	3	FADS3	1
DYNC1I1	1	EIF2AK4	1	EPHB1	1	FAH	2
DYNC1LI2	1	EIF2D	1	EPHB3	1	FAHD1	1
DYNLL1	1	EIF2S2	1	EPHB6	3	FAHD2A	2
DYNLL2	2	EIF3D	1	EPHX3	2	FAIM2	1
DYRK1A	3	EIF3J	1	EPM2AIP1	3	FAM102A	1
DYRK2	2	EIF4E3	3	EPN1	1	FAM107A	2
DYSF	1	EIF4G1	1	EPN2-IT1	1	FAM110C	1
DZIP1	2	EIF4G3	2	EPOP	2	FAM117B	3
EBI3	2	EIF5	2	EPS8L1	2	FAM120AOS	1
EBLN3P	2	ELAVL3	2	ERAS	1	FAM120B	1
EBP	1	ELF2	1	ERBB4	1	FAM122A	1
ECH1	2	ELFN1-AS1	2	ERC1	1	FAM124A	1
EDEM3	1	ELK3	1	ERC2	2	FAM131A	2
EDF1	1	ELOB	1	ERCC3	1	FAM131B	2
EDIL3	1	ELP6	1	ERF	1	FAM133B	1
EDN1	2	EMC3-AS1	1	ERFE	1	FAM13A-AS1	4
EDN2	2	EME2	2	ERH	2	FAM155A	1

FAM160B2	1	FAM83C	2	FBXW7-AS1	2	FMN2	5
FAM163B	2	FAM83E	1	FCGBP	1	FMNL2	1
FAM166B	2	FAM84A	3	FCGRT	1	FN1	1
FAM167A	2	FAM84B	2	FEM1A	7	FN3K	1
FAM168B	3	FAM89B	2	FEM1B	5	FNDC5	4
FAM171A2	1	FAM8A1	1	FEM1C	2	FNDC9	3
FAM171B	3	FAM90A1	1	FEN1	1	FNIP2	2
FAM173A	1	FAM92B	7	FERMT2	1	FNTA	1
FAM174A	1	FAM98B	1	FES	2	FOS	1
FAM174B	1	FAM98C	1	FEZ2	2	FOSB	2
FAM180B	2	FAN1	2	FEZF2	1	FOSL2	1
FAM181B	2	FANCB	1	FGD5-AS1	1	FOXC1	4
FAM183BP	2	FANCE	2	FGF12	4	FOXD1	1
FAM185A	1	FAR2P2	2	FGF12-AS1	1	FOXF1	1
FAM187A	#	FASN	1	FGF14	2	FOXG1	3
FAM189A2	1	FASTK	2	FGF2	1	FOXH1	2
FAM198A	1	FASTKD1	1	FGF22	1	FOXJ1	2
FAM198B-AS1	2	FASTKD5	1	FGF23	1	FOXJ2	1
FAM19A2	4	FAT1	2	FGFR1	2	FOXN3	2
FAM201A	1	FAT3	6	FGFR2	1	FOXN4	1
FAM208A	2	FAT4	2	FGFR3	2	FOXO3	1
FAM208B	1	FAXC	1	FGFR4	1	FOXO4	1
FAM20B	1	FBH1	3	FHAD1	1	FOXO6	1
FAM20C	3	FBLL1	2	FIBIN	2	FOXP1	1
FAM213A	2	FBLN2	2	FICD	3	FOXRED2	1
FAM217B	3	FBLN7	1	FIGNL2	6	FRAT1	1
FAM219B	2	FBRS	2	FITM2	1	FRAT2	3
FAM220A	2	FBXL12	1	FIZ1	2	FREM3	3
FAM222A	1	FBXL14	1	FJX1	3	FRMD4A	2
FAM222A-AS1	2	FBXL17	1	FKBP11	1	FRMD6	1
FAM25C	1	FBXL19	2	FKBP2	1	FRS3	2
FAM25E	1	FBXL19-AS1	1	FKBP4	1	FSCN1	2
FAM25G	1	FBXL3	3	FLG-AS1	1	FSTL4	1
FAM32A	2	FBXL4	1	FLJ20021	1	FTCD-AS1	1
FAM3A	1	FBXO10	4	FLJ23867	2	FTH1	1
FAM41C	1	FBXO22	1	FLJ31356	2	FTO	1
FAM43A	1	FBXO33	1	FLJ42102	1	FUT1	2
FAM43B	3	FBXO38	1	FLJ44635	1	FUT11	2
FAM50B	1	FBXO41	2	FLJ45513	1	FUT4	1
FAM53A	1	FBXO44	3	FLNB-AS1	1	FUT9	2
FAM53B-AS1	6	FBXO46	5	FLRT1	8	FUZ	2
FAM66C	1	FBXO6	1	FLRT2	8	FXYD2	4
FAM69C	1	FBXW11	1	FLT3LG	1	FXYD6	1
FAM78A	1	FBXW2	1	FLVCR1	1	FZD1	2
FAM81A	1	FBXW5	3	FLYWCH1	1	FZD4	2
		FBXW7	2	FMN1	4	FZD7	1

FZD8	1	GDF11	2	GMPR	3	GPR37	3
FZD9	2	GDF15	1	GNA12	2	GPR37L1	4
GAB1	1	GDF2	1	GNA15	4	GPR45	2
GABARAP	1	GDF7	1	GNAI3	1	GPR6	2
GABBR1	2	GDI1	1	GNAL	1	GPR61	3
GABPB1	1	GDI2	1	GNAZ	1	GPR62	2
GABPB1-AS1	1	GDPD4	1	GNB1	1	GPR68	2
GABPB2	1	GDPGP1	1	GNB3	1	GPR75	1
GABRA5	1	GEMIN4	4	GNE	1	GPR83	1
GABRB2	1	GEMIN8P4	1	GNPTG	1	GPR85	1
GABRB3	1	GET4	3	GNRHR2	1	GPR88	2
GABRD	1	GFAP	3	GOLGA3	1	GPRASP1	1
GABRG2	1	GFM2	1	GOLGA4	2	GPRC5B	3
GADD45B	4	GFOD1	1	GOLGA6A	1	GPRC5C	1
GADD45G	1	GFPT1	1	GOLGA6L10	1	GPRIN1	4
GADD45GIP1	1	GFRA2	2	GOLGA7B	2	GPRIN2	1
GAL3ST1	1	GFRA4	1	GOLGA8IP	1	GPS2	2
GAL3ST3	1	GFY	1	GOLIM4	1	GPSM1	2
GALE	1	GGA2	1	GOLM1	1	GPSM3	1
GALNT11	2	GGA3	4	GOLPH3	#	GPT	2
GALNT17	2	GGT1	1	GOLT1A	3	GPX2	2
GALNT18	1	GHRL	1	GON7	1	GRAMD2A	1
GANAB	3	GHRLOS	4	GOT1	3	GRAMD2B	1
GAP43	1	GID8	1	GP1BB	5	GRAMD4	2
GAPDH	3	GIMAP1-GIMAP5	2	GP6	1	GRASP	3
GAPVD1	1	GIMAP5	2	GP9	2	GRB10	4
GAREM2	4	GIMAP6	1	GPANK1	1	GREM2	1
GARS	1	GIMAP7	1	GPAT2	3	GRHL3	3
GAS1	2	GINS2	1	GPATCH2L	1	GRHPR	2
GAS2L1	1	GIT1	1	GPER1	2	GRIA2	3
GAS6-AS1	1	GJA10	2	GPI	1	GRID1-AS1	1
GATAD2A	2	GJB6	1	GPKOW	2	GRID2	1
GATD1	1	GJD3	1	GPM6B	1	GRIK2	1
GATM	1	GJD4	1	GPN2	3	GRIK3	7
GBA2	1	GLB1L3	1	GPR12	1	GRIK4	1
GBAT2	1	GLDN	1	GPR135	4	GRIN1	2
GBX1	1	GLIS3-AS1	1	GPR146	3	GRIN2A	3
GBX2	2	GLMN	1	GPR150	2	GRIN2B	1
GCC1	2	GLOD4	1	GPR158	2	GRIN2C	1
GCFC2	1	GLRX5	1	GPR158-AS1	1	GRIN2D	1
GCK	1	GLS	2	GPR161	1	GRIN3A	4
GCNA	1	GLTPD2	2	GPR176	2	GRIN3B	2
GCNT1	1	GLUD1	2	GPR179	1	GRIP2	2
GCNT4	1	GLUD1P3	1	GPR21	1	GRK2	1
GDE1	1	GLUL	1	GPR25	2	GRM1	1
GDF10	3	GMPPB	1	GPR26	1	GRM2	4

GRM3	3	HCG14	1	HIST1H4E	1	HSPA2	2
GRM4	2	HCG17	2	HIST3H2A	1	HSPA4	4
GRM5	2	HCG2040054	2	HK1	1	HSPB1	2
GRM5-AS1	#	HCLS1	1	HK3	1	HSPB8	1
GRM7	1	HCN2	2	HLA-A	3	HTD2	2
GRM7-AS1	1	HCN4	2	HLA-B	3	HTR1F	1
GRN	1	HCRTR1	1	HLA-C	1	HTR2A	1
GRPEL2	1	HDAC10	1	HLA-E	1	HTR2A-AS1	1
GRWD1	1	HDDC3	1	HLA-L	1	HTR5A-AS1	1
GSDMB	1	HDHD3	1	HLCS	1	HTR6	4
GSDMC	1	HEBP2	4	HLF	2	HTRA4	1
GSK3A	2	HECA	2	HMBOX1	2	HYAL2	4
GSK3B	1	HECTD1	3	HMBS	1	HYAL3	1
GSPT1	1	HECTD4	1	HMCN2	1	HYPK	1
GSTK1	1	HECW2	1	HMGCS1	2	IAH1	1
GSTO1	1	HEIH	1	HMGN1	1	IBA57	1
GSTZ1	1	HELZ2	4	HNRNPA0	2	IBA57-DT	2
GTDC1	3	HEPN1	1	HNRNPF	2	ICAM5	1
GTF2A1	1	HERC1	1	HNRNPH2	2	ICE1	2
GTF2IRD1	1	HERPUD1	1	HNRNPM	1	ICMT	1
GUCD1	1	HERPUD2	1	HNRNPU	1	ID2	3
GUCY1A1	1	HES3	1	HNRNPUL1	1	ID4	1
GUCY1A2	3	HES5	1	HOMER1	1	IDUA	1
GUSB	1	HES6	1	HPF1	1	IER2	4
GUSBP4	1	HEXB	3	HPS4	2	IER5	2
GUSBP5	1	HEXIM1	3	HPS6	4	IER5L	2
GVQW3	2	HEY1	1	HPX	2	IFI30	2
GYPC	1	HGC6.3	3	HR	3	IFIT1	1
GZF1	1	HGFAC	4	HRAS	1	IFIT5	1
GZMM	1	HGH1	2	HRC	1	IFITM10	1
H1FOO	1	HGSNAT	1	HRH1	1	IFNAR1	2
H1FX-AS1	1	HHAT	2	HRK	1	IFNGR1	1
H2AFJ	1	HHLA1	2	HS3ST1	1	IFNGR2	2
H2AFX	2	HIC1	2	HS3ST2	2	IFNK	1
H6PD	1	HIF1A	1	HS3ST4	2	IGFBP2	1
HACD3	1	HIF1AN	1	HS6ST1	6	IGFLR1	1
HAGHL	3	HILPDA	1	HS6ST3	1	IGHMBP2	1
HAO1	1	HINFP	1	HSD11B2	1	IGSF11-AS1	1
HAP1	1	HINT3	1	HSD17B1	4	IGSF21	1
HAPLN4	3	HIP1R	1	HSD17B8	1	IGSF22	1
HAR1B	3	HIPK1	1	HSF4	1	IGSF6	2
HAS3	1	HIPK1-AS1	1	HSF5	2	IGSF8	2
HBB	1	HIPK2	1	HSP90AA1	6	IKBKE	4
HCCS	2	HIPK3	1	HSPA13	1	IKZF4	2
HCFC1	2	HIST1H2AC	1	HSPA14	2	IL10	1
HCFC1-AS1	1	HIST1H4C	1	HSPA1B	2	IL10RA	2

IL10RB-DT	2	IRF2BPL	4	KANK3	1	KCNK15-AS1	2
IL15RA	2	IRF4	1	KANSL1	3	KCNK2	1
IL17B	1	IRF7	3	KANSL2	1	KCNK7	1
IL17D	5	IRGQ	5	KANSL3	2	KCNK9	5
IL17F	1	IRS1	4	KANTR	2	KCNMA1	1
IL18BP	2	IRS2	4	KAT14	4	KCNMB4	1
IL1RAP	1	ISG15	1	KAT6B	1	KCNN1	1
IL21R	1	ISG20L2	1	KAT8	1	KCNN3	1
IL21R-AS1	2	ISLR	2	KBTBD11	4	KCNQ3	1
IL34	1	ISLR2	5	KBTBD11-OT1	2	KCNQ5	1
IL4I1	4	ISM2	1	KBTBD2	1	KCNS1	3
IL6ST	3	ISOC2	1	KBTBD4	3	KCNS2	2
ILF3-DT	2	IST1	1	KBTBD6	2	KCNT1	3
IMP3	3	ISYNA1	2	KBTBD7	2	KCNV1	4
IMPAD1	1	ITGA1	1	KCNA1	4	KCTD1	1
IMPDH2	2	ITGA10	2	KCNA2	3	KCTD12	3
INAFM2	2	ITGA2B	1	KCNA3	3	KCTD15	5
INCENP	1	ITGA3	1	KCNA4	4	KCTD16	2
ING4	4	ITGAE	1	KCNA6	#	KCTD18	1
INIP	1	ITGB2	1	KCNAB1	2	KCTD2	3
INKA2	4	ITGB4	2	KCNAB2	6	KCTD21	7
INO80D	1	ITIH5	1	KCNB1	1	KCTD4	2
INPP1	1	ITM2C	2	KCNB2	1	KCTD6	1
INPP4A	1	ITPKA	1	KCNC1	7	KCTD8	1
INPP5E	3	ITPKB	3	KCNC2	5	KDM1A	1
INPP5F	2	ITPKC	1	KCNC3	1	KDM2A	2
INSM1	1	ITPRIPL2	4	KCNC4	3	KDM3B	4
INSR	1	IVD	2	KCND2	3	KDM4A-AS1	2
INTS10	1	JADE1	1	KCND3	1	KDM4B	1
INTS11	1	JADE2	2	KCNE1	1	KDM5C	2
INTS6	1	JAGN1	2	KCNE4	1	KDM8	1
IP6K2	1	JAKMIP2-AS1	2	KCNF1	4	KDR	2
IPO13	2	JCAD	5	KCNG1	2	KEAP1	1
IPO9	4	JDP2	1	KCNG2	4	KHDC1L	2
IPPK	1	JMJD7	5	KCNG3	4	KHDRBS1	1
IQCA1L	2	JMJD8	3	KCNH1-IT1	4	KHDRBS3	1
IQCG	1	JMY	3	KCNH2	2	KHK	3
IQCH-AS1	1	JPH3	2	KCNH3	1	KIAA0100	8
IQCJ-SCHIP1-AS1	1	JPH4	1	KCNJ11	4	KIAA0319	2
IQCK	4	JPT2	5	KCNJ12	2	KIAA0319L	1
IQSEC2	1	JRK	3	KCNJ3	1	KIAA0355	1
IQSEC3	1	JUN	4	KCNJ4	3	KIAA0408	#
IRAIN	1	JUNB	2	KCNJ6	2	KIAA0513	1
IRF2BP1	3	JUND	2	KCNJ8	1	KIAA0754	5
IRF2BP2	3	KANK1	2	KCNK10	1	KIAA0895	1
		KANK2	3	KCNK12	1	KIAA0895L	1

KIAA1107	4	KLHL23	1	LENG8	1	LINC00672	1
KIAA1109	1	KLHL24	1	LENG8-AS1	1	LINC00673	2
KIAA1147	1	KLHL32	1	LENG9	1	LINC00674	4
KIAA1191	1	KLHL34	3	LEPROT	1	LINC00676	1
KIAA1217	3	KLHL36	2	LETM1	1	LINC00685	1
KIAA1324L	2	KLHL41	1	LETMD1	1	LINC00691	1
KIAA1328	1	KLHL42	3	LGALS3BP	4	LINC00836	1
KIAA1522	2	KLHL8	1	LGI1	2	LINC00847	1
KIAA1549L	1	KLHL9	4	LHFPL2	1	LINC00920	2
KIAA1614	1	KMT2B	1	LHFPL4	2	LINC00921	1
KIAA1614-AS1	3	KMT2D	4	LHFPL6	1	LINC00938	1
KIAA1656	2	KMT2E	2	LHX3	1	LINC00942	4
KIAA1671	2	KNSTRN	1	LIG3	1	LINC00950	2
KIAA2013	1	KRBA1	2	LIMCH1	1	LINC00963	2
KIDINS220	1	KRBA2	2	LIMD1	1	LINC00982	3
KIF17	3	KRCC1	1	LIMD2	1	LINC01000	1
KIF1BP	1	KREMEN2	2	LIME1	2	LINC01003	2
KIF26A	2	KRI1	1	LIMK1	1	LINC01006	2
KIF26B-AS1	1	KRTAP5-2	2	LIMK2	3	LINC01007	3
KIF3B	1	KRTAP5-AS1	1	LIMS2	1	LINC01118	2
KIF3C	3	KTI12	2	LIN7B	1	LINC01123	1
KIF5A	2	L1CAM	2	LINC00051	2	LINC01127	1
KIF5B	1	L3HYPDH	1	LINC00052	2	LINC01140	1
KIF5C	1	LAMB4	1	LINC00092	1	LINC01158	1
KIRREL3	1	LAMC1	1	LINC00163	1	LINC01195	1
KITLG	1	LAMP3	1	LINC00200	1	LINC01227	1
KLC1	1	LAMP5-AS1	2	LINC00222	2	LINC01231	1
KLC2	1	LAMTOR1	1	LINC00235	1	LINC01250	1
KLF10	1	LAMTOR2	1	LINC00260	1	LINC01269	3
KLF11	2	LANCL2	1	LINC00266-1	1	LINC01336	1
KLF13	6	LARGE2	1	LINC00334	2	LINC01347	1
KLF15	2	LARS2-AS1	3	LINC00359	2	LINC01424	1
KLF2	2	LAT2	1	LINC00367	1	LINC01433	1
KLF3	1	LATS1	1	LINC00461	3	LINC01521	2
KLF4	2	LBHD1	1	LINC00467	1	LINC01529	1
KLF6	1	LBR	1	LINC00511	1	LINC01530	1
KLF7	1	LCOR	1	LINC00528	9	LINC01537	1
KLF9	3	LDB1	1	LINC00575	1	LINC01543	1
KLHDC2	1	LDHD	2	LINC00598	2	LINC01544	2
KLHDC4	1	LDLRAD4	2	LINC00620	1	LINC01559	3
KLHDC8B	1	LDLRAD4-AS1	1	LINC00622	1	LINC01578	1
KLHDC9	1	LDOC1	2	LINC00643	1	LINC01583	1
KLHL10	1	LEAP2	1	LINC00659	1	LINC01585	3
KLHL11	3	LEMD2	1	LINC00662	4	LINC01619	1
KLHL15	1	LEMD3	2	LINC00665	1	LINC01635	1
KLHL21	4	LENEP	1	LINC00667	3	LINC01637	4

LINC01645	1	LNP1	1	LOC100289333	1	LOC101927972	1
LINC01736	1	LNPEP	3	LOC100289511	1	LOC101927989	4
LINC01750	2	LNX1-AS1	1	LOC100291105	1	LOC101928052	4
LINC01767	1	LOC100128079	3	LOC100419583	1	LOC101928105	1
LINC01820	1	LOC100128253	1	LOC100505635	2	LOC101928120	1
LINC01861	3	LOC100128325	1	LOC100505912	1	LOC101928177	1
LINC01864	2	LOC100128494	6	LOC100506100	2	LOC101928323	5
LINC01909	2	LOC100128573	2	LOC100506271	5	LOC101928324	1
LINC01934	1	LOC100128653	2	LOC100506321	1	LOC101928416	1
LINC01963	1	LOC100128882	1	LOC100506472	1	LOC101928424	1
LINC01975	3	LOC100129434	1	LOC100506585	1	LOC101928525	3
LINC01983	2	LOC100129484	1	LOC100506691	4	LOC101928583	2
LINC01988	3	LOC100129534	3	LOC100507346	1	LOC101928659	3
LINC02012	3	LOC100129617	1	LOC100507351	3	LOC101928807	3
LINC02022	1	LOC100129917	1	LOC100507373	4	LOC101928943	1
LINC02033	1	LOC100129931	5	LOC100507472	1	LOC101929089	1
LINC02035	2	LOC100130283	3	LOC100507507	1	LOC101929106	2
LINC02068	1	LOC100130331	2	LOC100630923	1	LOC101929208	2
LINC02168	1	LOC100130357	1	LOC100652768	2	LOC101929295	3
LINC02210-CRHR1	1	LOC100130449	3	LOC100996263	1	LOC101929384	1
LINC02246	2	LOC100130587	4	LOC100996419	1	LOC101929528	3
LINC02283	1	LOC100130705	1	LOC100996693	2	LOC101929550	1
LINC02361	1	LOC100130744	3	LOC100996740	2	LOC101929563	1
LINC02387	2	LOC100130992	2	LOC100996842	1	LOC101929679	3
LINC02389	2	LOC100131315	1	LOC101926962	1	LOC101929901	2
LINC02424	1	LOC100132215	1	LOC101927000	2	LOC101930094	1
LINC02449	2	LOC100132249	1	LOC101927018	1	LOC102723566	1
LINC02497	1	LOC100133091	1	LOC101927070	4	LOC102723582	2
LINC02517	1	LOC100286925	1	LOC101927472	1	LOC102723692	1
LINC02585	1	LOC100287015	1	LOC101927550	2	LOC102723703	1
LINC02586	3	LOC100287049	3	LOC101927583	2	LOC102723729	2
LINC2194	1	LOC100287837	2	LOC101927751	1	LOC102724009	1
LINC-PINT	1	LOC100287944	1	LOC101927752	5	LOC102724058	3
LINGO1	4	LOC100288123	2	LOC101927815	2	LOC102724163	1
LIX1L	2	LOC100288175	2	LOC101927895	1	LOC102724659	3
LMAN1L	1	LOC100288254	2	LOC101927914	1	LOC102724784	1
LMAN2L	1	LOC100288778	1	LOC101927969	2	LOC102724804	1
LMBRD1	2	LOC100288911	1				
LMBRD2	1						
LMF1	3						
LMLN-AS1	1						
LMO3	1						
LMO4	3						
LMO7	1						
LMOD3	1						
LMTK3	1						

LOC102724927	2	LOC151484	1	LRG1	1	LUZP6	2
LOC103344931	1	LOC153910	9	LRIG1	2	LY6E	1
LOC105369431	7	LOC155060	3	LRIG2	1	LY6H	1
LOC105369595	1	LOC202181	1	LRP1	1	LYL1	1
LOC105370024	3	LOC283045	1	LRP10	2	LYNX1	3
LOC105370457	1	LOC284578	2	LRP1-AS	1	LYPD1	2
LOC105370697	1	LOC339059	2	LRP3	4	LYPD6B	2
LOC105370941	2	LOC339666	1	LRP4-AS1	2	LYPLA2	1
LOC105370943	1	LOC375196	2	LRPAP1	1	LYRM1	1
LOC105371038	1	LOC400541	3	LRRC10B	4	LYRM2	2
LOC105371184	1	LOC400627	2	LRRC14	2	LYSMD1	1
LOC105371414	4	LOC401320	1	LRRC24	2	LYSMD4	4
LOC105371485	2	LOC401442	1	LRRC27	1	LYVE1	1
LOC105371506	1	LOC401463	1	LRRC37B	1	LZTS1	4
LOC105371592	1	LOC401478	2	LRRC3B	1	LZTS2	3
LOC105371795	3	LOC401554	2	LRRC3-DT	2	MAD1L1	1
LOC105371899	2	LOC403312	2	LRRC4	3	MAD2L1BP	1
LOC105371998	1	LOC440040	1	LRRC41	1	MAF	3
LOC105372068	1	LOC440934	1	LRRC42	1	MAFB	1
LOC105372071	2	LOC441052	1	LRRC43	1	MAFG	1
LOC105372383	1	LOC441455	1	LRRC45	1	MAGEB2	1
LOC105373100	2	LOC554206	1	LRRC47	3	MAGED1	1
LOC105373156	1	LOC574538	3	LRRC49	2	MAGED2	3
LOC105373378	2	LOC642423	1	LRRC4C	2	MAGEE1	3
LOC105374338	1	LOC642852	3	LRRC55	1	MAGEF1	2
LOC105374952	1	LOC643542	3	LRRC58	1	MAGEH1	2
LOC105375787	1	LOC643802	2	LRRC73	2	MAGEL2	1
LOC105375843	4	LOC646548	2	LRRC8A	1	MAGI1-AS1	3
LOC105376114	1	LOC646762	1	LRRC8B	3	MAGOHB	1
LOC105376480	2	LOC651337	1	LRRK2	1	MALAT1	3
LOC105377146	1	LOC652276	2	LRRN2	4	MALINC1	1
LOC105378586	2	LOC653712	1	LRRTM1	2	MAMSTR	1
LOC105379192	1	LOC692247	1	LRRTM3	3	MAN1A1	2
LOC105379393	1	LOC728392	2	LRRTM4	3	MAN1A2	2
LOC105447645	1	LOC728743	4	LRSAM1	1	MAN1B1	1
LOC108783654	3	LOC729683	3	LRTM2	1	MAN1B1-DT	2
LOC148413	2	LOC729867	3	LSAMP	1	MAN1C1	2
LOC149684	1	LOC93622	4	LSM10	1	MAN2A1	1
		LONRF2	3	LSM11	2	MAN2C1	1
		LOXHD1	4	LSM4	1	MANEAL	3
		LPAR1	2	LSMEM2	2	MANF	2
		LPAR5	1	LTBR	1	MANSC1	1
		LRFN1	7	LTK	1	MAP1A	#
		LRFN3	2	LTV1	3	MAP1B	#
		LRFN4	2	LUARIS	3	MAP1LC3A	1
		LRFN5	4	LUC7L2	1	MAP1LC3B	3

MAP1S	2	MCL1	4	MIB2	3	MIR1914	3
MAP2	2	MCM3AP	2	MICAL2	1	MIR1915	2
MAP2K1	1	MCMBP	1	MICALL1	2	MIR193BHG	2
MAP3K1	1	MCOLN1	1	MICALL2	1	MIR194-2HG	1
MAP3K11	3	MCRS1	1	MID1	1	MIR1976	1
MAP3K12	1	MDGA1	2	MID1IP1-AS1	2	MIR2054	1
MAP3K3	1	MDK	1	MID2	1	MIR219A2	2
MAP3K4	2	MDM2	1	MIDN	1	MIR22	1
MAP3K5	1	MEA1	2	MIEF2	1	MIR2682	1
MAP4K2	1	MED10	1	MIIP	1	MIR26A2	1
MAP6	1	MED13	1	MINDY1	1	MIR26B	1
MAP6D1	1	MED18	1	MINDY2	1	MIR2861	1
MAP7D1	1	MED19	2	MINPP1	1	MIR3125	1
MAPK12	2	MED29	1	MIR103A1	1	MIR3134	1
MAPK13	1	MEIS3	3	MIR103A2	1	MIR3138	2
MAPK1IP1L	1	MEIS3P1	2	MIR103B2	1	MIR3145	2
MAPK4	2	MELTF-AS1	1	MIR107	1	MIR3176	1
MAPK6	1	MEMO1	1	MIR1180	1	MIR3179-2	1
MAPK8	1	MEP1B	2	MIR1182	1	MIR3183	1
MAPK8IP1P2	1	MEPCE	1	MIR1199	1	MIR3186	4
MAPK8IP2	4	MESD	1	MIR1200	1	MIR3187	2
MAPK8IP3	1	METRNL	1	MIR122	1	MIR3190	1
MAPKBP1	2	METTL7A	1	MIR1224	2	MIR3196	1
MAPRE2	1	MEX3C	1	MIR1225	1	MIR3198-1	1
MARCH2	2	MEX3D	4	MIR1226	2	MIR3199-1	2
MARCH4	3	MFAP3	1	MIR1227	1	MIR3202-2	1
MARCH9	1	MFAP3L	2	MIR1228	1	MIR328	1
MARCKSL1	1	MFHAS1	6	MIR1231	1	MIR331	1
MARK3	1	MFN2	1	MIR124-2	1	MIR33A	1
MARS2	2	MFSD10	3	MIR1249	1	MIR3616	2
MARVELD3	2	MFSD11	1	MIR1257	2	MIR3620	2
MATK	1	MFSD13A	2	MIR1260A	2	MIR3621	2
MATR3	2	MFSD3	2	MIR1262	1	MIR3622A	2
MAVS	1	MFSD4B	1	MIR1268A	1	MIR3649	1
MAZ	3	MFSD5	2	MIR1271	3	MIR3654	2
MBD3	1	MFSD6	3	MIR1273C	3	MIR3658	1
MBLAC1	1	MFSD9	2	MIR1275	1	MIR3682	2
MBLAC2	1	MGA	1	MIR1276	1	MIR3692	1
MBNL2	1	MGAT1	1	MIR1281	1	MIR3714	3
MBP	5	MGAT2	2	MIR128-2	1	MIR378B	3
MBTPS1	3	MGAT3	2	MIR1286	1	MIR378H	5
MC1R	1	MGAT5	4	MIR1306	1	MIR3911	1
MCAT	1	MGAT5B	1	MIR140	1	MIR3914-1	3
MCF2L2	1	MHENCR	2	MIR153-2	2	MIR3941	1
MCF2L-AS1	2	MIATNB	3	MIR1825	1	MIR4253	1
MCHR1	1	MIB1	1	MIR190A	1	MIR4254	2

MIR4256	1	MIR4687	1	MIR6069	1	MIR6795	1
MIR4279	2	MIR4688	1	MIR6080	1	MIR6796	1
MIR4284	1	MIR4690	1	MIR6083	1	MIR6803	1
MIR4285	1	MIR4697HG	2	MIR6084	1	MIR6808	3
MIR4287	1	MIR4701	1	MIR611	1	MIR6810	1
MIR4288	1	MIR4704	1	MIR6126	3	MIR6816	1
MIR4312	1	MIR4706	2	MIR620	2	MIR6818	6
MIR4315-2	2	MIR4715	2	MIR625	1	MIR6820	2
MIR4319	2	MIR4717	1	MIR629	1	MIR6821	1
MIR4326	3	MIR4718	1	MIR636	1	MIR6825	1
MIR4427	2	MIR4724	1	MIR637	2	MIR6827	3
MIR4428	1	MIR4726	2	MIR6501	8	MIR6829	1
MIR4432HG	2	MIR4728	2	MIR6506	2	MIR6832	2
MIR4440	1	MIR4742	1	MIR6511A2	2	MIR6841	1
MIR4444-2	1	MIR4743	1	MIR6511B1	5	MIR6843	2
MIR4446	1	MIR4746	2	MIR6515	1	MIR6845	2
MIR4453	1	MIR4753	1	MIR657	3	MIR6847	1
MIR4457	1	MIR4757	1	MIR671	3	MIR6851	1
MIR4466	1	MIR4761	1	MIR6716	2	MIR6853	1
MIR4477B	1	MIR4764	2	MIR6717	3	MIR6855	3
MIR4489	1	MIR4777	1	MIR6727	1	MIR6860	1
MIR4492	1	MIR4781	1	MIR6730	1	MIR6861	2
MIR4498	1	MIR4784	1	MIR6734	1	MIR6866	2
MIR4505	2	MIR4786	1	MIR6742	5	MIR6871	4
MIR4517	1	MIR4793	1	MIR6743	4	MIR6880	4
MIR4519	1	MIR4800	2	MIR6744	4	MIR6881	1
MIR4523	1	MIR488	1	MIR6752	2	MIR6883	1
MIR4531	1	MIR5003	1	MIR6756	1	MIR6887	1
MIR4535	1	MIR5004	2	MIR6757	1	MIR6891	1
MIR4632	1	MIR5094	2	MIR6760	2	MIR6895	2
MIR4635	2	MIR5187	2	MIR6764	1	MIR7106	1
MIR4636	1	MIR5193	1	MIR6765	2	MIR7107	2
MIR4640	1	MIR544B	1	MIR6770-1	2	MIR7109	1
MIR4647	1	MIR548A3	1	MIR6770-2	3	MIR7114	1
MIR4648	2	MIR548AU	1	MIR6771	6	MIR7156	1
MIR4656	1	MIR548AV	1	MIR6772	1	MIR7158	1
MIR4657	1	MIR548J	1	MIR6775	2	MIR718	3
MIR4659B	1	MIR548Q	2	MIR6776	3	MIR744	1
MIR4664	8	MIR548W	1	MIR6777	3	MIR765	1
MIR4665	1	MIR5572	2	MIR6779	1	MIR770	1
MIR4667	2	MIR5586	2	MIR6782	1	MIR7843	1
MIR4668	1	MIR5706	1	MIR6784	5	MIR7844	1
MIR4671	1	MIR589	1	MIR6785	1	MIR7848	1
MIR4677	2	MIR592	1	MIR6787	1	MIR7855	7
MIR4683	2	MIR597	1	MIR6790	1	MIR8072	1
MIR4684	1	MIR600	3	MIR6792	1	MIR8075	1

MIR8080	1	MPO	1	MSL2	3	MYLK-AS2	1
MIR8089	2	MPP4	1	MSMO1	1	MYO15B	1
MIR8485	1	MPV17	1	MSMP	1	MYO16-AS1	2
MIR874	1	MPV17L2	1	MSS51	1	MYO18A	1
MIR877	2	MRAP	1	MSX1	1	MYO18B	3
MIR885	2	MRAP2	1	MT3	2	MYO5C	1
MIR887	2	MRAS	1	MTA2	1	MYO7A	1
MIR9-1	3	MRFAP1	2	MTCL1	5	MYOG	1
MIR921	2	MRFAP1L1	2	MTDH	1	MYORG	6
MIR922	1	MRGBP	2	MTFR1	1	MYRF	1
MIR935	2	MRI1	1	MTFR1L	3	MYRIP	1
MIR9-3HG	2	MRLN	1	MTFR2	2	MZF1-AS1	2
MIR943	1	MRM1	1	MTG2	1	N4BP3	2
MIR98	2	MRO	1	MTHFD1L	2	NAA10	1
MIRLET7G	1	MROH3P	3	MTMR1	3	NAA20	2
MIRLET7I	1	MROH7	2	MTMR11	2	NAA30	1
MISP3	2	MRPL12	1	MTNR1A	6	NAA38	2
MKKS	1	MRPL14	1	MTPAP	1	NAA40	1
MKNK2	2	MRPL17	1	MTR	2	NAA50	1
MKRN1	1	MRPL27	2	MTRNR2L4	4	NAB1	1
MKRN2	2	MRPL28	3	MTSS1L	5	NAB2	3
MKX-AS1	1	MRPL34	1	MTURN	1	NACAD	5
MLC1	1	MRPL35	1	MTUS1	1	NAGLU	2
MLF2	2	MRPL36	1	MTUS2	1	NAGPA-AS1	2
MLLT1	6	MRPL37	1	MTUS2-AS1	3	NANOS2	4
MLNR	1	MRPL38	1	MUC13	2	NAP1L2	1
MLYCD	2	MRPL4	1	MUC6	2	NAP1L3	1
MMAB	1	MRPL41	3	MUL1	3	NAP1L5	2
MMP16	1	MRPL43	1	MUM1	2	NARF	1
MMP17	1	MRPL44	2	MUSTN1	2	NARS2	6
MN1	5	MRPL54	1	MXD1	1	NAT10	1
MNT	3	MRPL58	1	MXD4	2	NAT14	1
MOAP1	1	MRPS10	1	MXRA8	2	NAT2	2
MOB2	4	MRPS12	1	MYBBP1A	1	NAT8L	3
MOB4	1	MRPS18A	2	MYBL1	1	NAT9	1
MOCS3	2	MRPS21	1	MYBPC3	1	NAV2	1
MOGS	1	MRPS23	1	MYBPH	3	NAXD	1
MOK	1	MRPS24	6	MYCBP2	2	NBAT1	1
MON1B	1	MRPS25	2	MYCBP2-AS1	2	NBEA	2
MON2	1	MRPS26	1	MYCNOS	1	NBL1	1
MORC2-AS1	1	MRPS6	1	MYDGF	1	NBPF9	1
MORC3	1	MRTO4	1	MYH10	1	NCALD	2
MORN4	1	MSANTD1	4	MYL12B	1	NCAM2	1
MPEG1	2	MSANTD4	2	MYL6	1	NCAN	4
MPG	2	MSC-AS1	1	MYL9	1	NCAPD2	2
MPLKIP	2	MSL1	1	MYLK	1	NCBP1	1

NCBP2-AS2	6	NEUROD2	2	NOL4	2	NSD2	2
NCBP3	2	NEUROD6	1	NOL4L	6	NSD3	1
NCDN	2	NFATC2	3	NOP14-AS1	1	NSDHL	1
NCK1-DT	1	NFATC3	1	NOP53	1	NSG2	4
NCK2	3	NFATC4	1	NORAD	1	NSMAF	1
NCKAP1	1	NFE2L1	2	NOS1	3	NSMCE3	2
NCKAP5L	5	NFIA	1	NOS1AP	3	NSUN5P1	1
NCKIPSD	1	NFIB	1	NOTCH1	1	NSUN5P2	1
NCOA4	1	NFIC	3	NOV	1	NSUN6	1
NCOA5	1	NFKBIA	1	NOVA1	2	NT5C	1
NCOA7	2	NFKBIE	1	NPAS1	1	NT5C2	2
NDE1	1	NFKBIL1	1	NPAS3	1	NT5C3B	1
NDEL1	4	NFKBIZ	1	NPB	2	NT5DC3	2
NDN	3	NFRKB	1	NPBWR2	1	NT5E	1
NDP-AS1	1	NFU1	2	NPC1	1	NTM-IT	5
NDRG2	1	NGB	1	NPFFR1	1	NTN1	1
NDRG4	1	NHLRC1	1	NPHP1	1	NTN4	2
NDST1	3	NIM1K	2	NPM3	1	NTNG1	1
NDST2	5	NINJ1	1	NPR2	1	NTNG2	1
NDST3	1	NIPA2	1	NPRL2	1	NTPCR	2
NDUFA1	1	NIPAL3	1	NPTN-IT1	1	NTRK2	2
NDUFA3	1	NIT1	1	NPTX1	5	NTRK3	1
NDUFA6-DT	1	NKAIN3	1	NPTX2	1	NTSR2	2
NDUFAF3	1	NKAIN4	2	NPTXR	1	NUAK1	1
NDUFAF8	2	NKPD1	2	NPY1R	2	NUCB1-AS1	1
NDUFS7	3	NKRF	1	NR1D1	4	NUDT14	2
NEAT1	1	NKX6-2	1	NR1D2	2	NUDT16	1
NEBL-AS1	1	NKX6-3	3	NR1H3	1	NUDT16L1	1
NECAB1	1	NLGN1	1	NR2E1	1	NUDT18	1
NECAP1	1	NLGN3	3	NR2E3	2	NUDT2	1
NECTIN1	2	NLGN4Y	1	NR2F1	3	NUDT22	2
NECTIN3	1	NLGN4Y-AS1	1	NR2F2	1	NUDT3	1
NEFL	1	NLRC3	2	NR2F6	1	NUDT6	1
NEFM	4	NLRP2	1	NR3C1	2	NUFIP2	1
NEIL1	1	NLRP3	1	NR3C2	1	NUMBL	3
NEK9	2	NME2	1	NRARP	1	NUP153	2
NELL2	1	NME3	4	NRAV	1	NUP50-DT	1
NEMP2	1	NMRAL1	1	NRGN	1	NUTM2B-AS1	1
NET1	1	NMRK2	4	NRL	1	NWD2	1
NETO1	1	NMT2	3	NRN1	2	NXNL2	1
NETO2	1	NNMT	1	NRON	2	NXPE3	1
NEU1	1	NOA1	2	NRSN1	1	NXPH1	2
NEU3	2	NOB1	1	NRSN2	3	NXPH2	1
NEU4	1	NOCT	1	NRXN1	6	NXPH3	3
NEURL1-AS1	7	NOG	1	NRXN2	2	NYAP1	4
NEURL4	1	NOL3	2	NRXN3	2	NYNRIN	1

OACYLP	1	OXR1	1	PCDH11Y	1	PCMT1	2
OAZ1	3	P2RX4	4	PCDH17	8	PCNT	1
OAZ2	1	P2RY1	2	PCDH18	1	PCNX1	2
OBSCN-AS1	1	P2RY11	2	PCDH19	4	PCNX2	2
OBSL1	1	P3H1	1	PCDH20	8	PCNX3	1
OCA2	1	P3H3	1	PCDH7	3	PCP4	1
OCEL1	1	P3H4	1	PCDH8	4	PCSK9	1
OGA	1	P4HA3	2	PCDH9	4	PCYT1B	1
OGDHL	1	P4HTM	1	PCDHA1	2	PDCL	1
OGFRL1	1	PAAF1	1	PCDHA11	1	PDE12	1
OGG1	1	PABPN1	2	PCDHA3	1	PDE1A	1
OIP5-AS1	1	PACRGL	1	PCDHA4	4	PDE1B	1
OLFM1	2	PACSIN1	3	PCDHA5	1	PDE3B	1
OLFML2A	2	PAF1	1	PCDHA6	1	PDE4B	1
OLFML3	1	PAFAH1B1	1	PCDHAC1	2	PDE4D	2
OLIG1	3	PAFAH1B2	1	PCDHAC2	3	PDE4DIP	2
OLIG2	2	PAGR1	4	PCDHB11	4	PDE8A	1
OLMALINC	1	PAIP1	1	PCDHB12	6	PDF	5
OMG	4	PAK6	1	PCDHB13	1	PDGFA	1
OPA3	1	PALM	1	PCDHB14	8	PDGFB	1
OPCML	1	PAM	1	PCDHB15	1	PDGFRL	1
OPHN1	1	PANK2	1	PCDHB19P	5	PDIA2	2
OPN3	2	PANK3	1	PCDHB2	2	PDIA6	2
OPRK1	1	PANK4	4	PCDHB3	2	PDIK1L	1
OPRL1	1	PANX1	1	PCDHB4	4	PDK1	1
OPRM1	5	PANX2	1	PCDHB5	4	PDK2	1
OR1D5	1	PAPLN	1	PCDHB6	2	PDK4	1
OR7E47P	2	PAPPA-AS1	1	PCDHB9	1	PDLIM1	1
ORAI1	1	PAQR3	2	PCDHGA1	1	PDP1	1
ORAI2	4	PAQR4	7	PCDHGA10	1	PDP2	2
ORAI3	4	PAQR5	2	PCDHGA11	1	PDRG1	1
ORMDL1	1	PAQR9	1	PCDHGA12	1	PDXK	1
OSBP2	1	PARD6A	1	PCDHGA3	1	PDYN-AS1	2
OSBPL10-AS1	1	PARD6B	1	PCDHGA4	1	PDZRN3	3
OSBPL7	2	PARS2	3	PCDHGA5	2	PEA15	2
OSER1-DT	1	PARVB	1	PCDHGA6	1	PEAK3	3
OTUB2	1	PASK	3	PCDHGA7	1	PEG10	4
OTUD1	2	PATZ1	1	PCDHGA9	1	PEG13	6
OTUD4	1	PAXIP1-AS1	2	PCDHGB5	1	PEG3-AS1	2
OTUD5	1	PAXIP1-AS2	1	PCDHGC3	2	PELI2	1
OTULINL	1	PBOV1	2	PCDHGC4	4	PER1	1
OVCA2	3	PBX1	2	PCDHGC5	3	PEX26	4
OVCH1	1	PCBD1	1	PCED1B	1	PEX5L	1
OXER1	1	PCBP1	2	PCF11	2	PEX5L-AS2	2
OXLD1	5	PCDH1	6	PCIF1	1	PEX6	1
OXNAD1	1	PCDH10	5	PCLO	#	PFKFB3	2

PFKP	1	PIK3R2	6	PLXNA1	4	POSTN	1
PFN1	1	PIK3R3	1	PLXNA4	1	POU3F1	2
PGAM2	3	PIK3R4	1	PLXNB1	2	POU3F2	2
PGBD1	1	PILRA	2	PLXNB2	2	POU3F3	5
PGBD2	1	PILRB	1	PLXNB3	1	POU4F1	2
PGBD5	4	PIMREG	1	PLXNC1	1	POU5F1P4	3
PGD	3	PIN1	1	PMF1-BGLAP	1	PP7080	2
PGLS	1	PIN1P1	3	PMM1	3	PPARGC1A	1
PGM1	1	PINK1-AS	4	PMP2	1	PPARGC1B	3
PGM2L1	1	PISD	1	PMS2CL	1	PPCDC	1
PGM3	2	PITHD1	1	PMS2P3	1	PPIAL4C	1
PGP	3	PITPNA	3	PMVK	3	PPIF	6
PGPEP1L	2	PITPNC1	2	PNISR	1	PPIL2	5
PGRMC1	1	PITPNM1	1	PNKD	1	PPM1A	2
PGS1	1	PIWIL1	1	PNMA1	1	PPM1B	1
PHB	3	PJA1	2	PNMA2	2	PPM1E	1
PHETA1	1	PJA2	1	PNMA3	3	PPM1K	1
PHF12	1	PKD2	1	PNMA6A	1	PPM1L	1
PHF2	1	PKM	1	PNMA6F	1	PPP1R10	1
PHKG1	1	PKP4-AS1	1	PNMA8A	3	PPP1R15A	1
PHLDA1	1	PLA2G10	1	PNMA8B	5	PPP1R15B	3
PHLDA2	2	PLA2G12A	1	PNOC	2	PPP1R1A	1
PHLDA3	1	PLA2G4F	3	POC1B-GALNT4	1	PPP1R1B	1
PHLPP1	5	PLBD1-AS1	1	PODXL	3	PPP1R26	5
PHLPP2	1	PLCD4	1	POGK	1	PPP1R27	3
PHOX2A	1	PLCL1	1	POLB	1	PPP1R35	1
PHPT1	2	PLD4	#	POLD4	2	PPP1R37	1
PHTF1	1	PLD6	5	POLG	1	PPP1R3C	2
PHTF2	1	PLEC	5	POLL	3	PPP1R3D	2
PHYHD1	3	PLEKHA5	1	POLR1A	2	PPP1R3F	2
PHYHIP	2	PLEKHF1	2	POLR1B	1	PPP1R3G	2
PHYHIPL	1	PLEKHF2	2	POLR1D	1	PPP1R9A	1
PHYKPL	3	PLEKHG3	2	POLR2D	6	PPP1R9B	1
PI16	2	PLEKHM3	2	POLR2E	2	PPP2R1A	1
PI4KB	1	PLEKHO2	1	POLR2H	1	PPP2R1B	4
PIANP	1	PLK1	4	POLR3D	1	PPP2R2B	1
PIAS4	1	PLK2	2	POLR3E	1	PPP2R5B	1
PICALM	1	PLN	1	POLR3H	6	PPP3CB	1
PID1	1	PLOD3	1	POLRMT	2	PPP3CC	1
PIGG	2	PLP1	2	POM121C	2	PPP3R2	1
PIGM	2	PLPP2	1	POMC	2	PPP4R1	2
PIGV	2	PLPP3	1	POMGNT1	2	PPP6R1	1
PIK3C2B	2	PLPP6	1	POMGNT2	3	PPP6R2	1
PIK3CD	3	PLPP7	1	POMT1	3	PPRC1	1
PIK3IP1	1	PLPPR4	3	POP7	1	PQLC2	1
PIK3R1	2	PLPPR5	1	POPDC3	1	PQLC3	1

PRAG1	6	PRUNE2	4	PTPRN	2	RABIF	1
PRAM1	1	PSD	6	PTPRO	1	RAC1	1
PRDM1	1	PSD2	2	PTPRS	3	RAD18	4
PRDM14	1	PSD4	1	PTRHD1	3	RAD23A	1
PRDM2	2	PSMB3	3	PTTG1IP	1	RAD52	2
PRDM4	1	PSMB4	1	PUM1	1	RAD9B	1
PRDM8	3	PSMB5	2	PURA	1	RAET1E-AS1	2
PREX1	3	PSMC1	1	PURB	2	RALBP1	1
PRF1	1	PSMC3IP	1	PURG	1	RALGAPB	1
PRH1	1	PSMC5	1	PUS1	2	RALGDS	2
PRICKLE1	5	PSMD1	2	PVR	1	RAMP1	1
PRICKLE2-AS2	3	PSMD13	1	PVRIG	2	RANBP6	1
PRICKLE2-AS3	2	PSMD2	1	PWP1	1	RANGAP1	1
PRICKLE3	2	PSMD3	2	PWWP2A	1	RAP1GAP	2
PRIMA1	1	PSMD4	1	PWWP2B	2	RAP2A	2
PRKAB1	2	PSMD6-AS2	1	PXDC1	2	RAP2B	2
PRKAG1	6	PSMD7	1	PXDN	1	RAP2C	1
PRKAR1A	1	PSMG3	1	PXMP4	1	RAPGEF1	1
PRKAR2A	2	PSMG3-AS1	1	PXT1	1	RAPGEF2	1
PRKAR2B	1	PSMG4	2	PYCR3	3	RARA	2
PRKCE	1	PSPN	1	PYGB	4	RARRES2	1
PRKCZ-AS1	3	PSRC1	1	PYGL	1	RASA1	1
PRKG1	1	PTAR1	2	PYURF	3	RASA2	3
PRKXP1	1	PTCD1	2	QKI	1	RASA4CP	4
PRMT6	2	PTCD2	1	QPCTL	1	RASAL1	1
PRMT7	5	PTCH1	1	QRFP	4	RASAL2-AS1	1
PRMT9	1	PTCHD1	3	QRICH1	1	RASD1	5
PRNP	1	PTCHD4	1	QSOX1	1	RASD2	3
PROCA1	1	PTEN	1	QTRT1	3	RASGEF1B	1
PRPF18	3	PTGDR2	1	R3HCC1	1	RASGEF1C	1
PRPF19	1	PTGER1	1	RAB10	1	RASGRF1	1
PRPF8	1	PTGER3	1	RAB11FIP3	2	RASL10A	3
PRPH2	1	PTGIS	1	RAB1B	1	RASL10B	2
PRPS2	3	PTH2R	2	RAB21	1	RASL11B	1
PRR12	4	PTN	2	RAB24	3	RASSF2	3
PRR18	3	PTP4A1	1	RAB28	1	RASSF7	1
PRR25	1	PTPMT1	3	RAB30	1	RAVER1	4
PRR29-AS1	2	PTPN11	2	RAB32	3	RAVER2	1
PRR36	1	PTPN13	1	RAB35	5	RAX2	1
PRR7	3	PTPN23	3	RAB36	2	RB1CC1	1
PRRT2	3	PTPN4	1	RAB37	1	RBBP5	1
PRRT3	1	PTPN5	1	RAB3A	1	RBBP6	1
PRRT3-AS1	4	PTPRD	1	RAB40C	2	RBCK1	1
PRSS27	2	PTPRG-AS1	1	RAB5IF	3	RBFOX1	1
PRSS35	1	PTPRM	1	RAB6C	2	RBFOX2	1
PRSS38	1			RABGEF1	3		

RBM12B-AS1	2	RGS8	1	RNF40	1	RPTOR	1
RBM14	3	RHOB	2	RNF41	1	RPUSD1	1
RBM15	4	RHOBTB2	5	RNF44	2	RPUSD3	2
RBM15B	6	RHOC	1	RNF8	1	RPUSD4	1
RBM23	1	RHOG	1	RNH1	2	RRAGA	2
RBM3	3	RHOU	1	RNPS1	1	RRAS2	1
RBM4	2	RHOV	1	RNU105B	1	RRM1	1
RBM45	1	RHPN1	1	RNU6-2	1	RRNAD1	1
RBM4B	2	RIMKLA	1	RNU6ATAC	1	RRP1B	1
RBM6	1	RIMS1	2	ROBO2	1	RRP36	1
RBM7	3	RIMS3	1	ROCK1	1	RRP7A	2
RCAN3	1	RIN1	1	ROCK2	1	RRP7BP	1
RCC1L	1	RIN2	1	ROGDI	2	RRP8	1
RCE1	2	RING1	1	ROPN1B	1	RS1	1
RCOR2	2	RIOX1	2	RORA-AS1	1	RSAD1	2
RCVRN	3	RIPOR2	1	RORB-AS1	2	RSC1A1	1
RDH12	1	RLBP1	1	RPA1	1	RSPH10B2	1
RDH14	1	RLIM	2	RPAIN	3	RSPH14	3
RDH5	2	RMND5A	1	RPAP3	1	RSPH9	2
REEP2	2	RN7SK	2	RPE	2	RSPRY1	1
REEP4	2	RN7SL1	2	RPL13	2	RTL10	1
RELB	1	RNASE1	1	RPL13AP17	1	RTL5	3
RELL2	3	RNASEH2C	2	RPL19	1	RTL6	3
RELT	2	RNASET2	1	RPL19P12	1	RTL8B	1
RENBP	1	RNF103	1	RPL27	1	RTL8C	2
REPIN1	2	RNF112	1	RPL29	1	RTN1	1
RETREG1	2	RNF130	1	RPL31	2	RTN2	1
RETREG2	2	RNF135	1	RPL36	4	RTN3	2
REV1	3	RNF139	1	RPL37A	1	RTN4	2
REXO1	1	RNF144A	1	RPL7L1	1	RTN4RL2	4
RFFL	1	RNF145	2	RPP21	1	RTP1	1
RFLNB	4	RNF146	1	RPP25	1	RTP5	1
RFPL1	4	RNF150	2	RPP25L	1	RTRAF	1
RFPL1S	2	RNF166	2	RPRM	1	RUFY3	1
RFT1	1	RNF167	1	RPRML	1	RUNDC3A	2
RFXANK	1	RNF168	1	RPS14	1	RUNX1T1	1
RGCC	1	RNF169	1	RPS19	1	RUSC1	4
RGL2	2	RNF182	1	RPS19BP1	1	RUSC1-AS1	2
RGL4	2	RNF187	1	RPS21	1	RUSC2	1
RGMA	1	RNF19A	1	RPS23	1	RUVBL1-AS1	2
RGMB-AS1	2	RNF213	2	RPS26	1	RWDD3	2
RGS12	2	RNF216P1	1	RPS29	2	RXRA	3
RGS2	1	RNF217-AS1	2	RPS5	1	RXRB	1
RGS3	3	RNF223	2	RPS6KB2	2	RYBP	1
RGS4	2	RNF26	2	RPS6KL1	4	RYR2	1
RGS7BP	1	RNF32	2	RPS9	1	S100A1	1

S100A6	1	SCN3B	4	SERPINF2	2	SHISA6	1
S100B	2	SCN4B	1	SERPING1	1	SHISA7	4
S1PR1	3	SCO1	1	SERTAD1	1	SHISA9	3
SACS	8	SCO2	4	SERTAD2	1	SHISAL1	1
SALL2	1	SCRIB	1	SERTAD3	1	SHKBP1	3
SALL3	2	SCRN1	1	SERTM1	2	SHROOM2	1
SAMD1	1	SCRN3	1	SESN1	1	SIAH1	4
SAMD14	1	SCRT1	1	SETBP1	1	SIAH3	1
SAMD4A	2	SCX	1	SETD1B	2	SIGLEC15	2
SAMD5	2	SDAD1P1	1	SETD2	1	SIGMAR1	1
SAP30	1	SDC2	1	SETD3	1	SIK3	1
SAP30L	1	SDC3	2	SETD6	3	SIMC1	1
SAP30L-AS1	1	SDCBP2	5	SETD7	1	SIN3B	1
SAPCD2	2	SDCCAG3	1	SETMAR	1	SIPA1	1
SAR1B	2	SDCCAG8	1	SETX	2	SIPA1L1	3
SARAF	1	SDHAF1	1	SEZ6L	1	SIPA1L2	2
SARM1	2	SDHB	1	SF3B5	1	SKA3	1
SASH1	6	SDR39U1	1	SFPQ	1	SKI	2
SAT2	1	SEC16A	7	SFRP5	1	SKIL	1
SATB1	4	SEC22A	1	SFT2D3	7	SLA2	1
SATB2	3	SEC23IP	1	SFXN5	2	SLBP	1
SBK1	1	SECISBP2	3	SGK494	3	SLC12A1	2
SCAF1	3	SELENOM	1	SGPP1	1	SLC12A2	1
SCAI	1	SELENON	1	SGSH	1	SLC12A5	3
SCAMP1-AS1	1	SELENOO	2	SGSM3	1	SLC12A6	2
SCAND1	3	SELENOP	2	SH2B1	1	SLC12A8	1
SCAND2P	3	SELPLG	3	SH2B2	2	SLC13A3	1
SCARA3	2	SEMA3G	1	SH2B3	2	SLC15A2	1
SCARB1	1	SEMA4F	2	SH2D4A	2	SLC15A4	1
SCARF2	3	SEMA6A-AS1	3	SH3BP4	4	SLC16A14	2
SCARNA10	1	SEMA6C	1	SH3BP5L	3	SLC16A2	1
SCARNA14	1	SEMA6D	2	SH3D19	1	SLC16A8	2
SCARNA22	1	SENP2	1	SH3D21	2	SLC17A9	2
SCARNA26A	2	SENP3-EIF4A1	2	SH3RF1	1	SLC18A2	2
SCARNA6	1	SENP5	2	SH3RF3	2	SLC18B1	1
SCCPDH	2	SENP6	1	SH3TC1	3	SLC19A1	3
SCD5	1	SENP8	1	SHANK1	1	SLC1A2	1
SCG2	1	SEPHS2	1	SHARPIN	1	SLC1A4	2
SCGB1C2	1	SEPT5-GP1BB	1	SHB	2	SLC20A2	1
SCLY	2	SEPT7P2	3	SHC3	2	SLC22A12	1
SCML1	1	SEPT8	1	SHC4	2	SLC22A16	1
SCML4	4	SEPT9	1	SHE	1	SLC22A17	1
SCN2A	1	SERAC1	2	SHF	1	SLC22A20P	1
SCN2B	1	SERBP1	1	SHH	2	SLC22A23	2
SCN3A	2	SERPINF1	3	SHISA2	3	SLC22A7	6
				SHISA4	2	SLC24A2	1

SLC25A23	1	SLC39A10	1	SLCO4A1-AS1	1	SNORA11G	1
SLC25A24	2	SLC39A3	5	SLIT1	1	SNORA120	4
SLC25A25	1	SLC39A5	1	SLIT1-AS1	7	SNORA17B	2
SLC25A27	1	SLC39A6	1	SLITRK1	4	SNORA31	1
SLC25A28	1	SLC39A9	2	SLITRK2	9	SNORA4	1
SLC25A29	2	SLC3A2	1	SLITRK3	4	SNORA40B	1
SLC25A34	4	SLC41A1	1	SLITRK4	2	SNORA47	2
SLC25A37	1	SLC41A2	1	SLITRK5	4	SNORA50C	2
SLC25A39	1	SLC41A3	1	SLN	1	SNORA53	1
SLC25A41	3	SLC45A1	2	SMAD1-AS1	2	SNORA59B	1
SLC25A42	1	SLC45A2	2	SMAD2	1	SNORA5A	1
SLC25A44	2	SLC45A3	1	SMAD3	3	SNORA68B	1
SLC25A46	1	SLC45A4	3	SMAD6	1	SNORA70B	1
SLC25A48	1	SLC48A1	1	SMAD7	7	SNORA75	1
SLC25A51	2	SLC4A11	1	SMC6	1	SNORA77	1
SLC25A6	2	SLC4A3	1	SMCR5	2	SNORA80A	2
SLC26A4	1	SLC4A8	1	SMCR8	4	SNORA80B	1
SLC27A5	1	SLC50A1	1	SMG6	1	SNORA80C	3
SLC29A4	3	SLC51A	2	SMG8	3	SNORA89	2
SLC2A10	2	SLC51B	1	SMIM10L2A	1	SNORA92	1
SLC2A12	1	SLC5A11	1	SMIM10L2B	1	SNORC	2
SLC2A13	1	SLC5A2	2	SMIM12	4	SNORD108	1
SLC2A1-AS1	2	SLC5A5	1	SMIM17	3	SNORD12	4
SLC2A2	1	SLC6A13	1	SMIM22	1	SNORD124	1
SLC2A3	1	SLC6A17	3	SMIM24	2	SNORD129	1
SLC2A4RG	4	SLC6A1-AS1	2	SMIM29	3	SNORD143	1
SLC2A6	1	SLC6A20	1	SMIM32	3	SNORD145	1
SLC2A8	1	SLC6A3	2	SMKR1	1	SNORD148	1
SLC30A1	1	SLC6A7	3	SMPD1	2	SNORD14C	1
SLC30A2	3	SLC6A8	1	SMTNL1	1	SNORD14E	1
SLC30A3	1	SLC7A14	1	SMUG1	4	SNORD151	4
SLC31A2	2	SLC7A4	2	SNAI3	3	SNORD152	4
SLC32A1	3	SLC7A5	1	SNAP47	1	SNORD153	1
SLC33A1	1	SLC7A5P2	4	SNAP91	1	SNORD164	2
SLC35B4	1	SLC7A6	3	SNCA	1	SNORD170	3
SLC35C1	4	SLC8A1	4	SNCB	1	SNORD172	2
SLC35C2	3	SLC8A1-AS1	1	SNCG	4	SNORD31B	1
SLC35E1	1	SLC8A2	1	SNN	3	SNORD36B	1
SLC35E3	1	SLC8A3	1	SNORA10	1	SNORD53B	1
SLC35E4	2	SLC9A1	3	SNORA105A	1	SNORD54	1
SLC35F6	1	SLC9A3-AS1	7	SNORA11	1	SNORD60	1
SLC35G2	1	SLC9A3R2	1	SNORA115	2	SNORD62A	1
SLC37A3	2	SLC9A6	2	SNORA117	5	SNORD62B	4
SLC38A2	1	SLC9A7P1	1	SNORA118	1	SNORD65	1
SLC38A7	2	SLC9B2	1	SNORA11D	1	SNORD68	1
SLC38A8	1					SNORD88B	1

SNORD9	2	SPARCL1	3	SRGAP3	1	STK35	3
SNORD96A	1	SPART-AS1	1	SRP19	7	STMN3	1
SNRK	2	SPATA13-AS1	2	SRPRB	1	STMN4	1
SNRK-AS1	1	SPATA2	4	SRRD	2	STMP1	1
SNRNP35	2	SPATA25	1	SRRM2-AS1	4	STOML1	2
SNRNP70	1	SPATA2L	3	SRRM5	1	STOX2	6
SNRPE	1	SPATA33	2	SRSF11	1	STRN4	4
SNTA1	1	SPATA46	1	SRSF2	2	STS	1
SNU13	1	SPATA6L	1	SRSF5	1	STUB1	1
SNX18	2	SPCS3	1	SRSF8	2	STUM	2
SNX19	3	SPECC1	1	SRXN1	6	STX10	3
SNX21	1	SPECC1L	2	SSBP3-AS1	2	STXBP1	1
SNX22	2	SPEF1	1	SSBP4	1	STXBP4	2
SNX27	2	SPEG	1	SSFA2	2	SUGP2	2
SNX33	3	SPEM1	2	SSH1	1	SUGT1	1
SOCS1	4	SPEN	1	SSR2	2	SUMO1	1
SOCS3	1	SPHK1	3	SSR4	3	SUMO4	1
SOCS7	1	SPHK2	2	SSTR1	5	SUPT16H	1
SOD2	1	SPIN4	1	SSTR2	2	SUPT4H1	1
SOD3	1	SPIRE1	1	SSTR3	1	SUPT7L	1
SOGA1	2	SPOCK1	1	ST20	3	SURF2	1
SOGA3	3	SPOCK2	3	ST3GAL1	2	SURF6	1
SORBS2	2	SPPL2B	3	ST3GAL2	1	SUSD2	2
SORD	1	SPPL2C	3	ST3GAL4	3	SUV39H1	2
SOST	1	SPRED1	2	ST3GAL5	2	SV2A	2
SOWAHA	1	SPRED2	1	ST6GAL1	2	SV2B	2
SOWAHB	9	SPRED3	1	ST6GAL2	1	SWSAP1	1
SOWAHC	1	SPRN	5	ST6GALNAC1	1	SYBU	2
SOX1	2	SPRY1	1	ST6GALNAC6	1	SYCE1	1
SOX10	1	SPRY2	1	ST8SIA1	2	SYCP2	1
SOX11	1	SPRY4-IT1	4	ST8SIA3	1	SYCP3	2
SOX12	4	SPRYD4	2	ST8SIA5	2	SYDE1	1
SOX15	1	SPSB1	2	STAB1	3	SYDE2	1
SOX1-OT	1	SPTAN1	1	STAC2	1	SYN1	1
SOX2	3	SPTBN1	3	STAC3	1	SYNDIG1	3
SOX21	3	SPTBN2	2	STARD13	1	SYNE1	1
SOX21-AS1	1	SPTBN4	1	STARD4-AS1	2	SYNE1-AS1	2
SOX4	4	SPTBN5	1	STARD7-AS1	3	SYNGR1	1
SOX8	2	SQLE	1	STARD8	1	SYNGR2	1
SP3	3	SQSTM1	2	STAT3	1	SYNGR3	3
SP4	1	SRARP	3	STH	5	SYNM	7
SP8	1	SRC	3	STIM1	2	SYNPO	5
SP9	2	SRCIN1	2	STK11	1	SYNRG	1
SPACA3	1	SREBF1	3	STK17B	1	SYS1-DBNDD2	1
SPACA9	3	SRF	1	STK25	1	SYT11	5
SPAG5-AS1	1	SRGAP2	1			SYT13	4

SYT15	1	TBRG1	1	THAP3	2	TMCC1	4
SYT16	1	TBRG4	1	THAP4	2	TMCC2	3
SYT17	1	TBX1	1	THAP7-AS1	3	TMCO2	2
SYT3	2	TBX2	1	THBD	1	TMCO3	1
SYT4	1	TBX6	1	THBS3	2	TMED5	2
SYT5	1	TCAP	2	THEM5	1	TMED6	1
SYT7	1	TCF20	6	THEM6	2	TMED7-TICAM2	1
SYTL1	1	TCFL5	1	THEMIS	1	TMED9	1
SYTL5	1	TCP11	2	THOC1	1	TMEFF2	1
SZRD1	1	TCTE1	1	THOC2	2	TMEM106A	1
SZT2-AS1	1	TDRD6	1	THOC6	1	TMEM11	1
TAB1	1	TDRG1	4	THRIL	1	TMEM115	2
TACC1	3	TECPR1	1	THSD1	3	TMEM120A	1
TACC2	1	TECPR2	7	THUMPD1	1	TMEM121	3
TACO1	1	TEDC1	1	THY1	3	TMEM121B	6
TADA1	3	TEDC2	1	THYN1	2	TMEM125	3
TAF11	1	TEF	2	TIAF1	2	TMEM127	2
TAF1C	2	TELO2	1	TIAM1	4	TMEM129	1
TAF2	1	TEN1	1	TICAM1	2	TMEM130	3
TAF4B	1	TENT4A	2	TIGD5	3	TMEM132A	2
TAF5L	2	TENT4B	1	TIMM13	2	TMEM132B	5
TAF7	1	TERF1	1	TIMM22	3	TMEM132D	2
TAF8	1	TET2-AS1	1	TIMM44	1	TMEM132D-AS1	5
TAGLN3	1	TET3	1	TIMM8A	1	TMEM132E	3
TAL1	2	TEX10	1	TIMM8B	1	TMEM147	1
TANGO6	2	TEX2	2	TIMP3	2	TMEM151A	3
TAP2	3	TEX22	1	TIMP4	1	TMEM151B	2
TAPBP	4	TEX264	2	TINCR	1	TMEM155	1
TAPT1	1	TEX29	2	TINF2	1	TMEM158	1
TARBP1	2	TEX35	2	TIPARP	3	TMEM160	7
TARS2	3	TEX53	2	TJP2	2	TMEM161A	1
TAS1R3	1	TFAP2E	1	TLE1	1	TMEM165	1
TBC1D1	1	TFCP2	3	TLE2	1	TMEM170A	2
TBC1D10B	1	TFCP2L1	1	TLE3	1	TMEM170B	1
TBC1D12	2	TFE3	1	TLE4	1	TMEM177	1
TBC1D14	4	TFF3	1	TLL2	1	TMEM178A	2
TBC1D16	4	TGFB1	2	TLNRD1	3	TMEM178B	1
TBC1D2	1	TGFB1I1	1	TLR5	1	TMEM179	1
TBC1D20	2	TGFBR2	1	TLR9	1	TMEM179B	2
TBC1D22A	1	TGFBR3L	1	TM2D2	1	TMEM181	1
TBC1D7-LOC100130357	1	TGFBRAP1	1	TM7SF2	3	TMEM185B	2
TBCB	1	TGM2	1	TM9SF1	2	TMEM186	3
TBCC	2	TGOLN2	3	TM9SF3	1	TMEM191A	1
TBL2	1	THAP11	1	TMA16	1	TMEM191C	2
TBR1	3	THAP12	1	TMBIM7P	2	TMEM192	1
		THAP2	2	TMC4	2	TMEM196	1

TMEM198B	2	TNFAIP8L2	1	TPST1	2	TSC22D1	2
TMEM199	2	TNFRSF11A	1	TRA2B	1	TSC22D1-AS1	3
TMEM200A	2	TNFRSF13C	1	TRABD	1	TSC22D2	2
TMEM200C	5	TNFRSF1A	1	TRAF3IP2	2	TSC22D3	2
TMEM203	2	TNFRSF21	2	TRAF3IP2-AS1	1	TSFM	1
TMEM204	2	TNFRSF25	2	TRAF4	2	TSHZ1	4
TMEM211	2	TNFRSF4	1	TRAF6	1	TSHZ3	1
TMEM214	2	TNFRSF6B	1	TRAIP	1	TSKU	1
TMEM215	1	TNFSF14	1	TRAP1	3	TSNARE1	1
TMEM216	1	TNFSF9	1	TRAPPC10	2	TSPAN11	1
TMEM229A	1	TNIP1	1	TRAPPC12	1	TSPAN17	2
TMEM229B	3	TNK2	1	TRAPPC2L	1	TSPAN3	2
TMEM240	1	TNKS1BP1	5	TRAPPC3	3	TSPAN5	2
TMEM242	5	TNKS2	1	TRAPPC5	2	TSPOAP1	2
TMEM246-AS1	1	TNRC18	4	TRAPPC9	1	TSPOAP1-AS1	4
TMEM248	1	TNRC18P1	1	TREX1	2	TSPY26P	6
TMEM250	2	TNRC6C	3	TRG-AS1	1	TSPYL2	3
TMEM263	1	TNRC6C-AS1	1	TRHDE	2	TSPYL4	4
TMEM265	8	TNXB	2	TRIB1	3	TSPYL5	3
TMEM30A	1	TOGARAM1	4	TRIB2	3	TSR3	2
TMEM38A	1	TOMM40	1	TRIL	2	TSSC4	1
TMEM39A	3	TOMM6	2	TRIM11	1	TSSK2	1
TMEM41A	2	TONSL	2	TRIM17	1	TSSK3	1
TMEM42	1	TOR1AIP2	2	TRIM24	1	TSSK6	2
TMEM43	3	TOR1B	1	TRIM26	1	TST	2
TMEM44	1	TOR2A	2	TRIM28	1	TSTD1	1
TMEM44-AS1	1	TOR3A	2	TRIM3	1	TTC1	1
TMEM47	3	TOR4A	1	TRIM32	4	TTC19	1
TMEM51-AS1	6	TP53AIP1	3	TRIM35	1	TTC21A	2
TMEM65	1	TP53BP1	1	TRIM37	1	TTC36	3
TMEM74	2	TP53BP2	1	TRIM39	1	TTC9	1
TMEM74B	1	TP53I13	1	TRIM39-RPP21	2	TTC9B	2
TMEM81	2	TP53INP2	1	TRIM41	1	TTI1	2
TMEM86A	1	TP73-AS1	2	TRIM56	2	TTLL11	2
TMEM87B	1	TPBG	3	TRIM65	1	TTLL4	1
TMEM88	1	TPBGL	2	TRIM8	5	TTLL8	1
TMIGD3	1	TPGS1	3	TRIM9	2	TTPAL	1
TMOD3	1	TPI1	1	TRIO	1	TTR	1
TMPPE	2	TPM2	1	TRIR	1	TTYH3	4
TMSB4X	1	TPP1	9	TRMT12	2	TUB	3
TMTC2	3	TPP2	1	TRMT61B	1	TUBA1B	1
TMUB2	2	TPPP	2	TRNP1	1	TUBA4B	3
TNFAIP1	2	TPRG1L	4	TRPC1	1	TUBA8	3
TNFAIP2	1	TPRN	1	TRPS1	5	TUBB	3
TNFAIP8L1	3	TPSG1	1	TRPV1	5	TUBB2A	1
				TRUB2	1	TUBB3	4

TUBB4A	2	UCK2	1	VDAC1	1	WFS1	4
TUBB4B	2	UCKL1	1	VDAC3	1	WHAMM	1
TUBB6	2	UFSP1	1	VEGFA	2	WIPI2	2
TUBBP5	2	UGGT1	1	VGF	3	WIZ	1
TUBG2	1	UMPS	2	VHL	1	WLS	1
TUG1	7	UNC13C	2	VIM-AS1	3	WNK1	1
TULP4	2	UNC45A	1	VIPR1-AS1	2	WNT10A	1
TUSC1	1	UNC50	1	VOPP1	4	WNT11	1
TUSC8	1	UNC5C	2	VPS13C	1	WNT3	1
TWIST1	1	UNC80	7	VPS13D	1	WNT7A	1
TWISTNB	1	UNC93B1	1	VPS16	2	WNT7B	3
TWSG1	1	UNKL	1	VPS18	3	WRNIP1	1
TXLNA	2	UPF1	1	VPS33A	1	WSCD1	2
TXN2	1	UPRT	1	VPS37B	2	WSCD2	1
TXNDC12	1	UQCR10	1	VPS51	1	WTIP	1
TXNDC15	1	UQCRFS1	2	VPS9D1-AS1	2	WWC1	1
TXNDC2	1	URAHP	4	VSIG2	1	XBP1	1
TXNDC5	1	URB2	3	VSTM2A	2	XIAP	1
TYRO3	1	URI1	1	VSTM2A-OT1	1	XKR4	1
TYSND1	1	USB1	2	VSTM2B	2	XKR6	1
U2AF2	1	USE1	3	VSTM2L	2	XKR7	1
UBA5	2	USF2	1	VTI1B	1	XPC	1
UBAC1	1	USP10	1	VWA1	2	XPO1	1
UBALD1	1	USP11	2	VWC2	1	XPO6	1
UBALD2	1	USP12-AS1	1	VXN	2	XRCC5	1
UBB	3	USP2	1	WASL	1	XXYLT1-AS1	1
UBC	2	USP22	1	WBP2	1	YARS2	1
UBE2CP5	2	USP27X	2	WDCP	1	YBEY	1
UBE2D4	3	USP31	4	WDFY3-AS2	2	YBX1	1
UBE2G2	1	USP35	3	WDR13	1	YDJC	1
UBE2H	1	USP36	2	WDR20	1	YEATS2-AS1	4
UBE2M	1	USP38	2	WDR24	3	YIPF2	2
UBE2Q1	1	USP42	4	WDR26	1	YKT6	4
UBE2Q1-AS1	1	USP46	1	WDR34	3	YLPM1	1
UBE2QL1	2	USP49	1	WDR45B	5	YPEL5	1
UBE2V1	2	USPL1	1	WDR47	2	YRDC	1
UBFD1	2	UTF1	4	WDR54	1	YTHDF1	2
UBL3	3	UTP18	1	WDR6	4	YTHDF2	3
UBL4A	2	UTS2R	3	WDR7	1	YTHDF3	1
UBN1	5	UVSSA	2	WDR73	2	YWHAE	1
UBOX5	4	VAMP3	1	WDR81	5	YWHAH	1
UBOX5-AS1	1	VAPB	1	WDR86-AS1	1	YWHAQ	1
UBQLN2	2	VASH1-AS1	1	WDR92	1	YY1	1
UBR3	1	VASN	2	WDR97	1	ZACN	8
UBXN4	1	VCAN-AS1	3	WFIKKN1	2	ZADH2	6
UCK1	2	VCPIP1	2			ZAR1L	1

ZBED1	6	ZFP36L2	1	ZNF324B	3	ZNF594	1
ZBED5	1	ZFP41	6	ZNF32-AS1	1	ZNF609	1
ZBED9	1	ZFP64	3	ZNF333	1	ZNF622	2
ZBP1	1	ZFP91-CNTF	2	ZNF334	1	ZNF623	8
ZBTB10	3	ZFP92	2	ZNF337	4	ZNF629	5
ZBTB11-AS1	3	ZFX	4	ZNF34	1	ZNF638	2
ZBTB16	2	ZFYVE21	1	ZNF350-AS1	1	ZNF641	2
ZBTB17	1	ZFYVE9	1	ZNF382	1	ZNF646	5
ZBTB18	3	ZGLP1	2	ZNF397	1	ZNF648	2
ZBTB2	1	ZIC1	1	ZNF416	1	ZNF653	1
ZBTB20-AS1	4	ZIC2	2	ZNF428	1	ZNF664	1
ZBTB22	1	ZKSCAN1	1	ZNF436	4	ZNF667-AS1	1
ZBTB3	1	ZKSCAN2	1	ZNF445	1	ZNF668	3
ZBTB34	3	ZMAT3	1	ZNF446	8	ZNF669	1
ZBTB38	3	ZMAT4	1	ZNF451	1	ZNF671	1
ZBTB39	1	ZMPSTE24	1	ZNF460	3	ZNF672	2
ZBTB4	3	ZMYM2	1	ZNF467	1	ZNF687	4
ZBTB44	2	ZMYM3	1	ZNF469	8	ZNF688	2
ZBTB45	1	ZMYM5	1	ZNF470	1	ZNF691	2
ZBTB46	1	ZNF106	2	ZNF48	2	ZNF696	1
ZBTB6	1	ZNF12	2	ZNF483	5	ZNF703	1
ZBTB7A	3	ZNF121	1	ZNF484	1	ZNF704	1
ZBTB7B	2	ZNF132	1	ZNF488	1	ZNF706	1
ZBTB9	2	ZNF133	1	ZNF496	2	ZNF711	2
ZC3H10	1	ZNF134	1	ZNF497	2	ZNF718	1
ZC3H12C	1	ZNF142	4	ZNF500	1	ZNF720	1
ZC3H18	1	ZNF154	1	ZNF503-AS2	3	ZNF74	2
ZC3H3	1	ZNF17	3	ZNF513	3	ZNF747	2
ZCCHC2	2	ZNF18	1	ZNF517	5	ZNF75D	1
ZCCHC3	1	ZNF189	2	ZNF521	1	ZNF764	2
ZCCHC7	1	ZNF2	1	ZNF527	1	ZNF768	3
ZCCHC8	1	ZNF205-AS1	2	ZNF532	1	ZNF770	2
ZDHHC11B	1	ZNF212	2	ZNF536	4	ZNF772	1
ZDHHC14	2	ZNF22	1	ZNF543	1	ZNF777	4
ZDHHC22	1	ZNF24	1	ZNF544	1	ZNF780A	1
ZDHHC23	4	ZNF248	1	ZNF555	2	ZNF780B	2
ZDHHC3	2	ZNF250	1	ZNF557	2	ZNF781	1
ZDHHC7	2	ZNF251	1	ZNF559-ZNF177	1	ZNF783	2
ZER1	1	ZNF263	2	ZNF564	5	ZNF785	2
ZFAS1	3	ZNF276	3	ZNF565	1	ZNF786	3
ZFHX3	1	ZNF280D	1	ZNF570	1	ZNF791	1
ZFP1	1	ZNF282	1	ZNF574	2	ZNF792	1
ZFP14	1	ZNF3	1	ZNF576	1	ZNF8	1
ZFP28	1	ZNF302	1	ZNF579	2	ZNF805	2
ZFP36	1	ZNF316	5	ZNF584	2	ZNF827	1
ZFP36L1	2	ZNF324	1			ZNF831	2

ZNF84	1	ZNRF2P1	1	ZSCAN5A	2	ZXDA	3
ZNF853	4	ZRANB1	1	ZSWIM1	2	ZXDB	4
ZNF862	1	ZRANB2-AS1	1	ZSWIM5	1	ZXDC	1
ZNF865	4	ZSCAN18	6	ZSWIM6	1	ZYG11B	1
ZNF91	1	ZSCAN20	1	ZSWIM7	1	ZZZ3	1
ZNHIT2	1	ZSCAN21	4	ZSWIM8	1		
ZNRF1	1	ZSCAN23	1	ZSWIM8-AS1	2		
ZNRF2	1	ZSCAN25	1	ZSWIM9	2		

Appendix 2. Annotation of m^6A peaks from grey matter.

Gene name	m^6A peaks						
A1BG	3	ACKR3	1	ADGRL2	3	AHDC1	4
A2ML1	2	ACOT12	1	ADGRV1	6	AHI1	1
A3GALT2	2	ACOT2	1	ADHFE1	1	AHNAK	22
AACS	1	ACP6	4	ADIG	2	AHNAK2	1
AAK1	1	ACSL3	3	ADIPOR2	1	AHSA1	1
AANAT	1	ACSL4	1	ADIRF	1	AHSA2P	5
AAR2	5	ACTB	2	ADNP	3	AIG1	1
AASDH	1	ACTG1	1	ADO	3	AJAP1	2
AASDHPPT	1	ACTG1P4	2	ADORA2A	1	AJM1	1
AASS	3	ACTN1-AS1	4	ADORA3	3	AK1	1
AATBC	1	ACTR2	3	ADPGK-AS1	2	AK2	2
ABCA11P	6	ACTR5	1	ADPRHL1	1	AK3	1
ABCA4	2	ACTR8	2	ADPRHL2	2	AK5	2
ABCA8	1	ACVR1	1	ADPRM	1	AKAP1	2
ABCC10	1	ACVR2A	1	ADRA1A	2	AKAP10	1
ABCC3	1	ACY1	1	ADRA1B	1	AKAP11	3
ABCC5-AS1	2	ADA	1	ADRA2A	1	AKAP12	5
ABCD2	2	ADAL	2	ADRA2C	1	AKAP13	1
ABCD4	1	ADAM11	1	ADRB1	1	AKAP2	8
ABCF3	1	ADAM1A	2	ADRB2	3	AKAP5	3
ABCG8	1	ADAM22	1	ADRM1	1	AKAP6	2
ABHD11-AS1	1	ADAM30	3	ADSL	3	AKAP7	2
ABHD13	1	ADAMTS1	2	AFAP1-AS1	1	AKAP9	2
ABHD15	3	ADAMTS4	2	AFAP1L1	1	AKIRIN1	2
ABHD17A	1	ADAMTS8	1	AFAP1L2	2	AKIRIN2	1
ABHD8	1	ADAP1	2	AFF1	2	AKNA	1
ABI2	6	ADAR	8	AFF4	1	AKR7A2P1	1
ABL1	2	ADARB1	1	AFG3L1P	3	AKT1S1	1
ABRA	1	ADAT1	2	AGAP2	2	AKTIP	3
ABRAXAS2	1	ADAT2	1	AGAP2-AS1	7	ALCAM	5
ABT1	1	ADCK2	1	AGAP6	1	ALDH18A1	2
ABTB1	2	ADCY5	2	AGER	1	ALDH1A3	3
ACACA	1	ADCY7	1	AGK	3	ALDH1B1	3
ACAD9	1	ADCY8	1	AGMAT	1	ALDH3A1	1
ACADS	2	ADCYAP1R1	2	AGO1	2	ALDH3A2	1
ACADSB	3	ADD1	1	AGO2	2	ALDH5A1	4
ACAT1	3	ADGRA1	4	AGO3	1	ALDH6A1	1
ACAT2	2	ADGRA1-AS1	1	AGPAT4	1	ALDH8A1	1
ACER2	9	ADGRB1	1	AGPAT4-IT1	8	ALDOA	2
ACHE	2	ADGRB3	1	AGT	1	ALG10	1
ACIN1	1	ADGRG3	2	AHCTF1	1	ALG12	4

ALG1L	3
ALG2	2
ALG9	1
ALK	3
ALKBH1	1
ALKBH2	3
ALKBH3	4
ALKBH4	1
ALMS1-IT1	12
ALOX15	1
ALOX15P1	1
ALPK3	3
ALS2	1
ALS2CR12	1
ALX3	1
AMBP	1
AMBRA1	3
AMD1	2
AMDHD2	2
AMER2	7
AMER3	4
AMFR	6
AMHR2	1
AMIGO1	2
AMMECR1L	2
AMN	6
AMOT	1
AMOTL1	1
AMOTL2	1
AMT	4
AMZ1	4
AMZ2	1
AMZ2P1	1
ANAPC10	2
ANAPC7	2
ANGEL1	1
ANGEL2	3
ANGPTL1	1
ANGPTL2	3
ANGPTL5	1
ANK1	5
ANK2	9
ANK3	10
ANKAR	1
ANKDD1B	3
ANKIB1	1
ANKLE2	3
ANKMY2	1
ANKRD12	1
ANKRD13D	1
ANKRD19P	4
ANKRD30B	1
ANKRD33B	9
ANKRD34B	1
ANKRD36BP2	1
ANKRD39	1
ANKRD40	1
ANKRD49	3
ANKRD50	5
ANKRD63	1
ANKRD65	1
ANKRD9	4
ANKS1B	4
ANKZF1	1
ANO10	1
ANO5	1
ANO8	1
ANP32B	1
ANXA2P1	1
AP1G2	2
AP1M1	1
AP3M1	1
AP3M2	4
AP3S1	1
AP4S1	4
AP5B1	3
AP5M1	2
AP5S1	2
AP5Z1	3
APAF1	2
APBA1	2
APBA2	7
APBB1	2
APBB2	4
APBB3	1
APC2	2
APCDD1	2
APEH	12
APEX1	1
APH1A	1
APH1B	1
APLF	1
APLNR	4
APLP1	1
APOA1	3
APOD	1
APOE	1
APOL2	1
APOL5	2
APOLD1	1
APOPT1	1
APPBP2	1
APTR	1
APTX	1
AQP1	1
AQP12A	1
AQP4	5
AQP7	1
AQP8	1
AR	1
ARAP1	1
ARAP2	2
ARC	2
ARCN1	1
AREL1	1
ARF4-AS1	2
ARF5	1
ARF6	1
ARFGAP2	1
ARFGEF1	1
ARFIP2	2
ARHGAP1	2
ARHGAP11B	1
ARHGAP12	1
ARHGAP20	3
ARHGAP21	1
ARHGAP22	1
ARHGAP23	5
ARHGAP24	2
ARHGAP25	1
ARHGAP26-IT1	4
ARHGAP27	1
ARHGAP32	1
ARHGAP5	2
ARHGAP5-AS1	1
ARHGDIA	1
ARHGEF12	1
ARHGEF16	1
ARHGEF26	2
ARHGEF3	1
ARHGEF4	1
ARHGEF9	1
ARHGEF9-IT1	1
ARID1A	1
ARID2	2
ARID5B	4
ARIH2OS	1
ARL14EP	1
ARL16	1
ARL17A	1
ARL2BP	6
ARL3	1
ARL4A	1
ARL4C	6
ARL5A	1
ARL5C	1
ARL6	1
ARL6IP1	1
ARL6IP4	4
ARL9	1
ARMC1	3
ARMC10	1
ARMC5	2
ARMC8	1
ARMCX1	2
ARMCX2	2
ARMCX3	2
ARMCX4	1
ARMCX5	1
ARMCX5-GPRASP2	4
ARMCX6	1

ARMH4	1	ATM	4	AZIN1	1	BCDIN3D	3
ARNTL2	1	ATMIN	4	B2M	1	BCHE	2
ARPC3	1	ATOX1	1	B3GALNT1	4	BCKDK	1
ARPC5	2	ATP10D	1	B3GALT1	2	BCL10	1
ARPP19	2	ATP13A5	1	B3GALT2	2	BCL11B	2
ARPP21	2	ATP1A1	1	B3GALT6	3	BCL2	6
ARRDC1-AS1	1	ATP1A1-AS1	1	B3GAT1	3	BCL2L1	1
ARRDC2	2	ATP1A3	1	B3GAT2	3	BCL2L10	1
ARRDC3	1	ATP1A4	4	B3GLCT	3	BCL2L11	1
ARRDC4	1	ATP1B2	1	B3GNT10	3	BCL2L13	1
ARSG	4	ATP1B3	1	B3GNT2	1	BCL2L2	2
ART3	2	ATP2B1	2	B3GNT4	5	BCL7A	1
ARTN	2	ATP2B4	1	B3GNT5	1	BCLAF1	3
ASAH1	2	ATP4B	2	B3GNT9	4	BCLAF3	2
ASAH2	2	ATP5ME	1	B4GALNT4	1	BCOR	1
ASAP1-IT2	1	ATP5MF	2	B4GALT2	1	BCORL1	2
ASB1	2	ATP5MG	2	B4GALT4-AS1	1	BCR	2
ASB13	2	ATP5PF	3	B4GALT7	2	BCS1L	1
ASB6	4	ATP5PO	2	B4GAT1	1	BDKRB1	1
ASB7	1	ATP6V0A4	1	BAAT	3	BDNF	1
ASB8	1	ATP6V0C	6	BACE1	1	BDP1	3
ASCC1	1	ATP6V0E2	2	BACE1-AS	4	BEAN1-AS1	1
ASCC3	1	ATP6V0E2-AS1	1	BACH1	1	BEGAIN	1
ASCL3	2	ATP6V1C1	1	BACH1-IT2	2	BEND3P3	1
ASDURF	2	ATP6V1E1	1	BAG1	1	BEST2	1
ASH1L	1	ATP6V1G2	1	BAG2	2	BET1L	1
ASIC3	2	ATP8B2	1	BAG3	2	BEX1	1
ASMT	3	ATP8B5P	3	BAG5	1	BEX4	2
ASPDH	4	ATR	1	BAIAP2-DT	5	BEX5	1
ASPH	2	ATRIP	1	BAMBI	3	BFSP1	1
ASPHD2	8	ATRNL1	2	BARD1	1	BHLHA15	9
ASPM	1	ATRX	5	BASP1	3	BHLHB9	1
ASPRV1	1	ATXN1L	3	BATF3	1	BHLHE40-AS1	1
ASXL1	3	ATXN7L3	1	BAZ1B	2	BHLHE41	3
ASXL2	3	ATXN7L3B	2	BAZ2A	1	BICRAL	2
ASXL3	4	AUNIP	3	BBS10	1	BIRC2	1
ATAT1	1	AURKC	4	BBS12	2	BIRC3	2
ATF1	1	AUTS2	1	BCAN	1	BIRC5	1
ATF3	1	AVEN	2	BCAP29	1	BIRC6	1
ATF4	4	AVL9	2	BCAR3	3	BLCAP	3
ATF7IP	3	AXDND1	1	BCAR4	1	BLOC1S3	1
ATG14	4	AXIN1	1	BCAS1	1	BLOC1S4	1
ATG16L1	1	AXIN2	2	BCAS3	2	BLVRA	1
ATG16L2	3	AZI2	2			BMP10	1
ATG7	1						
ATL2	2						

BMP2	1	BTBD3	1	C17orf58	6	C2orf40	1
BMP7-AS1	1	BTBD7	2	C17orf75	2	C2orf42	1
BMP8A	1	BTBD9-AS1	7	C17orf80	1	C2orf49	1
BMPER	1	BTD	2	C17orf99	1	C2orf66	1
BMPR1A	2	BTF3	2	C18orf21	1	C2orf68	1
BMPR1B	4	BTG2	2	C18orf25	2	C2orf69	1
BMPR2	1	BTN2A1	2	C18orf54	2	C2orf71	1
BMS1P20	1	BTN2A2	1	C19orf12	1	C2orf72	1
BNIP1	1	BTN2A3P	2	C19orf18	1	C2orf73	1
BNIP3	2	BUD31	1	C19orf24	2	C2orf88	1
BNIPL	2	C10orf105	1	C19orf25	9	C2orf92	1
BOD1	1	C10orf25	4	C19orf44	1	C3	1
BOD1L1	8	C10orf82	6	C19orf66	2	C3AR1	1
BOK-AS1	1	C10orf88	1	C19orf71	1	C3orf18	1
BOLA1	1	C10orf90	1	C19orf81	3	C3orf20	1
BOLA3	3	C11orf24	3	C1GALT1C1	2	C3orf35	4
BOLA3-AS1	2	C11orf42	1	C1GALT1C1L	1	C3orf38	2
BORCS6	2	C11orf58	2	C1orf105	3	C3orf62	1
BPGM	1	C11orf65	1	C1orf115	3	C3orf70	3
BPHL	3	C11orf68	2	C1orf123	7	C3orf80	1
BPTF	2	C11orf71	1	C1orf131	2	C4BPB	1
BRAP	1	C11orf87	3	C1orf162	1	C4orf19	7
BRCC3	2	C11orf91	6	C1orf189	1	C4orf3	2
BRD1	2	C11orf94	3	C1orf198	4	C4orf33	1
BRD2	8	C11orf95	1	C1orf216	2	C4orf46	1
BRD3OS	2	C11orf96	2	C1orf226	1	C5orf22	1
BRD4	1	C11orf98	2	C1orf35	1	C5orf24	5
BRD8	1	C12orf40	1	C1orf50	1	C5orf30	1
BRF1	1	C12orf43	1	C1orf52	1	C5orf47	1
BRF2	1	C12orf49	1	C1orf56	2	C5orf49	2
BRICD5	1	C12orf57	1	C1orf74	1	C5orf64	3
BRINP1	1	C12orf66	2	C1QB	1	C6	1
BRINP2	1	C12orf76	2	C1QBP	1	C6orf120	2
BRINP3	2	C14orf132	4	C1QC	1	C6orf163	1
BRK1	1	C14orf28	1	C1QL3	2	C6orf203	1
BRMS1	1	C15orf40	1	C1QTNF12	1	C6orf226	1
BRPF1	1	C15orf59	3	C1QTNF5	2	C6orf47	2
BRPF3	3	C16orf46	2	C1QTNF9	6	C6orf62	1
BRSK1	1	C16orf58	1	C1S	1	C6orf89	1
BRWD1	1	C16orf72	1	C20orf144	3	C7orf25	2
BSCL2	1	C16orf86	2	C22orf23	1	C7orf26	3
BSN-DT	3	C16orf87	1	C22orf24	3	C7orf33	2
BTBD10	4	C16orf91	1	C22orf31	4	C7orf43	1
BTBD16	1	C17orf100	1	C22orf39	1	C8orf34	1
BTBD2	1	C17orf51	5	C2CD4C	1	C8orf37-AS1	1
						C8orf76	6

C8orf88	1	CANT1	1	CCDC169	1	CCNQ	2
C9	1	CAPN10-DT	1	CCDC17	2	CCNT2	2
C9orf131	1	CAPN11	1	CCDC181	1	CCP110	2
C9orf147	1	CAPN13	1	CCDC183-AS1	1	CCSAP	1
C9orf152	2	CAPN2	1	CCDC184	2	CCSER1	2
C9orf24	2	CAPN6	4	CCDC28B	2	CCSER2	2
C9orf3	1	CAPN7	1	CCDC30	1	CCT2	1
C9orf64	1	CAPRIN2	2	CCDC34	1	CD101	1
C9orf72	4	CAPS	2	CCDC40	1	CD14	1
C9orf92	1	CAPZA2	2	CCDC43	1	CD164	1
CA10	2	CARD8	1	CCDC62	1	CD180	5
CA3-AS1	1	CARD9	2	CCDC7	1	CD200	2
CA4	2	CARHSP1	2	CCDC70	2	CD22	2
CAAP1	1	CARMIL2	2	CCDC71	2	CD226	3
CABLES1	2	CASD1	2	CCDC71L	3	CD2BP2	3
CABP1	1	CASKIN1	6	CCDC74A	2	CD320	1
CABP5	1	CASKIN2	1	CCDC74B	3	CD34	5
CABP7	2	CASP16P	1	CCDC8	1	CD36	1
CACNA1C-AS1	1	CAV1	1	CCDC80	1	CD40	2
CACNA1E	2	CAV2	1	CCDC81	1	CD47	3
CACNA2D1	2	CAVIN2	3	CCDC82	1	CD53	1
CACNB3	3	CAVIN4	3	CCDC83	2	CD58	1
CACNG1	3	CBARP	1	CCDC85A	1	CD63	1
CACNG2	1	CBLN2	1	CCDC85B	1	CD68	2
CACNG3	2	CBLN4	2	CCDC88A	1	CD74	1
CACTIN	3	CBR1	1	CCDC88C	1	CD83	2
CACTIN-AS1	2	CBR4	2	CCDC90B	2	CD8A	3
CACUL1	1	CBX4	3	CCDC92	3	CDADC1	1
CACYBP	2	CBX6	2	CCDC93	1	CDAN1	12
CADM2	2	CBX7	2	CCDC96	4	CDC25C	1
CADM2-AS2	4	CC2D1B	2	CCDC97	1	CDC27	1
CADM3-AS1	3	CCAR1	2	CCK	3	CDC42BPA	1
CALCOCO1	2	CCAR2	2	CCKAR	1	CDC42BPG	1
CALHM2	1	CCDC107	2	CCKBR	1	CDC42EP1	3
CALHM6	1	CCDC115	1	CCNB2	2	CDC42EP2	4
CALM1	4	CCDC127	1	CCNDBP1	2	CDC42EP3	1
CALM3	3	CCDC138	6	CCNG1	1	CDC42SE2	3
CALML4	1	CCDC141	3	CCNH	1	CDC6	2
CAMK2B	4	CCDC144A	2	CCNI	1	CDCA7L	4
CAMK2D	1	CCDC144CP	2	CCNI2	1	CDH10	2
CAMLG	1	CCDC149	1	CCNK	1	CDH11	2
CAMSAP1	8	CCDC151	2	CCNL1	1	CDH18	2
CAND1	2	CCDC154	4	CCNL2	4	CDH19	1
CAND2	1					CDH2	1
						CDH20	1

CDH6	1	CENPBD1P1	3	CHAC1	2	CHST3	5
CDH8	3	CENPC	3	CHAC2	5	CHST5	1
CDIPTOSP	1	CENPI	1	CHADL	5	CHST7	4
CDK11B	3	CENPL	1	CHAF1A	1	CHSY1	3
CDK12	3	CENPO	3	CHAF1B	2	CHSY3	2
CDK13	3	CENPS-CORT	1	CHAMP1	2	CHTF8	1
CDK19	1	CENPU	2	CHCHD1	1	CIAO1	2
CDK2AP1	2	CEP135	1	CHCHD5	2	CIB1	3
CDK5R1	3	CEP164	1	CHCHD7	1	CIC	3
CDK5R2	1	CEP170	2	CHD1	1	CINP	1
CDK5RAP1	1	CEP170B	2	CHD1L	1	CIPC	3
CDK5RAP2	2	CEP19	1	CHD5	1	CIRBP-AS1	1
CDK9	1	CEP192	3	CHD6	3	CISD3	3
CDKAL1	2	CEP350	4	CHD7	4	CITED2	3
CDKL2	1	CEP57	2	CHD8	1	CKAP2	1
CDKN1C	1	CEP68	5	CHD9	1	CKAP4	1
CDKN2AIP	2	CEP85	1	CHDH	2	CKB	1
CDPF1	3	CERCAM	2	CHERP	2	CKM	1
CDR1	2	CERK	1	CHGA	5	CKMT1A	1
CDR2	3	CERS1	2	CHGB	3	CKMT1B	1
CDRT1	1	CERS2	3	CHKA	2	CKMT2	1
CDRT15P1	2	CERS5	1	CHL1	1	CLASP1	1
CDRT4	2	CERS6-AS1	1	CHL1-AS1	3	CLCA4	1
CDS1	2	CES2	2	CHML	8	CLCC1	5
CDS2	1	CES4A	2	CHMP1B	4	CLCN3	3
CDV3	3	CETN2	1	CHMP6	1	CLCN4	2
CEACAM19	1	CFAP20	1	CHMP7	1	CLCN6	1
CEBPB-AS1	1	CFAP298	1	CHN1	5	CLDN10	3
CEBPD	1	CFAP300	1	CHN2	4	CLDN11	2
CEBPG	1	CFAP53	1	CHPF	2	CLDN12	1
CEBPZ	1	CFAP69	1	CHPF2	1	CLDN20	1
CELA1	1	CFAP70	2	CHRAC1	3	CLDN34	1
CELA2B	1	CFAP97	3	CHRM1	3	CLDN5	3
CELF1	1	CFD	1	CHRM3-AS1	1	CLDND1	3
CELF2-AS1	2	CFDP1	1	CHRM4	2	CLEC14A	2
CELF5	1	CFL1	1	CHRM5	4	CLEC18B	3
CELP	2	CFL2	2	CHRNA2	1	CLEC19A	1
CELSR2	2	CFLAR	1	CHRNA4	3	CLEC2D	1
CELSR3	4	CFLAR-AS1	3	CHRNB1	3	CLEC2L	6
CEMIP	2	CFP	1	CHRNB2	2	CLEC3A	1
CEMIP2	2	CFTR-AS1	1	CHST1	3	CLEC3B	2
CEND1	2	CGGBP1	4	CHST10	3	CLIP1-AS1	2
CENPA	2	CGRRF1	1	CHST12	2	CLK1	3
CENPB	4	CH25H	1	CHST14	3	CLMAT3	2
				CHST15	5	CLN5	4
				CHST2	4		

CLN8	1
CLNS1A	3
CLP1	2
CLSTN2-AS1	1
CLSTN3	1
CLTA	1
CLTC	3
CLTCL1	1
CLUAP1	1
CLVS1	1
CLVS2	2
CMC2	1
CMC4	1
CMKLR1	1
CMPK1	1
CMTM4	1
CMTR2	4
CMYA5	1
CNDP1	1
CNDP2	1
CNFN	4
CNIH3	1
CNKSR2	1
CNNM1	1
CNNM2	1
CNNM3	1
CNNM3-DT	1
CNNM4	1
CNOT3	1
CNOT4	1
CNOT7	6
CNOT8	2
CNP	4
CNPY2	1
CNPY3	1
CNR1	4
CNRIP1	2
CNST	1
CNTF	2
CNTN1	1
CNTN2	5
CNTNAP5	1
COA3	1
COA5	6
COA7	1
COG1	6
COG7	1
COG8	1
COIL	1
COL11A2	1
COL14A1	1
COL16A1	2
COL18A1	1
COL21A1	4
COL8A2	1
COL9A1	3
COL9A2	2
COL9A3	1
COLGALT1	3
COLGALT2	5
COMMD5	4
COPS9	1
COQ10A	1
COQ3	1
COQ6	3
COQ8A	2
CORO6	9
COX10-AS1	1
COX14	3
COX15	1
COX16	3
COX18	5
COX19	1
COX6A1	1
COX6B2	1
COX7A1	3
COX7A2	3
COX7B2	1
CPD	1
CPEB2	2
CPEB4	5
CPED1	1
CPLANE2	2
CPLX2	1
CPNE1	5
CPQ	1
CPS1-IT1	4
CPSF4L	6
CPTP	1
CRAT37	3
CRB1	4
CRB2	3
CREBBP	1
CREBL2	2
CREBZF	3
CREG1	1
CREG2	1
CRIP3	2
CRIPAK	1
CRISPLD1	2
CRISPLD2	1
CRKL	1
CRMP1	1
CRNKL1	2
CRTC1	1
CRTC3	1
CRYAB	2
CRYBA1	2
CRYBB3	1
CRYBG3	5
CRYGS	1
CSAD	2
CSE1L	1
CSE1L-AS1	1
CSF1	3
CSF1R	5
CSGALNACT2	2
CSNK1A1	4
CSNK1G1	2
CSNK1G2-AS1	2
CSPG4	1
CSPG5	1
CSPP1	3
CSRNP1	2
CSRNP3	6
CSRP1	2
CSRP2	1
CSTB	2
CSTF2T	1
CTB-178M22.2	5
CTBP1-AS	1
CTBP1-DT	1
CTBP2	3
CTD-2201I18.1	1
CTDP1	2
CTDSPL2	2
CTGF	1
CTNNA1	7
CTNNA2	1
CTNNAL1	2
CTNNB1	2
CTNND1	3
CTSB	2
CTSC	1
CTSH	3
CTSL	1
CTSZ	1
CTTN	6
CTTNBP2	2
CUEDC1	1
CUL2	1
CUL9	1
CUTALP	4
CUTC	1
CWF19L2	2
CX3CL1	1
CX3CR1	2
CXCR4	3
CXCR5	3
CXorf36	2
CXorf38	1
CXXC4-AS1	1
CXXC5	3
CYB561	7
CYB561D1	3
CYB5B	1
CYB5D2	4
CYB5R2	3
CYBC1	2
CYBRD1	1
CYCS	1
CYCSP52	2
CYHR1	2
CYP17A1	2
CYP1B1	1

CYP26B1	2
CYP27A1	1
CYP2J2	1
CYP2T1P	2
CYP51A1	7
CYREN	5
CYTH1	3
CYTH2	2
CYYR1	1
D2HGDH	3
DAB2IP	3
DACT1	2
DACT3	1
DAGLB	1
DALRD3	4
DAO	1
DAP	2
DAPK3	1
DAW1	3
DAXX	1
DAZAP2	1
DBNDD1	3
DBNDD2	2
DBR1	1
DBX1	5
DBX2	2
DCAF13	1
DCAF16	1
DCAF4L2	3
DCAF7	1
DCAKD	1
DCHS1	2
DCHS2	10
DCLK2	3
DCLRE1A	1
DCLRE1B	5
DCP2	1
DCT	1
DCTD	6
DCTN5	1
DCTN6	1
DCUN1D5	1
DDA1	2
DDC	2
DDHD2	2
DDIT4	2
DDN-AS1	5
DDR2	1
DDX11L5	1
DDX18	1
DDX19A	4
DDX23	1
DDX24	2
DDX27	3
DDX31	4
DDX39B	1
DDX3X	1
DDX3Y	2
DDX41	1
DDX47	3
DDX51	1
DDX56	1
DDX6	2
DEDD2	2
DEGS1	3
DEGS2	2
DEK	1
DENND2A	2
DENND3	1
DENND4A	1
DENND5A	1
DENND5B-AS1	1
DEPDC1B	1
DEPDC7	1
DERL1	4
DESI2	1
DET1	3
DEXI	2
DFFA	1
DGCR10	1
DGCR11	2
DGCR5	2
DGCR8	2
DGCR9	3
DGKK	7
DHCR24	4
DHFR2	1
DHRS11	1
DHRS13	1
DHRS7	2
DHRS9	4
DHX15	1
DHX29	1
DHX36	1
DHX57	1
DHX58	1
DICER1	8
DIDO1	3
DIMT1	2
DIO2-AS1	6
DIP2A	1
DIP2C	2
DIRAS1	4
DIRAS2	1
DISC1-IT1	2
DISP2	4
DKFZP586I1420	2
DKK3	3
DLAT	2
DLC1	7
DLEU7-AS1	1
DLG3-AS1	4
DLG5	3
DLGAP3	2
DLGAP4	1
DLL3	1
DLSTP1	1
DLX1	2
DLX6	1
DMAC1	1
DMD	1
DMPK	3
DMRT2	1
DMXL2	1
DNAAF2	1
DNAAF4	1
DNAH11	2
DNAH7	1
DNAH9	1
DNAJA2	2
DNAJA4	1
DNAJB1	2
DNAJB12	2
DNAJB13	1
DNAJB4	1
DNAJB5-DT	3
DNAJB6	3
DNAJB8-AS1	1
DNAJC12	1
DNAJC13	1
DNAJC19	4
DNAJC22	1
DNAJC24	1
DNAJC27	1
DNAJC3	1
DNAJC5	2
DNAJC9-AS1	2
DNASE1L2	1
DNASE2	1
DND1	3
DNER	2
DNM1L	2
DNM3-IT1	1
DNTTIP2	1
DOCK10	1
DOCK4-AS1	1
DOCK9-AS1	2
DOHH	1
DOK1	1
DOPEY1	1
DPH3	1
DPH3P1	1
DPH7	1
DPM2	3
DPP10	1
DPP3	1
DPP7	1
DPY19L2P2	3
DPY19L3	1
DPYSL2	3
DPYSL4	2
DQX1	1
DR1	2
DRAM2	1
DRC1	1
DRD1	4

DRD4	1	EBPL	3	EIF2B2	1	EP400	1
DRD5	1	EDC4	1	EIF2D	1	EP400P1	3
DRG1	1	EDEM3	3	EIF2S1	1	EPAS1	2
DRG2	1	EDF1	1	EIF2S3	2	EPB41	1
DRGX	1	EDIL3	1	EIF3D	1	EPB41L2	1
DSCR9	1	EDN1	3	EIF3I	1	EPB41L5	1
DSE	2	EDN2	3	EIF3J	3	EPC1	2
DSN1	5	EDNRB	4	EIF3M	2	EPC2	5
DST	2	EDRF1-AS1	1	EIF4A2	1	EPG5	1
DSTN	2	EEF1AKMT1	1	EIF4E3	1	EPHA4	1
DTD2	1	EEF1D	1	EIF4EBP3	7	EPHA5	1
DTL	1	EEPD1	1	EIF4G1	1	EPHA5-AS1	3
DTNA	7	EFCAB10	1	EIF4G2	1	EPHA6	1
DTNB	3	EFCAB14	1	EIF4G3	2	EPHA7	2
DTNBP1	2	EFCAB14-AS1	3	EIF5B	1	EPHA8	1
DTX1	2	EFCAB6	2	ELAC1	1	EPHB1	3
DTX3	2	EFCAB6-AS1	1	ELAC2	1	EPHB3	1
DTYMK	2	EFCAB9	1	ELAVL3	1	EPHB6	1
DUBR	4	EFEMP1	1	ELAVL4	3	EPHX1	1
DUS2	1	EFHC1	2	ELF2	2	EPHX3	1
DUSP1	1	EFHD1	2	ELK3	1	EPHX4	1
DUSP10	4	EFNA5	1	ELK4	4	EPM2AIP1	3
DUSP14	4	EFNB2	4	ELOA	1	EPN2-IT1	1
DUSP16	5	EFNB3	1	ELOB	3	EPS8L1	1
DUSP26	1	EFR3A	1	ELOVL4	1	EQTN	1
DUSP3	1	EFS	1	ELP3	1	ERC1	2
DUSP5	1	EGF	1	ELP6	1	ERC2	1
DUSP6	2	EGFLAM	2	EMC4	2	ERCC4	2
DUSP7	4	EGFR-AS1	2	EME2	2	ERCC5	6
DUSP8	1	EGLN2	2	EMILIN3	4	ERF	1
DVL2	2	EGLN3	1	EML6	3	ERH	2
DYNC1H1	3	EGR1	2	EMSY	1	ERICH1	1
DYNC1I2	2	EGR2	2	EMX1	1	ERLIN1	1
DYNLL1	2	EGR3	3	EMX2	4	ERLNC1	1
DYNLL2	2	EHBP1	1	EMX2OS	1	ERMAP	1
DYNLRB1	2	EHD2	1	ENDOG	3	ERMN	3
DYNLT1	1	EHD3	3	ENDOU	1	ERMP1	2
DYNLT3	1	EID1	3	ENDOV	7	ERO1A	1
DYRK1A	4	EID2	2	ENOPH1	2	ERP29	2
DYRK2	4	EID2B	1	ENOSF1	1	ERRFI1	1
DYSF	3	EIF1	1	ENPP5	2	ERVFRD-1	2
DZIP1	1	EIF1AX	1	ENPP6	3	ERVK13-1	2
EAF1	2	EIF1B	1	ENSA	2	ERVK3-1	12
EBAG9	1	EIF2AK4	1	ENTPD4	1	ESCO1	3
EBLN2	3			ENY2	1	ESD	1
EBLN3P	2			EP300-AS1	4		

ESYT3	3
ETAA1	1
ETF1	1
ETFBKMT	1
ETFRF1	1
ETNK1	1
ETS1	1
ETS2	2
ETV4	1
ETV5	6
EVI2A	2
EVI2B	1
EVL	1
EVPL	2
EXO5	2
EXOC1	1
EXOC3	1
EXOC5	2
EXOC8	3
EXOG	3
EXOSC2	2
EXOSC6	4
EXT1	4
EXT2	1
EXTL1	2
EXTL2	2
EXTL3	3
EYA4	1
F13A1	3
F2RL3	3
F3	1
F7	3
FA2H	1
FAAP100	3
FADD	2
FAH	1
FAHD1	2
FAM102A	1
FAM106CP	4
FAM107A	4
FAM107B	1
FAM110C	1
FAM111A	3
FAM117B	2
FAM118A	1
FAM120AOS	4
FAM120B	2
FAM120C	1
FAM122A	1
FAM124A	3
FAM124B	2
FAM126A	1
FAM131A	2
FAM131B	3
FAM13A-AS1	3
FAM151B	1
FAM155A	1
FAM160B1	1
FAM163B	1
FAM167A	1
FAM168B	4
FAM170B	2
FAM171B	1
FAM173B	1
FAM177B	1
FAM180B	1
FAM181B	2
FAM183BP	1
FAM187A	1
FAM189A2	1
FAM192A	1
FAM198B-AS1	2
FAM199X	2
FAM19A2	1
FAM200A	6
FAM200B	2
FAM201A	1
FAM204A	1
FAM208A	4
FAM208B	3
FAM209A	1
FAM20B	1
FAM20C	1
FAM217B	1
FAM219B	1
FAM220A	3
FAM222A-AS1	3
FAM237A	1
FAM24A	1
FAM25E	2
FAM25G	1
FAM32A	1
FAM41C	5
FAM43B	2
FAM49A	3
FAM50B	1
FAM53A	1
FAM53B	1
FAM53B-AS1	3
FAM66C	1
FAM69C	1
FAM71C	1
FAM71D	1
FAM78A	1
FAM81B	1
FAM83C	2
FAM84A	4
FAM84B	3
FAM86C1	1
FAM86DP	1
FAM89B	2
FAM8A1	5
FAM92B	5
FAM98B	2
FAN1	5
FANCE	2
FANCL	2
FARP2	2
FARSB	3
FAS-AS1	1
FASLG	1
FASN	2
FASTKD1	1
FASTKD3	1
FASTKD5	2
FAT1	2
FAT3	2
FAT4	4
FAXC	1
FBH1	3
FBLL1	1
FBRS	2
FBXL12	2
FBXL14	1
FBXL19	1
FBXL20	2
FBXL22	2
FBXL3	1
FBXL4	1
FBXO10	3
FBXO22	1
FBXO25	1
FBXO30	3
FBXO32	1
FBXO33	2
FBXO39	3
FBXO4	1
FBXO41	1
FBXO46	1
FBXO7	2
FBXO8	1
FBXW11	2
FBXW2	1
FBXW4P1	1
FBXW7	2
FBXW7-AS1	1
FCF1P2	3
FDFT1	1
FDPS	1
FEM1A	6
FEM1B	4
FEN1	4
FERMT2	1
FES	2
FEZ2	3
FEZF1	1
FEZF2	3
FGD4	4
FGD5-AS1	1
FGD6	1
FGF1	3

FGF12	3	FNDC3A	1	GABPA	1	GBX2	5
FGF12-AS1	2	FNDC5	3	GABPB1	1	GC	1
FGF14	1	FNDC9	1	GABPB1-AS1	1	GCA	3
FGF14-AS2	1	FNIP2	4	GABPB2	3	GCC1	1
FGF16	1	FNTA	2	GABRA1	2	GCC2	4
FGF23	1	FOLH1	2	GABRA2	1	GCDH	1
FGF7	2	FOS	1	GABRB1	1	GCLC	2
FGF9	2	FOXF1	1	GABRB2	3	GCNA	3
FGFR1OP2	2	FOXG1	2	GABRB3	4	GCNT1	2
FGFR2	2	FOXH1	2	GABRD	1	GCNT4	3
FGFR3	1	FOXJ1	1	GABRG1	3	GCSHP3	3
FH	1	FOXJ2	1	GABRG2	1	GDAP2	1
FHAD1	1	FOXN2	1	GABRG3	2	GDE1	2
FHL1	1	FOXN3	4	GABRP	2	GDF11	3
FIBIN	1	FOXN4	1	GADD45A	1	GDF15	1
FICD	2	FOXO3	2	GADD45B	4	GDF7	1
FIGN	2	FOXO4	1	GADD45G	1	GDI2	3
FIGNL1	3	FOXO6	1	GAL3ST1	2	GDPD4	1
FIGNL2	7	FOXP1	1	GAL3ST3	1	GDPGP1	1
FIP1L1	1	FPGT	1	GALC	2	GEMIN6	1
FITM2	1	FRAT2	3	GALNT11	12	GEMIN7-AS1	1
FIZ1	1	FREM2-AS1	1	GALNT15	4	GEMIN8P4	2
FJX1	3	FREM3	2	GALNT16	3	GEN1	1
FKBP10	1	FRMD4A	1	GALNT17	4	GET4	2
FKBP11	1	FRMD6	2	GALNT4	2	GFAP	1
FKBP2	1	FRRS1L	1	GANAB	3	GFI1	1
FKBP9	1	FRS3	1	GANC	1	GFM2	3
FKBPL	1	FSD1L	2	GAP43	1	GFOD1	1
FLII	1	FTH1	5	GAPLINC	2	GFOD2	1
FLJ23867	3	FTO	1	GAPVD1	2	GFPT1	2
FLJ31356	1	FTO-IT1	1	GAREM2	3	GFRA2	2
FLJ37035	3	FUCA2	2	GARNL3	1	GFRA4	4
FLJ42102	1	FUNDC1	1	GAS1	1	GFRAL	1
FLJ44635	1	FUT10	3	GAS5	3	GFY	2
FLJ45513	1	FUT11	5	GAS5-AS1	1	GGA2	1
FLNB-AS1	1	FUT4	2	GASAL1	2	GGA3	4
FLRT1	6	FUT9	5	GATA3-AS1	1	GGPS1	1
FLRT2	5	FUZ	1	GATAD2A	1	GGTA1P	1
FLRT3	5	FXYD2	2	GATD3A	1	GHET1	1
FLT1	1	FYN	1	GATM	2	GHRLOS	4
FMN1	2	FZD1	2	GBA2	1	GID8	1
FMN2	2	FZD4	3	GBF1	1	GIGYF2	2
FMR1NB	1	FZD5	2	GBX1	1	GIMAP4	2
FN3K	2	FZD8	1			GIMAP5	2
		FZD9	2			GIMAP6	1
		GABARAP	1			GIMAP8	1

GINS2	2	GOLGA3	1	GPR34	1	GRN	1
GJA1	1	GOLGA5	1	GPR37	1	GRPEL1	1
GJA10	10	GOLGA7B	1	GPR37L1	2	GRPEL2	1
GJB1	2	GOLGA8IP	1	GPR45	2	GRSF1	2
GJB6	2	GOLIM4	1	GPR61	3	GS1-124K5.11	3
GJD3	1	GOLM1	2	GPR62	3	GSDMB	1
GJD4	2	GOLPH3	9	GPR63	2	GSG1	1
GK3P	1	GOLT1A	3	GPR68	1	GSG1L	2
GLB1L3	2	GON4L	1	GPR75-ASB3	1	GSK3A	1
GLCE	2	GON7	1	GPR83	1	GSK3B	2
GLDN	7	GOPC	1	GPR85	1	GSN	2
GLG1	1	GORASP2	3	GPRASP1	3	GSPT2	3
GLIS1	1	GOSR1	5	GPRC5B	5	GSTCD	1
GLIS2	2	GOSR2	1	GPRIN1	4	GSTK1	1
GLIS3-AS1	1	GOT1	3	GPRIN3	2	GSTM3	3
GLMN	1	GP1BB	3	GPX2	3	GTDC1	2
GLOD4	1	GPAT2	2	GRAMD1C	2	GTF2A1	1
GLRA3	1	GPATCH2	1	GRAMD2B	1	GTF2B	2
GLRX	1	GPATCH2L	4	GRAMD4	1	GTF2E1	1
GLRX2	1	GPBAR1	1	GRASP	2	GTF2H4	1
GLRX5	1	GPBP1	5	GRB10	3	GTF2H5	1
GLS	2	GPC5-AS1	1	GREM1	1	GTF2IRD1	2
GLUD2	1	GPD1L	1	GREM2	2	GTF2IRD1P1	2
GLUL	2	GPD2	1	GRHL3	1	GTF3A	2
GM2A	3	GPER1	1	GRHPR	3	GTPBP6	2
GMFB	1	GPHB5	1	GRIA2	3	GUCA2A	1
GMPPB	1	GPI	1	GRIA4	1	GUCD1	3
GMPR	7	GPM6B	1	GRID1	1	GUCY1B1	2
GMPS	1	GPR12	4	GRID1-AS1	1	GUSB	1
GNA12	3	GPR135	2	GRIK2	2	GUSBP5	1
GNA14	1	GPR137B	1	GRIK3	4	GVQW3	3
GNA14-AS1	2	GPR143	4	GRIK4	1	GXYLT1	1
GNA15	4	GPR151	2	GRIN2A	3	GYG1	1
GNAL	1	GPR155	2	GRIN2B	1	GYPC	1
GNAO1	1	GPR158	2	GRIN3A	2	GZF1	2
GNAS	2	GPR161	2	GRIN3B	3	GZMM	1
GNAZ	2	GPR162	3	GRK2	1	H1F0	1
GNE	1	GPR171	1	GRM1	1	H1FOO	3
GNG3	2	GPR179	2	GRM2	3	H1FX-AS1	1
GNL1	1	GPR183	1	GRM3	3	H2AFJ	2
GNPNAT1	1	GPR21	3	GRM5	2	H2AFV	1
GNRH1	4	GPR22	1	GRM5-AS1	5	H2AFX	2
GNRHR2	1	GPR25	4	GRM7-AS1	1	H6PD	1
GNS	1	GPR26	2	GRM8	1	HABP4	5
GOLGA1	1					HACD4	1

HACE1	1
HADH	1
HADHB	1
HAGHL	1
HAO1	1
HAPLN1	1
HAPLN2	1
HAPLN4	5
HARBI1	1
HAS3	2
HAUS3	1
HAVCR1P1	3
HAVCR2	1
HBEGF	2
HBP1	1
HCFC1	1
HCG14	1
HCG17	1
HCG2040054	3
HCLS1	9
HCN1	5
HCN2	2
HCN4	1
HCRTR1	1
HDHD3	2
HDLBP	1
HEBP2	4
HECA	1
HECTD1	2
HECTD2-AS1	1
HECTD4	1
HECW2	2
HEIH	1
HELQ	2
HELZ2	2
HERC4	1
HERPUD2	2
HES5	1
HEXB	1
HEXIM1	2
HEY1	2
HEY2	1
HGC6.3	3
HGSNAT	1
HHAT	5
HHIP-AS1	2
HHLA1	6
HIF1A-AS2	1
HIF1AN	2
HILPDA	1
HINFP	1
HIP1R	3
HIPK2	1
HIPK3	1
HIST1H1E	1
HIST1H2AC	1
HIST1H2BD	1
HIST1H4E	1
HIST2H2BE	3
HIVEP1	4
HK3	1
HKDC1	1
HLA-DMA	1
HLA-E	1
HLA-L	3
HLCS	2
HLF	3
HMBOX1	5
HMBS	1
HMCES	2
HMCN2	1
HMGB2	1
HMGCR	2
HMGCS1	4
HMGN2	2
HMGN2P46	1
HMGN3-AS1	1
HMGN4	1
HMGN5	1
HMGXB3	2
HMOX2	2
HNMT	1
HNRNPA0	3
HNRNPA1L2	2
HNRNPA2B1	2
HNRNPDL	1
HNRNPF	3
HNRNPH1	2
HNRNPH2	2
HNRNPK	1
HNRNPM	1
HNRNPUL1	1
HOMER1	1
HP1BP3	2
HPCAL4	1
HPF1	2
HPS3	1
HPS4	3
HPS6	3
HPX	1
HR	1
HRAS	1
HRASLS2	1
HRC	1
HRH1	4
HRH3	1
HRK	1
HS3ST1	1
HS3ST2	2
HS6ST1	5
HSBP1L1	1
HSD11B2	1
HSD17B1	2
HSD17B3	1
HSD17B8	1
HSF2	1
HSF5	2
HSFX1	1
HSH2D	5
HSP90AA1	5
HSP90AB4P	2
HSP90B2P	1
HSPA12A	2
HSPA14	3
HSPA1A	1
HSPA1B	1
HSPA2	3
HSPA4	1
HSPA5	3
HSPB1	3
HSPB8	1
HSPB9	1
HSPBAP1	2
HSPD1	1
HSPH1	3
HTATSF1	3
HTD2	3
HTR1F	1
HTR2A	1
HTR2A-AS1	2
HTR5A-AS1	1
HTR6	2
HTR7P1	4
HYAL2	2
HYPK	2
IAH1	1
IBA57-DT	2
IBTK	1
ICA1L	3
ICAM3	1
ICAM5	1
ICE1	7
ICE2	1
ICMT	3
ICOSLG	2
ID2	3
ID4	2
IDH3A	1
IDI1	2
IDNK	1
IDS	2
IER2	4
IER5	1
IER5L	1
IFFO1	1
IFI30	2
IFI44	1
IFIT1	2
IFIT2	1
IFIT3	4
IFIT5	2
IFITM10	1
IFNA2	1
IFNAR1	4
IFNGR1	1
IFT122	1

IFT20	2
IFT52	1
IGBP1	1
IGFBP2	2
IGFBP3	1
IGFLR1	1
IGSF11-AS1	1
IGSF22	1
IGSF3	1
IGSF6	1
IGSF8	2
IKBKE	5
IKZF4	1
IL10	1
IL10RB-DT	1
IL15RA	2
IL17C	1
IL17D	4
IL17F	1
IL18BP	1
IL20RB	1
IL21R-AS1	2
IL23A	1
IL34	1
IL4I1	3
IL6ST	5
ILF3-DT	2
IMMT	2
IMP3	2
IMPA1	1
IMPAD1	2
IMPDH2	2
IMPG1	3
INA	3
INAFM2	2
INE2	2
ING1	1
ING2	1
ING4	4
INHBA	2
INHBB	1
INIP	3
INKA2	8
INO80D	3
INPP1	2
INPP5E	2
INPP5F	1
INSM1	1
INSM2	2
INSR	1
INTS11	1
INTS14	2
INTS2	2
INTS8	1
IP6K2	1
IP6K3	1
IPCEF1	1
IPMK	1
IPO13	1
IPO4	1
IPO5	2
IPO8	3
IPO9	4
IPPK	1
IPW	1
IQCA1	1
IQCA1L	3
IQCH-AS1	1
IQCJ-SCHIP1-AS1	1
IQCK	1
IQGAP1	1
IQSEC1	2
IQUB	1
IRAIN	1
IRAK1BP1	7
IRF2BP1	4
IRF2BP2	2
IRF2BPL	3
IRF4	1
IRF7	3
IRGQ	3
IRS2	4
IRS4	1
ISCA2	1
ISCU	1
ISG20L2	2
ISLR	2
ISM2	1
ISOC2	1
IST1	1
ISY1	2
ISYNA1	1
ITGA1	1
ITGA10	2
ITGA2B	4
ITGA9-AS1	1
ITGAE	2
ITGB1BP1	1
ITGB4	1
ITM2C	1
ITPKA	3
ITPKB	2
ITPKC	1
ITPRIPL2	2
IVD	2
IVNS1ABP	1
IWS1	2
JADE1	1
JADE2	2
JAGN1	1
JAK1	1
JAKMIP2	1
JAKMIP2-AS1	3
JCAD	8
JDP2	1
JKAMP	1
JMJD1C	5
JMJD7-PLA2G4B	3
JMJD8	2
JMY	2
JOSD1	1
JPH1	1
JPH2	2
JPH3	1
JPT2	5
JRK	2
JRKL	2
JUN	2
JUNB	2
JUND	3
KANK1	4
KANSL1	1
KANSL1L	1
KANSL2	3
KANSL3	3
KANTR	5
KAT14	5
KAT6B	1
KAT8	1
KATNA1	1
KBTBD11	9
KBTBD11-OT1	4
KBTBD2	2
KBTBD3	1
KBTBD4	2
KBTBD6	2
KBTBD7	2
KBTBD8	1
KCCAT333	3
KCNA1	6
KCNA2	4
KCNA3	1
KCNA4	4
KCNA6	9
KCNAB1	1
KCNAB2	3
KCNB1	1
KCNB2	1
KCNC1	3
KCNC2	3
KCNC3	2
KCNC4	2
KCND2	2
KCND3	1
KCNE1	2
KCNE5	1
KCNF1	1
KCNG1	1
KCNG2	1
KCNG3	1
KCNH1-IT1	4
KCNH3	1
KCNH5	4
KCNJ1	1
KCNJ11	2
KCNJ14	1
KCNJ2	4
KCNJ2-AS1	2
KCNJ3	1

KCNJ4	3
KCNJ6	2
KCNJ8	1
KCNJ9	3
KCNK10	1
KCNK15-AS1	1
KCNK7	1
KCNK9	2
KCNMA1-AS1	3
KCNMB4	5
KCNQ4	1
KCNRG	1
KCNS1	2
KCNS2	3
KCNT1	2
KCNV1	3
KCTD1	1
KCTD11	1
KCTD12	2
KCTD15	2
KCTD16	4
KCTD17	1
KCTD18	1
KCTD2	2
KCTD21	5
KCTD3	2
KCTD4	1
KCTD6	1
KCTD8	1
KDELC2	1
KDELR3	1
KDF1	1
KDM2A	1
KDM3A	1
KDM3B	4
KDM4A	3
KDM4A-AS1	2
KDM5C	2
KDM5D	1
KDR	2
KEAP1	2
KHDC1L	1
KIAA0100	5
KIAA0319	3
KIAA0319L	1
KIAA0355	1
KIAA0391	2
KIAA0408	8
KIAA0513	1
KIAA0753	1
KIAA0754	9
KIAA0895	2
KIAA0895L	1
KIAA1024	1
KIAA1107	2
KIAA1147	4
KIAA1191	1
KIAA1217	5
KIAA1324L	2
KIAA1328	3
KIAA1522	2
KIAA1549	1
KIAA1549L	3
KIAA1551	9
KIAA1586	2
KIAA1614	1
KIAA1614-AS1	2
KIAA1656	2
KIAA1671	2
KIAA1958	2
KIAA2013	2
KIDINS220	2
KIF1B	1
KIF1BP	2
KIF26B-AS1	1
KIF27	1
KIF3B	2
KIF3C	3
KIF5B	1
KIRREL3	1
KIT	1
KIZ	1
KLC1	2
KLF11	1
KLF13	8
KLF15	2
KLF2	1
KLF3-AS1	1
KLF6	1
KLF7	1
KLF9	6
KLHDC2	3
KLHDC4	1
KLHL11	1
KLHL12	1
KLHL13	1
KLHL15	2
KLHL20	1
KLHL21	4
KLHL23	2
KLHL28	1
KLHL32	1
KLHL34	1
KLHL36	1
KLHL4	2
KLHL41	2
KLHL42	5
KLHL5	2
KLHL8	5
KLHL9	3
KLK5	1
KLKB1	2
KMT2A	5
KMT2C	2
KMT2D	3
KMT2E	6
KNDC1	1
KNSTRN	5
KPNA1	1
KPNB1	3
KRBA1	1
KRBA2	3
KRBOX4	1
KRCC1	1
KREMEN2	2
KRI1	1
KRR1	2
KRT222	1
KRT8P41	1
KTI12	1
KTN1	1
KYAT3	2
LACC1	4
LACTBL1	1
LAMB4	1
LAMC1-AS1	2
LAMP3	1
LAMP5	1
LAMP5-AS1	1
LAMTOR1	1
LAMTOR2	1
LANCL1	4
LAPTM4B	1
LARGE2	1
LARP1B	3
LARS2-AS1	2
LATS1	3
LAYN	2
LBHD1	1
LBR	1
LCA5	1
LCAT	1
LCNL1	1
LCOR	1
LDB1	1
LDHA	1
LDHC	1
LDHD	3
LDLR	1
LDLRAD3	3
LDLRAD4	6
LDLRAP1	4
LDOC1	2
LEAP2	1
LEMD2	1
LEMD3	2
LENEP	1
LENG9	2
LEPROT	3
LEPROTL1	1
LETMD1	3
LGALS3BP	5
LGALS8-AS1	1

LGALS9	2
LGALSL	1
LGI1	3
LGMN	1
LHFPL3-AS2	1
LHFPL4	2
LHFPL6	1
LHX2	1
LHX3	2
LHX6	1
LIG3	5
LIG4	5
LIMD2	2
LIME1	2
LIMK2	3
LIMS2	1
LIN54	1
LIN7C	1
LINC00032	1
LINC00051	1
LINC00052	2
LINC00092	4
LINC00159	1
LINC00200	2
LINC00216	2
LINC00222	5
LINC00235	2
LINC00260	4
LINC00294	6
LINC00317	2
LINC00320	2
LINC00324	1
LINC00334	1
LINC00342	1
LINC00348	1
LINC00359	3
LINC00367	1
LINC00400	3
LINC00411	1
LINC00423	1
LINC00445	3
LINC00461	3
LINC00467	1
LINC00483	3
LINC00511	3
LINC00526	3
LINC00528	#
LINC00539	1
LINC00562	1
LINC00565	1
LINC00575	2
LINC00597	4
LINC00598	3
LINC00635	7
LINC00641	1
LINC00643	3
LINC00652	1
LINC00662	3
LINC00665	1
LINC00667	4
LINC00674	5
LINC00676	1
LINC00689	2
LINC00691	3
LINC00706	1
LINC00836	4
LINC00839	1
LINC00844	1
LINC00847	2
LINC00889	1
LINC00909	1
LINC00920	1
LINC00938	1
LINC00942	6
LINC00950	2
LINC00958	1
LINC00963	1
LINC01000	2
LINC01003	1
LINC01006	3
LINC01007	1
LINC01018	3
LINC01030	1
LINC01039	1
LINC01054	2
LINC01072	2
LINC01094	1
LINC01103	1
LINC01114	1
LINC01118	1
LINC01123	2
LINC01127	3
LINC01140	2
LINC01181	1
LINC01184	1
LINC01195	4
LINC01227	1
LINC01231	1
LINC01234	1
LINC01269	4
LINC01279	1
LINC01291	1
LINC01341	2
LINC01347	7
LINC01352	2
LINC01355	2
LINC01393	1
LINC01431	1
LINC01465	2
LINC01490	1
LINC01501	2
LINC01504	2
LINC01507	3
LINC01530	3
LINC01535	2
LINC01537	1
LINC01543	1
LINC01544	5
LINC01553	2
LINC01554	1
LINC01559	6
LINC01561	1
LINC01563	1
LINC01583	2
LINC01585	1
LINC01619	1
LINC01635	1
LINC01637	3
LINC01645	1
LINC01671	1
LINC01719	1
LINC01725	2
LINC01729	1
LINC01730	1
LINC01767	1
LINC01772	2
LINC01798	1
LINC01806	2
LINC01820	3
LINC01848	1
LINC01861	5
LINC01909	2
LINC01923	1
LINC01934	1
LINC01975	2
LINC01983	3
LINC01988	6
LINC02003	1
LINC02012	2
LINC02017	1
LINC02022	2

LINC02033	1
LINC02035	1
LINC02060	1
LINC02065	2
LINC02068	1
LINC02073	1
LINC02133	1
LINC02168	3
LINC02210-CRHR1	1
LINC02246	4
LINC02275	3
LINC02282	1
LINC02283	1
LINC02322	1
LINC02361	1
LINC02362	1
LINC02387	2
LINC02389	2
LINC02424	2
LINC02449	3
LINC02495	1
LINC02497	3
LINC02517	1
LINC02548	1
LINC02556	1
LINC02562	1
LINC02567	1
LINC02574	1
LINC02585	1
LINC02586	2
LINC2194	1
LINC-ROR	2
LINGO1	2
LIPT1	1
LIPT2	1
LITAF	2
LIX1L	1
LIX1L-AS1	1
LLGL1	1
LLPH	1
LLPH-DT	1
LMAN1L	1
LMAN2L	1
LMF1	2
LMLN-AS1	1
LMNA	1
LMO2	1
LMO3	2
LMO4	2
LMO7	3
LMO7DN	2
LMOD3	2
LMTK3	1
LNPEP	4
LNX1-AS1	2
LOC100128079	3
LOC100128253	1
LOC100128494	8
LOC100128568	1
LOC100128653	2
LOC100128882	1
LOC100129034	3
LOC100129434	3
LOC100129534	2
LOC100129617	1
LOC100129917	5
LOC100129931	4
LOC100130111	3
LOC100130207	2
LOC100130283	1
LOC100130298	2
LOC100130331	4
LOC100130357	1
LOC100130449	1
LOC100130587	1
LOC100130705	1
LOC100130744	2
LOC100131315	6
LOC100131347	1
LOC100131496	2
LOC100132215	1
LOC100132249	1
LOC100190986	1
LOC100192426	1
LOC100286906	1
LOC100287015	1
LOC100287049	3
LOC100287837	2
LOC100287944	1
LOC100288123	3
LOC100288254	2
LOC100288911	1
LOC100289333	2
LOC100289511	3
LOC100291105	1
LOC100303749	1
LOC100379224	2
LOC100419170	2
LOC100419583	2
LOC100499489	1
LOC100505501	2
LOC100505635	7
LOC100505715	2
LOC100505795	1
LOC100505912	2
LOC100505921	1
LOC100506022	1
LOC100506071	2
LOC100506076	1
LOC100506100	2
LOC100506142	4
LOC100506258	1
LOC100506271	4
LOC100506321	2
LOC100506548	3
LOC100506691	4
LOC100506725	2
LOC100506804	1
LOC100506937	1
LOC100507250	1
LOC100507351	2
LOC100507373	4
LOC100507387	1
LOC100507388	2
LOC100507472	3
LOC100507516	1
LOC100507557	1
LOC100507599	3
LOC100652758	1
LOC100652768	2
LOC100652999	2
LOC100996263	3
LOC100996419	3
LOC100996635	2
LOC101926962	1
LOC101927000	1
LOC101927018	1
LOC101927021	1
LOC101927027	2
LOC101927040	2
LOC101927055	1
LOC101927070	2
LOC101927100	2
LOC101927151	1
LOC101927178	1
LOC101927189	1
LOC101927354	2
LOC101927356	1
LOC101927365	1
LOC101927410	2
LOC101927418	3
LOC101927472	2

LOC1019		LOC1019		LOC1027		LOC1053	
27482	1	28807	4	24804	1	77102	1
LOC1019		LOC1019		LOC1027		LOC1053	
27550	6	28936	1	24927	1	78047	1
LOC1019		LOC1019		LOC1030		LOC1053	
27572	1	28943	2	21295	1	78311	1
LOC1019		LOC1019		LOC1033		LOC1053	
27583	1	28988	1	44931	1	78397	1
LOC1019		LOC1019		LOC1036		LOC1053	
27746	1	29162	1	11081	1	78586	1
LOC1019		LOC1019		LOC1053		LOC1053	
27752	4	29295	6	69391	3	79183	2
LOC1019		LOC1019		LOC1053		LOC1053	
27811	4	29340	1	69431	5	79192	2
LOC1019		LOC1019		LOC1053		LOC1053	
27815	2	29341	1	69509	1	79393	2
LOC1019		LOC1019		LOC1053		LOC1056	
27854	1	29384	2	70024	4	16981	1
LOC1019		LOC1019		LOC1053		LOC1087	
27855	1	29452	2	70457	5	83654	2
LOC1019		LOC1019		LOC1053		LOC1458	
27895	1	29457	2	70489	4	45	4
LOC1019		LOC1019		LOC1053		LOC1484	
27972	1	29523	2	70697	1	13	3
LOC1019		LOC1019		LOC1053		LOC1496	
27974	3	29528	1	70829	1	84	1
LOC1019		LOC1019		LOC1053		LOC1520	
28000	1	29550	3	70941	3	48	1
LOC1019		LOC1019		LOC1053		LOC1539	
28020	1	29563	1	70943	3	10	#
LOC1019		LOC1019		LOC1053		LOC1547	
28021	1	29579	1	71414	6	61	1
LOC1019		LOC1019		LOC1053		LOC2021	
28042	1	29595	2	71433	1	81	1
LOC1019		LOC1019		LOC1053		LOC2207	
28052	2	29679	2	71485	2	29	1
LOC1019		LOC1019		LOC1053		LOC2573	
28063	2	29680	2	71506	1	96	1
LOC1019		LOC1019		LOC1053		LOC2840	
28105	1	29901	1	71899	2	09	1
LOC1019		LOC1019		LOC1053		LOC2843	
28120	1	30085	2	71998	6	95	1
LOC1019		LOC1027		LOC1053		LOC2845	
28123	2	23385	1	72068	2	78	1
LOC1019		LOC1027		LOC1053		LOC2858	
28140	1	23566	1	72069	1	04	1
LOC1019		LOC1027		LOC1053		LOC3396	
28177	1	23582	6	73064	3	66	1
LOC1019		LOC1027		LOC1053		LOC3398	
28191	1	23692	3	73100	2	03	1
LOC1019		LOC1027		LOC1053		LOC3405	
28307	2	23703	1	73156	3	12	3
LOC1019		LOC1027		LOC1053		LOC3430	
28323	3	23704	1	73185	1	52	1
LOC1019		LOC1027		LOC1053		LOC3449	
28371	2	23729	2	73378	6	67	1
LOC1019		LOC1027		LOC1053		LOC3751	
28386	2	23809	1	74338	2	96	3
LOC1019		LOC1027		LOC1053		LOC3997	
28404	2	23885	5	74727	3	16	1
LOC1019		LOC1027		LOC1053		LOC4005	
28424	1	24009	2	74952	4	41	3
LOC1019		LOC1027		LOC1053		LOC4005	
28525	1	24058	2	75218	1	53	1
LOC1019		LOC1027		LOC1053		LOC4006	
28530	1	24152	7	75787	2	27	4
LOC1019		LOC1027		LOC1053		LOC4006	
28583	3	24163	1	75843	5	84	1
LOC1019		LOC1027		LOC1053		LOC4013	
28595	1	24323	2	76114	1	20	1
LOC1019		LOC1027		LOC1053		LOC4014	
28626	1	24404	4	76480	2	63	1
LOC1019		LOC1027		LOC1053		LOC4014	
28659	3	24659	2	76736	1	78	3

LOC401554	3
LOC403312	1
LOC403323	1
LOC440028	2
LOC440040	2
LOC440934	1
LOC441666	2
LOC554206	1
LOC574538	3
LOC641367	2
LOC642423	1
LOC642852	2
LOC643542	#
LOC643802	1
LOC644189	3
LOC646471	3
LOC646548	1
LOC646730	1
LOC646762	1
LOC647070	1
LOC651337	1
LOC652276	5
LOC728158	1
LOC728392	1
LOC728485	1
LOC728743	1
LOC728989	2
LOC729218	1
LOC729683	2
LOC729867	3
LOC729970	1
LOC91548	2
LOC93622	1
LONRF2	2
LOX	1
LOXHD1	1
LOXL4	2
LPAR1	2
LPAR2	1
LPAR5	1
LPAR6	2
LRBA	2
LRFN1	3
LRFN3	1
LRFN4	3
LRFN5	2
LRG1	2
LRIF1	1
LRIG1	2
LRIT2	2
LRP1	1
LRP10	2
LRP2	1
LRP3	3
LRP4-AS1	1
LRPAP1	1
LRRC14	2
LRRC24	4
LRRC27	1
LRRC37B	2
LRRC3B	3
LRRC3-DT	1
LRRC4	4
LRRC41	1
LRRC43	2
LRRC47	1
LRRC49	2
LRRC4C	3
LRRC55	3
LRRC58	1
LRRC66	1
LRRC73	2
LRRC8B	2
LRRC8C	3
LRRN2	4
LRRN3	6
LRRN4	1
LRRTM1	2
LRRTM3	3
LRRTM4	4
LRTM2	5
LSAMP	1
LSM10	1
LSM11	1
LSM2	1
LSMEM2	1
LTBR	1
LTC4S	1
LTN1	2
LTV1	3
LUARIS	1
LUC7L2	1
LURAP1L	1
LURAP1L-AS1	1
LVRN	2
LXN	1
LY6H	1
LYL1	2
LYNX1	1
LYPD1	4
LYPD6B	3
LYPLAL1	1
LYRM1	1
LYRM2	6
LYRM4-AS1	1
LYRM7	1
LYSMD2	3
LYSMD4	7
LYVE1	1
LZTS1	3
LZTS2	4
MAB21L3	1
MACO1	1
MAD1L1	2
MAD2L1BP	1
MAF	4
MAGEB2	2
MAGED1	1
MAGEE1	3
MAGEF1	3
MAGEH1	2
MAGI1-AS1	3
MAGI2	1
MAGI2-AS3	3
MAGOH	1
MAGT1	1
MAL2-AS1	2
MALAT1	5
MAML1	1
MAML2	1
MAMLD1	1
MAMSTR	1
MAN1A2	2
MAN1B1-DT	1
MAN1C1	1
MAN2A1	2
MAN2C1	1
MANBA	1
MANEA	1
MANEAL	3
MANF	2
MANSC1	2
MAP10	1
MAP1A	9
MAP1B	#
MAP1LC3A	1
MAP1LC3B	8
MAP1S	2
MAP2K6	1
MAP3K10	2
MAP3K11	1
MAP3K13	2
MAP3K4	1
MAP3K7	1
MAP4K2	1
MAP6	1
MAPK12	2
MAPK13	2
MAPK1IP1L	2
MAPK3	1
MAPK4	1
MAPK6	3
MAPK8	1
MAPK8IP2	1
MAPK8IP3	1
MAPKBP1	6
MAPRE3	1
MARCH4	1
MARCH7	3
MARCH9	1
MARCKS	6

MARCKSL1	1
MARF1	1
MARS2	3
MARVELD2	2
MARVELD3	3
MAS1	2
MASCRNA	10
MASTL	1
MAT2A	4
MATN2	1
MAVS	1
MAZ	1
MBD3	1
MBNL1	3
MBP	5
MBTPS1	4
MCCC2	1
MCF2L-AS1	3
MCFD2	1
MCL1	2
MCM3AP	3
MCM7	1
MCOLN1	2
MCPH1	3
MCRS1	1
MCUB	1
MDFI	2
MDGA2	1
MDH1B	1
MDK	1
MDM2	4
MDM4	2
MDN1	1
MEA1	2
MED10	1
MED11	1
MED13	1
MED15	1
MED18	1
MED19	2
MED21	1
MED28	1
MED29	1
MED7	1
MEF2B	1
MEF2C-AS1	1
MEI1	1
MEIKIN	1
MEIS3	3
MEIS3P1	2
MEP1B	3
MEPCE	2
MERTK	1
MESD	1
MET	1
METAP2	1
METRNL	1
METTL13	1
METTL14	2
METTL21A	1
METTL21EP	2
METTL2B	2
METTL3	1
METTL4	1
METTL6	1
METTL7A	1
MEX3C	1
MEX3D	5
MFAP3	2
MFAP3L	2
MFHAS1	3
MFN1	2
MFN2	1
MFSD10	5
MFSD13A	1
MFSD14A	2
MFSD14B	2
MFSD2B	1
MFSD4B	3
MFSD5	2
MFSD6	2
MGAT1	3
MGAT2	2
MGAT3	3
MGAT3-AS1	1
MGAT4A	1
MGAT5	4
MGC16275	2
MGC27345	1
MGC34796	2
MGST2	4
MHENCR	1
MIA3	5
MIATNB	4
MIB2	3
MICAL1	1
MICAL2	1
MICALL1	2
MICALL2	1
MID1	1
MID1IP1	1
MID1IP1-AS1	3
MIEF2	1
MIGA1	1
MIIP	2
MINDY1	2
MINDY2	1
MINDY3	1
MINPP1	2
MIOS	3
MIR101-2	2
MIR103A2	2
MIR103B1	3
MIR103B2	2
MIR1180	2
MIR1182	1
MIR1184-3	2
MIR1200	3
MIR122	1
MIR1224	1
MIR1225	1
MIR1226	4
MIR1227	1
MIR1231	2
MIR124-2	2
MIR124-3	1
MIR1244-1	2
MIR1244-4	1
MIR1249	1
MIR1252	2
MIR1255B2	1
MIR1256	2
MIR1257	2
MIR125B1	1
MIR1260A	3
MIR1262	1
MIR1268A	1
MIR1271	3
MIR1273C	1
MIR1273H	2
MIR1276	1
MIR1279	1
MIR128-2	1
MIR1286	2
MIR130A	1
MIR1321	1
MIR133A1HG	1
MIR140	1
MIR146A	3
MIR153-1	1
MIR153-2	1
MIR1537	5
MIR1825	1
MIR183	2
MIR190A	1
MIR1914	2
MIR193BHG	4
MIR194-1	1
MIR194-2HG	1
MIR197	1
MIR1976	1
MIR199B	1
MIR2054	7
MIR2110	1
MIR219A2	1
MIR219B	1
MIR2355	2
MIR23C	1
MIR25	1
MIR2682	2
MIR26A2	1
MIR26B	1
MIR2909	3
MIR3064	1

MIR3074	1	MIR3918	2	MIR4664	2	MIR548Q	4
MIR3117	1	MIR3922	1	MIR4665	2	MIR548S	1
MIR3124	1	MIR3941	2	MIR4667	2	MIR550A3	1
MIR3125	2	MIR4254	1	MIR4675	2	MIR5572	2
MIR3134	2	MIR4256	2	MIR4677	3	MIR558	2
MIR3135A	3	MIR4262	1	MIR4684	1	MIR5582	1
MIR3136	2	MIR4264	1	MIR4687	1	MIR5586	1
MIR3138	2	MIR4273	1	MIR4690	1	MIR5685	1
MIR3139	1	MIR4279	2	MIR4701	1	MIR5687	2
MIR3145	4	MIR4284	1	MIR4704	2	MIR569	1
MIR3149	4	MIR4294	1	MIR4706	4	MIR5692A2	1
MIR3154	1	MIR4312	4	MIR4713HG	2	MIR5693	1
MIR3159	1	MIR4319	3	MIR4715	1	MIR5696	1
MIR3162	1	MIR4326	3	MIR4717	1	MIR5706	5
MIR3175	2	MIR4428	2	MIR4718	6	MIR570HG	1
MIR3186	3	MIR4432HG	2	MIR4720	3	MIR571	4
MIR3187	1	MIR4434	2	MIR4721	1	MIR576	1
MIR3190	1	MIR4440	2	MIR4723	2	MIR577	1
MIR3199-1	2	MIR4444-2	2	MIR4724	1	MIR584	6
MIR324	1	MIR4446	2	MIR4729	1	MIR590	1
MIR331	3	MIR4457	1	MIR4731	2	MIR592	2
MIR335	1	MIR4458	1	MIR4737	2	MIR597	3
MIR33A	1	MIR4473	2	MIR4743	1	MIR600	2
MIR3606	2	MIR4477B	1	MIR4753	3	MIR602	1
MIR3612	1	MIR448	1	MIR4764	3	MIR604	1
MIR3616	2	MIR4485	1	MIR4766	1	MIR6069	1
MIR3621	2	MIR4489	1	MIR4776-2	2	MIR611	2
MIR3622A	1	MIR4496	1	MIR4781	1	MIR6126	3
MIR3650	1	MIR4500HG	1	MIR4786	1	MIR6129	2
MIR3651	1	MIR4502	1	MIR4791	1	MIR616	1
MIR3652	1	MIR4505	2	MIR4793	1	MIR620	6
MIR3657	1	MIR4512	4	MIR488	2	MIR626	1
MIR365A	1	MIR4515	1	MIR493	1	MIR628	4
MIR3662	2	MIR4519	1	MIR5001	1	MIR629	1
MIR3666	1	MIR4535	2	MIR5004	3	MIR630	1
MIR3682	2	MIR4633	1	MIR5047	1	MIR634	2
MIR3690	1	MIR4635	1	MIR5094	2	MIR636	1
MIR3692	1	MIR4636	3	MIR5187	2	MIR637	1
MIR3714	4	MIR4639	1	MIR5196	1	MIR6499	1
MIR378B	4	MIR4640	1	MIR544B	2	MIR6501	8
MIR378D1	1	MIR4647	2	MIR548A3	3	MIR6506	3
MIR378H	6	MIR4648	1	MIR548AO	2	MIR6511A4	2
MIR3911	2	MIR4657	1	MIR548AU	1	MIR6511B1	4
MIR3913-2	1	MIR4659B	1	MIR548AV	2	MIR6515	1
MIR3914-1	5	MIR4660	1	MIR548N	1	MIR653	1

MIR657	3	MIR6832	3	MIR8089	1	MORF4L2	4
MIR670	1	MIR6839	2	MIR874	1	MOS	1
MIR671	2	MIR6841	2	MIR877	1	MOSPD2	2
MIR6716	4	MIR6843	3	MIR885	1	MOXD1	1
MIR6717	1	MIR6845	2	MIR887	3	MPC1L	2
MIR6719	1	MIR6847	1	MIR9-1	1	MPDZ	3
MIR6721	1	MIR6851	1	MIR921	1	MPEG1	5
MIR6727	1	MIR6853	1	MIR922	1	MPHOSPH10	1
MIR6730	1	MIR6855	3	MIR935	1	MPHOSPH8	2
MIR6731	2	MIR6857	2	MIR9-3HG	1	MPHOSPH9	2
MIR6734	1	MIR6860	2	MIR943	1	MPLKIP	2
MIR6738	1	MIR6861	1	MIR98	1	MPO	1
MIR6742	1	MIR6866	2	MIRLET7I	2	MPP4	2
MIR6743	4	MIR6867	1	MIS12	2	MPP5	1
MIR6744	3	MIR6869	1	MISP	1	MPPE1	2
MIR6747	2	MIR6870	3	MITF	1	MPV17	1
MIR6748	1	MIR6871	6	MKKS	2	MPV17L2	1
MIR6751	1	MIR6874	1	MKNK2	1	MPZL1	1
MIR6752	1	MIR6880	2	MKRN2	1	MR1	1
MIR6753	1	MIR6881	1	MLANA	5	MRAP	3
MIR6756	3	MIR6883	1	MLEC	1	MRAP2	1
MIR6757	3	MIR6886	1	MLF2	1	MRC2	2
MIR6761	1	MIR6887	1	MLH3	6	MRFAP1	3
MIR6762	1	MIR6888	3	MLLT1	5	MRFAP1L1	3
MIR6764	3	MIR7-1	1	MLYCD	3	MRGBP	2
MIR6765	1	MIR7106	1	MMAB	5	MRI1	1
MIR6766	2	MIR7107	5	MMACHC	1	MRLN	2
MIR6770-2	2	MIR7109	2	MMP16	1	MRO	5
MIR6771	2	MIR7114	1	MMP17	1	MROH3P	1
MIR6773	2	MIR7157	2	MN1	3	MROH7	2
MIR6775	2	MIR7160	1	MND1	3	MRPL12	1
MIR6776	3	MIR718	3	MOAP1	1	MRPL14	1
MIR6777	2	MIR744	2	MOB2	4	MRPL16	1
MIR6780A	1	MIR761	1	MOB3C	1	MRPL17	1
MIR6782	1	MIR770	2	MOB4	1	MRPL19	2
MIR6784	4	MIR7705	1	MOBP	9	MRPL27	1
MIR6787	1	MIR7843	2	MOCOS	2	MRPL3	1
MIR6800	1	MIR7844	3	MOCS3	2	MRPL30	1
MIR6808	1	MIR7848	1	MOK	2	MRPL32	1
MIR6816	2	MIR7855	3	MON1B	1	MRPL33	1
MIR6818	6	MIR7856	1	MON2	2	MRPL34	1
MIR6820	5	MIR8066	1	MORC2	1	MRPL35	2
MIR6821	1	MIR8068	1	MORC2-AS1	2	MRPL36	1
MIR6822	1	MIR8072	1	MORC3	2	MRPL41	2
MIR6827	1	MIR8075	1	MORF4L1	1	MRPL43	1
MIR6828	1	MIR8078	1				

MRPL44	1	MTFR2	3	MYO15B	1	NAXD	3
MRPL46	1	MTG2	1	MYO16-AS1	1	NBAT1	2
MRPL51	1	MTHFD1L	4	MYO18A	1	NBEA	1
MRPL54	1	MTMR1	2	MYO18B	2	NBL1	1
MRPL58	1	MTMR10	1	MYO19	1	NBN	1
MRPS10	1	MTMR11	3	MYO3B	2	NBPF11	1
MRPS12	1	MTMR2	2	MYO5A	1	NBPF9	1
MRPS14	1	MTMR6	1	MYO5C	4	NCALD	3
MRPS16	2	MTMR9	1	MYO6	3	NCAM1	1
MRPS17	5	MTNR1A	12	MYOC	2	NCAM1-AS1	4
MRPS18A	2	MTPAP	1	MYOG	1	NCAM2	1
MRPS21	1	MTR	3	MYORG	8	NCAN	2
MRPS22	1	MTRNR2L4	1	MYOZ2	6	NCBP1	2
MRPS23	2	MTRR	1	MYRF	1	NCBP2-AS1	3
MRPS24	6	MTSS1L	5	MYRFL	2	NCBP2-AS2	4
MRPS25	8	MTURN	5	MYSM1	2	NCBP3	1
MRPS26	1	MTUS1	5	MZF1-AS1	1	NCDN	1
MRPS28	1	MTUS2	1	N4BP1	2	NCF1	1
MRPS30	2	MTUS2-AS1	4	N4BP2L1	4	NCK1-DT	1
MRPS30-DT	1	MTVR2	1	N4BP2L2	3	NCK2	4
MRPS33	2	MTX2	1	NAA20	5	NCKAP5L	3
MRTO4	1	MTX3	1	NAA30	1	NCKIPSD	3
MSANTD1	5	MUC13	2	NAA40	1	NCOA3	1
MSANTD3-TMEFF1	2	MUC6	2	NAA50	1	NCOA4	2
MSANTD4	5	MUL1	2	NAALADL2-AS3	1	NCOA5	3
MSH6	6	MUM1	1	NAB1	1	NCOA6	2
MSL1	1	MUM1L1	4	NAB2	2	NCOA7	2
MSL2	3	MVP	2	NACAD	6	NDC1	1
MSMP	1	MXI1	4	NACC2	1	NDE1	3
MSRB1	1	MXRA7	1	NADK	1	NDEL1	4
MSRB2	1	MYADM	1	NADK2	1	NDN	2
MSS51	2	MYBBP1A	2	NAGPA-AS1	7	NDP-AS1	2
MSTO2P	1	MYBPH	3	NANOS1	3	NDRG2	1
MT1HL1	1	MYBPHL	1	NANOS2	2	NDRG4	1
MT2A	1	MYC	1	NANP	1	NDST1	4
MT3	1	MYCBP2-AS1	3	NAP1L2	1	NDST2	4
MTAP	2	MYCL	1	NAP1L3	1	NDST3	2
MTCL1	3	MYCNOS	2	NAP1L5	2	NDUFA12	2
MTERF1	1	MYH10	1	NARS2	5	NDUFA6	1
MTERF2	2	MYL12B	2	NAT10	2	NDUFAF1	1
MTERF4	2	MYL6	2	NAT2	3	NDUFAF3	1
MTF1	1	MYL6B	1	NAT8	2	NDUFAF7	1
MTFR1	2	MYL9	1	NAT8L	1	NDUFAF8	3
MTFR1L	3	MYLK	2	NAT9	2		
		MYNN	2	NAV3	1		

NDUFB2-AS1	1	NHLRC3	1	NOM1	1	NREP	1
NDUFB4	1	NHP2	1	NOP10	1	NRG1	1
NDUFB9	4	NIF3L1	3	NOP14-AS1	2	NRG3	1
NDUFC1	2	NIFK-AS1	2	NOP16	1	NRGN	1
NDUFS7	3	NIM1K	2	NORAD	4	NRN1	1
NEAT1	4	NINJ1	1	NOS1	1	NRON	3
NEBL	3	NIPA2	3	NOS2P3	1	NRP1	1
NECAP1	2	NIPBL	1	NOV	1	NRP2	1
NECTIN1	1	NIPSNAP2	1	NOVA1	2	NRSN1	3
NECTIN3	2	NIPSNAP3B	2	NPAP1	1	NRSN2	3
NEDD4	4	NIT1	1	NPAS1	1	NRXN1	7
NEDD9	2	NIT2	2	NPAS3	3	NRXN2	3
NEFH	1	NKAIN4	1	NPAT	3	NRXN3	2
NEFL	1	NKPD1	1	NPB	1	NSD1	3
NEFM	4	NKRF	6	NPBWR2	1	NSD2	1
NEK11	2	NKX2-2	1	NPC1	2	NSD3	2
NEK7	2	NKX6-2	1	NPEPL1	2	NSDHL	1
NEK9	2	NLGN1	1	NPIPA5	1	NSG1	3
NELL2	4	NLGN1-AS1	2	NPIPB5	1	NSG2	3
NEMP2	2	NLGN3	4	NPM2	1	NSMAF	1
NENF	1	NLGN4Y	1	NPPA-AS1	1	NSMCE3	1
NEO1	1	NLGN4Y-AS1	3	NPRL2	2	NSUN3	2
NEPRO	1	NLK	1	NPTN-IT1	1	NSUN4	1
NET1	2	NLRC3	2	NPTX1	3	NSUN6	2
NEU1	1	NLRC4	1	NPTX2	2	NT5C	1
NEU3	2	NLRP2	1	NPTXR	1	NT5C1A	1
NEURL1-AS1	4	NLRP3	1	NPY1R	1	NT5C2	7
NEUROD2	2	NLRX1	1	NPY6R	1	NT5C3A	1
NEUROD6	1	NMB	1	NR1D1	2	NT5DC3	2
NEXN	1	NME2	1	NR1D2	1	NTAN1	2
NFATC2	4	NME3	3	NR1H3	1	NTM	1
NFATC3	2	NME7	2	NR2E1	2	NTM-AS1	1
NFE2L1	7	NME9	1	NR2E3	4	NTM-IT	6
NFIA	1	NMNAT1	1	NR2F1	4	NTN4	1
NFIB	4	NMNAT2	2	NR2F1-AS1	1	NTNG1	2
NFIC	4	NMRK2	4	NR2F2	2	NTNG2	2
NFIL3	1	NMT2	1	NR3C1	1	NTPCR	2
NFKB2	1	NNT-AS1	2	NR3C2	2	NTRK1	1
NFKBIA	1	NOA1	1	NR4A2	1	NTRK2	#
NFKBIZ	1	NOCT	1	NRADDP	3	NTRK3	2
NFU1	5	NOL11	4	NRAS	1	NTS	1
NFX1	1	NOL4	4	NRAV	1	NTSR2	1
NGB	1	NOL4L	6	NRBF2	2	NUAK1	3
NHLRC1	1	NOL7	4	NRCAM	1	NUCB1-AS1	1
NHLRC2	1	NOLC1	2	NRDE2	1	NUCKS1	1
						NUDT10	1

NUDT12	1
NUDT14	2
NUDT16	1
NUDT16L1	1
NUDT18	2
NUDT2	1
NUDT4	1
NUDT6	2
NUDT9	2
NUMBL	1
NUP188	1
NUP210L	2
NUP214	3
NUP50-DT	1
NUP54	3
NUPL2	2
NUTM2D	1
NWD2	1
NXF5	1
NXNL2	1
NXPE3	2
NXPH1	2
NXPH3	6
NYAP1	3
NYAP2	1
NYX	1
OACYLP	1
OARD1	3
OAZ2	7
OAZ3	2
OBSL1	1
OCA2	1
OCEL1	1
OCIAD1-AS1	2
OFD1	3
OGFOD1	1
OGFRL1	3
OIP5-AS1	7
OLFM1	1
OLFM2	1
OLFML3	1
OLIG1	6
OLIG2	2
OLMALINC	5
OMG	5
OPA1-AS1	3
OPA3	1
OPALIN	3
OPHN1	1
OPN5	1
OPRK1	1
OPRL1	2
OPRM1	5
OPTC	1
OR14I1	1
OR1D5	1
OR2H2	1
OR7E47P	2
ORAI1	1
ORAI2	3
ORAI3	3
ORC2	1
ORC4	2
ORMDL1	1
OSBPL10-AS1	2
OSBPL7	1
OSER1-DT	1
OSGEPL1	1
OSGEPL1-AS1	1
OSGIN2	1
OSMR	2
OST4	1
OSTC	1
OTOP3	1
OTUB2	2
OTUD1	1
OTUD4	3
OTUD5	1
OTUD6B-AS1	1
OTULINL	1
OVCA2	3
OVCH1	1
OXA1L	1
OXCT1-AS1	1
OXER1	1
OXLD1	2
OXR1	1
P2RX4	6
P2RY1	4
P2RY11	1
P2RY12	1
P2RY13	1
P3H3	1
PA2G4	2
PAAF1	1
PABPC1L	2
PABPN1	1
PACRGL	2
PACSIN1	1
PAF1	1
PAFAH1B1	1
PAFAH2	1
PAGR1	1
PAICS	1
PAIP1	1
PAIP2	2
PALB2	3
PAM	1
PAN3-AS1	2
PANK2	1
PANK4	2
PANX1	1
PAOX	1
PAPLN	1
PAPOLA	1
PAPPA-AS1	1
PAPSS1	1
PAQR3	4
PAQR4	6
PAQR5	4
PAQR6	1
PAQR7	1
PARD6A	1
PARD6G-AS1	3
PARG	2
PARP12	1
PARP14	3
PARP4	1
PARP8	1
PARP9	2
PARS2	3
PATZ1	1
PAWR	1
PAXBP1	1
PAXBP1-AS1	2
PAXIP1-AS1	1
PAXIP1-AS2	2
PBLD	1
PBOV1	1
PBRM1	1
PBX1	1
PBXIP1	1
PCBD1	1
PCBP1	3
PCCB	1
PCDH1	5
PCDH10	5
PCDH11X	1
PCDH11Y	5
PCDH12	1
PCDH17	7
PCDH18	2
PCDH19	3
PCDH20	6
PCDH7	3
PCDH8	1
PCDH9	1
PCDHA3	1
PCDHA4	1
PCDHA6	1
PCDHAC1	2
PCDHAC2	1
PCDHB1	21
PCDHB10	2
PCDHB11	1
PCDHB12	1
PCDHB13	1
PCDHB14	8
PCDHB15	2
PCDHB16	1
PCDHB18P	1
PCDHB19P	2
PCDHB2	3
PCDHB3	2
PCDHB4	3
PCDHB6	4

PCDHB9	1	PDF	4	PGLS	1	PIGV	3
PCDHGA10	1	PDGFA	2	PGM1	1	PIK3C2A	1
PCDHGA11	1	PDGFB	1	PGM3	5	PIK3CA	1
PCDHGA12	3	PDHA1	1	PGP	3	PIK3CB	1
PCDHGA4	1	PDHB	3	PGPEP1L	6	PIK3CD	3
PCDHGA5	2	PDIA2	1	PGRMC1	1	PIK3IP1	2
PCDHGA6	3	PDIA6	2	PGS1	1	PIK3R1	1
PCDHGA9	3	PDIK1L	3	PHACTR3	1	PIK3R2	5
PCDHGB2	1	PDK1	1	PHB	2	PIK3R3	3
PCDHGB4	1	PDK2	2	PHF11	2	PIK3R4	2
PCDHGB5	2	PDK3	1	PHF12	1	PILRA	2
PCDHGB6	1	PDK4	2	PHF14	4	PILRB	2
PCDHGB7	2	PDLIM1	2	PHF19	2	PIN1P1	2
PCDHGC3	2	PDP1	2	PHF2	2	PIN4P1	1
PCDHGC5	24	PDP2	2	PHF20L1	1	PINK1-AS	3
PCED1B	1	PDXK	2	PHF3	5	PINLYP	2
PCF11	7	PDYN-AS1	2	PHF5A	1	PIP4K2A	1
PCF11-AS1	2	PDZRN3	1	PHF7	1	PIP4K2C	1
PCGF5	1	PDZRN4	2	PHF8	2	PISD	2
PCLO	11	PEBP1	3	PHKG1	1	PITPNA	2
PCMTD1	1	PEG10	4	PHLDA1	3	PITPNA-AS1	2
PCMTD2	1	PEG13	2	PHLDA2	1	PITPNM3	1
PCNP	1	PEG3-AS1	6	PHLDA3	1	PITRM1-AS1	1
PCNT	1	PELI1	2	PHLPP1	4	PIWIL1	2
PCNX1	1	PELI2	1	PHOSPHO2	1	PJA1	2
PCNX2	1	PER3	1	PHOX2A	2	PJA2	1
PCNX3	1	PEX1	1	PHOX2B	3	PKD2	1
PCNX4	3	PEX10	2	PHPT1	2	PKD2L2	3
PCP4	1	PEX19	3	PHTF1	3	PKIA-AS1	1
PCSK1	1	PEX26	1	PHTF2	1	PKM	2
PCSK6	1	PEX5L-AS2	2	PHYH	1	PKP4-AS1	2
PCSK9	2	PEX6	2	PHYHD1	3	PLA2G10	1
PCYOX1L	1	PFDN1	1	PHYHIP	3	PLA2G12A	1
PCYT2	1	PFKFB3	2	PHYHIPL	3	PLA2G16	1
PDCD6IP	2	PFN1	1	PHYKPL	1	PLA2G2E	1
PDCL	1	PFN2	2	PI16	3	PLA2G4F	2
PDCL3P4	1	PGAM1	2	PIAS1	1	PLAC8L1	1
PDE12	2	PGAM4	2	PIAS2	1	PLAC9	1
PDE1A	2	PGAM5	2	PICALM	2	PLAG1	1
PDE4B	2	PGBD1	6	PID1	2	PLBD1-AS1	1
PDE4D	8	PGBD2	2	PIGC	2	PLCD4	1
PDE4DIP	4	PGBD3	1	PIGH	4	PLCE1-AS1	1
		PGBD4	3	PIGM	9	PLCG1	2
		PGBD5	3	PIGO	1		
		PGD	3	PIGT	1		

PLCH1-AS2	3
PLCL1	2
PLCXD1	1
PLD4	5
PLD6	9
PLEC	11
PLEKHA5	2
PLEKHB1	6
PLEKHF1	1
PLEKHF2	2
PLEKHG1	1
PLEKHG3	5
PLEKHG5	1
PLEKHG7	2
PLEKHM1P1	1
PLEKHO2	1
PLIN1	1
PLK1	4
PLK2	2
PLK4	3
PLN	1
PLP1	2
PLPBP	2
PLPP3	1
PLPP5	4
PLPPR2	1
PLPPR4	4
PLXNA1	2
PLXNA2	2
PLXNA4	2
PLXNB1	2
PLXNB2	1
PMF1-BGLAP	2
PML	1
PMM1	1
PMP2	2
PMPCA	1
PMPCB	1
PMS1	1
PMS2CL	1
PMS2P3	2
PMVK	1
PNISR	1
PNKD	1
PNMA1	3
PNMA2	2
PNMA3	4
PNMA8A	1
PNMA8B	8
PNMT	1
PNN	1
PNO1	1
PNOC	2
PNPLA8	2
PNRC1	2
PNRC2	2
POC1B-GALNT4	1
PODN	1
PODXL	7
PODXL2	1
POGK	5
POLB	2
POLD3	2
POLD4	2
POLI	1
POLL	2
POLQ	2
POLR1A	1
POLR1B	3
POLR1C	1
POLR1D	2
POLR2A	1
POLR2C	1
POLR2D	5
POLR2E	1
POLR2L	1
POLR2M	1
POLR3B	1
POLR3H	3
POLRMT	1
POMC	3
POMGNT1	3
POMGNT2	1
POMK	1
POMT1	5
POMZP3	1
PON1	2
PON3	1
POP4	1
POP5	1
POP7	1
POPDC3	1
POSTN	2
POU1F1	1
POU2F1	1
POU2F3	1
POU3F2	2
POU3F3	2
POU4F1	2
POU5F1P4	3
POU6F1	1
PP2D1	1
PP7080	2
PPCDC	1
PPDPF	1
PPFIA4	1
PPIAL4C	1
PPIB	1
PPIC	1
PPIF	6
PPIG	2
PPIL2	5
PPM1A	1
PPM1B	1
PPM1K	2
PPM1L	1
PPP1CC	2
PPP1R10	2
PPP1R12B	4
PPP1R15B	3
PPP1R17	5
PPP1R26	5
PPP1R27	5
PPP1R35	1
PPP1R3C	3
PPP1R3E	1
PPP1R3F	1
PPP1R3G	1
PPP1R9A	2
PPP1R9B	1
PPP2CA	2
PPP2CB	1
PPP2R1B	3
PPP2R3A	3
PPP2R5B	1
PPP3CB	3
PPP3CC	1
PPP3R2	2
PPP4R1	2
PPP4R3A	1
PPP4R3B	1
PPP6R2	1
PPRC1	2
PPT1	1
PPWD1	2
PQLC2	1
PQLC3	2
PRAF2	1
PRAG1	2
PRAM1	1
PRCP	1
PRDM1	1
PRDM14	1
PRDM2	2
PRDM4	1
PRDM8	3
PREPL	5
PREX1	1
PREX2	1
PRH1-PRR4	2
PRH1-TAS2R14	2
PRICKLE1	5
PRICKLE2-AS2	6
PRICKLE2-AS3	1
PRIMA1	4
PRKAB1	1
PRKACA	1
PRKACB	5
PRKACG	1
PRKAG1	6
PRKAG2	1
PRKCE	2
PRKCG	1
PRKCQ	1

PRKCZ-AS1	3
PRMT2	1
PRMT6	1
PRMT7	1
PRMT9	1
PRNP	3
PROCA1	1
PRORSD1P	4
PROSER2-AS1	1
PROX1	3
PRPF18	3
PRPF3	1
PRPF38A	2
PRPF39	2
PRPF40A	2
PRPF4B	1
PRPH2	3
PRPS2	3
PRR12	1
PRR14L	7
PRR18	2
PRR3	1
PRR36	2
PRRC1	2
PRRC2C	6
PRRG1	2
PRRG3	1
PRRT1	1
PRRT2	3
PRRT3-AS1	3
PRSS23	1
PRSS27	1
PRSS35	2
PRSS38	1
PRSS47	1
PRSS53	1
PRUNE2	10
PSAT1	3
PSD	1
PSD2	1
PSD3	2
PSD4	1
PSEN1	1
PSIP1	1
PSKH1	1
PSMA4	1
PSMA7	1
PSMB3	3
PSMB4	4
PSMB5	1
PSMB8	1
PSMC1	2
PSMC3IP	2
PSMC5	1
PSMD1	1
PSMD12	1
PSMD13	1
PSMD4	2
PSMD6-AS2	3
PSMD7	4
PSMG3	1
PSMG4	3
PSPN	1
PSRC1	3
PSTK	1
PTBP2	2
PTCD2	1
PTCHD1	3
PTEN	4
PTGER4	1
PTGIS	1
PTH2R	2
PTK6	1
PTMA	1
PTN	3
PTP4A1	1
PTP4A2	1
PTPDC1	1
PTPMT1	2
PTPN13	1
PTPN23	4
PTPN4	1
PTPN9	1
PTPRA	1
PTPRB	1
PTPRD	5
PTPRG-AS1	2
PTPRK	1
PTPRO	3
PTPRS	2
PTPRZ1	1
PTRHD1	2
PTTG1IP	2
PURA	3
PURG	1
PUS1	2
PUS10	1
PUS3	2
PUS7L	1
PVRIG	6
PWAR6	1
PWWP2A	2
PWWP2B	1
PXDN	5
PXDNL	1
PXMP4	1
PXT1	4
PYGB	3
PYGL	6
PYGM	1
PYROXD2	1
PYURF	3
PYY2	2
QRFP	5
QRICH2	2
QSER1	4
QSOX1	4
QTRT1	3
QTRT2	2
R3HCC1	1
R3HDM1	2
RAB11FIP2	4
RAB11FIP4	3
RAB1A	1
RAB24	1
RAB27B	2
RAB28	1
RAB29	1
RAB30-AS1	1
RAB32	4
RAB33A	1
RAB33B	3
RAB35	4
RAB36	1
RAB39A	1
RAB39B	1
RAB40AL	2
RAB40C	1
RAB5IF	2
RAB8A	3
RAB9A	1
RAB9B	1
RABAC1	1
RABGEF1	3
RABIF	2
RAC1	2
RAD17	1
RAD18	4
RAD21-AS1	2
RAD23A	1
RAD23B	1
RAD50	2
RAD52	7
RAD54B	2
RAD9B	1
RADIL	1
RAET1E-AS1	3
RALB	1
RALBP1	3
RALY	1
RAMP1	1
RAN	1
RANBP6	6
RAP1GAP	2
RAP1GDS1	1
RAP2A	3
RAP2B	2
RAP2C-AS1	1
RAPGEF1	1
RAPGEF2	4
RAPGEF4	1
RAPGEF6	4
RAPGEFL1	1
RAPH1	1
RARA	1
RASA1	1
RASA2	4
RASA4CP	1

RASAL1	1
RASD1	2
RASGEF1B	1
RASGEF1C	2
RASGRP3	1
RASL10A	2
RASL10B	2
RASSF2	10
RASSF8	1
RAVER1	2
RAVER2	5
RB1CC1	4
RBAKDN	2
RBBP5	1
RBBP6	2
RBBP7	1
RBBP8	1
RBFA	1
RBFADN	1
RBFOX1	1
RBM12B-AS1	5
RBM14	3
RBM15	5
RBM15B	4
RBM17	2
RBM22	4
RBM23	1
RBM24	1
RBM3	1
RBM34	1
RBM4	2
RBM44	1
RBM48	1
RBM4B	3
RBM5	1
RBM6	2
RBM7	5
RBP7	1
RCAN3	2
RCC1	1
RCC1L	1
RCC2	4
RCN1	1
RCN2	1
RCOR2	1
RCVRN	2
RDH14	2
RDX	1
REEP2	2
REEP4	3
REEP5	2
RELB	1
RELL2	1
RELT	4
RENBP	1
REPIN1	4
REPS2	1
RERG-AS1	1
REST	3
RETREG1	4
RETREG2	1
RETREG3	1
REV1	3
REXO1	1
REXO5	2
RFC1	2
RFFL	1
RFLNB	3
RFPL1	3
RFPL1S	2
RFTN2	1
RFX4	1
RGL1	1
RGL2	2
RGL4	2
RGMA	1
RGMB-AS1	2
RGS1	3
RGS10	1
RGS2	1
RGS3	5
RGS4	2
RGS7BP	1
RGS8	1
RHBDD1	1
RHBDD3	1
RHEB	1
RHOB	4
RHOBTB1	1
RHOBTB2	4
RHOG	2
RHOU	4
RIC8A	1
RIF1	6
RIMKLA	2
RIMS1	2
RIMS2	3
RIMS3	1
RIN2	2
RIN3	1
RING1	1
RINT1	1
RIOX1	2
RIOX2	2
RIPK4	1
RIPOR2	1
RIT1	2
RLBP1	2
RLIM	5
RMC1	2
RNASE1	1
RNASEH2C	2
RND3	1
RNF103	2
RNF111	1
RNF130	1
RNF133	1
RNF135	2
RNF139	2
RNF14	2
RNF144A	2
RNF145	2
RNF146	3
RNF150	1
RNF167	1
RNF168	3
RNF169	3
RNF180	2
RNF182	1
RNF183	2
RNF187	1
RNF19A	2
RNF19B	1
RNF20	1
RNF213	1
RNF216P1	1
RNF217	2
RNF217-AS1	2
RNF220	1
RNF223	1
RNF26	2
RNF32	3
RNF34	1
RNF4	1
RNF40	4
RNF41	1
RNF44	3
RNF6	3
RNF7	1
RNFT1	1
RNH1	1
RNLS	1
RNMT	1
RNPS1	2
RNU105B	3
RNU6-1	2
RNU6-9	3
RNVU1-1	1
ROBO1	1
ROCK1	2
ROGDI	2
ROPN1L-AS1	1
ROR2	1
RORA-AS1	1
RORB-AS1	1
RPA1	2
RPAIN	2
RPE	4
RPH3A	2
RPL13	1
RPL13AP17	1
RPL15	1
RPL19	1
RPL19P12	1
RPL26L1	1
RPL27	3
RPL29	1
RPL31	3

RPL36	4	RSAD2	1	SAMD1	2	SCFD2	1
RPL36AL	1	RSBN1	1	SAMD14	2	SCG2	2
RPL37A	1	RSC1A1	5	SAMD4A	2	SCGB1A1	1
RPL41	3	RSL1D1	1	SAMD9	1	SCGB1B2P	1
RPL6	1	RSPH10B	1	SAMD9L	1	SCGB1C2	3
RPL7L1	1	RSPH14	2	SAP18	1	SCGB3A1	1
RPP21	1	RSPRY1	1	SAP30BP	1	SCHIP1	1
RPP25	1	RSRP1	1	SAR1B	3	SCLY	1
RPP25L	1	RTKN	1	SARS	1	SCML1	2
RPRD1B	1	RTL10	2	SASH1	3	SCML4	3
RPRM	1	RTL5	2	SASH3	1	SCN1A	1
RPRML	3	RTL6	3	SAT2	1	SCN2A	3
RPS13	1	RTL8A	1	SATB1	2	SCN2B	1
RPS15AP10	1	RTL8C	3	SATB2	4	SCN3A	3
RPS16	1	RTN2	1	SAV1	5	SCN3B	5
RPS17	1	RTN4	6	SAYSD1	2	SCN4B	1
RPS18P9	1	RTRAF	4	SBDS	3	SCN8A	2
RPS19BP1	1	RUNX1T1	3	SBF2-AS1	1	SCO1	1
RPS21	2	RUNX2	1	SC5D	1	SCO2	3
RPS23	2	RUSC1	4	SCAF1	5	SCRIB	1
RPS24	2	RUSC1-AS1	1	SCAF11	5	SCRN1	3
RPS27L	1	RUSC2	2	SCAI	2	SCRN3	3
RPS29	1	RUVBL1-AS1	2	SCAMP1-AS1	4	SCRT1	1
RPS4X	1	RWDD1	1	SCAND1	2	SCYL1	1
RPS6	2	RWDD3	2	SCAND2P	5	SCYL3	3
RPS6KB2	3	RXRA	1	SCARA3	1	SDAD1P1	2
RPS6KC1	3	RXRB	2	SCARB1	1	SDC1	1
RPS6KL1	4	RXYLT1-AS1	1	SCARF2	1	SDC3	4
RPSA	2	RYBP	2	SCARNA1	1	SDCBP	1
RPUSD1	1	S100A13	2	SCARNA14	2	SDCBP2	4
RPUSD2	1	S100A16	1	SCARNA18	1	SDCCAG3	1
RPUSD4	1	S100B	1	SCARNA18B	1	SDE2	1
RRAGA	2	S100PBP	1	SCARNA22	3	SDF4	1
RRAGC	2	S1PR1	3	SCARNA26A	2	SDHAF1	1
RRAS2	1	S1PR3	2	SCARNA26B	2	SDHAF2	1
RRBP1	1	S1PR5	2	SCARNA6	1	SDHAF4	3
RRM1	1	SAA1	2	SCARNA7	2	SDHB	3
RRNAD1	3	SAC3D1	1	SCARNA8	1	SDR39U1	1
RRP36	1	SACS	12	SCARNA9	1	SEC14L1	2
RRP7A	2	SACS-AS1	1	SCCPDH	2	SEC16A	7
RRP7BP	1	SALL1	4	SCD	1	SEC22A	3
RRP8	1	SALL2	4	SCD5	1	SEC23IP	1
RRS1	1	SALL3	4	SCFD1	1	SEC24A	1
RS1	2	SALRNA2	1			SEC61A2	1
RSAD1	2						

SEC62	2	SETD6	3	SHISA2	3	SLC17A8	1
SECISBP2	4	SETD7	1	SHISA3	1	SLC17A9	2
SELENOKP3	1	SETD9	3	SHISA4	2	SLC18A2	1
SELENON	1	SETDB2	1	SHISA7	3	SLC19A3	1
SELENOO	1	SETMAR	4	SHISA9	5	SLC1A2	1
SELENOP	2	SETSIP	1	SHKBP1	3	SLC1A3	4
SELPLG	3	SETX	7	SHPRH	1	SLC1A4	1
SEM1	1	SEZ6L	1	SHROOM1	1	SLC20A1	2
SEMA3A	2	SF3B1	1	SHTN1	1	SLC20A2	1
SEMA3B-AS1	2	SF3B4	1	SIAH1	5	SLC22A12	3
SEMA6A-AS1	1	SF3B5	1	SIDT2	1	SLC22A13	1
SEMA6A-AS2	1	SFRP1	1	SIGLEC15	1	SLC22A16	3
SEMA6D	3	SFRP2	1	SIM1	1	SLC22A17	3
SENP2	1	SFRP5	1	SIMC1	2	SLC22A23	1
SENP3	2	SFSWAP	1	SIN3A	1	SLC22A7	4
SENP5	2	SFT2D3	5	SIN3B	1	SLC22A9	1
SENP8	2	SFXN1	1	SIPA1L1	3	SLC23A1	1
SEPHS2	2	SFXN5	3	SIPA1L2	4	SLC24A2	1
SEPT4	1	SGCZ	1	SIRT1	1	SLC24A5	2
SEPT4-AS1	1	SGK1	3	SKA3	2	SLC25A18	2
SEPT7P2	4	SGK494	1	SKI	1	SLC25A19	1
SEPT8	1	SGMS2	1	SKIL	2	SLC25A28	1
SERAC1	5	SGPP1	1	SKP1	1	SLC25A29	2
SERBP1	1	SGSM3	1	SKP2	1	SLC25A34	2
SERINC1	3	SH2B1	1	SLA2	1	SLC25A37	1
SERPINE3	4	SH2B2	1	SLAIN1	1	SLC25A39	1
SERPINF1	1	SH2B3	3	SLAIN2	1	SLC25A41	4
SERPINF2	1	SH2D4A	2	SLAMF6	2	SLC25A44	1
SERTAD1	2	SH2D5	1	SLC10A4	1	SLC25A46	1
SERTAD2	3	SH3BGR	1	SLC10A6	3	SLC25A51	3
SERTAD3	1	SH3BGRL2	1	SLC11A2	3	SLC25A52	1
SERTAD4	1	SH3BGRL3	2	SLC12A1	2	SLC25A5-AS1	1
SERTAD4-AS1	1	SH3BP4	6	SLC12A2	5	SLC25A6	2
SERTM1	2	SH3BP5-AS1	3	SLC12A5	3	SLC26A1	1
SESN1	1	SH3BP5L	3	SLC12A6	2	SLC26A2	1
SESN2	1	SH3D19	1	SLC12A8	3	SLC26A4	2
SET	1	SH3D21	4	SLC13A3	1	SLC27A4	1
SETBP1	1	SH3GLB1	2	SLC14A1	1	SLC29A3	1
SETD1B	1	SH3KBP1	1	SLC15A2	1	SLC29A4	1
SETD2	5	SH3RF1	1	SLC15A4	3	SLC2A12	3
SETD3	1	SH3YL1	3	SLC16A14	1	SLC2A1-AS1	3
SETD5	1	SHB	1	SLC16A7	1	SLC2A2	2
		SHC4	3	SLC16A8	2		
		SHF	1	SLC16A9	1		
		SHH	2	SLC17A6	2		

SLC2A3	1	SLC50A1	1	SMAD1-AS1	1	SNAPC3	2
SLC2A6	1	SLC51A	2	SMAD3	4	SNAPC5	1
SLC30A1	2	SLC51B	2	SMAD4	1	SNCG	3
SLC30A2	2	SLC5A10	1	SMAD7	4	SNHG5	1
SLC30A4	1	SLC5A11	5	SMAP2	1	SNIP1	1
SLC31A2	4	SLC5A12	1	SMARCA2	1	SNN	3
SLC32A1	2	SLC5A2	2	SMARCA5	4	SNORA100	2
SLC33A1	1	SLC5A3	6	SMARCAD1	1	SNORA101B	2
SLC34A2	1	SLC6A13	3	SMARCAL1	1	SNORA105B	2
SLC35A1	3	SLC6A15	1	SMARCC2	2	SNORA11	1
SLC35B2	1	SLC6A17	3	SMARCE1	3	SNORA115	3
SLC35B3	1	SLC6A1-AS1	1	SMC3	1	SNORA117	1
SLC35B4	2	SLC6A3	2	SMCHD1	1	SNORA11C	1
SLC35C1	3	SLC6A4	2	SMCR5	3	SNORA11G	1
SLC35C2	5	SLC6A5	1	SMCR8	4	SNORA16B	3
SLC35E1	2	SLC6A7	1	SMG1P1	1	SNORA17B	2
SLC35E3	1	SLC6A8	1	SMG5	1	SNORA19	1
SLC35F4	1	SLC7A11	1	SMG6	2	SNORA24	1
SLC35F6	1	SLC7A14	1	SMG8	2	SNORA25	1
SLC35G5	1	SLC7A4	1	SMIM10L2A	2	SNORA28	2
SLC37A3	1	SLC7A6	1	SMIM10L2B	1	SNORA2C	1
SLC38A1	2	SLC8A1-AS1	4	SMIM12	2	SNORA30	2
SLC38A2	2	SLC8A2	1	SMIM15-AS1	1	SNORA31	1
SLC38A7	2	SLC9A3-AS1	6	SMIM17	2	SNORA38	2
SLC38A8	1	SLC9A3R2	1	SMIM20	1	SNORA4	2
SLC39A10	3	SLC9A6	2	SMIM22	1	SNORA40	2
SLC39A3	3	SLC9A7P1	4	SMIM23	2	SNORA40B	2
SLC39A6	2	SLC9A9-AS1	1	SMIM24	1	SNORA47	1
SLC39A8	1	SLC9B2	1	SMIM26	1	SNORA50C	1
SLC39A9	1	SLCO1A2	6	SMIM27	1	SNORA53	1
SLC3A1	2	SLCO1C1	1	SMIM3	1	SNORA54	1
SLC3A2	1	SLF1	2	SMIM30	1	SNORA58	1
SLC40A1	1	SLF2	2	SMIM32	2	SNORA59A	2
SLC41A1	1	SLFN5	2	SMIM4	1	SNORA5A	1
SLC41A2	2	SLIT1-AS1	7	SMIM5	1	SNORA63B	1
SLC45A1	3	SLITRK1	3	SMIM7	1	SNORA65	1
SLC45A2	2	SLITRK2	6	SMIM8	5	SNORA66	1
SLC45A3	1	SLITRK3	6	SMNDC1	1	SNORA68B	2
SLC45A4	1	SLITRK4	3	SMPD1	1	SNORA70F	3
SLC46A1	1	SLITRK5	4	SMTNL1	1		
SLC46A2	2	SLK	2	SMUG1	3		
SLC48A1	1	SLMAP	2	SMYD2	1		
SLC4A11	1	SLTM	4	SNAI3	2		
SLC4A1AP	2	SLX4	1	SNAP25-AS1	1		
SLC4A8	2						

SNORA74B	1
SNORA75	1
SNORA79	2
SNORA80C	1
SNORA80D	4
SNORA89	3
SNORA92	1
SNORA98	1
SNORA9B	3
SNORC	1
SNORD100	1
SNORD103A	1
SNORD103C	1
SNORD107	1
SNORD108	1
SNORD12	5
SNORD123	1
SNORD127	2
SNORD129	3
SNORD133	2
SNORD137	1
SNORD13D	2
SNORD13E	2
SNORD13F	1
SNORD13H	5
SNORD13J	1
SNORD141A	1
SNORD141B	1
SNORD143	1
SNORD148	1
SNORD14C	1
SNORD14E	2
SNORD151	5
SNORD152	1
SNORD153	3
SNORD155	4
SNORD163	1
SNORD164	6
SNORD168	1
SNORD170	1
SNORD172	4
SNORD18C	1
SNORD1A	1
SNORD20	1
SNORD21	1
SNORD31B	1
SNORD35A	1
SNORD35B	1
SNORD36B	1
SNORD42B	1
SNORD53B	1
SNORD54	3
SNORD57	1
SNORD60	1
SNORD61	2
SNORD62A	5
SNORD63B	1
SNORD66	1
SNORD68	1
SNORD69	1
SNORD72	1
SNORD73A	3
SNORD87	1
SNORD88B	1
SNORD91	1
SNORD90	1
SNORD96A	1
SNORD97	3
SNRK	1
SNRK-AS1	1
SNRNP25	1
SNRNP35	3
SNRPE	5
SNRPG	1
SNTG1	1
SNTN	1
SNU13	1
SNX14	1
SNX18	3
SNX19	3
SNX21	2
SNX22	5
SNX29	1
SNX33	3
SNX4	1
SOCS1	1
SOCS7	1
SOD1	1
SOD2	1
SOD3	4
SOGA3	4
SORBS2	2
SORL1	3
SOST	2
SOWAHA	4
SOWAHB	2
SOX12	2
SOX2	5
SOX5	1
SOX8	1
SOX9	1
SP1	2
SP3	3
SP4	3
SPACA3	1
SPACA9	4
SPAG9	2
SPART-AS1	1
SPATA13-AS1	6
SPATA2	6
SPATA22	3
SPATA24	3
SPATA25	1
SPATA2L	1
SPATA33	1
SPATA46	1
SPATA6L	1
SPATA7	1
SPDYA	1
SPDYE3	1
SPECC1	1
SPECC1L	2
SPEF1	1
SPEM1	3
SPEN	1
SPG11	1
SPHAR	1
SPHK1	2
SPHK2	1
SPIN3	1
SPIN4	2
SPINK13	1
SPOCK2	4
SPOPL	1
SPP1	1
SPPL2B	2
SPRED1	2
SPRED2	3
SPRED3	1
SPRN	4
SPRY1	1
SPRY2	1
SPRY4-IT1	2
SPSB1	2
SPTAN1	3
SPTBN2	1
SPX	1
SQLE	2
SQSTM1	2
SRCIN1	1
SRD5A3-AS1	1
SREBF1	2
SREK1	1
SRGAP2-AS1	1
SRGAP3	2
SRP19	7
SRP72	1
SRP9	1
SRPK1	1
SRPK2	1
SRPRB	2
SRRD	4
SRRM2-AS1	5
SRSF1	1
SRSF11	2
SRSF3	1

SRSF5	2	STIM1	2	SUSD2	2	TAF1C	3
SRSF6	1	STIM2	3	SUZ12P1	1	TAF2	1
SRSF8	5	STIMATE	1	SV2A	2	TAF5L	3
SRSF9	1	STIP1	1	SVIL-AS1	1	TAF7	4
SRXN1	6	STK11	1	SVOPL	1	TAGAP	2
SS18	1	STK17A	3	SWSAP1	1	TAGLN3	1
SSBP3-AS1	3	STK17B	1	SWT1	1	TAL2	1
SSFA2	5	STK25	1	SYBU	2	TANGO6	2
SSH1	1	STK35	2	SYCE1L	3	TAOK1	1
SSPN	2	STMN2	1	SYCP3	2	TAPBP	1
SSR2	2	STMN4	1	SYDE2	1	TAPT1	1
SSR3	1	STMP1	1	SYF2	1	TAPT1-AS1	1
SSR4	2	STOM	1	SYK	2	TARDBP	3
SSTR1	1	STOML1	2	SYN1	1	TARS2	7
SSTR2	4	STOML3	1	SYNC	1	TAS1R3	1
ST14	2	STOX2	7	SYNDIG1	3	TATDN2	1
ST18	4	STPG4	1	SYNE1	1	TAX1BP3	1
ST3GAL1	2	STRIP1	1	SYNE1-AS1	5	TBATA	1
ST3GAL2	1	STRN	2	SYNGR1	1	TBC1D1	1
ST3GAL4	1	STRN4	3	SYNGR2	1	TBC1D14	5
ST3GAL5	3	STS	2	SYNJ2	1	TBC1D16	2
ST3GAL5-AS1	1	STT3A-AS1	2	SYNM	#	TBC1D2	3
ST6GAL1	3	STUM	3	SYNPO	8	TBC1D20	2
ST6GAL2	1	STX10	2	SYNRG	2	TBC1D22A	1
ST6GALNAC3	1	STX17	1	SYS1-DBNDD2	2	TBC1D26	3
ST8SIA1	1	STXBP3	1	SYT11	7	TBC1D29	2
ST8SIA2	1	SUB1	1	SYT13	1	TBC1D7	1
ST8SIA3	1	SUCO	2	SYT15	2	TBC1D9	2
ST8SIA5	2	SUDS3	1	SYT16	1	TBCB	1
STAB1	2	SUGP2	3	SYT17	1	TBCC	1
STAC2	1	SUGT1	3	SYT2	4	TBCD	1
STAC3	1	SUGT1P3	2	SYT4	4	TBCEL	1
STAP1	1	SULF1	1	SYTL2	2	TBK1	1
STAR	3	SULF2	3	SYTL5	1	TBKBP1	1
STARD13	4	SUMO1	1	SZRD1	1	TBL1XR1	1
STARD4-AS1	3	SUMO1P1	1	SZT2-AS1	2	TBL2	1
STARD5	2	SUMO1P3	1	TAB2-AS1	2	TBPL1	1
STARD7-AS1	4	SUMO4	4	TAB3-AS1	1	TBR1	5
STAT3	2	SUOX	1	TACC1	1	TBRG4	1
STAU2	1	SUPT16H	4	TACC2	1	TBX6	1
STAU2-AS1	2	SUPT4H1	1	TACO1	2	TCAP	1
STEAP2	1	SUPT6H	1	TADA1	3	TCEAL1	1
STH	5	SURF2	1	TAF10	2	TCEAL2	2
		SURF6	2	TAF11	1	TCEAL3	1

TCEAL4	1
TCEAL5	1
TCEAL8	2
TCEAL9	1
TCF12	1
TCF20	5
TCF4	4
TCHP	3
TCP10L	1
TCP11	1
TCP11L1	1
TCTE1	1
TCTN1	1
TDP1	1
TDRD3	1
TDRD6	2
TDRG1	4
TEAD4	1
TECPR2	4
TECTA	1
TEF	5
TEFM	1
TEKT2	1
TENT2	1
TENT4A	2
TENT5A	1
TERF1	3
TERF2IP	1
TESC-AS1	1
TESPA1	2
TET2	5
TET2-AS1	3
TET3	1
TEX2	4
TEX22	1
TEX264	1
TEX29	5
TEX35	3
TEX43	1
TEX53	1
TFAM	1
TFAP2E	1
TFCP2	3
TFCP2L1	6
TFF3	2
TFG	1
TFRC	1
TGFA-IT1	2
TGFB1	1
TGFB1I1	1
TGFB2-OT1	2
TGFB3	3
TGFBR1	1
TGFBR2	2
TGM2	2
TGM4	1
TGOLN2	4
TH2LCRR	2
THADA	1
THAP1	1
THAP11	1
THAP12	3
THAP2	6
THAP3	4
THAP4	2
THAP5	3
THAP7-AS1	3
THAP9-AS1	2
THBS1	1
THCAT155	1
THEM5	1
THEMIS2	3
THNSL1	1
THOC1	2
THOC2	2
THOC5	1
THOC6	1
THRIL	4
THSD1	3
THTPA	1
THUMPD1	4
THUMPD2	1
THUMPD3	1
THUMPD3-AS1	1
THY1	3
THYN1	2
TIAF1	2
TIAL1	1
TIAM1	2
TIFA	1
TIGAR	1
TIGD5	3
TIMM13	1
TIMM21	2
TIMM22	4
TIMM44	1
TIMM8B	2
TIMMDC1	4
TIMP1	1
TIMP3	2
TIMP4	1
TINF2	2
TIPARP	1
TIRAP	1
TJP2	2
TLCD2	1
TLE1	1
TLE4	1
TLK1	2
TLL2	1
TLNRD1	3
TLR1	5
TLR2	1
TLR3	1
TLR4	5
TLR5	2
TM2D2	1
TM4SF19-TCTEX1D2	1
TM9SF1	2
TMA16	1
TMBIM6	1
TMBIM7P	1
TMC7	1
TMCC1	4
TMCC2	4
TMCO2	5
TMCO3	1
TMED10P1	4
TMED5	1
TMED6	1
TMED7-TICAM2	2
TMED9	2
TMEM100	2
TMEM106A	2
TMEM106B	1
TMEM11	1
TMEM115	2
TMEM121	1
TMEM121B	2
TMEM125	1
TMEM126B	1
TMEM127	2
TMEM129	1
TMEM132A	2
TMEM132B	3
TMEM132D	3
TMEM132D-AS1	4
TMEM132E	1
TMEM136	2
TMEM144	3
TMEM147	1
TMEM14C	1
TMEM14EP	3
TMEM151A	3
TMEM151B	2
TMEM155	1
TMEM158	1
TMEM160	5
TMEM165	2
TMEM167B	1
TMEM168	1
TMEM170A	2
TMEM170B	2
TMEM177	1
TMEM178A	1
TMEM179	1
TMEM181	3
TMEM184B	1
TMEM184C	2
TMEM185B	3
TMEM186	6

TMEM19	2
TMEM198B	2
TMEM199	2
TMEM200A	1
TMEM200B	1
TMEM200C	2
TMEM203	1
TMEM211	1
TMEM216	1
TMEM229A	2
TMEM229B	5
TMEM236	1
TMEM240	3
TMEM242	4
TMEM243	2
TMEM245	2
TMEM246-AS1	3
TMEM250	2
TMEM251	2
TMEM260	1
TMEM263	2
TMEM265	7
TMEM33	1
TMEM35B	2
TMEM39A	4
TMEM41A	3
TMEM42	1
TMEM43	4
TMEM44	1
TMEM47	1
TMEM50A	1
TMEM50B	1
TMEM51-AS1	10
TMEM52B	1
TMEM60	3
TMEM65	1
TMEM68	1
TMEM70	1
TMEM74	1
TMEM74B	2
TMEM81	4
TMEM86A	1
TMEM87B	1
TMEM95	1
TMEM97	1
TMEM98	1
TMOD1	1
TMOD2	1
TMOD3	3
TMOD4	1
TMPO-AS1	1
TMPPE	1
TMSB4X	1
TMTC2	2
TMTC3	2
TMUB2	2
TMX1	1
TMX3	1
TMX4	2
TNC	2
TNFAIP1	1
TNFAIP2	1
TNFAIP8	1
TNFAIP8L1	2
TNFRSF13C	1
TNFRSF19	1
TNFRSF1A	1
TNFRSF21	2
TNFRSF4	1
TNFRSF6B	1
TNFSF14	3
TNFSF4	1
TNIK	1
TNIP1	1
TNIP2	2
TNKS1BP1	3
TNRC18	4
TNRC18P1	1
TNRC6C	3
TNRC6C-AS1	8
TNS2	1
TOB1	1
TOB2	2
TOGARAM1	2
TOMM20	2
TOMM20L	3
TOMM22	3
TOMM40	1
TOMM5	2
TOMM70	1
TONSL	2
TOR1A	2
TOR1AIP1	2
TOR1AIP2	3
TOR1B	1
TOR3A	4
TOR4A	1
TP53AIP1	4
TP53BP1	2
TP53BP2	1
TP53I13	1
TP53INP2	4
TP73-AS1	4
TPBG	2
TPBGL	3
TPD52L1	1
TPGS1	1
TPI1	1
TPP1	5
TPPP	6
TPRG1L	2
TPRN	2
TPST1	2
TPT1	1
TRABD	1
TRABD2A	1
TRAF1	1
TRAF3IP2	4
TRAF3IP2-AS1	4
TRAF4	2
TRAF5	1
TRAF6	2
TRAFD1	1
TRAIP	1
TRAM1L1	1
TRAP1	3
TRAPPC10	2
TRAPPC12	1
TRAPPC13	2
TRAPPC2B	2
TRAPPC6B	3
TRAPPC9	1
TREX1	4
TRG-AS1	2
TRHDE-AS1	1
TRIAP1	1
TRIB1	3
TRIB2	3
TRIL	3
TRIM15	1
TRIM22	1
TRIM32	4
TRIM33	3
TRIM36	1
TRIM37	2
TRIM41	1
TRIM44	1
TRIM52	5
TRIM52-AS1	1
TRIM56	2
TRIM59-IFT80	2
TRIM62	1
TRIM8	2
TRIO	1
TRIP11	6
TRIR	1
TRMO	1
TRMT10C	2
TRMT12	3
TRMT5	1
TRMT6	1
TRMT61B	2
TRMT9B	3
TRNP1	1
TRNT1	1
TRO	1
TRPC1	1
TRPC4	1
TRPM6	2

TRPS1	5	TTC3-AS1	2	TXNIP	1	UGT3A2	2
TRPV1	3	TTC3P1	1	TXNL1	1	UHMK1	2
TRPV4	4	TTC7B	2	TYMSOS	3	ULK2	1
TRUB2	1	TTC9B	1	TYRO3	1	UMPS	4
TSC22D1	1	TTC9C	1	U2AF2	1	UNC119	1
TSC22D1-AS1	5	TTI1	4	U2SURP	1	UNC13C	3
TSC22D2	4	TTI2	1	UBA2	1	UNC45A	1
TSEN2	1	TTLL11	1	UBAC1	3	UNC50	2
TSFM	1	TTLL8	2	UBALD1	2	UNC5C	2
TSHZ1	3	TTN-AS1	2	UBALD2	1	UNC80	4
TSHZ2	3	TTPAL	3	UBAP1	1	UPF1	1
TSHZ3	4	TTR	2	UBAP2	1	UPF2	1
TSIX	1	TTTY23B	1	UBB	2	UQCC2	1
TSKU	1	TTYH3	4	UBC	3	UQCR10	1
TSL	1	TUB	4	UBE2A	1	UQCRB	2
TSN	1	TUBA1A	1	UBE2CP5	5	UQCRFS1	1
TSPAN17	1	TUBA1B	3	UBE2D3	1	UQCRH	1
TSPAN3	7	TUBA4B	3	UBE2G2	1	URAHP	2
TSPAN5	1	TUBA8	6	UBE2J1	1	URB2	3
TSPOAP1	2	TUBB	4	UBE2K	1	URI1	2
TSPOAP1-AS1	3	TUBB2A	2	UBE2L3	1	UROD	2
TSPY26P	5	TUBB3	1	UBE2N	2	USB1	1
TSPYL2	4	TUBB4A	4	UBE2Q1-AS1	1	USE1	1
TSPYL4	3	TUBB4B	2	UBE2QL1	2	USF2	1
TSPYL5	2	TUBB6	4	UBE2V1	5	USF3	5
TSR3	2	TUBBP5	2	UBE2V2	1	USO1	1
TSSK2	1	TUBG2	1	UBE4B	1	USP1	1
TSSK6	3	TUBGCP4	3	UBFD1	1	USP10	1
TST	3	TUG1	7	UBIAD1	1	USP11	1
TSTD1	1	TULP3	2	UBL3	2	USP12-AS1	1
TTBK1	1	TULP4	3	UBL4A	2	USP2	3
TTC14	1	TUNAR	1	UBLCP1	1	USP21	2
TTC17	1	TUSC1	2	UBN1	4	USP22	1
TTC21A	2	TUSC2	1	UBN2	3	USP25	1
TTC23L	1	TUSC8	1	UBOX5	3	USP27X	2
TTC27	1	TUT4	2	UBP1	2	USP31	4
TTC3	2	TUT7	1	UBQLN1	1	USP33	1
TTC30A	3	TWISTNB	1	UBQLN2	2	USP34	1
TTC30B	2	TWSG1	3	UBR3	1	USP35	2
TTC33	1	TXLNA	3	UBXN10-AS1	2	USP36	4
TTC36	6	TXLNGY	2	UBXN8	1	USP38	2
TTC39A	2	TXN2	1	UCHL5	2	USP3-AS1	4
TTC39B	1	TXNDC2	2	UCK1	2	USP40	1
TTC39C	1	TXNDC5	2	UCN	1	USP42	2
		TXNDC8	2	UFM1	2	USP46	2

USP49	1
USP51	1
USP6NL	1
USP9X	2
USPL1	3
UTF1	1
UTP14C	6
UTP25	2
UTP3	2
UTS2	2
UTS2B	1
UTY	1
UVSSA	2
VAMP3	1
VAPA	2
VAPB	4
VAV3	1
VCAN	1
VCAN-AS1	5
VCPIP1	2
VCPKMT	2
VCX3B	1
VDAC2	4
VDAC3	1
VEGFA	2
VEZF1	2
VEZT	1
VGF	2
VHL	1
VIPR1-AS1	3
VIRMA	2
VLDLR-AS1	1
VMP1	3
VOPP1	2
VPS13C	1
VPS13D	3
VPS16	1
VPS18	2
VPS29	1
VPS33A	1
VPS37B	1
VPS39	2
VPS45	1
VPS4A	1
VPS54	1
VPS8	1
VPS9D1-AS1	1
VSIG2	1
VSNL1	1
VSTM2A	1
VSTM2A-OT1	1
VSTM2B	1
VSTM2L	1
VTA1	1
VTI1B	3
VTRNA1-1	1
VWA1	2
VWA2	2
VWA3A	1
VWC2	1
VWC2L	1
VXN	3
WAC	1
WAC-AS1	2
WARS2-IT1	1
WASHC2A	1
WASHC4	1
WASHC5	1
WASL	2
WBP2	1
WBP2NL	1
WDCP	1
WDFY3-AS2	3
WDPCP	1
WDR11-AS1	1
WDR13	1
WDR24	2
WDR33	1
WDR36	1
WDR4	1
WDR41	1
WDR45B	7
WDR53	2
WDR54	1
WDR5B	3
WDR6	3
WDR73	2
WDR86-AS1	1
WDR89	3
WDR97	1
WDSUB1	5
WFIKKN1	2
WFS1	6
WHAMM	1
WIPI2	3
WLS	1
WNK1	1
WNT11	3
WNT3	1
WNT5A	1
WNT7A	1
WSB1	1
WSCD1	1
WSCD2	1
WTIP	1
WWC1	2
XBP1	2
XIAP	1
XK	1
XPO1	1
XPO6	1
XRCC3	1
XRCC5	2
XXYLT1-AS1	2
YAE1D1	1
YARS2	2
YBX1	2
YDJC	1
YEATS2	2
YEATS2-AS1	8
YIPF2	2
YIPF4	1
YIPF5	1
YIPF6	1
YKT6	3
YLPM1	2
YOD1	2
YPEL1	2
YPEL5	1
YTHDC1	1
YTHDF1	2
YTHDF2	5
YTHDF3	1
YWHAE	3
YWHAEP1	1
YWHAQ	1
YWHAZ	2
ZACN	9
ZADH2	1
ZAR1	3
ZAR1L	3
ZBED1	4
ZBED5	4
ZBED6	8
ZBED8	4
ZBP1	1
ZBTB10	6
ZBTB11	1
ZBTB11-AS1	5
ZBTB14	4
ZBTB16	1
ZBTB17	10
ZBTB18	3
ZBTB2	2
ZBTB20-AS1	4
ZBTB22	1
ZBTB25	4
ZBTB3	2
ZBTB33	2
ZBTB34	6
ZBTB38	5
ZBTB4	4
ZBTB41	1
ZBTB43	1
ZBTB44	1
ZBTB45	1
ZBTB47	5
ZBTB48	1
ZBTB6	4
ZBTB7A	2
ZBTB7B	1
ZC2HC1C	1
ZC3H10	2
ZC3H12B	3
ZC3H12C	5
ZC3H13	5
ZC3H14	1
ZC3H15	2
ZC3H6	4

ZC3HAV1	1
ZCCHC12	1
ZCCHC2	3
ZCCHC3	1
ZCCHC8	2
ZDBF2	10
ZDHHC11	1
ZDHHC11B	1
ZDHHC21	2
ZDHHC22	2
ZDHHC23	3
ZDHHC3	2
ZDHHC5	1
ZDHHC7	3
ZEB1	2
ZEB2	2
ZFAND5	2
ZFAS1	4
ZFHX3	1
ZFHX4-AS1	4
ZFP1	3
ZFP14	2
ZFP2	1
ZFP28	4
ZFP3	4
ZFP30	2
ZFP36L1	4
ZFP36L2	3
ZFP37	3
ZFP41	2
ZFP57	1
ZFP62	3
ZFP64	3
ZFP69B	1
ZFP90	4
ZFPM2-AS1	3
ZFX	1
ZFY	1
ZFY-AS1	1
ZFYVE1	2
ZFYVE16	3
ZFYVE21	1
ZFYVE9	2
ZGLP1	2
ZIC5	1
ZIK1	1
ZKSCAN1	1
ZKSCAN2	2
ZKSCAN4	1
ZKSCAN5	1
ZKSCAN8	1
ZMAT2	4
ZMAT4	2
ZMIZ2	1
ZMPSTE24	1
ZMYM1	2
ZMYM2	1
ZMYM4-AS1	3
ZMYM5	2
ZNF10	1
ZNF101	1
ZNF106	7
ZNF117	1
ZNF12	6
ZNF121	1
ZNF124	1
ZNF132	2
ZNF133	2
ZNF134	2
ZNF135	4
ZNF137P	4
ZNF138	2
ZNF14	2
ZNF142	3
ZNF148	1
ZNF154	2
ZNF16	1
ZNF160	7
ZNF17	4
ZNF174	1
ZNF177	4
ZNF18	2
ZNF180	2
ZNF181	1
ZNF182	2
ZNF184	2
ZNF189	1
ZNF192P1	1
ZNF195	2
ZNF2	1
ZNF20	6
ZNF202	3
ZNF204P	3
ZNF207	2
ZNF211	3
ZNF217	2
ZNF22	1
ZNF221	1
ZNF224	4
ZNF226	7
ZNF227	2
ZNF229	2
ZNF23	2
ZNF230	1
ZNF233	1
ZNF234	1
ZNF235	1
ZNF24	3
ZNF248	5
ZNF25	2
ZNF251	2
ZNF256	1
ZNF26	1
ZNF260	3
ZNF263	4
ZNF266	4
ZNF268	6
ZNF271P	3
ZNF273	1
ZNF276	3
ZNF280D	1
ZNF281	6
ZNF282	3
ZNF283	1
ZNF284	4
ZNF285	2
ZNF287	2
ZNF295-AS1	1
ZNF3	3
ZNF302	3
ZNF304	3
ZNF316	1
ZNF317	5
ZNF318	2
ZNF320	4
ZNF322	2
ZNF324B	2
ZNF32-AS1	1
ZNF331	2
ZNF333	2
ZNF334	3
ZNF337	2
ZNF35	6
ZNF350	5
ZNF350-AS1	3
ZNF354A	1
ZNF354C	2
ZNF37A	6
ZNF37BP	3
ZNF382	3
ZNF385C	1
ZNF391	1
ZNF394	2
ZNF396	1
ZNF397	6
ZNF398	1
ZNF407	7
ZNF41	4
ZNF410	1
ZNF415	2
ZNF416	2
ZNF417	4
ZNF418	3
ZNF426	2
ZNF428	1
ZNF429	1
ZNF43	1
ZNF431	5
ZNF432	7
ZNF436	3
ZNF439	7
ZNF44	2
ZNF441	3
ZNF443	1
ZNF446	3
ZNF449	1
ZNF451	2
ZNF451-AS1	5
ZNF454	2

ZNF460	4	ZNF561	3	ZNF660-ZNF197	1	ZNF780B	2
ZNF461	1	ZNF562	1	ZNF662	1	ZNF781	2
ZNF462	4	ZNF564	10	ZNF664	6	ZNF783	1
ZNF469	1	ZNF565	3	ZNF667	2	ZNF786	1
ZNF470	3	ZNF566	1	ZNF669	1	ZNF790	1
ZNF471	2	ZNF567	1	ZNF672	1	ZNF791	3
ZNF48	2	ZNF57	1	ZNF675	1	ZNF8	2
ZNF480	3	ZNF570	1	ZNF680	2	ZNF800	2
ZNF483	2	ZNF571-AS1	1	ZNF681	2	ZNF805	4
ZNF484	4	ZNF572	1	ZNF682	2	ZNF808	1
ZNF487	1	ZNF576	1	ZNF687	4	ZNF81	4
ZNF488	3	ZNF577	2	ZNF688	2	ZNF813	1
ZNF491	1	ZNF579	1	ZNF689	2	ZNF816-ZNF321P	1
ZNF493	6	ZNF581	1	ZNF691	1	ZNF818P	1
ZNF496	2	ZNF583	2	ZNF692	1	ZNF827	1
ZNF500	2	ZNF584	2	ZNF696	2	ZNF83	2
ZNF501	2	ZNF585A	7	ZNF697	1	ZNF830	2
ZNF503-AS2	1	ZNF594	2	ZNF699	1	ZNF839	2
ZNF507	4	ZNF595	3	ZNF70	1	ZNF84	3
ZNF510	2	ZNF596	3	ZNF701	6	ZNF841	1
ZNF513	4	ZNF597	2	ZNF704	3	ZNF844	4
ZNF514	3	ZNF600	1	ZNF708	3	ZNF846	1
ZNF518A	7	ZNF605	1	ZNF709	4	ZNF847P	1
ZNF518B	6	ZNF606	1	ZNF711	3	ZNF85	1
ZNF521	2	ZNF607	2	ZNF714	3	ZNF852	1
ZNF525	1	ZNF608	5	ZNF718	3	ZNF853	3
ZNF526	1	ZNF609	1	ZNF720	1	ZNF862	1
ZNF527	3	ZNF610	1	ZNF727	1	ZNF865	1
ZNF528-AS1	3	ZNF614	3	ZNF736	2	ZNF880	3
ZNF532	5	ZNF615	4	ZNF74	1	ZNF883	1
ZNF534	6	ZNF619	1	ZNF747	4	ZNF891	4
ZNF536	3	ZNF621	5	ZNF75A	1	ZNF91	3
ZNF540	1	ZNF622	3	ZNF75D	2	ZNF93	3
ZNF543	1	ZNF623	2	ZNF761	2	ZNHIT2	1
ZNF544	1	ZNF624	2	ZNF763	5	ZRANB1	2
ZNF546	2	ZNF626	1	ZNF764	1	ZSCAN12	3
ZNF547	1	ZNF627	4	ZNF765	2	ZSCAN16	2
ZNF548	1	ZNF629	1	ZNF768	2	ZSCAN18	6
ZNF549	3	ZNF638	2	ZNF770	3	ZSCAN20	4
ZNF551	1	ZNF639	1	ZNF772	3	ZSCAN21	6
ZNF555	6	ZNF641	2	ZNF773	1	ZSCAN25	1
ZNF557	9	ZNF644	7	ZNF774	1	ZSCAN26	1
ZNF558	1	ZNF646	3	ZNF776	6	ZSCAN29	2
ZNF559-ZNF177	2	ZNF648	1	ZNF777	3	ZSCAN31	2
ZNF56	3	ZNF649-AS1	1	ZNF778	4		
		ZNF655	1	ZNF780A	4		

ZSCAN32	2	ZSWIM1	3	ZSWIM9	1	ZYG11B	1
ZSCAN5A	3	ZSWIM6	1	ZXDA	3	ZZZ3	2
ZSCAN9	1	ZSWIM7	1	ZXDB	3		
		ZSWIM8-AS1	2	ZXDC	1		

Appendix 3. Annotation of m^{6}A peaks from foetal tissue.

A1BG	4	ACKR3	1	ADGRB1	1	AGPAT1	1
A2ML1	2	ACOT12	1	ADGRB2	1	AGPAT3	1
A3GALT2	2	ACP6	5	ADGRB3	4	AGPAT4-IT1	6
AADAT	1	ACRBP	1	ADGRG1	1	AGPAT5	1
AAR2	3	ACSF3	1	ADGRG3	2	AGPS	1
AASDH	4	ACSL3	1	ADGRL2	2	AGT	1
AASS	2	ACSL4	1	ADGRL3	1	AGTPBP1	1
AATBC	1	ACTB	2	ADI1	1	AGTRAP	3
AATF	2	ACTL6B	1	ADIG	2	AGXT2	1
ABCA11P	4	ACTN1	1	ADM5	1	AHCTF1	1
ABCA4	1	ACTN1-AS1	3	ADNP	5	AHCYL1	1
ABCB9	1	ACTN4	1	ADNP2	1	AHCYL2	2
ABCC10	1	ACTR2	3	ADO	2	AHDC1	7
ABCC3	2	ACTR5	1	ADORA3	1	AHNAK	9
ABCC5-AS1	2	ACVR1	1	ADPRHL1	1	AHNAK2	1
ABCC6	2	ACVR2A	2	ADPRHL2	2	AHSA1	1
ABCD2	1	ACVR2B	1	ADRA2A	5	AHSA2P	5
ABCF3	1	ACY1	1	ADRA2C	2	AIMP1	1
ABCG4	1	ADAD1	1	ADRB1	1	AIP	1
ABHD13	4	ADAL	6	ADRM1	3	AJAP1	2
ABHD15	2	ADAM22	1	ADSL	2	AJM1	2
ABHD17A	1	ADAM30	4	ADSSL1	2	AJUBA	1
ABHD17B	2	ADAMTS1	1	AEBP2	1	AK2	1
ABHD6	1	ADAMTS13	1	AEN	1	AK5	1
ABHD8	1	ADAMTS15	2	AFAP1-AS1	2	AKAP1	3
ABI2	3	ADAMTSL3	1	AFAP1L1	1	AKAP10	1
ABL1	4	ADAP1	2	AFAP1L2	3	AKAP11	4
ABL2	1	ADAR	3	AFDN	2	AKAP12	6
ABR	1	ADARB1	1	AFDN-DT	2	AKAP13	2
ABRAXAS2	1	ADARB2	1	AFF1	2	AKAP2	8
ABT1	1	ADARB2-AS1	2	AFF2	3	AKAP5	1
ABTB1	2	ADAT1	1	AFF3	2	AKAP6	6
ABTB2	1	ADAT2	1	AFF4	1	AKAP7	1
ACACA	1	ADCK2	1	AFG3L1P	2	AKAP8	5
ACAD11	2	ADCY3	1	AGAP11	1	AKAP8L	2
ACADS	2	ADCY5	3	AGAP2-AS1	4	AKIP1	1
ACAT2	2	ADCY7	1	AGAP3	1	AKIRIN1	1
ACBD3	1	ADCY8	2	AGAP6	3	AKNA	2
ACBD5	1	ADCY9	3	AGER	3	AKR7A2P1	2
ACBD6	1	ADCYAP1R1	3	AGFG2	1	AKT1S1	2
ACD	1	ADD1	3	AGK	3	AKT3	1
ACER2	1	ADD2	6	AGO1	4	AKTIP	1
ACHE	1	ADGRA1	2	AGO2	1	ALCAM	3
ACIN1	3	ADGRA3	1	AGO3	1	ALDH1B1	2

ALDH3A1	2	ANKLE1	1	APLP1	1	ARL17B	3
ALDH3A2	1	ANKLE2	4	APOA1	3	ARL2	1
ALDH4A1	1	ANKRD13D	1	APOD	1	ARL2BP	2
ALG1	1	ANKRD17	2	APOE	1	ARL3	2
ALG12	4	ANKRD28	1	APOL5	2	ARL4A	2
ALKBH1	1	ANKRD33B	6	APOLD1	2	ARL4C	3
ALKBH2	3	ANKRD36	1	APP	1	ARL4D	1
ALKBH4	4	ANKRD39	1	APTR	2	ARL5A	1
ALKBH5	1	ANKRD40	3	AQP12A	2	ARL5B	1
ALMS1	1	ANKRD46	1	AQP4	2	ARL5C	1
ALMS1-IT1	6	ANKRD49	1	ARAP1	1	ARL6IP1	2
ALOX15	2	ANKRD50	7	ARC	3	ARL6IP4	12
ALPK3	5	ANKRD62	2	AREL1	1	ARL8A	2
ALPP	3	ANKRD63	2	ARF3	1	ARMC1	1
ALS2	1	ANKRD9	4	ARF4-AS1	1	ARMC5	6
ALS2CR12	1	ANKS1A	1	ARF6	1	ARMCX1	1
ALX4	1	ANKS1B	4	ARHGAP1	2	ARMCX2	2
AMBP	5	ANKS6	1	ARHGAP12	1	ARMCX3	1
AMBRA1	3	ANKZF1	1	ARHGAP20	3	ARMCX5-GPRASP2	4
AMDHD2	2	ANO10	1	ARHGAP21	3	ARMCX6	1
AMER1	5	ANO8	3	ARHGAP23	5	ARPC4	1
AMER2	1	AOAH-IT1	1	ARHGAP27	1	ARPC5L	1
AMER3	2	AP1G2	3	ARHGAP32	1	ARPP21	1
AMFR	4	AP1M1	2	ARHGAP35	2	ARRDC2	2
AMIGO1	2	AP1S2	1	ARHGAP4	1	ARRDC4	1
AMIGO3	2	AP2B1	2	ARHGAP5	7	ARSD-AS1	1
AMMECR1L	3	AP2M1	3	ARHGAP8	1	ARX	2
AMN	6	AP3M1	1	ARHGDIG	1	ASAH1	1
AMOT	1	AP3M2	2	ARHGEF10	1	ASAH2	2
AMOTL1	1	AP4S1	1	ARHGEF11	2	ASAP1-IT2	1
AMT	4	AP5B1	4	ARHGEF12	2	ASB1	1
AMZ1	3	AP5M1	1	ARHGEF16	2	ASB6	4
AMZ2	3	AP5S1	1	ARHGEF26	1	ASB7	1
AMZ2P1	2	AP5Z1	4	ARHGEF3	2	ASB8	1
ANAPC15	2	APAF1	3	ARHGEF4	1	ASCL1	1
ANAPC2	1	APBA1	2	ARHGEF7	2	ASCL3	1
ANAPC7	1	APBA2	4	ARHGEF7-AS2	1	ASCL5	2
ANGEL1	2	APBB2	4	ARHGEF9	2	ASGR1	2
ANGPT2	1	APBB3	1	ARHGEF9-IT1	1	ASH1L	2
ANGPTL2	1	APC	1	ARID1A	1	ASH1L-AS1	1
ANGPTL4	1	APC2	2	ARID1B	3	ASIC1	1
ANK1	5	APCDD1	2	ARID2	3	ASIC3	1
ANK2	9	APEH	15	ARID5B	3	ASIC4	1
ANK3	13	APEX1	2	ARIH1	2	ASMT	4
ANKH	1	APEX2	1	ARIH2OS	1	ASNA1	1
ANKIB1	1	APH1B	1	ARL14EP	1	ASNSD1	1

ASPDH	1	ATXN7L3B	3	BCAR4	2	BMP6	1
ASPH	2	ATXN8OS	3	BCAS3	1	BMP8A	1
ASPHD1	1	AUNIP	3	BCCIP	1	BMPR1A	1
ASPHD2	5	AUP1	1	BCDIN3D	5	BMPR1B	1
ASRGL1	1	AURKAIP1	1	BCHE	1	BMPR2	1
ASXL1	3	AURKC	3	BCL11B	3	BOD1	1
ASXL2	2	AUTS2	2	BCL2	4	BOD1L1	6
ASXL3	6	AVL9	1	BCL2L1	2	BOLA1	1
ATAD2B	3	AXIN1	1	BCL2L12	1	BOLA3	3
ATF1	1	AXIN2	3	BCL2L13	2	BOLA3-AS1	1
ATF4	2	AZIN1	1	BCL2L14	2	BORCS6	3
ATF6B	1	B3GALNT1	4	BCL2L15	1	BRAP	1
ATF7IP	4	B3GALT1	1	BCL7C	1	BRD1	2
ATG14	4	B3GALT2	2	BCLAF1	1	BRD2	9
ATG16L2	2	B3GALT4	3	BCOR	1	BRD3OS	6
ATIC	1	B3GALT6	3	BCORL1	3	BRD4	3
ATMIN	1	B3GAT1	4	BCR	3	BRD8	1
ATOH1	2	B3GAT2	4	BCRP3	1	BRD9	1
ATOH8	1	B3GLCT	1	BCS1L	1	BRF1	2
ATP10A	1	B3GNT2	1	BDKRB1	1	BRF2	2
ATP11C	1	B3GNT4	4	BDNF	1	BRICD5	1
ATP1A1-AS1	1	B3GNT5	2	BECN1	1	BRINP1	2
ATP1A3	1	B3GNT9	1	BEGAIN	1	BRINP3	2
ATP1A4	2	B4GALNT4	2	BEND4	2	BRMS1	1
ATP1B1	2	B4GALT2	2	BEND5	1	BRPF1	2
ATP1B2	1	B4GALT7	1	BEX3	1	BRPF3	3
ATP1B3	2	B4GAT1	1	BEX5	1	BRWD1	1
ATP2B1	1	BAALC	1	BFSP1	2	BSCL2	1
ATP2B4	1	BAAT	1	BFSP2	1	BSN-DT	5
ATP2C2-AS1	1	BACE1	1	BHLHA15	12	BSX	1
ATP6AP1L	1	BACE1-AS	1	BHLHB9	1	BTBD17	2
ATP6V0A4	4	BAG1	1	BHLHE40-AS1	2	BTBD2	2
ATP6V0C	6	BAG5	2	BICD1	2	BTBD3	3
ATP6V0E2	8	BAG6	1	BICD2	3	BTBD7	2
ATP6V0E2-AS1	4	BAIAP2-DT	5	BICRAL	1	BTBD9-AS1	8
ATP6V1G2	1	BAMBI	3	BIRC2	2	BTD	3
ATP7B	1	BANF1	1	BIRC3	1	BTF3	1
ATP8B2	1	BAP1	2	BIRC6	1	BTG1	2
ATP9A	1	BARHL1	2	BLCAP	2	BTG2	2
ATPAF2	2	BASP1	2	BLOC1S3	3	BTN2A1	2
ATRN	1	BATF3	1	BLOC1S4	3	BTN2A3P	1
ATRNL1	1	BAZ1B	1	BLVRA	1	BUD13	1
ATRX	3	BAZ2A	2	BMF	1	BUD31	3
ATXN1	1	BBS10	1	BMI1	1	BYSL	1
ATXN1L	3	BCAR1	1	BMP2	2	C10orf105	1
ATXN7L3	3	BCAR3	4	BMP3	2	C10orf25	6

C10orf82	4	C1orf131	2	C6orf47	4	CACUL1	1
C10orf88	1	C1orf189	1	C6orf62	3	CACYBP	1
C11orf24	3	C1orf198	2	C7orf25	2	CADM2	2
C11orf42	2	C1orf21	1	C7orf26	1	CADM2-AS2	1
C11orf58	2	C1orf216	2	C7orf33	1	CADM3-AS1	2
C11orf68	1	C1orf226	2	C7orf43	1	CADPS	1
C11orf80	1	C1orf56	2	C8B	4	CALHM2	2
C11orf87	2	C1QB	1	C8orf76	2	CALHM6	1
C11orf91	6	C1QC	1	C8orf82	1	CALM1	2
C11orf94	5	C1QL2	1	C9	1	CALM3	3
C11orf95	4	C1QL3	2	C9orf129	1	CALML4	1
C11orf96	6	C1QL4	2	C9orf131	2	CALN1	1
C12orf49	1	C1QTNF12	1	C9orf147	1	CALY	1
C12orf57	2	C1QTNF9	4	C9orf152	2	CAMK1D	1
C12orf66	2	C1R	2	C9orf153	1	CAMK2B	4
C14orf132	7	C1S	1	C9orf16	2	CAMK2D	1
C14orf28	1	C2	2	C9orf24	3	CAMK2N2	1
C14orf93	1	C20orf144	2	C9orf3	1	CAMLG	1
C15orf59	3	C20orf173	7	C9orf40	1	CAMSAP1	8
C15orf59-AS1	1	C21orf2	4	C9orf43	1	CAMSAP2	1
C16orf72	2	C21orf58	1	C9orf72	4	CAND1	2
C16orf86	3	C22orf23	2	C9orf78	1	CAND1.11	1
C16orf91	1	C22orf24	1	CA10	1	CAND2	1
C16orf92	1	C22orf31	5	CA4	2	CANT1	1
C17orf100	1	C22orf39	1	CAAP1	1	CANX	1
C17orf107	2	C2CD4C	4	CAB39	1	CAPN10	1
C17orf49	1	C2orf16	1	CABP7	4	CAPN11	1
C17orf51	6	C2orf42	1	CACFD1	1	CAPN12	1
C17orf58	6	C2orf68	4	CACNA1A	1	CAPN13	1
C17orf67	2	C2orf72	1	CACNA1B	1	CAPNS1	2
C17orf80	1	C3orf18	2	CACNA1C-AS1	2	CAPRIN2	2
C18orf25	2	C3orf58	3	CACNA1D	1	CAPS	1
C19orf12	2	C3orf62	1	CACNA1E	3	CAPZA2	2
C19orf18	3	C3orf70	2	CACNA1G	2	CARD9	2
C19orf24	2	C3orf80	2	CACNA1G-AS1	1	CARM1	1
C19orf25	6	C4orf19	6	CACNA1H	1	CARMIL2	1
C19orf44	3	C4orf51	2	CACNA1I	3	CASC10	1
C19orf47	1	C5orf22	1	CACNB3	3	CASC15	1
C19orf53	2	C5orf24	2	CACNB4	1	CASC4	1
C19orf54	1	C5orf30	1	CACNG1	6	CASKIN1	10
C19orf57	3	C5orf49	1	CACNG3	2	CASTOR1	1
C19orf66	1	C5orf64	1	CACNG6	2	CASZ1	1
C19orf71	3	C6orf118	1	CACNG7	1	CATSPER2	1
C19orf81	3	C6orf120	2	CACNG8	1	CAVIN2	1
C1orf115	7	C6orf201	1	CACTIN	3	CAVIN4	2
C1orf123	2	C6orf203	2	CACTIN-AS1	4	CBARP	3

CBFB	1	CCDC88C	1	CDC42EP2	2	CEBPB-AS1	2
CBLN1	1	CCDC90B	4	CDC42EP3	1	CEBPD	2
CBLN2	2	CCDC92	5	CDC42EP4	2	CEBPG	1
CBR1	1	CCDC93	1	CDC42SE2	1	CEBPZ	2
CBR4	1	CCDC96	5	CDC6	2	CEL	1
CBS	1	CCDC97	1	CDC7	1	CELF1	2
CBX1	1	CCK	2	CDC73	1	CELF2-AS1	2
CBX2	3	CCKAR	1	CDCA7L	1	CELF3	1
CBX4	2	CCKBR	1	CDCP2	1	CELF5	1
CBX6	3	CCL19	1	CDH1	1	CELP	2
CBX8	3	CCM2L	1	CDH10	2	CELSR2	2
CC2D2B	2	CCNB2	3	CDH11	2	CELSR3	5
CCAR1	1	CCND2	1	CDH2	2	CEMIP	1
CCAR2	4	CCND3	1	CDH20	2	CEMIP2	2
CCDC107	2	CCNI	2	CDH24	3	CEMP1	1
CCDC115	1	CCNK	1	CDH6	2	CEND1	1
CCDC124	2	CCNL1	1	CDH8	3	CENPA	1
CCDC127	2	CCNL2	2	CDIPT	2	CENPB	1
CCDC136	2	CCNQ	1	CDIPTOSP	1	CENPI	1
CCDC137	1	CCNT2	3	CDK11B	5	CENPO	5
CCDC138	1	CCNYL1	1	CDK12	4	CENPX	1
CCDC144CP	1	CCP110	1	CDK13	4	CEP164	2
CCDC149	2	CCSER1	2	CDK20	1	CEP170	1
CCDC151	5	CCSER2	4	CDK2AP1	1	CEP170B	2
CCDC154	2	CD101	2	CDK3	2	CEP192	3
CCDC162P	1	CD14	1	CDK5R1	4	CEP250	1
CCDC17	1	CD180	4	CDK5R2	3	CEP350	3
CCDC177	3	CD200	1	CDK5RAP1	1	CEP68	5
CCDC184	2	CD226	1	CDK5RAP2	3	CERK	1
CCDC32	1	CD276	1	CDK7	1	CERS1	6
CCDC34	1	CD2BP2	4	CDK8	2	CERS2	5
CCDC40	2	CD320	2	CDK9	4	CERS6	1
CCDC43	1	CD34	5	CDKL2	1	CERS6-AS1	1
CCDC57	2	CD40	1	CDKN1B	1	CES2	2
CCDC70	1	CD58	4	CDKN1C	3	CES4A	2
CCDC71	2	CD81	1	CDKN2D	1	CETN2	1
CCDC71L	4	CD83	1	CDR1	2	CFAP298	1
CCDC77	1	CD8A	2	CDR2	1	CFAP53	2
CCDC8	3	CD93	3	CDRT1	1	CFAP97	2
CCDC80	2	CDAN1	6	CDRT3	1	CFDP1	1
CCDC81	1	CDC16	1	CDS1	2	CFL1	2
CCDC83	1	CDC25C	2	CDS2	2	CFLAR	2
CCDC85A	1	CDC27	1	CDV3	4	CFLAR-AS1	1
CCDC85B	2	CDC42BPA	1	CEACAM19	2	CFP	2
CCDC85C	2	CDC42BPB	1	CEBPA	2	CGGBP1	2
CCDC88A	1	CDC42BPG	1	CEBPB	1	CGREF1	1

CHAC1	1	CHST3	2	CLPB	1	COL4A2-AS1	1
CHADL	3	CHST5	3	CLPTM1	1	COL4A2-AS2	1
CHAF1A	3	CHST7	3	CLPTM1L	1	COL6A1	1
CHAMP1	2	CHSY1	5	CLSTN3	2	COL9A2	5
CHCHD1	1	CHSY3	2	CLTA	1	COL9A3	3
CHCHD5	2	CIAO1	1	CLTC	1	COLGALT1	6
CHD3	1	CIB1	10	CLTCL1	1	COLGALT2	3
CHD4	1	CIC	5	CLUAP1	1	COMMD10	1
CHD5	1	CINP	1	CLVS1	1	COMMD5	3
CHD6	1	CIP2A	1	CLVS2	1	COMMD8	1
CHD7	5	CIPC	2	CMTM1	1	COMP	2
CHD8	1	CISD3	2	CMTM4	2	COPS2	1
CHD9	2	CITED2	2	CMTR2	1	COPS7B	1
CHDH	1	CIZ1	2	CNDP1	2	COPS9	1
CHERP	2	CKAP2	1	CNFN	3	COQ10A	1
CHGA	2	CKAP4	3	CNIH3	2	COQ3	1
CHGB	2	CKM	1	CNKSR2	1	COQ8A	2
CHKA	4	CKMT2	4	CNN3	1	CORO2B	1
CHKB-CPT1B	2	CLBA1	1	CNNM2	1	CORO6	8
CHL1	3	CLCC1	2	CNNM3	1	COTL1	1
CHL1-AS1	1	CLCN3	2	CNNM3-DT	1	COX14	2
CHL1-AS2	1	CLCN4	2	CNNM4	1	COX16	2
CHML	3	CLCN6	1	CNOT3	1	COX18	2
CHMP1B	2	CLDN12	1	CNOT7	3	COX19	2
CHMP4A	1	CLDN20	2	CNOT8	1	COX6A1	2
CHMP6	3	CLDN23	1	CNP	3	COX6B2	1
CHMP7	3	CLDN34	2	CNR1	4	COX7A1	3
CHN2	4	CLDN5	4	CNRIP1	1	COX7A2	2
CHPF	3	CLDND1	2	CNST	1	COX7A2L	2
CHRAC1	2	CLEC14A	1	CNTD2	2	COX7B2	1
CHRM1	3	CLEC16A	1	CNTF	4	CPE	1
CHRM3	2	CLEC19A	1	CNTN2	5	CPEB2	3
CHRM3-AS1	2	CLEC2L	1	CNTN4	1	CPEB3	1
CHRM4	1	CLEC3A	2	CNTNAP1	1	CPEB4	2
CHRM5	3	CLEC3B	1	CNTNAP2	1	CPLANE2	2
CHRNA2	2	CLIC4	1	CNTNAP5	1	CPLX1	1
CHRNA4	6	CLINT1	1	CNTROB	1	CPLX2	2
CHRNB1	2	CLIP1-AS1	2	COA3	1	CPOX	2
CHRNB2	3	CLIP2	1	COA5	3	CPS1-IT1	1
CHST1	3	CLIP3	1	COA7	1	CPSF4	1
CHST10	1	CLK2	1	COG1	3	CPSF4L	2
CHST11	1	CLK3	5	COG7	2	CPSF6	1
CHST12	2	CLMAT3	1	COL11A2	2	CPT1C	1
CHST14	3	CLN5	2	COL16A1	2	CRAMP1	1
CHST15	3	CLNS1A	2	COL1A2	1	CRAT37	2
CHST2	2	CLP1	2	COL21A1	2	CRB1	1

CRB2	1	CTTNBP2	3	DALRD3	3	DDX46	1
CREB3	1	CTU1	1	DAO	1	DDX51	1
CREBBP	2	CTXN1	1	DAP	2	DDX56	1
CREBL2	1	CUEDC1	1	DAPK3	1	DDX6	3
CREG1	1	CUL1	2	DAW1	7	DECR2	1
CRHR1	1	CUL3	1	DAXX	1	DEGS1	3
CRIM1	1	CUL4A	1	DAZAP2	2	DENND2A	1
CRIP2	1	CUL7	1	DBN1	1	DENND3	1
CRIP3	3	CUL9	3	DBNDD1	3	DENND5A	2
CRIPAK	2	CUTALP	2	DBX1	3	DENND5B-AS1	1
CRMP1	4	CUTC	2	DCAF16	2	DEPDC7	1
CRTC1	2	CUX1	1	DCAF4L2	2	DEPP1	1
CRYAB	1	CWC15	1	DCAF5	1	DERL1	3
CRYBB3	1	CWC27	1	DCAKD	1	DEXI	4
CRYGS	1	CWF19L1	1	DCC	1	DFFA	2
CSAD	4	CX3CL1	3	DCHS1	1	DGCR2	1
CSE1L	1	CXCR4	1	DCLK1	1	DGKD	1
CSF1	1	CXCR5	2	DCLK3	1	DGKI	1
CSF1R	2	CXorf36	1	DCLRE1B	3	DGKQ	1
CSGALNACT1	1	CXorf40A	1	DCP2	2	DGKZ	1
CSGALNACT2	2	CXXC1	1	DCTD	6	DHCR24	4
CSNK1A1	1	CXXC4-AS1	2	DCTN5	1	DHRS13	2
CSNK1E	1	CXXC5	4	DCTN6	1	DHRS7	1
CSNK1G1	1	CYB561	6	DCUN1D1	1	DHRS7C	1
CSNK1G2-AS1	2	CYB561D1	1	DCUN1D2	1	DHX34	1
CSNK1G3	1	CYB561D2	1	DCUN1D5	1	DHX36	1
CSPG5	1	CYB5B	1	DCX	2	DHX58	1
CSPP1	1	CYB5D2	5	DDA1	1	DICER1	7
CSRNP1	3	CYBA	1	DDAH1	1	DIDO1	4
CSRNP3	5	CYBC1	2	DDAH2	3	DIO2-AS1	5
CSTB	2	CYCSP52	3	DDC	1	DIP2A	2
CSTF2T	1	CYHR1	1	DDHD1	1	DIP2C	1
CTB-178M22.2	4	CYP17A1	3	DDHD2	3	DIRAS1	3
CTBP2	5	CYP1B1	1	DDIT4	2	DIRAS2	2
CTD-2201I18.1	1	CYP26A1	1	DDN-AS1	8	DISP2	5
CTDP1	2	CYP2D7	1	DDR1	1	DISP3	4
CTDSP2	1	CYP2T1P	3	DDX11L16	1	DIXDC1	2
CTGF	1	CYP46A1	2	DDX11L5	1	DKFZP586I1420	2
CTNNA1	6	CYP51A1	4	DDX19A	6	DKK3	5
CTNNB1	1	CYREN	4	DDX23	3	DLAT	1
CTNND1	4	CYTH2	3	DDX24	3	DLC1	3
CTSB	1	D2HGDH	4	DDX31	5	DLG1-AS1	1
CTSH	1	DAB2IP	6	DDX3X	1	DLG2	1
CTSL	1	DACT1	2	DDX3Y	1	DLG3	1
CTSZ	3	DACT3	2	DDX41	4	DLG3-AS1	3
CTTN	7	DAGLB	2	DDX42	1	DLG4	1

DLG5	3	DNMT3A	2	DUSP16	1	EFNB2	3
DLG5-AS1	1	DNPH1	1	DUSP18	3	EFNB3	3
DLGAP2-AS1	1	DNTTIP1	1	DUSP26	1	EFS	1
DLGAP3	2	DOCK4	1	DUSP3	1	EGFLAM	1
DLGAP4	2	DOCK4-AS1	1	DUSP4	2	EGFR-AS1	2
DLL3	1	DOCK9	1	DUSP6	1	EGLN1	2
DLX1	5	DOCK9-AS1	1	DUSP7	3	EGLN2	5
DLX2	1	DOHH	1	DUSP8	1	EGR1	1
DLX6	5	DOK4	1	DUT	1	EGR3	1
DMAC1	1	DOLPP1	2	DVL1	1	EHBP1	2
DMAP1	3	DOPEY1	1	DVL2	2	EHBP1L1	1
DMBT1	2	DOPEY2	1	DYNC1H1	4	EHD2	1
DMPK	4	DPF1	3	DYNC1LI2	1	EID1	3
DMRTA2	1	DPH2	1	DYNLL1	2	EID2	3
DMXL2	1	DPH3P1	2	DYNLL2	4	EID2B	1
DNAAF2	3	DPH7	1	DYRK1A	3	EIF1AD	1
DNAAF4	3	DPM2	1	DYRK2	1	EIF2A	1
DNAH11	1	DPP10	1	DYRK3	3	EIF2AK1	1
DNAH9	1	DPP3	2	DYSF	3	EIF2AK4	1
DNAJA1	1	DPP6	1	DZIP1	2	EIF2S1	1
DNAJA2	2	DPP7	2	E2F5	1	EIF2S2	2
DNAJA4	1	DPYSL2	3	EAPP	1	EIF2S3	1
DNAJB1	2	DPYSL3	1	EBAG9	1	EIF3D	2
DNAJB12	2	DPYSL4	3	EBI3	1	EIF3G	2
DNAJB13	1	DQX1	1	EBLN2	2	EIF3I	1
DNAJB2	3	DRAP1	1	EBP	1	EIF3J	2
DNAJB4	1	DRAXIN	1	EBPL	1	EIF3J-DT	1
DNAJB5	4	DRD1	2	EDEM3	2	EIF4B	1
DNAJB5-DT	3	DRD4	1	EDF1	2	EIF4E2	3
DNAJB6	2	DRD5	1	EDN1	2	EIF4E3	3
DNAJB8-AS1	1	DRG1	1	EDN2	5	EIF4EBP1	2
DNAJC13	1	DSE	2	EDNRB	1	EIF4EBP3	1
DNAJC17	1	DSN1	10	EED	1	EIF4G1	1
DNAJC18	1	DST	11	EEF1A2	1	EIF4G3	2
DNAJC30	2	DSTYK	3	EEF1D	2	EIF5A	1
DNAJC3-DT	1	DTL	1	EEPD1	2	ELAC2	2
DNAJC6	1	DTNB	1	EFCAB10	2	ELAVL3	1
DNAJC9-AS1	3	DTNBP1	2	EFCAB14	1	ELAVL4	1
DNASE1	1	DTX1	2	EFCAB6	2	ELF2	1
DNASE1L2	1	DTX2	1	EFCAB6-AS1	1	ELFN1-AS1	5
DNASE2	1	DTX3	1	EFHC1	3	ELK3	1
DND1	2	DTX4	2	EFHD1	2	ELK4	3
DNER	2	DTYMK	2	EFHD2	1	ELOA	1
DNLZ	2	DUS2	1	EFL1P1	1	ELOB	3
DNM1L	1	DUSP1	2	EFNA2	1	ELOVL4	1
DNM2	1	DUSP14	5	EFNB1	2	ELP3	1

ELP6	1	EPS15	1	FA2H	1	FAM192A	1
EMC4	2	EPS8L1	2	FAAP24	1	FAM193B	1
EMC6	1	EQTN	1	FABP3	1	FAM196A	3
EME1	1	ERAS	1	FABP5	1	FAM198A	1
EME2	2	ERC1	2	FADD	3	FAM198B-AS1	1
EMG1	2	ERCC4	1	FADS2	1	FAM19A1	1
EMID1	1	ERCC5	4	FADS3	1	FAM19A2	4
EMILIN1	1	ERF	2	FAHD1	2	FAM200A	2
EMILIN3	4	ERH	2	FAIM	1	FAM208A	3
EML4	1	ERICH1	1	FAM102A	1	FAM20B	1
EML6	2	ERICH3-AS1	2	FAM102B	1	FAM20C	3
EMSY	2	ERLNC1	1	FAM107A	2	FAM213A	2
EMX1	5	ERMP1	1	FAM110A	2	FAM213B	1
EMX2OS	1	ERO1A	1	FAM110C	2	FAM214A	1
ENDOG	6	ERP29	1	FAM110D	1	FAM214B	2
ENGASE	2	ERRFI1	1	FAM117B	1	FAM217B	2
ENKD1	1	ERVFRD-1	2	FAM120AOS	1	FAM220A	2
ENO2	1	ERVK3-1	6	FAM120B	1	FAM222A	1
ENOPH1	2	ESYT3	5	FAM120C	1	FAM222A-AS1	1
ENPP4	1	ETF1	1	FAM122A	2	FAM237A	2
ENSA	3	ETNK1	1	FAM124A	3	FAM24A	1
ENTPD6	1	ETS1	1	FAM124B	2	FAM25E	1
EP300	1	ETS2	1	FAM126A	1	FAM25G	3
EP300-AS1	3	ETV5	1	FAM131A	2	FAM32A	1
EP400	3	EVA1B	2	FAM131B	3	FAM3A	1
EP400P1	2	EVI2A	1	FAM133B	1	FAM43A	1
EPAS1	3	EVL	2	FAM13A-AS1	3	FAM43B	1
EPB41	1	EXO5	3	FAM155A	1	FAM49A	1
EPB41L3	1	EXOC3	1	FAM155B	1	FAM50B	3
EPC1	2	EXOC3-AS1	3	FAM160A2	1	FAM53A	1
EPC2	4	EXOC5	1	FAM160B1	1	FAM53B	1
EPDR1	1	EXOC6B	1	FAM160B2	1	FAM53B-AS1	2
EPHA4	3	EXOC8	6	FAM163B	1	FAM57A	1
EPHA5	2	EXOG	2	FAM166B	2	FAM57B	1
EPHA6	3	EXOSC3	1	FAM167A	1	FAM66C	3
EPHA7	3	EXOSC4	2	FAM168B	6	FAM69C	1
EPHA8	6	EXOSC6	2	FAM171A2	2	FAM71E1	2
EPHB1	3	EXT1	5	FAM171B	1	FAM74A1	1
EPHB3	1	EXT2	1	FAM173A	1	FAM78A	1
EPHB6	2	EXTL1	2	FAM174A	1	FAM83G	2
EPHX3	2	EXTL3	3	FAM174B	2	FAM84B	3
EPM2AIP1	3	F11R	2	FAM180B	1	FAM85A	1
EPN1	1	F2R	4	FAM181B	2	FAM86B2	1
EPN2-IT1	1	F2RL3	3	FAM183BP	2	FAM86C1	1
EPOP	1	F3	1	FAM187A	12	FAM89B	4
EPPK1	9	F7	4	FAM189A2	1	FAM8A1	5

FAM90A1	4	FBXW5	2	FKBP1B	1	FRAT2	2
FAM92B	5	FBXW7	3	FKBP2	2	FREM2	1
FAM95C	2	FBXW7-AS1	1	FKBP8	1	FRMD3	1
FANCB	1	FBXW8	1	FKBP9	1	FRMD4A	2
FANCE	3	FCF1P2	6	FLAD1	1	FRMD4B	1
FANCF	2	FCGR3A	1	FLJ20021	1	FRMD5	1
FANCL	2	FCHO2	1	FLJ23867	2	FRMPD1	1
FARSA-AS1	1	FCHSD1	1	FLJ30901	7	FRS3	2
FASN	4	FDFT1	1	FLJ31356	2	FRZB	1
FASTK	2	FDPS	1	FLJ42102	1	FSD1L	1
FASTKD1	2	FEM1A	13	FLJ45513	1	FSTL3	1
FASTKD5	1	FEM1B	2	FLNB-AS1	1	FTCD-AS1	1
FAT1	4	FEM1C	2	FLNC	1	FTH1	1
FAT3	2	FEN1	3	FLOT2	2	FTL	1
FAT4	2	FERMT2	1	FLRT1	5	FTO	1
FBH1	5	FERMT3	1	FLRT2	6	FTSJ1	1
FBLL1	2	FES	2	FLT1	2	FUBP3	1
FBLN2	1	FEZ2	3	FLT3LG	1	FUNDC1	1
FBRS	3	FEZF2	2	FLVCR1	2	FUS	1
FBXL12	1	FGD1	1	FLYWCH1	2	FUT11	8
FBXL14	1	FGD3	1	FMN1	3	FUT4	5
FBXL17	2	FGD4	1	FMN2	3	FUT8-AS1	2
FBXL19	2	FGD5	3	FMNL2	1	FUT9	1
FBXL19-AS1	1	FGD5-AS1	2	FMNL3	1	FXR2	1
FBXL20	3	FGF11	1	FMR1	1	FXYD6	1
FBXL22	3	FGF12	3	FNDC3A	1	FYN	2
FBXL3	2	FGF12-AS1	1	FNDC5	3	FZD1	3
FBXL4	1	FGF13	1	FNDC9	1	FZD2	1
FBXL7	1	FGF14	2	FNIP2	2	FZD7	1
FBXO10	2	FGF7	2	FNTA	1	FZD8	1
FBXO11	1	FGF9	1	FOS	3	FZD9	4
FBXO22	1	FGFBP2	1	FOSL2	2	G6PC3	1
FBXO25	1	FGFBP3	3	FOXC1	2	GAB1	1
FBXO3	1	FGFR1OP2	1	FOXF1	1	GABARAP	1
FBXO30	3	FGFR3	2	FOXG1	2	GABBR1	2
FBXO32	2	FGFR4	1	FOXG1-AS1	2	GABPB1	2
FBXO33	1	FHL1	1	FOXH1	2	GABPB1-AS1	1
FBXO38	1	FIBIN	2	FOXI3	1	GABPB2	2
FBXO4	1	FICD	2	FOXJ1	3	GABRA5	1
FBXO41	1	FIGN	1	FOXJ2	3	GABRB2	1
FBXO45	1	FIGNL2	4	FOXJ3	1	GABRB3	3
FBXO46	3	FITM2	2	FOXN2	2	GABRG1	1
FBXO7	1	FIZ1	2	FOXN3	4	GABRG2	1
FBXW10	1	FJX1	4	FOXO3	1	GABRG3	1
FBXW11	2	FKBP10	1	FOXP4	1	GABRG3-AS1	1
FBXW2	1	FKBP11	2	FRAT1	4	GABRP	2

GADD45A	2	GET4	1	GNAO1	2	GPR61	2
GADD45B	2	GFAP	2	GNAS	1	GPR62	2
GADD45G	1	GFER	3	GNAT1	1	GPR63	2
GAL3ST1	1	GFM2	1	GNAZ	2	GPR68	4
GAL3ST3	1	GFOD1	1	GNB2	1	GPR75	1
GAL3ST4	1	GFRA2	2	GNB3	1	GPR75-ASB3	1
GALNT10	1	GFRA4	5	GNE	1	GPR85	1
GALNT11	7	GFY	1	GNL1	3	GPR88	1
GALNT15	1	GGA2	2	GNPAT	6	GPRASP1	3
GALNT17	4	GGA3	3	GNRHR	1	GPRC5B	5
GALNT18	1	GGNBP2	1	GOLGA3	1	GPRIN1	4
GALNT2	1	GGT1	1	GOLGA5	1	GPRIN2	2
GANAB	3	GHET1	1	GOLGA7B	4	GPRIN3	7
GAP43	1	GHRLOS	4	GOLIM4	2	GPS2	3
GAPVD1	1	GIMAP5	2	GOLM1	1	GPSM3	1
GAREM2	4	GIMAP6	1	GOLPH3	10	GPT	2
GARNL3	1	GINS1	3	GOLT1A	2	GPX2	4
GARS	1	GINS2	2	GON7	1	GPX3	1
GAS1	1	GJA1	1	GOSR1	1	GRAMD1B	2
GAS2L1P2	1	GJA10	7	GOT1	2	GRAMD2A	1
GAS2L3	1	GJC1	4	GP1BB	3	GRAMD4	2
GAS5	3	GJD3	1	GPANK1	1	GRASP	4
GATA3-AS1	1	GJD4	1	GPAT2	3	GRB10	2
GATAD2A	1	GLB1L2	1	GPATCH3	1	GREM2	3
GATM	1	GLB1L3	1	GPBAR1	1	GRHPR	4
GBA2	1	GLDC	1	GPBP1	2	GRIA1	1
GBAT2	2	GLDN	2	GPI	1	GRIA2	2
GBX1	1	GLG1	1	GPM6A	1	GRIA4	2
GBX2	3	GLIS3	2	GPN2	1	GRID1-AS1	2
GCA	4	GLMN	3	GPR12	4	GRID2	1
GCC1	2	GLOD4	4	GPR135	9	GRIK2	1
GCK	1	GLRX5	2	GPR143	1	GRIK3	5
GCNA	1	GLS	2	GPR146	2	GRIN2A	2
GCNT2	1	GLUD1	1	GPR151	2	GRIN2B	1
GDF10	1	GLUD1P3	2	GPR158	2	GRIN2C	1
GDF11	5	GLUL	2	GPR160	1	GRIN3A	2
GDF2	1	GLYR1	1	GPR161	5	GRIN3B	2
GDF7	1	GMCL1	1	GPR162	1	GRIP2	2
GDI1	1	GMPPB	1	GPR176	1	GRK4	1
GDI2	3	GMPR	6	GPR179	2	GRM1	1
GDPD4	1	GNA11	1	GPR19	2	GRM2	4
GDPGP1	1	GNA12	4	GPR25	4	GRM3	3
GEMIN4	3	GNA15	6	GPR26	1	GRM5	1
GEMIN6	1	GNAI1	1	GPR37	3	GRM5-AS1	6
GEMIN7-AS1	1	GNAI3	1	GPR37L1	3	GRM7	1
GEMIN8P4	3	GNAL	3	GPR45	2	GRM7-AS1	2

GRN	1	HCFC1	1	HINT3	1	HOMER1	3
GRPEL2	1	HCG14	1	HIP1R	1	HOMER3	1
GRSF1	2	HCG17	2	HIPK1	1	HP1BP3	1
GRWD1	2	HCG2040054	2	HIPK1-AS1	1	HPCAL4	1
GSDMB	1	HCLS1	1	HIPK2	1	HPF1	2
GSDMC	2	HCN1	3	HIPK3	4	HPS3	1
GSDME	2	HCN3	2	HIRIP3	2	HPS4	3
GSG1L	2	HCN4	4	HIST1H1B	1	HPS6	2
GSK3A	3	HDAC10	2	HIST1H1C	1	HPX	2
GSK3B	1	HDAC6	1	HIST1H1D	1	HR	1
GSPT1	2	HDAC9	1	HIST1H1E	1	HRAS	1
GSPT2	2	HDGFL3	1	HIST1H2BD	1	HRASLS5	1
GTDC1	3	HDHD3	2	HIST1H2BE	4	HRC	1
GTF2A1	3	HEBP2	3	HIST1H4E	1	HRH2	2
GTF2H5	1	HECA	1	HIST2H2BE	2	HRH3	1
GTF2IRD1	1	HECTD1	2	HIST3H2A	1	HRK	1
GTF2IRD1P1	2	HECTD3	1	HIVEP1	4	HS2ST1	1
GTF2IRD2B	1	HECTD4	2	HIVEP2	1	HS3ST1	1
GTF3C5	1	HECW2	2	HK1	1	HS3ST2	2
GTPBP2	2	HELB	1	HK3	1	HS3ST3A1	1
GTPBP6	3	HELLS	1	HLA-A	1	HS3ST4	1
GUCA2A	1	HELQ	1	HLCS	1	HS3ST5	3
GUCY1A1	1	HELZ2	2	HLF	1	HS6ST1	5
GUCY1A2	1	HENMT1	1	HM13-AS1	1	HS6ST3	1
GUCY1B1	1	HEPN1	1	HMBOX1	1	HSD11B1L	2
GUSB	2	HERC1	1	HMBS	1	HSD11B2	1
GVQW3	4	HERPUD1	1	HMCN2	1	HSD17B1	4
GYPC	1	HES1	1	HMGB1	2	HSD17B8	1
GZF1	2	HES3	1	HMGCR	1	HSF5	2
GZMM	1	HES4	1	HMGCS1	3	HSFX4	1
H1F0	2	HES5	1	HMGN3-AS1	1	HSH2D	5
H1FOO	2	HEXB	1	HMGN4	2	HSP90AA1	3
H1FX-AS1	3	HEXIM1	3	HMGXB3	1	HSP90AB1	1
H2AFX	2	HEY1	1	HMGXB4	1	HSP90AB4P	1
H2AFY	2	HGC6.3	2	HMOX2	2	HSPA12A	1
H2AFY2	1	HGFAC	4	HNRNPA0	3	HSPA1A	3
H6PD	4	HGH1	1	HNRNPA1	1	HSPA1B	1
HACE1	1	HGSNAT	2	HNRNPA1L2	2	HSPA2	3
HAGHL	2	HHIPL1	1	HNRNPA2B1	2	HSPA5	1
HAMP	2	HHLA1	3	HNRNPDL	3	HSPA6	3
HAPLN4	6	HIC1	3	HNRNPF	2	HSPA8	1
HAS3	2	HIF1A-AS1	1	HNRNPH1	3	HSPB1	5
HAVCR1P1	1	HIF1A-AS2	1	HNRNPH2	2	HSPB9	1
HBEGF	1	HIF1AN	1	HNRNPM	2	HSPD1	1
HBG1	1	HILPDA	1	HNRNPU	2	HSPH1	1
HBP1	1	HINFP	1	HNRNPUL1	1	HTATSF1	2

HTD2	3	IGSF6	1	INTS6	1	ITPKC	2
HTR1A	2	IGSF8	2	INTS8	1	ITPRIPL2	6
HTR6	2	IGSF9B	1	INTU	1	ITSN1	1
HTR7	4	IKBKE	5	IP6K2	1	IWS1	1
HUNK	1	IKZF4	1	IPO13	2	IZUMO4	3
HYAL2	2	IL10	1	IPO5	1	JADE1	2
HYI	3	IL10RB-DT	2	IPO8	1	JADE2	1
HYKK	1	IL15RA	1	IPO9	4	JAG2	1
HYPK	2	IL16	1	IPPK	2	JAGN1	2
IAH1	1	IL17B	1	IQCA1L	1	JAK1	1
IBA57-DT	1	IL17D	8	IQCG	1	JAKMIP1	1
IBTK	2	IL17F	1	IQCH-AS1	1	JAKMIP2-AS1	3
ICA1L	3	IL20RB	1	IQCJ-SCHIP1-AS1	1	JCAD	2
ICAM2	1	IL21R-AS1	2	IQCK	6	JDP2	1
ICAM3	1	IL34	1	IQSEC1	2	JMJD1C	1
ICE1	2	IL4I1	4	IQSEC2	1	JMJD6	2
ICE2	1	IL6ST	1	IRAK1BP1	1	JMJD7-PLA2G4B	5
ICMT	2	IL7	1	IRF2BP1	3	JMY	1
ID2	2	ILF3	1	IRF2BP2	3	JOSD1	1
ID4	1	ILF3-DT	3	IRF2BPL	4	JPH1	1
IDS	2	IMP3	2	IRF7	3	JPH2	2
IER2	3	IMPAD1	2	IRGQ	6	JPH3	1
IER3	1	IMPDH2	2	IRS1	4	JPH4	1
IER5	1	INA	4	IRS2	3	JPT2	5
IER5L	5	INAFM2	2	ISCA2	1	JRK	4
IFFO1	2	INCENP	1	ISG20L2	2	JRKL	1
IFFO2	1	ING1	1	ISLR2	4	JUN	4
IFIT1	1	ING2	2	ISM2	1	JUNB	2
IFIT5	3	ING4	7	ISOC2	1	JUND	2
IFITM1	1	ING5	1	IST1	2	KANK1	1
IFNAR1	5	INHBA	2	ISY1	1	KANK2	1
IFNGR1	2	INHBA-AS1	2	ISYNA1	2	KANSL1	1
IFNGR2	2	INHBB	1	ITFG2	1	KANSL1L	1
IFNK	1	INIP	1	ITGA1	1	KANSL2	1
IFT20	2	INKA2	4	ITGA2B	7	KAT14	7
IGBP1	1	INO80D	3	ITGA3	1	KAT2A	1
IGF2BP2	1	INPP1	1	ITGA7	1	KAT2B	1
IGFBP2	3	INPP4A	2	ITGAE	3	KAT6B	1
IGFBP3	2	INPP5E	5	ITGB1	1	KAT8	1
IGFBP5	1	INPP5F	2	ITGB1BP2	1	KATNA1	2
IGFLR1	1	INSM1	5	ITGB5	1	KAZN	1
IGHMBP2	2	INSM2	2	ITIH5	1	KBTBD11	8
IGSF11-AS1	1	INSR	1	ITM2B	1	KBTBD2	2
IGSF21	1	INTS11	1	ITM2C	1	KBTBD4	5
IGSF22	1	INTS14	1	ITPKA	1	KBTBD6	2
IGSF3	1	INTS2	3	ITPKB	4	KBTBD7	2

KBTBD8	1	KCNQ4	1	KIAA1217	2	KLHL12	1
KCNA1	2	KCNQ5	2	KIAA1324L	1	KLHL13	1
KCNA2	2	KCNRG	2	KIAA1328	3	KLHL14	1
KCNA3	4	KCNS2	1	KIAA1522	1	KLHL15	1
KCNA4	1	KCNT1	1	KIAA1549	4	KLHL20	1
KCNA5	1	KCNV1	5	KIAA1549L	2	KLHL21	3
KCNA6	8	KCTD1	1	KIAA1551	1	KLHL23	1
KCNAB1	1	KCTD11	2	KIAA1614-AS1	6	KLHL28	1
KCNAB2	1	KCTD12	3	KIAA1656	3	KLHL29	2
KCNAB3	1	KCTD15	4	KIAA1671	2	KLHL32	1
KCNB2	1	KCTD16	3	KIAA2013	4	KLHL34	1
KCNC1	4	KCTD17	1	KIF16B	2	KLHL35	1
KCNC2	5	KCTD21	3	KIF17	1	KLHL36	3
KCNC3	2	KCTD3	3	KIF1BP	1	KLHL4	1
KCNC4	1	KCTD6	2	KIF21B	1	KLHL41	1
KCND1	1	KCTD7	2	KIF26A	6	KLHL42	5
KCND2	3	KDELC1	2	KIF26B	1	KLHL5	1
KCND3	1	KDELR3	1	KIF26B-AS1	5	KLHL8	3
KCNE1	1	KDM2A	3	KIF27	1	KLHL9	3
KCNE4	1	KDM3A	1	KIF2A	1	KMT2A	4
KCNE5	1	KDM3B	4	KIF3B	1	KMT2B	3
KCNF1	3	KDM4A	4	KIF3C	1	KMT2C	1
KCNG1	5	KDM4A-AS1	2	KIF5A	1	KMT2D	2
KCNG2	1	KDM4B	2	KIF5C	1	KMT2E	6
KCNH2	2	KDM5C	1	KIFC2	2	KNDC1	1
KCNH5	3	KDM5D	1	KIRREL3	1	KNSTRN	4
KCNJ1	1	KDM8	1	KIT	1	KPNA4	1
KCNJ11	4	KDR	1	KITLG	1	KPNB1	1
KCNJ12	1	KHDC1L	1	KLC1	2	KRBA1	1
KCNJ14	2	KHK	3	KLC2	1	KRBA2	3
KCNJ2	1	KHNYN	5	KLF10	1	KREMEN2	2
KCNJ3	2	KIAA0040	5	KLF11	2	KRI1	1
KCNJ4	4	KIAA0100	7	KLF13	5	KRIT1	1
KCNJ6	1	KIAA0319	3	KLF15	1	KRTAP5-1	1
KCNJ9	6	KIAA0319L	1	KLF2	1	KYAT3	2
KCNK10	1	KIAA0355	1	KLF4	1	L1CAM	1
KCNK12	1	KIAA0408	10	KLF6	1	L3MBTL1	1
KCNK15-AS1	1	KIAA0513	1	KLF7	1	LAGE3	2
KCNK7	1	KIAA0754	14	KLF8	2	LAMB4	1
KCNK9	6	KIAA0895	5	KLF9	4	LAMC1	1
KCNMA1	1	KIAA0895L	1	KLHDC10	1	LAMC1-AS1	1
KCNMB3	1	KIAA0930	1	KLHDC2	1	LAMP3	1
KCNMB4	4	KIAA1024	3	KLHDC4	2	LAMP5-AS1	1
KCNN1	1	KIAA1107	4	KLHDC8A	2	LAMTOR2	1
KCNN2	1	KIAA1109	2	KLHL1	1	LARGE1	1
KCNQ3	1	KIAA1147	3	KLHL11	4	LARGE2	3

LARP1B	1	LINC00092	2	LINC01158	2	LINC02308	2
LARP4B	1	LINC00159	2	LINC01176	1	LINC02322	1
LARP6	1	LINC00163	1	LINC01195	1	LINC02361	2
LARS2-AS1	1	LINC00222	3	LINC01227	1	LINC02362	1
LAS1L	1	LINC00235	1	LINC01231	1	LINC02387	1
LATS1	3	LINC00260	1	LINC01234	1	LINC02389	5
LBH	1	LINC00294	3	LINC01269	4	LINC02424	1
LBHD1	2	LINC00342	1	LINC01347	4	LINC02495	2
LBR	1	LINC00359	3	LINC01352	1	LINC02517	1
LCOR	2	LINC00367	1	LINC01355	1	LINC02525	1
LDB1	3	LINC00392	2	LINC01433	1	LINC02556	1
LDHD	5	LINC00423	1	LINC01465	2	LINC02575	1
LDLR	2	LINC00445	1	LINC01501	1	LINC02586	4
LDLRAD4	3	LINC00461	4	LINC01529	1	LINC2194	1
LDLRAP1	2	LINC00467	3	LINC01535	2	LINCR-0001	4
LDOC1	3	LINC00476	1	LINC01537	2	LINGO1	2
LEAP2	1	LINC00483	2	LINC01543	1	LIPG	1
LEMD2	3	LINC00511	1	LINC01544	5	LIX1L-AS1	1
LENEP	1	LINC00526	1	LINC01553	1	LMAN1	1
LENG8	1	LINC00528	13	LINC01559	10	LMAN1L	1
LENG8-AS1	1	LINC00575	1	LINC01571	2	LMAN2L	1
LENG9	2	LINC00599	5	LINC01578	1	LMBRD1	2
LEO1	1	LINC00622	3	LINC01585	3	LMBRD2	1
LEPROT	2	LINC00641	1	LINC01637	4	LMNB1	1
LGALS3BP	4	LINC00643	2	LINC01645	2	LMO2	1
LGALS8-AS1	1	LINC00659	3	LINC01671	1	LMO3	2
LGALS9	3	LINC00667	4	LINC01704	1	LMO4	2
LGALSL	1	LINC00676	1	LINC01772	3	LMO7	3
LGI1	2	LINC00685	1	LINC01798	1	LMO7DN	2
LGI4	1	LINC00691	4	LINC01864	1	LMTK2	1
LHFPL2	1	LINC00847	2	LINC01909	2	LNPEP	6
LHFPL4	5	LINC00863	3	LINC01934	1	LNPK	1
LHFPL6	1	LINC00882	1	LINC01963	1	LNX1-AS1	1
LHX2	1	LINC00889	1	LINC01975	2	LOC100128079	4
LHX3	1	LINC00893	2	LINC01979	3	LOC100128253	1
LHX6	2	LINC00920	1	LINC01983	3	LOC100128325	1
LIG3	1	LINC00950	1	LINC01988	3	LOC100128361	4
LIMCH1	1	LINC00960	1	LINC02012	1	LOC100128494	12
LIMD1	1	LINC01006	3	LINC02022	1	LOC100128573	2
LIMD2	4	LINC01007	1	LINC02024	1	LOC100128653	2
LIME1	2	LINC01018	2	LINC02033	4	LOC100128882	1
LIMK1	1	LINC01054	1	LINC02068	1	LOC100129034	3
LIMS2	1	LINC01103	3	LINC02080	1	LOC100129434	3
LIN7B	1	LINC01111	2	LINC02168	1	LOC100129484	1
LINC00051	2	LINC01118	3	LINC02246	5	LOC100129534	3
LINC00052	4	LINC01127	2	LINC02283	2	LOC100129617	2

LOC100129917	1	LOC100506691	3	LOC101928626	1	LOC105369595	2
LOC100129931	4	LOC100506804	1	LOC101928659	3	LOC105370024	4
LOC100130111	1	LOC100507373	7	LOC101928786	1	LOC105370361	2
LOC100130207	4	LOC100507472	2	LOC101928807	5	LOC105370489	4
LOC100130283	3	LOC100507564	3	LOC101929066	1	LOC105370697	1
LOC100130298	1	LOC100652768	2	LOC101929089	1	LOC105370941	2
LOC100130331	1	LOC100996263	1	LOC101929106	1	LOC105370943	1
LOC100130357	1	LOC100996419	4	LOC101929162	1	LOC105371414	12
LOC100130417	2	LOC100996437	1	LOC101929208	2	LOC105371430	1
LOC100130449	2	LOC100996842	1	LOC101929295	3	LOC105371433	1
LOC100130548	1	LOC101926908	1	LOC101929340	2	LOC105371485	3
LOC100130587	4	LOC101927000	2	LOC101929415	1	LOC105371592	1
LOC100130705	1	LOC101927018	1	LOC101929439	1	LOC105371795	2
LOC100130744	1	LOC101927040	2	LOC101929452	1	LOC105371899	2
LOC100131315	1	LOC101927070	3	LOC101929528	3	LOC105371998	1
LOC100131496	1	LOC101927100	2	LOC101929550	1	LOC105372069	1
LOC100132111	1	LOC101927151	1	LOC101929563	1	LOC105372071	2
LOC100132215	2	LOC101927178	1	LOC101929577	1	LOC105372383	1
LOC100132249	1	LOC101927354	1	LOC101929595	3	LOC105372397	1
LOC100192426	1	LOC101927365	1	LOC101929679	5	LOC105373064	5
LOC100286925	1	LOC101927418	1	LOC101929882	1	LOC105373100	2
LOC100287015	1	LOC101927472	2	LOC101929901	1	LOC105373156	3
LOC100287837	2	LOC101927550	6	LOC102723692	2	LOC105373185	2
LOC100287944	1	LOC101927572	1	LOC102723703	2	LOC105373378	4
LOC100288123	2	LOC101927583	4	LOC102723704	1	LOC105374727	2
LOC100288175	3	LOC101927752	5	LOC102723729	2	LOC105374952	2
LOC100288254	6	LOC101927811	1	LOC102723809	1	LOC105375218	1
LOC100289333	1	LOC101927815	2	LOC102723885	1	LOC105375843	7
LOC100289511	3	LOC101927854	1	LOC102724009	3	LOC105376480	2
LOC100291105	1	LOC101927895	1	LOC102724034	1	LOC105376736	1
LOC100505635	2	LOC101927914	1	LOC102724152	2	LOC105377146	1
LOC100505715	3	LOC101927954	1	LOC102724163	1	LOC105377372	3
LOC100505795	2	LOC101927972	1	LOC102724323	2	LOC105378047	1
LOC100505912	2	LOC101927974	1	LOC102724659	2	LOC105378397	1
LOC100505915	1	LOC101927989	5	LOC102724784	2	LOC105378586	3
LOC100505921	1	LOC101928000	2	LOC102724804	1	LOC105379183	1
LOC100506022	1	LOC101928052	2	LOC102724927	1	LOC105379393	2
LOC100506071	3	LOC101928105	1	LOC103021295	1	LOC108783654	3
LOC100506076	1	LOC101928120	1	LOC103171574	6	LOC148413	2
LOC100506083	1	LOC101928140	1	LOC103344931	2	LOC151484	1
LOC100506100	2	LOC101928191	1	LOC104613533	2	LOC153910	11
LOC100506258	1	LOC101928266	1	LOC105369187	1	LOC155060	2
LOC100506271	6	LOC101928323	5	LOC105369340	2	LOC283045	2
LOC100506321	3	LOC101928324	1	LOC105369391	1	LOC284009	1
LOC100506472	2	LOC101928424	2	LOC105369431	7	LOC284454	2
LOC100506548	3	LOC101928525	3	LOC105369509	1	LOC284578	1

LOC285804	1	LPAR1	1	LRRTM1	4	MAML3	2
LOC339666	1	LPAR2	3	LRRTM3	3	MAMSTR	1
LOC340512	1	LPCAT4	1	LRRTM4	1	MAN1A1	1
LOC343052	2	LPL	1	LRSAM1	1	MAN1A2	1
LOC375196	2	LPP-AS1	1	LRTM2	4	MAN1C1	2
LOC400541	4	LRFN1	4	LSAMP	1	MAN2A1	1
LOC400627	2	LRFN3	3	LSM10	1	MAN2A2	1
LOC400684	1	LRFN4	4	LSM11	2	MAN2C1	2
LOC400940	1	LRFN5	2	LSM4	1	MANEAL	3
LOC401463	3	LRG1	2	LSS	1	MANF	2
LOC401478	3	LRIG1	2	LTBP2	1	MANSC1	1
LOC401554	2	LRIG2	1	LTBP4	1	MAOB	1
LOC403312	3	LRIT2	1	LTC4S	3	MAP10	1
LOC440028	2	LRP1	1	LTN1	1	MAP1A	6
LOC440934	2	LRP10	1	LTV1	1	MAP1B	9
LOC441052	1	LRP11	1	LUARIS	2	MAP1LC3A	1
LOC574538	2	LRP1B	1	LXN	1	MAP1LC3B	8
LOC643542	11	LRP3	4	LY6G5C	1	MAP1S	2
LOC643802	4	LRP4-AS1	2	LY6H	1	MAP2	1
LOC644189	1	LRP6	1	LYL1	1	MAP3K1	1
LOC644656	1	LRP8	1	LYNX1	2	MAP3K10	1
LOC646471	3	LRRC10B	3	LYPD1	5	MAP3K11	1
LOC646548	1	LRRC14	3	LYRM1	1	MAP3K12	1
LOC646762	1	LRRC17	1	LYRM2	4	MAP3K13	1
LOC646938	2	LRRC24	6	LYSMD2	1	MAP3K21	2
LOC652276	3	LRRC27	1	LYSMD4	3	MAP3K3	1
LOC653712	1	LRRC3	2	LYVE1	1	MAP3K4	4
LOC653786	1	LRRC37A3	1	LZTS1	4	MAP3K5	1
LOC692247	2	LRRC37B	3	LZTS1-AS1	1	MAP3K9	2
LOC727896	1	LRRC39	1	LZTS2	3	MAP4K2	2
LOC728024	1	LRRC3B	1	MAD1L1	2	MAP4K3	1
LOC728392	1	LRRC4	3	MAD2L1BP	1	MAP4K5	1
LOC728743	5	LRRC41	1	MAD2L2	1	MAP6	1
LOC728989	1	LRRC47	1	MAF	4	MAPK11	1
LOC729603	1	LRRC49	1	MAFB	1	MAPK12	2
LOC729683	7	LRRC4C	6	MAFG	2	MAPK1IP1L	2
LOC729867	4	LRRC55	7	MAGED1	2	MAPK4	1
LOC729968	1	LRRC58	1	MAGEE1	4	MAPK6	1
LOC91450	1	LRRC7	1	MAGEF1	1	MAPK7	3
LOC93622	4	LRRC73	1	MAGEH1	2	MAPK8IP1P2	1
LONP1	1	LRRC8A	1	MAGI1	1	MAPK8IP2	2
LONRF1	1	LRRC8B	4	MAGI1-AS1	2	MAPK8IP3	3
LONRF2	2	LRRC8C	2	MAGI2-AS3	1	MAPKAPK2	1
LOX	1	LRRN1	1	MAGOHB	1	MAPKAPK5	2
LOXHD1	3	LRRN2	3	MALAT1	7	MAPKBP1	5
LOXL2	1	LRRN3	2	MAML1	1	MAPRE2	2

MAPRE3	2	MED19	3	MGAT3	4	MIR124-3	1
MARCH2	1	MED26	2	MGAT4A	1	MIR1244-1	1
MARCH4	2	MED28	1	MGAT4B	2	MIR1244-2	3
MARCH7	1	MED6	1	MGAT5	3	MIR1249	1
MARCH8	1	MED7	1	MGAT5B	1	MIR1256	1
MARCH9	2	MEF2A	1	MGC32805	3	MIR1257	3
MARCKS	2	MEF2C-AS1	1	MGC34796	1	MIR1260A	3
MARCKSL1	1	MEF2C-AS2	1	MGST2	2	MIR1260B	1
MARK2	1	MEIS2	3	MHENCR	1	MIR1262	1
MARK3	1	MEIS3	3	MIA3	1	MIR1268A	1
MARS2	1	MELTF-AS1	1	MIATNB	8	MIR1271	4
MARVELD1	1	MEMO1	1	MIB1	1	MIR1273C	2
MARVELD3	1	MEN1	1	MIB2	3	MIR1273H	3
MASCRNA	7	MEP1B	6	MICAL1	1	MIR1276	1
MAT2A	3	MEPCE	2	MICALL1	2	MIR1277	2
MATR3	2	MESD	2	MICALL2	1	MIR1279	3
MAZ	3	MET	2	MICU3	1	MIR1281	1
MB21D2	1	METRNL	3	MID1	3	MIR128-2	1
MBD2	2	METTL13	2	MID1IP1	1	MIR1286	1
MBD3	1	METTL21EP	2	MID1IP1-AS1	3	MIR1306	2
MBLAC1	1	METTL26	1	MID2	2	MIR1321	1
MBLAC2	1	METTL2B	3	MIDN	2	MIR1343	1
MBNL2	1	METTL3	2	MIEF2	3	MIR137	1
MBP	3	METTL6	1	MIGA1	1	MIR137HG	1
MBTD1	1	METTL7A	2	MIIP	1	MIR140	1
MBTPS1	5	MEX3A	4	MINDY2	1	MIR153-2	2
MC1R	4	MEX3B	5	MINDY3	1	MIR1537	1
MCAT	1	MEX3C	2	MINPP1	1	MIR181A1HG	1
MCF2L2	1	MEX3D	5	MIOS	2	MIR1825	1
MCF2L-AS1	2	MFAP2	1	MIR100HG	2	MIR183	1
MCFD2	2	MFAP3	2	MIR101-2	1	MIR190A	1
MCL1	2	MFAP3L	2	MIR103A2	1	MIR1914	2
MCM3AP	2	MFHAS1	4	MIR103B1	2	MIR1915	2
MCM7	4	MFN2	1	MIR103B2	1	MIR193BHG	3
MCOLN1	1	MFSD10	3	MIR107	2	MIR194-2HG	1
MCPH1	3	MFSD13A	2	MIR1180	1	MIR197	1
MCRS1	1	MFSD14A	2	MIR1181	1	MIR1976	1
MCTP1	1	MFSD14B	1	MIR1184-1	1	MIR2054	9
MDC1-AS1	1	MFSD2B	1	MIR1199	1	MIR223	1
MDFI	2	MFSD4B	4	MIR122	1	MIR2682	1
MDGA1	3	MFSD5	2	MIR1225	1	MIR26A2	1
MDK	3	MFSD6	3	MIR1226	5	MIR2909	4
MDM2	3	MFSD9	1	MIR1227	1	MIR3064	1
MEA1	4	MGA	1	MIR1231	3	MIR3125	1
MED17	1	MGAT1	3	MIR1238	1	MIR3136	2
MED18	1	MGAT2	4	MIR124-2	2	MIR3138	1

MIR3145	6	MIR4281	1	MIR4694	1	MIR5582	1
MIR3154	1	MIR4284	1	MIR4697HG	2	MIR5586	2
MIR3162	1	MIR4288	1	MIR4701	1	MIR563	2
MIR3175	1	MIR4304	1	MIR4704	1	MIR5685	1
MIR3176	2	MIR4315-1	1	MIR4706	2	MIR569	1
MIR3181	1	MIR4319	6	MIR4717	2	MIR5706	1
MIR3183	1	MIR4428	1	MIR4718	5	MIR570HG	1
MIR3186	6	MIR4432HG	2	MIR4720	1	MIR573	1
MIR3187	3	MIR4434	3	MIR4723	2	MIR576	1
MIR3190	2	MIR4440	1	MIR4724	2	MIR5787	1
MIR3196	1	MIR4444-2	2	MIR4728	2	MIR579	2
MIR3199-1	3	MIR4453	1	MIR4737	1	MIR581	1
MIR324	3	MIR4457	1	MIR4742	1	MIR590	2
MIR328	2	MIR4466	1	MIR4749	1	MIR597	1
MIR331	1	MIR4473	2	MIR4755	1	MIR600	4
MIR33A	1	MIR4477B	2	MIR4761	4	MIR600HG	2
MIR3616	2	MIR4489	1	MIR4764	2	MIR602	1
MIR3621	2	MIR4500HG	1	MIR4775	1	MIR612	2
MIR3622A	2	MIR4502	1	MIR4776-2	1	MIR6126	2
MIR3649	3	MIR4505	4	MIR4777	1	MIR6129	3
MIR3652	1	MIR4519	2	MIR4784	1	MIR6132	1
MIR3654	1	MIR451B	1	MIR4793	1	MIR616	1
MIR3655	1	MIR4523	2	MIR4800	1	MIR6165	1
MIR3658	1	MIR4531	2	MIR4804	1	MIR620	3
MIR3661	2	MIR4535	2	MIR486-2	1	MIR626	2
MIR3665	1	MIR4632	1	MIR488	1	MIR629	2
MIR3682	2	MIR4635	1	MIR493	1	MIR634	1
MIR3692	2	MIR4636	2	MIR5001	1	MIR636	1
MIR3714	3	MIR4639	2	MIR5003	2	MIR637	1
MIR378B	4	MIR4640	1	MIR5004	2	MIR6499	1
MIR378D1	9	MIR4644	1	MIR5008	1	MIR6501	6
MIR378H	7	MIR4647	3	MIR5047	1	MIR6506	1
MIR3910-2	1	MIR4648	1	MIR5187	3	MIR6511B1	4
MIR3911	2	MIR4649	1	MIR5193	1	MIR657	2
MIR3913-2	1	MIR4656	1	MIR548A3	3	MIR671	3
MIR3914-1	10	MIR4657	1	MIR548AO	1	MIR6716	5
MIR3916	1	MIR4659B	3	MIR548AU	3	MIR6717	2
MIR3917	1	MIR4664	3	MIR548AV	1	MIR6719	1
MIR3918	2	MIR4665	2	MIR548E	2	MIR6726	1
MIR3922	1	MIR4667	3	MIR548N	2	MIR6727	1
MIR3940	1	MIR4668	1	MIR548P	1	MIR6731	1
MIR3941	1	MIR4675	1	MIR548Q	1	MIR6738	1
MIR4253	1	MIR4677	3	MIR548W	1	MIR6742	6
MIR4254	1	MIR4683	4	MIR555	2	MIR6743	5
MIR4256	2	MIR4687	1	MIR5572	2	MIR6744	2
MIR4279	1	MIR4690	1	MIR558	1	MIR6746	1

MIR6748	1	MIR6867	1	MLLT1	6	MRFAP1L1	3
MIR6752	1	MIR6870	2	MLLT10	1	MRGBP	1
MIR6753	1	MIR6871	7	MLLT11	1	MRI1	1
MIR6757	1	MIR6874	1	MLLT6	1	MRLN	2
MIR6760	2	MIR6880	4	MLX	1	MRM1	1
MIR6763	1	MIR6881	1	MLYCD	3	MRO	2
MIR6764	4	MIR6883	1	MMAA	1	MROH3P	3
MIR6765	2	MIR6886	2	MMAB	2	MRPL12	1
MIR6771	2	MIR6887	1	MMP14	2	MRPL14	1
MIR6773	1	MIR6888	1	MMP15	1	MRPL15	1
MIR6775	3	MIR6895	2	MMP16	3	MRPL16	1
MIR6776	2	MIR7106	1	MMP17	1	MRPL17	1
MIR6777	2	MIR7107	4	MMP23A	1	MRPL19	1
MIR6780A	1	MIR7108	2	MMP23B	1	MRPL27	2
MIR6782	1	MIR7109	2	MMS22L	1	MRPL28	2
MIR6784	4	MIR7114	1	MN1	8	MRPL32	1
MIR6785	1	MIR718	5	MND1	1	MRPL34	1
MIR6787	2	MIR744	1	MNT	2	MRPL35	1
MIR6792	2	MIR762	1	MOAP1	1	MRPL36	1
MIR6795	1	MIR7844	2	MOB2	4	MRPL37	1
MIR6805	1	MIR7848	1	MOB3C	1	MRPL40	1
MIR6806	2	MIR7855	2	MOCS3	2	MRPL41	4
MIR6807	1	MIR8066	1	MOGS	1	MRPL43	3
MIR6808	1	MIR8072	1	MOK	3	MRPL44	2
MIR6816	1	MIR8075	1	MON1B	1	MRPL51	1
MIR6818	5	MIR8089	1	MON2	1	MRPL53	2
MIR6819	1	MIR877	1	MORC2	1	MRPL54	1
MIR6821	1	MIR885	1	MORC2-AS1	1	MRPL58	1
MIR6827	4	MIR887	3	MORC3	2	MRPS10	1
MIR6831	1	MIR9-2	1	MORF4L1	1	MRPS12	1
MIR6832	2	MIR922	3	MORF4L2	3	MRPS16	1
MIR6837	1	MIR935	4	MORN4	1	MRPS17	3
MIR6840	2	MIR937	1	MPEG1	3	MRPS18A	2
MIR6841	2	MIR943	1	MPLKIP	1	MRPS18B	1
MIR6843	3	MIR98	2	MPND	1	MRPS21	1
MIR6845	2	MIRLET7F2	1	MPO	1	MRPS23	3
MIR6847	1	MIRLET7G	1	MPP4	2	MRPS24	4
MIR6848	1	MIS12	1	MPP5	1	MRPS25	2
MIR6851	1	MISP	2	MPRIP	1	MRPS30	1
MIR6853	2	MKNK2	2	MPV17	1	MRPS31	1
MIR6855	5	MKRN2	1	MPV17L2	1	MRTO4	1
MIR6857	2	MKRN3	2	MPZL1	2	MSANTD1	5
MIR6860	1	MLANA	5	MRAP	1	MSANTD3	1
MIR6861	1	MLEC	1	MRAS	1	MSANTD4	3
MIR6862-1	1	MLH1	1	MRC2	2	MSH6	5
MIR6866	3	MLH3	2	MRFAP1	3	MSL1	2

MSL2	4	MYCN	1	NACC2	1	NCKAP5L	5
MSMP	4	MYCNOS	2	NADK	1	NCKIPSD	3
MSRB2	2	MYDGF	1	NADSYN1	1	NCOA3	1
MSS51	1	MYH10	1	NAGK	2	NCOA4	1
MST1R	2	MYL12B	1	NAGLU	1	NCOA5	2
MSTN	1	MYL6	4	NAGPA-AS1	1	NCOA6	2
MSTO2P	1	MYLIP	1	NANOS1	3	NCOA7	2
MT2A	1	MYLK	1	NANOS2	3	NDEL1	5
MT3	1	MYNN	2	NANOS3	1	NDN	3
MTA2	1	MYO15B	3	NAP1L2	2	NDNF	1
MTA3	1	MYO16-AS1	1	NAP1L3	2	NDRG2	4
MTCL1	3	MYO18A	1	NAP1L5	1	NDRG4	1
MTERF2	1	MYO18B	2	NAPG	1	NDST1	2
MTERF4	1	MYO1F	1	NAPRT	3	NDST2	5
MTF1	1	MYO5A	1	NARS2	10	NDST3	3
MTFR1	1	MYO5C	1	NAT10	1	NDUFA1	2
MTFR2	1	MYO6	1	NAT14	1	NDUFA6	1
MTG2	2	MYO7A	2	NAT16	1	NDUFA6-DT	1
MTHFR	2	MYO9A	1	NAT2	2	NDUFAF1	1
MTMR1	4	MYOC	1	NAT8	1	NDUFAF8	2
MTMR11	1	MYOG	1	NAT8L	3	NDUFB2-AS1	1
MTMR2	3	MYORG	4	NATD1	1	NDUFB7	1
MTMR9	1	MYOZ3	2	NAV1	1	NDUFB9	5
MTNR1A	4	MYRF	1	NAV2-AS2	1	NDUFC1	1
MTPAP	1	MYRIP	1	NAV3	2	NDUFS1	1
MTR	2	MYSM1	1	NBAT1	1	NDUFS6	1
MTSS1L	6	MYT1	1	NBEA	2	NDUFV2-AS1	1
MTURN	2	MZF1	3	NBPF1	1	NEAT1	7
MTUS2	4	MZF1-AS1	1	NBPF15	1	NEBL-AS1	1
MTUS2-AS1	2	MZT2A	1	NBPF3	1	NECTIN1	2
MTX1	1	MZT2B	2	NBPF9	2	NECTIN2	1
MUC13	1	N4BP1	4	NCALD	3	NECTIN3	2
MUL1	3	N4BP2L1	1	NCAM1-AS1	5	NEDD4	4
MUM1	3	N4BP2L2	2	NCAM2	1	NEDD4L	1
MUSTN1	2	N4BP3	1	NCAN	4	NEFL	1
MVP	1	N6AMT1	1	NCAPD2	1	NEFM	6
MXD4	2	NAA15	1	NCAPG	1	NEGR1	1
MXRA7	2	NAA20	2	NCBP1	5	NEIL1	3
MYBBP1A	3	NAA30	1	NCBP2-AS1	1	NEK11	1
MYBL1	1	NAA38	2	NCBP2-AS2	2	NEK9	1
MYBPH	4	NAA40	1	NCBP3	1	NELFB	1
MYBPHL	1	NAA50	1	NCDN	1	NELL2	1
MYC	2	NAB1	3	NCF1	1	NEMP2	2
MYCBP2	1	NAB2	3	NCF1C	1	NEO1	2
MYCBP2-AS1	7	NACA	3	NCK1-DT	1	NES	4
MYCL	2	NACAD	5	NCK2	3	NET1	1

NETO1	1	NLGN1-AS1	2	NPTXR	1	NTNG1	2
NETO2	2	NLGN3	3	NPY1R	2	NTNG2	4
NEU1	1	NLGN4Y	1	NR1D1	4	NTPCR	3
NEU3	2	NLGN4Y-AS1	3	NR1D2	2	NTRK1	1
NEURL1-AS1	8	NLRP2	1	NR1H3	1	NTRK2	3
NEURL4	2	NLRX1	1	NR2C2	1	NTRK3	2
NEUROD1	1	NME3	4	NR2E1	2	NTSR1	1
NEUROD2	3	NMNAT2	3	NR2E3	3	NUAK1	4
NEUROD6	1	NMRK2	4	NR2F1	4	NUAK2	1
NEXMIF	1	NMT1	1	NR2F2	3	NUCB1-AS1	1
NFATC2	3	NMT2	3	NR3C1	1	NUDT11	1
NFATC2IP	1	NNMT	1	NR4A2	1	NUDT14	2
NFATC3	1	NNT-AS1	1	NRADDP	2	NUDT16	1
NFATC4	1	NOA1	3	NRARP	3	NUDT18	2
NFE2L1	5	NOC2L	1	NRBF2	1	NUDT19	1
NFIA	1	NOCT	2	NRBP2	5	NUDT2	1
NFIB	4	NOG	1	NRDC	1	NUDT3	1
NFIC	4	NOL4	5	NRDE2	1	NUDT4	4
NFIL3	1	NOL4L	8	NREP	1	NUMBL	2
NFIX	1	NOL7	1	NRG1	3	NUP188	1
NFKBIA	2	NOLC1	1	NRGN	1	NUP210L	1
NFKBIE	1	NOM1	2	NRIP2	1	NUP214	1
NFKBIL1	1	NOP10	1	NRN1	2	NUPL2	1
NFKBIZ	1	NOP14	1	NRON	3	NUTM2B-AS1	1
NFRKB	2	NOP14-AS1	2	NRP2	3	NUTM2F	1
NFU1	2	NOP53	1	NRSN1	2	NWD2	1
NFX1	2	NOS1	1	NRXN1	4	NXF1	2
NGB	1	NOSIP	1	NRXN2	4	NXPE3	3
NGEF	1	NOTCH2	1	NRXN3	5	NXPH1	1
NHLRC1	1	NOV	1	NSD1	4	NXPH2	1
NHLRC2	1	NOVA1	3	NSD2	2	NXPH3	4
NHP2	1	NOXO1	2	NSD3	1	NXT1	1
NIF3L1	3	NOXRED1	1	NSDHL	1	NYAP1	2
NIM1K	4	NPAS1	4	NSG1	3	NYAP2	3
NINJ1	1	NPAS3	2	NSG2	4	NYNRIN	2
NIPA2	3	NPB	1	NSMAF	1	OACYLP	2
NIPBL	2	NPBWR2	1	NSMCE3	2	OARD1	1
NIT1	1	NPEPL1	1	NSUN6	1	OAZ2	7
NIT2	1	NPFFR2	1	NT5C	2	OBSCN-AS1	2
NKAIN1	2	NPIPA5	1	NT5C1A	1	OBSL1	2
NKAIN3	1	NPLOC4	1	NT5C2	4	OCA2	1
NKPD1	2	NPM3	2	NT5DC3	2	OCEL1	1
NKRF	4	NPNT	1	NTAN1	3	OGFOD1	1
NKX6-2	1	NPR2	1	NTF3	2	OGFRL1	1
NKX6-3	3	NPR3	1	NTM-IT	4	OIP5-AS1	3
NLGN1	1	NPTX2	1	NTN4	2	OLFM1	2

OLFM2	2	P2RY11	2	PAXIP1-AS2	1	PCDHB2	8
OLFM3	1	P2RY12	1	PBDC1	1	PCDHB3	2
OLIG1	5	P3H3	1	PBLD	2	PCDHB4	2
OLIG2	2	P4HA3	1	PBOV1	2	PCDHB5	3
OLMALINC	2	PA2G4	1	PBRM1	2	PCDHB6	5
OMG	2	PAAF1	1	PBX1	1	PCDHB7	2
OPA1-AS1	1	PABPC5	1	PBX2	1	PCDHB9	5
OPA3	1	PABPC5-AS1	2	PCBD1	1	PCDHGA1	2
OPCML	1	PABPN1	3	PCBD2	2	PCDHGA10	3
OPHN1	1	PACRGL	2	PCBP1	3	PCDHGA11	5
OPN5	3	PACS1	1	PCBP4	2	PCDHGA12	3
OPRK1	2	PACSIN1	1	PCDH1	6	PCDHGA2	2
OPRL1	1	PAF1	1	PCDH10	4	PCDHGA3	1
OPTN	1	PAFAH1B1	1	PCDH11X	5	PCDHGA4	2
OR13J1	1	PAGR1	1	PCDH11Y	4	PCDHGA5	5
OR1D5	1	PAH	1	PCDH12	2	PCDHGA6	5
OR1F2P	1	PAIP1	1	PCDH17	7	PCDHGA7	3
OR2S2	1	PAIP2	2	PCDH18	2	PCDHGA9	2
OR4B1	1	PAK6	1	PCDH19	5	PCDHGB2	2
OR52I1	1	PALM	1	PCDH20	6	PCDHGB3	3
OR7C2	1	PALM3	2	PCDH7	3	PCDHGB4	2
OR7E47P	2	PAM	1	PCDH8	7	PCDHGB5	3
ORAI1	1	PAN2	1	PCDH9	3	PCDHGB6	4
ORAI2	4	PAN3-AS1	2	PCDHA1	2	PCDHGB7	4
ORAI3	2	PANK2	2	PCDHA10	4	PCDHGC3	3
ORC2	1	PANK4	3	PCDHA11	3	PCDHGC4	2
OSBP	1	PANX1	2	PCDHA12	5	PCDHGC5	26
OSBPL10-AS1	1	PANX2	1	PCDHA13	2	PCED1B	3
OSBPL2	1	PAOX	1	PCDHA2	4	PCF11	3
OST4	1	PAPLN	1	PCDHA3	2	PCIF1	1
OTOP3	1	PAPOLA	2	PCDHA4	5	PCLO	12
OTUB2	1	PAPPA2	1	PCDHA5	6	PCM1	1
OTUD1	2	PAPPA-AS1	1	PCDHA6	3	PCMTD1	1
OTUD3	1	PAQR3	3	PCDHA7	3	PCMTD2	2
OTUD4	3	PAQR4	5	PCDHA8	1	PCNP	1
OTUD5	1	PAQR5	3	PCDHA9	4	PCNT	2
OTULINL	2	PAQR7	1	PCDHAC1	3	PCNX1	2
OXA1L	1	PARD6A	1	PCDHAC2	2	PCNX2	4
OXCT1-AS1	1	PARD6B	1	PCDHB1	28	PCNX3	1
OXER1	2	PARD6G-AS1	6	PCDHB10	3	PCNX4	4
OXLD1	2	PARG	1	PCDHB11	7	PCSK1N	1
OXSM	1	PARP6	3	PCDHB12	7	PCSK2	1
OXSR1	1	PARP8	1	PCDHB13	2	PCSK9	3
P2RX2	1	PASK	1	PCDHB14	7	PCYT2	1
P2RX4	2	PATZ1	1	PCDHB15	4	PDCL	1
P2RY1	1	PAWR	1	PCDHB16	5	PDE12	1

PDE2A	1	PGAM4	1	PIAS2	1	PLCE1	1
PDE3B	2	PGAM5	2	PIAS3	1	PLCE1-AS1	1
PDE4A	2	PGBD1	3	PICALM	1	PLCH1-AS2	1
PDE4D	3	PGBD3	1	PID1	2	PLCL1	4
PDE4DIP	6	PGBD4	2	PIGC	2	PLCL2	1
PDE9A	1	PGBD5	5	PIGM	1	PLCXD2	1
PDF	4	PGD	3	PIGV	1	PLD4	10
PDGFA	1	PGLS	1	PIK3C2A	1	PLD6	6
PDGFB	1	PGM3	3	PIK3CD	3	PLEC	15
PDGFRA	1	PGP	2	PIK3IP1	2	PLEKHA3	1
PDHA1	1	PGPEP1L	4	PIK3R3	1	PLEKHB1	3
PDIA2	3	PGRMC1	1	PIK3R4	1	PLEKHF2	1
PDIA6	2	PGRMC2	3	PIM1	1	PLEKHG1	1
PDIK1L	1	PHACTR3	1	PIM2	1	PLEKHG2	3
PDK1	1	PHACTR4	1	PIMREG	2	PLEKHG3	1
PDK2	1	PHC3	1	PIN1	1	PLEKHG4B	1
PDLIM1	2	PHETA1	4	PIN1P1	1	PLEKHG5	3
PDLIM7	1	PHF10	1	PIN4P1	1	PLEKHH3	1
PDP1	4	PHF12	2	PINK1-AS	2	PLEKHM2	1
PDP2	4	PHF14	2	PIP4K2A	1	PLEKHM3	1
PDXK	4	PHF2	1	PIP4K2B	1	PLEKHO1	1
PDYN-AS1	2	PHF20	1	PIP4K2C	3	PLEKHO2	2
PDZD8	1	PHF20L1	1	PIP4P1	1	PLK1	6
PDZRN3	5	PHF3	4	PIP5K1A	1	PLK2	2
PDZRN4	2	PHF5A	1	PITHD1	1	PLN	1
PEA15	2	PHF8	1	PITPNA	1	PLOD3	1
PEAK3	1	PHKG1	1	PITPNC1	2	PLP1	1
PEBP1	2	PHLDA1	2	PIWIL1	2	PLPP2	1
PEG10	5	PHLDA2	1	PJA1	3	PLPP3	1
PEG3-AS1	7	PHLDB1	1	PJA2	2	PLPP5	1
PELI1	1	PHLDB2	1	PKD2	1	PLPP6	2
PELI2	1	PHLPP1	4	PKD2L2	3	PLPPR1	1
PER2	1	PHLPP2	2	PKDCC	1	PLPPR2	1
PEX1	1	PHOSPHO2	2	PKDREJ	1	PLPPR4	3
PEX10	1	PHOX2A	2	PKIA	1	PLPPR5	1
PEX14	1	PHOX2B	1	PKM	2	PLS3	1
PEX19	2	PHPT1	3	PKP4	1	PLXNA1	5
PEX26	4	PHTF1	2	PKP4-AS1	2	PLXNA2	1
PEX5L-AS2	2	PHTF2	2	PLA2G10	1	PLXNA3	1
PEX6	1	PHYH	2	PLA2G12A	1	PLXNA4	2
PFDN1	1	PHYHD1	4	PLA2G2E	1	PLXNB1	2
PFKFB3	3	PHYHIP	2	PLA2G4F	2	PLXNB2	2
PFKP	1	PHYHIPL	1	PLAGL1	3	PLXNC1	2
PFN1	1	PI16	1	PLCB1	1	PM20D2	2
PGAM1	1	PI4KB	1	PLCB4	1	PMM1	4
PGAM2	1	PIAS1	1	PLCD4	1	PMPCA	1

PMS2P3	3	POU3F3	2	PPP4R3A	2	PRPS2	2
PMVK	3	POU3F4	4	PPP4R3B	3	PRR12	2
PNMA1	3	POU5F1P4	2	PPP5C	1	PRR14L	3
PNMA2	3	PP7080	3	PPP5D1	1	PRR16	1
PNMA3	4	PPCDC	1	PPP6R2	1	PRR19	1
PNMA8A	3	PPDPF	1	PPRC1	2	PRR3	2
PNMA8B	4	PPFIA3	1	PPWD1	1	PRR36	2
PNMT	1	PPIB	2	PQBP1	1	PRR7	1
PNN	2	PPIF	5	PQLC2	2	PRRC1	2
PNOC	2	PPIL2	5	PRAF2	1	PRRC2B	1
PNRC1	1	PPIL6	1	PRAG1	2	PRRC2C	4
POC1B	1	PPM1A	3	PRDM14	2	PRRT2	4
PODXL	4	PPM1B	2	PRDM2	8	PRRT3-AS1	2
POGK	2	PPM1K	2	PRDM4	1	PRRT4	1
POGZ	1	PPM1L	2	PRDM8	3	PRSS23	2
POLG	1	PPM1M	2	PREX1	1	PRSS27	2
POLG2	1	PPOX	1	PRF1	1	PRSS35	1
POLH	1	PPP1CB	1	PRH1-PRR4	1	PRSS53	1
POLI	2	PPP1CC	2	PRICKLE1	9	PSAT1	1
POLL	3	PPP1R12B	3	PRICKLE2-AS3	1	PSD	4
POLR1A	2	PPP1R12C	1	PRICKLE3	1	PSD2	4
POLR1B	2	PPP1R14B	1	PRIMA1	4	PSEN2	1
POLR1D	3	PPP1R14C	2	PRKAB1	1	PSMA7	1
POLR1E	1	PPP1R15A	3	PRKAG1	7	PSMB3	2
POLR2C	1	PPP1R15B	5	PRKAR1A	2	PSMB4	2
POLR2D	5	PPP1R18	3	PRKAR2A	2	PSMC1	1
POLR2E	2	PPP1R1B	1	PRKCA	1	PSMC3IP	1
POLR2G	1	PPP1R26	5	PRKCE	2	PSMC5	3
POLR2M	3	PPP1R27	4	PRKCZ-AS1	2	PSMD1	1
POLR3B	1	PPP1R37	2	PRKD3	1	PSMD13	1
POLR3D	2	PPP1R3C	1	PRKG2	1	PSMD2	1
POLR3GL	1	PPP1R3D	1	PRKXP1	3	PSMD3	2
POLR3H	3	PPP1R3E	1	PRMT2	1	PSMD4	2
POLRMT	2	PPP1R3F	2	PRMT6	3	PSMD6-AS2	1
POM121	1	PPP1R8	1	PRMT7	10	PSMD7	4
POM121C	2	PPP1R9A	3	PRNP	2	PSME2	1
POMC	2	PPP2R1B	3	PROCA1	1	PSMG1	2
POMGNT1	2	PPP2R3A	1	PROKR2	1	PSMG3	1
POMGNT2	1	PPP2R5A	1	PROM1	1	PSPN	1
POMT1	5	PPP2R5B	1	PRORSD1P	2	PSRC1	1
PON1	2	PPP2R5C	1	PROX1	2	PTAR1	1
POP1	1	PPP3CA	1	PRPF18	3	PTCHD1	2
POP7	1	PPP3CC	1	PRPF3	1	PTCHD4	1
POPDC3	1	PPP3R2	1	PRPF38A	2	PTEN	5
POU3F1	2	PPP4C	1	PRPF40A	1	PTENP1	1
POU3F2	1	PPP4R1	3	PRPH2	1	PTGER4	1

PTGFRN	1	PYCARD-AS1	1	RAMP1	1	RBM15	3
PTH2R	1	PYCR1	2	RAN	1	RBM15B	7
PTMA	1	PYGB	3	RANBP1	3	RBM17	1
PTN	1	PYM1	1	RANBP6	3	RBM22	2
PTP4A1	1	PYURF	3	RAP1GAP	1	RBM23	1
PTP4A2	2	QKI	1	RAP2A	1	RBM24	3
PTPDC1	3	QRFP	2	RAP2B	3	RBM26	1
PTPMT1	2	QRICH2	4	RAPGEF1	2	RBM3	1
PTPN1	1	QSER1	3	RAPGEF2	4	RBM4	2
PTPN11	1	QTRT1	5	RAPGEFL1	1	RBM44	1
PTPN12	1	RAB10	1	RAPH1	1	RBM48	1
PTPN18	2	RAB11FIP2	1	RAPSN	1	RBM4B	2
PTPN23	4	RAB11FIP3	1	RARA	3	RBM5	1
PTPN4	1	RAB11FIP4	2	RARRES2	2	RBM5-AS1	1
PTPN5	1	RAB12	1	RARS	1	RBM7	4
PTPN9	1	RAB21	2	RASA1	1	RBMS3	1
PTPRA	1	RAB24	3	RASA2	5	RBMX2	1
PTPRD	4	RAB27B	1	RASA4CP	4	RBP1	3
PTPRF	1	RAB30-AS1	1	RASAL1	2	RBSN	1
PTPRG	2	RAB32	2	RASAL2-AS1	1	RC3H1	2
PTPRG-AS1	1	RAB33A	1	RASD1	5	RCAN1	1
PTPRJ	1	RAB33B	1	RASD2	1	RCC1L	1
PTPRK	1	RAB35	3	RASGEF1B	1	RCC2	3
PTPRM	1	RAB39A	1	RASGEF1C	2	RCE1	1
PTPRO	5	RAB39B	2	RASGRF1	1	RCN1	1
PTPRS	3	RAB3D	1	RASGRP2	1	RCOR2	2
PTPRT	1	RAB40C	2	RASL10A	2	RDH14	1
PTPRZ1	1	RAB43	1	RASL10B	4	RDX	1
PTRH2	1	RAB5A	2	RASL11B	1	REEP2	2
PTX3	1	RAB5IF	2	RASSF10	1	REEP4	1
PURA	2	RAB8A	2	RASSF2	5	RELB	1
PURB	2	RAB9B	1	RAVER2	3	RELT	3
PURG	3	RABAC1	1	RAX2	1	RENBP	1
PUS1	2	RABGEF1	3	RB1CC1	2	REPIN1	3
PUS10	3	RABIF	1	RBAK	1	REPS1	1
PUS3	1	RABL6	1	RBAKDN	1	REPS2	1
PUSL1	1	RAC1	4	RBBP4	1	RETREG1	3
PVRIG	9	RAC3	2	RBBP5	1	RETREG2	2
PWWP2A	4	RAD18	6	RBBP6	1	RETREG3	1
PWWP2B	2	RAD23A	1	RBBP7	1	REV1	3
PXDC1	4	RAD23B	2	RBCK1	1	RFFL	1
PXDN	5	RAD52	6	RBFA	2	RFLNB	7
PXDNL	1	RAD9A	1	RBFOX1	1	RFPL1	4
PXMP4	1	RADIL	1	RBM10	1	RFPL1S	5
PXT1	3	RAI14	1	RBM12B-AS1	4	RFXANK	2
PXYLP1	2	RALBP1	2	RBM14-RBM4	3	RGL1	1

RGL2	1	RNF130	2	RPL13	1	RSL1D1	2
RGL4	4	RNF139	3	RPL13AP17	1	RSPH14	2
RGMA	1	RNF14	1	RPL14	2	RSPRY1	1
RGMB-AS1	2	RNF145	1	RPL15	1	RTL10	1
RGS12	3	RNF146	3	RPL19	1	RTL5	2
RGS16	1	RNF150	1	RPL23AP82	1	RTL6	2
RGS3	2	RNF157-AS1	1	RPL27	2	RTL8A	1
RGS7	1	RNF166	1	RPL29	1	RTL8C	1
RGS8	3	RNF167	1	RPL36	3	RTN1	1
RGS9BP	3	RNF168	2	RPL36AL	1	RTN2	1
RHBDD1	1	RNF169	4	RPL37A	1	RTN3	4
RHBDD3	1	RNF182	1	RPL41	2	RTN4	5
RHOB	4	RNF187	1	RPL6	2	RTN4RL2	2
RHOBTB1	2	RNF19A	2	RPL7	1	RTRAF	4
RHOBTB2	6	RNF19B	1	RPL7L1	1	RUFY3	1
RHOF	3	RNF2	1	RPP21	1	RUNDC3A	2
RHOQ	1	RNF20	1	RPP25	2	RUSC1	3
RHOT2	1	RNF213	1	RPP25L	1	RUSC1-AS1	2
RHOU	2	RNF217	1	RPRD1B	1	RUSC2	2
RHOV	2	RNF217-AS1	2	RPRM	2	RUVBL1-AS1	1
RIC8A	2	RNF223	1	RPRML	4	RXRA	3
RIF1	1	RNF227	2	RPS15	2	RXRB	4
RILPL1	1	RNF26	1	RPS16	1	S100A13	2
RIMKLA	1	RNF31	1	RPS2	1	S100A6	1
RIMS1	2	RNF34	1	RPS21	3	S100B	3
RIMS2	3	RNF4	4	RPS25	1	S1PR1	2
RIMS3	1	RNF40	5	RPS27L	1	S1PR3	2
RIN2	3	RNF44	3	RPS29	2	SAA1	1
RING1	2	RNF5	1	RPS6	3	SAC3D1	2
RIOX1	2	RNFT2	1	RPS6KC1	2	SACS	9
RIPK4	1	RNU6-1	1	RPS6KL1	3	SACS-AS1	1
RIPOR1	2	RNU6-8	2	RPSA	1	SALL1	3
RIPOR2	2	RNU6ATAC	1	RPUSD1	1	SALL2	5
RIT1	3	ROBO1	1	RPUSD2	1	SALL3	2
RITA1	1	ROBO2	5	RPUSD4	1	SAMD1	1
RLBP1	1	ROCK1	1	RRAGA	1	SAMD14	2
RLIM	8	ROCK2	1	RRAGC	1	SAMD4A	3
RN7SK	1	ROGDI	3	RRAGD	1	SAMD5	3
RNASE1	1	ROPN1L-AS1	1	RRAS2	1	SAP18	1
RNASEH2C	3	ROR2	1	RRNAD1	1	SAP25	1
RNASET2	1	RORA-AS1	2	RRP1B	1	SAP30	2
RND3	1	RORB	1	RRP7A	2	SAP30L	2
RNF103	3	RORB-AS1	2	RRP8	1	SAP30L-AS1	1
RNF111	2	RPA1	1	RS1	3	SAR1B	1
RNF112	1	RPAIN	4	RSBN1L	1	SARDH	1
RNF114	1	RPH3A	1	RSC1A1	2	SARM1	2

SART1	2	SCP2	1	SEPT3	1	SH2B1	2
SART3	1	SCRIB	1	SEPT5	1	SH2B2	3
SASH1	3	SCRN1	2	SEPT7P2	6	SH2D1A	3
SATB1	3	SCRN3	1	SEPT9	1	SH2D4A	2
SATB2	5	SCRT1	1	SERAC1	1	SH2D5	1
SAV1	1	SCX	1	SERBP1	2	SH3BGRL2	1
SAYSD1	1	SCYL1	2	SERF2	1	SH3BGRL3	1
SBF1	5	SCYL2	1	SERINC1	1	SH3BP1	1
SBF2	1	SCYL3	1	SERP2	1	SH3BP2	3
SBK1	2	SDAD1P1	1	SERPINA3	2	SH3BP4	3
SC5D	1	SDC2	1	SERPINE3	1	SH3BP5-AS1	2
SCAF1	2	SDC3	4	SERPINH1	2	SH3BP5L	3
SCAF11	1	SDCBP2	2	SERPINI1	2	SH3D19	1
SCAF8	1	SDCCAG3	1	SERTAD2	1	SH3D21	2
SCAMP1-AS1	2	SDCCAG8	1	SERTAD3	1	SH3GLB1	1
SCAMP4	1	SDE2	2	SERTAD4-AS1	1	SH3KBP1	1
SCAND1	3	SDHAF1	1	SERTM1	1	SH3PXD2A	1
SCAND2P	9	SDHAF2	2	SESN1	2	SH3RF1	1
SCARA3	1	SDK1	1	SESN2	1	SH3RF3	2
SCARB1	1	SDR39U1	1	SET	1	SH3TC1	2
SCARNA11	1	SEC14L1	1	SETBP1	1	SH3YL1	2
SCARNA14	1	SEC16A	6	SETD1B	2	SHARPIN	1
SCARNA18	1	SEC22A	1	SETD2	4	SHB	2
SCARNA22	2	SEC23IP	1	SETD3	1	SHC4	1
SCARNA26A	2	SEC24A	1	SETD5	2	SHF	3
SCARNA26B	1	SEC62	1	SETD7	2	SHH	3
SCARNA8	1	SECISBP2	4	SETD9	4	SHISA2	6
SCCPDH	3	SEL1L3	1	SETX	3	SHISA4	2
SCD5	1	SELENOKP3	1	SEZ6	1	SHISA6	1
SCFD2	1	SELENOO	4	SEZ6L	1	SHISA7	2
SCG2	1	SEMA3A	1	SEZ6L2	1	SHISA9	4
SCGB1A1	1	SEMA3B-AS1	1	SF1	1	SHISAL1	2
SCGB1C2	3	SEMA4C	1	SF3B1	1	SHKBP1	3
SCGB3A1	1	SEMA4F	1	SF3B4	1	SHROOM1	1
SCGN	1	SEMA6A-AS1	1	SF3B5	1	SHROOM2	2
SCLT1	1	SEMA6A-AS2	2	SFRP1	1	SHROOM3	1
SCML4	5	SEMA6C	2	SFRP5	1	SIAH1	4
SCN1A	1	SEMA6D	2	SFSWAP	1	SIAH3	2
SCN1B	1	SENP3-EIF4A1	3	SFT2D3	7	SIGLEC15	1
SCN2A	3	SENP5	5	SGCZ	1	SIMC1	2
SCN3A	4	SENP6	2	SGK1	1	SIN3A	2
SCN3B	4	SENP8	1	SGK494	1	SIN3B	1
SCN8A	1	SEPHS1	1	SGPP1	2	SIPA1L1	2
SCN9A	2	SEPHS2	2	SGSH	2	SIPA1L2	3
SCO1	1	SEPT10	2	SGSM2	1	SIRT1	2
SCO2	6	SEPT11	1	SGSM3	1	SIRT4	1

SIRT7	1	SLC25A27	1	SLC38A7	1	SLF2	2
SIX5	1	SLC25A28	1	SLC38A8	1	SLFN5	1
SKA3	1	SLC25A29	1	SLC39A10	1	SLFNL1	1
SKI	2	SLC25A30-AS1	1	SLC39A3	5	SLIRP	1
SKIDA1	3	SLC25A34	1	SLC39A9	1	SLIT1	1
SKIL	2	SLC25A37	2	SLC3A1	1	SLIT1-AS1	6
SKOR1	1	SLC25A39	1	SLC3A2	2	SLITRK1	2
SKP2	1	SLC25A41	3	SLC41A1	2	SLITRK2	6
SLAIN1	1	SLC25A44	3	SLC41A2	3	SLITRK3	5
SLAIN2	1	SLC25A46	1	SLC45A1	3	SLITRK4	3
SLC10A4	1	SLC25A51	2	SLC45A3	2	SLITRK5	3
SLC10A6	2	SLC25A6	2	SLC45A4	1	SLMAP	1
SLC12A2	1	SLC26A1	2	SLC46A1	1	SLTM	2
SLC12A5	3	SLC26A2	1	SLC48A1	1	SMAD1	1
SLC12A6	1	SLC26A4	2	SLC4A11	1	SMAD2	1
SLC12A8	2	SLC27A3	1	SLC4A1AP	2	SMAD4	4
SLC13A3	1	SLC27A4	2	SLC4A3	1	SMAD5-AS1	1
SLC15A4	2	SLC27A5	1	SLC4A8	1	SMAD7	4
SLC16A14	3	SLC28A1	1	SLC51A	2	SMAD9	1
SLC16A1-AS1	2	SLC29A4	5	SLC52A2	1	SMARCA2	1
SLC16A2	1	SLC2A10	2	SLC5A11	5	SMARCA5	4
SLC16A8	1	SLC2A13	1	SLC5A2	2	SMARCC1	1
SLC16A9	2	SLC2A1-AS1	2	SLC5A3	3	SMARCD3	1
SLC17A8	1	SLC2A2	1	SLC5A6	2	SMC6	1
SLC17A9	3	SLC2A3	1	SLC6A13	5	SMCR5	5
SLC18A2	3	SLC2A4RG	4	SLC6A15	1	SMCR8	3
SLC19A1	1	SLC2A6	1	SLC6A17	3	SMG5	1
SLC1A3	1	SLC30A1	1	SLC6A1-AS1	1	SMG6	2
SLC1A4	2	SLC31A2	1	SLC6A3	2	SMG8	5
SLC20A1	1	SLC32A1	2	SLC6A4	1	SMIM10L2A	3
SLC20A2	1	SLC33A1	1	SLC6A7	1	SMIM10L2B	1
SLC22A12	1	SLC34A2	1	SLC6A8	2	SMIM12	2
SLC22A13	1	SLC35A5	1	SLC7A5	1	SMIM17	2
SLC22A16	2	SLC35B2	1	SLC7A6	1	SMIM20	1
SLC22A17	2	SLC35B4	1	SLC7A9	1	SMIM22	1
SLC22A23	2	SLC35C1	5	SLC8A1	1	SMIM26	1
SLC22A5	1	SLC35C2	4	SLC8A1-AS1	2	SMIM27	1
SLC22A7	4	SLC35E1	4	SLC8A2	1	SMIM4	1
SLC24A2	1	SLC35E3	1	SLC8A3	2	SMIM8	7
SLC24A3	1	SLC35E4	2	SLC9A3-AS1	5	SMLR1	1
SLC24A5	2	SLC35F2	1	SLC9A3R2	1	SMN1	1
SLC25A10	1	SLC35F6	1	SLC9A6	2	SMO	1
SLC25A17	1	SLC35G5	2	SLC9B2	1	SMPD1	1
SLC25A18	2	SLC37A3	1	SLCO3A1	1	SMTNL1	2
SLC25A23	1	SLC38A1	6	SLCO5A1	2	SMUG1	2
SLC25A24	4	SLC38A2	1	SLF1	1	SMURF1	1

SNAI3	1	SNORA79	1	SNORD69	1	SOX10	2
SNAP25	1	SNORA80A	1	SNORD72	1	SOX11	4
SNAP25-AS1	1	SNORA80C	2	SNORD73B	1	SOX12	4
SNAP47	5	SNORA80D	3	SNORD82	1	SOX2	4
SNAP91	2	SNORA89	1	SNORD88B	1	SOX21	1
SNAPC3	1	SNORA92	1	SNORD9	1	SOX3	2
SNAPIN	2	SNORA9B	1	SNORD94	1	SOX4	2
SNCAIP	2	SNORC	4	SNORD97	2	SOX5	1
SNCG	1	SNORD12	4	SNRK	1	SOX8	1
SNHG20	1	SNORD128	1	SNRK-AS1	1	SOX9	1
SNHG22	2	SNORD129	1	SNRNP25	2	SP1	2
SNHG5	1	SNORD135	1	SNRNP35	3	SP3	4
SNN	3	SNORD13D	1	SNRNP70	1	SP4	4
SNORA10	1	SNORD13E	1	SNRPB2	1	SP5	1
SNORA100	2	SNORD13F	1	SNRPE	9	SP8	1
SNORA101B	1	SNORD13J	1	SNRPN	1	SP9	2
SNORA105B	1	SNORD141A	1	SNTA1	1	SPACA3	1
SNORA11	1	SNORD141B	1	SNU13	1	SPACA6P-AS	2
SNORA117	7	SNORD145	1	SNX12	1	SPACA9	5
SNORA11C	1	SNORD148	2	SNX14	2	SPAG7	1
SNORA11G	2	SNORD14C	1	SNX18	4	SPARCL1	2
SNORA120	1	SNORD14E	2	SNX19	4	SPART-AS1	1
SNORA16B	1	SNORD151	2	SNX21	3	SPATA13-AS1	3
SNORA17B	2	SNORD152	2	SNX22	4	SPATA2	2
SNORA20B	1	SNORD153	1	SNX32	1	SPATA2L	2
SNORA21B	1	SNORD155	1	SNX33	3	SPATA46	1
SNORA28	1	SNORD163	1	SNX4	1	SPATA5	1
SNORA30	2	SNORD164	1	SNX7	1	SPATA6L	2
SNORA31	1	SNORD167	1	SOCS1	1	SPATA7	1
SNORA36C	1	SNORD170	2	SOCS2	2	SPATA9	1
SNORA38	2	SNORD172	6	SOCS3	1	SPCS1	1
SNORA4	2	SNORD20	1	SOCS7	1	SPDYA	2
SNORA40B	2	SNORD23	1	SOD1	2	SPECC1	3
SNORA47	2	SNORD31B	1	SOD2	1	SPECC1L	6
SNORA50C	2	SNORD35A	1	SOD3	3	SPEG	1
SNORA53	1	SNORD35B	1	SOGA1	2	SPEM1	3
SNORA54	1	SNORD36B	1	SOGA3	4	SPG11	1
SNORA59B	1	SNORD42B	1	SORBS2	2	SPHK1	5
SNORA5A	1	SNORD51	1	SORCS1	1	SPIDR	1
SNORA65	3	SNORD53B	1	SORCS3	1	SPIN3	2
SNORA66	1	SNORD54	2	SOST	1	SPIN4	1
SNORA67	3	SNORD57	1	SOSTDC1	1	SPINDOC	1
SNORA70B	1	SNORD61	3	SOWAHA	3	SPIRE1	1
SNORA74B	1	SNORD62A	4	SOWAHB	4	SPNS2	1
SNORA75	1	SNORD66	1	SOWAHC	1	SPOCK2	3
SNORA77	1	SNORD68	1	SOX1	3	SPP1	1

SPPL2B	3	SSH3	1	STOX2	5	SYS1-DBNDD2	2
SPPL2C	1	SSNA1	1	STPG4	1	SYT11	4
SPPL3	1	SSR1	2	STRAP	1	SYT13	4
SPRED2	2	SSR2	4	STRN3	1	SYT16	1
SPRN	4	SSR4	4	STRN4	3	SYT17	1
SPRTN	1	SSTR1	3	STUB1	1	SYT2	2
SPRY1	1	SSTR2	7	STUM	1	SYT3	1
SPRY2	1	ST14	2	STX10	2	SYT4	2
SPRY4-IT1	1	ST20	4	STX16	4	SYT5	2
SPSB1	1	ST20-MTHFS	1	STX4	1	SYT6	1
SPSB2	1	ST3GAL1	6	STX7	1	SYT7	1
SPSB3	1	ST3GAL2	4	SUGP2	3	SZRD1	1
SPTBN2	2	ST3GAL4	1	SULF1	3	SZT2-AS1	2
SPTBN4	2	ST3GAL5	2	SULF2	2	TAB1	1
SQLE	1	ST3GAL6	1	SULT4A1	1	TAB2	2
SQSTM1	2	ST6GAL1	3	SUMF2	1	TAB3-AS1	1
SRA1	1	ST6GAL2	2	SUMO1	1	TACC1	2
SRC	3	ST7-OT3	1	SUMO4	2	TACC2	1
SRCIN1	2	ST8SIA1	1	SUN2	1	TACO1	1
SRD5A1	1	ST8SIA2	2	SUOX	1	TACR1	1
SREBF1	2	ST8SIA3	2	SUPT16H	2	TADA1	3
SREK1	3	ST8SIA4	1	SUPT6H	1	TAF10	1
SRF	1	ST8SIA5	3	SUPT7L	1	TAF11	2
SRGAP2	1	STAB1	4	SURF2	1	TAF1C	1
SRGAP2-AS1	1	STAC3	1	SURF6	2	TAF2	1
SRGAP3	1	STAG1	1	SUSD2	2	TAF4	1
SRP14	1	STAP1	1	SUV39H2	1	TAF6	1
SRP19	11	STARD4-AS1	2	SUZ12P1	1	TAF7	3
SRPK1	2	STARD7-AS1	4	SV2A	1	TAGAP	1
SRPRB	1	STAT3	1	SV2B	1	TAGLN3	2
SRRD	2	STH	3	SWI5	1	TANGO6	2
SRRM2-AS1	5	STIM1	2	SYBU	1	TAOK2	1
SRRM3	1	STIM2	1	SYCP3	2	TAOK3	2
SRRM5	1	STIP1	1	SYDE2	2	TAPBP	1
SRSF1	1	STK11	1	SYNC	2	TAPT1	1
SRSF11	2	STK17A	1	SYNCRIP	1	TAPT1-AS1	1
SRSF5	1	STK17B	1	SYNDIG1	3	TARBP1	1
SRSF6	1	STK24	1	SYNE1	1	TARDBP	2
SRSF9	2	STK25	2	SYNE1-AS1	3	TARS2	6
SRXN1	6	STK35	2	SYNGR1	1	TAS1R3	2
SS18	1	STK38	1	SYNGR2	1	TATDN2	1
SSBP3-AS1	4	STK40	1	SYNGR3	3	TAX1BP1	2
SSBP4	1	STMN2	1	SYNM	11	TBC1D1	2
SSC5D	1	STMN3	2	SYNPO	7	TBC1D10A	1
SSFA2	5	STMN4	1	SYNRG	2	TBC1D10B	1
SSH1	1	STOML1	2	SYP-AS1	1	TBC1D12	1

TBC1D14	5	TDRG1	4	THEM6	2	TM6SF1	1
TBC1D16	4	TEAD4	2	THEMIS2	2	TM7SF2	1
TBC1D20	4	TECPR2	2	THNSL1	1	TM9SF1	2
TBC1D22A	2	TEDC1	1	THOC1	1	TMA16	1
TBC1D24	1	TEDC2	1	THOC2	2	TMA7	3
TBC1D26	3	TEF	6	THOC5	2	TMBIM6	1
TBC1D29	2	TEKT2	1	THOC6	1	TMBIM7P	1
TBC1D4	1	TELO2	2	THOP1	1	TMCC1	2
TBC1D7-LOC100130357	1	TENM4	1	THRIL	2	TMCC2	4
TBC1D9	1	TENT4A	4	THSD1	5	TMCO2	1
TBC1D9B	5	TERF1	4	THSD7A	2	TMED5	1
TBCC	2	TERF2	1	THSD7B	2	TMED6	1
TBKBP1	2	TERF2IP	2	THTPA	1	TMED7-TICAM2	2
TBL1XR1	1	TET2	1	THUMPD1	1	TMED9	1
TBL2	1	TET2-AS1	2	THY1	3	TMEFF2	1
TBP	1	TET3	3	THYN1	2	TMEM106A	1
TBPL1	1	TEX10	1	TIAF1	2	TMEM11	4
TBR1	7	TEX2	2	TIAM1	2	TMEM110-MUSTN1	1
TBRG1	1	TEX22	1	TIAM2	1	TMEM115	1
TBRG4	1	TEX264	1	TICAM1	2	TMEM120B	1
TBX2	1	TEX29	4	TIGAR	1	TMEM121	3
TBX3	1	TEX35	3	TIGD3	1	TMEM121B	5
TBX6	1	TEX43	1	TIGD5	4	TMEM127	2
TCAF2	1	TEX53	4	TIMM10	1	TMEM129	1
TCAP	2	TFAP2C	1	TIMM13	3	TMEM132A	3
TCEAL1	1	TFCP2L1	4	TIMM22	5	TMEM132B	2
TCEAL2	1	TFE3	1	TIMM44	1	TMEM132D	2
TCEAL3	1	TFG	2	TIMM8A	1	TMEM132D-AS1	3
TCEAL4	1	TFPT	1	TIMM8B	1	TMEM132E	2
TCEAL5	1	TGFA	1	TIMMDC1	1	TMEM136	1
TCEAL6	1	TGFB1	1	TIMP2	1	TMEM147	2
TCEAL7	1	TGFB1I1	2	TINF2	2	TMEM150B	2
TCEAL8	1	TGFB2-OT1	2	TIPARP	2	TMEM151A	1
TCEAL9	1	TGFB3	3	TIPRL	1	TMEM151B	4
TCERG1	1	TGFBR1	2	TJP1	2	TMEM158	2
TCF12	1	TGFBR3L	2	TJP2	1	TMEM160	7
TCF15	2	TGFBRAP1	1	TKT	1	TMEM168	1
TCF20	5	TGIF1	1	TLE1	2	TMEM170A	1
TCF25	1	TGOLN2	4	TLE2	2	TMEM177	1
TCF4	4	THAP11	2	TLE3	1	TMEM178A	1
TCHP	1	THAP2	2	TLE4	1	TMEM178B	1
TCIM	1	THAP3	5	TLL2	1	TMEM179	1
TCP11	2	THAP4	1	TLNRD1	4	TMEM179B	3
TCTE1	1	THAP5	1	TLR5	2	TMEM181	2
TDP1	1	THAP7-AS1	3	TLR9	2	TMEM184B	2
TDRD6	1	THBS1	2	TM2D2	1	TMEM184C	1

TMEM185B	2	TMEM74	1	TOMM6	4	TRG-AS1	2
TMEM186	4	TMEM74B	3	TONSL	2	TRHDE	2
TMEM19	1	TMEM80	1	TOP2B	1	TRIB1	1
TMEM191C	5	TMEM81	3	TOR1A	2	TRIB2	2
TMEM196	1	TMEM82	1	TOR1AIP1	1	TRIL	3
TMEM198B	2	TMEM86A	1	TOR1AIP2	2	TRIM14	1
TMEM199	2	TMEM88	2	TOR1B	3	TRIM15	2
TMEM200A	2	TMEM8A	1	TOR2A	1	TRIM22	1
TMEM200B	2	TMEM95	1	TOR3A	3	TRIM24	1
TMEM200C	3	TMEM97	1	TOR4A	2	TRIM28	1
TMEM201	2	TMOD3	1	TOX3	2	TRIM3	1
TMEM203	1	TMOD4	1	TP53AIP1	5	TRIM32	3
TMEM211	1	TMPPE	1	TP53BP1	2	TRIM33	1
TMEM214	1	TMSB4Y	1	TP53BP2	3	TRIM35	1
TMEM215	1	TMTC1	1	TP53I11	5	TRIM36	3
TMEM216	1	TMTC2	4	TP53I13	2	TRIM37	3
TMEM217	1	TMUB1	1	TP53INP2	4	TRIM41	2
TMEM229A	1	TMUB2	1	TP73-AS1	2	TRIM44	2
TMEM229B	2	TMX4	2	TPBG	1	TRIM45	1
TMEM236	1	TNC	1	TPGS1	3	TRIM52	4
TMEM240	3	TNFAIP1	2	TPI1	1	TRIM67	3
TMEM242	4	TNFAIP2	2	TPM2	1	TRIM69	1
TMEM243	1	TNFAIP8L1	2	TPP1	9	TRIM8	6
TMEM245	1	TNFRSF1A	1	TPPP	9	TRIO	1
TMEM246-AS1	1	TNFRSF21	2	TPRG1L	2	TRIOBP	3
TMEM248	1	TNFRSF25	4	TPRN	1	TRIP11	1
TMEM250	2	TNFRSF4	2	TPSG1	1	TRIP12	1
TMEM251	2	TNFRSF6B	2	TPST1	1	TRIP6	2
TMEM256	1	TNFSF8	1	TRAF1	1	TRIR	1
TMEM259	1	TNIP1	1	TRAF3	1	TRIT1	1
TMEM263	2	TNIP2	2	TRAF3IP1	2	TRMT12	3
TMEM265	7	TNK2	2	TRAF3IP2	2	TRMT44	4
TMEM30A	1	TNKS1BP1	5	TRAF3IP2-AS1	1	TRMT61B	1
TMEM39A	2	TNKS2	1	TRAF4	4	TRMT9B	1
TMEM41A	1	TNRC18	7	TRAF5	1	TRNP1	2
TMEM42	1	TNRC18P1	1	TRAF6	3	TRO	3
TMEM43	4	TNRC6C	3	TRAFD1	1	TRPC1	1
TMEM44	2	TNRC6C-AS1	3	TRAIP	1	TRPC3	1
TMEM44-AS1	1	TNS2	2	TRAM2	1	TRPC4	1
TMEM47	2	TNXB	3	TRAP1	3	TRPC5OS	1
TMEM50A	2	TOB1	2	TRAPPC10	3	TRPS1	2
TMEM54	1	TOB2	1	TRAPPC12	1	TRPV1	2
TMEM59	1	TOGARAM1	2	TRAPPC3	1	TRPV4	1
TMEM60	2	TOMM20L	1	TRAPPC5	2	TRUB2	1
TMEM65	1	TOMM22	3	TRAPPC6B	1	TSC22D1	2
TMEM70	1	TOMM40	1	TREX1	2	TSC22D1-AS1	3

TSC22D2	3	TTN-AS1	3	UBE2N	1	UQCRHL	1
TSC22D3	1	TTPAL	1	UBE2Q1	1	URAHP	2
TSC22D4	1	TTYH3	4	UBE2QL1	2	URB2	2
TSEN2	1	TUBA1A	1	UBE2V1	4	UROD	3
TSFM	1	TUBA1B	2	UBE3A	2	USB1	1
TSHZ1	6	TUBA4B	1	UBE4B	1	USE1	4
TSHZ2	1	TUBA8	3	UBFD1	2	USF2	1
TSHZ3	6	TUBB	3	UBIAD1	1	USF3	3
TSKU	2	TUBB2A	3	UBL3	2	USP10	1
TSNARE1	1	TUBB2B	1	UBL4A	2	USP11	2
TSPAN17	1	TUBB3	7	UBN1	4	USP19	1
TSPAN3	2	TUBB4A	3	UBN2	3	USP21	3
TSPAN4	1	TUBB4B	3	UBOX5	3	USP22	1
TSPAN5	1	TUBB6	4	UBP1	3	USP27X	2
TSPOAP1	2	TUBBP5	3	UBQLN2	4	USP31	3
TSPOAP1-AS1	3	TULP3	1	UBQLN4	1	USP35	5
TSPY26P	8	TULP4	3	UBR2	1	USP36	1
TSPYL1	1	TUSC1	1	UBR3	2	USP38	2
TSPYL2	4	TUT1	1	UBR5	1	USP3-AS1	2
TSPYL4	3	TUT4	1	UBXN4	1	USP40	1
TSPYL5	3	TXLNA	2	UCHL1	1	USP42	4
TSR2	1	TXN2	1	UCHL5	2	USP46	1
TSR3	2	TXNDC15	1	UCK1	4	USP6NL	1
TSSC4	3	TXNDC17	1	UCK2	1	USP7	1
TSSK2	5	TXNDC2	1	UCKL1	2	USP9X	1
TSSK3	1	TXNDC5	1	UCN	1	USPL1	5
TSSK6	2	TXNIP	1	UFSP1	1	UTF1	1
TST	1	TXNL4B	2	UGP2	1	UTP14C	3
TSTD1	1	TYRO3	1	ULK1	1	UTP18	1
TTBK1	1	TYSND1	1	ULK2	1	UTP3	1
TTBK2	1	U2AF2	1	UMPS	3	UTS2B	1
TTC1	1	UBA5	2	UNC119	1	UTY	2
TTC27	1	UBAC1	2	UNC119B	1	VAMP2	1
TTC3	1	UBALD1	1	UNC13A	1	VAMP3	1
TTC30A	1	UBALD2	1	UNC13C	1	VANGL1	1
TTC31	3	UBAP1	1	UNC50	2	VARS2	2
TTC36	7	UBAP2	1	UNC5B	1	VASH1	2
TTC3-AS1	2	UBB	2	UNC5C	2	VASH1-AS1	3
TTC5	1	UBE2CP5	8	UNC80	7	VASN	1
TTC9B	3	UBE2D3	1	UNK	1	VAT1	1
TTF1	1	UBE2E2	1	UPK3A	1	VAT1L	1
TTI1	4	UBE2G2	1	UPRT	1	VAV2	1
TTLL11	2	UBE2H	1	UQCR10	1	VAV3	1
TTLL12	1	UBE2J1	1	UQCR11	1	VCAN	2
TTLL7	1	UBE2K	1	UQCRB	2	VCAN-AS1	15
TTLL8	1	UBE2L3	1	UQCRFS1	2	VCPIP1	3

VCPKMT	2	WDPCP	1	XKR4	1	ZBTB14	3
VCX3B	1	WDR11	1	XKR6	2	ZBTB16	1
VDAC3	2	WDR13	2	XKR7	2	ZBTB17	7
VEGFA	4	WDR24	2	XPC	1	ZBTB18	1
VEZF1	1	WDR25	2	XPO1	1	ZBTB2	1
VGF	3	WDR26	1	XPO6	1	ZBTB20-AS1	3
VGLL4	2	WDR33	1	XPR1	1	ZBTB22	1
VHL	3	WDR34	1	XRCC5	2	ZBTB25	2
VIM-AS1	1	WDR45B	11	XXYLT1-AS1	1	ZBTB3	1
VIPR1-AS1	1	WDR47	2	YAE1D1	1	ZBTB34	4
VIRMA	2	WDR55	1	YBEY	1	ZBTB38	4
VKORC1L1	1	WDR6	4	YBX1	1	ZBTB39	5
VLDLR	1	WDR81	3	YDJC	2	ZBTB4	2
VMAC	1	WDR86-AS1	2	YEATS2	1	ZBTB44	2
VMP1	1	WDR89	3	YEATS2-AS1	10	ZBTB45	1
VOPP1	4	WDR92	2	YIPF2	3	ZBTB46	1
VPS13C	1	WDR97	2	YIPF5	1	ZBTB48	2
VPS13D	4	WDSUB1	1	YIPF6	1	ZBTB49	2
VPS16	2	WDTC1	1	YKT6	3	ZBTB6	3
VPS18	3	WEE1	1	YLPM1	4	ZBTB7A	4
VPS33A	2	WFIKKN1	2	YOD1	1	ZBTB8A	4
VPS35L	1	WFIKKN2	2	YPEL1	2	ZBTB8B	5
VPS37B	1	WFS1	4	YPEL5	2	ZBTB8OS	2
VPS37C	1	WHAMM	2	YRDC	2	ZBTB9	5
VPS37D	3	WIPF2	1	YTHDC1	2	ZC2HC1C	1
VPS53	1	WIPI2	3	YTHDF1	2	ZC3H10	4
VPS54	2	WISP1	1	YTHDF2	5	ZC3H12B	2
VPS9D1-AS1	1	WIZ	1	YTHDF3	3	ZC3H12C	4
VSIG10L	1	WLS	1	YWHAE	1	ZC3H13	2
VSIG2	1	WNK1	2	YWHAH	1	ZC3H14	1
VSNL1	1	WNT10B	1	YWHAQ	1	ZC3H15	1
VSTM2A	1	WNT11	3	YWHAZ	4	ZC3H18	2
VSTM2B	1	WNT3	2	YY1	2	ZC3H3	1
VSTM2L	1	WNT4	1	ZACN	6	ZC3H6	3
VTA1	1	WNT5A	1	ZADH2	6	ZC3H7A	1
VTI1B	3	WNT5B	1	ZAP70	1	ZC3H7B	1
VWA1	3	WNT7A	2	ZAR1	1	ZCCHC14	1
VWA2	1	WNT7B	2	ZAR1L	3	ZCCHC2	3
WAC	3	WRAP53	1	ZBED1	8	ZCCHC3	1
WAPL	2	WRNIP1	1	ZBED3	1	ZCCHC7	1
WASF1	1	WSCD1	3	ZBED4	2	ZCCHC8	2
WASHC2A	1	WTAP	1	ZBED5	3	ZDBF2	1
WBP1	3	WTIP	1	ZBED6	6	ZDHHC14	1
WBP2NL	2	WWC1	3	ZBP1	1	ZDHHC18	1
WDCP	1	XBP1	1	ZBTB10	5	ZDHHC22	4
WDFY3-AS2	2	XIAP	1	ZBTB11-AS1	3	ZDHHC23	2

ZDHHC5	2	ZNF138	1	ZNF3	2	ZNF460	1
ZDHHC7	2	ZNF14	1	ZNF300	1	ZNF462	7
ZEB1	3	ZNF140	2	ZNF302	1	ZNF470	1
ZEB2	2	ZNF160	1	ZNF304	3	ZNF48	5
ZFAND5	3	ZNF17	3	ZNF316	4	ZNF480	2
ZFAS1	2	ZNF174	1	ZNF317	5	ZNF483	2
ZFHX2	1	ZNF18	2	ZNF318	4	ZNF487	2
ZFHX4-AS1	3	ZNF180	1	ZNF320	3	ZNF488	1
ZFP1	2	ZNF189	1	ZNF324	1	ZNF493	1
ZFP3	1	ZNF192P1	1	ZNF324B	2	ZNF496	3
ZFP36	1	ZNF195	2	ZNF32-AS1	1	ZNF500	1
ZFP36L1	3	ZNF197	1	ZNF331	1	ZNF501	1
ZFP36L2	1	ZNF2	2	ZNF333	3	ZNF503-AS2	2
ZFP41	6	ZNF20	2	ZNF337	6	ZNF510	1
ZFP62	2	ZNF202	2	ZNF341-AS1	1	ZNF512	2
ZFP64	2	ZNF205-AS1	2	ZNF35	3	ZNF513	7
ZFP69B	2	ZNF207	2	ZNF350	2	ZNF514	4
ZFX	3	ZNF211	4	ZNF354C	4	ZNF517	2
ZFY-AS1	1	ZNF212	3	ZNF362	1	ZNF518B	6
ZFYVE1	2	ZNF217	2	ZNF37A	2	ZNF519	1
ZFYVE21	2	ZNF221	1	ZNF37BP	4	ZNF521	1
ZFYVE26	1	ZNF224	1	ZNF382	3	ZNF526	2
ZFYVE9	2	ZNF226	5	ZNF385A	1	ZNF528-AS1	1
ZGLP1	2	ZNF227	1	ZNF385B	1	ZNF532	4
ZGPAT	2	ZNF230	1	ZNF385C	1	ZNF536	3
ZIC1	3	ZNF233	3	ZNF394	2	ZNF543	1
ZIC2	1	ZNF234	1	ZNF397	2	ZNF544	1
ZKSCAN1	1	ZNF236	1	ZNF398	1	ZNF546	1
ZKSCAN2	4	ZNF24	2	ZNF407	2	ZNF548	3
ZKSCAN4	1	ZNF248	2	ZNF41	2	ZNF549	2
ZKSCAN5	2	ZNF250	2	ZNF415	1	ZNF555	4
ZMAT2	2	ZNF251	2	ZNF416	1	ZNF556	2
ZMAT4	1	ZNF256	1	ZNF417	5	ZNF557	5
ZMIZ2	2	ZNF26	3	ZNF418	3	ZNF558	2
ZMPSTE24	1	ZNF260	2	ZNF419	1	ZNF561	3
ZMYM3	1	ZNF263	5	ZNF428	1	ZNF564	10
ZMYM4-AS1	3	ZNF266	2	ZNF432	5	ZNF565	1
ZMYM5	1	ZNF273	4	ZNF433	1	ZNF570	2
ZNF101	1	ZNF280B	1	ZNF436	2	ZNF571-AS1	2
ZNF106	3	ZNF280D	1	ZNF439	4	ZNF574	6
ZNF12	1	ZNF281	2	ZNF44	2	ZNF576	1
ZNF121	3	ZNF282	3	ZNF445	1	ZNF577	1
ZNF132	1	ZNF284	3	ZNF446	9	ZNF579	3
ZNF133	2	ZNF285	1	ZNF449	1	ZNF581	1
ZNF134	3	ZNF292	1	ZNF451	3	ZNF583	1
ZNF135	4	ZNF295-AS1	1	ZNF454	2	ZNF585A	1

ZNF586	3	ZNF711	4	ZRANB1	2
ZNF593	2	ZNF713	2	ZSCAN12	3
ZNF594	1	ZNF717	1	ZSCAN18	9
ZNF595	1	ZNF718	1	ZSCAN20	3
ZNF606	1	ZNF720	1	ZSCAN21	8
ZNF607	1	ZNF736	1	ZSCAN25	2
ZNF608	2	ZNF737	2	ZSCAN26	1
ZNF609	1	ZNF747	4	ZSCAN29	2
ZNF614	1	ZNF749	1	ZSCAN31	3
ZNF619	1	ZNF763	2	ZSCAN32	2
ZNF621	1	ZNF764	2	ZSCAN9	2
ZNF622	2	ZNF768	2	ZSWIM1	3
ZNF623	3	ZNF770	1	ZSWIM4	1
ZNF627	2	ZNF771	1	ZSWIM5	1
ZNF629	12	ZNF772	3	ZSWIM6	2
ZNF638	2	ZNF773	1	ZSWIM7	4
ZNF639	1	ZNF777	4	ZSWIM8	1
ZNF641	1	ZNF778	4	ZSWIM9	4
ZNF644	1	ZNF780A	1	ZXDA	3
ZNF646	4	ZNF780B	1	ZXDB	5
ZNF648	1	ZNF781	1	ZYG11B	1
ZNF649-AS1	1	ZNF782	1	ZZZ3	3
ZNF652	1	ZNF783	2		
ZNF653	1	ZNF785	3		
ZNF660-ZNF197	1	ZNF786	3		
ZNF662	1	ZNF791	2		
ZNF664	2	ZNF792	3		
ZNF668	3	ZNF8	4		
ZNF669	1	ZNF804A	2		
ZNF671	2	ZNF805	3		
ZNF672	3	ZNF81	2		
ZNF675	1	ZNF827	2		
ZNF687	5	ZNF83	2		
ZNF688	2	ZNF830	2		
ZNF689	1	ZNF839	1		
ZNF69	1	ZNF84	1		
ZNF691	2	ZNF847P	2		
ZNF692	1	ZNF852	1		
ZNF696	1	ZNF853	4		
ZNF70	5	ZNF862	1		
ZNF701	2	ZNF865	3		
ZNF703	1	ZNF891	4		
ZNF704	2	ZNF91	5		
ZNF706	1	ZNF93	5		
ZNF709	3	ZNHIT2	1		
ZNF710	1	ZNRF1	1		

Appendix 4. Optimisation of anti-YTHDF3 antibody for immunocytochemistry in differentiated TE671 cells. 40x objective.

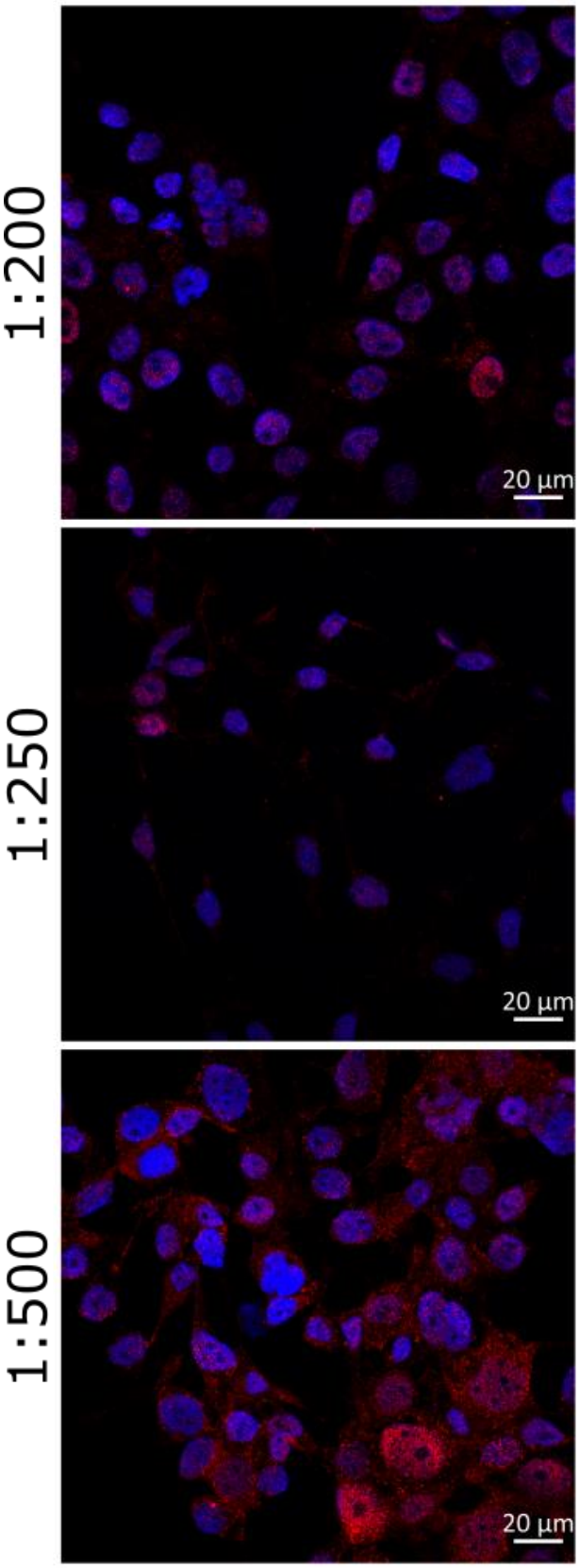

Appendix 5. Optimisation of anti-YTHDF3 antibody for immunohistochemistry in differentiated TE671 cells. 63x objective.

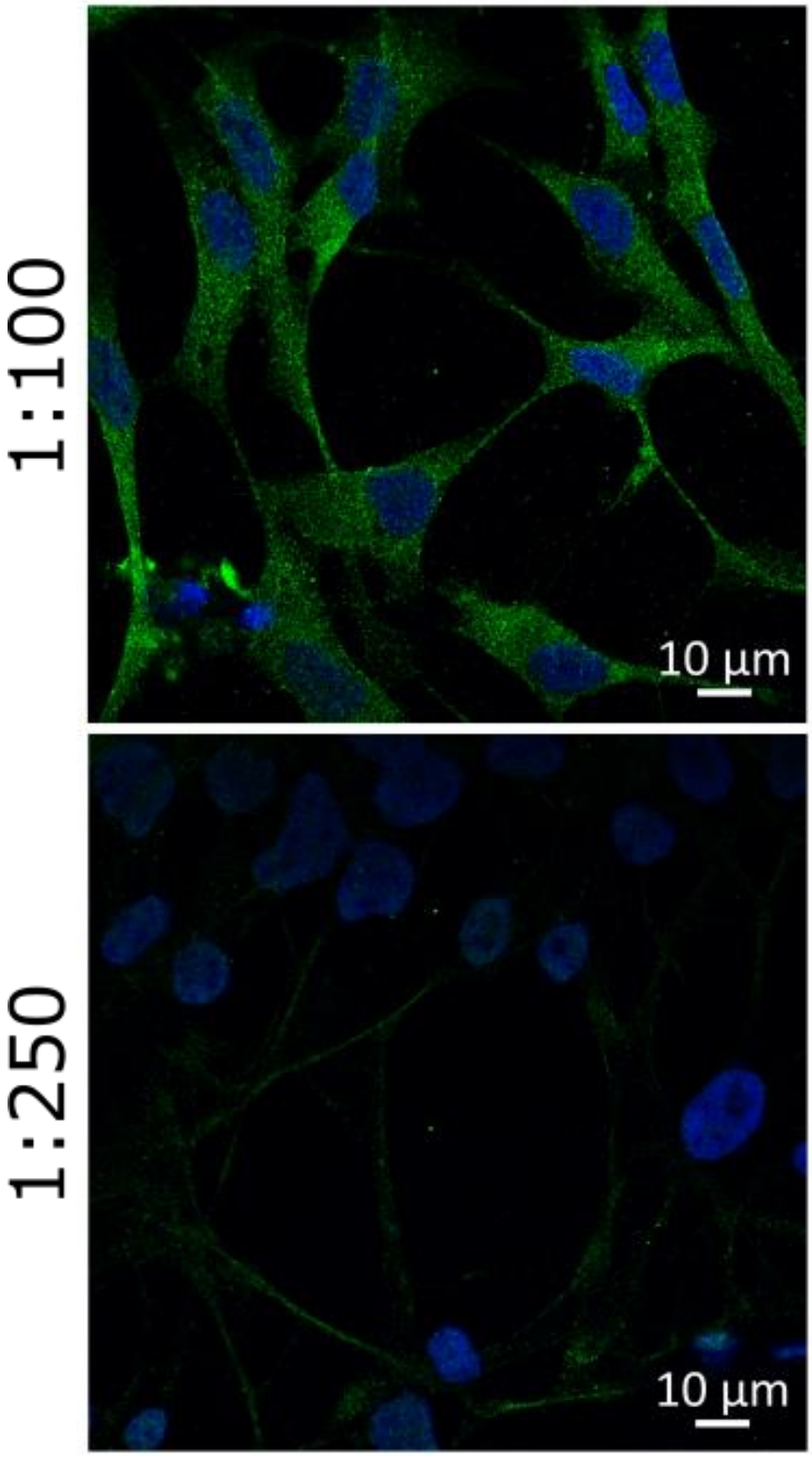

Appendix 6. Sample immunocytochemistry figures of quiescent and 15 min NMDA-activated differentiated TE671 cells.

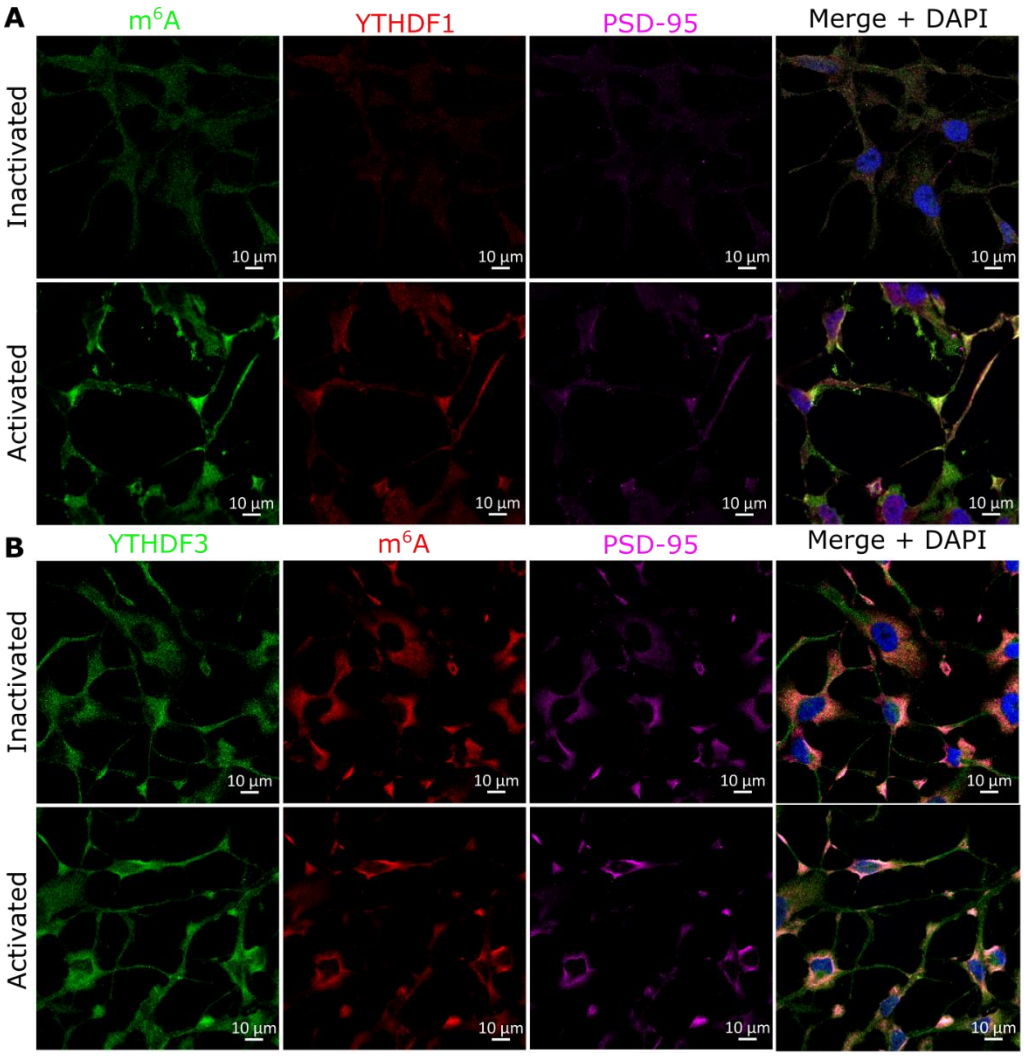

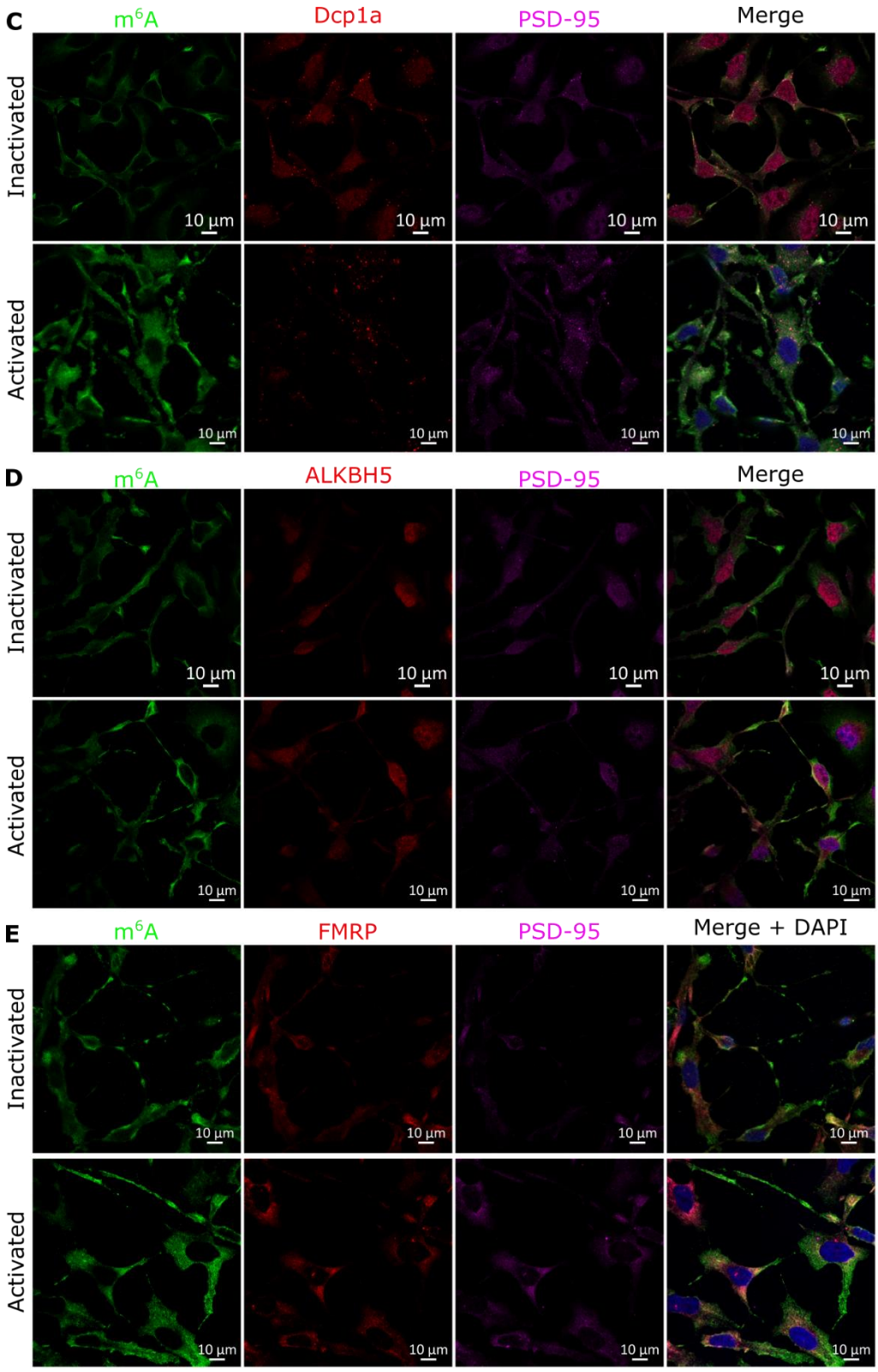
C
m6A
Dcp1a
PSD-95
Merge
Inactivated
Activated
10 μm
D
m6A
ALKBH5
PSD-95
Merge
Inactivated
Activated
10 μm
E
m6A
FMRP
PSD-95
Merge + DAPI
Inactivated
Activated
10 μm